Principles of Stable Isotope Geochemistry

2nd Edition

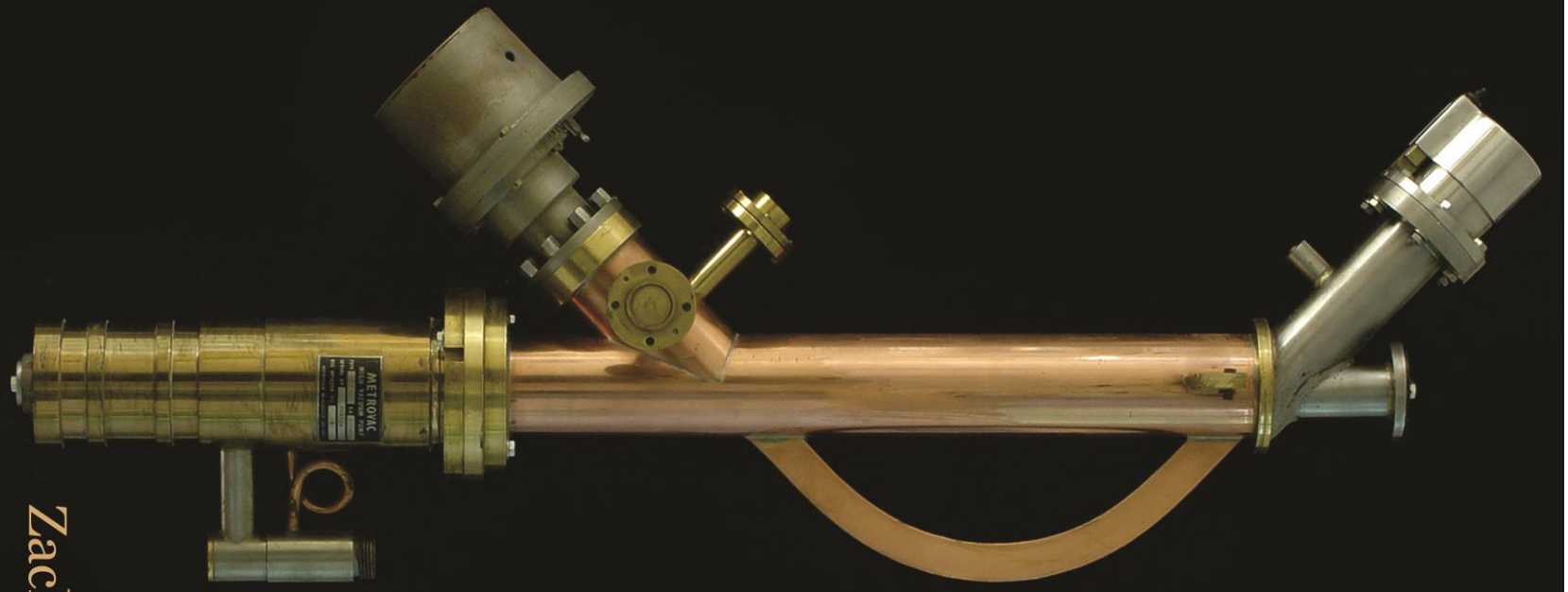

Zachary Sharp

Abstract

Principles of Stable Isotope Geochemistry is written as a textbook to accompany a one semester course in Stable Isotope Geochemistry. There are 13 chapters, each dealing with a specific subtopic of the field. Other than Chapters 1 and 2 – introduction and definitions – most of the remaining chapters can be read without reliance on the preceding ones. It is also hoped that the book will serve as a general reference volume for researchers in the field.

Principles of Stable Isotope Geochemistry has been organized in such a way that major concepts are explained and accompanied by numerous examples. In most cases, the first published examples are used for illustration, giving both a broad base of understanding and an appreciation for the historical development of the field. Chapters are organized according to broad classifications. In some cases this is done by discipline such as Chapter 4 – Hydrology and in others by isotope, such as Chapter 10 – Sulfur.

The new revised version is online. In this way, it can be modified as new advances are made in the field. Comments regarding errors, omissions or suggestions for improvements are welcome in order to keep the book up to date. This new online version is free of charge, available in PDF format. A hardcopy is also available.

Table of Contents

Chapter 1: Introduction

Chapter 2: Terminology, Standards and Mass Spectrometry

Chapter 3: Equilibrium Isotope Fractionation

Chapter 4: The Hydrosphere

Chapter 5: The Oceans

Chapter 6: Biogenic Carbonates: Oxygen

Chapter 7: Carbon in the Low-Temperature Environment

Chapter 8: Low Temperature Minerals, Exclusive of Carbonates

Chapter 9: Nitrogen

Chapter 10: Sulfur

Chapter 11: Igneous Petrology

Chapter 12: Metamorphic Petrology

Chapter 13: Extraterrestrial Materials

Appendix 1: Standard Reference Materials for Stable Isotopes

Appendix 2: Sample calculation of the correction procedure for adjusting measured isotope data to accepted IAEA reference scales

About the cover: A Metropolitan Vickers MS 2 mass spectrometer, bought by the Ecole de Géologie, Nancy France in 1958 for analyses of Pb, and later Rb/Sr at the CNRS, Nancy. Similar mass spectrometers were used for oxygen isotope analyses. The mass spectrometer consists of a copper vertical tube pumped by a diffusion pump (bottom center). The flight tube cuts through the central vacuum tube, allowing it to be pumped essentially at both ends. This is the predecessor of the early VG Micromass spectrometers. Photograph by Andreas Pack.

About the cover: A Metropolitan Vickers MS 2 mass spectrometer, bought by the Ecole de Géologie, Nancy France in 1958 for analyses of Pb, and later Rb/Sr at the CNRS, Nancy. Similar mass spectrometers were used for oxygen isotope analyses. The mass spectrometer consists of a copper vertical tube pumped by a diffusion pump (bottom center). The flight tube cuts through the central vacuum tube, allowing it to be pumped essentially at both ends. This is the predecessor of the early VG Micromass spectrometers. Photograph by Andreas Pack.

Chapter 1

INTRODUCTION

Contents

1.1 About this book 1
1.2 Historical Background 1
1.3 Scope of the Discipline 5
1.3.1 What are stable isotopes? 6
1.3.2 Which elements and why? 8
1.4 Abundances of the Rare Isotopes of Light Elements 9
1.5 Characteristics of Elements that Undergo Significant Isotopic Fractionation 10
1.6 Applications in the Earth Sciences 12
1.7 Isotope Effects 13
1.7.1 Kinetic isotope effects 13
1.7.2 Equilibrium isotope effects 14
References 16

Chapter 1

INTRODUCTION

1.1 About this book

The first edition of this book was written as a general introduction to stable isotope geochemistry. It was meant primarily as a guide and general resource for an upper division and graduate level stable isotope course. Since it was first published in 2007, the scope of stable isotopes has grown tremendously. New fields, not envisioned in the first edition, have developed and blossomed, and existing fields have grown considerably. The motivation for the original book was to provide a useful, inexpensive textbook that could also be used as foundation for new practitioners to the field. However things are changing so fast that it is impossible to keep up with new developments using the traditional publishing format. Turn-around times are too long, and the cost to the end-user are too high. This new 'live' edition is meant to overcome these problems. The book is online and freely available to all. Because it is electronic, it can be (and hopefully will be) modified easily and frequently, so that new developments can be incorporated as they become available. It is my hope that this 'live' version will remain up-to-date and be a valuable no-cost resource for stable isotope practitioners around the world.

1.2 Historical Background

The published early 'discussions' by scientists studying the structure of the atom and significance of isotopes make for remarkable reading. The early practitioners, including J.J. Thomson, E. Rutherford, F. Soddy and F.W. Aston, J. Chadwick, G. Gamow and others were generally concerned with radioactivity – the spontaneous disintegration of large atoms to smaller fragments. But in their efforts to understand the structures of atoms, they were also keenly aware of departures of elemental masses from Aston's 'whole number rule' – the idea that all elements have masses that are multiples of the mass of hydrogen. In a round-table discussion by E. Rutherford, F. W. Aston, J. Chadwick, and others, Rutherford states: "*The essential point brought out in the earlier work of Dr. Aston was that the masses of the elements are approximately expressed by whole numbers, where oxygen is taken as 16-with the exception of hydrogen itself. But the real interest, as we now see it, is not the whole number rule*[1] *itself, but rather the departures from it"* (Rutherford et al., 1929). Of particular interest was the element Cl, with a mass of 35.5. In an earlier 'discussion' in 1921, J.J. Thomson stated "*Mr. Aston, who has measured the atomic weight of chlorine by a different method, cannot find any chlorine – or any other substance – with an atomic weight of 35.5, but he does find substances with atomic weights of 35 and 37. Accepting the numbers on both sides, there does not seem to be any explanation other than that either chlorine is a mixture of these two substances of atomic weight 35 and 37, or else that, in the discharge tube which Mr. Aston employs to measure the atomic weight, some decomposition or integration – or both – of the chlorine atom has occurred."* (Thomson et al., 1921). Aston had identified the two isotopes of Cl, masses 35 and 37. There was no problem with his mass

[1] The whole number rule is that the masses of the elements are multiples of the mass of hydrogen or as Rutherford states above, relative to oxygen with a mass of 16.

spectrograph! In 1931 James Chadwick published the results of his discovery of the neutron in the modestly titled paper "*Possible existence of a neutron*" (Chadwick, 1931), and the fundamental building blocks of atoms were firmly in place.

The first suggestion that physical chemical processes could cause isotopic fractionation of light elements in natural substances was made in 1925 by British scientists H. Briscoe and P. Robinson (Briscoe and Robinson, 1925). Before that time, it was generally assumed that the isotopic compositions of all substances were homogeneously distributed throughout the Earth. Briscoe and Robinson observed a variation in the atomic weight of boron in minerals from various localities. They proposed that processes like solution, crystallization, melting, and volatilization would likely cause such isotopic variations in nature. In the following year the eminent Russian scientist V. Vernadsky suggested that isotopic fractionation of the light elements should occur in living matter as well, but there were no experimental or natural data to support this hypothesis at that time. Variations in the hydrogen and oxygen isotope ratios of water in the hydrologic cycle of the Earth were recognized crudely as early as the mid-1930s on the basis of precise density measurements (Gilfillan, 1934). In that same decade, H. Urey[2] and his colleagues at Columbia University were conducting experiments and developing the theory for isotope exchange reactions and equilibria (Urey and Greiff, 1935), and A. Nier and his colleagues at the University of Minnesota were making significant improvements to Aston's early mass spectrometer designs, and were discovering variations in the stable isotope ratios of several light elements in natural materials (Fig. 1.1).

Probably the first *bona fide* application of light stable isotope measurements to a major geochemical problem was published by F. Wickman (1941) who calculated the total amount of bitumen and coal in the Earth on the basis of carbon isotope analyses of these materials. Titles of several articles written in the 1930s and 1940s show clearly that the power of stable isotope measurements in resolving problems in earth science was recognized long ago by outstanding scientists throughout the world (Table 1.1).

Light stable isotope geochemistry as we know it today arguably began in 1946. During that year, Harold Urey traveled to several prominent universities in Europe to deliver a lecture sponsored annually by the Royal Society of London. Urey presented results of calculations of the isotopic fractionation of stable isotope ratios of the

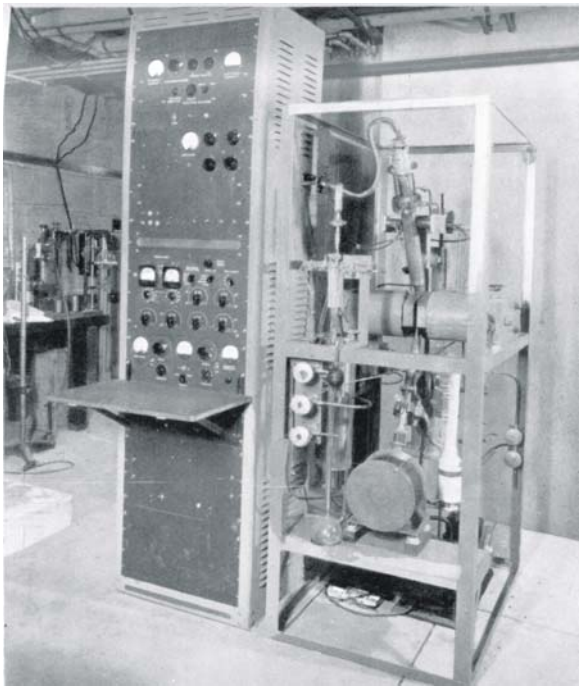

Fig. 1.1. Nier's 60° sector mass spectrometer, 1947. From Rankama (1954).

[2] H.C. Urey (1893-1981) won the Nobel Prize in chemistry in 1934 for his discovery of deuterium. He is considered the father of modern stable isotope geochemistry.

light elements among ideal gases and simple aqueous ions from spectroscopic data and the methods of statistical mechanics. The results of his calculations, published in the now classic paper entitled *The Thermodynamic Properties of Isotopic Substances* (Urey, 1947) remain to this day a valuable resource for isotope fractionation factors of simple compounds. At this lecture in Zurich in December of 1946, the renowned crystallographer Paul Niggli wondered if it might be possible to determine the fresh water or marine origin of ancient deposits of limestone, coral or shells from oxygen isotope analysis of the carbonate. At that time it was already known that $^{18}O/^{16}O$ ratios of marine limestones were about 3% higher than those of the ocean and that ocean water was isotopically heavier than fresh waters. Prompted by Niggli's remarks, Urey turned his attention to the temperature coefficient of the oxygen isotope fractionation between $CaCO_3$ and H_2O. On the basis of estimates made from his calculations, he concluded that this coefficient might be large enough to determine the temperatures of ancient oceans from oxygen isotope analyses of $CaCO_3$ in fossil shells. As Urey recounted the story later: "I suddenly found myself with a geological thermometer in my hands." And the games began.

Table 1.1. *Selected early publications in stable isotope chemistry and geochemistry.*

Year	Title	Reference
1921	Discussion on isotopes	Thomson *et al. Proc. Roy. Soc. Lond.* **99**, 87-104
1932	A hydrogen isotope of mass 2 and its concentration.	Urey, H.C., Brickwedde, F.G. and Murphy, G.M., *Phys. Rev*. **40**, 1.
1934	The natural separation of the isotopes of hydrogen.	Dole, M., *J. Amer. Chem. Soc*. **56**, 999.
1935	Isotopic exchange equilibria.	Urey, H.C. and Greiff, L.J., *J.Amer. Chem. Soc*. **57**, 321
1936	The relative atomic weight of oxygen in water and air.	Dole, M., *J. Chem. Phys.* **4**. 268-275.
1939	Isotopic composition of rain water.	Teis, R.V., *Compt. Rend. Acad. Sci. U.R.S.S*. **23**, 674.
1940	A mass spectrometer for routine isotope abundance measurements	Nier, A.O. *Rev. Sci. Inst.* **11**, 212-216
1941	Determination of the isotopic composition of [hydroxyl] waters in metamorphic rocks and minerals.	Vernadsky, W.I., Vinogradov, A.P., and Teis, R.V., *Compt. Rend. Acad. Sci. U.R.S.S.* **31**, 573.
1941	On a new possibility of calculating the total amount of coal and bitumen.	Wickman, F.E., *Geol. Fören. i Stockholm Förh*. **63**, 419.
1947	Calculation of equilibrium constants for isotopic exchange reactions.	Bigeleisen, J., Mayer, M.G. *J. Chem. Phys.* **15**, 261-267.
1947	The thermodynamic properties of isotopic substances	Urey, H.C. *J. Chem. Soc.* 562-581.
1949	Natural variations in the isotopic content of sulfur and their significance.	Thode, H.G., MacNamara, J. and Collins, C.B., *Can. J. Res*. **27B**, 361.
1950	Isotopic composition of oxygen in silicate rocks.	Baertschi, P., *Nature* **166**, 112. Baertschi, P. and Silverman, S.R., *Geochim. Cosmochim. Acta* **1**, 4-6.
1951	Carbonate-water isotopic temperature scale.	Epstein, S., Buchsbaum, R., Lowenstam, H., Urey, H.C. *J. Geol.* **62,** 417-426.
1951	Relative abundance of oxygen and carbon isotopes in carbonate rocks.	Baertschi, P., Nature **168**, 288.
1952	Variation in the relative abundance of carbon isotopes in plants.	Wickman, F.E., Geochim. Cosmochim. Acta, **2**, 243.
1953	The geochemistry of the stable carbon isotopes.	Craig, H., Geochim. Cosmochim. Acta, **3**, 53-92.

The overall precision of the isotopic measurements required to make temperature estimates that were meaningful in paleoclimatology was not attainable in the 1940s. At that time the precision of mass spectrometric measurements of $^{18}O/^{16}O$ ratios was about a factor of ten less than required to determine temperatures to ± 0.5°C. In addition, there was no reproducible technique for extracting CO_2 from $CaCO_3$, and there were no experimental data relating the oxygen isotope fractionation between calcium carbonate and water to temperature. Urey was not to be deterred from proceeding with this ambitious project, and he assembled an outstanding group of young scientists to work on it. This research team included postdoctoral fellow Sam Epstein, doctoral students Harmon Craig, and John McCrea, paleontologist Heinz Lowenstam and an electronics engineer Charles McKinney. By 1950, this group had successfully improved the precision of the Nier isotope ratio mass spectrometer (Nier, 1947; McKinney et al., 1950) by the necessary factor of 10, developed reproducible analytical extraction methods for biogenic carbonates and established standards and protocols that are still being followed for the most part today. The development of the oxygen isotope paleotemperature scale (Urey et al., 1948; Epstein et al., 1951; Urey et al., 1951) has been heralded as one of the outstanding scientific achievements of the twentieth century.

Concurrent with work on oxygen isotope analyses of carbonate shells, members of the Chicago group conducted survey studies of oxygen isotope variations in silicate rocks and minerals (Baertschi, 1950; Baertschi and Silverman, 1951), carbon isotope variations in nature (Craig, 1953), stable isotope ratios of natural waters (Epstein and Mayeda, 1953; Friedman, 1953) and oxygen isotope compositions of biogenic phosphates (Tudge, 1960). Important early stable isotope research was also conducted in Hamilton, Ontario on sulfur isotope ratios of rocks and minerals (Thode, 1949), in Copenhagen on oxygen isotope variations in natural waters (Dansgaard, 1954), and in Moscow on oxygen and sulfur isotope ratios of rocks and minerals (Vinogradov and Dontsova, 1947; Trofimov, 1949). Tom Hoering and his group in Arkansas investigated isotopic variations of nitrogen and chlorine in natural substances (Hoering, 1956; Hoering and Moore, 1958; Hoering and Parker, 1961). Within a few short years, it was recognized that oxygen isotope fractionations between cogenetic minerals were large enough to register temperatures of formation of high-temperature rocks (Clayton and Epstein, 1958) and that hydrogen and oxygen isotope measurements of rocks and minerals were powerful petrologic tools (Taylor and Epstein, 1962).

From these beginnings, stable isotope research has blossomed to the point where thousands of isotope ratio mass spectrometers are in operation in laboratories all over the world. Stable isotope measurements are being made to resolve problems in many diverse fields including geochemistry, climatology, hydrology, plant physiology, ecology, archaeology, meteorology, meteoritics, palaeobiology, bacteriology and the origin of life.

Almost all the early achievements in the field of isotope geology were made by gifted chemists and physicists who developed the theory and techniques, improved the mass spectrometers and extraction methods, and thought and wrote about many fundamental scientific questions of geologic interest. It is well to keep in mind that, despite developments in isotope ratio mass spectrometry, most notably very stable electronics and increased sensitivity of sources, there have been only modest improvements in the overall precision of modern stable isotope analyses over those made in the early 1950s. There are certainly exceptions to this claim. Sample sizes have come

down considerably and some of the more exotic, cutting-edge analyses could not have been made on the early machines. Most importantly however, the ease of analysis has improved dramatically. Thanks to the efforts of the mass spectrometer manufacturers to produce more user-friendly machines, many types of analyses that used to take the better part of a day can now be done in minutes. This has opened up the field of stable isotopes to a whole new class of researchers, particularly biologists, who need large numbers of analyses to see through the inherent variability of natural populations.

The new rapid techniques do not necessarily translate to better precision or accuracy. The old laborious extraction techniques for a stable isotope analysis were developed by analytical chemists who were very concerned about reproducible, quantitative chemical reactions. I have been asked by students whether the 'old' data are any good and can be used. I would say that data from much of the old literature is as good or better than data collected today. (The only question would be whether the old data are calibrated to known reference materials).

It is instructive to read the early papers. One comes to the enlightening realization that many questions being examined with the aid of stable isotope measurements today were already addressed by these early workers. Similar or identical conclusions reached from analyses of several or even only a few carefully selected materials 40-50 years ago are reappearing in recent publications that may contain hundreds of analyses, many of them superfluous. It is worthwhile, both from an historical standpoint and as proper scientific procedure to be aware of pertinent observations and conclusions published in the older literature. In this spirit, I have made an attempt to cite primary references whenever possible in this book.

1.3 Scope of the Discipline

Stable isotope measurements have an extremely wide range of applications and the principles employed are relatively easy to grasp. There are gross similarities between some of the approaches and scientific goals of stable isotope geochemistry and other geochemical systems. The basic principle of stable isotope geochemistry was first recognized by Briscoe and Robinson (1925) when they identified differences in the boron isotope ratios of natural materials. The fundamental principle is this: ***In any multiphase system, there is a preferential fractionation of isotopes, with one phase preferentially incorporating the heavy (or light) isotope relative to other coexisting phases.*** This isotope fractionation is due to subtle differences in the masses and thermodynamic properties of the different isotopes, and occurs in both equilibrium and kinetic processes. Evaporation of water into undersaturated air and incorporation of CO_2 during photosynthesis are examples of irreversible kinetic processes with large isotope fractionations. High temperature crystal growth and mineral recrystallization are processes that often approach thermodynamic equilibrium and have generally smaller isotopic fractionations. Unlike the kinetic fractionations, equilibrium fractionations follow well-understood thermodynamic rules. The traditional isotopic systems apply to the elements H, C, N, O, S. Recent analytical advances have added a whole host of additional elements to the isotope geochemists arsenal, including B, Cl, Si and the 'non-traditional' isotopes of Li, Mg, Ca, Cr, Fe, Cu, Zn, Se, and Mo (Johnson et al., 2004; Teng et al., 2017). Given that most natural materials contain one or more of these elements, the applications of stable isotopes to natural systems are extraordinarily broad

based, with new ideas being developed all the time. Figure 1.2 gives a broad-brush overview of the various fields and types of applications of stable isotopes.

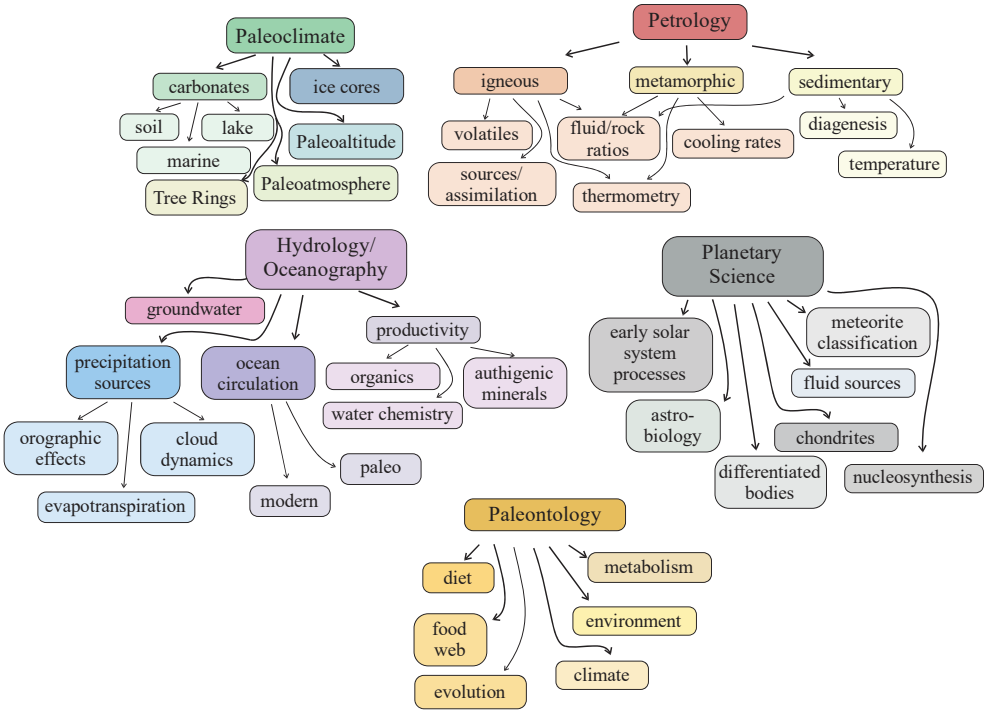

Fig. 1.2. Examples of the types of fields that are studied using stable isotopes.

1.3.1 What are stable isotopes?

In the most simple description, atoms consist of the subatomic particles ***protons, electrons*** and ***neutrons***. Protons are positively charged, electrons are negatively charged and neutrons have no charge. The mass of a neutron is about equal to that of a proton and the mass of an electron is negligible relative to protons and neutrons (Table 1.2). The mass of an atom, therefore is determined by the total number of protons and neutrons.

An element is defined by the number of protons in its nucleus. In a neutral atom, the number of protons is balanced by an equal number of electrons which are present as a negatively charged cloud around the nucleus. The configuration of the electron cloud imparts to the atom its gross chemical properties. For a given element, the number of protons (**atomic number** Z) is always the same, but the number of neutrons (**neutron number** N) may vary. The **mass number** A is the sum of Z + N (Table 1.3). The number of neutrons in the nucleus of an element does not affect the gross chemical properties of the element and its compounds, but mass differences due to changing N can cause subtle chemical and physical differences which results in isotopic fractionation. It is these small differences comprise the subject of this discipline.

An **isotope**[3] of a given element differs from another isotope of the same element by the number of neutrons in its nucleus. Most elements in the Periodic Table have two or more naturally occurring isotopes (either stable or radioactive) but 21 elements, including fluorine and sodium, are **monoisotopic**. The nucleus of the single natural isotope of fluorine, contains 9 protons (Z = 9) and 10 neutrons (A = 19). Oxygen has three naturally occurring isotopes: ^{16}O with 8 protons and 8 neutrons, ^{17}O with 8 protons and 9 neutrons, and ^{18}O with 8 protons and 10 neutrons.

Table 1.2. *Charge and mass of the proton, neutron and electron.*

Particle	Charge	Mass (g)	Mass (amu)
Proton	+1	$1.6726219 \times 10^{-24}$	1.0072766
Neutron	0	$1.6749275 \times 10^{-24}$	1.0086654
Electron	-1	$9.1093836 \times 10^{-28}$	0.000548597

Consider the three isotopes of hydrogen. **Protium** has one proton, one electron and a mass of 1.0078 atomic mass units, or amu. The nucleus of **deuterium**, a second isotope of hydrogen, contains one proton and one neutron. It has almost the same chemical properties as protium, but a mass of 2.0141 amu (Fig. 1.3), equal to the additional mass of a neutron less the nuclear binding energy of deuterium. **Tritium**, the third naturally occurring isotope of hydrogen, has one proton and two neutrons in its nucleus and thus has a mass of ~3 amu. Whereas both protium and deuterium are stable isotopes of hydrogen, the additional neutron in tritium imparts instability to the nucleus so that tritium is radioactive with a half life of 12.3 years. Neither protium nor deuterium will undergo spontaneous radioactive decay, although strictly speaking, any **nuclide**[4] could undergo spontaneous decay, but the *probability* of such decay is negligible for these so-called stable isotopes. For example, ^{50}V, which was assumed to be stable, actually has a half-life of 1.5×10^{17} y, far longer than the age of the Universe. The three isotopes of hydrogen have very similar chemical properties but different masses, and these slight differences in mass result in slightly different strengths of bonds to other elements. These slight differences in mass and bond strengths are responsible for fractionation of the different isotopes between coexisting phases undergoing a physical or chemical reaction and provide the foundation for all of stable isotope geochemistry.

An example of important effects that can arise as a result of small differences in bond strengths is provided by the chemical and physical properties of the various **isotopologues** of water (Table 1.4), where an 'isotopologue' refers to the mass of a given compound. Although the physical and chemical properties of the isotopologues of water are clearly distinct and large, pure isotopologues are not found in nature. Rather, there exist mixtures of the end-member isotopologues which are each determined by the

[3] The word *isotope* was coined in 1913 by Frederick Soddy, an English scientist who was awarded the 1921 Nobel Prize in chemistry for his investigations into the origin and nature of isotopes.

[4] Truman Kohman of Carnegie Mellon University coined the word **nuclide** as a general term for a *specific* isotope. Including those artificially produced, there are >2500 known nuclides and most of them are radioactive. That is, stable isotopes are relatively rare in nature.

isotopes of the elements in the compound. Isotopic variations that occur in our Solar System are much smaller than the isotopic differences between artificially produced pure isotopologues.

Table 1.3 *Isotopic abundances and relative atomic masses of the pertinent elements in stable isotope geochemistry. Symbols for the main elements in the discipline are emboldened.*

Symbol	Atomic Number **Z**	Neutron number **N**	Mass Number **M**	Abundance (per cent)	Atomic Weight (12C = 12.)
H	1	0	1	99.985	1.007825
D	1	1	2	0.015	2.0140
Li	3	3	6	7.42	6.01512
		4	7	92.58	7.01600
B	5	5	10	19.78	10.0129
		6	11	80.22	11.00931
C	6	6	12	98.89	≡12.
		7	13	1.11	13.00335
N	7	7	14	99.63	14.00307
		8	15	0.37	15.00011
O	8	8	16	99.759	15.99491
		9	17	0.037	16.99914
		10	18	0.204	17.99916
Si	14	14	28	92.21	27.97693
		15	29	4.70	28.97649
		16	30	3.09	29.97376
S	16	16	32	95.0	31.97207
		17	33	0.76	32.97146
		18	34	4.22	33.96786
		20	36	0.014	35.96709
Cl	17	18	35	75.53	34.96885
		20	37	24.47	36.96590

1.3.2 Which elements and why?

It often comes as a surprise to learn that classical stable isotope geochemistry concerns, for the most part, variations in the stable isotope ratios of only five elements: H, C, N, O, and S (or SNOCH). Although small in number, these elements comprise the bulk of tissues in living organisms. The isotope ratios of Si and Cl in natural materials were first measured in 1954 (Allenby, 1954) and 1961 (Hoering and Parker, 1961), respectively, but only recently has interest in these systems jumped substantially. The most unexpected developments in stable isotope geochemistry is the explosive rise in the non-traditional isotopes of metals, including Li, B, Mg, Ca, Ti, V, Cr, Fe, Cu, Zn, Se, Sr, and Mo (Johnson et al., 2004). Most of these isotope ratios are measured using multi-collector inductively coupled plasma mass spectrometer (MC-ICP-MS) and to a lesser

extent thermal ionization mass spectrometry (TIMS) or secondary ion mass spectrometery (SIMS). The isotopic variability in these systems is generally low (except for Li, which has enormous fractionations), but the analytical methodologies allow for differences of less than 0.1‰ to be measured with confidence.

Except for certain stable isotope relations in extraterrestrial materials and gases in the upper atmosphere of Earth, stable isotope geochemistry deals mainly with those

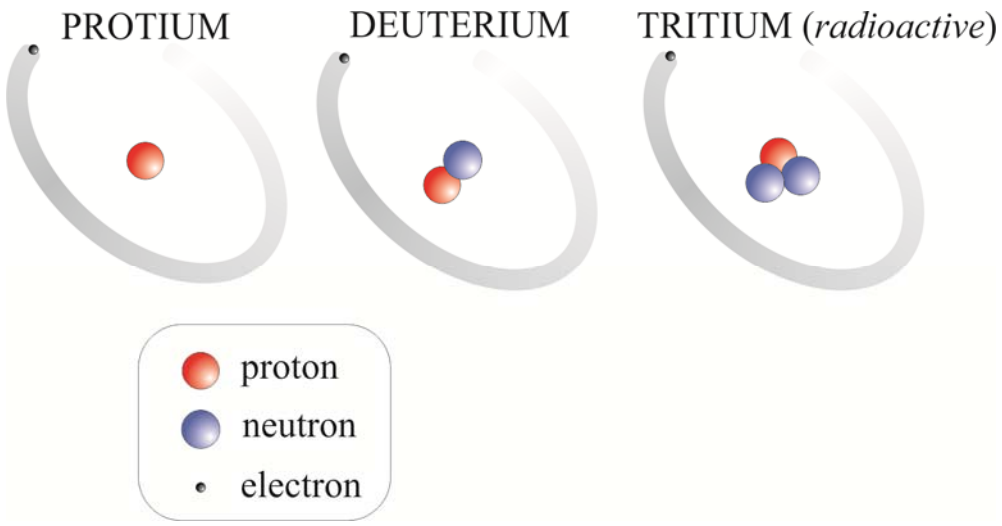

Fig. 1.3. Cartoon of the three isotopes of hydrogen. All have one proton (red sphere) and one electron but differ in the number of neutrons in the nucleus (blue sphere). The three isotopes have very similar chemical properties, but they have very different relative masses and subtly different bond strengths. This phenomenon gives rise to hydrogen isotope fractionation in physical and chemical reactions.

isotopic variations that arise either from isotopic exchange reactions or from mass-dependent fractionations that accompany biological and physical chemical processes occurring in nature or in the laboratory. While ultimately *quantum mechanical* in origin, such isotope effects are governed by kinetic theory and the laws of thermodynamics. Natural variations in the stable isotope ratios of heavy elements of geological interest like Sr, Nd, and Pb involve nuclear reactions and are governed by other factors including the ratio of radioactive parent and daughter, decay constants, and time.

1.4 Abundances of the Rare Isotopes of Light Elements

Isotopic ratios of the most of the elements of primary interest for light stable isotope geochemistry are written conventionally as the ratio of the heavy (and rare) isotope to the light (and more abundant) isotope as in $^{18}O/^{16}O$, $^{34}S/^{32}S$, *etc.* Early workers wrote these ratios in the opposite sense and reported values of absolute ratios. For example, $^{12}C/^{13}C$ or $^{32}S/^{34}S$ ratios were reported as relatively large numbers like 91.16 and 22.51, respectively. With our present knowledge of the absolute stable isotope ratios of certain international reference standards, it is now possible to compare these old analyses with modern analyses of similar materials. There is no accepted convention for writing isotopic ratios of other elements of geochemical interest. Sometimes the heavier

isotope is the more abundant isotope and is still written in the numerator, as in $^{11}B/^{10}B$. In other cases the lighter isotope is written in the numerator regardless of its relative abundance, as in $^{3}He/^{4}He$. The moderately heavy isotope systems violate the 'rare is heavy' rule. Johnson *et al.* (2004) recommend that all isotope systems should report 'heavy/light' isotope ratios to be consistent with the traditional stable isotope terminology. He isotopes will remain forever an exception. The traditional $^{3}He/^{4}He$ nomenclature, where the R value is the $^{3}He/^{4}He$ ratio of a sample relative to the $^{3}He/^{4}He$ ratio of air ($R_a = 1.4 \times 10^{-6}$) will live on.

Table 1.4 *Chemical and physical properties of three of the nine isotopologues of water. (From Hutchinson, 1957 and Handbook of Chemistry and Physics)*

Property	**$H_2{}^{16}O$**	**$D_2{}^{16}O$**	**$H_2{}^{18}O$**
Boiling Point (°C)	100.00	101.42	
Freezing Point (°C)	0.00	3.82	
Density at 0°C (gm/cm^2)	0.999841	1.10469	
Vapor Pressure at 20°C (bars × 10^2)	2.3379	2.0265	2.3161
Temperature of Maximum Density (°C)	4.0	11.6	
Critical Temperature (°C)	374.1	371.5	
Critical Pressure (bars)	220.6	221.5	
Ionization Product, K_w at 25°C	1×10^{-14}	0.3×10^{-14}	
Dielectric Constant at 20°C	80.36	79.755	
Surface Tension at 19°C (dynes/cm)	73.66	72.83	
Viscosity at 20°C (centipoise)	1.009	1.260	
Refractive Index, η_d at 20°C	1.33300	1.32844	
Representative Solubilities at 25°C (g/g of water)			
NaCl	0.359	0.305	
$BaCl_2$	0.357	0.289	

The elements under discussion in this text have one common isotope, like ^{16}O or ^{32}S, and one or more rare isotopes, like ^{17}O, ^{18}O, or ^{33}S, ^{34}S, and ^{36}S whose *average* abundances range from fractions of a per cent to a few per cent. The isotopic abundances and relative atomic weights of elements whose isotopic ratios vary as a result of mass-dependent processes are given in Table 1.3. Note that boron and chlorine are exceptions to the general rule given above concerning disparity in the abundances of the heavy and light isotopes of an element. In these two cases the abundances of the *rare* isotopes ^{10}B and ^{37}Cl are relatively high at 19.78 and 24.47 per cent, respectively.

1.5 Characteristics of Elements that Undergo Significant Isotopic Fractionation

The named elements share several characteristics that are not possessed by other elements whose isotopic ratios are not fractionated to any significant extent in nature or in the laboratory. These characteristics, enumerated below, are only *observed* characteristics and are not rigorously tied to theoretical principles.

1. *They have a relatively low atomic mass*. Significant mass-dependent isotopic variations in terrestrial materials have been looked for but not clearly demonstrated in heavier elements like Cu, Sn, and Ag. These heavier elements do have small fractionations that can now be measured with sufficient precision to have geological relevance, but they generally only have a total range in nature of a few per mil or less.

2. *The relative mass difference between the rare (heavy) and abundant (light) isotope is large.* Compare, for example, the values of 8.3 per cent and 12.5 per cent for the pairs ^{13}C-^{12}C and ^{18}O-^{16}O, respectively, with the value of only 1.2 per cent for ^{87}Sr-^{86}Sr. The relative mass difference between D (deuterium) and H (protium) is almost 100 per cent and hydrogen isotope fractionations are accordingly about ten times larger than those of the other elements of interest. The condition of large relative mass difference is by no means sufficient to promote isotopic fractionation; the $^{48}Ca/^{40}Ca$ ratio varies little in terrestrial rocks despite the large relative mass difference between the isotopes (only that of D-H is larger).

3. *They form chemical bonds that have a high degree of covalent character.* Elements like K, Ca, and Mg that occupy cation sites in minerals form ionic bonds to other elements and experience little or no site preference that could give rise to significant isotopic fractionations. Mg^{2+}, for example, is almost always surrounded by the same atomic environment in nature: an octahedron of oxygen. Nonetheless, small Ca isotope variations observed in biogenic carbonates may have an origin in mass dependent fractionation.

4. *They can exist in more than one oxidation state (C, N, S), form a wide variety of compounds (notably O), and are important constituents of naturally occurring solids and fluids.* Some of the largest fractionations in nature arise from differences in the nature of the chemical bonds to elements in different oxidation states as in the carbon isotope fractionation between CO_2 and CH_4, and sulfur isotope fractionation between sulfide and sulfate. Silicon occurs in a number of naturally occurring compounds, but is almost always bonded to the same element (oxygen) in one oxidation state (+4). Consequently its isotopic ratios vary little in nature, outside of biological processes. Hydrogen is also bonded exclusively to oxygen in inorganic minerals as -OH groups but its isotopic composition is influenced greatly by the other ions bonded to the OH oxygen (Mg^{2+}, Al^{3+}, Fe^{2+}, *etc*.).

5. *The abundance of the element and rare isotope is sufficiently high (tenths to a few atom per cent) to assure the ability to make precise determinations of the isotopic ratios by mass spectrometry.* Measurements of isotopic ratios in materials at trace levels are difficult. Large amounts of material are needed and problems with blanks and contamination become quite serious. With recent advances in the sensitivity of conventional isotope ratio mass spectrometers and the introduction of continuous flow mass spectrometers, low abundance is less of an issue than it

has historically been. The abundance of the rare isotope still separates certain elements, such as He, which has a rare isotope abundance of 0.000137 %, from the elements commonly considered the 'light stable isotopes'.

1.6 Applications in the Earth Sciences

Stable isotope measurements have been applied successfully to the resolution of fundamental problems in the earth sciences, human sciences, biological sciences and several subdisciplines of chemistry. Applications in the earth sciences can be broadly classified into four main types:

1. *Thermometry*	Formation temperatures of rock, mineral and gas systems are determined on the basis of temperature-dependent equilibrium fractionations of the isotopic ratios between two or more cogenetic phases. Stable isotope thermometry has played a major role in studies of paleoclimatology. Recent development of 'clumped isotopes' results in a single-mineral thermometer.
2. *Tracers*	Large reservoirs like the ocean, the mantle, meteoric waters and organic matter have distinct stable isotope signatures that can be used to trace the origin of rocks, fluids, plants, contaminants, and food sources. Isotopic ratios can also be used as biomarkers.
3. *Reaction mechanisms*	Distinctions can be made between diffusion and recrystallization, open and closed systems, and bacterial and thermogenic processes. Certain isotope values can be used to identify kinetic, non-equilibrium processes.
4. *Chemostratigraphy*	Abrupt changes (excursions) in the stable isotope ratios of minerals and organic matter in ocean sediments and certain other terrestrial materials are used as stratigraphic markers, indicators of ocean productivity, and atmospheric chemistry.

The applications of stable isotopes are driven partly by technology and partly by the changing interests in scientific disciplines. Some applications, such as the new non-traditional isotopes, are exciting and high profile, but are also very difficult analytically and costly. An MC-ICP-MS is a very expensive instrument and clean labs are also required for many of the non-traditional measurements. This necessarily limits the number of practitioners in the field. On the other hand, the oxygen and hydrogen isotope ratio of waters can now be measured using low-cost desktop laser spectroscopy devices. As a result, far more researchers are able to measure waters than exotic non-traditional isotopes. The fields are also driven by the science, and interests wax and wane in different disciplines. Climate change concerns drive more people towards water issues and paleoclimate, so research in these fields has increased. Some fields, have 'matured' and consequently, related publications have decreased. There are also completely new techniques which have led to large number of unanticipated study fields. These include

triple isotope analyses of sulfur and oxygen and most notably, the single mineral carbonate thermometer based on 'clumped isotopes' (Eiler, 2007).

1.7 Isotope Effects

1.7.1 Kinetic isotope effects

Kinetic isotope effects are common both in nature and in the laboratory and their magnitudes are comparable to and often much larger than those of equilibrium isotope effects. Kinetic isotope effects are irreversible, and normally associated with fast, incomplete, or unidirectional processes like evaporation, diffusion, and dissociation reactions. Biological reactions such as photosynthesis are clearly irreversible, defying tradition thermodynamics which assume chemical equilibrium. Isotope effects attendant on diffusion and evaporation are explained (in part) by the different translational velocities possessed by the different isotopic forms of molecules as they move through a phase or across a phase boundary. Classical kinetic theory tells us that the average kinetic energy (K.E.) per molecule is the same for all gases at a given temperature. Consider, for example, the molecules $^{12}C^{16}O$ and $^{12}C^{18}O$ that have molecular weights of 28 and 30, respectively. Equating their kinetic energies at some T

$$\text{K.E.}\left(^{12}\text{C}^{16}\text{O}\right) = \text{K.E.}\left(^{12}\text{C}^{18}\text{O}\right) \tag{1.1}$$

and

$$\text{K.E.} = \tfrac{1}{2}mv^2 \tag{1.2}$$

where m is mass and v is velocity. Substituting the masses of these isotopologues of CO, the above equations reduce to

$$\tfrac{1}{2}(28)(v_{28})^2 = \tfrac{1}{2}(30)(v_{30})^2 \tag{1.3}$$

$$v_{28} = \sqrt{30/28}\,v_{30} = 1.035v_{30}. \tag{1.4}$$

That is, regardless of T, the average velocity of $^{12}C^{16}O$ molecules is 3.5 per cent greater than the average velocity of $^{12}C^{18}O$ molecules in the same system.

Such velocity differences can lead to isotopic fractionations in a variety of ways. For example, isotopically light molecules will preferentially diffuse out of a system and leave the reservoir enriched in the heavy isotope. On average, more $^{12}CO_2$ molecules than $^{13}CO_2$ molecules strike the surfaces of leaves and enter the stomates, an effect partially responsible for the low $^{13}C/^{12}C$ ratios of plants relative to other carbon-containing substances in nature. In the case of evaporation, the greater average translational velocities of isotopically lighter water molecules allow them to break through the liquid surface preferentially and diffuse across a boundary layer, resulting in an isotopic fractionation between vapor and liquid that is superimposed on the equilibrium isotopic fractionation between liquid and gaseous H_2O. Attesting to this phenomenon is the fact that water vapor over the oceans or over a large lake has $^{18}O/^{16}O$ and D/H ratios that are significantly lower than the ratios that would obtain at equilibrium (at 100% relative humidity). These lower ratios arise from kinetic isotope effects associated with evaporation.

While it is important to be aware of kinetic isotope effects, they are relatively rare in high-temperature processes occurring on Earth. By contrast, transient processes can occur whereby differing rates of isotopic exchange between coexisting minerals themselves, or between the minerals and an external fluid, can result in assemblages that are grossly out of isotopic equilibrium. Such examples are explained, not by kinetic isotope effects, but rather by a series of equilibrium isotope exchange reactions that have not gone to completion.

1.7.2 Equilibrium isotope effects

Equilibrium isotope effects can be considered in terms of the effect of atomic mass on bond energy. Substituting a light for heavy isotope in a molecular site does not affect the nuclear charges or electronic distribution of the molecule. It does, however, affect the bond strength. The energy required to break a bond is slightly higher for a heavy isotope than it is for a light one. This subtle difference in bond strength results in a predictable isotope fractionation between any two phases. The magnitude of this equilibrium isotopic effect is related to the bonding environment of the phases in question. Most importantly, the fractionation is dependent on temperature, so that for appropriate systems, such as calcite-water, the equilibrium oxygen isotope fractionation between the two phases is a function of temperature alone.

Equilibrium isotopic fractionations between two substances or between two phases of the same substance is the basis of stable isotope thermometry. The temperature dependence on isotope fractionation spawned the first major application of stable isotope chemistry to geological problems: the calcite oxygen isotope thermometer. first used for paleotemperature estimates over 50 years ago (Urey et al., 1948; Epstein et al., 1951; Urey et al., 1951). Figure 1.4 illustrates the equilibrium oxygen isotope fractionations between selected silicate minerals as a function of temperature. The fractionation between any two phases (roughly given by the difference in the isotopic composition of the two phases) generally follows a $1/T^2$ relationship (T in Kelvins). This means that the fractionations become smaller with increasing temperature and that the *temperature dependence* on the fractionation becomes greater at lower temperatures. The calcite-water fractionation is 28.8 ‰ at 25°C, but less than 1‰ at 600°C. The inverse temperature relationship means that a thermometer becomes more precise at lower temperature. The calcite-water thermometer has a precision of better than 1/2°C at room temperature, whereas the precision for quartz-mineral fractionations at metamorphic temperatures is an order of magnitude less precise (Fig. 1.4). (That said, being able to constrain the temperature of metamorphism to ±10°C is a remarkable achievement. Fractionations of not only oxygen isotopes, but those of hydrogen, carbon, nitrogen and sulfur have been used successfully over the years to place constraints on formation temperatures of both high and low temperature systems in nature. These concepts are discussed in more detail in later chapters of this text.

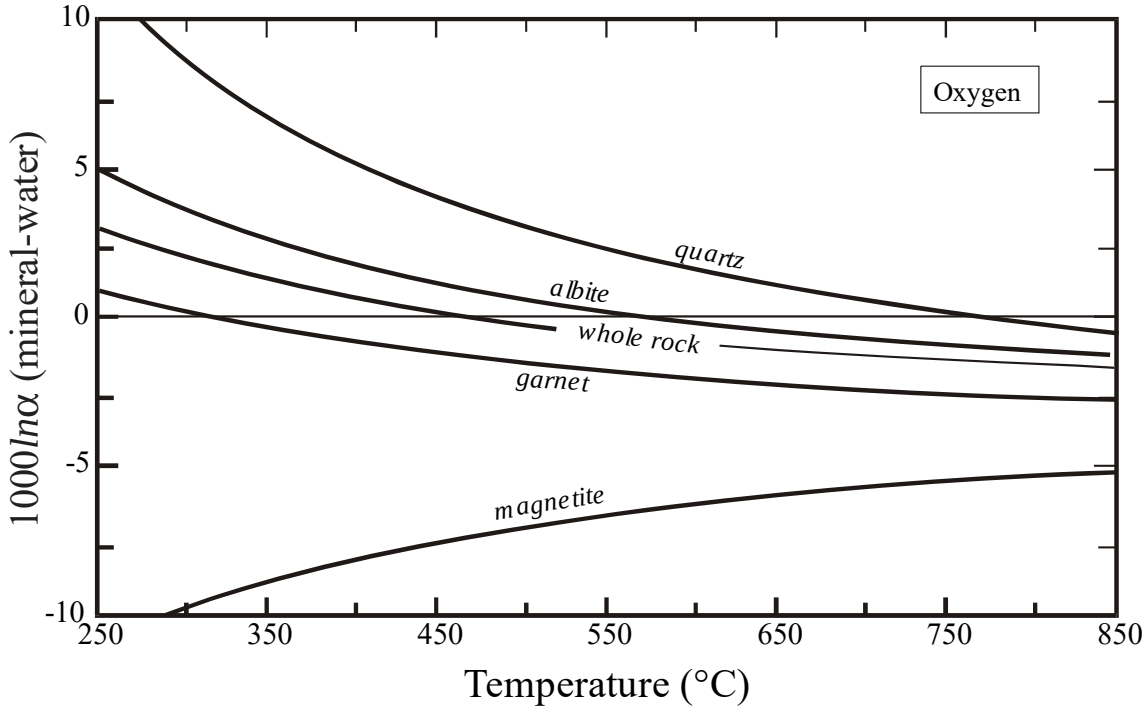

Fig. 1.4. Oxygen isotope fractionation between selected minerals as a function of temperature. In addition to oxygen, regular variations occur for most isotopic systems, including hydrogen, carbon, nitrogen and sulfur. Under certain circumstances to be discussed later, knowledge of the $\delta^{18}O$ values of two cogenetic phases allows the temperatures of formation to be determined. Note: $1000ln\alpha_{a\text{-}b} \approx \delta_a - \delta_b$.

References

Allenby, R.J. (1954) Determination of the isotopic ratios of silicon in rocks. *Geochimica et Cosmochimica Acta* **5**, 40-48.

Baertschi, P. (1950) Isotopic composition of the oxygen in silicate rocks. *Nature* **166**, 112-113.

Baertschi, P. and Silverman, S.R. (1951) The determination of relative abundances of the oxygen isotopes in silicate rocks. *Geochimica et Cosmochimica Acta* **1**, 4-6.

Briscoe, H.V.A. and Robinson, P.L. (1925) A redetermination of the atomic weight of boron. *Journal of the Chemical Society, Transactions* **127**, 696.

Chadwick, J. (1931) Possible existence of a neutron. *Nature* **192**, 312.

Clayton, R.N. and Epstein, S. (1958) The relationship between O^{18}/O^{16} ratios in coexisting quartz, carbonate, and iron oxides from various geological deposits. *Journal of Geology* **66**, 352-373.

Craig, H. (1953) The geochemistry of the stable carbon isotopes. *Geochimica et Cosmochimica Acta* **3**, 53-92.

Dansgaard, W. (1954) The O^{18}-abundance in fresh water. *Geochimica et Cosmochimica Acta* **6**, 241-260.

Eiler, J.M. (2007) "Clumped-isotope" geochemistry—The study of naturally-occurring, multiply-substituted isotopologues. *Earth and Planetary Science Letters* **262**, 309-327.

Epstein, S., Buchsbaum, R., Lowenstam, H. and Urey, H.C. (1951) Carbonate-water isotopic temperature scale. *Journal of Geology* **62**, 417-426.

Epstein, S. and Mayeda, T.K. (1953) Variation of ^{18}O content of waters from natural sources. *Geochimica et Cosmochimica Acta* **4**, 213-224.

Friedman, I. (1953) Deuterium content of natural water and other substances. *Geochimica et Cosmochimica Acta* **4**, 89-103.

Gilfillan, E.S.J. (1934) The isotopic composition of sea water. *Journal of the American Chemical Society* **56**, 406-408.

Hoering, T. and Parker, P.L. (1961) The geochemistry of the stable isotopes of chlorine. *Geochimica et Cosmochimica Acta* **23**, 186-199.

Hoering, T.C. (1956) Variations in the nitrogen isotope abundance, [Chap. 6] of Nuclear Processes in Geologic Settings. *Natl. Research Council, Comm. Nuclear Sci., Nuclear Sci. Ser. Rept. no.* **19**, 39-44.

Hoering, T.C. and Moore, H.E. (1958) The isotopic composition of the nitrogen in natural gases and associated crude oils. *Geochimica et Cosmochimica Acta* **13**, 225-232.

Johnson, C.M., Beard, B.L. and Albarède, F. (2004) Overview and General Concepts, in: Johnson, C.M., Beard, B.L., Albarède, F. (Eds.), Geochemistry of Non-Traditional Stable Isotopes. Mineralogical Society of America, Washington, D.C., pp. 1-24.

McKinney, C.R., McCrea, J.M., Epstein, S., Allen, H.A. and Urey, H.C. (1950) Improvements in mass spectrometers for the measurement of small differences in isotope abundance ratios. *Review of Scientific Instruments* **21**, 724-730.

Nier, A.O. (1947) A mass spectrometer for isotope and gas analysis. *Review of Scientific Instruments* **18**, 398-411.

Rankama, K. (1954) Isotope Geology. McGraw-Hill Book Co., Inc., New York.

Rutherford, E., Aston, F.W., Chadwick, J., Ellis, C.D., Gamow, G., Fowler, R.H., Richardson, O.W. and Hartree, D.R. (1929) Discussion on the structure of atomic nuclei. *Proceedings of the Royal Society of London, Series A* **123**, 373-390.

Taylor, J., H.P. and Epstein, S. (1962) Relationship between O^{18}/O^{16} ratios in coexisting minerals of igneous and metamorphic rocks Part 2. Application to petrologic problems. *Geological Society of America Bulletin* **73**, 675-694.

Teng, F.-Z., Watkins, J.M. and Dauphas, N. (2017) Non-Traditional Stable Isotopes, Reviews in Mineralogy and Geochemistry. Mineralogical Society of America, p. 885.

Thode, H.G. (1949) Natural variations in the isotopic content of sulphur and their significance. *Canadian Journal of Research* **27B**, 361.

Thomson, J.J., Aston, F.W., Soddy, F., Merton, T.R. and Lindeman, F.A. (1921) Discussion on isotopes. *Proceedings of the Royal Society of London, Series A* **99**, 87-104.

Trofimov, A. (1949) Isotopic constitution of sulfur in meteorites and in terrestrial objects. *Doklady Akademii nauk SSSR* **66**, 181-184.

Tudge, A.P. (1960) A method of analysis of oxygen isotopes in orthophosphate; its use in the measurement of paleotemperatures. *Geochimica et Cosmochimica Acta* **18**, 81-93.

Urey, H.C. (1947) The thermodynamic properties of isotopic substances. *Journal of the Chemical Society*, 562-581.

Urey, H.C., Epstein, S., McKinney, C. and McCrea, J. (1948) Method for measurement of paleotemperatures. *Bulletin of the Geological Society of America (abstract)* **59**, 1359-1360.

Urey, H.C., Epstein, S. and McKinney, C.R. (1951) Measurement of paleotemperatures and temperatures of the Upper Cretaceous of England, Denmark, and the southeastern United States. *Geological Society of America Bulletin* **62**, 399-416.

Urey, H.C. and Greiff, L.J. (1935) Isotopic exchange equilibria. *Journal of the American Chemical Society* **57**, 321-327.

Vinogradov, A.P. and Dontsova, E.I. (1947) Izotopnyi sostav kisloroda alyumosilikatnykh gornykh porod. *Doklady Akademii nauk SSSR*, 83-84.

Wickman, F.E. (1941) On a new possibility of calculating the total amount of coal and bitumen. *Geol. Foren. i Stockholm Forh.* **63**, 419-422.

Chapter 2

TERMINOLOGY, STANDARDS AND MASS SPECTROMETRY

Contents

2.1 Overview 1
2.2 Isotopes, Isotopologues, Isotopomers, and Mass Isotopomers 1
2.2.1 'Isotope' vs. 'Isotopic' 2
2.3 The Delta Value 2
2.4 The Fractionation Factor α 8
2.5 1000lnα, Δ, and the ε Value 10
2.6 Reference Standards 12
2.6.1 Hydrogen 13
2.6.2 Carbon 17
2.6.3 Nitrogen 17
2.6.4 Oxygen 18
2.6.5 Sulfur 19
2.6.6. Silicon 19
2.6.7. Chlorine 20
2.7 Isotope Ratio Mass Spectrometry 20
2.7.1 Components of a mass spectrometer 21
2.7.1.1 The ion source 22
2.7.1.2. The analyzer 23
2.7.1.3. Collector assembly 25
2.7.1.4 Dual inlet mass spectrometer inlet system 26
2.7.2 Gas Chromatograph Isotope Ratio Mass Spectrometry (GC-IRMS) 27
2.7.3 Gases measured in isotope ratio mass spectrometry 28
2.7.4 Relations between measured and desired isotopic ratios 29
2.8 Laser absorption mass spectroscopy 30
REFERENCES 33

Chapter 2

TERMINOLOGY, STANDARDS AND MASS SPECTROMETRY

2.1 Overview

Most of the accepted terms and symbols used in stable isotope geochemistry are precise and were developed by the earliest workers who gave the matter considerable thought. Arguably, some of the terms could be improved, and some recent workers have unilaterally coined new symbols and expressions for reasons known only to themselves. Unfortunately this practice has caused considerable confusion among new workers and more and more improper usage is finding its way into the literature and into oral presentations. In this text the terms established by the founders of our discipline will be used, both in homage to them and because these terms are, for the most part, logical and grammatically correct. In Table 2.1 a number of terms and phrases are presented that are considered to be mistakes, with the reasons why they are unacceptable, and recommended alternatives. All examples were culled from the literature. Although some of these common mistakes can be seductive in their simplicity, they should be avoided, in part to preserve the historical purity of the discipline but, most importantly, because they are indeed mistakes and not simply a matter of style.

In this chapter, the nomenclature commonly used in stable isotope geochemistry is developed, the mysterious and arcane standardization protocols and reference standards are explained and the principles of the mass spectrometer are presented.

2.2 Isotopes, Isotopologues, Isotopomers, and Mass Isotopomers

Most definitions of the word **isotope** include something to the extent '*one of two or more forms of an element*' due to differing numbers of neutrons. Or '*one of two or more atoms having the same atomic number but different mass numbers*'. However these definitions fail to describe monoisotopic elements such as fluorine. A better definition might be '*a particular form of an element defined by a specific number of neutrons*' or '*a variety an element with a fixed number of neutrons*". In applications to natural processes, we are obviously not concerned with monoisotopic elements, so perhaps both definitions are equally valid.

All stable isotope studies report the stable isotope composition of a particular element in a molecule or compound. For example, we measure the carbon isotope composition of CO_2 or calcite, and the hydrogen isotope composition of water. According to recommendations made in 1994 by the International Union of Pure and Applied Chemistry (IUPAC), **isotopologues** are molecules that differ from one another only in isotopic composition. It is therefore appropriate to talk about the different 'isotopologues' of water, but not the different 'isotopes' of water because water doesn't have isotopes – its constituent elements H and O do. Writing about 'water isotopes' may sound short and concise, but it is wrong. Just as petrologists don't talk about 'rock isotopes', so hydrologists should avoid talking about 'water isotopes'.

Isotopologues *can have the same or different masses*. For example, $^{12}C^{17}O$ has the same mass as $^{13}C^{16}O$. Although they have the same mass, they are distinctly different isotopologues of carbon monoxide. The word isotopologue, when used with care, is the

appropriate term to describe molecules that are encountered in stable isotope geochemistry and will be employed frequently in this text.

Isotopomers (contraction of isotopic isomers) are isotopologues that differ from one another only in the positions or locations of the isotopic elements. Studies of isotopomers is common in pharmaceutical and biochemical research, where the position of atoms provides important information about metabolic processes. Isotopomers always comprise the same number of each isotope and thus *always have the same mass*. They differ from one another in the positions or locations of the isotopic elements and thus the connection to isomerism. Two different isotopic forms of acetaldehyde provide an example of isotopomers: $CH_2DCH{=}O$ and $CH_3CD{=}O$. They have the same isotopic composition, but the D atom is bonded to the methyl group carbon in the first case and to the carboxyl carbon in the second. Isotopic forms of nitrous oxide ($^{15}N^{14}NO$ and $^{14}N^{15}NO$), and ozone ($^{16}O^{18}O^{16}O$ and $^{18}O^{16}O^{16}O$) are among the few isotopomers studied by stable isotope geochemists (e.g., Michalski and Bhattacharya, 2009). In mass spectrometry, the expression mass isotopomer, normally an organic compound, is used to describe a family of isotopologues that *have the same mass*. Because mass isotopomers are collected simultaneously on the same collectors of a mass spectrometer, they pose a problem in isotopic analysis. The molecules $^{13}C^{16}O$ and $^{12}C^{17}O$ are mass isotopomers that each have mass 29.

2.2.1 'Isotope' vs. 'Isotopic'

These two words appear to be used randomly and interchangeably because the proper use of one or the other is not immediately clear. My mentor, Jim O'Neil, was confronted with this dilemma as a U.S.G.S. employee. He consulted the Technical Reports Unit at the USGS for guidance. After some research, it was decided that 'isotope' is used when modified and 'isotopic' is used as a stand-alone adjective. One therefore should write "The oxygen isotope composition of . . ." and "The isotopic composition of . . .". In the first case, 'oxygen' modifies 'isotope' and in the second 'isotopic' stands alone.

2.3 The Delta Value

Relative differences in isotopic ratios can be determined far more precisely than absolute isotopic ratios. McKinney *et al.* (1950) introduced the delta (δ) notation to report stable isotope data for all materials except certain extraterrestrial materials whose isotopic ratios and variations are occasionally so large that absolute ratios are used in publications (see Chapter 13). The delta value is given by[1]

$$\delta = \left(\frac{R_x - R_{std}}{R_{std}} \right) \times 1000 \qquad 2.1a$$

[1] Some people have suggested that the '× 1000' part of the definition of delta should be left out. The delta numbers would then be very small, and they would be reported in per mil (‰), percent (%) or per meg (ppm), with the actual δ value being multiplied by 1,000, 100 or 10^6, respectively. There is some sense to this argument, but the 50+ years of defining the delta with the ×1000 part has worked wonderfully, and as the saying goes 'if it ain't broke, don't fix it'.

or equivalently

$$\delta = \left(\frac{R_x}{R_{std}} - 1 \right) \times 1000 \qquad 2.1b$$

where R is the ratio of the abundance of the heavy to light isotope, x denotes the sample, and *std* is an abbreviation for standard. For the elements, hydrogen, carbon, nitrogen, oxygen, sulfur,, silicon and chlorine, R is given by $^{2}H/^{1}H$ (or D/H), $^{13}C/^{12}C$, $^{15}N/^{14}N$, $^{18}O/^{16}O$ (and $^{17}O/^{16}O$), $^{34}S/^{32}S$ (and $^{33}S/^{32}S$, $^{36}S/^{32}S$), $^{30}Si/^{28}Si$ (and $^{29}Si/^{28}Si$), and $^{37}Cl/^{35}Cl$, respectively. The notation $^{2}H/^{1}H$ is strictly correct for hydrogen isotope ratios (Coplen, 1994) and is used almost exclusively in the hydrological literature, but, for historical reasons, D/H is routinely used by many workers in geological studies.

Delta values are reported in per mil, or parts per thousand, and the symbol for per mil is ‰. A positive δ value means that the ratio of heavy to light isotope is higher in the sample than it is in the standard, and a negative δ value has the opposite meaning. A sample with a $\delta^{18}O$ value of +19.7‰ has an $^{18}O/^{16}O$ ratio that is 19.7 per mil, or 1.97 per cent, higher than that of the standard. Similarly, a negative δD value of –65.2‰ means that the D/H ratio of the sample is 65.2 per mil or 6.52 per cent lower than that of the standard. The δ value is computed from the intensities of ion signals measured in the

Table 2.1. *Common Mistakes in Terminology and Phraseology*

Mistake	**Recommended Expressions**	**Explanation**
referring to the symbol δ as 'del'	Since the time of the early Greeks, the name of this symbol has been and remains **delta**.	The word *del* describes either of two things in mathematics and science: an operator (∇) or the partial derivative (∂)
$\delta^{13}C$ composition	$\delta^{13}C$ value; carbon isotope composition	$\delta^{13}C$ values are numbers and a *composition of numbers* has no meaning.
Isotopically depleted water	^{18}O (or D) depleted water	A given sample of water is neither depleted nor enriched in isotopes.
Stable water isotopes have been widely used as tracers. . .	Stable O and H isotope ratios in water have been used. . .	Only elements have isotopes. It is the H and O that has the isotopes, not H_2O.
heavy (light) $\delta^{18}O$ values	high (low) $\delta^{18}O$ values	As numbers, δ-values can be high or low, positive or negative, but not heavy or light.
Isotopically negative	relatively low δ values	Isotopic ratios are not negative or positive; they are lower or higher than those of the standards.
depleted $\delta^{13}C$ value enriched (depleted) carbonates. enriched (depleted) compositions depleted carbon reservoir	low $\delta^{13}C$ value (relative to another) isotopically heavy (light) carbonates (relatively) ^{18}O-rich or ^{13}C-poor carbonates reservoir of (isotopically) light carbon	$\delta^{13}C$ values are numbers and, as such, they cannot be depleted or enriched. The words *enrich* and *deplete* are overused and much abused. These words should be reserved for describing a **process** that changes the content of the heavy isotope of the element in some substance.
oxygen isotopes **in** chert; inferred from carbon isotopes; isotopes of soil water	oxygen isotope **ratio** (**composition) of** chert; inferred from carbon isotope **measurements**; isotopic composition of soil water	Such written mistakes are a carryover from loose oral communication.

The isotopic composition of the water was $\delta^{18}O = -4.3‰$.	The $\delta^{18}O$ value of the water was –4.3‰.	A matter of redundancy.
The isotopic value changed.	The isotopic composition changed. The $\delta^{18}O$ value changed.	The phrase *isotopic value* is ambiguous. R?, δ? Which element?
The isotopic signature of the rock was $\delta^{18}O = 5.7‰$.	The $\delta^{18}O$ value of the rock was 5.7‰. Thus this rock has the oxygen isotope signature of the mantle.	The word **signature** should be used to describe the isotopic composition of a significant reservoir like the mantle, the ocean, or a major part of the system being studied, not to the isotopic composition of ordinary samples.
δ^{15}, δ^{18}, δ^{13}, *etc.;* $^{15}\delta$, $^{18}\delta$, $^{13}\delta$, *etc.*; δ–15, δ–18, δ–13, *etc.*	$\delta^{15}N$, $\delta^{18}O$, $\delta^{13}C$, *etc.*	Introduction of new symbols that save one character of space is unnecessary at best and confusing at worst.
Sulfur was measured	the sulfur **isotope composition** was measured	Misleading because the sulfur **content** of a rock or mineral may be understood.
The ^{13}C content of . .	The $^{13}C/^{12}C$ ratio of ..	^{13}C content refers to how much ^{13}C there is in a rock. A sample of coal has a lot of ^{13}C (high ^{13}C content) but a low $^{13}C/^{12}C$ ratio compared to most materials.
In general the water isotopes are valuable proxies of temperature variations in high latitudes	In general the **isotopologues of** water are valuable proxies of temperature variations in high latitudes	Water does not have isotopes. It is composed of H and O that have multiple isotopes.
. . . using data assimilation of water-isotope ratios . .	Same as above	Just as it would be wrong to say "using data of fish-isotope ratios" so it is wrong to say 'water-isotope ratios'.

mass spectrometer (see section 2.8). Mass spectrometric analyses of pure gases other than H_2 are *reproducible* to ± 0.01‰ or better. Excellent reproducibility like this does not necessarily represent the precision of an actual sample because errors can be introduced from the collection and chemical preparation procedures employed. To get a true precision of ± 0.01‰ requires extreme care. Reporting a precision for an analysis based on the precision obtained on the measurement of the gas in a mass spectrometer will always result in a precision that is higher than the actual precision of the overall analysis and should be avoided. Oxygen isotope compositions are reported using the symbol $\delta^{18}O$, those of carbon by $\delta^{13}C$, and so forth. The symbol δ is the lower case Greek letter **delta** and is commonly used in many disciplines to express a difference. The unrelated symbol ∂ (*del*) crept into the parlance of stable isotope geochemistry about 20-30 years ago, presumably as some kind of abbreviation for the correct word delta[2]. This incorrect usage should be abandoned because the word del has been used for centuries to denote the symbol ∂, the partial derivative sign and is not the greek letter 'delta'.

The delta notation provides a very convenient means to express the small **relative differences** in isotopic ratios between samples and standards that are measured by isotope ratio mass spectrometry. The effective precision of a stable isotope measurement is much higher than is immediately apparent from the stated precision of a δ value, which in the best case is ±0.01‰. For example, the absolute $^{18}O/^{16}O$ ratio of one of the international reference standards SMOW is $(2005.20\pm0.45)\times10^{-6}$. This ratio was

[2] I first encountered students using ∂ in place of δ because the symbol took only one stroke of a keyboard (on a Mac) instead of two for the δ. Needless to say, this was not a convincing reason to abandon the correct notation.

determined by comparing the isotopic value of a sample of SMOW to synthetic mixtures of pure $D_2{}^{18}O$ and $H_2{}^{16}O$ (Baertschi, 1976b), and is known to five significant figures, or to four parts in 10^5. The $^{18}O/^{16}O$ ratio of a gas whose $\delta^{18}O$ value is +2.06‰ *relative* to SMOW ($\delta^{18}O$ of SMOW = 0.00‰ by definition) is 0.00200933, the value obtained by substituting 2.06 in equation 2.1

$$2.06 = \frac{^{18}O/^{16}O_{sample} - 2005.20\times10^{-6}}{2005.20\times10^{-6}} \times 1000, \qquad 2.2$$

A $\delta^{18}O$ value of +2.05‰ corresponds to an absolute ratio of 0.002009311, different from a $\delta^{18}O$ value of +2.06‰ by ±0.00000002. Obviously, given the uncertainties in the absolute value of our reference, the absolute ratio is not known anywhere near the calculated precision. Nevertheless, by accepting a value for the absolute $^{18}O/^{16}O$ ratio of a reference standard (SMOW in this case), we can determine *relative* differences in the $^{18}O/^{16}O$ ratios of two substances at the remarkable level of two parts in the eighth decimal place! The ability to determine relative differences in small isotopic ratios at this level of precision makes stable isotope measurements among the most precise attainable in all of geochemistry.

The delta scale leads to some interesting peculiarities which fortunately, for the most part, can be ignored. Consider the oxygen isotope composition of a gas, given by

$$\delta^{18}O = \left(\frac{\left(^{18}O/^{16}O\right)_{sample}}{\left(^{18}O/^{16}O\right)_{standard}} - 1 \right) 1000 \qquad 2.3.$$

If we have a sample with no ^{18}O, then the $^{18}O/^{16}O$ ratio of the sample is 0, and the $\delta D\delta^{18}O$ value is -1000‰. The isotope scale 'bottoms out' at -1000‰. At the other extreme, a sample containing only ^{18}O has a $^{18}O/^{16}O$ ratio of ∞, and the $\delta^{18}O$ value is ∞‰. The δ value of a mixture of two materials can be approximated by taking the average of the two delta values of the unmixed materials in their relative proportions, and in practice, this works well, although mathematically it is not correct. Just consider mixing equal proportions of pure $H_2{}^{18}O$ and pure $H_2{}^{16}O$. The mixture has a composition of $H^{16}O^{18}O$, with a $\delta^{18}O$ value of 497753‰, but if we were just to take the average of the two endmember delta values (-1000 and ∞‰), the answer would not be correct. Fortunately, the rare isotope is generally in low concentrations, so that for most geological applications we can use delta values additively because the denominator (the common isotope) has a fraction close to 1.

Isotopic compositions of samples are measured relative to the isotopic composition of a reference gas, the **working standard**, in a mass spectrometer. To convert the δ value of sample X from one scale (reference standard A – the working gas δ value) to another scale (reference standard B – the international standard δ value), the following equation is used:

$$\delta_{X-B} = \delta_{X\text{-}A} + \delta_{A-B} + 0.001\left(\delta_{X\text{-}A} \times \delta_{A\text{-}B}\right) \qquad 2.4.$$

This simple calculation, analogous to converting temperatures on the Celsius scale to temperatures on the Fahrenheit scale, is made in every stable isotope laboratory in the world[3]. Laboratory working standards are calibrated relative to international reference standards, precious materials which are distributed to qualified workers by the International Atomic Energy Agency (IAEA) or the National Institute of Standards and Technology (NIST). In most stable isotope laboratories there are supplies of gases like CO_2, N_2, H_2, *etc*. contained in metal or glass tubes and tanks that are fitted with appropriate valves to allow aliquots of the gases to be taken for use as working standards or for calibration purposes. The δ values of the gases are well known from repeated measurements relative to the values of primary or secondary reference standards, which are analyzed sparingly.

Suppose that the CO_2 working standard (WS) used in a given mass spectrometer has a $\delta^{13}C$ value of +4.75‰ relative to the international standard PDB ($\delta_{WS\text{-}PDB}$). When an unknown sample is analyzed in the mass spectrometer, the difference in the isotopic composition of the sample and the working standard is measured. If sample X has a $\delta^{13}C$ value of –22.32‰ relative to WS ($\delta_{X\text{-}WS}$), the $\delta^{13}C$ value of X on the PDB scale is

$$4.75 - 22.32 + 0.001(4.75)(-22.32) = -17.68‰. \qquad 2.5$$

That is, δ values are converted from the working standard of the mass spectrometer to PDB, or to any international reference standard, by simply adding a scaling term $10^{-3}(\delta_{X\text{-}WS})(\delta_{WS\text{-}PDB})$ to the sum of the two delta values $\delta_{X\text{-}WS}$ and $\delta_{WS\text{-}PDB}$. Another equation (essentially the same equation rearranged in a slightly different format) frequently used to calculate a scale change like this has, for the case above, the form

$$1.00475(-22.32) + 4.75 = -17.68‰ \qquad 2.6$$

The difference of 4.75‰ between the isotopic composition of the working standard and PDB must be added to the measured *raw* value (-22.32), but only after the raw value has been corrected for scale expansion, equivalent in this case to a multiplicative factor of 1.00475 (equal to $1 + 0.001\times\delta_{WS\text{-}PDB}$). Note that there is a contraction or expansion of scales involved in these calculations and this term is directly related to the magnitude of the difference in δ values between the two standards. The *size* of δ values changes from one scale to another. When converting between scales, one must apply both an additive and multiplicative factor to the raw data. If the δ value of a working standard is 12.34‰, the multiplicative factor is 1.01234 (*i.e.,* $1 + 0.001\times\delta$) and the additive factor is 12.34. If the δ value of another working standard is –6.78‰, the multiplicative factor is 0.99322 (1 + 0.001 × -6.78), which in this case contracts the scale, and the additive factor is –6.78. The application of this equation is familiar to many geochemists analyzing carbonates. There are two references scales for oxygen, the SMOW and PDB scale. The value of

[3] Certainly, many workers are not aware that such calculations are being made, as the conversion equations are hidden in the software packages provided with their mass spectrometers.

PDB on the SMOW scale (or VPDB on the VSMOW scale) is 30.91‰. In order to convert a $\delta^{18}O$ value from the SMOW to PDB scale the equation

$$\delta^{18}O_{SMOW} = 1.03091 \times \delta^{18}O_{PDB} + 30.91 \qquad 2.7$$

is used.

In order to reduce the size of the multiplicative factor, international reference standards are prepared with isotopic compositions that are as close as possible to the range of isotopic compositions of natural materials expected to be analyzed by most workers. In the same vein, a researcher can choose working standards whose isotopic compositions are close to those of the materials most commonly met in the research at hand. If given the choice, it would be better to have a working gas with a higher delta value (higher proportion of rare isotope) than the sample gas to minimize extrapolation. The practice of having similar reference and sample gas compositions results in only small improvements in precision, but is a worthwhile practice in any case.

Over the years, stable isotope geochemists have tacitly developed a certain uniformity in the presentation of their data. Some notations used in the past have all but disappeared in the modern literature, but are noted for the sake of completeness. In the early literature you will see the expressions $\delta(O^{18}/O^{16})$, δO^{18} δ(D/H), and so forth, but these strictly more correct notations soon gave way to the simpler expressions $\delta^{18}O$ and δD. Prior to the mid-1970s the mass number was always written as a right superscript of the symbol of the element as in O^{18}, C^{14}, U^{235}, *etc*. It is for this reason that one usually *hears* the element name (or symbol) and number spoken in that order, as in "C-14 dating", "Sr-90 contamination", or "delta O-18 values". Subsequently, IUPAC officially changed the order in which mass number and symbol are written to allow oxidation states and other identifying marks to be written to the right of the element symbol. In the early literature, δD and $\delta^{13}C$ values were often given in per cent rather than in per mil.

Box 2.1 *Why ^{12}C is the official reference mass for atomic mass units?*

Prior to the 1970s, two conventions were used for determining relative atomic masses. Physicists related their mass spectrometric determinations to the mass of ^{16}O, the most abundant isotope of oxygen, and chemists used the weighted mass of all three isotopes of oxygen ^{16}O, ^{17}O, and ^{18}O. At an international congress devoted to standardization of scientific weights and measures, the redoubtable A.O. Nier proposed a solution to these disparate conventions whose negative consequences were becoming serious. He suggested that the carbon-12 isotope (^{12}C) be the reference for the atomic mass unit (amu). By definition, its mass would be *exactly* 12 amu, a convention that would be acceptable to the physicists. By adopting this convention, the average mass for oxygen (the weighted sum of the three naturally occurring isotopes) becomes 15.9994 amu, a number close enough to 16 to satisfy the chemists.

2.4 The Fractionation Factor α

The isotopic fractionation factor between two substances A and B is defined as

$$\alpha_{A-B} = \frac{R_A}{R_B} \qquad 2.8.$$

The α value is the ratio of the ratios for the rare to heavy isotope in any two substances A and B. In terms of δ values this expression becomes

$$\alpha_{A-B} = \frac{1 + \frac{\delta_A}{1000}}{1 + \frac{\delta_B}{1000}} = \frac{1000 + \delta_A}{1000 + \delta_B} \qquad 2.9.$$

The α value is a measure of the isotope fractionation between any two phases and is extremely important in terms of understanding equilibrium isotope exchange. This concept is the foundation of our field, where the early practitioners realized that the enrichment of the heavy isotope in one phase relative to coexisting phase in isotopic equilibrium is a function almost exclusively of temperature. Isotope exchange reactions are considered in terms of equilibrium thermodynamics in which isotopes of a single element are exchanged between two substances until equilibrium is reached. (Kinetic reactions that do not reach equilibrium are important for understanding the mechanisms of chemical reactions or mineral formation, but should not be considered in terms of the equilibrium fractionation factor α). The chemical makeup of reactants and products in an isotope exchange reaction are identical. For the general case of an isotope exchange reaction between substances A and B, where the subscripts 1 and 2 refer to molecules *totally substituted* by the light and heavy isotope, respectively and *a* and *b* refer to the coefficients necessary to balance the reaction, we have

$$aA_1 + bB_2 = aA_2 + bB_1 \qquad 2.10a.$$

An example of such a reaction is given by

$$^{12}CH_4 + {}^{13}CO_2 = {}^{13}CH_4 + {}^{12}CO_2 \qquad 2.10b.$$

In a real system, there would be only one methane phase and one CO_2 phase, nevertheless it is thermodynamically valid to consider the *components* $^{12}CH_4$ and $^{13}CH_4$ as making up the CH_4 *phase*. The equilibrium constant for equation 2.10a the above reaction is written in the usual way

$$K = \frac{(A_2)^a (B_1)^b}{(A_1)^a (B_2)^b} = \frac{(A_2/A_1)^a}{(B_2/B_1)^b} \qquad 2.11.$$

The terms in parentheses are activities but, in practice, ratios are normally used. The difference between concentrations and ratios of isotopologues is normally negligible (*i.e.*

the activity coefficient $\gamma \sim 1$), so that substituting ratio for activities is valid. For the reaction given by equation 2.10b, the equilibrium constant is

$$K = \frac{\left({}^{13}CH_4\right)\left({}^{12}CO_2\right)}{\left({}^{12}CH_4\right)\left({}^{13}CO_2\right)} = \frac{\left({}^{13}CH_4/{}^{12}CH_4\right)}{\left({}^{13}CO_2/{}^{12}CO_2\right)} \qquad 2.12.$$

Finally, because the reaction is written with the hydrogen (in methane) and oxygen (in CO_2) as having the same value in the numerators and denominators (we are considering their isotopic composition fixed), equation 2.12 becomes simply

$$K = \frac{\left({}^{13}C/{}^{12}C\right)_{methane}}{\left({}^{13}C/{}^{12}C\right)_{CO2}} \qquad 2.13,$$

which is identical to the α value

If the isotopes are randomly distributed over all possible sites or positions in substances A and B, the fractionation factor (α) is related to the equilibrium constant (K) for isotope exchange reactions in the following way:

$$\alpha = K^{1/n} \qquad 2.14$$

where n is the number of atoms exchanged, normally 1 as in the example above. For the isotope exchange reaction between CO_2 and SiO_2, we have

$$K = \alpha = \frac{\left({}^{18}O/{}^{16}O\right)_{CO_2}}{\left({}^{18}O/{}^{16}O\right)_{SiO_2}} \qquad 2.15.$$

Values of α are normally very close to unity, typically 1.00*X*, and the fractionation is often considered informally to be equal to *X*. As a true thermodynamic equilibrium constant, α is a function of temperature[4], so values of α are meaningful only when temperature is specified. For example, the sulfur isotope fractionation between sphalerite (ZnS) and galena (PbS) is 1.00360 **at 200°C**. It is accepted parlance to state that, at 200°C, (1) the sphalerite-galena fractionation is 3.60 per mil, or (2) sphalerite concentrates ^{34}S by 3.60 per mil relative to galena[5]. It is common to report the difference in the isotopic composition as

[4] Chemical thermodynamic reactions are a function of both temperature and pressure. Because the volume change for the isotope exchange reactions 2.10a is extremely small, pressure can be ignored except in extreme cases. See Horita *et al.*(2002).

[5] Note that the difference of 3.60‰ is only correct if the $\delta^{34}S$ value of the galena is 0.

$$\Delta_{A-B} = \delta_A - \delta_B \qquad 2.16.$$

Δ is the upper case symbol for the Greek letter delta and is frequently expressed orally as **"big delta"** or "**cap delta**".

2.5 1000*ln*α, Δ, and the ε Value

For the $^{34}S/^{32}S$ example mentioned above, if the $\delta^{34}S$ values of sphalerite and galena are 3.6‰ and 0.0‰, respectively, then α = 1.0036 and the difference between the $\delta^{34}S$ values of sphalerite and galena is 3.6‰. It is a useful mathematical fact that 1000*ln*(1.00*X*) is approximately equal to *X*. For our sphalerite-galena example, 1000*ln*α = 3.594. That is, 1000*ln*α *is* the fractionation between sphalerite and galena. It is close the difference in the isotopic composition of the two phases, and is independent on their actual isotopic composition. It is sometimes called the **per mil fractionation**, but this terminology is strictly not correct because α is unitless. This logarithmic function has added theoretical significance. For perfect gases, lnα varies as $1/T^2$ and $1/T$ in the high and low temperature regions, respectively. As in any expressions or calculations in thermodynamics, *T* is absolute temperature in kelvins.

The fractionation expressed as 1000*ln*α is of prime importance in stable isotope geochemistry. This quantity is very well approximated by the Δ value, but it is important to realize that the two are not exactly the same:

$$\Delta_{A-B} = \delta_A - \delta_B \approx 1000 ln\alpha_{A-B} \qquad 2.17.$$

That is, merely subtracting δ values is a good approximation to the per mil fractionation given by 1000*ln*α and identical to it within the limits of analytical error **when the individual values of δ_A and δ_B as well as Δ_{A-B} are less than about 10‰**. As the numbers in Table 2.2 indicate however, the differences between Δ_{A-B} and 1000*ln*α become significant when the fractionations or the δ values are greater than 10. For all fractionations that are assumed to be at thermodynamic equilibrium, 1000*ln*α should be reported. Reporting the differences in delta values is valid when non-equilibrium fractionations are being studied, such as in biological processes. A few authors have used the symbol ε to designate an isotopic fractionation and define it as ε = (α – 1)1000. Again, for small values of ε, this function is almost identical to 1000*ln*α (Table 2.2). It is recommended that ε not be used for equilibrium reactions. Instead ε is more commonly used in kinetic, non-equilibrium processes, where the isotopic composition of two phases can be measured, but because they are out of chemical equilibrium, do not follow the rules of classical thermodynamics.

***Table 2.2**. Comparison between values obtained using different expressions for isotopic fractionations.*

δ_A	δ_B	α	Δ_{A-B}	ε_{A-B}	$10^3 ln\alpha_{A-B}$
1.0	0.0	1.00100	1.00	1.00	1.000
5.0	0.0	1.00500	5.00	5.00	4.988
10.0	5.0	1.00498	5.00	4.98	4.963

10.0	0.0	1.01000	10.00	10.00	9.950
12.0	0.0	1.01200	12.00	12.00	11.929
15.0	0.0	1.01500	15.00	15.00	14.889
20.0	0.0	1.02000	20.00	20.00	19.803
20.0	5.0	1.01493	15.00	14.93	14.815
30.0	5.0	1.02488	25.00	24.88	24.571
30.0	20.0	1.00980	10.00	9.80	9.756
30.0	15.0	1.01478	15.00	14.78	14.670
30.0	10.0	1.01980	20.00	19.80	19.608

The α function is an integral part of a variety of analytical techniques. For example, the $\delta^{18}O$ value of a sample of liquid (*l*) water is determined by equilibrating the water with a small amount of CO_2 gas at a constant temperature and then measuring the oxygen isotope composition of the equilibrated CO_2 gas in a mass spectrometer. At 25°C, the fractionation factor α between $CO_{2(gas)}$ and H_2O_l is 1.04120. This is approximately equivalent to stating that CO_2 is 40.37‰ ($10^3 \ln\alpha = 40.37‰$) heavier than the water with which it was equilibrated, but the actual $\delta^{18}O$ value of the water is not equal to the $\delta^{18}O$ value of CO_2 - 40.37‰. The $\delta^{18}O$ value of CO_2 in equilibrium with H_2O is determined using equation 2.9.

As another example, the isotopic compositions of carbon and oxygen in carbonates are determined by reacting the carbonates with 100% phosphoric acid and measuring the CO_2 that is released during the decarbonation reaction. All of the carbon is released during this procedure and the $\delta^{13}C$ value of the CO_2 gas is identical to the $\delta^{13}C$ value of the original carbonate. Only 2/3 of the oxygen in the carbonate is transferred to the CO_2 gas. There is a temperature dependent isotopic fractionation between the oxygen in the evolved CO_2 and the oxygen in the original carbonate. To a first-approximation, as long as the temperature of acid dissolution reaction is held constant, the fractionation between the carbonate and liberated CO_2 is constant. This provides us with the so-called **acid fractionation factor**, α for CO_2 liberated from a carbonate sample. If we know the α value between evolved CO_2 gas and carbonate at the reaction temperature, we can calculate the $\delta^{18}O$ value of the carbonate itself. At 25°C, $\alpha(CO_2\text{-calcite})$ for the phosphoric acid reaction is 1.01025. That is, the liberated CO_2 is about 10‰ heavier than the calcite. From equation 2.9, we have

$$\alpha = 1.01025 = \frac{1000 + \delta_{CO_2}}{1000 + \delta_{calcite}} \qquad 2.18.$$

If the $\delta^{18}O$ value of the calcite is -6.78‰, then the liberated CO_2 gas will have a $\delta^{18}O$ value of 3.40‰. Interestingly, this α value is not the same as the equilibrium fractionation between CO_2 and calcite. At 25°C, the equilibrium $\alpha_{CO2\text{-calcite}}$ value is 1.01258. The 1.01025 value is an empirical determination of the fractionation between a calcite sample and the CO_2 liberated in a non-equilibrium, but repeatable, fractionation that occurs during acid dissolution. It would probably be more correct to use ε for this equation, because the fractionation is not the same as the equilibrium α value for CO_2 and calcite.

2.6 Reference Standards

Very precise comparisons of isotopic compositions of materials can be determined in a given laboratory, but to allow for accurate intercomparisons of data obtained in different laboratories, an internationally accepted set of reference standards is available to all workers in the field. The measured isotopic composition of any substance should be the same in all laboratories after calibrations have been made with these international reference standards. Beginning in the 1970s, committees of stable isotope geochemists convened periodically in Vienna to select standard materials and to establish protocols for calibrating mass spectrometer analyses and presenting stable isotope data (Coplen and Clayton, 1973; Coplen et al., 1983; Hut, 1987; Coplen, 1996). These reference materials (Appendix 1) are available from the National Institute for Standards and Technology (NIST) in Gaithersburg, Maryland and from the International Atomic Energy Agency (IAEA) in Vienna. International reference standards are in limited supply and are not intended for use as working standards. They are provided in small quantities to allow workers to establish larger supplies of secondary reference materials (solids, liquids and gases) that in turn can be used on a daily basis as working standards, for calibrating extraction techniques, and so on.

The history of stable isotope reference materials is long and complex and unfortunately has led to considerable confusion. The early Chicago group reported $\delta^{13}C$ and $\delta^{18}O$ values of carbonates relative to the carbon and oxygen isotope compositions of a powdered specimen of *Belemnitella americana* from the Upper Cretaceous Peedee formation of South Carolina. They called this calcite standard PDB (**P**ee**D**ee **B**elemnite). When the original supply of this material became exhausted, another sample was prepared and named PDB II, a standard that was later replaced by PDB III. In each case the new standard was carefully calibrated against the isotopic composition of the original sample of PDB. Despite the fact that the original supply of PDB is exhausted, PDB remains the standard used in reporting all carbon isotope analyses and most of the oxygen isotope analyses of low-temperature carbonates. Secondary standards have been developed with isotopic compositions that are calibrated to the original PDB.

The Chicago group also created an Mean Ocean Water by taking the average ocean water samples collected at depths ranging from 500 and 2000 meters, with the goal of creating a sample that was representative of the average oxygen isotope composition of the ocean (Epstein and Mayeda, 1953). Each ocean has a slightly different $\delta^{18}O$ and δD value (Table 2.3). In order to standardize the average ocean water value, Harmon Craig compared the $\delta^{18}O$ and δD values of these ocean waters to the National Bureau of Standards Potomac River water (NBS-1). He coined the term Standard Mean Ocean Water, or SMOW as the average of the different ocean waters, with δ values defined in terms of NBS 1 by the following relationships:

$$\begin{aligned} D/H\ (SMOW) &\equiv 1.050\ D/H\ (NBS\text{-}1) \\ {}^{18}O/{}^{16}O\ (SMOW) &\equiv 1.008\ {}^{18}O/{}^{16}O\ (NBS\text{-}1) \end{aligned} \qquad 2.20.$$

This allowed workers everywhere to standardize their 'ocean water' values to the widely distributed NBS-1 (Fig. 2.1). Ultimately an actual water standard with δD and $\delta^{18}O$ values equal to the defined SMOW was made by mixing waters with different isotopic

compositions. This physical sample is called VSMOW (or V-SMOW), where the V is an abbreviation for 'Vienna', the headquarters for the International Atomic Energy Agency that distributes the standard. Unfortunately the original VSMOW has been used up, and a second standard VSMOW2 was made by the IAEA Isotope Hydrology Laboratory in 2006. It is thought to be essentially identical to the original VSMOW (except perhaps for its $\delta^{17}O$ value) and is available for distribution through the IAEA. Many other accepted standards are available from the IAEA, so that standardization procedures are now relatively routine and stable isotope analyses made anywhere in the world are, for the most part, easily comparable.

Table 2.3. *$\delta^{18}O$ and δD values of the average deep water samples from the different oceans. Compilation from Craig (1961).*

Location (sample)	δD‰	$\delta^{18}O$ (‰)
Atlantic	-0.7	+0.14
Pacific	+0.9	+0.04
Indian	+0.1	-0.07
NBS-1	-47.60	-7.94

A further complication has developed because of the use of non-quantitative techniques for determining stable isotope ratios. Carbon and nitrogen isotope analyses of organic matter, and to a lesser extent sulfur isotope analyses, are now made almost exclusively using an elemental analyzer. This methodology consists of combusting organic matter (or S-bearing phase) in a helium stream and excess oxygen gas. The C is converted to CO_2, N is converted to N_2 and S is converted to SO_2. The gases are separated in a gas chromatograph using He as a carrier gas and measured in 'continuous flow mode' in the mass spectrometer (see section 2.7.2 for a discussion of continuous flow mass spectrometry). Unfortunately, the measured isotopic composition is often not the same as the actual composition of the sample due to a number of factors, including incomplete reaction, contamination from other C and N sources in the organic matter and fractionation at the open split. Many laboratories and the IAEA have developed standards that can be used to compare the isotopic compositions of specific isotopic compounds, including cellulose, benzoic acid and caffeine. An outline of the reference materials for selected elements is given below.

2.6.1 Hydrogen

In much of the early literature on the abundance of deuterium in natural materials, a sample of Lake Michigan water was used as a reference standard. The δD value of the Lake Michigan standard is –42.4‰ on the modern VSMOW scale. Today, all hydrogen isotope analyses are reported relative to VSMOW, a logical geochemical reference material because ocean water is by far the largest terrestrial reservoir of water. By definition, the δD value of VSMOW is equal to zero. VSMOW has a D/H ratio that is higher than the ratios of most other materials on Earth, an interesting geochemical fact in itself. Thus most δD values of natural materials on our planet are negative on this scale in

Fig. 2.1. Picture of an ampoule (glass break-seal tube) containing NBS-1 standard, a reference standard that was formerly distributed by the National Bureau of Standards (now NIST).

The label reads:
Isotope Reference Sample #1.
PROTIUM OXIDE (Ordinary Water)

contrast to δD values of extraterrestrial substances which can be extremely positive for reasons explained in Chapter 13.

SMOW was originally defined relative to NBS-1 (Fig. 2.1) by equation 2.19. A physical sample of water with an isotopic composition equal to SMOW was made by Harmon Craig and Ray Weiss, who distilled a large sample of ocean water (Fig. 2.2 and Fig. 2.3) and adjusted its hydrogen and oxygen isotope compositions to match SMOW by carefully adding appropriate amounts of other waters of different isotopic compositions. This was the original VSMOW sample. By definition, it has a δD value ≡ 0‰ on the VSMOW scale. Practitioners in the field should realize that data presented in older literature using the SMOW reference are identical to those using the VSMOW or VSMOW2 reference. No additional corrections are needed in order to compare data reported relative to either reference. In other words, the δD and $\delta^{18}O$ values of SMOW and VSMOW are identical[6].

All hydrogen isotope ratios are measured using H_2 gas in the mass spectrometer and H_2O gas with laser spectroscopy[7] (Table 2.4). The raw δD value of a sample whose D/H ratio is quite different, say 20-30‰ or more from that of the working standard, will generally be very slightly different when measured on different mass spectrometers. The factor most responsible for this effect is the inevitable production of the ion H_3^+ (the same mass 3 as DH^+) in the source of the mass spectrometer (or non-linearities in the case of laser spectroscopy). In order to resolve this problem, an isotopically light natural water from Antarctica was selected as an additional reference standard for use in determining the *stretching factor* for individual mass spectrometers (see Appendix 2 for further discussion). The stretching factor is especially important for hydrogen isotope measurements because the variation in δD values of natural materials are about ten times larger than variations in any other element. This standard was given the acronym SLAP (**S**tandard **L**ight **A**ntarctic **P**recipitation) and has a δD value of –428‰ on the basis of a comparison study made in many of the major stable isotope laboratories in the world in the 1970s. (SLAP2 has a δD value of -427.5±0.3‰). In order to calibrate a machine for

[6] see https://nucleus.iaea.org/rpst/Documents/VSMOW2_SLAP2.pdf for details of VSMOW2
[7] See sections 2.7 and 2.8 for methodological details

Fig. 2.2. The ocean pier at the Scripps Institute in San Diego, where Harmon Craig and Ray Weiss collected water for VSMOW. Photo by author.

Table 2.4*. Gases commonly measured in conventional gas source isotope ratio mass spectrometers.*

Element	Gas	Masses of Isotopologues Measured
Hydrogen	H_2 H_2O (g)	2 , 3 (interference from H_3^+) (H_2O, HDO in laser spectroscopy systems)
Carbon	CO_2	44, 45
Nitrogen	N_2	28, 29 (and 30 for artificially enriched samples)
Oxygen	CO_2 O_2 (fluorination) CO (pyrolysis) H_2O (g)	44, 46 32, (33), 34 28, 30 ($H_2{}^{16}O$, $H_2{}^{18}O$ in laser spectroscopy systems)
Sulfur	SO_2 SF_6	64, 66 146, (147), 148, (150)
Silicon	SiF_4	85, 86, 87
Chlorine	CH_3Cl	50, 52

Fig. 2.3. The original container of VSMOW. From https://en.wikipedia.org/wiki/Vienna_Standard_Mean_Ocean_Water.

δD determinations, hydrogen isotope analyses of both SMOW and SLAP are analyzed relative to the working standard, and the difference obtained multiplied by a factor so that $\delta D_{SLAP-SMOW} = -428‰$ (Coplen, 1988).

Absolute ratios of D/H determined for both SMOW and SLAP and the absolute ratio of $^{18}O/^{16}O$ and $^{17}O/^{16}O$ determined for SMOW are given in Table 2.5. The absolute values were determined by mixing waters that were extremely pure samples of $^{1}H_2{}^{16}O$, $^{1}H_2{}^{18}O$, $D_2{}^{16}O$ and $H_2{}^{17}O$. It is very difficult to prepare water that has no deuterium or ^{18}O and ^{17}O in it, but the best job possible was done at the time the determination was made. By careful mixing, the D/H and $^{18}O/^{16}O$ ratios of these synthetic waters were *known*, but with significant uncertainty. SMOW and SLAP were then measured relative to the isotopic compositions of these waters to derive their absolute D/H and $^{18}O/^{16}O$ ratios. While it is desirable to have reliable determinations of the absolute ratios of these standards, keep in mind that knowledge of the absolute ratios is not necessary to conduct research in stable isotope geochemistry and is not used in determining stable isotope ratios on a mass spectrometer.

Table 2.5*. Determinations of the absolute ratios of the isotope ratios of selected elements and internationally accepted standards.*

Ratio	Standard	Value	Reference
D/H	SMOW	$(155.76\pm0.05)\times10^{-6}$	(Hagemann et al., 1970)
D/H	SMOW	$(155.75\pm0.08)\times10^{-6}$	(de Wit et al., 1980)
D/H	SMOW	$(155.60\pm0.12)\times10^{-6}$	(Tse et al., 1980)
$^{13}C/^{12}C$	PDB	$(11179\pm20)\times10^{-6}$	(Zhang et al., 1990)
$^{15}N/^{14}N$	AIR	$(3670\pm40)\times10^{-6}$	(Junk and Svec, 1958)
$^{17}O/^{16}O$	SMOW	$(379.9\pm0.8)\times10^{-6}$	(Li et al., 1988)
$^{18}O/^{16}O$	SMOW	$(2005.20\pm0.45)\times10^{-6}$	(Baertschi, 1976a)
$^{33}S/^{32}S$	VCDT	$(78.77\pm0.03)\times10^{-4}$	(Ding et al., 2001)
$^{34}S/^{32}S$	VCDT	$(441.626\pm0.039)\times10^{-4}$	(Ding et al., 2001)
$^{29}Si/^{28}Si$	NBS-28	$(508.1\pm0.1)\times10^{-4}$	(De Bièvre et al., 1994)
$^{30}Si/^{28}Si$	NBS-28	$(335.3\pm0.7)\times10^{-4}$	(De Bièvre et al., 1994)
$^{37}Cl/^{35}Cl$	SMOC (ISL 354)	0.31977±0.00009	(Xiao et al., 2002)

2.6.2 Carbon

Carbon isotope ratios are reported relative to the PDB standard described above and, by definition, the $\delta^{13}C$ value of PDB is zero. The calculated $^{13}C/^{12}C$ ratio for VPDB is given in Table 2.5. Several secondary carbonate standards (*e.g.* Carrara marble and Solenhofen limestone) were measured relative to PDB in the early years and these standards are still in use in some older laboratories. The international isotope reference standard NBS-19 (and most recently IAEA-603) is now the accepted means of calibrating to the PDB scale. NBS-19 was originally the TS (**T**oilet **S**eat) limestone working standard used in the laboratory of Irving Friedman and colleagues at the U. S. Geological Survey (Friedman et al., 1982). It has a $\delta^{13}C$ value of +1.95‰ relative to PDB and VPDB. In other words, the $\delta^{13}C$ value of NBS-19 ≡ +1.95‰ on the VPDB scale. Unfortunately, NBS-19 is now out of stock, and a new calcite standard IAEA-603, a sample of the Carrara marble is available with a $\delta^{13}C$ value of +2.46‰ ± 0.01 on the VPDB scale[8]. Other IAEA carbon isotope standards include oil, graphite and caffeine.

As in the case for SMOW, it is recommended to append the letter V to the acronym PDB.

Carbon isotope geochemistry has remained a very active discipline since its inception, and many thousands of carbon isotope analyses are reported every year. The carbon analyzed is present in a variety of substances including the various carbonate minerals, organic matter in sediments, organic matter in meteorites, petroleum products, collagen extracted from plant material, graphite, carbonate in the apatite of bones and teeth, carbon present in trace quantities in rocks (*e.g.*, basalts) and minerals (*e.g.*, goethite) and in archaeological and anthropological specimens. There are major differences in the extraction techniques used for these various carbonaceous materials and the errors assigned to an analysis depend on the complexities of the extraction method employed. In almost all cases, however, the carbon is put into the form of CO_2 for mass spectrometric analysis (Table 2.4), and therefore can be compared to the CO_2 liberated from one of the IAEA standards calibrated to PDB.

2.6.3 Nitrogen

Nitrogen isotope values are measured using N_2 gas in the mass spectrometer. The reference standard for nitrogen isotope analyses is atmospheric nitrogen and is called AIR. The $\delta^{15}N$ value of atmospheric nitrogen is almost constant everywhere on Earth and is 0‰ by definition (Mariotti, 1983). The $^{15}N/^{14}N$ ratio of air is given in Table 2.5. One N_2 gas standard called NSVEC ($\delta^{15}N$ = -2.8‰ vs AIR) is distributed by IAEA. Several other solid standards (nitrates) are also available from IAEA. Any laboratory can produce their own nitrogen reference by purifying air. Oxygen is removed by combusting the air sample with Cu metal, but contaminant Ar in the product can interfere with the nitrogen isotope analyses[9].

[8] For details, see:
https://nucleus.iaea.org/rpst/referenceproducts/referencematerials/Stable_Isotopes/13C18and7Li/IAEA-603/RM603_Reference_Sheet_2016-08-16.pdf

[9] Note that V-AIR has not yet been proposed.

2.6.4 Oxygen

Two international reference standards are used to report variations in oxygen isotope ratios, VPDB and VSMOW. SMOW was originally defined in terms of NBS-1

$$\left(\frac{^{18}O}{^{16}O}\right)_{SMOW} = 1.008\left(\frac{^{18}O}{^{16}O}\right)_{NBS-1} \qquad 2.21.$$

SMOW has a $\delta^{18}O$ value of 8.00‰ relative to NBS-1, and NBS-1 has a $\delta^{18}O$ value of -7.94‰ versus SMOW. As with hydrogen, a stretching factor should be applied to oxygen isotope analyses and this factor is calibrated by analyzing VSMOW whose $\delta^{18}O \equiv 0$‰ and SLAP (**S**tandard **L**ight **A**ntarctic **P**recipitation) whose $\delta^{18}O = -55.5$‰ (See Appendix 2). By calibrating in this manner, analyses of water reported on the VSMOW scale are reliable. The stretching factor is much smaller for oxygen isotope analyses than for hydrogen isotope analyses and is often ignored.

Use of the PDB standard for reporting oxygen isotope compositions is restricted to analyses of carbonates of low-temperature origin (oceanic, lacustrine, or pedogenic) in studies of paleoclimate, paleoceanography and carbonate diagenesis. As mentioned above, oxygen isotope compositions of carbonates are determined by analyses of CO_2 generated from them by reaction with 100% H_3PO_4 at a fixed temperature. It is emphasized that the *PDB standard is the solid carbonate*, not the acid-liberated CO_2 that is actually introduced to the mass spectrometer. The $\delta^{18}O$ of PDB is 0‰ on the VPDB scale by definition and analysis of NBS-19 is the accepted means of relating oxygen isotope analyses to VPDB. The $\delta^{18}O$ value of NBS-19 is $\equiv -2.20$‰ on the VPDB scale. Additional international secondary reference standards for carbonates are available (Appendix 1), and relating analyses to PDB no longer poses any ambiguities.

Because the $\delta^{18}O$ value of VPDB is 30.91‰ higher than VSMOW (on the VSMOW scale), the conversion between VSMOW and VPDB scales is given by equation 2.7. There is a difference of 0.28‰ (Fig. 6.1) between CO_2 in equilibrium with VSMOW ($\alpha_{CO2\text{-}H2O} = 1.04120$) at 25ºC and CO_2 liberated from PDB at 25ºC ($\alpha_{CO2\text{-}CaCO3} = 1.01025$) and all these values were used in deriving equation 2.7 (See Chapter 6 for further explanation). Marine carbonates have $\delta^{18}O$ values near zero on the VPDB scale, while ocean waters have $\delta^{18}O$ values near zero on the VSMOW scale. As a result of this relationship, it is not uncommon to see the two scales mixed in published reports, with data for carbonates reported on the VPDB scale and data for waters reported on the VSMOW scale. If their $\delta^{18}O$ values were replotted on the same scale, however, they would be approximately 30‰ apart! Care must be taken not to mix scales when presenting oxygen isotope data.

Traditionally, the $^{17}O/^{16}O$ ratios of terrestrial materials are not measured, because they provide no additional information than the $^{18}O/^{16}O$ ratios alone. The $^{17}O/^{16}O$ ratio correlates well with the $^{18}O/^{16}O$ ratio by the equation

$$\left(^{17}O/_{^{16}O}\right) = \left(^{18}O/_{^{16}O}\right)^{\lambda} \qquad 2.22,$$

where the lambda (λ) is an empirical best fit of ~0.527 for solids and 0.528 for waters. Recently, it has been recognized that there are small departures in the $\delta^{17}O$ values

predicted by equation 2.22 (Luz and Barkan, 2010; Pack and Herwartz, 2014), so that high precision $\delta^{17}O$ studies have relevance and are beginning to be made on a more routine basis. The $\delta^{17}O$ value of VSMOW is by definition 0‰.

Oxygen isotope measurements are made on one of several gases. Generally, samples are converted to or equilibrated with CO_2, which is analyzed in the mass spectrometer. O_2 is routinely used for analyses of silicates which are fluorinated to produce O_2 gas. Analysis of O_2 is required for $\delta^{17}O$ analyses. Finally, oxygen from organic matter is frequently analyzed as CO by reaction with carbon at very high temperatures.

2.6.5 Sulfur

Sulfur has four stable isotopes ^{32}S, ^{33}S, ^{34}S and ^{36}S (Chapter 10). Like the triple oxygen isotope system, to a first approximation the four isotopes of sulfur fractionate in predictable proportions, so that measuring all four isotopes is redundant. (In some cases multiple sulfur isotopes can provide important information about low temperature processes – e.g., Farquhar and Wing, 2003; Ono et al., 2003). In general, only the $^{34}S/^{32}S$ ratios are measured, as these are the two most abundant isotopes of sulfur. Sulfur isotope ratios are given by $\delta^{34}S$ notation. $\delta^{34}S$ values are reported relative to the CDT (**C**añon **D**iablo **T**roilite) standard, a sample of meteoritic troilite (FeS) from Meteor Crater in Arizona. The $^{34}S/^{32}S$ value of CDT is given in Table 2.5. As with the other primary standards, $\delta^{34}S(CDT) \equiv 0.0‰$ by definition. Unfortunately, the CDT standard is not as homogeneous as originally thought, at least on a scale smaller than several milligrams (Beaudoin et al., 1994). The IAEA now distributes two synthetic Ag_2S standards with defined $\delta^{34}S$ values relative to CDT (Appendix 1). Sulfur isotope analyses are calibrated to CDT in each laboratory by analyses of these Ag_2S standards whose $\delta^{34}S$ values differ by 22‰. CDT now joins the ranks of PDB in the sense that they are the accepted international reference standards for reporting all sulfur and carbon isotope analyses, but neither is distributed and both are defined in terms of recommended δ values of secondary solid standards.

Sulfur analyses are made on either SO_2 gas or SF_6 gas (Table 2.4). The advantage of each is discussed in Chapter 10. The $\delta^{34}S$ values of SO_2 gas are determined by measuring masses 66 ($^{34}SO_2$) and 64 ($^{32}SO_2$). Unfortunately, there is an isobaric interference at mass 66 from $^{32}S^{16}O^{18}O$, which must be corrected for. This problem does not exist with SF_6 because F is monoisotopic, however SF_6 is more difficult to produce in the laboratory and requires a mass spectrometer specially configured for the high masses (Table 2.4).

2.6.6. Silicon

Silicon has three stable isotopes, ^{28}Si, ^{29}Si, and ^{30}Si. The abundance of the major isotope ^{28}Si is 92.2%, while ^{29}Si and ^{30}Si have abundances of 4.6 and 3.0%, respectively. The three isotope system follows well-established mass dependent fractionation for terrestrial materials, so that there is no need to measure all three isotopes. In general, the $^{30}Si/^{28}Si$ ratios are measured, reported in terms of $\delta^{30}Si$ values. The total range of $\delta^{30}Si$ values for terrestrial materials range from ~-4 to +4‰. Silicon isotope ratios are reported relative to the NIST standard NBS 28 quartz, with a defined value ≡0‰. Si isotope ratios are measured using either gas source mass spectrometery with SiF_4 as the sample gas or

using multicollector ICPMS. Each method has equivalent precision. Samples measured with gas source mass spectrometry measure the ion fragment SiF_3^+ at masses 85, 86 and 87.

2.6.7. Chlorine

Chlorine has two stable isotopes, ^{35}Cl and ^{37}Cl. Unlike the other isotope systems commonly studied, the abundance the rare isotope is very high, leading to a non-integer mass for the average atomic weight of Cl (35.453 amu). Originally analyzed as HCl (*g*) (Hoering and Parker, 1961) or CsCl on a thermal ionization mass spectrometer (Magenheim et al., 1994), Cl isotope ratios are now analyzed exclusively using CH_3Cl (Long et al., 1993). Seawater, with an extremely long residence time for Cl^- is well mixed, and is therefore the accepted standard, defined as **S**tandard **M**ean **O**cean **C**hloride (SMOC) with a $\delta^{37}Cl$ value ≡ 0.0‰. Several Cl isotope standards have been made (Appendix 1), although any ocean sample has a Cl isotope composition equal to 0.0‰, unless extreme contamination has occurred. The ocean has an essentially constant Cl isotope composition, although some publications suggest that there are variations, a conclusion that I believe in general is not correct.

2.7 Isotope Ratio Mass Spectrometry

The mass spectrometer is the heart of nearly all stable isotope laboratories Some labs are beginning to employ laser spectroscopy systems, but for the last century, most analyses have been made using a mass spectrometer. The foundations of the mass spectrometer can be traced to the Cavendish Laboratory, University of Cambridge, where noted scientists including J.J. Thomson, E. Rutherford and F.W. Aston developed some of the first mass spectrographs[10]. By 1927, Aston had built a second generation machine that allowed for the discovery of isotopes and accurate determinations of their atomic weights. A description of Aston's early machine is discussed in detail and is worth reading (Aston, 1927). In the early to mid-20th century, most isotope ratios were determined gravimetrically, where the mass of a sample was determined using a precise density balance. The difference in the atomic weight of oxygen in air and water – the basis for the 'Dole Effect' – was determined in this way (Dole, 1936). Major improvements were made in the sensitivity and precision of mass spectrometers in the 1940's so that variations in the isotopic composition of natural materials could be measured with the necessary precision. These machines were operated by talented physicists, and extracting high-quality data required skilled practitioners. Only starting in the 1970s and 80s did the mass spectrometer manufacturers begin to offer mass spectrometers that could be used without a great deal of training and infrastructure. Today, there are a wide range of mass spectrometers available, from simple desktop units for low-precision analyses used for simple tracer experiments, to complex doubly-focusing machines that have high sensitivities and mass resolution for analyses of exotic isotopologues from natural samples. At the same time, there is a growing industry of laser spectroscopy systems in which the isotope ratios are measured based on the absorption of infrared radiation by the different isotopologues of a particular gas, such as CO_2, H_2O, CH_4 and N_2O (see section 2.8 for further details).

[10] Mass spectrographs used photographic plates to measure the position and intensity of ion beams. Mass spectrometers use electronic collectors which measure the intensity (current) of the ion beam.

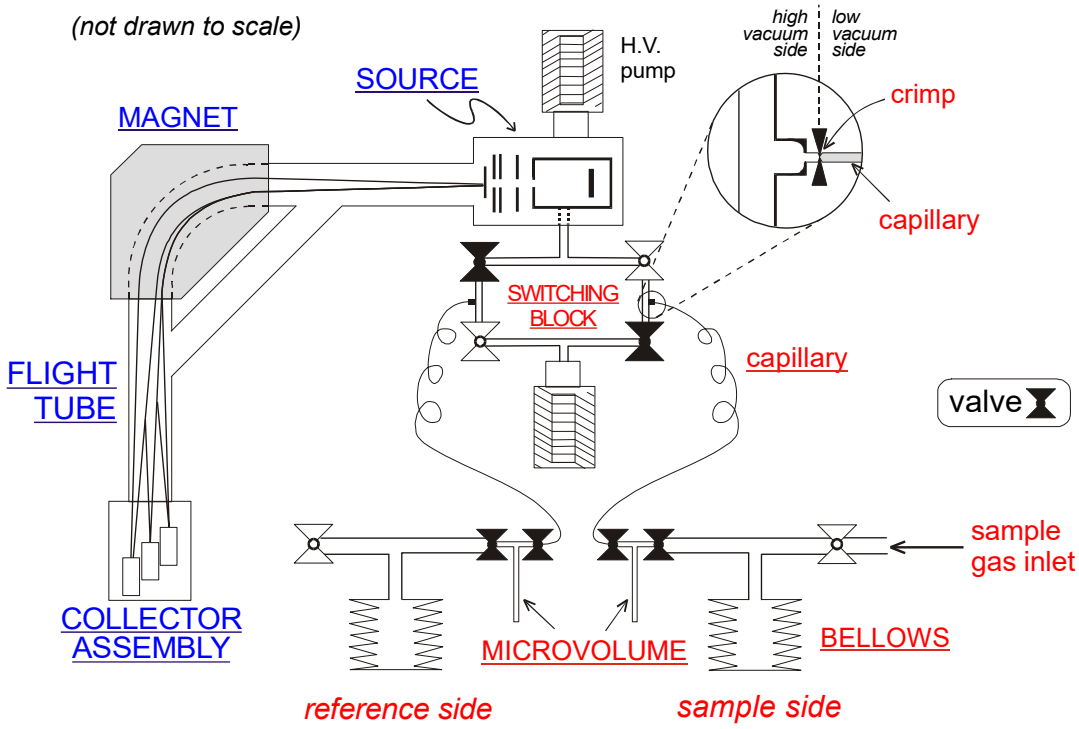

Fig. 2.4. Schematic of a typical modern mass spectrometer. The isotopic composition of two gases (reference and sample) are measured relative to one another. The pressures of both gases in the source region are adjusted to the same value by compressing or expanding the bellows. The gas passes through a capillary about 1 meter long with a crimp at the mass spectrometer end to help reduce the flow rate and to assure viscous flow. The capillary/crimp prevents a fractionation of the gas as it enters the high vacuum of the mass spectrometer. The bleed rate of the gas into the mass spectrometer is slow enough so that the reference gas will remain in the bellows system for a full day of measurement (except for hydrogen). The gas enters the source region, where it is ionized, focused into a coherent beam and accelerated down the flight tube. The ion beams are deflected in a magnetic field in relation to the charge/mass ratio of the ion. The lighter ions are deflected to a greater degree than the heavy ones of the same charge. The ions enter the various collectors (Faraday cups) where the current developed is sent through resistors to produce voltages that are amplified and registered on a recording system (not shown). The intensities of these ion beams are proportional to the abundance of the isotopologue collected. The isotopic ratios and delta values are automatically calculated and recorded by the software that operates the machine.

2.7.1 Components of a mass spectrometer

All mass spectrometers are based on the principle of deflecting an energetic, focused ion beam in a magnetic and/or electrostatic field. The degree of deflection is a function of mass and charge. The relative intensities of the ion beams of different masses can then be used to calculate isotopologue masses or isotope ratios. The mass spectrometer consists of three primary components (Fig. 2.4): 1) the source, where a sample is ionized, accelerated to a given energy and collimated into a well-focused beam; 2) the analyzer, which acts to deflect the ion as a function of mass. It is the 'prism' of the system (See Criss, 1999 for a nice review); and 3) the collector assembly for measuring the relative intensities of the different ion beams. In addition, the mass spectrometer system also has an inlet system for introducing the gas into the source without

fractionation. (see Sharp, 2014 for a detailed discussion of gas source mass spectrometers).

2.7.1.1 The ion source

The ion source both ionizes the sample gas, accelerates it to a near-constant energy and focuses the beam in the direction of the analyzer. Sample gas is admitted into the source at low pressures and a fraction of the gas is ionized (~0.1%) with an unknown but significant isotope fractionation. The ideal ion source has high ionization efficiency, a well collimated ion beam and a near-constant, or at least linear isotope source fractionation over a wide range of source pressures .

The gas source mass spectrometer uses **electron impact ionization**, in which a hot tungsten filament generates electrons in the ionization box. The ionization box has a filament on one side and an anode on the other, so that the electrons are accelerated towards an anode with an energy of ~90eV (Fig. 2.5). This energy is more than enough to cause the sample gas to reach its first ionization potential, which ranges from 12.08eV for O_2 to 15.58 for N_2. Interestingly, above 100eV, ionization efficiencies begin to decrease as molecules become 'transparent' to the electrons (de Hoffmann et al., 1996). A magnetic field is applied to the electron beam with two small permanent magnets on either side of the ionization box which causes the electrons to spiral towards the anode, thereby increasing ion efficiency. The electron impact knocks an electron off a molecule of sample gas causing it to become positively charged. The source is held at a positive electric potential of 2 and 10 kV relative to ground. The positively ionized gas is accelerated out of the ionization box by the repeller plate and towards a stack of electrostatic lenses which focus the ions into a tight beam. Each lens is at a higher potential relative to the ionization box, so that the ions reach a nearly mono-energetic value equal to the electric potential of the source relative to ground. In addition to imparting energy to the ions, the lens stack acts as a telescope, focusing the beam at the collector assembly.

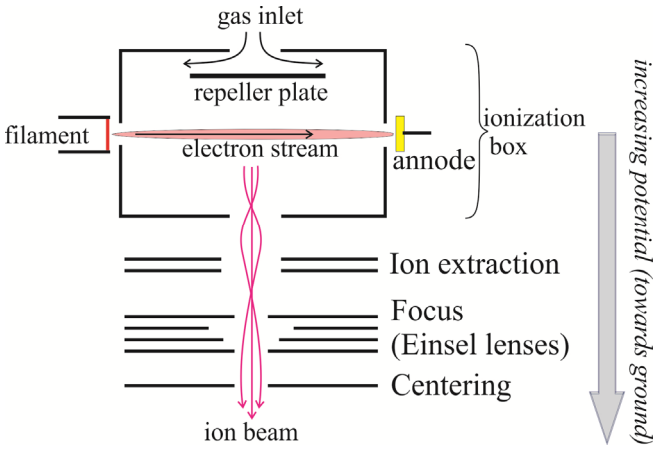

Fig. 2.5. Schematic of the ion source. Gas is bled into the ionization box and is ionized by a stream of energetic electrons generated at the hot (2000°C) tungsten filament. The electrons strike the gas, knocking off one (or more) electrons, producing positively charged ions. The ions are accelerated out of the ionization box by a combination of repulsion from the repeller plate and acceleration towards the focusing electrostatic lenses. Each lens is at an ever-higher potential relative to the trapping box (closer to ground), thereby further increasing both the energy and the focus of the ion beam.

While the ideal electron impact source ionizes the sample gas by removing one electron, ion fragmentation and double ionization (removal to two or more electrons) invariably occur. If the source conditions remain nearly identical for both sample and reference gas, the fragmentation problems can generally be ignored, because it

will affect both gases to the same extent. Consider CO_2 as an example. CO_2 will ionize primarily to CO_2^+, but other ion fragments, such as such as CO^+, C^+, and O^+ and CO_2^{2+}. A mass spectrum of CO_2 gas will show peaks at masses 12, 16, 22 (doubly ionized CO_2), 28 and 44.

The ionization efficiency of an electron impact source is on the order of 0.1 to 0.15% (for CO_2), with a large and generally unknown isotope fractionation. Again, if source conditions (i.e., pressure) are kept the same both for sample and standard, this fractionation will not affect the relative isotopic ratios of reference and sample gas. How the isotope fractionation changes with source pressure is known as **linearity**. Increasing the draw-out potential from the ionization box increases linearity by minimizing ion-ion interactions, but also reduces the sensitivity of the source. A tradeoff must be made between linearity and sensitivity. If gas quantities are not an issue, then the source should be focused for highly linear conditions.

2.7.1.2. The analyzer

The mass analyzer is the portion of the mass spectrometer where the ion beams are separated from each other on the basis of their mass. It is equivalent to a prism, which separates light according to wavelength. Most stable isotope mass spectrometers use a magnetic field to separate ions by mass, but doubly-focusing mass spectrometers also use an electrostatic lens in order to attain very high mass resolution. The effects of electric and magnetic fields on an ion beam is given by Lorentz's law by

$$F = q\left(E + v \times B\right) \qquad 2.23,$$

where F is the force acting on the ion, (which determines the degree of deflection in a circular field), q is the ion charge, v is velocity and E and B are the electric and magnetic forces, respectively.

The energy imparted by the ion source is given by

$$qV = \tfrac{1}{2}\, mv^2 \qquad 2.24,$$

where q is the charge, V is the voltage potential between the source and ground, m is the ion mass and v is the ion velocity. The force imparted by an electrostatic field, composed of two charged plates in a semi-circular arc results in a deflection of the ion beam given by

$$r = \frac{mv^2}{qE} \qquad 2.25,$$

where E is the electric force. All ions of equal charge traveling through a curved electrostatic field with radius r will have a constant kinetic energy ($\frac{1}{2}mv^2$). Higher or lower energetic ions will have a different radius of curvature and can be physically removed from the beam with proper placement of slit apertures. An electrostatic field is therefore an energy filter, imparting a constant energy to the ion beam.

A magnetic field generates a force equal to qvB which imparts a centripetal force equal to mv^2/r. The radius of curvature is given by

$$r = \frac{mv}{qB} \qquad 2.26.$$

Unlike an electrostatic field, where the deflection is related to mv^2, a magnetic field deflects ions proportional to mv or momentum. The radius of singly charged particles at constant velocity is therefore related to the mass. For a constant energy ion beam, ions with a smaller mass will be deflected more than ions with a higher mass.

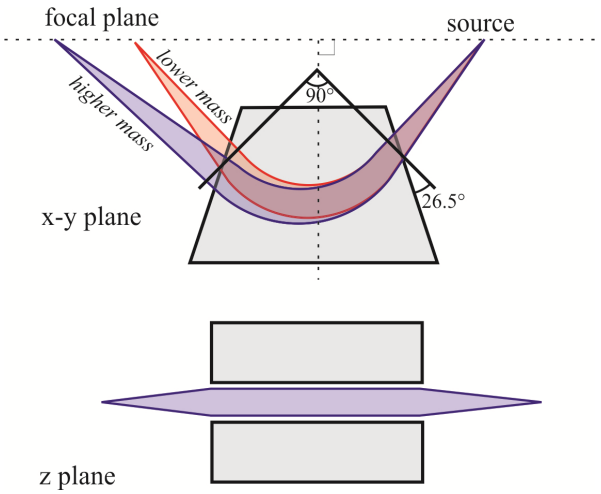

Fig. 2.6. Schematic of mass spectrometer focusing. The dispersion of the beam from the source is eliminate by focusing through the analyzer in the x-y plane (2.4a top). The beam will refocus on a line perpendicular to the magnetic arc which includes the source. In the z-plane, focusing is made by 'fringe focusing', in which the edge of the magnet is designed to be non-perpendicular to the ion beam (2.4b bottom).

High resolution doubly focusing mass spectrographs have been around for close to a century (e.g., Bainbridge and Jordan, 1936). For most stable isotope studies, sufficient mass separation is achieved with a magnetic field alone. However, for very high mass resolution and when the ions are produced with variable energy, the addition of energy filtering using an electrostatic field is required. Both an ion microprobe and high resolution ICP MS require both electrostatic and magnetic field focusing.

In a magnetic sector mass spectrometer, the magnet separates ions of different masses, but also focuses the ion beam at the point of the collector assembly (Fig. 2.6). Interestingly, it is the radius of the magnetic field, and not the total arc fraction (e.g., 60° vs. 180°) that defines the degree of separation and focus (Nier, 1940)[11]. An ion beam leaving the source will necessarily have some degree of divergence. As shown in Fig. 2.6a, the beam will enter the magnetic field and be deflected in such a way as to be refocused on a plane perpendicular to the arc of the magnetic field that includes the ion source and the point of refocusing. Beam divergence also occurs perpendicular to the plane defined by the ion path (the z direction). It has been shown that if the beam crosses the fringing field (edge) of a magnetic field non-perpendicular to the edge of the magnet, the beam will be deflected perpendicular to the median plane (in a vertical direction in a flat-lying magnetic arc – 26.5° angle in Fig. 2.6b). By adjusting the angle of the fringing field, the beam can be deflected – and thereby focused – in a vertical plane at the point of

[11] Commercially available mass spectrometers use 60° or 90° sector field with comparable results.

the collector assembly. The angle between the beam and magnet edge is a function of the arc and the path lengths on either side of the magnet. If properly designed, the deflection that occurs upon entering the magnet causes the beam to become parallel to the magnetic plates, and during the exit deflection, the beam is deflected to focus at the focal plane of the ion beam (e.g., at the collector).

2.7.1.3. Collector assembly

The final component of the gas source mass spectrometer is the collector assembly. The early machines were mass spectrographs, in which the ion beams were focused on photographic plates. The intensity and position of the exposed images gave the position and abundance of the isotopologues. The accuracy attained with photographic film was so high that Francis Aston in 1937 was able to determine the atomic weights of over twenty isotopes to better than 0.008 amu of today's accepted value (when corrected for different scales) (Aston, 1937). All modern mass spectrometers use electronic detectors to measure the intensity (current) of an ion beam. Positive ions enter a collector which acts as an electron source for charge compensation. Neutralization of the collectors generates an extremely small electric current. The current (total charge per unit time) is related to the intensity of the ion beam. Current is related to voltage by Ohm's law

$$V = IR \qquad 2.27$$

where V is voltage, I is current and R is resistance. By using a very large resistor (10^8 to 10^{12} Ω), a high voltage can be generated from a very small current. A voltage-to-frequency converter is then employed to give a signal that is related to the beam strength. When multiple beams from different isotopologues are collected simultaneously, each collector is fitted with appropriate resistors so that the output voltage (current) of each ion beam are close to the same. For example, the relative abundance of the isotopologues of CO_2 are roughly the following: $^{12}C^{16}O^{16}O$ – 0.984; $^{13}C^{16}O^{16}O$ – 0.011; $^{12}C^{18}O^{16}O$ – 0.004. Voltages for these three beams will be similar if resistors of $1 \times 10^8\Omega$, $1\times10^{10}\Omega$ and $3\times10^{10}\Omega$ are used for masses 44, 45 and 46, respectively.

For most applications in gas source mass spectrometry, Faraday collectors are used to measure beam intensity. Positive ions are neutralized in the collector and draw an electron for charge compensation. Ideally, the collector acts as a perfect black body surface for reception of the ions. Reflection of ions is minimized by coating the inside of the collector with soft carbon. Some sputtering of the ions occurs, generating secondary electrons. The loss of such an electron would negate the charge contribution from a positive

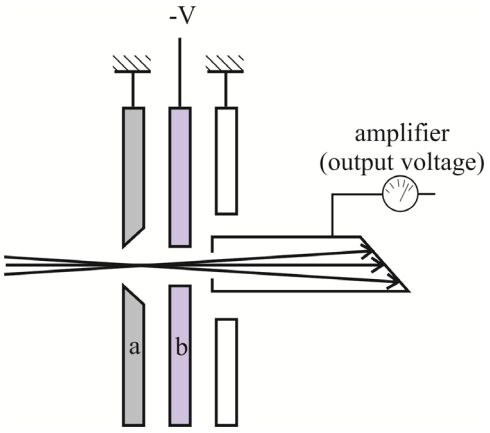

Fig. 2.7. Schematic of a Faraday collector. The ion beam passes through a narrow slit a and is neutralized in the collector, generating a current. A charged electrode b prevents secondary electrons generated in the collector cup from exiting the assembly.

ion. Collectors are therefore manufactured as deep wells with narrow entrance slits to prevent the loss of secondary electrons. The collector consists of a narrow slit to prevent the introduction of stray ions and a charged electrode at the entrance to the collector to help prevent the secondary ions produced in the collector from escaping back through the entrance slit (Fig. 2.7). Multiple collectors are generally used in order to simultaneously measure the intensities of all relevant isotopologues of a given gas. In this way, electronic drift in the system is minimized. Instrumental designs include either multiple narrow detectors positioned for analysis of a single gas type or 'universal collectors', in which several wide cups are paired with a narrow cup. The multiple, narrow collector design is unquestionably superior to the universal collector system, but it can be costly, and flexibility is limited because the positioning of the collectors is generally fixed. For users wishing to be able to analyze multiple gases on a single instrument, the number of collectors required can be quite high. The universal collector design is simple and less costly, but inherently runs the risk of having a greater loss of secondary electrons or reflected ions and the possibility of stray ions entering the cup. In practice, by comparing standard and sample, these effects are minimized.

2.7.1.4 Dual inlet mass spectrometer inlet system

In gas source mass spectrometry, a dynamic inlet system is used. Gas continuously bleeds into the source, is partially ionized, and the excess non-ionized gas is pumped away. A dynamic inlet system avoids the problems of drift due to preferential ionization of one isotopologue relative to another by continuously streaming fresh sample gas into the source. Source pressures must be kept low to avoid molecular collisions in the flight tube which would otherwise broaden the well-focused beam. Therefore some method of pressure reduction is required between the gas reservoir and the source. Whereas the gas pressure in the sample reservoir is on the order of 10^2-10^3 mbar, pressures are reduced to 10^{-4} bars in the ionization chamber and 10^{-6} to 10^{-8} bars in the flight tube. The pressure drop from sample volume to source could be accomplished by having a pinhole orifice between the gas volume and the source, but such a geometry causes an isotopic fractionation, with the lighter isotopologues preferentially passing through the orifice due to their higher translational velocities (Graham's Law). To eliminate this fractionation, gas source mass spectrometers are equipped with a capillary inlet system. A long (~1 m) 0.1mm I.D. capillary is connected to the gas volume adjusted to between 10-100 mbar pressure. At the other end – the interface with the high vacuum of the mass spectrometer – the capillary is crimped, so that the pressure drops to 10^{-4} bar in the source. The light molecules will preferentially pass through the crimp, but because the mean free path of individual molecules in the capillaries is a fraction of the capillaries' internal diameter (~10^{-7} m), the gas migrates along the capillary into the mass spectrometer under viscous flow conditions. Like leaves floating on a swift moving stream, the random motion of individual molecules is overwhelmed by the overall flow direction of the gas through the capillary into the mass spectrometer. Using this type of geometry, there is no fractionation in the capillary inlet system as long as the pressure in the capillary is kept in the 10-100 mbar range.

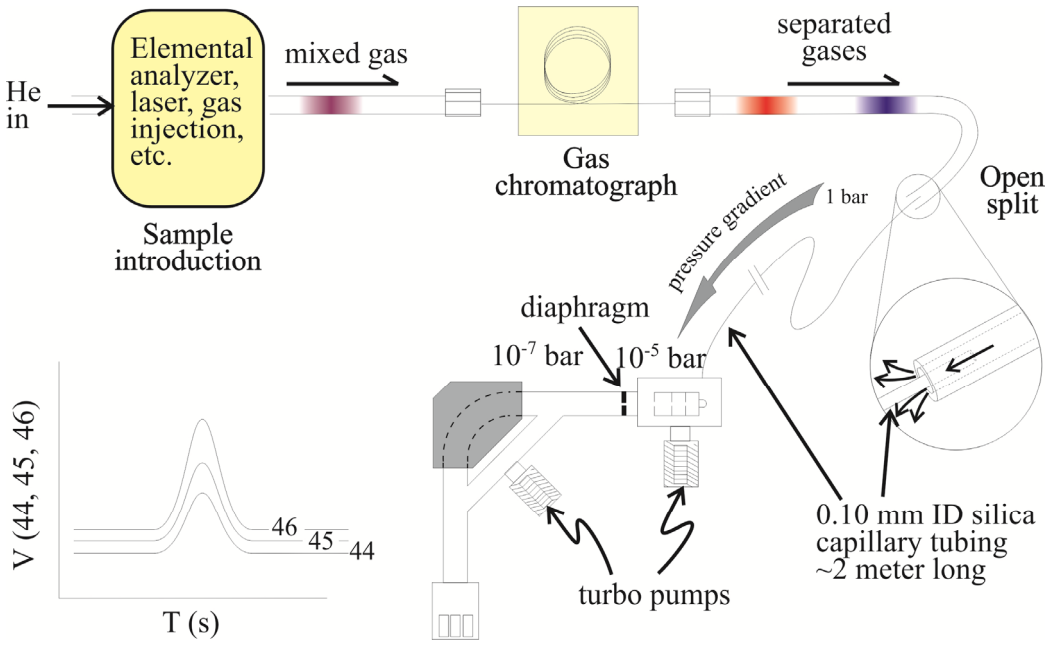

Fig. 2.8. Schematic of a GC-IRMS system. Samples are introduced into a He stream and the different gases are separated on a gas chromatographic column. They pass through an open split into the mass spectrometer. The open split allows for a constant pressure to be maintained in the source. A pressure drop from 1 bar at the open split to 10^{-5} - 10^{-6} bars occurs along the length of the capillary. Multiple turbomolecular pumps separated by a diaphragm slit keeps the pressure in the flight tube low. Signals for the different isotopolouges of a given gas are measured simultaneously as Gaussian-shaped peaks. The integrated area of each peak relative to those of a reference gas or standard sample can be used to determine the isotope ratio in conventional delta format.

High precision is achieved by rapidly switching between sample and reference gas using a system of changeover valves ('switching block' in Fig. 2.4). First described by Murphey (1947) and then McKinney et al. (1950), two identical capillary systems feed through a system of four change-over valves so that either the reference gas or the sample gas enters the mass spectrometer. Gas always flows through the two capillaries to achieve steady state flow. The switching valves change the flow path between the source and a waste pump. Switching between reference and sample gas can be accomplished rapidly, so that the intensities of all ion beams for the sample and reference gas can be compared almost simultaneously. This rapid switching minimizes any errors associated with drifting electronics. In order to keep conditions in the source as similar as possible, both reference and sample gas are adjusted to be nearly the same pressure. This was originally accomplished using mercury pistons, but is now done using flexible steel bellows controlled by stepping motors ('bellows' in Fig. 2.4).

2.7.2 Gas Chromatograph Isotope Ratio Mass Spectrometry (GC-IRMS)

In recent years, the **continuous flow** method of gas introduction has revolutionized isotope ratio mass spectrometry and opened up a panoply of research avenues (Matthews and Hayes, 1978). In place of analyzing gas using the dual inlet method of measurement, samples of gas are entrained in a He stream, purified in a gas

chromatograph and (with or without first oxidizing or reducing the gas by passage through an oven) introduced directly into the source of the mass spectrometer. Initial applications of the GC were mainly to purify the gas. Early online applications included the now routine high temperature combustion of very small C and/or N-bearing samples in an elemental analyzer or equivalent oxidation furnace (Fig. 2.8). Another important application is compound specific analysis of organic molecules (Hayes et al., 1989). Organic species are separated on a GC column and oxidized (or reduced) sequentially before being analyzed in the mass spectrometer. A simple example would be the analysis of a natural gas sample. The gas consists of methane (CH_4), ethane (C_2H_6), propane (C_3H_8), etc. The lighter alkanes pass through the GC column faster than heavier ones, and with a judicious choice of GC columns, flow rates, temperatures, etc, it is possible to get a quantitative separation of the different alkanes. The methane exits the GC column first and is carried by the He stream through a copper oxide furnace where it is oxidized to CO_2 and introduced into the mass spectrometer. The $\delta^{13}C$ vale of the methane-derived CO_2 is determined as it flows into the source. Ethane and higher alkanes follow sequentially, allowing for the $\delta^{13}C$ values of each species to be determined. The range of isotopic variations within a single sedimentary organic sample can often exceed the total variation of different bulk samples (Freeman et al., 1990). This information has been used extensively for paleoclimate reconstruction, ecology and metabolic studies.

GC-IRMS (**G**as **C**hromatography- **I**sotope **R**atio **M**ass **S**pectrometry) technology has been modified so that it can be used in place of conventional extraction techniques for almost every material that has been analyzed conventionally. The advantages of GC-IRMS is that gases can be purified easily and efficiently, analysis is extremely rapid, and sample sizes are reduced by several orders of magnitude. Systems that combine gas chromatography and continuous flow technology continue to find important applications in the earth and biological sciences. Recent improvements in analyses of water and carbonates effectively replace analytical methods that have been in use with only minor modification for over half a century. There is a slight loss of precision relative to the traditional dual inlet system, although the gap is reduced every year.

2.7.3 Gases measured in isotope ratio mass spectrometry

Gases that are commonly introduced into isotope ratios mass spectrometers and masses of the isotopologues measured are given in Table 2.4. Hydrogen isotope ratios are almost always determined from the 3/2 ratios of H_2. Carbon isotope ratios are almost always determined from 45/44 ratios of CO_2 gas. Nitrogen isotope ratios are determined from 29/28 and 30/28 ratios of N_2. Because the concentration of $^{15}N^{15}N$ is negligible in nature, measurements are made of mass 30 only when materials artificially enriched in ^{15}N are being studied. Oxygen isotope ratios are most commonly determined from measurements of 46/44 ratios of CO_2 but, more and more frequently, the gases CO and O_2 are being used. $^{18}O/^{16}O$ ratios are determined from the 30/28 mass ratio of CO and the 34/32 mass ratio of O_2. $^{17}O/^{16}O$ ratios are determined from 33/32 ratios of O_2. CO is the gas of choice for emerging pyrolysis applications.

As discussed in section 2.6.5., sulfur isotope ratios can be measured on either SO_2 or SF_6. SO_2 is easily produced from most samples and can be analyzed in most mass spectrometers, but has a number of disadvantages, most notably, it quickly dirties the source of the mass spectrometer (see section 10.2). This problem is reduced significantly

in continuous flow systems where only minor amounts of SO_2 are introduced into the mass spectrometer. SF_6 is cleaner and allows for the rare isotope ratios to be measured, but it is difficult to produce and requires a large-radius mass spectrometer especially configured for SF_6.

Silicon isotope ratios are measured on SiF_4 gas. The fragment SiF_3^+ is analyzed because it is the major isobar produced in the source. Masses 85 ($^{28}SiF_3^+$), 86 ($^{29}SiF_3^+$) and 87 ($^{30}SiF_3^+$) are analyzed. Chlorine isotope ratios are made using CH_3Cl. Masses 50 ($CH_3{}^{35}Cl$) and 52 ($CH_3{}^{37}Cl$) are analyzed. Many normal triple collector assemblies are not quite configured correctly for simultaneous analysis of masses 50 and 52, so that mass spectrometers must be fitted with special collectors for CH_3Cl analysis.

2.7.4 Relations between measured and desired isotopic ratios

The relationship between intensities of measured gasses in a mass spectrometer and the actual isotopic ratio of a given element is different for each gas. A few of the salient points pertinent to the analyses of three gases (H_2, N_2, and CO_2) will be made here to gain an appreciation of this important aspect of isotope ratio mass spectrometry.

After experimenting with various hydrogen containing gases, Irving Friedman (1953) concluded that diatomic hydrogen was the most suitable for determination of hydrogen isotope ratios and H_2 remains the gas of choice to this day. Isotopic analysis of hydrogen poses a unique analytical problem. One of the ionic fragments produced in the source of the mass spectrometer is H_3^+ which has the same mass 3 as HD^+. Collection of this ion results in an apparent 3/2 ratio that is higher than the true HD/HH ratio. The production of H_3^+ is proportional to the pressure of hydrogen gas in the source because this ion is produced by the reaction $H_2 + H_2^+ \rightarrow H_3^+ + H$. The H_3^+ contribution to mass 3 can be minimized, but not eliminated, by using a high accelerating voltage and a low gas pressure. The contribution of H_3^+ is evaluated by measuring the 3/2 ratio as a function of source pressure, a procedure that is done routinely on modern mass spectrometers. The correlation is linear on most modern machines (at low pressures, less H_3^+ is produced). Once the relationship between pressure and contribution of H_3^+ is determined, a correction algorithm can be applied that removes the mass 3 contribution from the H_3^+ ion (*i.e.,* extrapolate back to zero pressure).

Nitrogen isotope analysis is relatively straightforward. Measurements are made of two isotopologues of molecular nitrogen whose masses are 28 and 29. The isotopologue with mass 28 consists solely of $^{14}N^{14}N$ while that of mass 29 is a sum of the two possible orientations of ^{15}N and ^{14}N atoms in the molecule, $^{15}N^{14}N$ and $^{14}N^{15}N$. The desired mass ratio is then obtained from the relatively simple relation[12]:

$$\frac{29}{28} \approx 2 \times \frac{^{15}N}{^{14}N} \qquad 2.28$$

[12] The actual relationship is $\left(\frac{29}{29+28}\right) = 2 \times \frac{15}{14}$ or $\frac{29}{28} = \frac{2 \times 15/14}{1 - 15/14}$. If the 15/14 ratio is 3670×10^{-6}, the actual stochastic 29/28 ratio is 7367×10^{-6}, whereas equation 2.28 gives a 29/28 ratio of 7340×10^{-6}.

The molecular mass ratio 29/28 is twice the atomic mass ratio of 15/14 and is the one used to determine nitrogen isotope ratios. This same mathematical correction is used for CO_2 as well.

The nine isotopologues of CO_2 that are measured on a mass spectrometer are given in Table 2.7. An additional 5 are included when mass 47 is measured in 'clumped isotope' studies (see section 6.7). Deconvolution of the three masses 44, 45 and 46 to $^{13}C/^{12}C$ and $^{18}O/^{16}O$ ratios can be made assuming that the relationship between $^{17}O/^{16}O$ and $^{18}O/^{16}O$ ratios (equation 2.2) is valid. Given that $(^{17}O/^{16}O) \cong (^{18}O/^{16}O)^{0.5x}$, the three masses 44, 45 and 46 of CO_2 can be used to determine both $^{13}C/^{12}C$ and $^{18}O/^{16}O$ ratios (Craig, 1957; Santrock et al., 1985). The 46/44 ratio measured in the mass spectrometer is close to the $^{18}O/^{16}O$ ratio, because $^{12}C^{16}O^{18}O$ makes up >99.7% of the total isotopologues at mass 46. On the other hand, the $^{13}C/^{12}C$ ratio of CO_2 gas is not the same as the 45/44 ratio because the $^{12}C^{17}O^{16}O$ isotopologue is on the order of 7% of the total mass 45 isobar. For $\delta^{13}C$ analyses, the common '*^{17}O correction*' must be made. The $\delta^{17}O$ value of the CO_2 sample is estimated from the measured $\delta^{18}O$ value and the relationship between $^{17}O/^{16}O$ and $^{18}O/^{16}O$ (equation 2.2). The $^{12}C^{17}O^{16}O$ contribution to mass 45 is then subtracted from the total 45 isobar intensity in order to obtain the contribution of just $^{13}C^{16}O_2$.

Table 2.6 *Masses and possible configurations of CO_2 isotopologues.*

Mass	Isotopologue
44	$^{16}O^{12}C^{16}O$
45	$^{16}O^{13}C^{16}O$, $^{17}O^{12}C^{16}O$, $^{16}O^{12}C^{17}O$
46	$^{17}O^{13}C^{16}O$, $^{16}O^{13}C^{17}O$, $^{17}O^{12}C^{17}O$, $^{18}O^{12}C^{16}O$, $^{16}O^{12}C^{18}O$
47	$^{16}O^{13}C^{18}O$, $^{18}O^{13}C^{16}O$, $^{17}O^{13}C^{17}O$, $^{17}O^{12}C^{18}O$, $^{18}O^{12}C^{17}O$
48	$^{18}O^{12}C^{18}O$, $^{18}O^{13}C^{17}O$, $^{17}O^{13}C^{18}O$
49	$^{18}O^{13}C^{18}O$,

2.8 Laser absorption mass spectroscopy

In recent years, laser absorption spectroscopy has been modified for use in stable isotope analysis. This method involves measuring the absorption of electromagnetic radiation (generally infrared) generated by a laser at a frequency specific to the absorption of a single isotopologue of a gas molecule (Fig. 2.9). There are a large number of absorption bands for any molecule that has a dipole[13], and bands are chosen in the frequency range of the laser which are close to one another without any interferences from other absorption lines. Absorption is directly related to concentration following Beer-Lambert law, given by

$$I = I_o \exp(-\sigma C l) \qquad 2.29,$$

where I_o and I are the intensity of the electromagnetic radiation entering and leaving the chamber containing the gas, C is the concentration of the absorber, l is the sample path length and σ is the absorption cross section at the appropriate wavelength. The laser light

[13] A dipole has a permanent bond polarization – two atoms with different electronegativity. O_2 and N_2 consist of two atoms with the same electronegativity and have no dipole.

is directed through the input mirror (with most being reflected back to the laser) and reflects back and forth between two parallel mirrors. The intensity of the reflecting light is measured by a photo-sensitive detector behind the output mirror. The concentration of a molecular species is determined from the I/I_o value.

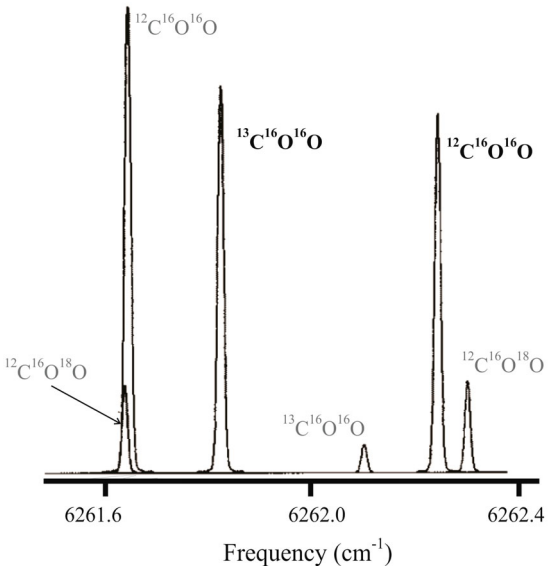

Fig. 2.9. Illustration of several absorption bands for CO_2 gas for different isotopologues. There are a large number of bands to chose from. Ideally, absorption bands will be chosen for the isotopologues of interest that are close to each other and do not have any other interferences. The $^{13}C^{16}O^{16}O$ and $^{12}C^{16}O^{16}O$ in bold are ideal pairs to analyze.

Several systems are now commercially available that take advantage of low-cost tunable diode lasers. Two distinct methods are employed. The first, called *off axis cavity output spectroscopy*, measures changes in intensity of the laser beam as it scans across the wavelength of interest (Baer et al., 2002). By having the beam reflect multiple times between the two mirrors in the sample cavity, it is possible to achieve path lengths of several km, thereby drastically increasing the degree of absorption (Fig. 2.10). The second method, called *cavity ring-down laser absorption spectroscopy*, measures changes in the intensity of the reflecting beam as a function of time. A pulse of laser light charges the cavity and the laser is quickly shut off. The rate of decay (the 'ring-down' time) of the laser beam (on the order of several microseconds) is a function of the concentration of the absorbing species. The higher the concentration, the more rapid the ring-down time. Each method has certain advantages and disadvantages, and at present, it appears that the precision of the two systems are more-or-less equivalent (Johnson et al., 2011).

The tunable diode laser systems are used primarily for H and O isotope ratios of water and C and O isotope ratios of CO_2, carbon from methane, and N and O in N_2O (Baer et al., 2002; Crosson et al., 2002; Lis et al., 2008; Brand et al., 2009). Analyses can only be made on gases which are transferred into the laser cavity in a carrier gas, either N_2 or dry air. Precision is only slightly lower than that attainable from conventional mass spectrometry. At low concentrations of water vapor, serious analytical bias is observed, however. Care must be taken to avoid interferences from contaminant gases (Brand et al., 2009). For all of the commercially available laser systems, the sample flows through the chamber continuously throughout the measurement, although efforts to introduce a small

amount of gas into the cavity in a static mode has met with success (Berryman et al., 2011).

The future outlook for laser spectroscopy systems is quite favorable. Simultaneous analyses of both D/H and $^{18}O/^{16}O$ ratios are possible because the absorption bands of $^{1}H_2{}^{16}O$, $^{1}H^{2}H^{16}O$, and $^{1}H_2{}^{18}O$ are all distinct and large enough for accurate analysis, and recently manufactures have added ^{17}O to the total analysis (although non-linearity problems persist). Similarly, analyses of N_2O and CO_2 may allow for isotopologues of the rare isotopes to be measured with far greater ease than by traditional mass spectrometry methods. Ono *et al.* (2014) have successfully developed a laser absorption spectroscopy system that is able to measure the isotopic composition of the rare methane isotopologue $^{13}CH_3D$. Laser spectroscopy systems have also been used for measuring the rare 'clumped' isotope $^{13}C^{16}O^{18}O$ (mass 47) and $^{17}O/^{16}O$ ratios in CO_2 gas (Sakai *et al.*, 2017) The ability to measure rare isotopologues and separate the contributions of different same-mass isotopologues (*e.g.,* $^{13}CH_4$ and $^{12}CH_3D$) suggests exciting applications yet to come. It is doubtful that the laser systems will supplant the gas source methods entirely, although for routine analyses, the cost of the instruments are far lower than for gas source mass spectrometers and the off-line preparation of samples such as water is virtually eliminated. The laser systems are compact and easily deployable to the field. It is likely that continued advancements to the laser systems will be made, resulting in lowered price and greater versatility.

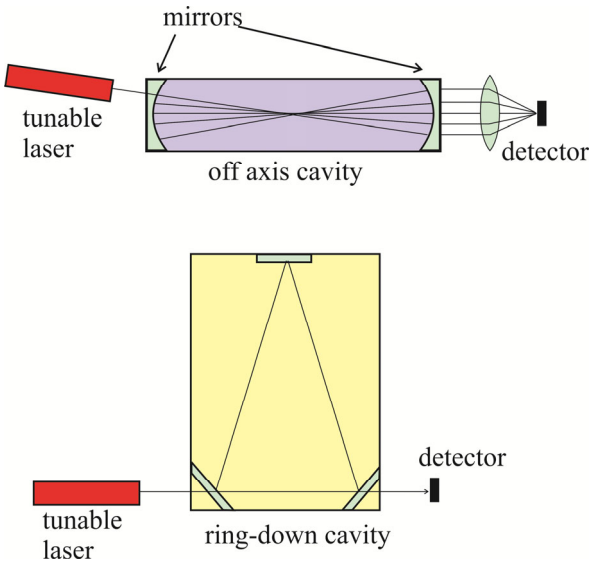

Fig. 2.10. Different configurations for laser absorption spectroscopy. Off axis cavity spectroscopy (top) causes the laser beam to reflect between two parallel mirrors multiple times before being analyzed at the detector, thereby increasing the effective cavity length (Baer et al., 2002). The second method (bottom) is the cavity ringdown laser, in which the cavity is charged with 'light' which reflects between several mirrors. The light source is switched off and the rate at which the light intensity decays (rings down) is measured by a detector, which allows a fraction of the radiation to pass through the mirror to the detector. The rate of decay (ringdown rate) is a function of the concentration of the absorbing gas in the cavity (Crosson et al., 2002).

REFERENCES

Aston, F.W. (1927) Bakerian Lecture. A new mass-spectrograph and the whole number rule. *Proceedings of the Royal Society of London, Series A* **115**, 487-514.

Aston, F.W. (1937) A Second-Order Focusing Mass Spectrograph and Isotopic Weights by the Doublet Method. *Proceedings of the Royal Society of London. Series A* **163**, 391-404.

Baer, D.S., Paul, J.B., Gupta, M. and O'Keefe, A. (2002) Sensitive absorption measurements in the near-infrared region using off-axis integrated-cavity-output spectroscopy. *Applied Physics B* **DOI: 10.1007/s00340-002-0971-z**.

Baertschi, P. (1976a) Absolute 18-O content of standard mean ocean water. *Earth and Planetary Science Letters* **31**, 341-344.

Baertschi, P. (1976b) Absolute ^{18}O content of standard mean ocean water. *Earth and Planetary Science Letters* **31**, 341-344.

Bainbridge, K.T. and Jordan, E.B. (1936) Mass spectrum analysis 1. The mass spectrograph. 2. The existence of isobars of adjacent elements. *Physical Review* **50**, 282-296.

Beaudoin, G., Taylor, B.E., Rumble, D.I. and Thiemens, M. (1994) Variations in the sulfur isotope composition of troilite from the Cañon Diablo iron meteorite. *Geochimica et Cosmochimica Acta* **58**, 4253-4255.

Berryman, E.M., Marshall, J.D., Rahn, T., Cook, S.P. and Litvak, M. (2011) Adaptation of continuous-flow cavity ring-down spectroscopy for batch analysis of $\delta^{13}C$ of CO_2 and comparison with isotope ratio mass spectrometry. *Rapid Communications in Mass Spectrometry* **25**, 2355-2360.

Brand, W.A., Geilmann, H., Crosson, E.R. and Rella, C.W. (2009) Cavity ring-down spectroscopy versus high-temperature conversion isotope ratio mass spectrometry; a case study on δ^2H and $\delta^{18}O$ of pure water samples and alcohol/water mixtures. *Rapid Communications in Mass Spectrometry* **23**, 1879-1884.

Coplen, T.B. and Clayton, R.N. (1973) Hydrogen isotopic composition of NBS and IAEA stable isotope water reference samples. *Geochimica et Cosmochimica Acta* **37**, 2347-2349.

Coplen, T.B., Kendall, C. and Hopple, J. (1983) Comparison of stable isotope reference samples. *Nature* **302**, 236-238.

Coplen, T.B. (1988) Normalization of oxygen and hydrogen isotope data. *Chemical Geology* **72**, 293-297.

Coplen, T.B. (1994) Reporting of stable hydrogen, carbon, and oxygen isotopic abundances (Technical Report). *Pure and Applied Chemistry* **66**, 273-276.

Coplen, T.B. (1996) New guidelines for reporting stable hydrogen, carbon, and oxygen isotope-ratio data. *Geochimica et Cosmochimica Acta* **60**, 3359-3360.

Craig, H. (1957) Isotopic standards for carbon and oxygen and correction factors for mass-spectrometric analysis of carbon dioxide. *Geochimica et Cosmochimica Acta* **12**, 133-149.

Craig, H. (1961) Standard for reporting concentrations of deuterium and oxygen-18 in natural waters. *Science* **133**, 1833-1834.

Criss, R.E. (1999) Prinicples of stable isotope distribution. Oxford University Press, New York.

Crosson, E.R., Ricci, K.N., Richman, B.A., Chilese, F.C., Owano, T.G., Provencal, R.A., Todd, M.W., Glasser, J., Kachanov, A.A. and Paldus, B.A. (2002) Stable Isotope Ratios Using Cavity Ring-Down Spectroscopy: Determination of $^{13}C/^{12}C$ for Carbon Dioxide in Human Breath. *Analytical Chemistry* **74**, 2003–2007.

De Bièvre, P., Valkiers, S. and Peiser, H.S. (1994) New values for silicon reference materials, certified for isotope abundance ratios. *Journal of research of the National Institute of Standards and Technology* **99**, 201-202.

de Hoffmann, E., Charette, J. and Stroobant, V. (1996) Mass Spectrometry. Principles and Applications. John Wiley & Sons, Chichester.

de Wit, J.C., van der Straaten, C.M. and Mook, W.G. (1980) Determination of the absolute hydrogen isotopic ratio of V-SMOW and SLAP. *Geostandards Newsletter* **4**, 33-36.

Ding, T., Valkiers, S., Kipphardt, H., De Bièvre, P., Taylor, P.D.P., Gonfiantini, R. and Krouse, R. (2001) Calibrated sulfur isotope abundance ratios of three IAEA sulfur isotope reference materials and V-CDT with a reassessment of the atomic weight of sulfur. *Geochimica et Cosmochimica Acta* **65**, 2433-2437.

Dole, M. (1936) The relative atomic weight of oxygen in water and in air. A discussion of the atmospheric distribution of the oxygen isotopes and the chemical standard of atomic weights. *The Journal of Chemical Physics* **4**, 268-275.

Epstein, S. and Mayeda, T.K. (1953) Variation of ^{18}O content of waters from natural sources. *Geochimica et Cosmochimica Acta* **4**, 213-224.

Farquhar, J. and Wing, B.A. (2003) Multiple sulfur isotopes and the evolution of the atmosphere. *Earth and Planetary Science Letters* **213**, 1-13.

Freeman, K.H., Hayes, J.M., Trendel, J.-M. and Albrecht, P. (1990) Evidence from carbon isotope measurements for diverse origins of sedimentary hydrocarbons. *Nature* **343**, 254-256.

Friedman, I. (1953) Deuterium content of natural water and other substances. *Geochimica et Cosmochimica Acta* **4**, 89-103.

Friedman, I., O'Neil, J.R. and Cebula, G. (1982) Two new carbonate stable-isotope standards. *Geostandards Newsletter* **6**, 11-12.

Hagemann, R., Nief, G. and Roth, E. (1970) Absolute isotopic scale for deuterium analysis of natural waters - absolute D/H ratio for SMOW. *Tellus* **22**, 712-715.

Hayes, J.M., Freeman, K.H., Hoham, C.H. and Popp, B.N. (1989) Compound-specific isotopic analyses: a novel tool for reconstruction of ancient biogeochemical processes. *Organic Geochemistry* **16**, 1115-1128.

Hoering, T. and Parker, P.L. (1961) The geochemistry of the stable isotopes of chlorine. *Geochimica et Cosmochimica Acta* **23**, 186-199.

Horita, J., Cole, D.R., Polyakov, V.B. and Driesner, T. (2002) Experimental and theoretical study of pressure effects on hydrogen isotope fractionation in the system brucite-water at elevated temperatures. *Geochimica et Cosmochimica Acta* **66**, 3769-3788.

Hut, G. (1987) Consultants' group meeting on stable isotope reference samples for geochemical and hydrological investigations. International Atomic Energy Agency, Vienna.

Johnson, L.R., Sharp, Z.D., Galewsky, J., Strong, M., Van Pelt, A., Dong, F. and Noone, D. (2011) Isotope correction for laser instrument measurement bias at low water

vapor concentration using flasks: application to measurements from Mauna Loa Observatory, Hawaii. *Rapid Communications in Mass Spectrometry* **25**, 608-616.

Junk, G. and Svec, H.J. (1958) The absolute abundance of the nitrogen isotopes in the atmosphere and compressed gas from various sources. *Geochimica et Cosmochimica Acta* **14**, 234-243.

Li, W.J., Ni, B.L., Jin, D.Q. and Zhang, Q.G. (1988) Measurement of the absolute abundance of O-17 in V-SMOW. *Kexue Tongbao* **33**, 1610-1613.

Lis, G., Wassenaar, L.I. and Hendry, M.J. (2008) High-precision laser spectroscopy D/H and $^{18}O/^{16}O$ measurements of microliter natural water samples. *Analytical Chemistry* **80**, 287-293.

Long, A., Eastoe, C.J., Kaufmann, R.S., Martin, J.G., Wirt, L. and Finley, J.B. (1993) High-precision measurement of chlorine stable isotope ratios. *Geochimica et Cosmochimica Acta* **57**, 2907-2912.

Luz, B. and Barkan, E. (2010) Variations of $^{17}O/^{16}O$ and $^{18}O/^{16}O$ in meteoric waters. *Geochimica et Cosmochimica Acta* **74**, 6276–6286.

Magenheim, A.J., Spivack, A.J., Volpe, C. and Ransom, B. (1994) Precise determination of stable chlorine isotopic ratios in low-concentration natural samples. *Geochimica et Cosmochimica Acta* **58**, 3117-3121.

Mariotti, A. (1983) Atmospheric nitrogen is a reliable standard for natural ^{15}N abundance measurements. *Nature* **303**, 685-687.

Matthews, D.E. and Hayes, J.M. (1978) Isotope-ratio-monitoring gas chromotagraphy-mass spectrometry. *Analytical Chemistry* **50**, 1465-1473.

McKinney, C.R., McCrea, J.M., Epstein, S., Allen, H.A. and Urey, H.A. (1950) Improvements in mass spectrometers for the measurement of small differences in isotope abundance ratios. *Review of Scientific Instruments* **21**, 724-730.

Michalski, G. and Bhattacharya, S.K. (2009) The role of symmetry in the mass independent isotope effect in ozone. *Proceedings of the National Academy of Sciences* **106**, 5493-5496.

Murphey, B.F. (1947) The Temperature Variation of the Thermal Diffusion Factors for Binary Mixtures of Hydrogen, Deuterium, and Helium. *Physical Review* **72**, 834-837.

Nier, A.O. (1940) A mass spectrometer for routine isotope abundance measurements. *Review of Scientific Instruments* **11**, 212-216.

Ono, S., Eigenbrode, J.L., Pavlov, A.A., Kharecha, P., Rumble, D., Kasting, J.F. and Freeman, K.H. (2003) New insights into Archean sulfur cycle from mass-independent sulfur isotope records from the Hamersley Basin, Australia. *Earth and Planetary Science Letters* **213**, 15-30.

Ono, S., Wang, D.T., Gruen, D.S., Sherwood Lollar, B., Zahniser, M.S., McManus, B.J. and Nelson, D.D. (2014) Measurement of a doubly substituted methane isotopologue, $^{13}CH_3D$, by tunable infrared laser direct absorption spectroscopy. *Analytical Chemistry* **86**, 6487-6494.

Pack, A. and Herwartz, D. (2014) The triple oxygen isotope composition of the Earth mantle and $\Delta^{17}O$ variations in terrestrial rocks. *Earth and Planetary Science Letters* **390**, 138-145.

Sakai, S., Matsuda, S., Hikida, T., Shimono, A., McManus, J.B., Zahniser, M., Nelson, D.D., Dettman, D.L., Yang, D. and Ohkouchi, N. (2017) High-Precision

Simultaneous $^{18}O/^{16}O$, $^{13}C/^{12}C$, and $^{17}O/^{16}O$ Analyses for Microgram Quantities of $CaCO_3$ by Tunable Infrared Laser Absorption Spectroscopy. *Analytical Chemistry* **89**, 11846-11852.

Santrock, J., Studley, S.A. and Hayes, J.M. (1985) Isotopic analyses based on the mass spectrum of carbon dioxide. *Analytical Chemistry* **57**, 1444-1448.

Sharp, Z.D. (2014) Stable Isotope Techniques for Gas Source Mass Spectrometry-15.16, in: McDonough, W.F. (Ed.), Treatise on Geochemistry. Elsevier, pp. 291-307.

Tse, R.S., Wong, S.C. and Yuen, C.P. (1980) Determination of deuterium/hydrogen ratios in natural waters by Fourier transform nuclear magnetic resonance spectrometry. *Analytical Chemistry* **52**, 2445-2445.

Wang, Z., Nelson, D.D., Dettman, D.L., McManus, J.B., Quade, J., Huntington, K.W., Schauer, A.J., Sakai, S., 2020. Rapid and Precise Analysis of Carbon Dioxide Clumped Isotopic Composition by Tunable Infrared Laser Differential Spectroscopy. *Analytical Chemistry* **92**, 2034-2042.

Xiao, Y.K., Yinming, Z., Qingzhong, W., Haizhen, W., Weiguo, L. and Eastoe, C.J. (2002) A secondary isotopic reference material of chlorine from selected seawater. *Chemical Geology* **182**, 655-661.

Zhang, Q.L., Chang, T.L. and Li, W.J. (1990) A calibrated measurement of the atomic-weight of carbon. *Chinese Science Bulletin* **35**, 290-296.

Chapter 3

EQUILIBRIUM ISOTOPE FRACTIONATION

Contents

3.1 Introduction 1
3.2 Theoretical determination of stable isotope fractionation factors 3
3.2.1 Free energy of reaction 3
3.2.2 The internal energy of a molecule 4
3.2.3 Vibrational Partition Function 5
3.2.4 Translational and Rotational Partition Function 7
3.2.5 The complete Partition Function Ratio 7
3.2.6 Extension to more complex molecules 8
3.2.7 'Empirical' theoretical methods 8
3.3 Relationship to temperature 9
3.4 Experimental determination of fractionation factors 10
3.4.1 Introduction 10
3.4.2 Mineral-water exchange reactions 11
3.4.3 Mineral-calcite exchange reactions 13
3.4.4 Mineral-CO_2 exchange reactions 13
3.4.5 The three-phase approach 14
3.5 Empirical determination of fractionation factors 14
3.6 Other factors controlling isotope partitioning 15
3.6.1 Pressure effect 15
3.6.2 Oxidation state 16
3.6.3 Composition 17
3.6.4 Salinity 18
3.6.4 Polymorphism 18
3.7 Multiple isotope system: The "Big Δ" notation 19
3.8 Distribution of isotopologues: Clumped Isotopes 22
References 24

Chapter 3

EQUILIBRIUM ISOTOPE FRACTIONATION

3.1 Introduction

We can classify isotope exchange reactions as either kinetic or equilibrium. Kinetic reactions are irreversible, and by definition, cannot be treated using the methods of classical thermodynamics. Evaporation of water into unsaturated air cannot be reversed; the isotopic fractionation that occurs during evaporation is a combination of equilibrium fractionation and that related to the different translational velocities of the isotopologues of water. The extent of processes such as evaporation and diffusion can be calculated for certain conditions, using kinetic-based theories. Other kinetic isotope effects, such as those associated with bacterial metabolism, are extremely complex, and mostly defy quantification (although qualitative models can be constructed). Products from bacterial reaction tend to be enriched in the light isotope, because the dissociation energies are lower and bonds are more easily broken. As the title of this chapter suggests, we will not consider kinetic-based reactions at this point, although discussions of kinetic effects are addressed at various places in this book. The remainder of this chapter is devoted to quantifying the fractionation associated with reversible, equilibrium processes. Chacko *et al.* (2001b) provide an excellent detailed overview of the subject and should be consulted for additional information.

Many processes involving isotope exchange can be modeled by classical equilibrium thermodynamics, because they are near-equilibrium phenomena. High temperature processes, such as crystallization, generally approach isotopic equilibrium, as do a number of low temperature processes, including precipitation of *some* carbonate, phosphate and silica phases in water. Equilibrium fractionation between two phases is based on the differences in bond strength of the different isotopes of an element. The heavier isotope will form a stronger bond, and will be concentrated in the phase with higher bond energy or 'stiffness'. Qualitative rules for equilibrium isotope fractionation are given by Schauble (2004):

1) Equilibrium fractionation between two phases generally decreases with increasing temperature, proportional to $1/T^2$.
2) The degree of fractionation is generally larger for elements whose mass ratio is large $\frac{m_{heavy} - m_{light}}{m_{heavy}\, m_{light}}$, where m_{heavy} and m_{light} are the heavy and light isotopes, respectively. Therefore, the isotopes of lighter elements generally show larger fractionation than those of heavier elements.
3) The heavy isotope is preferentially partitioned into the site with the stiffest bonds (strong and short chemical bonds). Bond stiffness increases qualitatively for
    a. high oxidation state, or high oxidation state in which the element is bonded,
    b. lighter elements
    c. covalent bonds

d. low coordination number.

From rule #1, fractionation varies regularly with temperature, which forms the basis for stable isotope thermometry. In order to have a *useful* isotope thermometer, we need to be able to measure the isotopic composition of the phases with the necessary precision, determine that they are indeed in isotopic equilibrium (often a daunting task), have a quantification of the fractionation as a function of temperature and have a mineral pair for which the fractionation changes significantly in response to temperature. In this chapter, we are concerned only with determining the fractionation factors. Quantification of fractionation factors has been made using three methods: 1) theoretical calculations based on statistical mechanics, 2) experimental determinations based on measured fractionations of phases equilibrated under known laboratory conditions, and 3) empirical calculations, based on measured fractionations of natural samples where independent temperature estimates can be obtained.

Each method of determining fractionation factors has benefits and limitations. Theoretical fractionation factors for simples gases have been calculated with a high degree of precision (Richet et al., 1977). At present, theoretical statistical mechanical calculations applied to complex minerals do not have the same precision as experimental determinations, although computational refinements continue to improve. A number of approximations must be made regarding the energy state of a phase because the quantum states of the individual molecules in solids and liquids do not behave independently from one another, and therefore approximate solutions to Schrödinger's equations cannot be used to calculate accurate fractionations (see Denbigh, 1971 for a general introduction). Also the magnitude of frequency shifts for the isotopically substituted molecule are not well known. However, the form of a theoretically-derived curves often allow for extrapolation of experimental fractionations beyond the temperature range of the experimental conditions. They may also be used for reactions that are difficult or impossible to duplicate in the laboratory, or have simply not-yet been done.

Experimental methods allow us to control most variables, such as temperature, reaction time, and chemical and isotopic composition. Experiments are difficult however, and many experiments are impractical, impeded by kinetic limitations. Empirical estimates take advantage of the fact that Nature provides us with very long-term experiments. A metamorphic rock heated to 500°C for 100 million years is an experiment that cannot be duplicated in the laboratory! At the same time, however, it is difficult to constrain temperatures very precisely in natural systems, and problems with isotopic inheritance and retrograde resetting always need be considered when empirical estimates are used. A nice website created by Georges Beaudoin and Pierre Therrien tabulates the results of a large number of published fractionations and allows for $1000 ln\alpha$ or temperatures to be estimated for any two phases. The site can be found at: http://www2.ggl.ulaval.ca/cgi-bin/alphadelta/alphadelta.cgi The reader should realize that this compilation does not assess the accuracy of each calibration and that it is appropriate to go back to the original sources to assess the reliability of relevant calibrations.

3.2 Theoretical determination of stable isotope fractionation factors

3.2.1 Free energy of reaction

Fractionation factors can be calculated using the methods of statistical mechanics. The basic principles are not complicated, but the mathematics are complex, and only the basic concepts are presented here. The reader is referred to the following articles for additional details (Denbigh, 1971; Richet et al., 1977; O'Neil, 1986; Criss, 1999; Chacko et al., 2001a; Schauble, 2004).

The fundamental concept of the equilibrium exchange reaction was introduced in Chapter 2, section 4. A typical reaction is of the form

$$aA_1 + bB_2 = aA_2 + bB_1 \qquad 3.1$$

where A_1 and A_2 are the two isotopologues of the molecule A, with similar notation for molecule B. An example would be exchange between CO and O_2, written as

$$C^{16}O + \tfrac{1}{2}{}^{18}O^{18}O = C^{18}O + \tfrac{1}{2}{}^{16}O^{16}O \qquad 3.2.$$

A_1 is $C^{16}O$, A_2 is $C^{18}O$, B_1 is $^{16}O^{16}O$, and B_2 is $^{18}O^{18}O$. Obviously the above reaction does not occur in nature as written. We do not have individual phases $C^{16}O$ and $C^{18}O$, instead only one inseparable, mixed $C^{18}O$ – $C^{16}O$ phase. The reaction does make sense from a thermodynamic standpoint, however, because it is possible to assign activities to each of the components $C^{16}O$, $C^{18}O$, $^{16}O^{16}O$, and $^{18}O^{18}O$ on the basis of concentrations. In this case, the equilibrium constant K is defined as

$$K = \frac{\prod (a_i)^{n_i}{}_{products}}{\prod (a_i)^{n_i}{}_{reactants}} = \frac{\left[a\left({}^{16}O^{16}O\right)\right]^{1/2} a(C^{18}O)}{\left[a\left({}^{18}O^{18}O\right)\right]^{1/2} a(C^{16}O)} \qquad 3.3,$$

and because the activity coefficients are close to 1, equation 3.3 can be simplified as

$$K = \frac{\left(\frac{{}^{18}O}{{}^{16}O}\right)_{CO}}{\left(\frac{{}^{18}O}{{}^{16}O}\right)_{O_2}} = \alpha_{CO-O_2} \qquad 3.4.$$

The equilibrium for exchange reaction 3.2 is given by

$$\Delta G^o_{r,T} = -RT\ln(K) \qquad 3.5.$$

At 300 K, α_{CO-O_2} is 1.028, so the free energy change for the reaction is -69 J (substituting α for K). Note that this energy change is miniscule compared to those

associated with chemical reactions. For the reaction ½O_2 + CO = CO_2, for example, the free energy change (@ 298 K) is –257,200 J.

3.2.2 The internal energy of a molecule

We can calculate the energy of a reaction by considering the total energy of each molecule in reaction 3.1, The total internal energy (E_{tot} or E_i) is the sum of all forms, including translational energy (E_{tr}), rotational energy (E_{rot}), vibrational energy (E_{vib}), electronic energy (E_{el}) and nuclear spin (E_{sp}). The last two terms are negligible, so the E_{tot} is given by

$$E_{tot} = E_{tr} + E_{rot} + E_{vib} \qquad 3.6.$$

At equilibrium, the ratio of molecules having energy E_i (energy at quantum state i) to those having zero point energy (discussed in following section) is given by

$$\frac{n_i}{n_0} = g_i e^{-E_i/kT} \qquad 3.7.$$

In equation 3.7, k is Boltzmann's constant (1.381×10^{-23}J/K or 0.6951 $cm^{-1}K^{-1}$), T is temperature in K and g is a statistical term to account for possible degeneracy, or different states. The sum over all possible quantum states i accessible to the system is defined as the partition function Q, given by

$$Q = \sum g_i e^{-E_i/kT} \qquad 3.8.$$

We can relate the partition function Q back to our equilibrium constant K (and ultimately our fractionation factor α) in equation 3.3 as

$$K = \frac{\prod (Q_i)^{n_i}{}_{products}}{\prod (Q_i)^{n_i}{}_{reactants}} = \frac{Q\left[C^{18}O\right]\left[Q(^{16}O^{16}O)\right]^{½}}{Q\left[C^{16}O\right]\left[Q(^{18}O^{18}O)\right]^{½}} \qquad 3.9.$$

The total partition function Q_{tot} can be split up into the partition functions relating to the different forms of energy, translation, vibration and rotation,

$$Q_{tot} = Q_{vib}Q_{rot}Q_{tr} \qquad 3.10.$$

The end result is that each of these components can be solved using quantum mechanics. The rotation and translation contributions for the different isotopologues are related only to mass difference. While the vibrational contribution to simple diatomic molecules is well known, the vibrations of atoms in complex multi-element compounds (especially solids and liquids) have contributions from interactions with multiple other atoms, and calculations become extremely complex. With accurate spectroscopic data, the fractionation between phases as a function of temperature can be computed. All that needs to be done is to compute the different components of the partition functions to determine our fractionation factors.

3.2.3 Vibrational Partition Function

We start by considering the potential energy of a diatomic molecule, such as H_2. As a first approximation, the energy can be approximated as a simple harmonic oscillator, illustrated by the harmonic potential curve in Fig. 3.1. The two atoms will have an average distance between each other so as to minimize the energy. That is, they will tend towards the energy well in Fig. 3.1. If we bring two H atoms from far apart towards one another, there is an attraction. If they are moved too close to one another, repulsive forces overwhelm the attractive forces, and the atoms are pushed apart. The average spacing is at the base of the energy well. The energy for a harmonic oscillator is then given by

$$E = (n + ½)h\nu \qquad 3.11$$

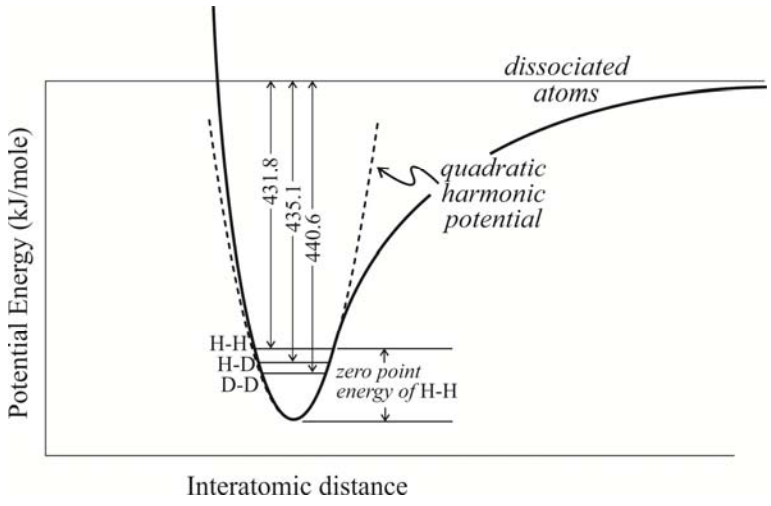

Fig. 3.1. Potential energy curve for diatomic hydrogen. Shown are the zero-point energies for the three isotopologues H-H, H-D, D-D. Note that D-D sits lower in the potential energy well than H-D or H-H and has a higher dissociation energy. The result is that the D-D bond is stronger than the H-H bond.

where n is the vibrational energy level (n = 0, 1, 2, etc.), h = Planck's constant (6.626×10^{-34} J·sec, ν = frequency (sec^{-1}). At low temperatures, n = 0, the ground vibrational state; at higher temperatures, higher energy levels are reached. But even at absolute zero, the vibrational energy is given by $E = ½h\nu$, and the atoms move[1]. This is the **zero point energy**, given by the difference between the bottom of the potential energy well and the energy at the ground vibration state. The difference in the zero-point energy of H-H and D-D illustrates the difference in their bond strengths. The amount of energy needed to dissociate a D-D molecule is larger than for an H-H molecule because the former resides lower in the potential well. More refined calculations of the vibrational energies take account of the deviation of the potential energy curve from the simple harmonic oscillator, but they will not be considered here.

For a diatomic molecule a-b, the frequency ν can be expressed by

[1] The atoms must move or they would violate the uncertainty principle, a fundamental law of quantum mechanics. If the atom had no motion, then we could tell exactly where it is and know its momentum, in violation of this law. . . something to do with a cat.

$$\nu = \frac{1}{2\pi}\sqrt{\frac{k_s}{\mu}} = \frac{1}{2\pi}\sqrt{k_s\left(\frac{1}{m_a}+\frac{1}{m_b}\right)} \qquad 3.12.$$

Here, k_s is the effective spring constant (related to stiffness), and μ is the reduced mass of molecule a-b ($\mu = \frac{1}{\frac{1}{m_1}+\frac{1}{m_2}} = \frac{m_1 m_2}{m_1+m_2}$). We can visualize this as two balls attached to either end of a rigid spring. They vibrate towards and away from each other with the frequency ν. When substituting the heavy isotope, the reduced mass changes, but the spring constant is unchanged. Imagining our two-ball model, the frequency is reduced due to substitution by the heavier mass – the balls vibrate more slowly. ν is related to the wave number ω by $\nu = \omega c$, where c is the speed of light (2.998×10^{10} cm/sec). Wave numbers are measured from spectroscopic data, or for our purposes, taken from published tabulations. For $^{12}C^{16}O$, $\omega = 2167.4$ cm^{-1}, and the spring constant (from 3.12 above) is easily calculated (see problem 5). The wave number for $^{12}C^{18}O$ is simply given by the relationship

$$\frac{\nu^*}{\nu} = \sqrt{\frac{\mu}{\mu^*}} \qquad 3.13$$

where the * refers to the isotopically substituted molecule. The frequency of $^{12}C^{18}O$ is calculated to be 2115.2 cm^{-1}.

If we consider the simple harmonic oscillator equation 3.8 becomes

$$Q_{vib} = \sum_i e^{-E_{vib}/kT} = \sum_{n=0}^{\infty} e^{-(n+1/2)h\nu/kT} \qquad 3.14.$$

Separating the terms, 3.14 is given by

$$Q_{vib} = e^{-U/2}\sum_{n=0}^{\infty} e^{-(n)U} \qquad 3.15$$

where $U = \frac{h\nu}{kT} = \frac{hc\varpi}{kT}$. The following approximation can be applied (Criss, 1999):

$$\sum_{n=0}^{\infty} x^n = \frac{1}{1-x} \quad (\text{for } 0 < x < 1) \qquad 3.16,$$

such that

$$Q_{vib} = e^{-U/2}\frac{1}{1-e^{-U}} \qquad 3.17.$$

The E_{vib} values for $C^{16}O$ and $C^{18}O$ are 2.1527×10^{-20} J/mole and 2.10084×10^{-20} J/mole (from Equation 3.11). The ratio Q_{vib} ($C^{18}O$)/ Q_{vib} ($C^{16}O$), called **the vibrational partition function ratio,** is 1.1343, which we will return to in equation 3.20.

3.2.4 Translational and Rotational Partition Function

The translational partition function ratio is dependent on a number of terms, but ultimately, the translational partition function ratio of a diatomic molecule with different masses simplifies to

$$\frac{Q_{2\,tr}}{Q_{1tr}} = \left(\frac{M_2}{M_1}\right)^{3/2} \qquad 3.18.$$

Here M_1 and M_2 are the molecular masses of the two molecules. Note that it is independent of temperature.

The rotational partition function is also a function of a number of terms which cancel out when we take the ratio of the two isotopically-substituted molecules. For a diatomic molecule, the rotational partition function ratio is given by

$$\frac{Q_{2rot}}{Q_{1rot}} = \frac{\sigma_1 I_2}{\sigma_2 I_1} \qquad 3.19,$$

where σ is the symmetry number, and I is the moment of inertia. For CO, where only one molecule is exchanged, σ =1. For O_2, where ^{18}O can occupy one of two sites, σ = 2. $I = \mu r^2$, where μ is the reduced mass, and r is the average interatomic distance.

3.2.5 The complete Partition Function Ratio

Combining all partition function ratios into one complete term gives

$$\frac{Q_2}{Q_1} = \left(\frac{M_2}{M_1}\right)^{3/2} \frac{\sigma_1 I_2}{\sigma_2 I_1}\frac{e^{-U^*/2}}{e^{-U/2}}\frac{1-e^{-U}}{1-e^{-U^*}} \qquad 3.20$$

(U^* is the isotopically substituted species). The above equation can be simplified using the Teller-Redlich spectroscopic theorem (see O'Neil, 1986, page 9) to give a final solution

$$\frac{Q_2}{Q_1} = \left(\frac{m_2}{m_1}\right)^{3/2} \frac{\sigma_1}{\sigma_2}\frac{\varpi_2}{\varpi_1}\frac{e^{-U^*/2}}{e^{-U/2}}\frac{1-e^{-U}}{1-e^{-U^*}} \qquad 3.21$$

Here, *m* is atomic mass, and this term will cancel out, as will the term σ_1/σ_2. For $C^{16}O$-$C^{18}O$, we have the following: $\omega_2/\omega_1 = 0.9759$, and $\frac{e^{-U^*/2}}{e^{-U/2}} = 1.134$, ($\frac{1-e^{-U}}{1-e^{-U^*}} = 1$) giving the total partition function ratio of 1.1069. A similar calculation for O_2 gives a partition function ratio of 1.08304. Partition function ratios can be divided by one another to give respective α values. The $\alpha_{CO\text{-}O2}$ is therefore 1.1069/1.08304 = 1.022 at 25 °C.

3.2.6 Extension to more complex molecules

Polyatomic gases, and solids can be treated in a similar manner to the above sets of equations, treating all possible modes of vibration in the summation terms. A number of assumptions and simplifications need to be made because the quantum states of molecules in liquids and solids (and high pressure gases) are not independent from each other. Extensions of the above models have been considered by a number of authors for relatively simple phases such as calcite, quartz, and UO_2 (e.g., Bottinga, 1968; Hattori and Halas, 1982). Kieffer (1982) made some simplifying assumptions and was able to predict relative isotopic enrichments of more complex minerals. The largest uncertainty in calculating partition function ratios for complex solids is estimating the frequency shifts for the isotopically-substituted molecule. Schauble (2004, and references therein) has predicted stable isotope fractionation for some elements other than those in the H-C-N-O-S system. Polyakov and Mineev (2000) used Mössbauer spectroscopy for estimating isotopic fractionation, and Driesner and Seward (2000) made simulations of salt effects on liquid-vapor partitioning.

3.2.7 'Empirical' theoretical methods

Several methods of determining fractionation factors have been developed that take advantage of the empirical relationship between bond strength and relative isotope enrichment (Schütze, 1980; Richter and Hoernes, 1988; Smyth, 1989; Zheng, 1993; Hoffbauer et al., 1994). These techniques are based on ordering minerals according to their increasing anionic bond strength. Smyth's method involved calculating electrostatic site potentials for anionic sites, a function related to the bond strength of the oxygen in different crystallographic locations. Variations on this method include consideration of the effects of cation site and coordination. These latter methods are called 'the increment method'. They require that the relative bond strength data be calibrated to some independently (experimentally or theoretically) determined oxygen isotope fractionation relationship and then the correlations are extended to the entire data set. The general enrichment obtained with this method is mostly consistent with experimental data, but there are a number of notable exceptions, such as an overemphasis of polymorphic substitution (e.g., Sharp, 1995). The major advantage of the technique is that it can be applied to almost any mineral, is 'internally consistent' and is easy to use. As a result, the increment method has been widely embraced. It should be pointed out, however, that these methods are not based on any known physical or chemical laws relating isotope fractionation to anionic bond strengths, and they should be used with caution, as their results sometimes are in serious disagreement with other calibrations.

Savin and Lee (1988) devised an empirical bond-type approach for determining fractionation factors for phyllosilicates, particularly clay-forming minerals. They assume

that oxygen in a given chemical bond has similar isotopic fractionation behavior regardless of the mineral in which it is located. Once fractionations are assigned to each bond type (*e.g.,* Si-O-Si, Al-O-Si, Al-OH, etc.), the fractionation for the entire mineral can be determined by summing the proportions of each bond. In general, the agreement between their method and experimental and empirical calibrations is good. In the case of low-temperature clay minerals, such methods are necessary, because experimental data are limited by the sluggish reaction rates of minerals in low-temperature range defining their stability field and the structures are too complex to treat using statistical mechanics.

3.3 Relationship to temperature

Bigeleisen and Mayer (1947) derived the following expression for partition function ratios:

$$\frac{Q_2}{Q_1} = 1 + \left(\frac{1}{2} + \frac{1}{U_2} + \frac{1}{e^{U_2} - 1} \right) \Delta U \qquad 3.22.$$

$U_i = \frac{hc\varpi_i}{kT}$, and ΔU is $U_1 - U_2$. If U is large, then $\frac{Q_2}{Q_1} \approx 1 + \frac{1}{2}\Delta U$. This would be the case when vibrational frequencies are high (such as reactions involving hydroxyl groups or water) or temperature are low. Under such conditions, $\frac{Q_2}{Q_1}$ is clearly proportional to $1/T$. When U is less than 5, the terms in parentheses approaches a value of U/12. In this case, $\frac{Q_2}{Q_1}$ will be proportional to $1/T^2$. At room temperature and above, for anhydrous minerals (where wave numbers are less than 1000 cm^{-1}), the $1/T^2$ relationship holds. As a result, the fractionation between phases m and n is defined as

$$1000 \ln \alpha_{m-n} = \frac{a \times 10^6}{T^2} + b \quad \text{(T in K)} \qquad 3.23$$

at high temperatures and

$$1000 \ln \alpha_{m-n} = \frac{a \times 10^6}{T} + b \quad \text{(T in K)} \qquad 3.24$$

at low temperatures, where a and b are constants. The temperature at which the crossover between 3.24 and 3.23 occurs is not known, but is probably below room temperature for most phases as discussed in section 3.2.7.

At infinite temperatures, the fractionation between any two phases approaches 0‰. Yet from equation 3.23, at $T = \infty$, $1000 ln\alpha = b$, which is clearly not correct. The b term cannot be constant over the complete temperature interval and must approach 0 at extremely high temperatures. Fractionation equations using both a $1/T^2$ and $1/T$ have been used (Zheng, 1993) as well as polynomials of $1/T^2$ such as (Clayton and Kieffer, 1991)

$$1000 \ln \alpha_{m-n} = a\left(\frac{10^6}{T^2}\right) + b\left(\frac{10^6}{T^2}\right)^2 + c\left(\frac{10^6}{T^2}\right)^3 \ldots \qquad 3.25.$$

Bottinga and Javoy (1973) argued that equation 3.23 applies to all rocks. The *b* constant is 0 for fractionation between anhydrous phases, phases for which the vibrational frequencies vary from 900 to 1200cm^{-1}. For water, the vibrational frequencies are far higher, ranging from ω_2 = 1647 to ω_3 = 3939 cm^{-1}. Fractionation between an anhyrous mineral and water will have a *b* term = 3.7[2]. Finally, for fractionation between anhydrous minerals and hydrous minerals, the *b* term is proportional to the number of OH bonds in the phase. Others have questioned the validity of this term when applied to solid-solid equilibria (e.g., Chacko et al., 1996).

3.4 Experimental determination of fractionation factors

3.4.1 Introduction

The first application of stable isotope thermometry was to the calcite-water system. McCrea (1950) synthesized calcite in water at room temperature and also estimated fractionation factors between calcite and water using statistical mechanical methods. Epstein *et al.* (1951; 1953) were able to determine the apparent equilibrium calcite-water fractionation at 29 and 31ºC by drilling small holes into living snails and bivalves (*Pinna* sp.). The organisms repaired their shells in an aquarium held at constant temperature where the $\delta^{18}O$ value of ambient water was held to a constant and known value. The newly-repaired material was removed and analyzed in order to determine the calcite-water fractionation at those specific temperatures (see section 6.3 for a more detailed discussion of carbonate-water fractionation).

More commonly, experiments are made by synthesizing or equilibrating two phases at high temperatures. O'Neil *et al*. (1969) expanded on McCrea's earlier work, both by synthesizing calcite at room temperature conditions and by equilibrating calcite and water at high temperatures in hydrothermal bombs. Their results agreed with the earlier low-temperature calibration of Epstein's earlier work using shells.

All high-temperature experiments are made by isotopically equilibrating two phases. There are several issues that must be overcome for a successful calibration:

1) Isotopic equilibrium must be achieved, or at least a quantification of the degree of equilibration must be known.
2) The phases must be separable for isotopic analysis. Fine grained intergrowths of two silicate minerals may be inseparable for traditional bulk analysis and therefore not amenable to the experimental technique.

The first of these concerns is met by employing one of several strategies. Commonly, starting materials are extremely fine-grained. Many experimental papers describe 'floating the minerals on acetone' which results in micron-size particles. During the subsequent heating experiment, grains recrystallize and grow. During this process,

[2] The value of 3.7 was determined from averaging data from experimental studies. See original paper for details.

oxygen exchange occurs as a result of the bond breaking and reforming. Other strategies include using metastable starting materials (such as silica gel which recrystallizes to quartz during prolonged heating) or equilibrating a mineral in a fluid that is not in chemical equilibrium with the starting material. For example, O'Neil and Taylor (1967) reacted sodium feldspars with a KCl solution. In the course of the analysis, the cations exchanged so that by the end of the reaction, the sodium feldspar had been converted to potassium feldspar. The high free energy of the cation exchange reaction was found to drive oxygen bond breaking so that oxygen isotope equilibration between the fluid and mineral would occur.

The use of fine-grained starting materials leads to the second problem. If the run products consist of intimately intergrown minerals, separation for bulk isotope analysis can be virtually impossible. Partly for this reason, most exchange experiments have been made with water or more rarely CO_2 gas, so that there is only one solid phase. Clayton *et al.* (1989) developed a calcite-mineral exchange technique, where at high pressure and temperature, recrystallization led to a high degree of oxygen isotope exchange. The calcite could then be easily separated from the silicate by reaction with phosphoric acid – the typical method for analyzing carbonates. Oftentimes, an experimental calibration may not be of geological interest – for example albitie-CO_2 gas fractionations – but the combination of two experiments can give a third fractionation that is geologically relevant. Consider the following example. Experimental fractionation factors have been measured for quartz-water and muscovite-water. Combining the results of these experiments gives the important quartz-muscovite equation, a widely-used isotope thermometer. Quite simply, the *a* and *b* terms can be subtracted from one another to eliminate the intermediate phase:

$$\begin{array}{lrcl} \text{If} & 1000\ln\alpha_{(\text{qz-water})} & = & 4.10\times10^6/T^2 - 3.70 \\ \text{and} & \underline{1000\ln\alpha_{(\text{musc-water})}} & = & \underline{1.90\times10^6/T^2 - 3.10}, \\ \text{then} & 1000\ln\alpha_{(\text{qz-musc})} & = & 2.20\times10^6/T^2 - \ \ 0.6. \end{array}$$

The choice of exchange medium (water, calcite, CO_2) is determined on the basis of a number of factors. Each has advantages and disadvantages as discussed below.

3.4.2 Mineral-water exchange reactions

Most early exchange experiments were made for mineral-water pairs. 10 to 20 mg. of a finely-ground solid, and ~200 mg. of water are sealed in a noble-metal tube and heated to reaction temperature at a confining pressure of 1-2 kbar[3]. The experiments are relatively easy to perform, reaction rates are moderately rapid, and the initial isotopic composition of the water starting material can be varied.

In order to test for equilibrium, mineral-water exchange reactions are made by starting with waters that have δ values both higher and lower than the presumed equilibrium value. In this way, the equilibrium fractionation is approached from both directions (Fig. 3.2). Because the rates of reaction are independent of the direction of

[3] Some experiments have been made in piston-cylinder apparatus at much higher pressures, with smaller sample charges. Although more difficult, exchange rates are generally enhanced (Matthews et al., 1983), and certain mineral stability fields may be extended to higher temperatures at high pressures.

approach, the results can be extrapolated to infinite time to find the exact equilibrium value[4].

In theory, experiments need be made only at a single temperature. From equation 3.23, the a constant can be determined (assuming b = 3.7) and extended over the entire temperature range. In practice, experiments are made at a series of temperatures, and the best-fit line through the data are used to calculate both a and b (Fig. 3.3).

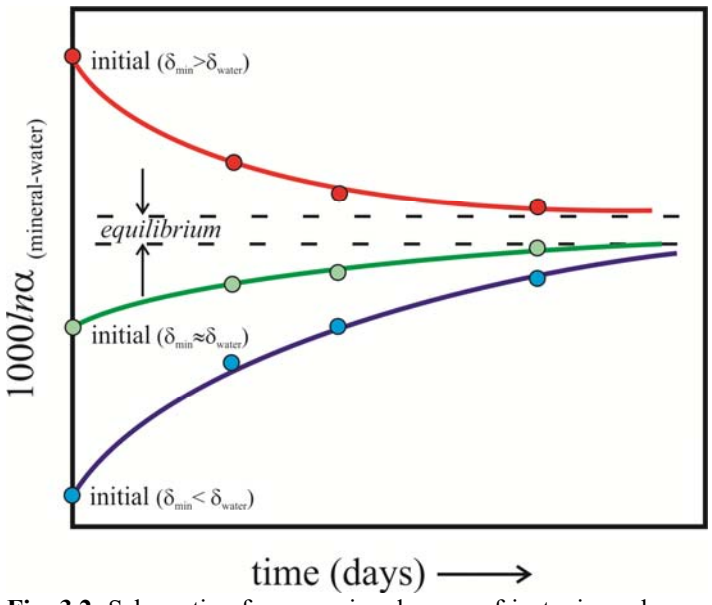

Fig. 3.2. Schematic of progressive degrees of isotopic exchange between a mineral and water as a function of time. Experiments are made with waters of different initial isotopic compositions. Multiple capsules can be put into a high P-T charge together and the different experiments all approach a single 1000$ln\alpha$ value with increasing time.

There are several important considerations regarding the mineral-water experimental method. First, there are both low and high temperature limits on exchange experiments. If the temperatures are too low, reaction kinetics are too sluggish and little exchange occurs. If the reactions are run at temperatures that are very high, then significant dissolution of the solid (*e.g.*, quartz) will occur into the fluid phase. During subsequent quench, the dissolved phase will rapidly precipitate, causing disequilibrium. The dissolved species may even have a different fractionation with water than the equivalent crystal. At very high temperatures, fractionations between the mineral and water become very small, so that the uncertainties in the measurements become an important problem. The general solution is to run the fractionation experiments over a range of temperatures and fit the data to the appropriate equations (Fig. 3.3). Nevertheless, as numerous authors have discussed, it is impossible to know if the recrystallization-based exchange is actually being driven towards the equilibrium value. Recrystallization is the thermodynamic driving force in these hydrothermal exchange experiments and it is not clear that isotopic equilibrium follows the recrystallization.

[4] See Northrop and Clayton (1966) and O'Neil (1986) for the mathematical treatment of this approach.

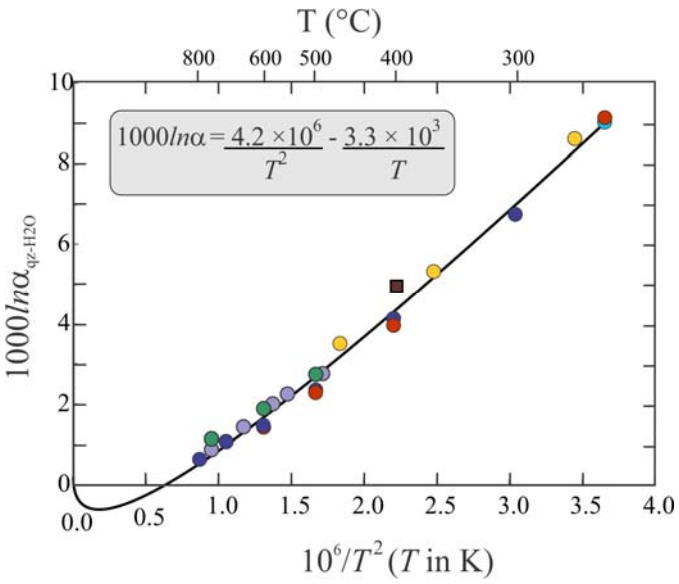

Fig. 3.3. Best fit line of equation $1000 \ln \alpha = a/T^2 + b/T$ to published quartz-water exchange experiment data. The studies were made using different techniques and yet still give similar results. The negative $1/T$ term results in a best-fit that has a reversal in the $1000lnT$ value at high temperatures, a result that is consistent with many mineral-water fractionation studies. The square symbol is a combination of CO_2-silica and CO_2-H_2O fractionations. Modified from (Sharp et al., 2016).

3.4.3 Mineral-calcite exchange reactions

Clayton *et al.* (1989) developed a new method for high pressure exchange experiments using calcite as the exchange medium. Starting materials were finely admixed calcite and mineral. During the course of the experiment, recrystallization occurred and there was presumably an approach towards isotopic equilibrium. The novel method, which has since been employed for a number of minerals, has two striking advantages over earlier experiments, but several potential problems as well.

The main advantage, of course, is that water is eliminated as a reactant. This removes the complication from the high O-H stretching frequencies characteristic of water, and the *b* term in equation 3.23 reduces to 0. Also dissolution in aqueous solutions and recrystallization during quench are eliminated.

There are several drawbacks to this method as well. It is clear that at all but the highest temperatures, isotopic equilibration occurs only because the solids undergo recrystallization. Like the mineral-water experiments, the driving force towards equilibrium is recrystallization, and there is no way to know if the changes in stable isotope ratios are trending towards the equilibrium values or are controlled by kinetically based recrystallization. A second limitation is that exchange rates are far slower than for the mineral-water system. This raises the lower-limits on the temperatures at which significant exchange occurs, and hence reduces the possible temperature range of calibration.

3.4.4 Mineral-CO_2 exchange reactions

The idea of measuring the fractionation between a solid and CO_2 gas was pioneered by O'Neil and Epstein (1966) and resurrected over two decades later (Chacko et al., 1991; Stolper and Epstein, 1991). Mineral-CO_2 exchange has the distinct advantage over other experimental methods in that, except at high very high temperatures and pressure (Chacko et al., 1991), no recrystallization of the solid phases occurs during the reaction. Exchange should be purely diffusional in nature, and therefore tend towards equilibrium. The experimental setup is simple as well. Finely powdered samples are

loaded in silica or metal tubes, CO_2 is introduced and the tube is sealed. After heating, the $\delta^{18}O$ value of the CO_2 is measured, which should be in equilibrium with the solid phase. Combining the experimental CO_2-silica (Stolper and Epstein, 1991) and theoretical CO_2-H_2O (Richet et al., 1977) fractionations gives a silica-water fractionation only slightly higher than the quartz-H_2O fractionations (Fig. 3.3).

The major limitation of this type of experiment is that exchange is very slow. Only phases that have very high oxygen diffusion rates, such as carbonates, albite, and silica glass, are accessible to this approach.

3.4.5 The three-phase approach

Several studies have used both calcite and water ($\pm CO_2$) as the exchange medium (Zheng et al., 1994b; Hu and Clayton, 2003). With judicious proportions of H_2O and CO_2, exchange experiments for mineral phases that would otherwise be unstable (e.g., hydrous phases, Zheng et al., 1994a) can be made. The presence of water also enhances reaction rates between the mineral and carbonate.

3.5 Empirical determination of fractionation factors

Empirical determinations are made by measuring the fractionation between two natural phases with temperatures either measured (for modern samples) or calculated (for example, when using metamorphic rocks). Some of the most successful, low temperature calibrations have been made using empirical calibrations, notably the calcite-water (Epstein et al., 1953), phosphate-water (Longinelli and Nuti, 1973), and silica-water (Leclerc and Labeyrie, 1987) systems. The isotopic composition of shells (or diatoms for silica) and coexisting water were measured, and then compared to measured temperatures of growth. The original (calcite, phosphate, silica) - water equations have withstood the test of time with very little modification.

Other low temperature equations have been made for clay minerals, where temperatures of formation are estimated from the depositional environment. Savin and Epstein (1970) estimated the oxygen and hydrogen isotope fractionation for kaolinite-water, montmorillonite-water and glauconite-water at low temperature. Other low temperature examples include gibbsite (Bird et al., 1994), and silica (Leclerc and Labeyrie, 1987). These empirical studies are particularly successful because exchange experiments are virtually impossible at room temperature; the only experimental avenue to low temperature exchange is mineral synthesis.

Modern empirical estimates have also been made at higher temperatures, often taking advantage of unique and unusual conditions. Amorphous silica-water fractionation was determined from deposits of thermal waters from power plants (Kita et al., 1985) and quartz-water, calcite-water and adularia-water fractionations were measured from the Broadlands geothermal field, New Zealand in drill cores where water could be samples and temperatures measured (Blattner, 1975).

Finally, fractionation factors have been made from minerals in metamorphic or igneous rocks where independent temperature estimates are available. In some cases, empirical estimates are the only option available to the isotope geochemist. For certain

'refractory' phases[5], the experimental approach is limited due to extremely sluggish reaction rates, so that empirical estimates are our only option. A good example is for the quartz-aluminum silicate system, where empirical estimates have been applied to a number of metamorphic terranes (Sharp, 1995). The effect of complex chemical substitutions can also be estimated from natural assemblages (Taylor and O'Neil, 1977; Kohn and Valley, 1998), bypassing the huge effort that would be required to make such measurements experimentally. In all cases, multiple samples from multiple localities should be analyzed to avoid any problems that might inadvertently exist within a single, potentially 'anomalous' site. Consider the case of trying to determine the equilibrium fractionation between orthopyroxene and clinopyroxene from mantle xenoliths. The minerals equilibrated at high temperatures, over an inordinately long time period, and cooled rapidly following eruption. A perfect natural laboratory. And yet we find that in some xenoliths, the clinopyroxene has a higher $\delta^{18}O$ value than coexisting orthopyroxene, and in other samples it is reversed (Perkins et al., 2004). Clearly empirical estimates should not be made by analyzing a single rock, with the thought that the results are universally applicable.

There are a number of advantages to making empirical estimates. First and foremost, the amount of time that a mineral has had to reach equilibrium with its surrounding far exceeds anything that could be accomplished in the laboratory. A metamorphic rock heated to 500°C for millions of years provides a nice contrast to the same system heated to 900°C in the laboratory for a period of hours or days. Also, many of the potential pitfalls inherent in experimental studies, such as quench recrystallization, metastable equilibria, and difficulty of separating fine-grained materials can be avoided by measuring natural materials.

As with all calibration methods, numerous concerns exist as well. The most serious of these are 1) knowing the precise temperature at which equilibrium was attained, 2) that the minerals of interest were indeed in equilibrium and did not 'inherit' their isotopic composition from an earlier metamorphic event and 3) insuring that no retrograde exchange occurred during cooling. This is particularly a concern for slowly-cooled metamorphic rocks, where some diffusional resetting is expected. The problem is illustrated when considering the $\Delta^{18}O$ (quartz-feldspar) values commonly measured in igneous rocks (Chapter 11). Fractionations commonly range from 1.5 to 2.5‰, corresponding to temperatures of 430-640°C, clearly lower than the crystallization temperature of the granite, indicating that post-crystallization isotopic exchange occurred.

3.6 Other factors controlling isotope partitioning

3.6.1 Pressure effect

The effect of pressure on the equilibrium constant is given by

$$\left(\frac{\partial \ln K}{\partial P}\right)_T = -\frac{\Delta V_R}{RT} \qquad 3.26,$$

[5] Minerals fitting into this category include kyanite, garnet, zircon, corundum, and staurolite for oxygen and certainly diamond and graphite for carbon.

where ΔV_R is the volume change of the reaction. For an isotope exchange reaction such as Equation 3.1, the ΔV_R term is close to zero, so that pressure will have a minimal effect on the fractionation between coexisting species. Hoering (1961) first demonstrated the insensitivity of fractionation to pressure when he measured the $^{16}O/^{18}O$ fractionation between and H_2O and HCO_3^- at 1 atmosphere and at 4 kilobars (both at 43.5°C). There was a change of 0.2 (± 0.2) ‰ fractionation between 4 kb and 1 atm, which he concluded was negligible. Later, calcite-water and quartz-water exchange experiments were made over a pressure range of 1 to 20 kbar, with no detectable pressure effect (Clayton et al., 1975; Matthews et al., 1983). Polyakov and Kharlashina (1994) devised a statistical mechanical method of estimating pressure effects. For most rocks exposed at the Earth's surface, the pressure effect will be near the detection limits of analysis. At very high pressures, however, the effects can be significant. Using the Polyakov and Kharlashina method, Sharp *et al.* (1992) found that quartz is particularly sensitive to pressure. For most minerals, the electrostatic site potentials increase slightly with pressure, but the reverse is found for quartz. As a result, $\Delta^{18}O_{qz\text{-}min}$ values will change by ~0.5 ‰ at 1200°C and 40 kbar. Fortunately, the unusual behavior of quartz becomes redundant because coesite is the stable SiO_2 polymorph above ~27 kbar.

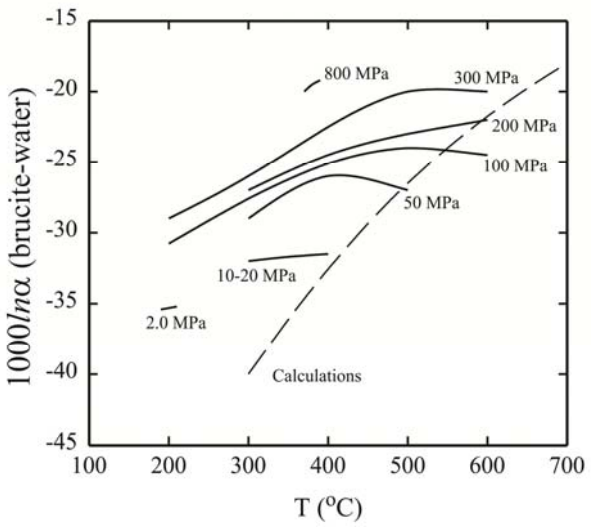

Fig. 3.4. Hydrogen isotope fractionation between brucite and water as a function of temperature for various pressures. The dashed line labeled 'Calculations' is the theoretical fractionation between brucite and water at 1 bar, based on statistical mechanical calculations. With increasing pressures there is an increase in brucite-water fractionations; the effect decreases with increasing temperature. From (Horita et al., 2002). Used with permission.

The effect of pressure is larger for graphite-diamond (Polyakov and Kharlashina, 1994). But the really striking pressure effects are seen for D/H fractionation between hydrous minerals and water. Fig. 3.4 shows the effect of pressure on the brucite-water fractionation as a function of pressure and temperature. In their combined experimental-theoretical study, Horita *et al.* (2002) conclude that water is much more strongly affected than hydrous minerals, so that hydrogen isotope fractionation pressure effects should exist for all water - hydrous mineral pairs.

3.6.2 Oxidation state

The largest effect on fractionation is oxidation state. The $1000ln\alpha$ value (at 20°C) for carbon in the C^{4+} (CO_2) *vs* C^{4-} (CH_4), for sulfur in the S^{6+} (SO_3) *vs* S^{2-} (H_2S) and for chlorine in the Cl^{7+} (ClO_4^-) *vs* Cl^- are all around 70‰. This explains why biological redox reactions have such large isotopic fractionations as evidenced by reduction of sulfate to sulfide and CO_2 to methane. The theoretical fractionations for hydrogen far outweigh any

other element. The calculated $1000 ln\alpha$ value for H_2O and H_2 at 20°C is over 1000‰ (Richet et al., 1977).

Oxygen has one oxidation state and so is not affected by the redox changes that occur in most of the other elements used for stable isotope studies. The heavy isotope of oxygen will be preferentially fractionated into short, strong chemical bonds (such as Si^{4+}) generally with a high oxidation state. Note however that uraninite ($U^{4+}O_2$) strongly incorporates ^{16}O relative to quartz, so that oxidation state alone does not always correlate with oxygen isotope enrichment.

3.6.3 Composition

Taylor and Epstein (1962) devised a simple relationship between composition and isotopic enrichment, recognizing that bond strength – and oxygen isotope enrichment – decrease from Si-O bonds through Al-O to M^{2+}-O = M^{1+}-O bonds. Minerals follow this rule quite well and it should be kept in mind as a qualitative guide to oxygen isotope enrichment in rocks. Quartz almost always has the highest $\delta^{18}O$ value, followed by feldspar and continuing down to the Si- and Al-free oxides such as magnetite, rutile and hematite. Rough estimates of relative isotopic enrichment are easily made by keeping this rule in mind. Consider olivine and clinopyroxene. Which one will concentrate ^{18}O relative to the other? Mg_2SiO_4 has a lower proportion of Si-O bonds than $MgSiO_3$ (or $CaMgSi_2O_6$), and consequently a lower $\delta^{18}O$ value. In general, substitution of identically-charged cations (*e.g.,* Na ⇔ K, Fe ⇔ Mg, Ca ⇔ Mn) has a minimal effect on isotopic fractionation[6]. There is no oxygen isotope fractionation between albite and potassium feldspar ($NaAlSi_3O_8$ vs. $KAlSi_3O_8$), nor between almandine and pyrope ($Fe_3Al_2Si_3O_{12}$ vs. $Mg_3Al_2Si_3O_{12}$), and only a small effect of Ca ⇔ (Mg, Fe) substitution.

A much larger fractionation exists for coupled substitutions, such as NaSi ⇔ CaAl in plagioclase ($NaAlSi_3O_8$ ⇔ $CaAl_2Si_2O_8$), and NaAl ⇔ Ca(Mg,Fe) in pyroxene ($NaAlSi_2O_6$ ⇔ $CaMgSi_2O_6$). The temperature coefficient of fractionation (*a* term in equation 3.23) is 0.94 for quartz-albite, increasing by 1.05*x* (*x* = fraction of anorthite in plagioclase) up to 1.99 for pure anorthite. Other substitutions that affect isotopic fractionation are F ⇔ OH in phlogopite and Al^{3+} ⇔ Fe^{3+} in garnet. See Chacko *et al* (2001a) for more details.

The effect of composition on hydrogen isotope fractionation has not been thoroughly studied, but in a seminal paper on the subject, Suzuoki and Epstein (1976) found that Al has the strongest affinity for deuterium, followed by Mg and Fe. They proposed a general equation to predict hydrogen isotope exchange between hydrous minerals and water given by[7]

$$1000 \ln \alpha_{\text{mineral}-H_2O} = \frac{-22.4\times10^6}{T^2} + 26.3 + \left(2X_{Al} - 4X_{Mg} - 68X_{Fe}\right) \qquad 3.27,$$

[6] Note that Fe has a strong effect of H isotope fractionation (see equation 3.27).

[7] Equation 3.26 contained a printing error in the original publication. The constant 26.3 was originally given as 28.2 (Morikiyo, 1986).

where X refers to the portion of each element in the octahedral site. The above equation generally predicts the correct degree of enrichment, but not necessarily the correct temperature dependence (Chacko et al., 2001a).

3.6.4 Salinity

There is a great deal of confusion about the effect of salinity on the isotope fractionation between water and coexisting phases. Many authors refer to 'the salinity effect' when discussing the carbonate-water paleothermometer. Unfortunately, many practitioners mistakenly assume that the addition of dissolved cations changes the oxygen isotope fractionation between calcite and water. The 'salinity effect', as discussed in Chapter 6, is actually related to the loose correlation between salinity and the degree of freshwater contamination (and hence lowering of the $\delta^{18}O$ value) in the ocean.

The actual effects of salinity are variable both for different dissolved salts and as a function of temperature. The fractionation between a salt solution and pure water varies linearly with molality and has a large positive value for salts with a high degree of 'structure making' electrolytes, and a negative fractionation for salts with 'structure-breaking' electrolytes (O'Neil and Truesdell, 1991), roughly correlating to cation charge (Fig. 3.5). Importantly, the effect of salinity (mostly related to dissolved NaCl) on the ocean has a completely negligible effect on the equilibrium fractionation between H_2O and authigenic minerals (*e.g.*, calcite). For all but concentrated $(Ca,Mg)Cl_2$ and $MgSO_4$ solutions, however, the effects for both hydrogen and oxygen can be ignored at low temperature. At temperatures above 200°C, a concentrated NaCl solution is enriched in the heavy isotope relative to pure water (Driesner and Seward, 2000). Studies of salt effects are extremely useful in understanding the solvation of dissolved cations in aqueous solutions. An elegant set of experiments on hydrogen and oxygen isotope salt effects was made in a series of papers by Horita *et al.* (Horita et al., 1993a; Horita et al., 1993b; Horita et al., 1995) and should be consulted for further information.

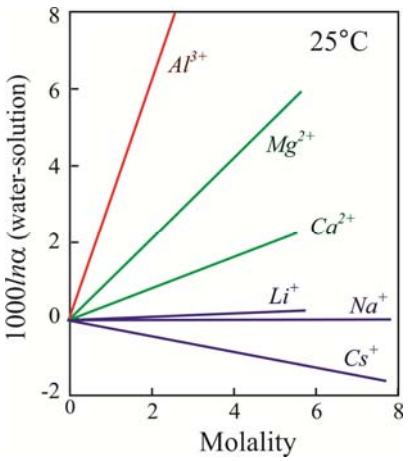

Fig. 3.5. The fractionation of dissolved salt solutions relative to pure water. Modified from (O'Neil and Truesdell, 1991)

3.6.4 Polymorphism

The effect of polymorphism generally has a 'second-order' effect on fractionation. unimportant for the most part. For example, no oxygen isotope fractionations have been seen between the different aluminum silicate polymorphs andalusite, kyanite, and sillimanite, where coexisting polymorphs are found to have nearly identical $\delta^{18}O$ values (Cavosie et al., 2002; Larson and Sharp, 2003). There are several notable exceptions, where a polymorphic transition has a significant isotope effect, including graphite-diamond (Bottinga, 1969), calcite-aragonite (oxygen, Rubinson and Clayton, 1969), and perhaps quartz and coesite. For most polymorphic transitions, the effects are negligible.

3.7 Multiple isotope system: The "Big Δ" notation

Oxygen and sulfur have three and four stable isotopes, respectively. Many of the non-traditional isotope systems also have multiple isotopes (Sn has the record with 10!). The early practitioners of stable isotope geochemistry recognized that there were fundamental mass dependent fractionation processes that appeared to make measurements of the rare isotopes redundant. For example, Craig (1957) noted the following relationship between $^{17}O/^{16}O$ and $^{18}O/^{16}O$:

$$\left(\frac{R^{18}_{sample}}{R^{18}_{standard}}\right)^{\lambda} = \left(\frac{R^{17}_{sample}}{R^{17}_{standard}}\right) \qquad 3.28,$$

where R^x = is the $^xO/^{16}O$ ratio and λ (for oxygen) is close to 1/2. This means that the $\delta^{17}O$ value is related to the $\delta^{18}O$ value of a sample that can be approximated by $\delta^{17}O \approx ½\ \delta^{18}O$. As a result, there was no need to measure the isotopic abundances of all three isotopes because the $\delta^{17}O$ and $\delta^{18}O$ values of Terrestrial materials plot on a straight line with a slope that is close to 0.5 (Fig. 3.6), and is called the Terrestrial Fractionation Line (TFL).

The close fit to the Terrestrial Fractionation Line is observed for most Earth-sourced materials. Extraterrestrial samples (Chapter 13) and terrestrial samples that have undergone photochemical reactions (Farquhar and Wing, 2003; Thiemens, 2006) often lie off of the TFL. The vertical displacement in per mil units from the TFL is the is the $\Delta^{17}O$ value[8], discussed below (see also Chapter 13).

When recast in a linear format (see Text box 3.1), the relationship between the $\delta'^{18}O$ and $\delta'^{17}O$ (or $\delta'^{34}S$ and $\delta'^{33}S$) of a set of data can be fit with a straight line of the form

$$\delta'^{17}O = \lambda \cdot \delta'^{18}O + \gamma \qquad 3.29.$$

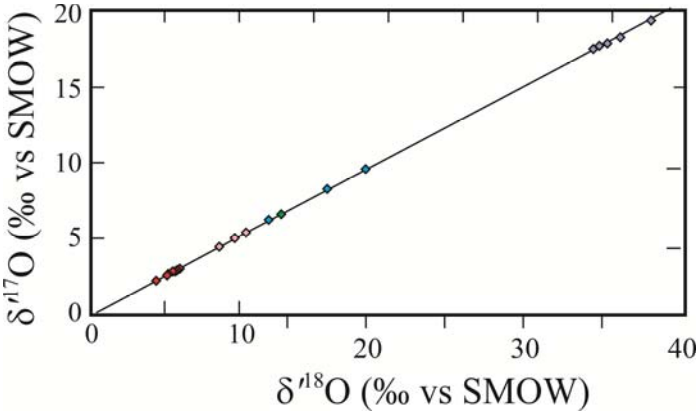

Fig. 3.6. Plot of the $\delta'^{17}O$ *vs.* $\delta'^{18}O$ values of assorted minerals from rocks of low and high temperatures. The data fall on a straight line, termed the Terrestrial Fractionation Line (TFL) with a slope = λ ≈ 0.525. Data from Pack and Herwartz (2014).

The λ term is the slope of the chosen or best-fit line and the γ is the *y* intercept. (Note that the γ term will be equal to 0 if the best fit crosses the origin at $\delta^{18}O = \delta^{17}O = 0$). Fig. 3.6 shows the results of a number of rock samples. A λ slope of 0.524 to 0.526 is obtained for most Earth materials (Miller, 2002; Rumble et al., 2007) with a *y* intercept (γ) assumed to be 0. In fact, careful analyses of terrestrial materials shows that the best fit actually has a *y* intercept that is slightly different from 0 (Pack and Herwartz, 2014; Sharp et al., 2016).

[8] In spoken English, one refers to this $\Delta^{17}O$ as 'Big delta' or 'Cap delta', where the 'big' and 'cap' indicate a capital δ, which is a Δ.

The choice of λ is somewhat arbitrary, determined by a best fit to the data set. For rocks, the best fit results in a slope of approximately 0.525 and for meteoric water samples, the best fit results in a λ value of 0.528 (Luz and Barkan, 2010). The reason that there is no single 'correct value' for λ is that there are a number of processes that affect the triple oxygen isotope fractionation (Matsuhisa et al., 1978), and hence the relationship between $\delta^{17}O$ and $\delta^{18}O$. There is no one 'correct answer' because there is no single process that determines the slope.

Text box 3.1: Linearization of isotope data.
Isotope data for multiple isotope systems are commonly linearized, where the δ value is redefined in a logarithmic form and is symbolized by δ′ (pronounced 'delta prime') in place of δ. The linearization changes the δ values only slightly and because the delta prime values follow the relationship given by equation 3.28, linearized data will plot in a linear array in $\delta'^{17}O$ - $\delta'^{18}O$ space. Hulston and Thode (1965) first proposed this linearization given by

$$\delta' = 1000 \times ln(R_{sa}/R_{std}) \qquad 3B1.1$$

which, in δ notation becomes (Miller, 2002)

$$\delta' = 1000 \times ln(\delta/1000 + 1) \qquad 3B1.2.$$

Whereas $1000ln\alpha_{A\text{-}B} \approx \delta_A - \delta_B$ (equation 2.17), in a linearized format

$$1000ln\alpha_{A\text{-}B} = \delta'_A - \delta'_B \qquad 3B1.3.$$

Under equilibrium conditions, the λ is replaced by θ to indicate that the fractionation between any two phases follows well established thermodynamic rules. In some cases the θ is also used for *reproducible* kinetic isotope fractionations (Barkan and Luz, 2007). For an equilibrium fractionation between two phases A and B with the three isotopes 1, 2, and 3, θ_{A-B} is given by

$$\theta_{A-B} = \frac{\ln \alpha_{3/1}}{\ln \alpha_{2/1}} \qquad 3.30,$$

where α_3 is the fractionation between the isotopes 3 and 1 (Young et al., 2002). For the triple oxygen isotope system, the equilibrium value of θ for fractionation between quartz and water is

$$\theta_{(SiO_2-H_2O)} = \frac{\ln \alpha_{(17_O)}}{\ln \alpha_{(18_O)}} = \frac{\left(\delta'^{17}O_{qz} - \delta'^{17}O_{H_2O}\right)}{\left(\delta'^{18}O_{qz} - \delta'^{18}O_{H_2O}\right)} \qquad 3.31.$$

Graphically, the θ value is simply the slope of the line given by the fractionation between the two phases quartz and water (Fig. 3.7).

The equations governing θ are discussed in detail by Young *et al.* (2002). At infinite temperatures, the θ value for the triple oxygen isotope system is given by

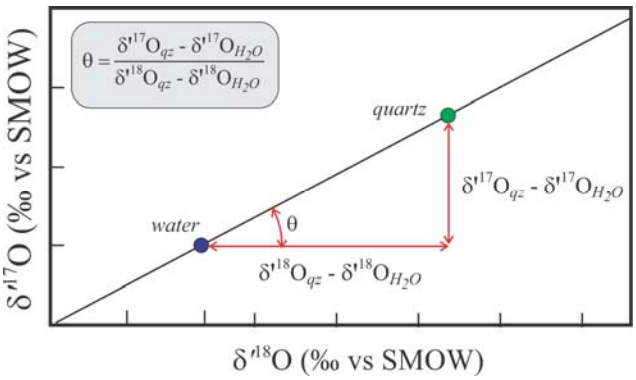

Fig. 3.7. Graphical representation of θ. For two phases in isotopic equilibrium, the triple isotope fraction is given by equation 3.31. Graphically, it is equal to the slope defined by the isotopic compositions of the two phases.

$$\theta = \frac{\left(\frac{1}{m^{17}O - m^{16}O}\right)}{\left(\frac{1}{m^{18}O - m^{16}O}\right)} = 0.5305 \qquad 3.32,$$

where $m^{16}O$ is the mass of ^{16}O, etc. (For the three isotopes ^{32}S, ^{33}S, ^{34}S, the θ value (at infinite temperatures) is 0.5159). With decreasing temperatures, the value of θ decreases, so that at 0°C, the θ oxygen value for quartz-water fractionation is 0.524 (Cao and Liu, 2011; Sharp et al., 2016). In kinetic fractionation processes, the θ value can be as low as 0.5.

Because θ varies with temperature and also according to the type of fractionation that has occurred (kinetic *vs.* equilibrium), the combined $\delta'^{17}O$ and $\delta'^{18}O$ values of a particular sample may plot slightly off the 'best fit' line for an assumed λ value. These deviations are referred to as $\Delta^{17}O$ values (or $\Delta'^{17}O$ values in a linearized format) given by the following equation (Fig. 3.8)

$$\Delta'^{17}O = \delta'^{17}O - \lambda \times \delta'^{18}O - \gamma \qquad 3.33,$$

and more commonly

$$\Delta'^{17}O = \delta'^{17}O - \lambda \times \delta'^{18}O \qquad 3.34$$

when $\gamma = 0$. Although the $\Delta^{17}O$ value will change for different assumed values of λ, the interpretations based on the $\Delta^{17}O$ values will not (see Sharp et al., 2016, Appendix A). The temperature dependent variations of θ have been used as a 'single mineral thermometer' (Sharp et al., 2016).

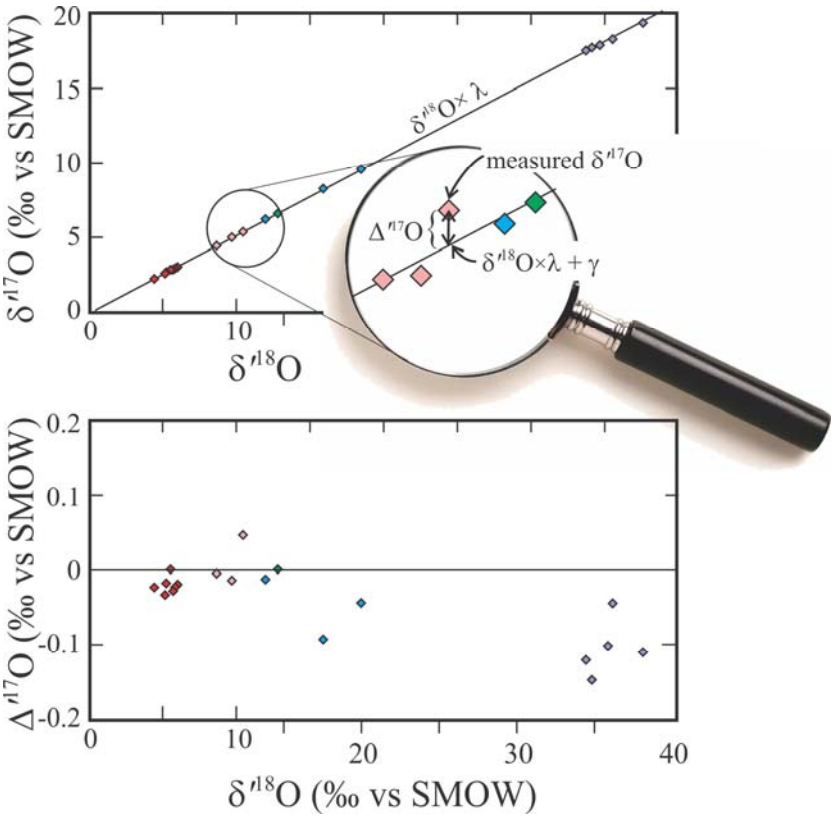

Fig. 3.8. Top: Illustration of small deviations from a best fit line. The vertical displacement is the $\Delta'^{17}O$ value. Bottom: When recast with $\Delta'^{17}O$ on the y-axis, subtle variations can be observed.

3.8 Distribution of isotopologues: Clumped Isotopes

For the simple molecule H_2, there are three possible combinations of D and H: H-H, H-D and D-D. If the two isotopes were randomly distributed in a sample of SMOW, then the abundance of each isotopologue would be the following:

$H_2 = [H]^2$;	$HD = 2 \times [H]\,[D]$;	$D_2 = [D]^2$
0.9997	2.979×10^{-4}	2.219×10^{-8}

where [H] and [D] are the fraction of each of the two isotopes. The exchange between the three isotopologues can be written as a disproportionation reaction given by 2 HD = H_2 + D_2 , where the equilibrium constant is $K = \frac{[HH][DD]}{[HD]^2}$. If the disproportionation were purely stochastic (random), then $K = 0.25$. In fact, the molecule D_2 is slightly more stable than would be expected on the basis of the reduced masses, so that sum of the energies of D_2 and H_2 are slightly lower than twice the energy of the HD molecule. At low temperatures, therefore, D_2 and H_2 will be slightly favored over 2 HD. As temperatures increase the entropy of the system overwhelms the slight energy favorability of D_2, so that the K value approaches the stochastic values given above (Eiler, 2007). The

difference from the stochastic value is given by Δ_I. The differences can be a result of temperature or kinetic fractionations (Eiler, 2007).

Clumped isotopes studies have been made on CO_2 (both gas and the CO_2 liberated from carbonates), CH_4 and O_2. The most highly studied system is for carbonates, where the difference in the abundance of the isotopolougue $^{13}C^{18}O^{16}O$ (mass 47) from the stochastic value (given by Δ_{47}) can be used as a single mineral thermometer (e.g., Ghosh et al., 2006). Specially configured mass spectrometers are required to measure the low abundance of the rare isotopolouge $^{13}C^{18}O^{16}O$, and long counting times are needed to get the necessary precision to make precise temperature estimates. A more detailed discussion on applications of this method are given in Chapter 7.

References

Barkan, E. and Luz, B. (2007) Diffusivity fractionations of $H_2{}^{16}O/H_2{}^{17}O$ and $H_2{}^{16}O/H_2{}^{18}O$ in air and their implications for isotope hydrology. *Rapid Communications in Mass Spectrometry* **21**, 2999-3005.

Bigeleisen, J. and Mayer, M.G. (1947) Calculation of equilibrium constants for isotopic exchange reactions. *Journal of Chemical Physics* **15**, 261-267.

Bird, M.I., Longstaffe, F.J., Fyfe, W.S., Tazaki, K. and Chivas, A.R. (1994) Oxygen-isotope fractionation in gibbsite: Synthesis experiments versus natural samples. *Geochimica et Cosmochimica Acta* **58**, 5267-5277.

Blattner, P. (1975) Oxygen isotopic composition of fissure-grown quartz, adularia, and calcite from Broadlands geothermal field, New Zealand, with an appendix on quartz-K-feldspar-calcite-muscovite oxygen isotope geothermometers. *American Journal of Science* **275**, 785-800.

Bottinga, Y. (1968) Calculation of fractionation factors for carbon and oxygen isotopic exchange in the system calcite-carbon dioxide-water. *Journal of Physical Chemistry* **72**, 800-808.

Bottinga, Y. (1969) Carbon isotope fractionation between graphite, diamond and carbon dioxide. *Earth and Planetary Science Letters* **5**, 301-307.

Bottinga, Y. and Javoy, M. (1973) Comments on oxygen isotope geothermometry. *Earth and Planetary Science Letters* **20**, 250-265.

Cao, X. and Liu, Y. (2011) Equilibrium mass-dependent fractionation relationships for triple oxygen isotopes. *Geochimica et Cosmochimica Acta* **75**, 7435-7445.

Cavosie, A., Sharp, Z.D. and Selverstone, J. (2002) Co-existing aluminum silicates in quartz veins: A quantitative approach for determining andalusite-sillimanite equilibrium in natural samples using oxygen isotopes. *American Mineralogist* **87**, 417-423.

Chacko, T., Cole, D.R. and Horita, J. (2001a) Equilibrium oxygen, hydrogen and carbon isotope fractionation factors applicable to geologic systems, in: Valley, J.W., Cole, D.R. (Eds.), Stable Isotope Geochemistry. Mineralogical Society of America, Washington, D.C., pp. 1-81.

Chacko, T., Cole, D.R. and Horita, J. (2001b) Equilibrium oxygen, hydrogen and carbon isotope fractionation factors applicable to geological systems. *Reviews in Mineralogy and Geochemistry* **43**, 1-81.

Chacko, T., Hu, X., Mayeda, T.M., Clayton, R.N. and Goldsmith, J.R. (1996) Oxygen isotope fractionations in muscovite, phlogopite, and rutile. *Geochimica et Cosmochimica Acta* **60**, 2595-2608.

Chacko, T., Mayeda, T.K., Clayton, R.N. and Goldsmith, J.R. (1991) Oxygen and carbon isotope fractionations between CO_2 and calcite. *Geochimica et Cosmochimica Acta* **55**, 2867-2882.

Clayton, R.N., Goldsmith, J.R., Karel, K.J., Mayeda, T.K. and Newton, R.C. (1975) Limits on the effect of pressure on isotopic fractionation. *Geochimica et Cosmochimica Acta* **39**, 1197-1201.

Clayton, R.N., Goldsmith, J.R. and Mayeda, T.K. (1989) Oxygen isotope fractionation in quartz, albite, anorthite and calcite. *Geochimica et Cosmochimica Acta* **53**, 725-733.

Clayton, R.N. and Kieffer, S.W. (1991) Oxygen isotopic thermometer calibrations, in: Taylor Jr., H.P., O'Neil, J.R., Kaplan, I.R. (Eds.), Stable Isotope Geochemistry: A Tribute to Samuel Epstein. The Geochemical Society Special Publication, pp. 1-10.

Craig, H. (1957) Isotopic standards for carbon and oxygen and correction factors for mass-spectrometric analysis of carbon dioxide. *Geochimica et Cosmochimica Acta* **12**, 133-149.

Criss, R.E. (1999) Prinicples of stable isotope distribution. Oxford University Press, New York.

Denbigh, K. (1971) The Principles of Chemical Equilibrium, 3 ed. Cambride University Press, Cambridge.

Driesner, T. and Seward, T.M. (2000) Experimental and simulation study of salt effects and pressure/density effects on oxygen and hydrogen stable isotope liquid-vapor fractionation for 4-5 molal aqueous NaCl and KCl solutions at 400 degrees C. *Geochimica et Cosmochimica Acta* **64**, 1773-1784.

Eiler, J.M. (2007) "Clumped-isotope" geochemistry—The study of naturally-occurring, multiply-substituted isotopologues. *Earth and Planetary Science Letters* **262**, 309-327.

Epstein, S., Buchsbaum, R., Lowenstam, H. and Urey, H.C. (1951) Carbonate-water isotopic temperature scale. *Journal of Geology* **62**, 417-426.

Epstein, S., Buchsbaum, R., Lowenstam, H.A. and Urey, H.C. (1953) Revised carbonate-water isotopic temperature scale. *Geological Society of America Bulletin* **64**, 1315-1326.

Farquhar, J. and Wing, B.A. (2003) Multiple sulfur isotopes and the evolution of the atmosphere. *Earth and Planetary Science Letters* **213**, 1-13.

Ghosh, P., Adkins, J., Affek, H., Balta, B., Guo, W., Schauble, E.A., Schrag, D.P. and Eiler, J.M. (2006) ^{13}C–^{18}O bonds in carbonate minerals: A new kind of paleothermometer. *Geochimica et Cosmochimica Acta* **70**, 1439-1456.

Hattori, K. and Halas, S. (1982) Calculation of oxygen isotope fractionation between uranium dioxide, uranium trioxide and water. *Geochimica et Cosmochimica Acta* **46**, 1863-1868.

Hoering, T.C. (1961) The effect of physical changes on isotopic fractionation. *Carnegie Institution of Washington Yearbook* **60**, 201-204.

Hoffbauer, R., Hoernes, S. and Fiorentini, E. (1994) Oxygen isotope thermometry based on a refined increment method and its application to granulite-grade rocks from Sri Lanka. *Precambrian Research* **66**, 199-220.

Horita, J., Cole, D.R., Polyakov, V.B. and Driesner, T. (2002) Experimental and theoretical study of pressure effects on hydrogen isotope fractionation in the system brucite-water at elevated temperatures. *Geochimica et Cosmochimica Acta* **66**, 3769-3788.

Horita, J., Cole, D.R. and Wesolowski, D.J. (1993a) The activity-composition relationship of oxygen and hydrogen isotopes in aqueous salt solutions: II. Vapor-liquid water equilibration of mixed salt solutions from 50 to 100°C and geochemical implications. *Geochimica et Cosmochimca Acta* **57**, 4703-4711.

Horita, J., Cole, D.R. and Wesolowski, D.J. (1995) The activity-composition relationship of oxygen and hydrogen isotopes in aqueous salt solutions: III. Vapor-liquid water

equilibration of NaCl solutions to 350°C. *Geochimica et Cosmochimica Acta* **59**, 1139-1151.

Horita, J., Wesolowski, D.J. and Cole, D.R. (1993b) The activity-composition relationship of oxygen and hydrogen isotopes in aqueous salt solutions: I. Vapor-liquid water equilibration of single salt solutions from 50 to 100°C. *Geochimica et Cosmochimca Acta* **57**, 2797-2817.

Hu, G. and Clayton, R.N. (2003) Oxygen isotope salt effects at high pressure and high temperature and the calibration of oxygen isotope geothermometers. *Geochimica et Cosmochimica Acta* **67**, 3227-3246.

Hulston, J.R. and Thode, H.G. (1965) Variations in the S^{33}, S^{34}, and S^{36} contents of meteorites and their relation to chemical and nuclear effects. *Journal of Geophysical Research* **70**, 3475-3484.

Kieffer, S.W. (1982) Thermodynamics and lattice vibrations in minerals: 5. Applications to phase equilibria, isotopic fractionation, and high-pressure thermodynamic properties. *Reviews of Geophysics and Space Physics* **20**, 827-849.

Kita, I., Taguchi, S. and Matsubaya, O. (1985) Oxygen isotope fractionation between amorphous silica and water at 34-93ºC. *Nature* **314**, 83-84.

Kohn, M.J. and Valley, J.W. (1998) Oxygen isotope geochemistry of the amphiboles; isotope effects of cation substitutions in minerals. *Geochimica et Cosmochimica Acta* **62**, 1947-1958.

Larson, T. and Sharp, Z.D. (2003) Stable isotope constraints on the Al_2SiO_5 'triple-point' rocks from the Proterozoic Priest pluton contact aureole, New Mexico. *Journal of Metamorphic Geology* **21**, 785-798.

Leclerc, A.J. and Labeyrie, L. (1987) Temperature dependence of oxygen isotopic fractionation between diatom silica and water. *Earth and Planetary Science Letters* **84**, 69-74.

Longinelli, A. and Nuti, S. (1973) Revised phosphate-water isotopic temperature scale. *Earth and Planetary Science Letters* **19**, 373-376.

Luz, B. and Barkan, E. (2010) Variations of $^{17}O/^{16}O$ and $^{18}O/^{16}O$ in meteoric waters. *Geochimica et Cosmochimica Acta* **74**, 6276–6286.

Matsuhisa, Y., Goldsmith, J.R. and Clayton, R.N. (1978) Mechanisms of hydrothermal crystallization of quartz at 250°C and 15 kbar. *Geochimica et Cosmochimica Acta* **42**, 173-182.

Matthews, A., Goldsmith, J.R. and Clayton, R.N. (1983) On the mechanisms and kinetics of oxygen isotope exchange in quartz and feldspars at elevated temperatures and pressures. *Geological Society of America Bulletin* **94**, 396-412.

McCrea, J.M. (1950) On the isotopic chemistry of carbonates and a paleotemperature scale. *Journal of Chemical Physics* **18**, 849-857.

Miller, M.F. (2002) Isotopic fractionation and the quantification of ^{17}O anomalies in the oxygen three-isotope system: an appraisal and geochemical significance. *Geochimica et Cosmochimica Acta* **66**, 1881-1889.

Morikiyo, T. (1986) Hydrogen and carbon isotope studies on the graphite-bearing metapelites in the northern Kiso District of central Japan. *Contributions to Mineralogy and Petrology* **94**, 165-177.

Northrop, D.A. and Clayton, R.N. (1966) Oxygen-isotope fractionations in systems containing dolomite. *Journal of Geology* **74**, 174-196.

O'Neil, J.R. (1986) Theoretical and experimental aspects of isotopic fractionation., in: Valley, J.W., Taylor Jr., H.P., O'Neil, J.R. (Eds.), Stable Isotopes in High Temperature Geological Processes, 1 ed. Mineralogical Society of America, Chelsea, pp. 1-40.

O'Neil, J.R., Clayton, R.N. and Mayeda, T.K. (1969) Oxygen isotope fractionation in divalent metal carbonates. *Journal of Chemical Physics* **51**, 5547-5558.

O'Neil, J.R. and Epstein, S. (1966) Oxygen isotope fractionation in the system dolomite-calcite-carbon dioxide. *Science* **152**, 198-200.

O'Neil, J.R. and Taylor Jr., H.P. (1967) The oxygen isotope and cation exchange chemistry of feldspars. *American Mineralogist* **52**, 1414-1437.

O'Neil, J.R. and Truesdell, A.H. (1991) Oxygen isotope fractionation studies of solute-water interactions, in: Taylor Jr., H.P., O'Neil, J.R., Kaplan, I.R. (Eds.), Stable isotope geochemistry: A tribute to Samuel Epstein. The Geochemical Society, pp. 17-25.

Pack, A. and Herwartz, D. (2014) The triple oxygen isotope composition of the Earth mantle and $\Delta^{17}O$ variations in terrestrial rocks. *Earth and Planetary Science Letters* **390**, 138-145.

Perkins, G., Sharp, Z.D. and Selverstone, J. (2004) Oxygen isotopic compositions of ultramfic xenoliths from the Rio Puerco volcanic necks, NM, and implications for the source of metasomatic fluids in the lithospheric mantle. *Geological Society of America, Abstracts with Programs* **36**, 57-54.

Polyakov, V.B. and Kharlashina, N.N. (1994) Effect of pressure on equilibrium isotopic fractionation. *Geochimica et Cosmochimica Acta* **58**, 4739-4750.

Polyakov, V.B. and Mineev, S.D. (2000) The use of Mössbauer spectroscopy in stable isotope geochemistry. *Geochimica et Cosmochimica Acta* **64**, 849-865.

Richet, P., Bottinga, Y. and Javoy, M. (1977) A review of hydrogen, carbon, nitrogen, oxygen, sulphur, and chlorine stable isotope fractionation among gaseous molecules. *Annual Review of Earth and Planetary Science* **5**, 65-110.

Richter, R. and Hoernes, S. (1988) The application of the increment method in comparison with experimentally derived and calculated O-isotope fractionations. *Chemie der Erde* **48**, 1-18.

Rubinson, M. and Clayton, R.N. (1969) Carbon-13 fractionation between aragonite and calcite. *Geochimica et Cosmochimica Acta* **33**, 997-1002.

Rumble, D., Miller, M.F., Franchi, I.A. and Greenwood, R.C. (2007) Oxygen three-isotope fractionation lines in terrestrial silicate minerals: An inter-laboratory comparison of hydrothermal quartz and eclogitic garnet. *Geochimica et Cosmochimica Acta* **71**, 3592-3600.

Savin, S.M. and Epstein, S. (1970) The oxygen and hydrogen isotope geochemistry of clay minerals. *Geochimica et Cosmochimica Acta* **34**, 25-42.

Savin, S.M. and Lee, M. (1988) Isotopic studies of phyllosilicates, in: Bailey, S.W. (Ed.), Hydrous phyllosilicates. Mineralogical Society of America, Chelsea, pp. 189-223.

Schauble, E.A. (2004) Applying stable isotope fractionation theory to new systems, in: Johnson, C.M., Beard, B.L., Albarède, F. (Eds.), Geochemistry of Non-Traditional Stable Isotopes. Mineralogical Society of America, Washington, D.C., pp. 65-111.

Schütze, H. (1980) Der Isotopenindex -- eine Inkrementenmethode zur näherungsweise Berechnung von Isotopenaustauschgleichgewichten zwischen kristallinin Substanzen. *Chemie der Erde* **39**, 321-334.

Sharp, Z.D. (1995) Oxygen isotope geochemistry of the Al_2SiO_5 polymorphs. *American Journal of Science* **295**, 1058-1076.

Sharp, Z.D., Essene, E.J. and Smyth, J.R. (1992) Ultra-high temperatures from oxygen isotope thermometry of a coesite-sanidine grospydite. *Contributions to Mineralogy and Petrology* **112**, 358-370.

Sharp, Z.D., Gibbons, J.A., Maltsev, O., Atudorei, V., Pack, A., Sengupta, S., Shock, E.L. and Knauth, L.P. (2016) A calibration of the triple oxygen isotope fractionation in the SiO2 - H2O system and applications to natural samples. *Geochimica et Cosmochimica Acta* **186**, 105-119.

Smyth, J.R. (1989) Electrostatic characterization of oxygen sites in minerals. *Geochimica et Cosmochimica Acta* **53**, 1101-1110.

Stolper, E. and Epstein, S. (1991) An experimental study of oxygen isotope partitioning between silica glass and CO_2 vapor, in: Taylor Jr., H.P., O'Neil, J.R., Kaplan, I.R. (Eds.), Stable Isotope Geochemistry: A Tribute to Samuel Epstein. The Geochemical Society, San Antonio, pp. 35-51.

Suzuoki, T. and Epstein, S. (1976) Hydrogen isotope fractionation between OH-bearing minerals and water. *Geochimica et Cosmochimica Acta.* **40**, 1229-1240.

Taylor, B.E. and O'Neil, J.R. (1977) Stable isotope studies of metasomatic skarns and associated metamorphic and igneous rocks, Osgood Mountains, Nevada. *Contributions to Mineralogy and Petrology* **63**, 1-49.

Taylor, H.P., Jr. and Epstein, S. (1962) Relationship between O^{18}/O^{16} ratios in coexisting minerals of igneous and metamorphic rocks Part 1. Principles and experimental results. *Geological Society of America Bulletin* **73**, 461-480.

Thiemens, M. (2006) History and applications of mass-independent isotope effects. *Annual Reviews of Earth and Planetary Sciences* **34**, 217–262.

Young, E.D., Galy, A. and Nagahara, H. (2002) Kinetic and equilibrium mass-dependent isotope fractionation laws in nature and their geochemical and cosmochemical significance. *Geochimica et Cosmochimica Acta* **66**, 1095-1104.

Zheng, Y.-F., Metz, P. and Satir, M. (1994a) Oxygen isotope fractionation between calcite and tremolite: an experimental study. *Contributions to Mineralogy and Petrology* **118**, 249-255.

Zheng, Y.F. (1993) Calculation of oxygen isotope fractionation in anhydrous silicate minerals. *Geochimica et Cosmochimica Acta* **57**, 1079-1091.

Zheng, Y.F., Metz, P., Satir, M. and Sharp, Z.D. (1994b) An experimental calibration of oxygen isotope fractionation between calcite and forsterite in the presence of a CO_2-H_2O fluid. *Chemical Geology* **116**, 17-27.

Chapter 4

THE HYDROSPHERE

Contents

4.1 Overview 1
Reservoir 1
4.2 Natural Abundances of the Isotopologues of Water. 2
Isotopomer of Water 3
4.3 Meteoric Water 3
4.4 The Meteoric Water Line 4
4.4.1 General features of the GMWL 5
4.4.2 Variations in slopes and intercepts of local MWLs 7
4.4.3 Meteoric waters in arid and semi-arid environments 8
4.5 The Deuterium Excess Parameter 10
4.6 Evaporation and Condensation 12
4.6.1 Evaporation over oceans 13
4.6.2 Condensation and precipitation 15
4.6.3 Condensation: open system (Rayleigh) isotopic fractionation 16
4.7. Factors Controlling the Isotopic Composition of Precipitation. 19
4.7.1 Temperature 19
4.7.2 Distance or continentality effect 21
4.7.3 Latitude effect 21
4.7.4 Altitude effect 21
4.7.5 Amount effect 22
4.7.6 Seasonal effects 24
4.8 Groundwater 24
4.9 Geothermal Systems 26
4.10. Basinal Brines and Formation Waters 28
4.11 Glacial Ice 30
4.11.1 Underlying bases for glacial paleoclimatology 30
4.11.2 Determining the age of glacial ice 31
4.11.3 Thinning of ice layers 31
4.11.4 The example of Camp Century, N. Greenland 33
4.11.5 Example of the GRIP Summit Core: Flickering climates 35
4.12 Triple oxygen isotope geochemistry of meteoric water 36
References 39

Chapter 4

THE HYDROSPHERE

4.1 Overview

The hydrosphere constitutes an astonishing 5.9 weight per cent of the crust of Earth and a significant amount of water is present in hydrous and nominally anhydrous minerals in the mantle as well. Water and aqueous solutions play a major role in the formation and development of rocks and minerals, the development of physiographic features, meteorological patterns, and all life processes. Thus it is understandable that more stable isotope analyses have been made of water, collected from its myriad of reservoirs on Earth, than of any other naturally occurring substance. Despite the pronounced reactivity of water, the stable isotope compositions of large and relatively well-mixed bodies of water like the ocean or large lakes vary little. In contrast, those of waters in minor abundance, and especially those that form as a result of evaporation (*e.g.,* meteoric origin), vary widely. This behavior reflects a simple mass-balance principle that we shall meet over and over again in this text: *during an interaction between two reservoirs of the same element, the isotopic composition of the element will change more in the smaller reservoir than it will in the larger reservoir and by an amount that is proportional to the relative sizes of the reservoirs*. Finally, it should be recognized that the wide range of $\delta^{18}O$ and δD values of meteoric water are fundamentally related to fractionation associated with phase change. As stated by Gat (1996) "*In the water cycle, the most significant process in this respect is that of phase changes, from vapor to liquid or ice and vice versa*"

Variations in the hydrogen and oxygen isotope compositions of modern natural waters are presented in Table 4.1. Ocean water is a logical reference material (SMOW = Standard Mean Ocean Water) for stable isotope analyses of natural waters because it comprises over 97% of the hydrosphere, is the source of essentially all atmospheric moisture, appears to be buffered to a relatively constant $^{18}O/^{16}O$ ratio by both high and low temperature interactions with mantle-derived rocks on the ocean floor (see Chapter 5), and controls the stable isotope compositions of authigenic minerals that form in it and the tissues of life forms that inhabit it.

Table 4.1. *Representative isotopic compositions and approximate volumes of natural waters (after Criss, 1999)* .

Reservoir	Volume (%)	δD(‰) SMOW	$\delta^{18}O$(‰) SMOW
Ocean	97.2	0±5	0±1
Deep Atlantic			+0.05
Deep Pacific			-0.15
Deep Antarctic			-0.40
Ice Caps and Glaciers	2.15	-230 ± 120	-30 ± 15
Groundwater	0.62	-50 ± 60	-8 ± 7
Fresh surface water	0.017	-50 ± 60	-8 ± 7
Atmospheric water vapor	0.001	-150 ± 80	-20 ± 10

While gross variations in stable isotope ratios of natural aqueous fluids were known from relatively precise density measurements made over 60 years ago, it was not until the publication of two landmark papers in 1953 (Epstein and Mayeda, 1953; Friedman, 1953) that we began to understand the relations between isotopic compositions of natural waters and the physical chemical processes that modify them: *evaporation, condensation, mixing, and exchange reactions*. Epstein and Mayeda measured only oxygen isotope ratios and Friedman measured only hydrogen isotope ratios, but trends in both isotopic ratios of natural waters are, with subtle but important exceptions, almost the same. Relations governing variations in the isotopic compositions of meteoric waters were put on a quantitative basis by Dansgaard (1964) and will be examined below in detail. An additional excellent summary of fractionation processes in the meteoric water cycle is given by Gat (1996).

The beauty of stable isotope measurements of natural waters is the fact that hydrogen and oxygen isotopes comprise the water molecules themselves and thereby constitute *built-in* tracers for water. They are most often conservative tracers, particularly for low-temperature surface waters, but the original isotopic compositions of natural waters can be changed by physical processes and by chemical reactions with rocks and other fluids.

4.2 Natural Abundances of the Isotopologues of Water.

Because there are two stable isotopes of hydrogen, protium (^{1}H or H) and deuterium (^{2}H or D), and three stable isotopes of oxygen (^{16}O, ^{17}O and ^{18}O), there are nine possible isotopologues of water: $H_2{}^{16}O$, $H_2{}^{17}O$, $H_2{}^{18}O$, $HD^{16}O$, $HD^{17}O$, $HD^{18}O$, $D_2{}^{16}O$, $D_2{}^{17}O$, and $D_2{}^{18}O$. It is a simple matter to calculate the approximate abundance of each of these forms on Earth using the average terrestrial abundance of each of the isotopes. The average terrestrial abundances of hydrogen and oxygen isotopes *in atom per cent* are (Coplen et al., 2002):

$^{16}O = 99.7621$	$H = 99.9844$
$^{17}O = 0.03790$	$D = 0.01557$
$^{18}O = 0.20004$	

The abundance of a particular isotopologue is determined by multiplying together the average abundances *of each atom* comprising the compound, taking into account symmetry considerations when appropriate. For example:

$$\mathbf{H_2{}^{16}O} \quad (0.999844)^2(0.997621) = 0.997310 \qquad 4.1.$$

That is, $H_2{}^{16}O$ comprises 99.7% of all water on Earth. In contrast,

$$\mathbf{HD^{16}O} \quad (2)(0.999844)(0.0001557)(0.99759) = 0.0003106 \qquad 4.2$$

compromises only 0.03% of all water is $HD^{16}O$ (note *caveat* below) and it is the variation about this average value that is measured in hydrogen isotope geochemistry.

The squared term in equation 4.1 arises from the fact that there are two atoms of hydrogen in the water molecule and each atom in the molecule must be accounted for in

the product of the abundances. The factor of 2 that appears in equation 4.2 is required because of the symmetry of the HDO molecule – both the HDO and DHO are possible. In the strictest sense, this symmetry factor is valid only for gaseous or monomeric HDO[1]. Monomeric water vapor in nature exists almost exclusively in the atmosphere and arises from evaporation of standing bodies of water and as emanations from volcanoes, fumaroles, hot springs and the like. Thus the symmetry consideration has no obvious practical implications. Nonetheless it is instructive to introduce the concept of molecular symmetry at this point.

The average natural abundances of the various isotopologues of water on Earth are given in Table 4.2. Only four isotopologues have sufficient abundance in nature to have any practical consequence to isotope geochemistry: $H_2{}^{16}O$, $H_2{}^{17}O$, $HD^{16}O$, and $H_2{}^{18}O$ (molecular weights = 18, 19, 19, and 20, respectively). Forms of any natural substance containing two rare stable isotopes, like $HD^{18}O$ or $D_2{}^{16}O$, are to all intents and purposes absent in nature (See however Eiler and Schauble, 2004).

Table 4.2. *Average natural abundances of the nine isotopomers of water vapor.*

Isotopomer of Water	Average Abundance (%)
$H_2{}^{16}O$	**99.73098**
$H_2{}^{18}O$	**0.199978**
$H_2{}^{17}O$	**0.037888**
$HD^{16}O$	**0.031460**
$HD^{18}O$	0.0000006
$HD^{17}O$	0.0000001
$D_2{}^{16}O$	0.00000002
$D_2{}^{17}O$	0.00000000001
$D_2{}^{18}O$	0.00000000005

4.3 Meteoric Water

Meteoric water is liquid or solid water that falls or has fallen from the sky and includes rain, fog, hail, sleet, and snow. Meteoric water resides on Earth principally in glaciers, groundwater systems, rivers and lakes. Using reasonable estimates of mean amounts and isotopic compositions of precipitation around the world, global meteoric water has $\delta^{18}O = -4‰$ and $\delta D = -22‰$. The development of precipitation can be discussed in general terms, with isotopic effects assigned to each part of the process. Most worldwide precipitation on Earth occurs over the oceans. About 90% of oceanic water vapor condenses after minimal horizontal movement of the confining air mass and falls back into the ocean. The remaining 10% is carried by winds over the continents where air masses pick up additional water vapor from sources of fresh water on land. Supersaturation occurs upon cooling of the air masses, and much of the vapor condenses and precipitates on land. Transport of atmospheric vapor over the continents helps regulate heat balance on Earth and provides plants and animals with life-sustaining fresh

[1] Liquid water is a complicated and constantly changing mixture of isotopically variable water molecules that are weakly joined by hydrogen bonds into clusters of different sizes.

water. Because of the extreme importance of these processes, particularly changes in precipitation in response to anthropogenic climate change, much attention has been given to the study of stable isotope variations of meteoric waters.

Using generally accepted estimates of vapor sources over land, one concludes that only about one-third of continental precipitation is derived *directly* from oceanic water vapor. The remaining two-thirds of continental water vapor enters the atmosphere through evaporation of large lakes and rivers and, significantly, by transpiration of plants (Fig. 4.1). Relatively minor amounts of water are introduced into the atmosphere by volcanic activity and from extraterrestrial sources like cometary material. Such waters have distinct isotopic compositions but, under normal circumstances, they can never be identified simply because they immediately become part of the vast amount of vapor in Earth's atmosphere and enter into the hydrologic cycle. They are mentioned primarily for the sake of completeness. Long term, however, they may contribute somewhat to the δD value of terrestrial waters.

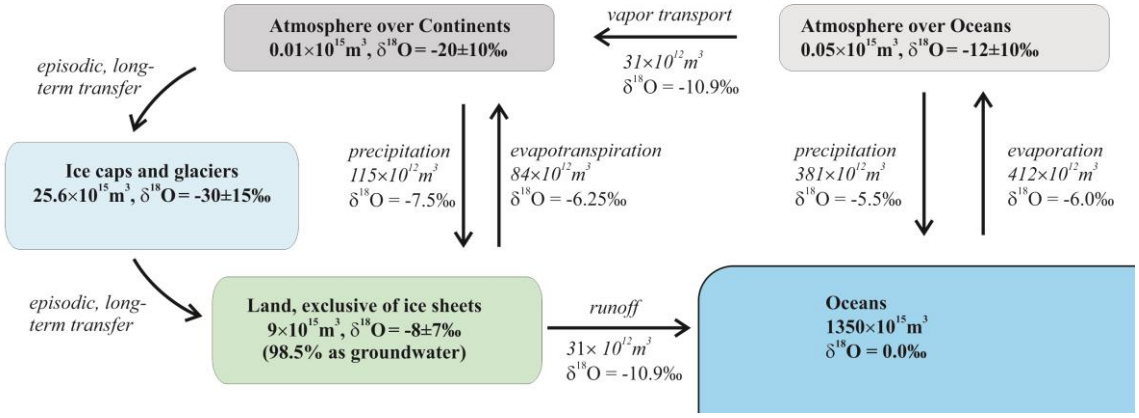

Fig. 4.1. Reservoirs and fluxes for the meteoric water cycle. All meteoric water is ultimately sourced from evaporation from the ocean. Most of this evaporation is returned directly to the ocean as precipitation. The small fraction that is blown over the continents is the source of all continental precipitation. A large fraction of land-based precipitation is returned to the atmosphere *via* evapotranspiration, with the remainder returning to the ocean in rivers. Note that the fluxes between all reservoirs are balanced.

The vast majority of freshwater is locked in the ice caps. Extensive transfer to and from the ice caps depends on climatic conditions. At present, warming is resulting in a diminution of the ice caps and an increase in flow to the oceans. When the ice caps melt completely, the $\delta^{18}O$ value of the oceans will be ~0.6‰ lower than they are today. Flux rate and isotope values from Good *et al.* (2015), converted from hydrogen isotope calculations using the relationship $\delta D = \delta^{18}O + 10$.

4.4 The Meteoric Water Line

One of the most remarkable relations observed in the geochemistry of natural substances is the near linear relation between δD and $\delta^{18}O$ values of the majority of waters of meteoric origin. Friedman (1953) first reported the covariance between δD and $\delta^{18}O$ values of natural waters, comparing his hydrogen isotope data with the oxygen isotope data reported by Epstein and Mayeda (1953). He proposed that the observed linear relationship between δ values was controlled by the covariations of relative vapor pressures of $HD^{16}O$ *versus* $H_2{}^{16}O$ and $H_2{}^{18}O$ *versus* $H_2{}^{16}O$ that prevail during the various processes that characterize cloud dynamics – particularly condensation. His relation and

explanation were fundamentally correct, but the isotopic fractionations that occur upon initial evaporation and transport away from seawater and those attendant on subsequent processes of evaporation, precipitation and exchange, as well as additions of water from sources on the continents, are to this day not understood in detail (see Criss, 1999). Because the correlation between $\delta^{18}O$ and δD values of natural waters was recognized early (and therefore analyzing both seemed redundant) and, more importantly, because the equipment necessary to analyze both stable isotope ratios was rarely available at a single institution, measurements were normally made of only one stable isotope ratio (D/H or $^{18}O/^{16}O$) of water in the early years.

In 1961 Craig (1961) published precise analyses made in a single laboratory of both isotopic ratios of many samples of meteoric water and defined the Meteoric Water Line (Fig. 4.2), often abbreviated simply as MWL. Related abbreviations commonly used are LMWL (Local Meteoric Water Line) and GMWL (Global Meteoric Water Line).

4.4.1 General features of the GMWL

1. A plot of the $\underline{\delta}D$ vs $\delta^{18}O$ values of most meteoric waters plot on a line with a slope of 8. The lowest delta values are found at high latitudes, inland, and at high altitudes. The highest delta values are found in tropical regions. Evaporated waters (*e.g.*, closed basins) plot at higher $\delta^{18}O$ values (to the right) relative to the global meteoric water line. See Gat (1996) for a thorough review of isotopic effects of meteoric water.

2. Despite the fact that the ocean is the ultimate source of all meteoric water, the GMWL does not pass through the ocean water value (δD and $\delta^{18}O = 0‰$, by definition). A best fit of global-scale meteoric water data have a δD value of ~10‰ for a $\delta^{18}O$ value of 0‰. The explanation for this phenomenon lies in the fact that the atmosphere above the oceans is unsaturated with respect to water. Evaporation into unsaturated air is a kinetic, irreversible process as explained below.

3. Regression of these data, and many other data accumulated subsequently, results in an expression that represents the isotopic compositions of the majority of meteoric waters that fall in regions on Earth where climates are temperate:

$$\delta D = 8\,\delta^{18}O + 10 \qquad 4.3.$$

Equation 4.3 represents very well the modern day *global* meteoric water line[2]. If the stable isotope compositions of ocean water were different in the past, and global circulation patterns were roughly similar to those prevailing today, the GMWL at that time would be parallel to the modern GMWL. That is, the slope of the line would remain near a value of 8 but the intercept would be different.

To a first approximation, the slope of the GMWL is related to the hydrogen and oxygen isotope fractionation associated with condensation of water and ice. Air masses cool as they rise and move away from their source. If the temperature of an air mass drops to the point of supersaturation, condensation and eventually precipitation occur.

[2] An *unweighted* GMWL generated from thousands of analyses of precipitation samples from the International Atomic Energy Agency network sites ((Rozanski et al., 1992) is represented by an equation that can be considered a refinement of equation 4.3: $\delta D = 8.17\ \delta^{18}O + 10.35$. An analogous expression generated by Kendall and Coplen (2001) for samples from the 48 contiguous states of the USA has a similar slope but an intercept that is 1.4‰ lower: $\delta D = 8.11\ \delta^{18}O + 8.99$.

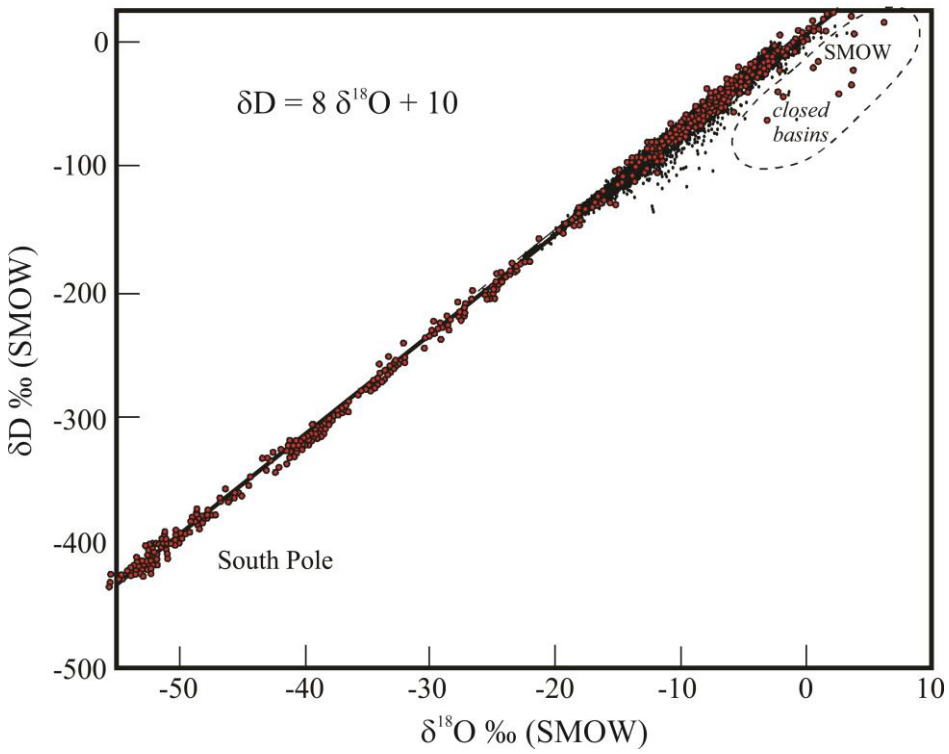

Fig. 4.2. Global Meteoric Water Line. Shaded circles after Craig (1961); black spots after Kendall and Coplen (2001).

The $\delta^{18}O$ and δD values of the condensate will be substantially more positive than those of the parent vapor. Condensation is generally considered to be an equilibrium process and thus equilibrium fractionation factors can be used to model it. (Note: At very low temperatures, supersaturation may occur, and kinetic isotope effects during ice crystallization will result in non-equilibrium formation of ice crystals (Jouzel and Merlivat, 1984)). At equilibrium (100% relative humidity), hydrogen and oxygen isotope fractionation factors between liquid or solid (*l*, *s*) and vapor (*v*) are nearly equal to the ratios of the vapor pressures of the pertinent isotopologues of water at a given value of T. For example, for the oxygen isotopologues $H_2{}^{16}O$ and $H_2{}^{18}O$

$$\alpha_{l-v} = \frac{\left({}^{18}O/{}^{16}O\right)_l}{\left({}^{18}O/{}^{16}O\right)_v} = \frac{p}{p'} = pH_2{}^{16}O/pH_2{}^{18}O \qquad 4.4,$$

where p' is the vapor pressure of the heavy isotopologue and p is the vapor pressure of the light isotopologue. Determinations of $\alpha_{l\text{-}v}$ have been made both by vapor pressure measurements and by exchange experiments between water, ice and water vapor. The ratios for $1000 ln\alpha_{s\text{-}v}$ and $1000 ln\alpha_{l\text{-}v}$ for D/H divided by ${}^{18}O/{}^{16}O$ are shown in figure 4.3. The average values are close to 8, the empirical slope for the GMWL.

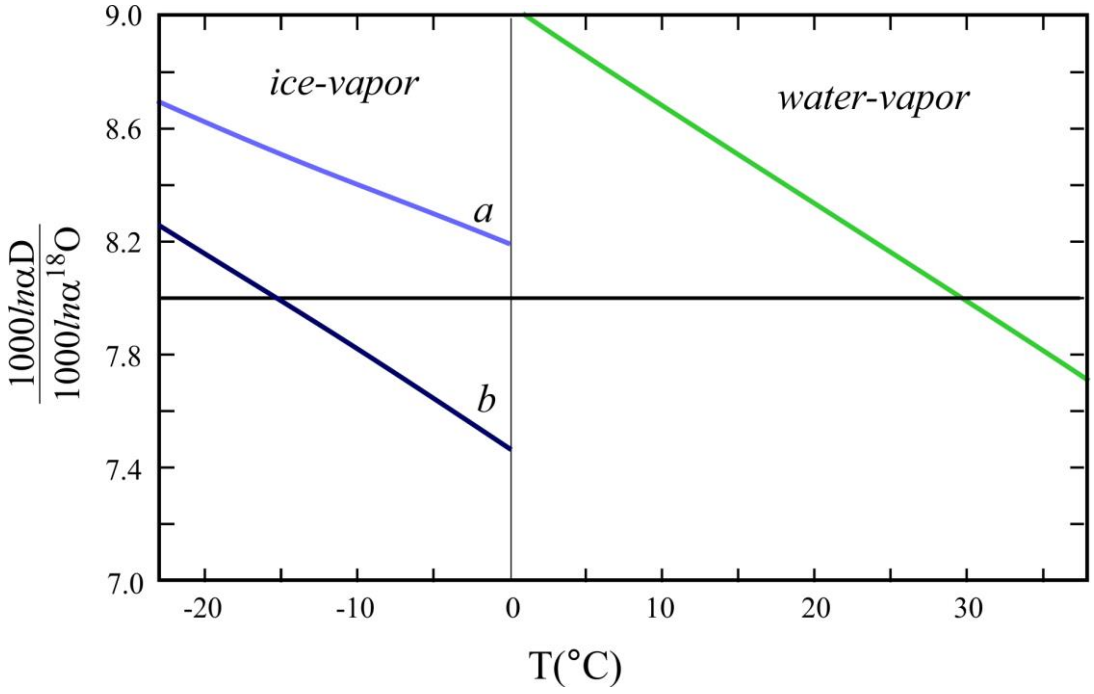

Fig. 4.3. Ratios of the fractionation between ice-vapor and water-vapor as a function of temperature. The ratio is close to 8 over a wide range of temperatures, explaining the slope of the global meteoric water line. Data sources: Water-vapor: (Horita and Wesolowski, 1994); ice-vapor (a) (Merlivat and Nief, 1967); (b) (Méheut et al., 2007).

5. Within the limits of analytical error, no data falling to the left of the GMWL were published for almost 20 years after the GMWL was defined. As a result, this region in δD-$\delta^{18}O$ space was considered a *forbidden region*. While we are now aware of a few important exceptions, this forbidden region continues to place constraints on possible processes undergone by meteoric waters.

4.4.2 Variations in slopes and intercepts of local MWLs

Analyses of a given sample of water collected during a single storm event may or may not lie on the MWL, but analyses of samples that are weighted averages of precipitation over a relatively long period of time (groundwater is a good example) at a specific site in temperate regions will almost certainly lie on or very near the MWL. Kendall and Coplen (2001) published stable isotope analyses of >4800 stream samples from 391 sites in the continental USA and demonstrated that such samples are normally very good proxies for modern local precipitation and corroborated earlier findings that local meteoric water lines usually have slopes that are lower than 8 (Fig. 4.4). In fact LMWLs that characterize very large areas of the southern and western USA have slopes that are <6. The ***GMWL represents a weighted average of LMWLs whose slopes are uniformly lower than 8 and whose intercepts vary widely from values as negative as about –2 to values as positive as about +15***. It is not surprising that the many attempts to derive a general expression for the MWL from first principles have been met with frustration.

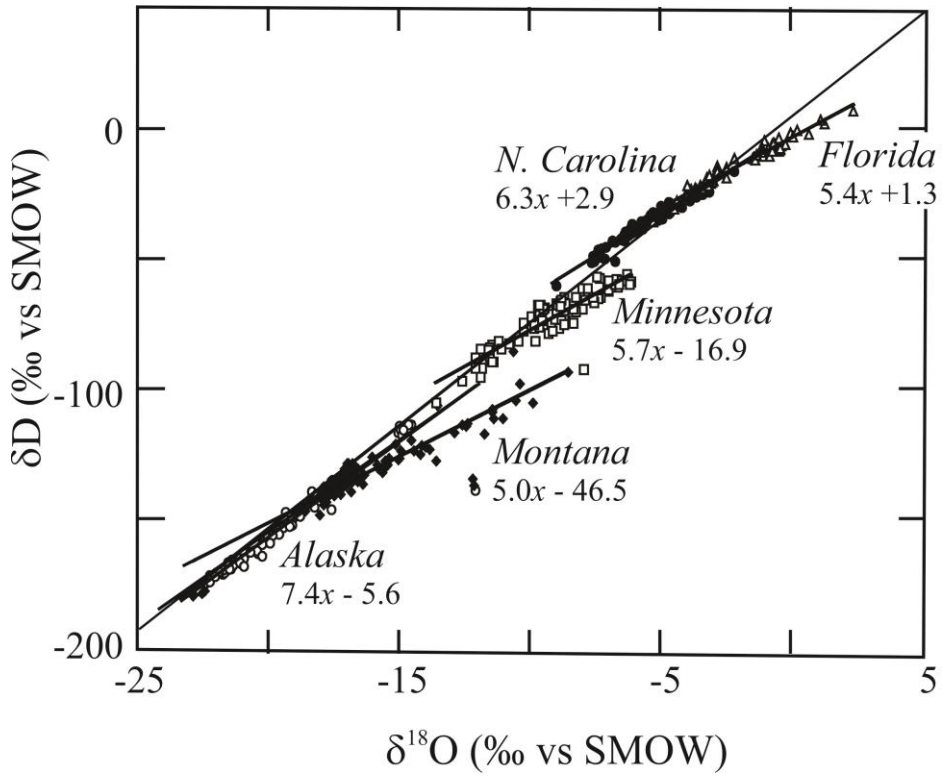

Fig. 4.4. Local meteoric water lines for selected regions of the United States. In almost all cases, the slope of the LMWL is less than the global meteoric water line value of ~8. After Kendall and Coplen (2001).

4.4.3 Meteoric waters in arid and semi-arid environments

The isotopic fractionation during evaporation into unsaturated air is a combination of equilibrium and kinetic (diffusion-based) fractionation between water and vapor. Craig and Gordon (1965) developed an evaporation model that explains and adequately predicts fractionation associated with evaporating air (Fig. 4.5). The model treats the water-vapor interface as a series of discrete layers. In each layer a specific transport mechanism overwhelms all others, allowing for a series of equations to be used to quantify the overall isotope fractionation as a function of humidity and the δ value of the free air. Horita *et al.* (2008) explain the model in detail and their paper should be consulted for additional information.

In regions where significant evaporation takes place, waters of meteoric origin can have quite unusual isotopic compositions. Data for waters in arid regions commonly have a $\delta D/\delta^{18}O$ slope of ~ 5, in strong contrast to the slope of 8 for the GMWL. As stated above, isotopic fractionations between liquid and vapor in these cases differ from the equilibrium fractionations due to kinetic isotope effects. In fact, $d\delta D/d\delta^{18}O$ slopes for evaporating waters are quite variable, typically 4-6, and depend on local conditions of humidity, isotopic composition of water vapor, and fraction of water evaporated. For the simple case where the isotopic composition of evaporating water is in isotopic equilibrium with the water vapor, the following relation applies (Criss, 1999):

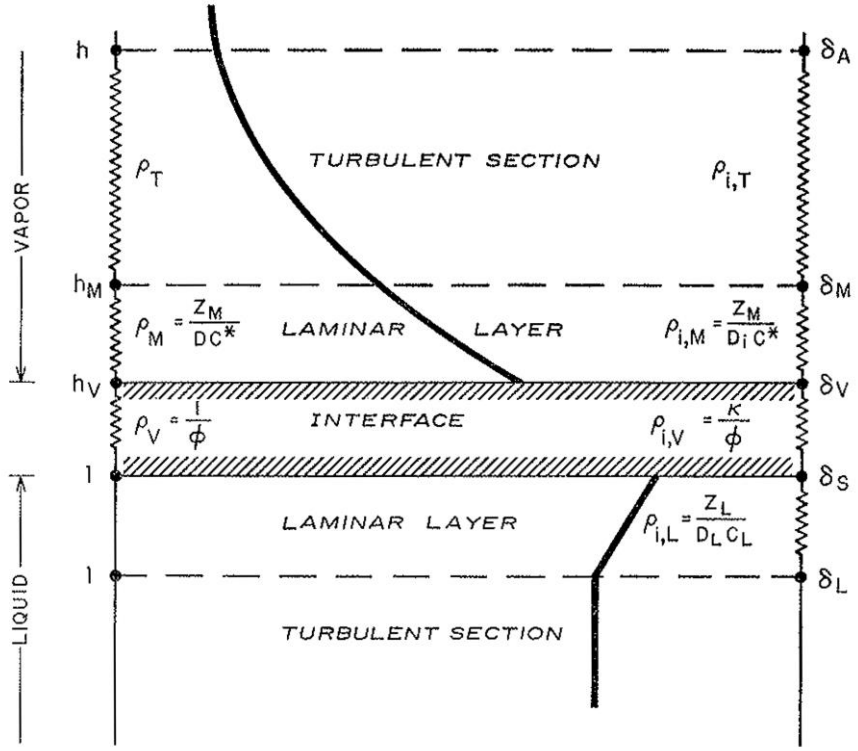

Fig. 4.5. Craig and Gordon's 'laminar layer model' for evaporation of H_2O into unsaturated air. The model consists of discreet layers in which a single transport mechanism dominates over all others, thereby greatly simplifying the overall evaporation process. The isotopic compositions of the liquid and vapor layers are shown by the thick black lines. A thin laminar layer in the liquid has an increasing δ value approaching the interface due to preferential loss of the light isotope to the vapor. The ρ values are the 'transport resistance' of each layer. The δ value of the vapor decreases towards the free air value away from the interface. Horita *et al.* (2008) provide a detailed description of the model. Figure from Craig and Gordon (1965).

$$\frac{d\delta \mathrm{D}}{d\delta^{18}\mathrm{O}} \cong \frac{\left(1-1/\alpha^{o}_{evap,D}\right)\left(1000+\delta \mathrm{D_w}\right)}{\left(1-1/\alpha^{o}_{evap,ox}\right)\left(1000+\delta^{18}\mathrm{O_w}\right)} \qquad 4.5,$$

where δD_w and $\delta^{18}O_w$ are the initial delta values of water prior to evaporation, and α^{o}_{evap} is the fractionation factor between water and vapor at zero humidity. At 20°C, values of α^{o}_{evap} are 1.0260 and 1.094 for the oxygen and hydrogen isotopologues, respectively, corresponding to a $\delta D/\delta^{18}O$ slope of only 3.4. When the humidity changes, or the isotopic composition of the water changes in response to Rayleigh effects, the equations become substantially more complicated (Criss, 1999).

Under conditions of extreme evaporation, such as is seen in lake water from the Sahara Desert, extraordinary $\delta^{18}O$ and δD values of +31‰ and +129‰, respectively, have been recorded (Fontes and Gonfiantini, 1967). Extreme evaporation does not necessarily lead to extremely heavy values of the residual liquid as in the Sahara case. For example, the $\delta^{18}O$ values of ocean water evaporating in the salt pans near San

Francisco only reach $\delta^{18}O$ values of 6‰ (Lloyd, 1966). In contrast to the situation in the Sahara Desert where vapor leaves the system with minimal back exchange with the liquid, vapor in the San Francisco atmosphere ultimately reaches isotopic equilibrium with water vapor. That is, the $\delta^{18}O$ values of the evaporating water increase but not indefinitely. Eventually, the back diffusion of water vapor into the remaining liquid exactly offsets the evaporation of the light isotope from the water to the vapor. The system has reached steady state and further evaporation will not cause an increase in the δ value of the remaining liquid. This experiment is easily done in the laboratory. Place a large container of water out to evaporate. The $\delta^{18}O$ value will rise as evaporation occurs but will eventually plateau at a value that is buffered by the $\delta^{18}O$ value of air.

Evaporation effects are seen commonly in lakes and rivers in regions of low relative humidity. For example, melt waters feeding Lake Tahoe have $\delta^{18}O$ values of about −16‰ whereas Lake Tahoe itself has a $\delta^{18}O$ value of about –5.5‰. Despite the relatively large volume of water in Lake Tahoe, it undergoes an amazing amount of evaporation during the year and the $^{18}O/^{16}O$ and D/H ratios of the water increase dramatically in response to this process. In like fashion, $\delta^{18}O$ values of rivers downstream can be several per mil higher than those of the head waters due to evaporation effects as the water moves to lower and warmer elevations.

4.5 The Deuterium Excess Parameter

In spite of many complex processes operating in the hydrological cycle, the relative vapor pressures of the hydrogen and oxygen isotopologues of water normally vary sympathetically, creating the linear relationship defining the global meteoric water line given by equation 4.3. Rearranging equation 4.3 results in the following equation:

$$d = \delta D - 8\,\delta^{18}O \qquad 4.6.$$

The parameter *d* was given the name *deuterium excess parameter* by Dansgaard (1964), and is also referred to as the *deuterium excess value*, or simply, *deuterium excess*. The *d* value mathematically expresses how far a sample plots above or below a slope 8 line in δD-$\delta^{18}O$ space. A *d* excess value of 10‰ fits the data for *modern* worldwide samples rather well (Fig. 4.3).

The deuterium excess parameter is primarily controlled by kinetic effects associated with evaporation of water at the surface of the oceans or inland and increases with an increase in the *moisture deficit* $(1 - h)$ of the oceanic air masses, where *h* is the relative humidity at the surface temperature of the water (Merlivat and Jouzel, 1979). As shown in Fig. 4.6, the isotopic composition of water vapor evaporating from a large water body will lie to the left of the meteoric water line (blue hexagon) following the fractionation given in equation 4.5. Evaporation drives the remaining water to higher δD and $\delta^{18}O$ values, with a $\delta D/\delta^{18}O$ slope of less than 8 (red circles in Fig. 4.6). The removal of water vapor with isotopic compositions that lie to the *left* of the GMWL results in the remaining water lying to the *right* of the meteoric water line. The extreme evaporation into dry air seen in the Sahara ephemeral lakes results is a *d* value as low as -120‰.

While removal of light water vapor will cause the remaining water body to shift to lower *d* excess values, the vapor itself will have high *d* excess values, and later condensation will result in precipitation with similarly high *d* excess values (blue circles in Fig. 4.6). Such a phenomenon is seen in the lake effect precipitation 'downwind' from the Great Lakes. Water vapor coming off the Great Lakes will lie to the left of the meteoric water line. When these air masses then cool as they migrate eastward, precipitation follows a slope 8 trend intersecting the water vapor composition. The combined $\delta^{18}O$ and δD values will be higher than the initial water vapor, but will have a similar *d* excess value. Winter precipitation in Michigan has *d* excess values in excess of 40‰ in the winter (Machavaram and Krishnamurthy, 1995).

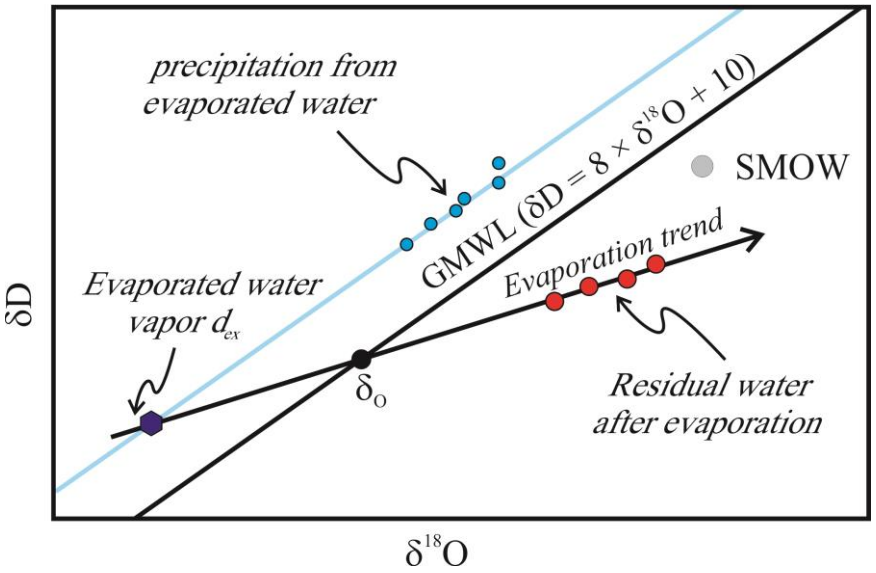

Fig. 4.6. Isotope effect of evaporation into dry air. The evaporated water is more strongly fractionated for oxygen relative to hydrogen compared to equilibrium fractionation. This is due to the larger mass difference between $H_2{}^{18}O$ (mass 20) and $H_2{}^{16}O$ (mass 18) *vs*. $HD^{16}O$ (mass 19) and $H_2{}^{16}O$ (mass 18). Condensation from the evaporated water will lie on a line with slope ~8 and intersecting the evaporated water vapor (source) value. The residual lake water following evaporation will lie to the right of the GMWL.

On a global scale, there is a profound seasonal effect on the *d* excess parameter for precipitation. The major driver for this variation appears to be variations in relative humidity of the sea surface rather than temperature (Pfahl and Sodemann, 2014). Figure 4.7 shows the excellent negative correlation between relative humidity and *d* excess, and also the annual variation in *d* excess. The deuterium excess value of 10‰ that characterizes the modern GMWL corresponds to a mean relative humidity over the oceans of 81%. The mean relative humidity of air masses over the oceans is about 10% lower in winter (colder air masses) than in summer, an effect that explains in part the seasonal shift from higher values of *d* in winter to lower values of *d* in summer precipitation over temperate continental regions. There is a difference of 10‰ in the deuterium excess parameter between meteoric waters that developed during glacial and interglacial periods (Harmon and Schwarcz, 1981). This latter difference reflects extreme differences in humidity over the oceans under glacial and interglacial conditions. In the

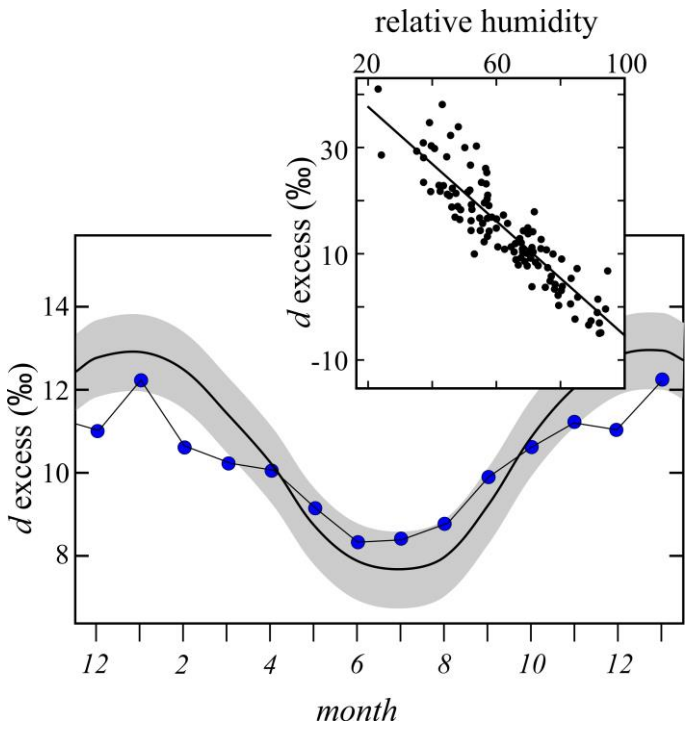

Fig. 4.7. Seasonal variation in the *d* excess value of meteoric water. The global *d* excess value is clearly related to relative humidity at the oceanic moisture source (inset). Blue spots are the northern hemispherically averaged *d* values. Modified from Pfahl and Sodemann (2014).

United States, the deuterium excess parameter varies strongly with geographic position, but is not explained by a single parameter. Instead it is related to different source air masses, differences in temperature, aridity and contribution from lakes and evapotranspiration (Fig. 4.8).

As mentioned above, LMWLs vary considerably around the earth in response to local and regional meteorological conditions. Dansgaard (1964) found that LMWLs in tropical and subtropical islands pass through SMOW (*i.e.* $d \sim 0$) according to the relationship

$$\delta D = 4.6(\pm 0.4)\delta^{18}O + 0.1(\pm 1.6) \qquad 4.7.$$

This relation develops if the bulk of such precipitation arises from condensation of vapor that is initially generated from rapid evaporation of ocean water. Data for certain other island stations fall off the trend in equation 4.7 because the islands are located on the equatorial side of the subtropical high pressure zone.

4.6 Evaporation and Condensation

Natural waters undergo evaporation in a variety of settings including clouds, large and small bodies of standing waters, soil, and respiratory sites in animals and plants. **Evaporation is a kinetic process**. The stable isotope fractionations associated with evaporation depend on a number of factors and can be surprisingly large. **Condensation, on the other hand, is generally considered to be an equilibrium process**. The fractionation factors attendant on condensation depend on temperature alone and consequently the isotopic systematics of condensation processes are relatively easy to treat mathematically. Knowledge of the isotopic effects associated with evaporation and condensation in air masses and in other reservoirs of water like flowing streams, plants, and lakes is fundamental to our understanding of the isotopic systematics of the hydrologic cycle.

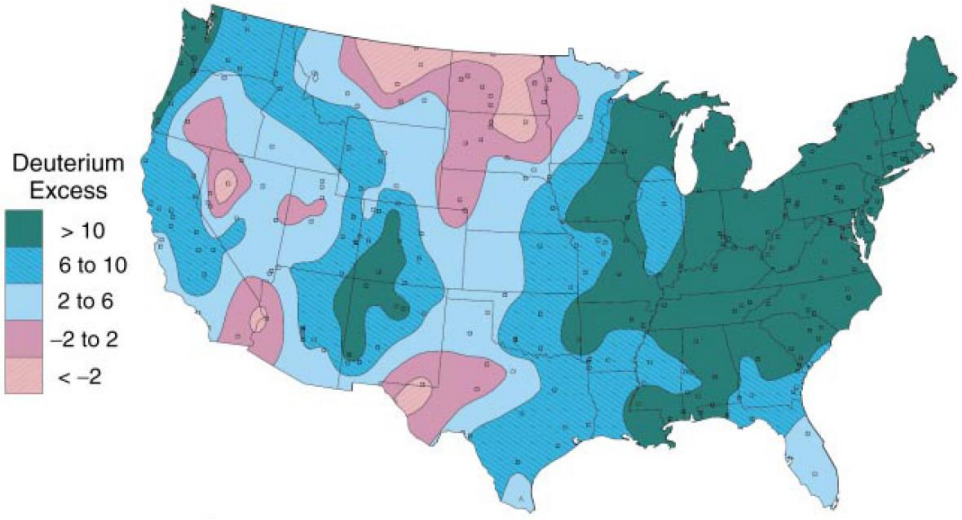

Fig. 4.8. Deuterium excess values of river waters from across the United States. There is a striking N-S gradient close to the Mississippi River. From Kendall and Coplen (2001).

4.6.1 Evaporation over oceans

The vapor pressures of the different isotopologues of water decrease in the order of increasing molecular weight: $H_2{}^{16}O > HD^{16}O \cong H_2{}^{17}O > H_2{}^{18}O$. In simple terms then, lighter isotopologues of water preferentially escape from the surface of the liquid into the vapor phase upon evaporation and the opposite occurs upon condensation, with heavier isotopologues preferentially condensing out and leaving a vapor phase relatively enriched in isotopically lighter water.

The explanation is fairly straightforward in a general sense. Isotopically lighter forms of H_2O species that constitute liquid water (monomers and various hydrogen-bonded clusters) have higher translational velocities than heavier forms, and are thus more likely to escape or *rattle free* from the surface of liquid water into the vapor phase. Evaporation is dominantly a unidirectional process when relative humidity is low, so that back isotopic exchange between departing vapor and remaining liquid is restricted. If the air above the ocean were to become saturated, then net evaporation would cease. At this point isotopic exchange between vapor and liquid would become a natural consequence of the dynamic processes of evaporation and condensation that take place at the interface of any liquid and vapor in equilibrium with each other. Such exchange would then rapidly force an equilibrium distribution of isotopes between the two phases. This process does *not* occur over the oceans.

Failure to attain *complete* or *equilibrium* isotopic exchange between vapor and liquid causes vapor above the oceans to be isotopically lighter than what would be expected for equilibrium. Measured oxygen isotope fractionations between ocean water and non-equilibrium vapor vary with temperature and relative humidity, but a typical value is $\alpha_{liquid\text{-}vapor} = 1.013$. That is, vapor over the oceans has a $\delta^{18}O$ value of about –13‰ instead of an equilibrium $\delta^{18}O$ value of about – 9‰ (Majoube, 1971). (In accordance with the idea of 'alpha' referring to equilibrium processes, the kinetic, non-equilibrium fractionation over the ocean might better be designated with an 'epsilon' terminology, such as $\varepsilon_{liquid\text{-}vapor} = 13‰$).

At this juncture we have no exact formulation for the difference of approximately 4 per mil between the observed kinetic fractionation between liquid water and water vapor ($\alpha_{l\text{-}v}$) and the equilibrium $\alpha_{l\text{-}v}$. During evaporation into unsaturated air, hydrogen and oxygen isotope fractionations depend not only on the vapor pressures of the different isotopologues of water, but also on the relative humidity of the air, turbulence in the liquid, and relative rates of diffusion of hydrogen and oxygen isotopes from deeper layers in the liquid (Craig and Gordon, 1965). Evaporation into a *vacuum* depends strongly on the relative diffusion rates of the different isotopologues of water, but that condition is vastly different from the case of evaporation of ocean water into air.

One can calculate *effective* fractionation factors that take into account estimates of relative diffusion rates (translational velocities) for the different isotopologues of the H_2O molecule, but these fractionation factors do not model well what is observed in nature. They overestimate the degree of kinetic fractionation. Actual diffusion rates are significantly lower than predicted on the basis of simple kinetic theory because the molecules in liquid water move as clusters, not as monomers. For example, the relative mass difference between $H_2{}^{18}O$ and $H_2{}^{16}O$ is 20/18 = 1.11. But if water is considered as a polymerized chain of H_2O molecules, then the relative mass difference between two chains, each consisting of (for example) 5 molecules, with one of the two chains containing an ^{18}O isotope, is only 92/90 = 1.02. Calculations using a 5 molecule chain as our parameter for kinetic diffusion gives a reasonable value for the fractionation between water and water vapor (see Dansgaard, 1964).

Measured $\delta^{18}O$ values of most vapor over the oceans are between −13 and −11‰, whereas equilibrium $\delta^{18}O$ values would be 3-4‰ more positive. The disequilibrium effect is less for hydrogen isotope fractionation because the difference in mass of the two hydrogen isotopologues of H_2O is smaller than the corresponding difference in the mass of the pertinent oxygen isotopologues (*i.e.*, HDO/H_2O; 19/18 *vs.* $H_2{}^{18}O/H_2{}^{16}O$; 20/18). The predicted lower sensitivity of the hydrogen isotopologues to diffusion effects is indeed observed in nature.

The departure from equilibrium in nature is maximum at latitudes of 18-26° (Fig. 4.9), where evaporation is highest and relative humidity is lowest (Craig and Gordon, 1965). Craig and Gordon (1965) proposed the following relation between the degree of disequilibrium evaporation and humidity:

$$\delta_l - \delta_v \approx \left[\left(1-\frac{1}{\alpha'}\right)(2-h)+\left(\frac{1}{\alpha'}-\frac{1}{\alpha}\right)\right]1000 \qquad 4.8,$$

where δ_l and δ_v are delta values of liquid water at the ocean surface and atmospheric vapor, respectively, h is the relative humidity, α is the equilibrium fractionation between liquid and vapor at a given temperature[3], and α' is the effective fractionation factor corrected for diffusion in the surface water. Note that when h = 1, equation 4.8 gives the equilibrium fractionation.

[3] Always note the *direction* that a fractionation factor is stated. In this case it is a liquid-vapor fractionation not a vapor-liquid fractionation, *i.e.*, $\alpha_{l\text{-}v}$, not $\alpha_{v\text{-}l}$

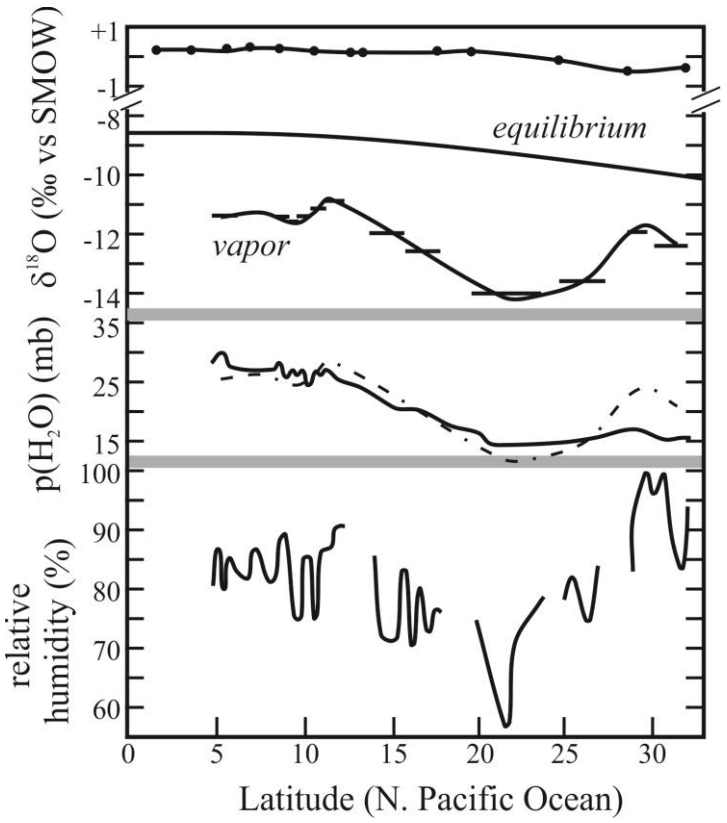

Fig. 4.9. Oxygen isotope variations of water vapor collected on N-S transect in the N. Atlantic Ocean. The top curve depicts $\delta^{18}O$ values of surface water. The curve labeled *equilibrium* is the calculated $\delta^{18}O$ value of vapor in equilibrium with the surface water at the appropriate temperature. The calculated equilibrium $\delta^{18}O_v$ values decrease with latitude due to decreasing temperature, however a much larger effect on the $\delta^{18}O$ values of water vapor is the relative humidity. The curve labeled $\delta^{18}O$ (vapor) is the measured $\delta^{18}O$ value of water vapor. The measured $\delta^{18}O$ values (repeated in this panel as dotted line to show form only) correlate well with measured $p(H_2O)$ and humidity, illustrating the non-equilibrium evaporation effect. Modified from Craig and Gordon, (1965).

4.6.2 Condensation and precipitation

It is generally assumed that condensation of water in a cloud is an equilibrium process. If condensation were allowed to take place in a closed system (a sealed box for example), then the weighted sum of the liquid and vapor at any time would always equal δ value equal to that of the initial vapor. For example, if the isotopic composition of the initial vapor $\delta^{18}O_{v,i}$ is -14.0‰ and the $\alpha_{l\text{-}v}$ = 1.00935 at 25°C, then the first droplet of liquid would have a composition of -4.78‰. Under equilibrium conditions $\delta^{18}O$ values of the liquid and vapor at any time in the condensation process are easily calculated from a material balance equation, for any assumed $\alpha_{l\text{-}v}$ value.

As an example we calculate values of $\delta^{18}O_l$ and $\delta^{18}O_v$ when the fraction of vapor *remaining* (*F*) is 0.4. The material (or mass) balance equation is

$$(F)\delta^{18}O_v + (1 - F)\delta^{18}O_l = \delta^{18}O_{total} \qquad 4.9.$$

The $\delta^{18}O_{total}$ value is the bulk oxygen isotope composition of our system and is equal to -14%, the $\delta^{18}O$ value of the initial vapor. Accordingly, the material balance equation for F = 0.4 is

$$(0.4)\delta^{18}O_v + (0.6)\delta^{18}O_l = -14.0 \qquad 4.10.$$

The relationship between the $\delta^{18}O$ values of liquid and vapor come from our α value, where at 25°C

$$\alpha_{l-v} = \frac{1000 + \delta^{18}O_l}{1000 + \delta^{18}O_v} = 1.00935 \qquad 4.11,$$

and rearranging terms

$$\delta^{18}O_l = (1.00935)(1000 + \delta^{18}O_v) - 1000 \qquad 4.12.$$

Combining equations 4.9 and 4.11, we solve for the delta values:

$$\delta^{18}O_v = -19.5‰ \quad \delta^{18}O_l = -10.3‰$$

As expected, $\delta^{18}O_v$ becomes increasingly lighter as the isotopically heavier liquid condenses and preferentially removes the heavy isotopologues of water. (Fig. 4.10). When *F* proceeds all the way to a value of 0 (all vapor is converted to liquid), the $\delta^{18}O$ value of the liquid equals that of the initial vapor, namely -14‰. The constant fractionation between δ_v and δ_l is maintained throughout the condensation process. Generalized equations relating δ_v and δ_l values to *F* at any point in the condensation process *at constant T* are

$$\delta_1 = \frac{\alpha\delta_{tot} + 1000F(\alpha - 1)}{\alpha(1 - F) + F} \qquad 4.13$$

and

$$\delta_v = \delta_l - 1000(\alpha - 1) \qquad 4.14.$$

These equations are linear on a plot of δ versus *F* (δ_{v*} and δ_{c*} in Fig. 4.10).

In fact the process of condensation is never isothermal. Condensation of a parcel of air *requires* cooling, which means that α must increase as the process proceeds. The isotopic trajectory during condensation with falling temperature is shown qualitatively by the dashed line in Figure 4.10. The non-isothermal model is a better approximation to nature, but is still not a valid model for condensation and precipitation that occurs in clouds because the real system is not 'closed'. Water leaves the cloud and no longer participates in any isotopic exchange. The closed-system model is presented here as an end-member case for the sake of completeness and because it illustrates the mass balance principle. In addition, it provides examples of simple mathematical manipulations that are used frequently in stable isotope geochemistry.

4.6.3 Condensation: open system (Rayleigh) isotopic fractionation

Open system Rayleigh fractionation is the other end member fractionation model that complements the closed system batch fractionation model described above. In the batch fractionation model, the condensed liquid and remaining vapor are always in contact with each other and in exchange equilibrium. Under Rayleigh conditions, condensate is continuously removed from the system as it is produced, thus prohibiting

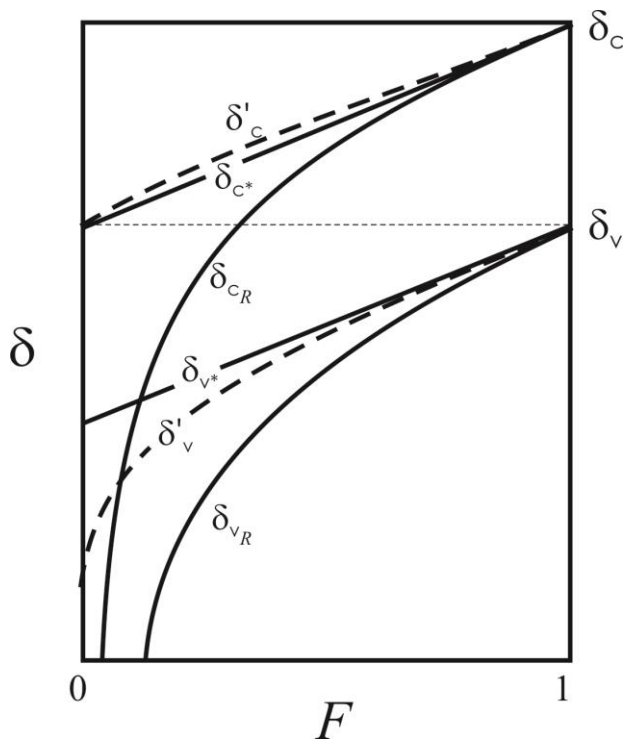

Fig. 4.10. Correlation between isotopic composition and fraction of vapor remaining during equilibrium isothermal condensation of a liquid from vapor. At F = 1, there is only vapor, while F = 0 represents all liquid and no vapor. The curves δ_v* and δ_c* are the trajectories of vapor and condensate for equilibrium isothermal processes. The difference between the two is the equilibrium fractionation $1000 ln\alpha_{l\text{-}v}$. The curves δ'_v and δ'_c are vapor and condensate trajectories for condensation during cooling. Curves $\delta_{v,R}$ and $\delta_{c,R}$ are vapor and condensate trajectories for condensation under Rayleigh conditions. After Dansgaard, (1964).

back exchange between the two phases after separation. Each increment of liquid condenses in isotopic equilibrium with the parent vapor, but is then forever removed from the system (*i.e.*, the cloud) as precipitation. Because 'heavy' water is continuously lost, the δ value of remaining vapor becomes progressively more negative with increasing degree of condensation and the δ value of newly formed condensate becomes correspondingly lower and lower by an amount dictated by the fractionation factor at the temperature of condensation.

Rayleigh fractionation in an air mass can lead to very large depletions of the heavy isotopes in precipitation, particularly after the air mass has lost most of its vapor. Mathematically, as the fraction of vapor remaining approaches zero, the δ value of the vapor approaches the limiting value of -1000‰. Very low δD values of water vapor at very high altitudes are an example of an effective Rayleigh fractionation process. From observations made over many years, it appears that gross isotopic variations in precipitation on Earth are explained for the most part by Rayleigh fractionation in air masses. Nonetheless, we are far from understanding these processes in detail. For further information on the Rayleigh equation and models developed to explain MWLs, the student is referred to the following articles: (Jouzel and Merlivat, 1984; Gat, 1996; Criss, 1999; Galewsky et al., 2016).

The Rayleigh equation is used to model many naturally occurring equilibrium processes other than precipitation in which a newly-formed phase is removed or isolated from the 'parent' from which it forms. Examples include crystals precipitating from a magma, decarbonation in a metamorphic system, and volcanic degassing to name a few. In modeling precipitation, a constant fractionation factor is normally used despite the obvious fact that temperatures of condensation in real systems must be decreasing (see Dansgaard, 1964 for a more detailed discussion). For the stable isotope relations attendant on equilibrium precipitation of liquid water from water vapor in clouds, the relevant Rayleigh expression *with constant* α is

$$\left(\frac{R}{R_i}\right) = F^{\alpha - 1} \qquad 4.15,$$

where R = the isotopic ratio (D/H) or ($^{18}O/^{16}O$), α is the fractionation factor *between liquid and vapor*, F is the fraction of vapor remaining, and i stands for *initial* ratio[4]. In the δ-notation, equation 4.15 reduces to

$$\delta_v = \left[\delta_{v,i} + 1000\right] F^{(\alpha - 1)} - 1000 \qquad 4.16,$$

where δ_v is the isotopic composition of the vapor for a given value of F, and $\delta_{v,i}$ is the isotopic composition of the initial vapor.

The corresponding equation for liquid[5] water condensed *at this value of F* is

$$\delta^{18}O_l = \alpha(\delta^{18}O_v + 1000) - 1000 \qquad 4.17.$$

The integrated δ value of the precipitation at any F is determined from mass balance using equation 4.9. The trajectories of vapor and liquid undergoing Rayleigh fractionation are shown in Fig. 4.10 as $\delta_{v,R}$ and $\delta_{c,R}$.

Temperatures of condensation in real air masses are not constant, and the α value is continuously changing. The Rayleigh equation cannot be integrated with varying α values unless the relationship between α (a function of temperature) and F is known. To address this problem, Dansgaard (1964) proposed the following expressions to model Rayleigh fractionation under conditions of varying temperature

$$\delta_l = \frac{\alpha}{\alpha_i}(\delta_i + 1000)F^{(\alpha_m - 1)} - 1000 \qquad 4.18$$

and

$$\delta_v = \frac{1}{\alpha_i}(\delta_i + 1000)F^{(\alpha_m - 1)} - 1000 \qquad 4.19,$$

where α, α_i and α_m refer to the momentary condensation temperature at T, at the initial temperature T_i, and at $(T + T_i)/2$, respectively. A more quantitative treatment of Rayleigh fractionation with changing temperatures can be found in Rowley and Garzione (2007).

Real air masses experience a series of precipitation cycles during which both the vapor remaining and the precipitation become progressively lighter. A cartoon of meteoric water precipitating from an air mass generated over ocean water is given in Figure 4.11. The water vapor over the ocean has a $\delta^{18}O$ value of about -13‰. Some vapor condenses, and rains out with a $\delta^{18}O$ value of -5‰, 8 per mil heavier than the vapor. The

[4] See Criss (1999, pg. 106) for a derivation of the Rayleigh equation.

[5] Strictly speaking, the Rayleigh condensation model crudely explains the slope of 8 for the MWL, but only if the condensate is liquid. Slopes < 8 obtain when ice is the condensate.

removal of this relatively heavy water leaves behind vapor with a lower $\delta^{18}O$ value of -15‰, so that the next cycle of rainout has a $\delta^{18}O$ of –7‰ (for example) instead of –5‰. As the air mass moves farther inland, and more and more precipitation cycles occur, the $\delta^{18}O$ values of vapor and condensate become progressively more negative, effectively following the Rayleigh curves of Figure 4.10. Remember that as the temperature of condensation decreases, the fractionation *increases*.

4.7. Factors Controlling the Isotopic Composition of Precipitation.

There are a number of factors that control the oxygen and hydrogen isotope composition of meteoric water as outlined in the following sections. Isotopic variations occur over long time periods, between seasons, and even within a single storm. Isotopic gradients exist with latitude and altitude and as a function of the amount of precipitation. An excellent database of existing stable isotope analyses for various meteoric waters is http://wateriso.utah.edu/waterisotopes/.

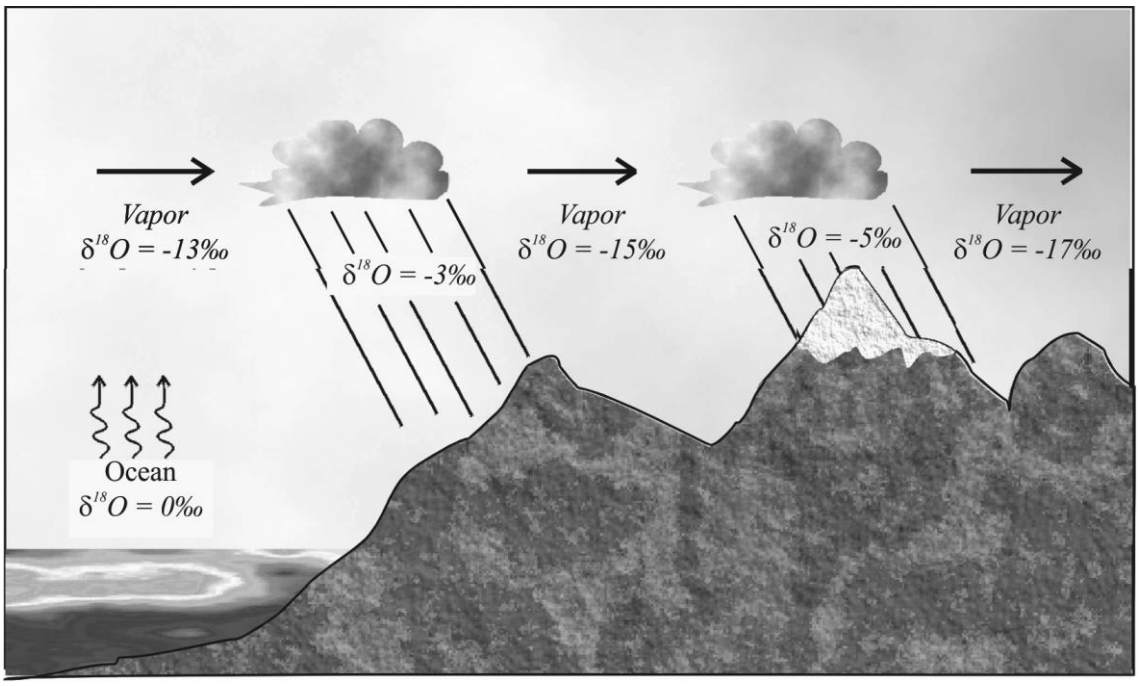

Fig. 4.11. Schematic of distillation effect for meteoric water. A large kinetic fractionation occurs between ocean and vapor. Liquid condensing in clouds is in equilibrium with vapor and is heavier than coexisting vapor. Remaining vapor becomes progressively lighter, leading to lower $\delta^{18}O$ and δD values farther from the water source.

4.7.1 Temperature

Surface temperature, especially at high latitudes where precipitation forms near the ground surface, is correlated with the isotopic composition of meteoric water. This phenomenon is easily explained by the temperature dependence on $\alpha_{l\text{-}v}$. Values of $1000\ln\alpha_{l\text{-}v}$ for H and O vary strongly with temperature, but the ratio of the two has a nearly constant value of 8 (Fig. 4.3). **The dominant control on the isotopic composition of precipitation from a given air mass is the fraction of vapor**

remaining. By the time an airmass reaches a region located at high latitudes, high altitudes or significantly inland it has generally become significantly colder and cannot hold as much water as it held or could have held in warmer regions that are closer to the ocean or at lower elevations and latitudes. The loss of the heavy isotope to the liquid lowers the isotopic composition of the remaining vapor and the effect becomes larger at low temperature because the fractionations are larger. Thus temperature is indeed a control on the isotopic compositions of local meteoric water, but mainly in the sense that it controls the amount of water that a given air mass has lost. In fact, the apparent controlling factors or effects on the isotopic composition of meteoric water that will be discussed below are merely different expressions of this same thing.

Dansgaard (1964) first recognized the good correlation between the weighted mean isotopic composition of precipitation *in temperate climates* and mean annual surface temperature at the collection site. This correlation, shown in Figure 4.12, provides the basis for many paleoclimate studies where analyses are made of proxies for local precipitation in a given area in the past. Since this early publication, the correlation has been refined through thousands of analyses of meteoric water from all over the world. Dansgaard's *global* correlations between $\delta^{18}O$, δD and mean annual surface temperature are

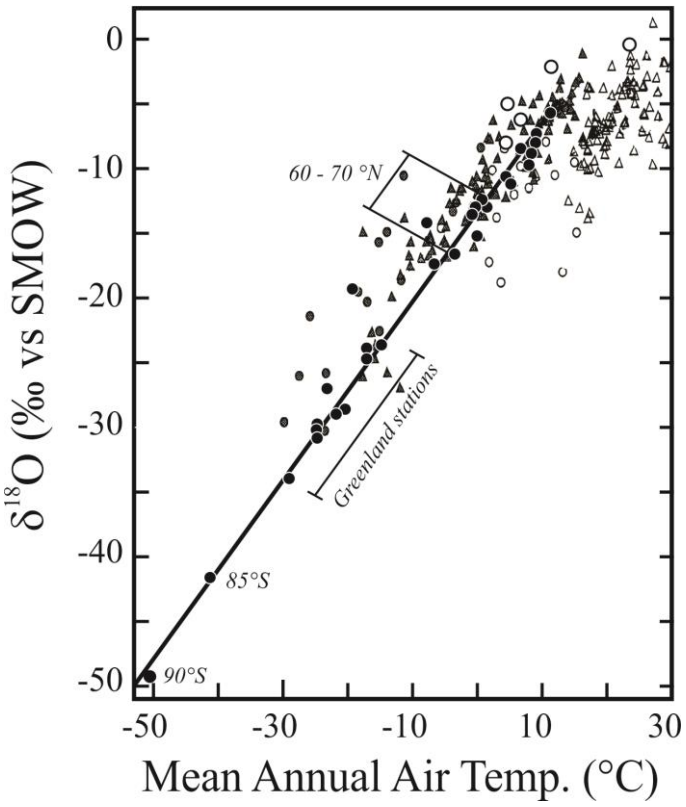

Fig. 4.12. Effect of mean annual air temperature on the oxygen isotope composition of meteoric water. The effect is largest, and most linear at high latitudes, where condensation occurs close to the land surface. Circles are annual data from Dansgaard (1964); Open diamonds are summer, closed diamonds are winter data from Fricke and O'Neil (1999).

$$\delta^{18}O = 0.69T_{average} - 13.6 \qquad 4.20$$

and

$$\delta D = 5.6T_{average} - 100 \qquad 4.21.$$

The temperature coefficient of $\left(\frac{d\delta^{18}O}{dT}\right) = 0.69$ is in good agreement with predictions made from experimental and theoretical considerations. The relationship is strongest at high latitudes with far more scatter at mid- and equatorial regions (Fig. 4.12). Clearly the temperature coefficient varies from place to place in response to a number of meteorological factors. For meaningful paleoclimate reconstructions in a given region, attempts must be made to evaluate this temperature coefficient in that

region at the time of interest (Fricke and O'Neil, 1999). The combination of Rayleigh fractionation and temperature effects result in a strong latitudinal gradient in $\delta^{18}O$ and δD values of meteoric water. As an extreme example of the effect of latitude and temperature (not independent parameters) on the isotopic composition of precipitation, δD and $\delta^{18}O$ values of snow samples from the South Pole are as low as –495‰ and –62.8‰, respectively (Aldaz and Deutsch, 1967; Jouzel et al., 1987).

4.7.2 Distance or continentality effect

Precipitation becomes isotopically lighter as the parent air masses move farther from their sources and over the continents simply because they have undergone more cycles of precipitation and *F* approaches ever-lower values. The continentality effect is obviously associated with the temperature decrease (ΔT) between the source of atmospheric vapor and point of precipitation. The ΔT parameter is logically tied to the seasons, such that the continentality effect is greater during the colder months. In Eurasia, $\delta^{18}O$ values of meteoric water drop very regularly with distance eastward, the effect being more pronounced in wintertime (about –3‰/1000 km) than in summertime (about –1.5‰/1000 km). In summertime, the continentality effect is lower because temperature (and hence the α value) differences are less and because recycling of precipitation by evapotranspiration is more intense in the summer. In some cases, the continentality effect is minimal because there is strong recycling of moisture *via* evaporation from the same region as precipitation. The effect is particularly strong in the Amazon basin, where intense evaporation and reprecipitation occurs over the entire region and the inland gradient is only 0.75‰/1000 km (Salati et al., 1979).

4.7.3 Latitude effect

$\delta^{18}O$ and δD values of precipitation decrease with increasing latitude again because the degree of rainout of air masses increases and temperatures decrease with latitude. While decreases in delta values with latitude are regular, they are by no means linear as many topographic and local meteorological conditions are operative as well in the process of rainout. Global scale circulation patterns also differ over oceans and continents as well as over eastern vs. western seaboards. The gross magnitude of the latitude effect in mid-latitude regions is about – 0.5‰ per degree of latitude. (Fig. 4.13).

4.7.4 Altitude effect

The isotopic composition of water becomes lighter with increasing altitude. As an air mass is deflected upward by a mountain, it decompresses, cools adiabatically, and more rainout occurs. The percentage of vapor remaining in the air mass will decrease rapidly if the relief is high. In fact, topographic relief has an intensely strong effect on the isotopic composition of the precipitation.

Both continentality and altitude effects are illustrated nicely by isotopic compositions of precipitation falling in and around the Sierra Nevada Mountains in western South America. In this region, where prevailing winds are easterly, $\delta^{18}O$ values of precipitation drop slowly (about – 1‰/1000 km) as air masses travel westward across the Amazon basin (the continentality effect), but drop rapidly to about – 0.2‰/100m as the remaining atmospheric moisture is carried up the Andes (the altitude effect). Poage and Chamberlain (2001) compiled data from many investigations of the altitude effect

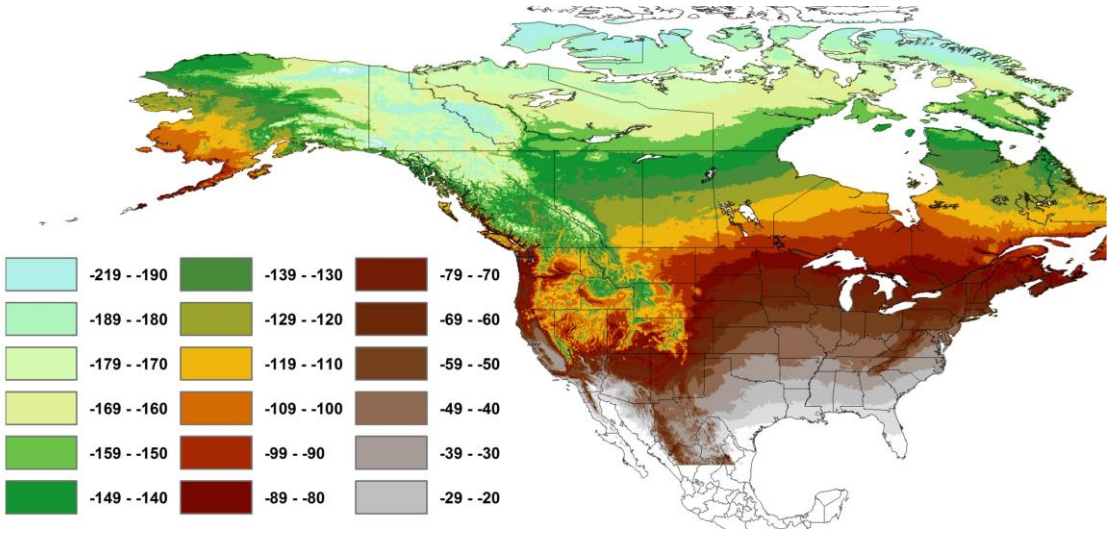

Fig. 4.13. Contours of hydrogen isotope composition of annual average precipitation. There is a regular lowering in the δD values of precipitation with latitude with regional orographic effects superimposed. Modified from Meehan *et al.*(2004).

and concluded that a gradient of –0.26 ‰/100 m characterizes the effect at most places in the world for elevations up to about 5000 m (Fig. 4.14). Numerous authors have used the very strong altitude effect as the basis for determining paleoaltitudes (see Reviews in Mineralogy v. 66 Paleoaltimetry: Geochemical and Thermodynamic Approaches for an overview of applications).

4.7.5 Amount effect

The amount effect is a negative correlation between mean δ values and amount of monthly precipitation **in tropical regions**. Note that in higher latitude regions, this negative correlation disappears or can even show a weak positive correlation (Kendall and Coplen, 2001). For the tropical stations, the δ values of rain falling at a given tropical station are high in months with little rain and low during the rainy season (Fig. 4.15). In accordance with principles already established, the more rainout that occurs from a given air mass, the lower the delta value of subsequent precipitation. But the behavior of

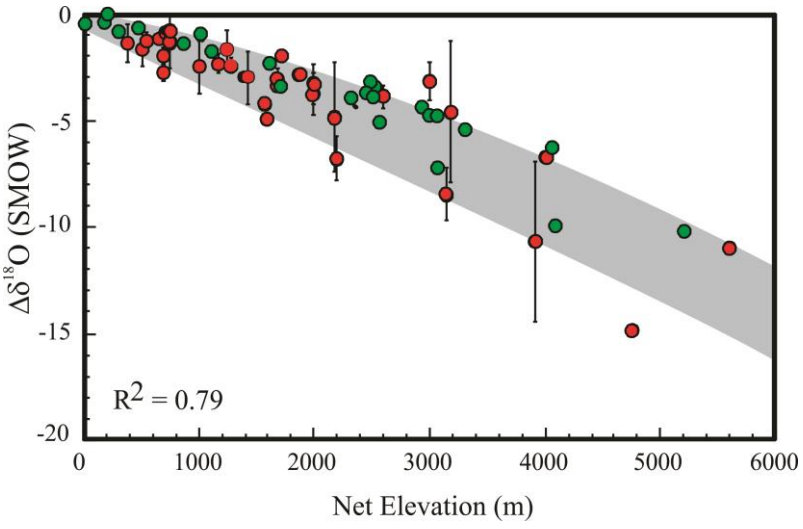

Fig. 4.14. Changes in the $\delta^{18}O$ values of meteoric water relative to the local sea level $\delta^{18}O$ values (hence the $\Delta\delta^{18}O$ terminology). Data are Poage and Chamberlain (red circles, 2001) and Rowley (green circles, 2007).

water in convecting air masses is very complicated and explanations for the amount effect are given only in qualitative terms. There are four processes associated with convecting air mass systems that should be considered in attempts to understand the amount effect: (1) as air rises and cools to saturation, condensate falls through other droplets that formed below, and can exchange with them, (2) the droplets can grow larger by taking on more vapor as they fall, (3) upon exiting the cloud the droplets can evaporate into dry air, and (4) droplets can exchange with vapor present in unsaturated air below the cloud.

When droplets evaporate into very dry air, isotopically light molecules vaporize preferentially and with a kinetic isotope effect. The liquid that reaches the surface in gentle rains will thus be relatively heavy. The lower the humidity the greater is this effect. At times when air is more humid, the probability of encounters between falling droplets and vapor molecules in the air increases and exchange can occur between them. As a result of such exchange reactions, the liquid becomes richer in the heavier isotopes simply because of the positive direction of the isotopic fractionation between liquid and vapor. Thus the two processes of evaporation and exchange explain the enrichment of heavy isotopes in gentle tropical rain. These same processes must *not* be operating during periods of intense tropical rainfall. At those times, rapidly ascending air masses result in deep cooling of the air mass, massive rainout, low values of *F*, and isotopically light precipitation. The $\delta^{18}O$ values of vapor over the tropical oceans are about –13 to -11‰ and that mean $\delta^{18}O$ values of precipitation in the rainy months in tropical regions approach such values. Light isotope ratios of precipitation from hurricanes attest to the efficiency of large 'fractionation chambers' in these massive storms (Gedzelman et al., 2003).

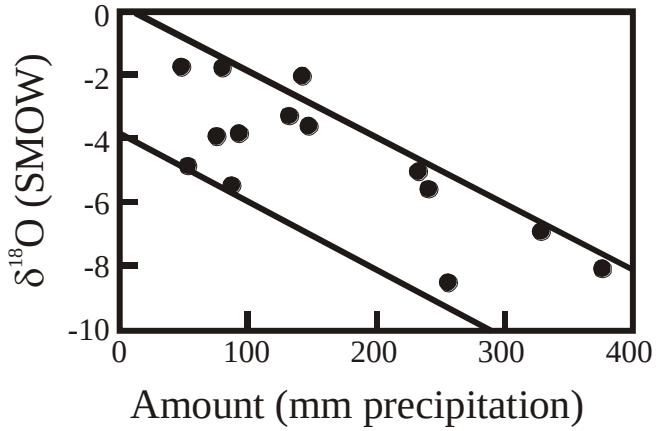

Fig. 4.15. Amount effect at Binza, Congo. mm precipitation vs. $\delta^{18}O$ value. After Dansgaard, (1964),

Isotopic effects associated with the processes undergone by water droplets falling through saturated or dry air deserve further consideration. When the amount of precipitation is low, the degree of cooling below the cloud mass is minimal. Under these conditions, the below-cloud air temperature can be relatively high and significant evaporation will take place. Evaporation is obviously most pronounced when rainwater falls through dry, hot air. The frequently beautiful natural phenomenon called virga (rain that never arrives to the ground) develops under these conditions.

A water droplet falling through saturated air will undergo no evaporation, but will exchange with vapor in the surrounding air. At saturation, the rate of evaporation of a falling water drop equals the rate of condensation on the surface of the drop. Many studies have been made of the equilibration time between a raindrop and the vapor in its environment. Using HDO as a tracer, (Friedman et al., 1962) determined that the rates of

exchange between droplets and vapor are rapid for all but the largest raindrops. The interplay between evaporation and exchange is obviously complex. It is natural to assume that rates of evaporation increase with a decrease in humidity, but there is a feedback mechanism that limits the degrees of evaporation and exchange processes. Large droplets fall rapidly and thus have a greater tendency to evaporate than do small droplets. But, evaporation causes a diminution in the size of the droplet which, in turn, reduces its rate of descent and therefore, the degree of evaporation. At the same time, because the water droplet is falling more slowly, it has more time to exchange with the water vapor in the air. A rigorous overview of the atmospheric physics of water vapor and how it controls the isotopic composition of water vapor is given in a recent paper by Galewsky *et al.* (2016).

4.7.6 Seasonal effects

Many environmental parameters change with the seasons. Seasonal changes in temperature clearly affect the isotopic composition of precipitation. In fact all the factors discussed above are influenced by seasonal change. Both the continentality effect and the deuterium excess factor are higher in winter than in summer for reasons explained above. The amount of rain in one season can be far more than in others, so that the amount effect can have a major effect on the isotopic composition of precipitation.

Differences in stable isotope compositions between summer and winter precipitation are seen all over the world. There are three primary processes that contribute to this effect (Gat, 1996). The most pronounced of these is almost certainly related to seasonal temperature variations. The Rayleigh effect is more pronounced at lower temperatures, explaining the low isotope values in winter. The seasonal effect tends to be more pronounced with increasing latitude (Fig. 4.16). Evapotranspiration is also higher in summer. The return of moisture to the atmosphere by evapotranspiration will reduce the 'distance' or 'continentality' effect. Finally, different moisture sources in summer and winter will affect the isotopic composition of precipitation. For example, in New Mexico, masses carrying winter precipitation originate over the Pacific Ocean and approach New Mexico from the west, while those carrying monsoonal rains in the summer originate in either the Gulf of Mexico or the Gulf of California and approach the area from the south and east. In St. Louis, there is a regular seasonal variation in the $\delta^{18}O$ values of precipitation. Criss (1999) proposed that this seasonality is related to the annual migration of the Gulf Stream, with different sources of precipitation being tapped in summer and winter. There are a number of additional minor complications that can arise with seasonal change and the reader is referred to Dansgaard (1964) and Criss (1999) for further details on seasonal effects.

The *d* excess values also change with season. Seasonal air temperature and humidity variations at the ocean source of precipitation will result in higher *d* excess values in the winter months. In cold climates, precipitation of snow rather than water will affect the evaporation of falling raindrops, which will also contribute to higher *d* excess values in winter (Gat, 1996).

4.8 Groundwater

Combined hydrogen and oxygen isotopic data provide us with a unique geochemical tool for evaluating the sources and flow paths of groundwaters. In most

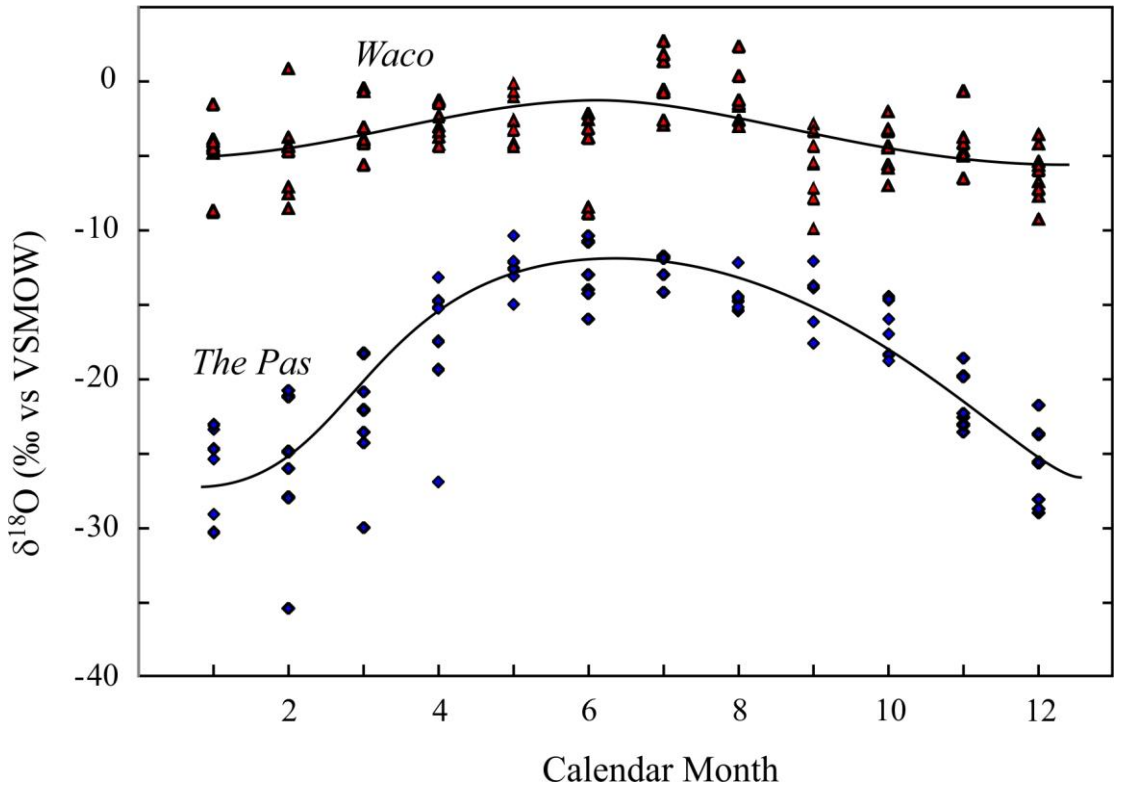

Fig. 4.16. Compilation of average monthly precipitation over a number of years for Waco Texas and The Pas, Manitoba. Larger seasonal variations are seen at the more northerly site, due to a combination of larger seasonal temperature variations and distance from source. Data from GNIP (https://nucleus.iaea.org/wiser/gnip.php).

cases, isotopic compositions of groundwaters represent the average isotopic compositions of precipitation that fell relatively recently in the local recharge areas. In some areas, water in deep aquifers can have isotopic compositions that are completely different from those of modern precipitation and may provide important paleoclimate information (e.g., Jasechko et al., 2015). Sometimes this difference is a result of recharge regions being very distant from the collection site, but commonly such waters are very old and were trapped in the aquifer when local climatic conditions were very different, as in the Pleistocene.

In areas of high topographic relief or those close to rivers fed from higher altitudes, groundwaters are often a mixture of local precipitation and distal (high altitude) waters with much lower $\delta^{18}O$ values. These differences can be exploited nicely in environmental and hydrological studies. For example, groundwater pumping for domestic usage in the region of Sacramento has lowered the head in the region and induced flow of water into that system from the nearby Sacramento and American rivers whose sources lie high in the Sierra Nevada Mountains. Unperturbed groundwaters there have $\delta^{18}O$ values of about −7‰ whereas the $\delta^{18}O$ values of the two rivers are about −11‰. With such a sharp contrast in isotopic compositions, it is easy to monitor the extent of infiltration of the river waters into this groundwater system. A $\delta^{18}O$ contour map of the

region shows a clear gradient in $\delta^{18}O$ values from –7‰ for waters sampled far from the rivers to –10.5‰ for waters sampled closer to the rivers (Criss and Davisson, 1996).

Sources and flow paths of groundwaters can be traced on very large scales in major aquifer systems. A remarkable example is provided by groundwater that discharges from natural springs and artesian wells in central Missouri. Stable isotope analyses of all these waters lie on the MWL so the waters were not altered isotopically during their passage from recharge area to discharge area (Fig. 4.17). The freshwater springs have $\delta^{18}O$ values of about –7‰ and δD values of about –50‰, typical of modern precipitation in the region. Springs with higher salinities have $\delta^{18}O$ and δD values as low as -15‰ and -108‰, respectively. These low-$\delta^{18}O$ waters most likely originated at high elevations in the Front Range of Colorado and traveled in the Western Plains Aquifer system to the central lowlands of Missouri, a distance of more than 1000 km (Banner et al., 1989; Musgrove and Banner, 1993). The high salinity of these waters occurred during passage through the Permian salt deposits in Kansas, without concomitant isotopic exchange with the enclosing rocks. Knowing that the Front Range was uplifted at about 65 Ma, flow rates in this system are at least 0.015 m/y, a value that is compatible with model flow rates calculated independently. Stable isotope data can be very useful in understanding origins and flow patterns of large aquifer systems and in developing generalized models for such systems.

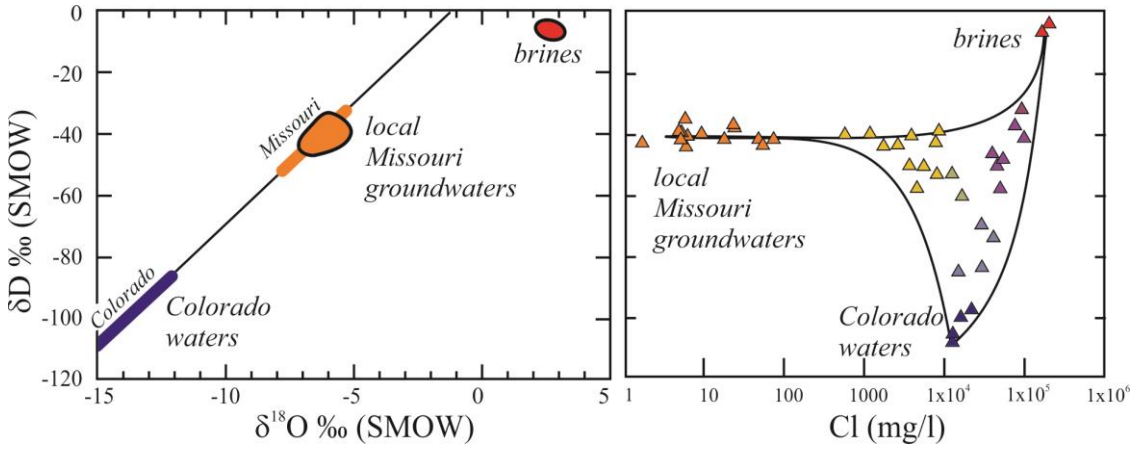

Fig. 4.17. Example of groundwater mixing from mid-continent of the United States. Three distinct waters can be identified; a) local Missouri groundwaters (orange), distal waters sourced from the Rocky Mountains with low δD values and moderate salinities (blue) and brines with high salinities and δD values (red). Groundwaters plot in the mixing field of δD vs chlorinity $1/[Cl^-]$ within the three endmembers. After Musgrove and Banner (1993).

4.9 Geothermal Systems

Geothermal fields exist in volcanic regions all over the world. Some are exploited for geothermal energy and all hold the fascination of scientists and laymen alike. A well-defined body of magma has been identified under the system at Yellowstone National Park and exotic chemical compositions characterize the waters of many systems in the world. It is understandable that many early workers believed that geothermal waters contained a significant component of primitive magmatic fluid whose components had never seen the surface of the Earth. Such a fluid is called *juvenile water* and the quest to

identify juvenile water occupied the research activities of many leading scientists in the first half of the twentieth century. The origin of geothermal fluids was determined unambiguously by stable isotope measurements and remains one of the crowning achievements of the discipline. Friedman (1953) first recognized the dominance of

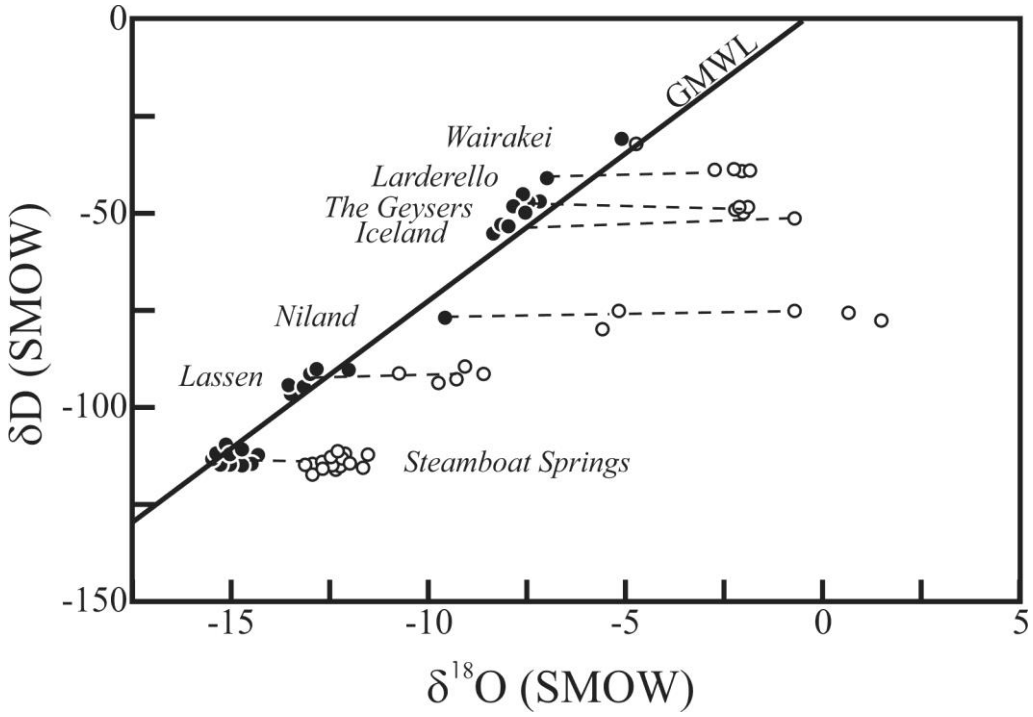

Fig. 4.18. δD-δ^{18}O values for geothermal waters (open circles) and equivalent local meteoric waters (filled circles). The δD values of the geothermal waters are the same as the local meteoric water, clearly identifying their origin. The δ^{18}O values of the geothermal waters, on the other hand, are shifted to higher δ^{18}O values, consistent with a meteoric source that has been modified by high temperature interaction with the host rock. After Craig (1963).

meteoric water in these fluids by noting that δD values of certain hot springs were very similar to those of local meteoric waters. A full understanding of the origin of the aqueous component of these fluids came through combined hydrogen and oxygen measurements by Craig *et al*. (1963) who showed that δD values of geothermal waters are nearly identical to those of the local meteoric water, while the δ^{18}O values are usually shifted (the *^{18}O-shift*) to more positive values (Fig. 4.18). The important conclusion was drawn that geothermal waters all over the world are dominated by local meteoric waters. Juvenile waters, if present at all, cannot constitute more than about 1% of these fluids.

The modifications to the oxygen, but not hydrogen isotope values of meteoric water can be understood in terms of hydrothermal interaction at depth. Volcanic terranes are riddled with cracks and fissures. Precipitation easily enters the ground through these cracks and descends to significant depth where it interacts with hot rocks. As a result of water/rock interactions, isotopes are exchanged and chemical constituents are taken into solution. The evolved fluids ascend to the surface in convection systems that are numerous and varied in geothermal fields.

Oxygen in descending meteoric waters undergoes exchange reactions with crystalline igneous rocks at depth and other rocks (often carbonates) that the fluid encounters on its journey back to the surface. Because rocks have very high $\delta^{18}O$ values relative to the negative $\delta^{18}O$ values of meteoric waters, high temperature interaction will *raise* the $\delta^{18}O$ values of the water and *lower* the $\delta^{18}O$ value of the rock. In contrast, hydrogen isotope compositions of neutral[6] geothermal waters are not different from those of local precipitation. This observation is explained by the simple fact that there is very little hydrogen in igneous rocks and none in carbonate rocks. There is simply no reservoir of hydrogen with which the water can exchange. The concept of fluid-rock ratios and high temperature isotopic exchange between rocks and fluids will be considered in more detail in Chapters 11 and 12.

4.10. Basinal Brines and Formation Waters

Large sedimentary basins host old, highly saline waters called *basinal brines* or *formation waters*, if associated with oil. These brines are of particular interest because they are commonly encountered in regions hosting oil or economically important ore deposits. These fluids share a number of characteristics: (1) they are commonly found at depths between 500 and 3700m, (2) the reservoir rocks are of marine origin, and (3) salinities range from 5 to 30‰. Given the host rock and high salinities, it is natural to conclude that such fluids have a marine origin, and are simply *connate* waters trapped during sedimentation. But such is not the case. The scientific literature is replete with studies of the origin of these important natural fluids and stable isotope analyses have played a major role in understanding them. Isotopic analyses have been made of formation waters from California, the Gulf Coast, and the Paris Basin and brines from the Illinois, Michigan, Delaware, and Alberta basins among others. $\delta^{18}O$ and δD values of these fluids covary in a systematic way (Fig. 4.19). Typically data for the lowest salinity and lowest temperature fluids plot near the LMWL, and there is a systematic, though scattered, increase in both $\delta^{18}O$ and δD values with increasing salinity and temperature. Because of significant scatter in the data initially published for brines from mid-latitude basins, there was some doubt about the connection of such brines to locally derived meteoric water. Such doubts were removed by the publication of data for brines from the high-latitude Alberta basin (Hitchon and Friedman, 1969). In Alberta the light isotopic compositions of local meteoric waters provide strong contrast with the isotopic compositions of marine components to the brines. At least 30% of the water in Alberta brines is meteoric water and the other component(s) may be marine waters that were diagenetically altered.

The increase in $\delta^{18}O$ values and salinity of basinal brines with temperature is due primarily to the effect of temperature on the rate or extent of oxygen isotope and chemical exchange between water and enclosing rocks. Sedimentary rocks have very high $\delta^{18}O$ values, typically 20-30‰, and the main reservoir of oxygen in these systems resides in the rock. Therefore, for reasons explained above, the water becomes enriched in ^{18}O as a result of exchange reactions with the rocks. Increase in evaporation with

[6] Some hydrothermal waters are acidic and δD values of such waters are normally more positive than those of local meteoric waters. This effect arises because of the isotopic properties of the H_3O^+ ion.

increase in temperature may also play a role in this ^{18}O enrichment process.

The increase in δD values of basinal brines with increase in temperature is less well understood. Possible explanations include (1) exchange with hydrous minerals, because D concentrates in water relative to minerals, (2) exchange reactions with or loss

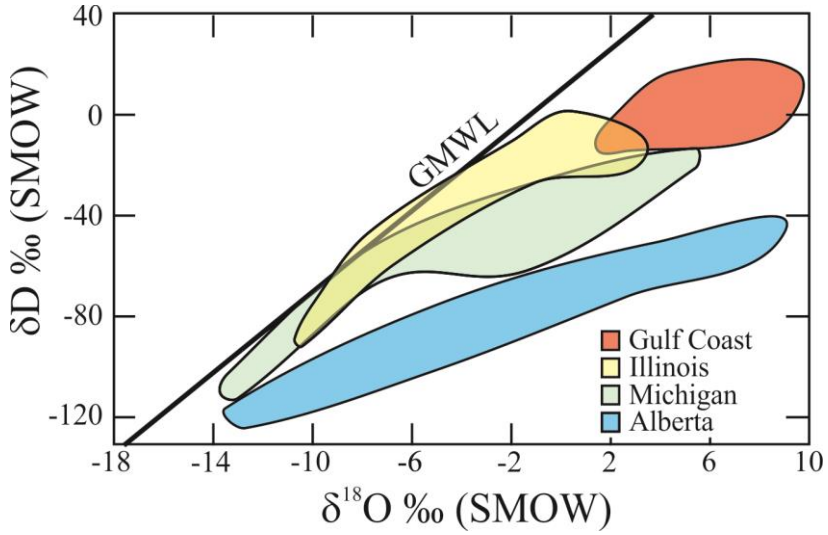

Fig. 4.19. $\delta^{18}O$–δD values of basinal brines. The combined delta values track back to those of local meteoric water. The most saline brines are generally those with the highest combined $\delta^{18}O$-δD values. After Clayton *et al.*, (1966).

of H-bearing gases like H_2S, CH_4 or H_2 because D concentrates in water relative to these gases, and (3) membrane filtration because isotopically lighter water is preferentially squeezed out of sediments when they are compacted (Coplen and Hanshaw, 1973).

In summary, the following explanations for the stable isotope systematics of basinal brines have been proposed:

1. With the passage of time, original connate waters were flushed away by meteoric waters that entered the system. In addition to this flushing process, water/rock interactions altered the chemical and isotopic compositions of the fluids (Clayton et al., 1966).

2. The original marine waters underwent evaporation and diagenetic alterations before being trapped and provide one component of a 2-component system. The other component is locally derived meteoric water whose isotopic composition could vary with time (Hitchon and Friedman, 1969).

3. Basinal brines are mixtures of meteoric water and evolved seawaters. One component brine develops from the release of water of crystallization in gypsum.

4. Basinal brines developed early during extensive evaporation of seawater. Under certain conditions of humidity and chemical composition of the evaporating brine, the combined δD-$\delta^{18}O$ values define a *hook*, such that the data *fall back* on lines of various slopes that are characteristic of those measured for basinal brines. Meteoric water could have entered the system with the passage of time (Knauth and Beeunas, 1986).

5. The present brines are mixtures of several components, one of which is meteoric water. The other components are relatively unaltered sea water and brines of different degrees of evolution from seawater (Fontes and Matray, 1993).

These explanations are basin specific but certain features, most notably the involvement of meteoric water and an evolved marine component, are common to brines in all basins. A proper understanding of the stable isotope systematics and evolution of basinal brines must include a careful consideration of the chemical compositions of the brines.

4.11 Glacial Ice

At various times in the history of our planet, including the present, glacial ice has been an important reservoir of fresh water on Earth. Because glaciers form at high latitudes and altitudes, they are isotopically unusually light. During periods of maximum glaciation in the past, the oceans had significantly higher $^{18}O/^{16}O$ and D/H ratios because so much light water was locked-up on land. Stable isotope measurements have always loomed in importance as a means of attacking classic problems in glaciology and paleoclimatology. In his classic paper on oxygen isotope variations in fresh waters, Dansgaard (1954) wrote *"Greenland Ice Cap . . , in the opinion of this author, offers the possibility . . . to determine climatic changes over a period of time of several hundred years of the past. . . . An investigation will be undertaken as soon as an opportunity exists"*. These words must surely register among the greatest understatements in the history of geochemistry. At that time, he had no idea how wildly successful this idea would prove to be! The hope to evaluate climatic variations on a scale of several hundred years underestimated the success of this avenue of research by three orders of magnitude. Ice cores from Greenland and Antarctica provide a continuous record of precipitation that reaches over 130,000 years in Greenland and >800,000 years in Antarctica.

4.11.1 Underlying bases for glacial paleoclimatology

The basic premise of glacial paleoclimatology is that mean $\delta^{18}O$ and δD values of precipitation falling in a given season or longer period are related to mean ambient temperatures. This correlation is especially robust at high latitudes where condensation occurs near to the ground surface (Fig. 4.20).

Requisite conditions for successful application of isotopic analyses of glacial ice to climate (temperature) reconstruction are the following:

1. Significant accumulation must occur in both winter and summer in order to be able to 'count' annual bands.
2. The pattern of precipitation, or trajectory of air masses, is the same year round, or is known to vary in a predictable manner.
3. Ablation (sublimation) of snow is minimal.
4. The topography at the site of accumulation remains constant (no elevation changes).
5. A method for determining the age of the ice layers is available.

Stable isotope compositions of glacial ice in Antarctica and Greenland indeed vary with the seasons as expected: $\delta^{18}O$ (and δD) values of summer samples are higher than those of winter samples. Differences in $\delta^{18}O$ values between summer and winter ice, $\Delta\delta^{18}O_{summer\text{-}winter}$, range from >10‰ for samples only decades old to 2 to 3‰ for samples that are several hundred years old (Fig. 4.21). Dansgaard determined a $\delta^{18}O$/temperature gradient for modern Antarctic ice of $d\delta^{18}O/dT$ = ~0.69‰/°C, with higher $\delta^{18}O$ values

corresponding to higher temperatures. dδD/d*T* from Antarctica gives a slope of 6.04‰/°C (Jouzel and Merlivat, 1984) from Antarctica. In recent accumulations, summer ice is visibly different from winter ice because summer ice undergoes a certain amount of melting. With increasing age, the distinction between summer and winter layers becomes blurred but seasonal isotope variations are still recognizable. Ice recrystallizes and flattens, the layers become thinner and optical distinctions between summer and winter ice disappear. Diffusion also has a small effect, such that differences between summer and winter layers are significantly reduced (Johnsen et al., 1972).

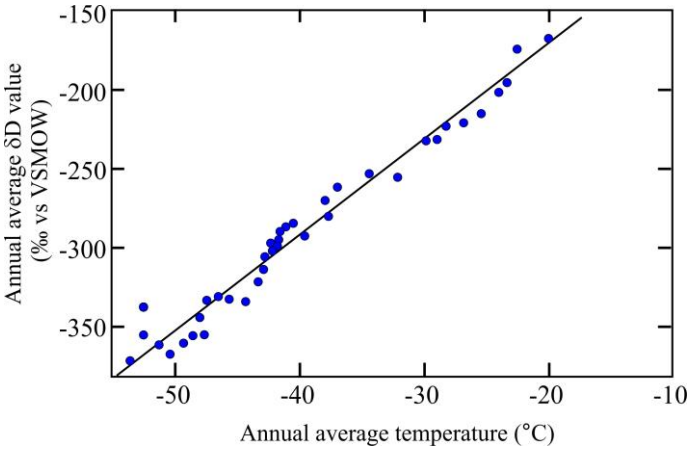

Fig. 4.20. Correlation between the mean annual surface temperature and δD value of snow in East Antarctica. Best fit line is δD = 6.04 *t* -51. *t* in °C. After Jouzel and Merlivat (1984)

4.11.2 Determining the age of glacial ice

Assigning reliable ages to the ice poses a major challenge in isotopic studies of glacial ice. Tritium and ^{210}Pb dating is used frequently for samples of ice that are younger than about 100 years. For somewhat older samples, ^{14}C dating can be used but this technique requires large samples of fracture free ice. Annual layers can be counted by visual inspection but, for samples older than several hundred years, the task becomes increasingly difficult. For each year, the isotopic composition of about 8 samples must be measured to establish clear seasonal variation. In addition, parts of the core may be missing and the annual layers ultimately become intractably thin.

An important method of dating ice is to link the age of ice layers containing volcanic ash or sulfurous aerosols to historic dates of the eruptions. Zielinski *et al*. (1994) identified 43 layers in the 8,000 years of the Greenland GISP 2 (Greenland Ice Sheet Project) core whose ice had relatively high acidity (SO_4 in excess of 20 ppb). Stuiver *et al.* (1995) correlated over 80% of these layers with historic accounts of eruptions worldwide. Depending on distance to the volcano, there may be a lag of several years for sulfurous aerosols to reach Greenland, but the correlations made to date appear to be excellent. For many eruptions, there is a lowering of temperature of ~ 1°C for several years preceding the appearance of the aerosol, due to the lag in arrival of the dust to the extreme boreal regions (Stuiver et al., 1995).

4.11.3 Thinning of ice layers

With established differences between the isotopic compositions of summer and winter ice, it should be possible to combine layer thickness with isotopic composition to estimate accumulation rates of summer and winter ice. This approach has been used with some success, but layer thickness decreases with time due to flattening or thinning imposed by the load of ice above and recrystallization. Typical decreases in thickness

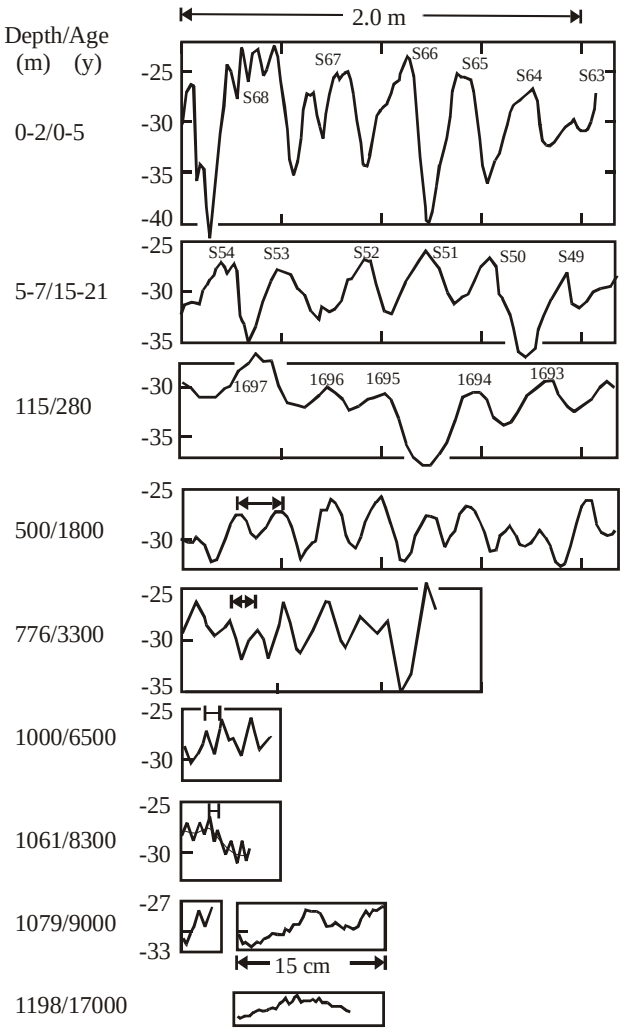

Fig. 4.21. $\delta^{18}O$ values (SMOW) in firn and ice as a function of depth at Camp Century, Greenland deep ice core. As the ice ages and becomes compressed, seasonal differences are reduced due to homogenization, and annual cycles become thinner. Y-axis is $\delta^{18}O$ vs SMOW. Years corresponding to summer values are given for first three curves. After Johnsen *et al.* (1972).

with time are 0.35 m/y for ice less than 280 years old, 0.20 m/y for ice 1800 years old, and 0.054 m/y for ice that is 8,300 years old. Dansgaard *et al*. (1969) proposed a mathematical model for evaluating the thinning of glacial ice as a function of age assuming 1) constant rate of accumulation, 2) constant thickness of the total ice sheet, 3) constant flow rate with time, and 4) the same geographic position of deposition for each layer. In order to minimize uncertainties with these calculations, samples are taken from a glacial divide where there is little or no lateral flow and changes in elevation are minimal. Classic, well known sites in Greenland and Antarctica meet these criteria and have been investigated (Johnsen et al., 1972).

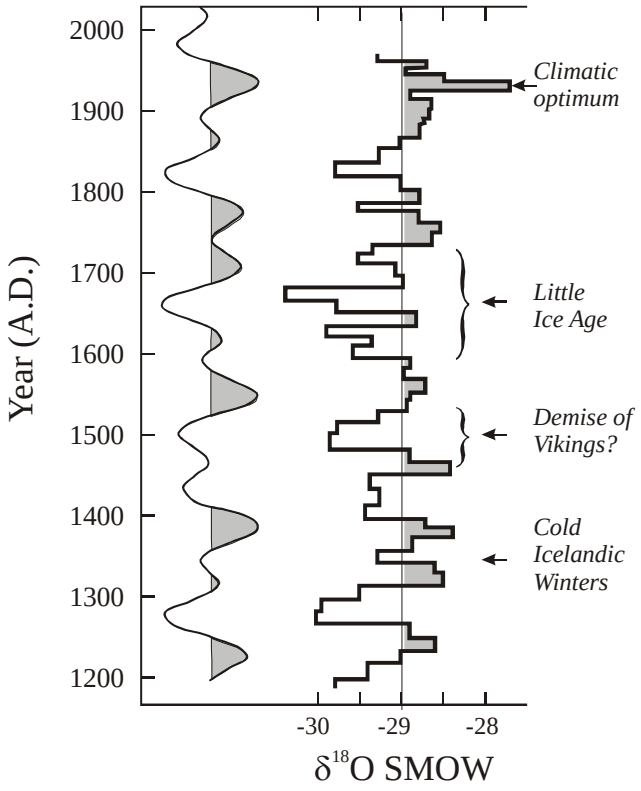

Fig. 4.22. The upper 283 m of the ice core at Camp Century, Greenland. The shaded areas represent warmer times, the curve on the left is a Fourier transform fit to the data given at right. The arrows refer to specific known cold and warm periods. See text for details. After Dansgaard *et al*. (1971).

4.11.4 The example of Camp Century, N. Greenland

An example of the information retrievable from ice cores is seen in results from Camp Century, N. Greenland (Dansgaard et al., 1971). The following discussion is divided into three parts, on the basis of distinct depths of the ice core.

0 to 283 meters The age of the ice over this core distance ranges from 0 to 780 b.p. (Fig. 4.22). Dansgaard *et al*. originally sampled the core at the decadal scale[7]. A number of cold and warm periods can be identified in the data shown in Figure 4.22.

a) a climatic optimum in 1930
b) the Little Ice Age (1600 – 1740).
c) a cold period in the 15th century that may have been responsible for the demise of the Viking settlements in Greenland.
d) especially cold years in 1352 and 1355. Recorded dates for severe Icelandic winters are 1350, 1351, and 1355

[7] Investigators now are able to sample at the annual scale going back in excess of 1000 years (e.g., Stuiver et al., 1995).

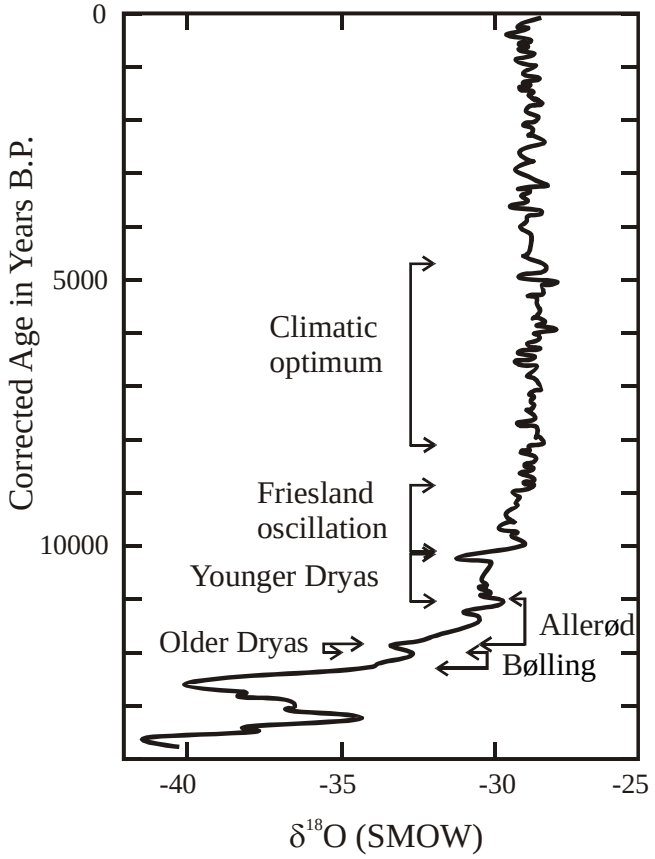

Fig. 4.23. Most recent 14 thousand years of Camp Century Ice core. Dramatic shifts to lower $\delta^{18}O$ values in Pleistocene samples. The last millennium appears to be colder than the preceding one. The $\delta^{18}O$ values during the climatic optimum are higher than at any other time. The rapid oscillations in the Pleistocene are due to glacial events, the overall lowering of $\delta^{18}O$ values with increasing age may be in part related to changing local circulation patterns. After Dansgaard *et al.* (1971).

296 to 1150 meters The ages of the ice at these greater depths are not well determined, but most likely cover the last 15,000 years of ice formation. There are significant results that can be extracted from the older core (Fig. 4.23).

a) The last millennium was cold, as were the first half of the third and fourth millennia.
b) The post-glacial Climatic optimum from 4,100 to 8,000 y.b.p. has consistently high $\delta^{18}O$ values.
c) The end of the Younger Dryas (the end of the Wisconsonian glaciation) is clearly visible
d) There is a strong shift to lower $\delta^{18}O$ values in the late Plistocene, that may be in part related to changing local circulation patterns.

0 to 1373 meters The annual layers of the core get significantly compressed with age (Fig. 4.24). Although it is difficult to know ages precisely, it appears that the core is over 126,000 years old at the bottom (Dansgaard et al., 1982), a conclusion supported by

comparison with other Greenland ice cores. Correlations with Antarctic ice cores are more difficult due to the complex ocean circulation patterns around Antarctica. Several features are apparent.

a) The entire Wisconsonian glaciation is visible, from 73,000 to 13,000 ybp. These can be divided into an early, middle and late events.
b) The Barbados I, II and III high sea-level stands are apparent in the lower parts of the diagram, resulting in the highest $\delta^{18}O$ values measured in the entire section.
c) There is a rapid and sudden change to significantly higher $\delta^{18}O$ values at the Pleistocene-Holocene boundary.

4.11.5 Example of the GRIP Summit Core: Flickering climates

Perhaps the most significant development in stable isotope studies of glacial ice, and one that may bear on governmental policies regarding global warming, is the indication that changes in climate can be more rapid than generally assumed (Alley et al., 2003). Members of the Greenland Ice Core Project (GRIP) observed remarkable changes in the $\delta^{18}O$ values of ice from the Eemian period (133,000 to 114,000 b.p.), an interglacial period that was previously thought to be one of stable warmth (Johnsen et al., 1997). The GRIP data record three warm substages in the Eemian that were about 7°C higher than the intervening cold stages. But, even more striking was the finding that temperatures dropped about 14°C over a period of only a decade or two at the end of the Eemian. If the interpretation of these data is correct, our present stable climate over the last 8000 years should be considered an exception to the possible norm of rapid climate change on Earth.

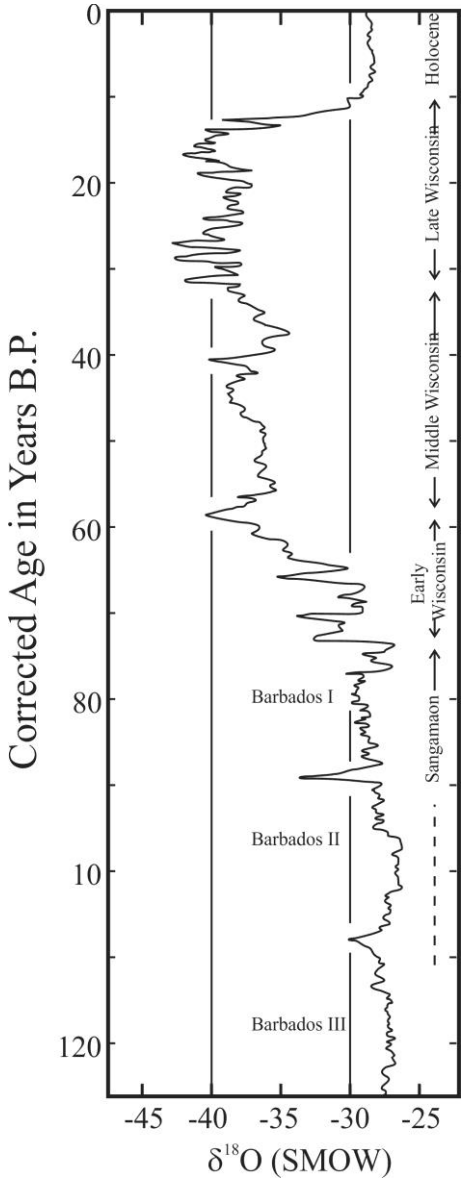

Fig. 4.24. The full record of the Camp Century Core, plotted against corrected time scale. A rapid warming is seen at the end of the Pleistocene, and a more gradual cooling starting at the beginning of the Wisconsin. Numerous glacial events can be identified on the isotope curve (Dansgaard et al., 1971).

An abrupt temperature change is also seen at the end of the Younger Dryas (Dansgaard et al., 1989). Rapid changes in humidity and dust accumulation occurred in a period of about 20 years, while temperatures

increased by 7°C in a 50 year period in South Greenland (Fig. 4.25). Such changes indicate the fragility of the surface temperature of our planet, and the need to be concerned with the effects of our anthropogenic activity.

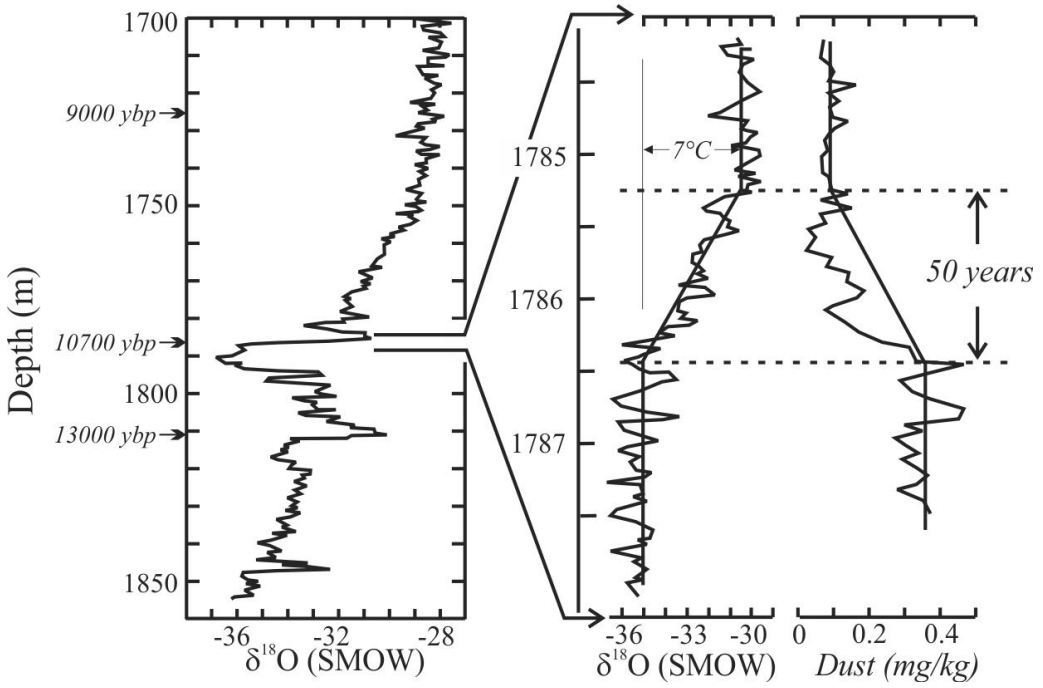

Fig. 4.25. Rapid increase in $\delta^{18}O$ values and concomitant decrease in dust (warmer, less arid) indicate a rapid change in both temperature and humidity during the Pleistocene-Holocene transition. A temperature change of ~7‰ in 50 years is indicated from the $\delta^{18}O$ record of the S. Greenland ice core at the Younger Dryas-Pre-Boreal transition. The changing dust concentration and deuterium excess parameter (not shown) over a 20 year period indicates rapid changes in climate, possibly related to changing ocean circulation patterns. After Dansgaard (1989).

4.12 Triple oxygen isotope geochemistry of meteoric water

The $\delta^{18}O$ and $\delta^{17}O$ values of most waters are generally well correlated, with $\delta'^{17}O = 0.528 \times \delta'^{18}O + 0.037$ for global meteoric waters. Nevertheless, there are subtle departures from this relationship, which, though small, have geological significance (see section 3.7 for the basics of triple isotope systems). Luz and Barkan (2010) conducted an extensive study of meteoric waters and pointed out the similarities between the triple isotope system and the *d* excess parameter. The analogy to the *d* excess parameter is the $\Delta^{17}O$ value (eq. 3.35), where

$$\Delta'^{17}O = \delta'^{17}O - 0.528 \times \delta'^{18}O + 0.037 \qquad 4.22.$$

Variations in the $\Delta'^{17}O$ value are related to the relative humidity at the source of precipitation. The effect is illustrated in Fig. 4.27. Luz and Barkan explain the effect using the Craig-Gordon model, where there is a thin layer of water-saturated air at 100% relative humidity overlying the water layer and then a diffusion boundary into the unsaturated air above that. The overall fractionation can be explained as a two-stage

process. First, water vapor in equilibrium with liquid water (point *a*) will plot at point *b* in Fig. 4.26 following an equilibrium $\theta_{(water - water\ vapor)}$ fractionation of 0.529. Second is the diffusion of water vapor into unsaturated air. The θ value for diffusion is a function of relative humidity. The oxygen isotope fractionation is larger for $H_2{}^{18}O/H_2{}^{16}O$ than $H_2{}^{17}O/H_2{}^{16}O$, and the slope (θ) is on the order of 0.518. This drives the vapor from *b* to *c*. Condensation will plot along the dashed line with a slope of 0.528 – the global meteoric water line for triple oxygen isotopes. Combined Rayleigh fractionation for $^{18}O/^{16}O$ and $^{17}O/^{16}O$ results in an effective θ of 0.528 (insensitive to temperature), explaining the slope of global meteoric waters. The $\Delta^{17}O$ value is fundamentally a function of the relative humidity at the ocean source. The near-zero $\Delta^{17}O$ value for extreme high latitude snow from Antarctica (SLAP and Dome F) is explained by the kinetics of H_2O diffusion through air to the deposition site in growing ice crystals (Jouzel and Merlivat, 1984). At the other extreme, low $\Delta^{17}O$ values for high $\delta^{18}O$ value waters is explained by extreme evaporation which is equivalent of driving water droplets from *c* to *b*.

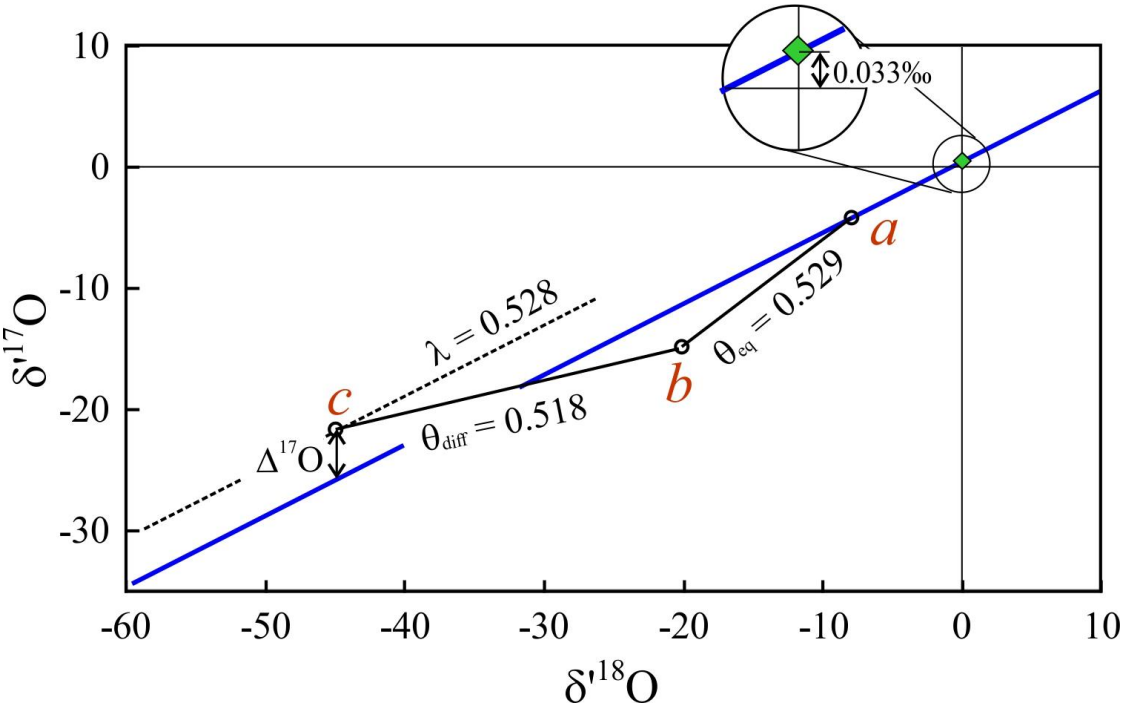

Fig. 4.26. The water vapor in equilibrium with ocean water at point *a* will plot at point *c*. This can be envisioned as a two-step process. First, the water vapor boundary layer at 100% relative humidity fractionates with a θ value of 0.529 (*a* → *b*). Second, diffusion into the unsaturated overlying air follows a shallow slope of ~0.518, driving it to a positive $\Delta'^{17}O$ value.

The contoured $\Delta^{17}O$ values for waters in the United States (based on tap water values) is shown in Fig. 4.27 (Li et al., 2015). Although it is assumed that both *d* excess and $\Delta^{17}O$ values of meteoric waters are related to water source relative humidity, the preliminary $\Delta^{17}O$ values for tap waters do not correlate strongly with *d* excess (compare Fig. 4.27 with Fig. 4.8). Cleary more work is warranted in terms of comparing these two ratios.

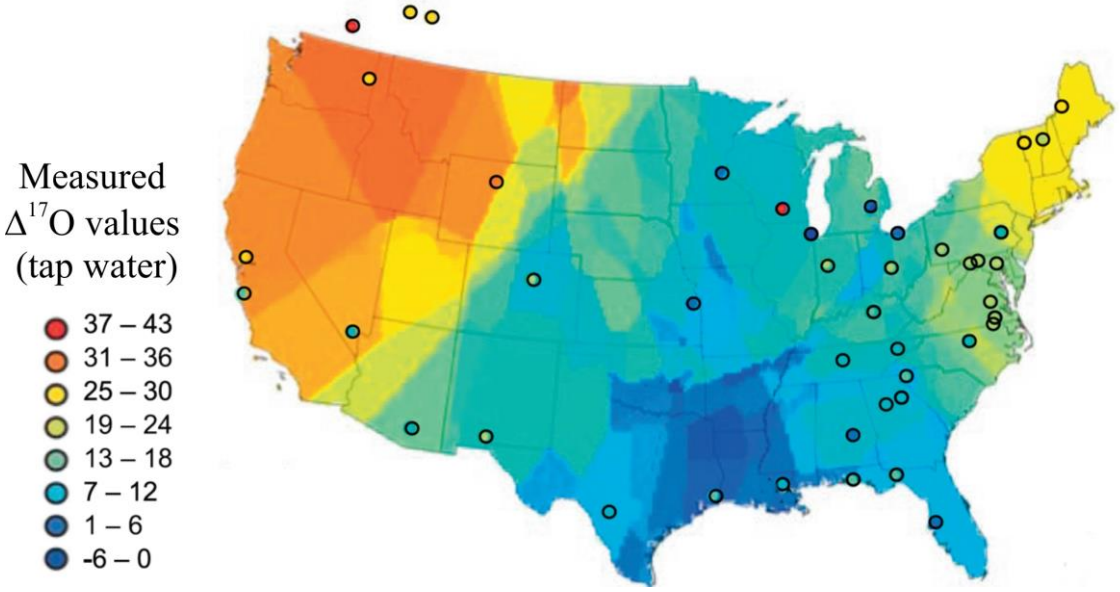

Fig. 4.27. Contoured $\Delta^{17}O$ values for the United States based on data from a number of tap water locations. Tap water samples that do not match the assumed average $\delta^{18}O$ values of the region are excluded from the contouring (and not shown on this figure). Modified from Li *et al.* (2015).

References

Aldaz, L. and Deutsch, S. (1967) On a relationship between air temperature and oxygen isotope ratio of snow and firn in the South Pole region. *Earth and Planetary Science Letters* **3**, 267-274.

Alley, R.B., Marotzka, J., Nordhaus, W.D., Ovrepeck, J.T., Peteet, D.M., Pielke, R.A., Jr., Pierrehumbert, R.T., Rhines, P.B., Stocker, T.F., Talley, L.D. and Wallace, J.M. (2003) Abrupt climate change. *Science* **299**, 2005-2010.

Banner, J.L., Wasserburg, G.J., Dobson, P.F., Carpenter, A.B. and Moore, C.H. (1989) Isotopic and trace element constraints on the origin and evolution of saline groundwaters from central Missouri. *Geochimica et Cosmochimica Acta* **53**, 383-398.

Clayton, R.N., Friedman, I., Graf, D.L., Mayeda, T.K., Meents, W.F. and Shimp, N.F. (1966) The origin of saline formation waters, I: Isotopic composition. *Journal of Geophysical Research.* **71**, 3869-3882.

Coplen, T.B. and Hanshaw, B.C. (1973) Ultrafiltration by a compacted clay membrane-I. Oxygen and hydrogen isotopic fractionation. *Geochimica et Cosmochimica Acta* **37**, 2295-2310.

Coplen, T.B., Hopple, J.A., Böhlke, J.K., Peiser, H.S., Rieder, S.E., Krouse, H.R., Rosman, K.J.R., Ding, T., Vocke, R.D.J., Révész, K.M., Lamberty, A., Taylor, P. and DeBièvre, P. (2002) Compilation of Minimum and Maximum Isotope Ratios of Selected Elements in Naturally Occurring Terrestrial Materials and Reagents. United States Geological Survey, Reston, p. 98.

Craig, H. (1961) Isotopic variations in meteoric waters. *Science* **133**, 1702-1703.

Craig, H. (1963) The isotopic geochemistry of water and carbon in geothermal areas, in: Tongiorgi, E. (Ed.), Nuclear geology in geothermal areas. Consiglio Nazionale della Ricerche, Laboratorio de Geologia Nucleare, Pisa, pp. 17-53.

Craig, H. and Gordon, L.I. (1965) Deuterium and oxygen-18 variations in the ocean and the marine atmosphere, Stable Isotopes in Oceanographic Studies and Paleotemperatures. Consiglio Nazionale delle Richerche, Pisa, Spoleto, Italy, pp. 9-130.

Criss, R.E. (1999) Prinicples of stable isotope distribution. Oxford University Press, New York.

Criss, R.E. and Davisson, M.L. (1996) Isotopic imaging of surface water/ groundwater interactions, Sacramento Valley, California. *Journal of Hydrology* **178**, 205-222.

Dansgaard, W. (1954) The O^{18}-abundance in fresh water. *Geochimica et Cosmochimica Acta* **6**, 241-260.

Dansgaard, W. (1964) Stable isotopes in precipitation. *Tellus* **16**, 436-468.

Dansgaard, W., Clausen, H.B., Gundestrup, N., Hammer, C.U., Johnsen, S.F., Kristinsdottir, P.M. and Reeh, N. (1982) A new Greenland deep ice core. *Science* **218**, 1273-1277.

Dansgaard, W., Johnsen, S.J., Clausen, H.B. and Langway, C.C., Jr. (1971) Climatic record revealed by the camp century ice core, in: Turekian, K.K. (Ed.), The late cenozoic glacial ages. Yale University Press, New Haven, pp. 37-56.

Dansgaard, W., Johnsen, S.J., Moller, J. and Langway, C.C., Jr. (1969) One thousand centuries of climatic record from Camp Century on the Greenland ice sheet. *Science* **166**, 377-381.

Dansgaard, W., White, J.W.C. and Johnsen, S.J. (1989) The abrupt termination of the Younger Dryas climate event. *Nature* **339**, 532-534.

Eiler, J.M. and Schauble, E. (2004) $^{18}O^{13}C^{16}O$ in Earth's atmosphere. *Geochimica et Cosmochimica Acta* **68**, 4767-4777.

Epstein, S. and Mayeda, T.K. (1953) Variation of ^{18}O content of waters from natural sources. *Geochimica et Cosmochimica Acta* **4**, 213-224.

Fontes, J.C. and Gonfiantini, R. (1967) Comportement isotopique au cours de l'évaporation de deux bassins Sahariens. *Earth and Planetary Sciences* **3**, 258-266.

Fontes, J.C. and Matray, J.M. (1993) Geochemistry and origin of formation brines from the Paris Basin, France; 2, Saline solutions associated with oil fields. *Chemical Geology* **109**, 177-200.

Fricke, H.C. and O'Neil, J.R. (1999) The correlation between $^{18}O/^{16}O$ ratios of meteoric water and surface temperature; its use in investigating terrestrial climate change over geologic time. *Earth and Planetary Science Letters* **170**, 181-196.

Friedman, I. (1953) Deuterium content of natural water and other substances. *Geochimica et Cosmochimica Acta* **4**, 89-103.

Friedman, I., Machta, L. and Soller, R. (1962) Water vapor exchange between a water droplet and its environment. *Journal of Geophysical Research* **67**, 2761-2770.

Galewsky, J., Steen-Larsen, H.C., Field, R.D., Worden, J., Risi, C. and Schneider, M. (2016) Stable isotopes in atmospheric water vapor and applications to the hydrologic cycle. *Reviews of Geophysics* **54**, doi:10.1002/2015RG000512.

Gat, J.R. (1996) Oxygen and hydrogen isotopes in the hydrologic cycle. *Annual Review of Earth and Planetary Sciences* **24**, 225-262.

Gedzelman, S., Lawrence, J.R., Gamache, J., Black, M., Hindman, E., Black, R., Dunion, J., Willoughby, H. and Zhang, X. (2003) Probing hurricanes with stable isotopes of rain and water vapor. *Monthly Weather Review* **131**, 1112-1127.

Good, S.P., Noone, D., Kurita, N., Benetti, M. and Bowen, G.J. (2015) D/H isotope ratios in the global hydrologic cycle. *Geophysical Research Letters* **42**, 5042-5050.

Harmon, R.S. and Schwarcz, H.P. (1981) Changes of ^{2}H and ^{18}O enrichment of meteoric water and Pleistocene glaciation. *Nature* **290**, 125-128.

Hitchon, B. and Friedman, I. (1969) Geochemistry and origin of formation waters in the western Canada sedimentary basin: I. Stable isotopes of hydrogen and oxygen. *Geochimica et Cosmochimica Acta* **33**, 1321-1349.

Horita, J., Rozanski, K. and Cohen, S. (2008) Isotope effects in the evaporation of water: a status report of the Craig–Gordon model. *Isotopes in Environmental and Health Studies* **44**, 23-49.

Horita, J. and Wesolowski, D.J. (1994) Liquid-vapor fractionation of oxygen and hydrogen isotopes of water from the freezing to the critical temperature. *Geochimica et Cosmochimica Acta* **58**, 3425-3437.

Jasechko, S., Lechler, A., Pausata, F.S.R., Fawcett, P.J., Gleeson, T., Cendón, D.I., Galewsky, J., LeGrande, A.N., Risi, C., Sharp, Z.D., Welker, J.M., Werner, M. and Yoshimura, K. (2015) Late-glacial to late-Holocene shifts in global precipitation $\delta^{18}O$. *Climate of the Past* **11**, 1375-1393.

Johnsen, S.J., Clausen, H.B., Dansgaard, W., Gundestrup, N.S., Hammer, C.U., Andersen, U., Andersen, K.K., Hvidberg, C.S., Dahl-Jensen, D., Steffensen, J.P., Shoji, H., Sveinbjornsdottir, A.E., White, J., Jouzel, J. and Fisher, D. (1997) The $\delta^{18}O$ record along the Greenland Ice Core Project deep ice core and the problem of possible Eemian climatic instability. *Journal of Geophysical Research, C, Oceans* **102**, 26397-26410.

Johnsen, S.J., Dansgaard, W., Clausen, H.B. and Langway, C.C., Jr. (1972) Oxygen Isotope Profiles through the Antarctic and Greenland Ice Sheets. *Nature* **235**, 429-434.

Jouzel, J., Lorius, C., Petit, J.R., Genthon, C., Barkov, N.I., Kotlyakov, V.M. and Petrov, V.M. (1987) Vostok ice core; a continuous isotope temperature record over the last climatic cycle (160,000 years). *Nature* **329**, 403-408.

Jouzel, J. and Merlivat, L. (1984) Deuterium and oxygen 18 in precipitation; modeling of the isotopic effects during snow formation. *Journal of Geophysical Research. D. Atmospheres* **89**, 11,749-711,757.

Kendall, C. and Coplen, T.B. (2001) Distribution of oxygen-18 and deuterium in river waters across the United states. *Hydrological Processes* **15**, 1363-1393.

Knauth, L.P. and Beeunas, M.A. (1986) Isotope geochemistry of fluid inclusions in Permian halite with implications for the isotopic history of ocean water and the origin of saline formation waters. *Geochmica et Cosmochimica Acta* **50**, 419-433.

Li, S., Levin, N.E. and Chesson, L.A. (2015) Continental scale variation in ^{17}O-excess of meteoric waters in the United States. *Geochimica et Cosmochimica Acta* **164**, 110-126.

Lloyd, R.M. (1966) Oxygen isotope enrichment of sea water by evaporation. *Geochimica et Cosmochimica Acta* **30**, 801-814.

Luz, B. and Barkan, E. (2010) Variations of $^{17}O/^{16}O$ and $^{18}O/^{16}O$ in meteoric waters. *Geochimica et Cosmochimica Acta* **74**, 6276–6286.

Machavaram, M.V. and Krishnamurthy, R.V. (1995) Earth surface evaporative process: A case study from the Great Lakes region of the United States based on deuterium excess in precipitation. *Geochimica et Cosmochimica Acta* **59**, 4279-4283.

Majoube, M. (1971) Fractionnement en oxygene 18 et en deuterium entre l-eau et sa vapeur. *Journal de Chimie et Physique* **68**, 1423-1436.

Meehan, T.D., Giermakowski, J.T. and Cryan, P.M. (2004) GIS-based model of stable hydrogen isotope ratios in North American growing-season precipitation for use in animal movement studies. *Isotopes in Environmental and Health Studies* **40**, 291-300.

Méheut, M., Lazzeri, M., Balan, E. and Mauri, F. (2007) Equilibrium isotopic fractionation in the kaolinite, quartz, water system: Prediction from first-principles density-functional theory. *Geochimica et Cosmochimica Acta* **71**, 3170-3181.

Merlivat, L. and Jouzel, J. (1979) Global climatic interpretation of the deuterium-oxygen 18 relationship for precipitation. *Journal of Geophysical Research: Oceans* **84**, 5029-5033.

Merlivat, L. and Nief, G. (1967) Fractionnement isotopique lors des changements d'état solide-vapeur et liquide-vapeur de l'eau à des températures inférieures à 0 C. *Tellus* **19**, 122-127.

Musgrove, M. and Banner, J.L. (1993) Regional ground-water mixing and the origin of saline fluids; Midcontinent, United States. *Science* **259**, 1877-1882.

Pfahl, S. and Sodemann, H. (2014) What controls deuterium excess in global precipitation? *Climate of the Past* **10**, 771-781.

Poage, M.A. and Chamberlain, C.P. (2001) Empirical relationships between elevation and the stable isotope composition of precipitation and surface waters; considerations for studies of paleoelevation change. *American Journal of Science* **301**, 1-15.

Rowley, D.B. (2007) Stable Isotope-Based Paleoaltimetry: Theory and Validation, Reviews in Mineralogy and Geochemistry, pp. 23-52.

Rowley, D.B. and Garzione, C.N. (2007) Stable isotope-based paleoaltimetry. *Annual Review of Earth and Planetary Sciences* **35**, 463-508.

Rozanski, K., Araguas, A.L. and Gonfiantini, R. (1992) Relation-between long-term trends of oxygen-18 isotope composition of precipitation and climate. *Science* **258**, 981-985.

Salati, E., Dall'Olio, A., Matsui, E. and Gat, J.R. (1979) Recycling of water in the Amazon Basin: An isotopic study. *Water Resources Research* **15**, 1250-1258.

Stuiver, M., Grootes, P.M. and Braziunas, T.F. (1995) The GISP2 $\delta^{18}O$ climate record of the past 16,500 years and the role of the sun, ocean and volcanoes. *Quaternary Research* **44**, 341-354.

Zielinski, G.A., Mayewski, P.A., Meeker, L.D., Whitlow, S., Twickler, M.S., Morrison, M., Meese, D.A., Gow, A.J. and Alley, R.B. (1994) Record of volcanism since 7000 B.C. from the GISP 2 Greenland ice core and implications for the volcano-climate system. *Science* **264**, 948-952.

Chapter 5

THE OCEANS

Contents

5.1 Overview 1
5.2 Oxygen Isotope Variations in Modern Oceans 2
5.2.1 Salinity-$\delta^{18}O$ relations in shallow marine waters 2
5.2.2 Salinity-$\delta^{18}O$ relations in deep ocean waters 3
5.3 Depth Profiles in Modern Oceans: $\delta^{18}O$ $(O_2)_{aq}$ and $\delta^{13}C$ (ΣCO_2) 6
5.4 Stable isotope ratios as monitors of productivity 7
5.5 Isotopic Compositions of Ancient Oceans 9
5.5.1 Primitive oceans 9
5.5.2 Secular changes in $\delta^{18}O$ of marine sediments 10
5.6 Seawater-Basalt Interactions – buffering the $\delta^{18}O$ value of the ocean 11
5.6.1 Low-temperature alteration 12
5.6.2 High temperature alteration 13
5.6.3 Evidence from drill core material 13
5.6.4 Evidence from obducted material 14
5.7 Buffering the $^{18}O/^{16}O$ Ratio of Ocean Water 15
5.7.1 Summing the processes affecting the $^{18}O/^{16}O$ ratio of seawater 15
5.7.2 Unresolved controversy 16
5.7.3. Model calculations 16
5.7.4. An alternative explanation for the early-Earth low $\delta^{18}O$ values 17
References 18

Chapter 5

THE OCEANS

5.1 Overview

The $\delta^{18}O$ values of *surface* marine waters vary by several per mil, particularly in coastal regions at high latitudes where isotopically light glacial and stream waters feed into the ocean. Surface water variations are due to three processes: 1) evaporation, 2) influx of fresh water and 3) melting or freezing of sea ice. In contrast to the shallow waters, the oxygen isotope compositions of *deep* ocean waters are nearly constant, varying by less than 1‰. Salinities at depth are also nearly constant at 34 to 35‰[1]. Nonetheless, the subtle variations in both salinity and isotopic composition of these waters can be used to provide valuable information on mass accumulations and circulation patterns in the deep oceans.

The earliest study of oxygen isotope variations in ocean waters was made by Epstein and Mayeda (1953) whose main interest at that time was focused on the extent of oxygen isotope variability of ocean water as it pertained to determining paleotemperature estimates from $\delta^{18}O$ values of carbonates (see Chapter 6). They quickly realized that failure to consider possible variations in $\delta^{18}O$ values of surface waters could lead to a disturbingly large uncertainty of up to about 10°C in temperature estimates using the carbonate-water oxygen isotope thermometer. Further uncertainty is introduced when possible and probable temporal variations in the oxygen isotope composition of the oceans are taken into consideration.

How has the oxygen isotope composition of ocean water changed over geologic time? From simple mass balance considerations involving the amount and isotopic composition of water now locked up on land in glaciers, we *know* that $\delta^{18}O$ values of ocean waters were about 1‰ lower in ice-free times than they are at present. But were variations in the past larger than this? Urey *et al.* (1951) realized that the formation of low temperature sedimentary rocks, enriched in ^{18}O, would cause the oceans to get lighter over time. They conclude with the following: "*Perhaps it is a conclusion based on little more than prejudice, but we believe that it is most likely that the major part of this change occurred before the Cambrian. Until more data are available we will make no correction for this effect*." In the ensuing half century, the community is still divided on the isotopic composition of the early ocean. On the basis of oxygen isotope analyses of marine sediments deposited at different times in the geologic past, $\delta^{18}O$ values of the early ocean as low as −15‰ have been proposed. A change of this magnitude in the isotopic composition of the vast quantity of water in the oceans would reflect an enormous change in some major (plate tectonic?) process operating on Earth, but the evidence presented for such changes is highly controversial. On the other hand, if the isotopic composition of the ocean has remained constant, then early ocean temperatures would have been arguably too high to support life. The question of major oxygen isotope variability in ancient oceans remains one of the most important unresolved problems in earth science. We will return to this intriguing subject later in this chapter.

[1] Salinity is often reported in per mil notation, where 34‰ salinity is equivalent to 3.4 wt % dissolved solids. It should not be confused with isotopic compositions.

5.2 Oxygen Isotope Variations in Modern Oceans

5.2.1 Salinity-$\delta^{18}O$ relations in shallow marine waters

Epstein and Mayeda (1953) first recognized the almost linear correlation between salinity (*S*) and $\delta^{18}O$ value of ocean waters, and the anticipated sympathetic correlation between salinity and δD was documented a few years later by Friedman *et al*. (1961). The correlation between salinity and stable isotope ratios of ocean waters is explained by two simple processes: evaporation and addition of fresh water. Evaporation from the ocean surface preferentially removes light isotopologues from the water and increases its salinity, so values of both $\delta^{18}O$ and *S* of surface waters increase with increasing degree of evaporation. Introduction of fresh water from melting ice, river systems or rain lowers the salinity and $\delta^{18}O$ value of the affected parcel of ocean. The $\delta^{18}O$ and δD values of this water are lowered because meteoric waters virtually always have lower stable isotope compositions than ocean water. The magnitude of the isotopic effect is related to the water source. $\delta^{18}O$ values of glacial waters are very low (a typical value is −30‰), while those of rivers in temperate zones are much higher (*e.g.* –4.9‰ for the Mississippi River). Thus, for a given dilution factor, high-latitude glacial waters will shift $\delta^{18}O$ values to a greater extent than low-latitude river waters for the same shift in salinity. In an ice-free world, $\delta^{18}O$ would change by about 0.2‰ per unit change in salinity (although this will vary in accordance with the $\delta^{18}O$ value of the fresh water), so that a 5‰ fluctuation in salinity would be accompanied by a 1.0‰ fluctuation in the O^{18}/O^{16} ratio of the oceans.

The carbonate-water paleothermometer is a function of the difference between the $\delta^{18}O$ values of the carbonate and water. Its applicability requires that the $\delta^{18}O$ value of the water from which the carbonates precipitated is known or can somehow be estimated. Large variations in $\delta^{18}O$ values of surface waters resulting from evaporation and influx of meteoric waters could bear significantly on estimates of ocean paleotemperatures that are made from analyses of carbonate from the shells of planktonic organisms. The rather loose relation observed between salinity and $\delta^{18}O$ values is called the *salinity effect* and implies that we can approximate one parameter from knowledge of the other. That is, if the paleosalinity can be determined by some means, then an appropriate correction for the departure of $\delta^{18}O$ from values of normal marine waters can be made (Railsback et al., 1989). A surprising number of authors have misused this term, assuming that salinity itself affects the oxygen isotope fractionation between carbonates and ocean water, which is not the case. There is indeed a small effect on the fractionation between water in highly saline solutions and other phases (see section 3.6.4) but, at the relatively low salinities of ocean water, the effect on oxygen isotope fractionation is negligible. The *salinity effect* employed in paleotemperature studies is not related to salinity-fractionation effects.

Craig and Gordon (1965) measured isotopic compositions of both water vapor and surface waters along N-S and E-W transects across the Atlantic Ocean. These data, shown in Figure 4.9, reflect the non-equilibrium nature of the evaporation process and also point to relative humidity as a dominant control on vapor compositions. As one travels in a northerly direction in the Atlantic Ocean, there is little change in $\delta^{18}O$ values of liquid water, but $\delta^{18}O$ values of the overlying water vapors decrease with increasing latitude due to decreasing sea-surface temperatures and concomitant increases in the magnitude of the isotopic fractionation between liquid and vapor. The measured $\delta^{18}O$

values of the vapor are, however, about 4.5‰ more negative than those expected at equilibrium because of kinetic isotope effects. During the process of evaporation, light molecules preferentially diffuse through the near-surface layers of liquid water and into the vapor phase, with little back-exchange. Kinetic effects also favor the diffusion of the light isotopologues from the saturated layer just above the liquid into the unsaturated air layer above that. The lowest $\delta^{18}O_{vapor}$ values are, as expected, found in the region of the trade winds, where evaporation is highest and relative humidity is lowest. Variations in the $\delta^{18}O$ value of water vapor are minimal in an E-W direction.

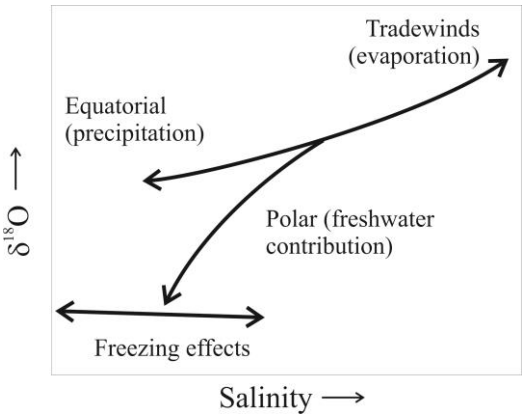

Fig. 5.1. Schematic illustration of various effects on the isotopic composition-salinity of ocean surface waters.

The factors that contribute to changes in *S* and $\delta^{18}O$ are summarized in Figure 5.1. Intense evaporation in the region of the trade winds causes both $\delta^{18}O$ and *S* values to increase, whereas intense precipitation at equatorial latitudes lowers both $\delta^{18}O$ and *S* values. At high latitudes, meltwater entering the ocean has very low $\delta^{18}O$ values, so that oxygen isotope ratios are accordingly more strongly affected than salinity (note the steeper slope in Fig. 5.1). In contrast, the formation of sea ice, a particularly important process in the Weddell sea off Antarctica, affects salinity more strongly than oxygen isotope ratios. This is because the oxygen isotope fractionation between ice and seawater is negligible (O'Neil, 1968), but formation of ice – which essentially incorporates no salt – will strongly increase the salinity of the remaining water. The salinity of the surrounding water thus increases while its $\delta^{18}O$ value decreases, but only very slightly. Assuming $\Delta^{18}O_{ice\text{-}water} = 2‰$, a quantity of ice formation that changes the salinity by 2‰ will only change the $\delta^{18}O$ value by 0.1‰.

The salinity - $\delta^{18}O$ values of waters from the N. Atlantic surface waters plot on a nearly linear array, with low salinity - low $\delta^{18}O$ values becoming especially pronounced towards Greenland (Fig. 5.2). The nearly perfect linear correlation is partly an artifact of the huge range of $\delta^{18}O$ and *S* plotted in Fig. 5.2. When we look at the Pacific waters at a smaller scale (Fig. 5.4) it become apparent that salinity and $\delta^{18}O$ do not correlate quite as well as suggested by Fig. 5.2. Compare the N. and S. Pacific waters in Fig. 5.4.

5.2.2 Salinity-$\delta^{18}O$ relations in deep ocean waters

Craig and Gordon (1965) developed deep ocean circulation models using the combined $\delta^{18}O$-*S* data. Because the total variation in the isotopic composition of deep ocean water is only about 0.5‰, the researchers needed to be able to measure the $\delta^{18}O$ values at an unprecedented level of precision. To meet this challenge, Craig and Gordon developed a procedure to greatly increase the precision of their $\delta^{18}O_{water}$ determinations. It is worth detailing here because, although many researchers may quote extremely high precision, the protocol developed by Craig and Gordon illustrate just how hard it is to really achieve such a goal.

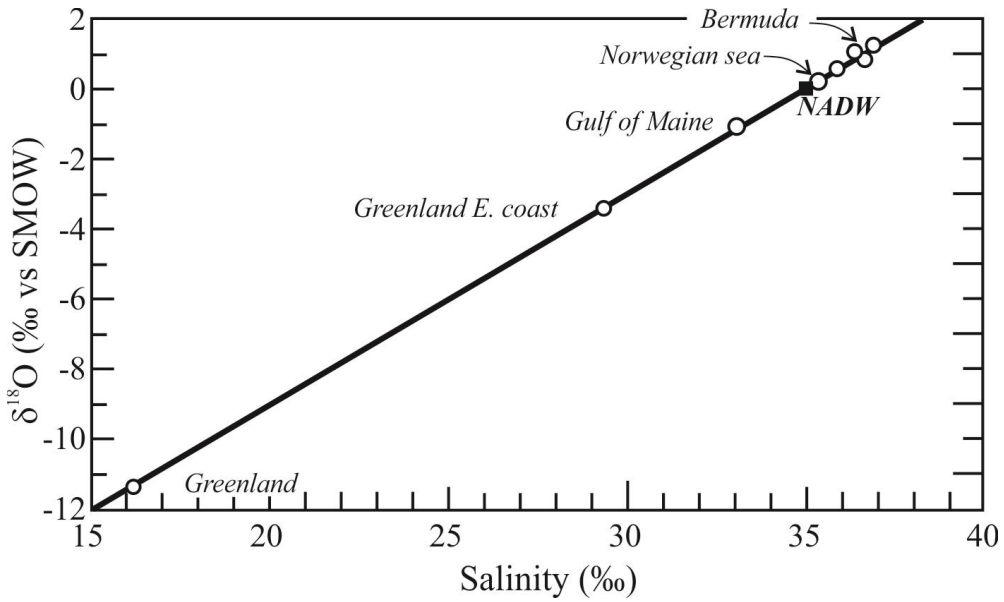

Fig. 5.2. δ^{18}O-*S* values for Atlantic surface waters and North Atlantic Deep Water (NADW - black square). The NADW δ^{18}O-*S* values fall on the mixing trend line for surface waters. After Craig and Gordon (1965) with data from Epstein and Mayeda (1953).

Craig and Gordon analyzed relatively large samples of water to limit the effects of vapor loss and contamination during sample manipulation. In addition, they equilibrated their water samples with CO_2 that had previously been isotopically equilibrated with a water of 'normal' marine composition. In this way, changes in the δ^{18}O value of the equilibrating CO_2 gas would be very small during exchange with their 'actual' samples, thus minimizing changes in the isotopic composition of the water sample during the equilibration process. The mass spectrometer working standard was CO_2 that had also been equilibrated with water of marine composition, and both reference and sample gas were introduced through the *sample* inlet side of the mass spectrometer, thus eliminating any fractionation effects that might arise when switching between standard and sample inlets. By adopting this protocol, they were able to reach an overall precision of better than ±0.02‰.

The isotopic compositions and salinities of near surface waters vary considerably with latitude as we have already seen in figures 5.2 and 5.4. But with increasing depth, there is a convergence at or below ~1000 m to values that are remarkably constant for large distinct ocean basins. Values of δ^{18}O and *S* for ten samples of water that spanned 40° of latitude were identical to within 1σ standard deviations of 0.04 and 0.03‰, respectively. δ^{18}O-*S* values for deep oceans basins are given in Table 5.1. Although subtle, the distinctions are significant, and can be explained completely by specific circulation patterns as discussed in the following section.

The δ^{18}O-*S* values of North Atlantic Deep Waters (NADW) plot directly on the linear array defined by N. Atlantic surface waters (Fig. 5.2). The deep waters are thus consistent with downwelling of cold, surface-waters in the Norwegian sea, in accord with independently developed circulation models. In the South Atlantic region near the Weddell Sea (59-65°S), the slope $d\delta^{18}O/dS$ is close to zero (dashed line in Fig. 5.3),

consistent with the relations associated with the formation of sea ice, explained above (Fig 5.1). Salinities range from 33.4 to 34.7 per mil, while $\delta^{18}O$ values are constant at -0.4 to -0.5 ‰ for all but the most saline waters. The $\delta^{18}O$-*S* values for the Antarctic Bottom Waters (AABW) are distinct from those of the NADW because the mechanism of their formation differs from that occurring in the North Atlantic. North Atlantic waters achieve sufficient density to sink by cooling and evaporation (increase in salinity) of Gulf Stream waters. In contrast, waters in the Weddell sea are so cold that significant freezing occurs, increasing salinity and density, but not changing $\delta^{18}O$ values. Combining salinity and isotopic data, two distinct bodies of downwelling waters (AABW and NADW) are clearly identified (Fig. 5.3).

Table 5.1. *Salinity and $\delta^{18}O$ values of principal deep water ocean masses. From (Craig and Gordon, 1965).*

	Salinity(‰)	**$\delta^{18}O$(‰)**
North Atlantic Deep Water (NADW)	34.93	+0.12
Antarctic Bottom Waters (AABW)	34.65	-0.45
Indian Deep Waters (IDW)	34.71	-0.18
Pacific Deep Waters (PDW)	34.70	-0.17*

*Antarctic samples have a slightly lower $\delta^{18}O$ value of -0.21‰

In contrast to the compositions of North Atlantic waters, data for the Pacific Deep Waters (PDW) do not lie on the $\delta^{18}O$-*S* line for surface Pacific waters (Fig. 5.4), implying an *exotic* source for the PDW. In addition, neither of the two Atlantic downwelling sources (NADW or AABW) match the combined $\delta^{18}O$-*S* values of the PDW. Instead, the PDW data lie intermediate to the NADW and AABW data, and are explained by simple mixing of these two deep water sources (Fig. 5.3). Such mixing is consistent with our current understanding of global ocean circulation patterns. Appreciable ocean

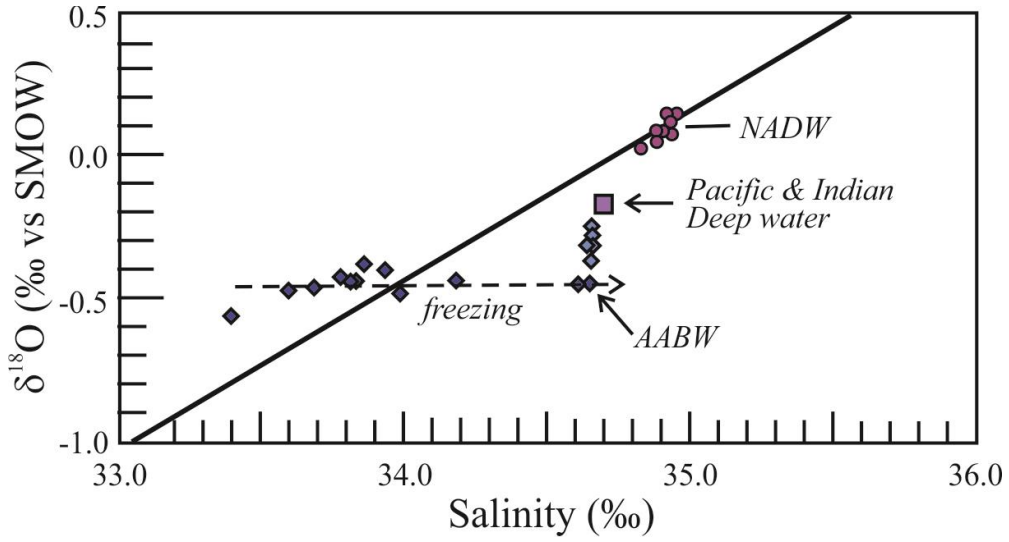

Fig. 5.3. $\delta^{18}O$ vs. salinity for Atlantic waters and Antarctic bottom waters (AABW). The near-horizontal trend for deep waters in the Weddell Sea indicates a freezing-related trajectory. The Antarctic Bottom Waters appear to have their source in the downwelling waters of the Weddell Sea. The Pacific and Indian Deep waters can be explained by a simple mixing relation between the NADW and AABW. After Craig and Gordon, (1965)

downwelling occurs only in the North Atlantic and the Antarctic. The North Atlantic data reflect the downwelling source in the Norwegian Sea and the AABW reflect a source in the Weddell Sea associated with ice production and downwelling of cold high-salinity waters. These two downwelling waters move eastward and mix, eventually traversing both the Pacific and Indian Oceans.

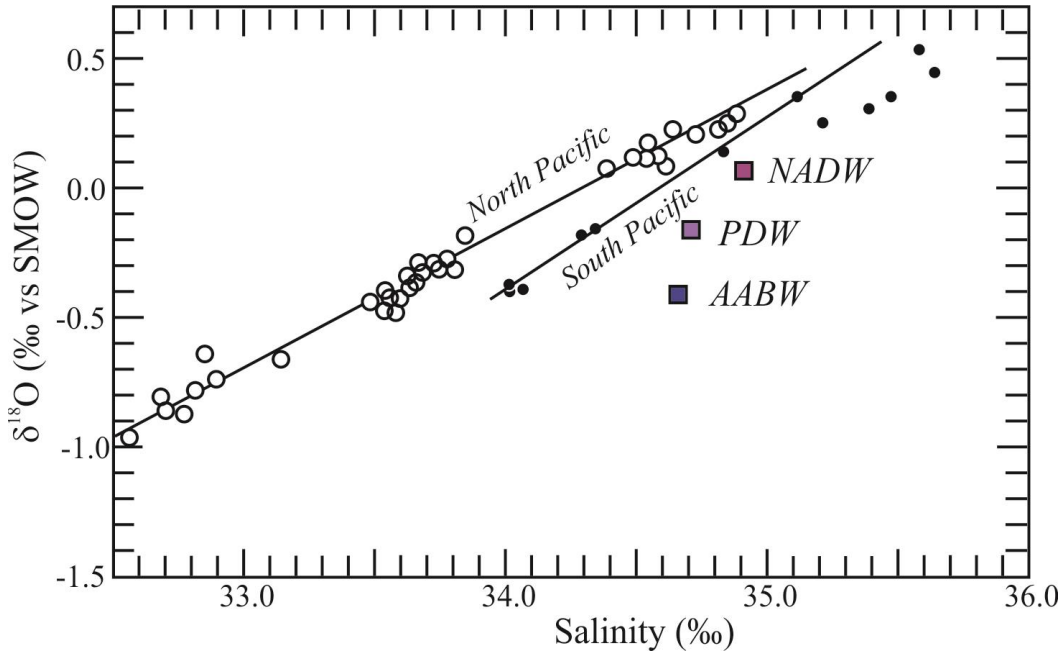

Fig. 5.4. δ^{18}O-*S* data for North and South Pacific surface waters and various deep waters. Pacific Deep Waters (*PDW*) cannot be generated by any combination of Pacific surface waters, but can be generated by mixing Antarctic Bottom Waters (*AABW*) with North Atlantic Deep Waters (*NADW*). After Craig and Gordon (1965).

5.3 Depth Profiles in Modern Oceans: $\delta^{18}O\ (O_2)_{aq}$ and $\delta^{13}C\ (\Sigma CO_2)$

Atmospheric oxygen all over the globe has a constant δ^{18}O value of 23.8±0.3‰ (Luz and Barkan, 2011). The oxygen isotope fractionation between O_2 dissolved in seawater and O_2 in the atmosphere is 0.6‰ at 25°C (note direction of this fractionation; δ^{18}O of O_2 dissolved in seawater is 0.6‰ higher than in air), and is reflected in measured δ^{18}O values of O_2 in shallow seawater. Because of the huge production of O_2 during photosynthesis, and the relatively low amounts of dissolved O_2 in the oceans, the δ^{18}O value of dissolved O_2 in the shallow marine environment is controlled by atmospheric oxygen and ultimately the isotopic fractionation associated with photosynthesis (see Box 5.1). With increasing depth, the abundance of dissolved oxygen in the ocean decreases from a value of ~210 μmoles/kg to a minimum of 150 μmoles/kg at about 1 km depth (Fig. 5.5). This decrease is due to oxidation of sinking organic matter. With increasing depth, the O_2 concentration increases again to 270 μmoles/kg because of the O_2 contribution of downwelling waters from the North Atlantic and Antarctic. δ^{18}O values of dissolved oxygen mirror the oxygen concentration profile. O_2 dissolved in surface waters has δ^{18}O values in excess of 24‰ as a result of equilibrium exchange with O_2 in the atmosphere. δ^{18}O values increase with depth because light oxygen is preferentially consumed in the oxidation of organic matter. At a depth of ~ 1km, dissolved oxygen

attains maximum $\delta^{18}O$ values in excess of 30‰. $\delta^{18}O$ values then decrease to a near constant value of 26‰, related to the continual contribution of fresh O_2 in downwelling waters.

Text Box 5.1. The Dole Effect

The $\delta^{18}O$ value of atmospheric CO_2 is ~41‰, and is explained by equilibrium fractionation between (primarily) ocean water and CO_2 gas. The equilibrium fractionation between CO_2 and H_2O is given by $\alpha = 1.0412$ @ 25°C. In contrast, the $\delta^{18}O$ value of atmospheric O_2 is 23.8‰, far higher than what would be expected based on the equilibrium isotope fractionation between O_2 (g) and H_2O (~13‰). The high $\delta^{18}O$ value of O_2 gas was first measured gravimetrically by Dole (1935, 1936). The explanation for the high $\delta^{18}O$ value of O_2 is explained in terms of photorespiration in plants. While the conversion of $H_2O \rightarrow O_2$ occurs with minimal fractionation, the incorporation of O_2 during respiration preferentially incorporates ^{16}O, leaving the remaining O_2 reservoir enriched in ^{18}O (Lane and Dole, 1956). The disequilibrium between O_2 CO_2 and H_2O vapor is maintained because the exchange rates between these gaseous species are far slower than the exchange rates between CO_2 and liquid water and O_2 cycled through the photosynthesis-respiration cycle. See Keeling (1995), Welp *et al.* (2011) and Luz and Barkan (2011) for a more detailed review.

The $\delta^{13}C$ curve for total dissolved inorganic carbon (ΣCO_2) is a mirror image of the $\delta^{18}O$ curve for dissolved O_2. The abundance of ΣCO_2, which is primarily HCO_3^-, steadily increases with depth as sinking organic matter is oxidized. The concentration increases from ~2000 μmoles/kg near the surface to ~2160 μmoles/kg at 1 km depth, after which it remains essentially constant. The $\delta^{13}C$ values of ΣCO_2 decrease from 2‰ at the surface to 0.7‰ at ~1 km depth and then rise back up to an almost constant value of about 1‰ below 2 km ocean depth (Fig. 5.5). In the absence of biological activity, $\delta^{13}C$ of HCO_3^- in surface waters would be about −1‰, a value appropriate to equilibrium exchange with atmospheric CO_2 (see Chapter 7 for a further explanation of this value). But isotopically light HCO_3^- is preferentially used by organisms in the formation of their soft tissues, driving the $\delta^{13}C$ values of remaining HCO_3^- in the upper (photic) zone to +2‰, or even higher in regions of intense biological productivity. The return to more negative $\delta^{13}C$ values at depth is caused by the addition of light carbon to these waters from the oxidation of sinking organic matter. The formation of organic matter in the productive region of shallow waters, and its systematic removal by oxidation at depth comprises the *biological carbon pump* (box 7.1). (See section 9.3.5 for nitrogen isotope variability with depth).

5.4 Stable isotope ratios as monitors of productivity

Stable isotopes are a powerful tool for evaluating ocean productivity and, using sedimentary materials, paleoproductivity. Carbon isotopes have long been used for this purpose. Light carbon is preferentially incorporated into organic matter, leaving the residual HCO_3^- dissolved in the ocean enriched in ^{13}C. Variations in the $\delta^{13}C$ values of

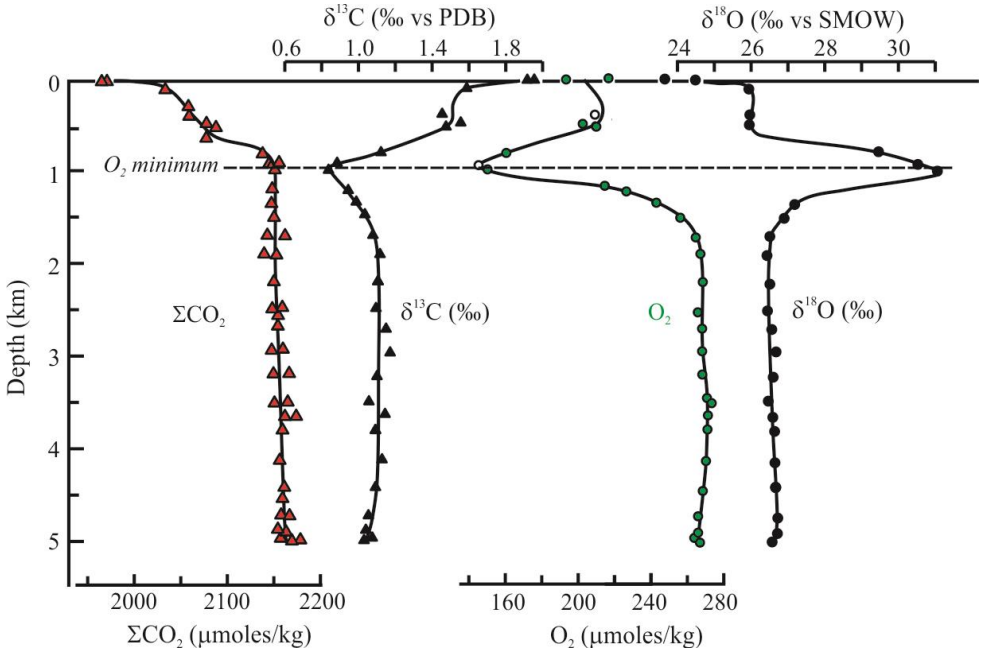

Fig. 5.5. Profiles of dissolved $\Sigma(CO_2)$ and its $\delta^{13}C$ values (left) and dissolved O_2 and its $\delta^{18}O$ values (right). The profile changes are due to oxidation of organic matter and, at depth, to mixing with deep waters. Corrected for $\alpha_{CO_2\text{-}H_2O}$ fractionation of 1.0412. After Kroopnick and Craig (1972).

carbonates can then be used as a proxy for paleoproductivity (Chapter 7). Similarly, the $\delta^{34}S$ values of evaporitic sulfates can be used as a measure ocean productivity (Chapter 10). This is because light sulfur is removed by bacterial sulfate reduction. The light isotope of sulfur is preferentially incorporated in the organic matter and ultimately as iron sulfide. The removal of light sulfur *raises* the $\delta^{34}S$ value of the remaining sulfate. Times of high organic matter burial will lead to more intense sulfate reduction and hence a higher $\delta^{34}S$ value of sulfate dissolved in the ocean.

Non-traditional isotopes have also filled this role. Silicon isotope ratios in diatom frustules have been used as a proxy for paleoproductivity (De La Rocha et al., 1998). Diatoms preferentially incorporate ^{28}Si relative to ^{30}Si by approximately 1‰ independent of temperature and diatom species (De La Rocha et al., 1997). The $\delta^{30}Si$ value of diatoms will vary depending on the conditions of formation. Four endmembers can be envisioned: 1) a small amount of diatoms are produced and their $\delta^{30}Si$ value will be 1‰ lower than the Si source (silicic acid dissolved in water). 2) The diatoms consume all of the dissolved silica. In this case, the $\delta^{30}Si$ values of the diatoms will be equal to that of the initial silicic acid. 3) In a steady state system, where Si is removed from the water column at the same rate it is being replaced from continental or upwelling sources, the $\delta^{30}Si$ value will be equal to that of the silicic acid entering the system. 4) Under conditions of closed system (finite input) Rayleigh fractionation (see 4.6.3 for a more detailed discussion of Rayleigh fractionation), the $\delta^{30}Si$ value of the diatoms will increase with increasing degree of diatom production (higher productivity). The $\delta^{30}Si$ values of diatom separates in marine sediment cores from the Southern ocean show a decrease as the last glacial period began consistent with decreased productivity. The $\delta^{30}Si$ values then increase at the end of the last glacial as higher productivity resumed (De La Rocha et al., 1998).

5.5 Isotopic Compositions of Ancient Oceans

How much has the isotopic composition of the global oceans changed through time? Why does present day seawater have the isotopic composition that it does? What exchange mechanisms or buffering capacity exist in the oceans to cause $^{18}O/^{16}O$ and D/H ratios to change or remain the same through time? These questions are important for a number of reasons, the most compelling being that ancient ocean temperature estimates using stable isotope fractionations are remarkably high if the oxygen isotope composition of the ocean has remained unchanged.

5.5.1 Primitive oceans

If the earliest oceans had equilibrated with hot primitive mantle-derived igneous rocks, they would have had $\delta^{18}O$ and δD values of ~7 ± 1‰ and –60 ± 20‰, respectively (Silverman, 1951). As primitive Earth cooled, interactions between ocean water and basalt would have led to the formation of hydrous minerals. At this stage of development, the δD value of the ocean may have raised the δD of the primitive waters to a small extent, but the effect of this process on $\delta^{18}O$ would have been negligible.

Marine *sediments* and alteration minerals formed by low temperature weathering of terrestrial rocks have D/H ratios that are considerably lower than the D/H ratio of ocean water, so formation of hydrous minerals at low temperatures is a very efficient way to raise the D/H ratio of the world oceans. The effect is somewhat lessened by the fact that marine sediments are subducted into the mantle and some fraction of the water entrained within them is returned to the surface in volcanic emanations.

In contrast to hydrogen, oxygen isotope ratios of the ocean will be lowered significantly by formation of marine sediments and minerals from weathering of igneous rocks. Oxygen isotope fractionations between sedimentary materials (carbonates, silica, phosphates, clays) and water are so large at low temperatures (~20-30‰) that locking up ^{18}O in weathering minerals and in marine sediments should have played a major role in lowering the $\delta^{18}O$ value of the initial oceans from the putative high initial values to those near 0‰. The degree to which $^{18}O/^{16}O$ ratios were lowered and D/H ratios were raised by weathering and sedimentary processes depends once again on material balance considerations and how much sedimentary material was reworked over time.

The hydrogen isotope history of primitive oceans is seldom addressed and, for the most part, remains unresolved. Limited hydrogen isotope analyses of rocks that formed in ancient oceans (greenstones and ophiolites) are similar to those of modern equivalents (Sheppard and Epstein, 1970; Yui et al., 1990; Lécuyer et al., 1996) suggesting that D/H values of the ocean have remained fairly constant throughout geologic time, except during glacial times when light water is locked up in continental ice sheets. Modeling of hydrogen fluxes into and out of the ocean led Lécuyer *et al* (1996) to conclude that the δD of the Archean ocean may have been several tens of per mil lower than the modern value. A similar conclusion was reached by Pope *et al.* (2012) based on the δD values of Archean serpentinites.

The oxygen isotope history of ancient oceans, on the other hand, has received considerable attention using a number of approaches. In the early years of stable isotope geochemistry, much attention was devoted to the carbonate-water isotope thermometer, and the lack of knowledge regarding the $\delta^{18}O$ values of ancient oceans was a major

concern. The oxygen isotope composition of ancient oceans has relevance not only to ocean paleotemperatures, but to understanding ocean hydrothermal systems, models of ocean growth, plate tectonic histories, and reconstruction of environmental conditions in the past.

5.5.2 Secular changes in $\delta^{18}O$ of marine sediments

Marine sediments have been used to address the question of oxygen isotope compositions of ancient oceans. The $\delta^{18}O$ values of cherts, iron formations, phosphorites, and limestones provide information on how $\delta^{18}O$ values of ancient oceans may have differed from those of the modern oceans. In every suite of samples examined to date, measured $\delta^{18}O$ values of marine sediments decrease with increasing age (Fig. 5.6).

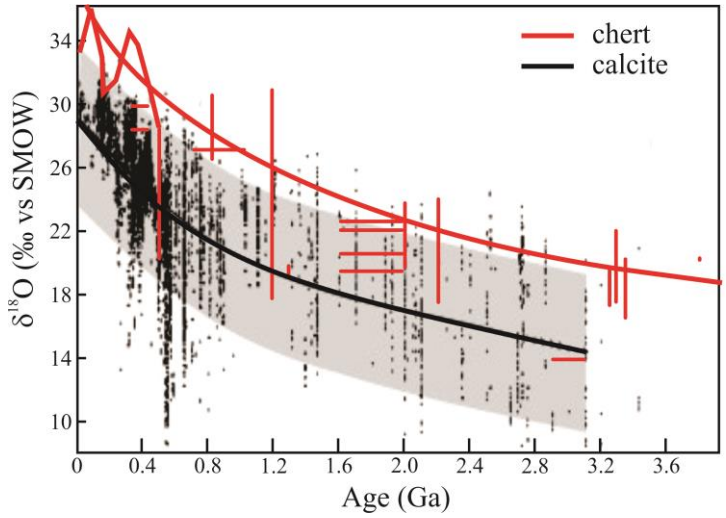

Fig. 5.6. Schematic variation in the $\delta^{18}O$ values of cherts and carbonates. Carbonate compilation from (Kasting et al., 2006) based on compilation from Ján Veizer. Chert data from references in Figure caption 8.8. The length of the lines refers to the range of analyses (*y* axis) and the range of potential age (*x* axis). The lower $\delta^{18}O$ values of ancient sediments may be due to lower $\delta^{18}O_{ocean}$ values in the past, higher ocean temperatures in the past or more intense diagenesis of the older samples.

Using oxygen isotope ratios of marine sediments to reconstruct conditions in ancient oceans is plagued with uncertainty. Consider that the $\delta^{18}O$ value of a chemical sediment in the ocean is a function of both temperature and $\delta^{18}O$ value of the water – two variables and only one analysis (the $\delta^{18}O$ value of the sediment). To complicate matters even further, the sediments examined may not have retained their original isotopic ratios through time. There are three ways to explain the observed secular trends for marine sediments seen in Fig. 5.6:

- $\delta^{18}O$ values of the oceans were more negative in the past
- Temperatures of ancient oceans were higher in the past
- Sediments become lighter with time through diagenetic reactions.

If explanation 1 is correct, mammoth and, for the most part unidirectional, changes occurred in the way the Earth operates, specifically in plate tectonic processes including cessation of activity for very long periods. Explanation 2 is attractive because temperatures were quite likely higher in the very old oceans. Some data, however, require marine organisms to have thrived at temperatures as high as about 70°C, a temperature most biologists would find unacceptable[2]. Many workers in the field favor (at least in part) explanation 3 – diagenesis – but it too is fraught with uncertainty. Most importantly, certain sedimentary minerals are grossly more resistant to oxygen isotope exchange with diagenetic fluids than others. As a consequence, rates of diagenetic alteration are expected to be different as well. Nonetheless, the same secular trend is seen in the oxygen isotope compositions of all sedimentary rocks. It is well to point out that there are rare but important exceptions to these systematics documented in the literature. That is, there are reported cases of ancient sedimentary minerals whose oxygen isotope compositions are similar to those of modern equivalents.

Some combination of all three processes might explain the trends, but assigning relative contributions of each process is not possible with the data at hand. Understanding these secular trends *and* the exceptions, bears importantly on our understanding of how the Earth worked in the past and poses an exciting challenge to earth scientists.

5.6 Seawater-Basalt Interactions – buffering the $\delta^{18}O$ value of the ocean

Muehlenbachs and Clayton (1976) forever changed the '*ocean composition*' landscape with their landmark paper on interactions between seawater and oceanic crust. These authors measured oxygen isotope compositions of samples dredged from the ocean floor as well as samples from Deep Sea Drilling Project (DSDP) boreholes. Confirming early measurements of Garlick and Dymond (1970), they reported that $\delta^{18}O$ values of ocean crust covered a broad range, from <4‰ to >25‰. The variability was explained by seawater alteration of oceanic crust at both low and high temperatures. Combining the two alteration regimes, Muehlenbachs and Clayton devised a model of ocean-crust interaction that effectively buffers the $\delta^{18}O$ value of the ocean to its present steady-state value of 0‰. Further investigations of this model (Gregory, 1991) indicate that drastic and *long-term* (many tens of millions of years) changes in plate tectonic activity would be required to cause significant changes of several per mil in the $^{18}O/^{16}O$ ratio of the ocean. Kasting *et al.* (2006) suggested that changes in ocean depth and rate of pelagic sediment accumulation since the beginning of the Paleozoic Era (~550 Ma) may explain the changing oxygen isotope composition of the ocean in the deep past. Their idea is discussed in section 5.7.4.

The buffering of the $\delta^{18}O$ values of the ocean work in the following way. Pristine Mid Ocean Ridge Basalt (MORB) has a very uniform $\delta^{18}O$ value of 5.7‰. Oceanic basalts with lower and higher values than this contain hydrous alteration phases. Muehlenbachs and Clayton recognized two types of alteration of oceanic crust – a low temperature alteration with $\delta^{18}O$ values that are higher than the source mid-ocean ridge basalts (MORB) and a high-temperature alteration with $\delta^{18}O$ values that are lower than

[2] However, recent discovery of thermophilic bacteria thriving in near-boiling waters lessens the force of this argument.

MORB. Each of these alteration mechanisms affects the $\delta^{18}O$ value of the ocean. Alteration of continental crust by meteoric water will also affect the oxygen isotope composition of the ocean. The combined effects of these three alteration processes results in a buffering of the $\delta^{18}O$ value of the ocean to its present-day value of 0‰ (Muehlenbachs, 1998).

5.6.1 Low-temperature alteration

The vast majority of oceanic basalts are altered to some extent at low temperature and have $\delta^{18}O$ values that are more positive than 5.7‰. Only the youngest glassy MORB preserves its primary $\delta^{18}O$ value of 5.7±0.2‰ (Ito et al., 1987). Most alteration of this type occurs between 0 and 15°C but some occurs at temperatures as high as 50°C. The $\delta^{18}O$ values of basalts that were intensely altered at the lowest temperatures near 0°C can be as high as 25‰. This is because equilibrium fractionations between clay minerals and water are very large at low temperature. The altered rock has a high $\delta^{18}O$ value, which has the effect of *lowering* the $\delta^{18}O$ value of the ocean. The positive correlation between $\delta^{18}O$ values and H_2O^+ contents of the rock illustrates this point (Fig. 5.7). The high $\delta^{18}O$ values are unambiguously explained by the presence of hydrous phases that form during low-temperature alteration of anhydrous basalt on the ocean floor. In most cases, measurements are made of mixtures, hereafter written as *basalt*, of pristine MORB and alteration phases. In the initial stages of alteration, the alteration phases may only be incipient precursors to smectite minerals and are not visible under the microscope. But even minor degrees of alteration can be easily determined by a measurement of H_2O^+ (water given off by heating).

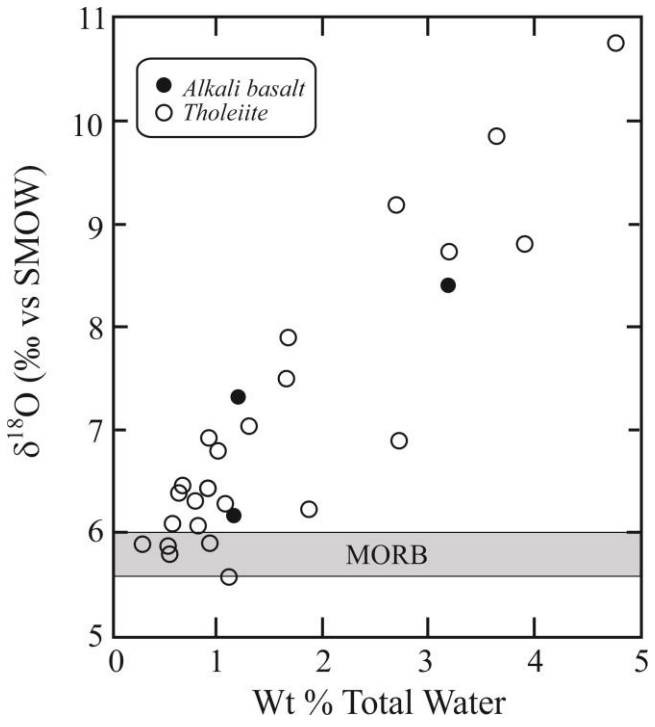

Fig. 5.7. Variation in the $\delta^{18}O$ values and wt% water of ocean basalts. The increase in both parameters is related to low temperature interaction with seawater. After Muehlenbachs and Clayton, (1972).

Low-temperature alteration starts almost immediately after extrusion of the basalt and is a very heterogeneous process that normally affects about 10% of the rock to depths of about 600 meters in the crust. After several million years the basalts reach a relatively constant $\delta^{18}O$ value of 8 to 10‰. Lack of further change with time indicates effective cessation of circulation of low-temperature seawater through the rocks. The low-T interaction between basalt and seawater causes an

increase in the $\delta^{18}O$ value of the rock and a corresponding *decrease* in the $\delta^{18}O$ value of the water, the magnitudes of which are determined by the ratios of water to rock, or W/R ratio. Stakes and O'Neil (1982) suggested that these low-T systems are water dominated with W/R > 50/1.

5.6.2 High temperature alteration

Low temperature alteration represents one half of the picture. Heat flow measurements at mid-ocean ridges show that newly formed crust is rapidly cooled by extensive penetration of vast quantities of water into the rock. The geophysical predictions were confirmed with the discovery of black smokers, ephemeral plumes of superheated water near mid ocean ridges. Petrographic evidence for high-temperature alteration is provided by greenschist-facies rocks that are found on the seafloor. $\delta^{18}O$ values of these *submarine greenstones* or *spilites* are lower (down to ~1.8‰) than those of unaltered MORB, in contrast to what is observed for the vast majority of seafloor basalts that were altered at much lower temperatures. The low $\delta^{18}O$ values of the basalt are consistent with high-temperature reactions and isotopic exchange between basalt and seawater, where $\Delta^{18}O$(*basalt*-water) values are very small. Above 300 to 350°C, equilibrium oxygen isotope fractionations between *basalt* and water are *less* than the 5.7‰ difference between unaltered MORB and ocean water. Therefore, seawater-basalt interactions at high temperatures *decrease* the $\delta^{18}O$ value of the basalt and *increase* the $\delta^{18}O$ value of the water. These high-T systems extend to crustal depths in excess of 1 km and tend to be rock dominated with W/R ratios ranging from extreme highs of about 50/1 to values as low as about 1/1.

Together these two alteration mechanisms along with continental weathering and other minor contributors buffer the $\delta^{18}O$ value of the ocean to a value close to 0‰ (section 5.7). Perturbations from the near-zero value of the modern ocean are countered by the buffering effects of rock alteration, so that a constant value is expected over time.

5.6.3 Evidence from drill core material

Preliminary conclusions about the oxygen isotope systematics of seawater-basalt interactions in the modern oceanic crust were made on the basis of analyses of samples dredged from the ocean floor. Further work has shown that alteration processes in the crust are extremely heterogeneous and can be seen on millimeter scales in tiny veinlets and on kilometer scales along extensive fracture zones. Our understanding of the vertical distribution of $\delta^{18}O$ values in seafloor basalts was greatly improved by the recovery of deep sea drillcores. Unfortunately, the cores are often incomplete, especially lacking extremely altered material. Accepting these constraints, Alt *et al.* (1986) measured an oxygen isotope depth profile of samples from DSDP borehole 504B. They presented evidence for low-temperature alteration in the upper 600 meters of core, followed by an abrupt change in mineralogy and isotopic composition that is consistent with high-temperature metamorphism (Fig. 5.8). The sharp division between styles of alteration at this site can be explained by a model whereby hot seawater migrated up through the relatively impermeable dike section and cold seawater descended through the more permeable upper layers.

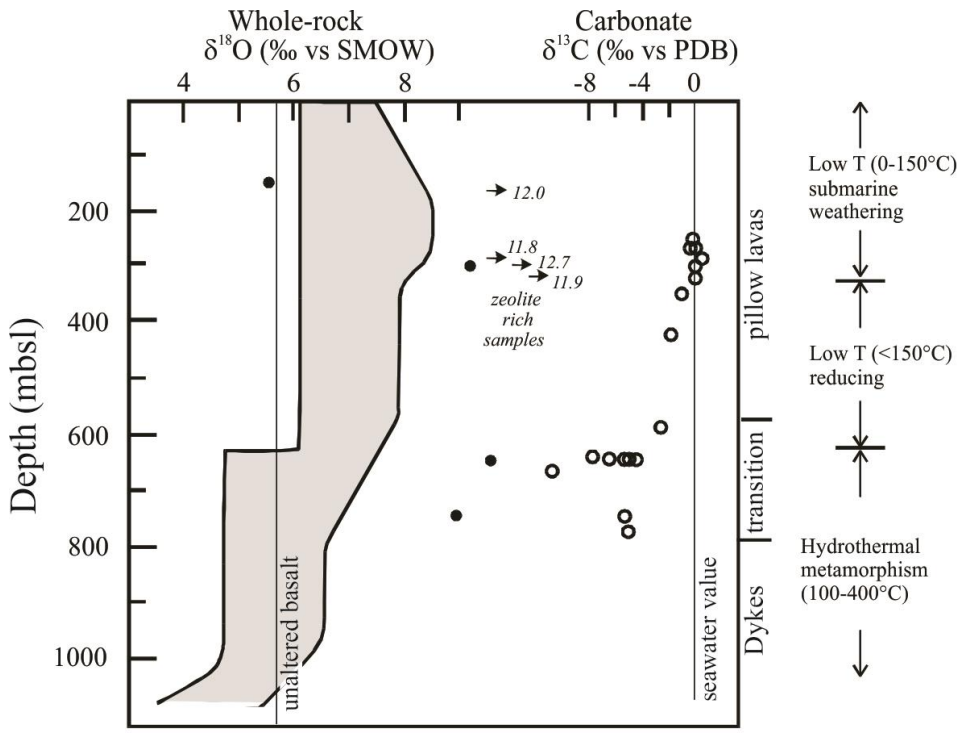

Fig. 5.8. $\delta^{18}O$ values of DSDP Hole 504B. There is an abrupt change from values higher than to values lower than the $\delta^{18}O$ value of normal MORB at 624m, a depth that marks an interface between hot upwelling waters and cold downwelling waters. $\delta^{13}C$ values of carbonate in the rocks below 624 m have a mantle signature. The grey region reflects the majority of values measured. After Alt *et al.* (1986).

5.6.4 Evidence from obducted material

Obducted equivalents of oceanic crust, the ophiolites, pose no problem of sampling and offer a way of studying the problem of seawater-crust interaction in ancient materials. Because the nature of both high-T and low-T alteration on the seafloor is almost certainly time-invariant, the patterns and $\delta^{18}O$ values of seafloor alteration should be the same in ancient ophiolites as they are in the modern crust, and indeed, this is the case (Muehlenbachs, 1986)[3]. The ophiolitic sequence from the 3.5 Ga Onverwacht Group has $\delta^{18}O$ values whose ranges are indistinguishable from modern ocean samples (Hoffman et al., 1986) and similar patterns are seen in other ancient ophiolites and hydrothermal deposits (e.g., Holmden and Muehlenbachs, 1993). The most complete and best exposed section of obducted oceanic crust is provided by the Samail ophiolite in Oman (Fig. 5.9). Gregory and Taylor (1981) found that $\delta^{18}O$ variations in this ophiolite are consistent with the seafloor interactions proposed by Muehlenbachs and Clayton. Pillow basalts and the diabase dike complex have $\delta^{18}O$ values that are higher than 5.7‰ and gabbros deeper down in the section have $\delta^{18}O$ values that are lower than 5.7‰. The amount of ^{18}O depletion by high-T alteration appears to be balanced by the amount of ^{18}O

[3] Ophiolites are not exactly analogous to mid ocean ridge spreading centers, but they are all that is available.

enrichment by low-T alteration in the Samail rocks providing strong evidence for the buffering capacity of these alteration processes.

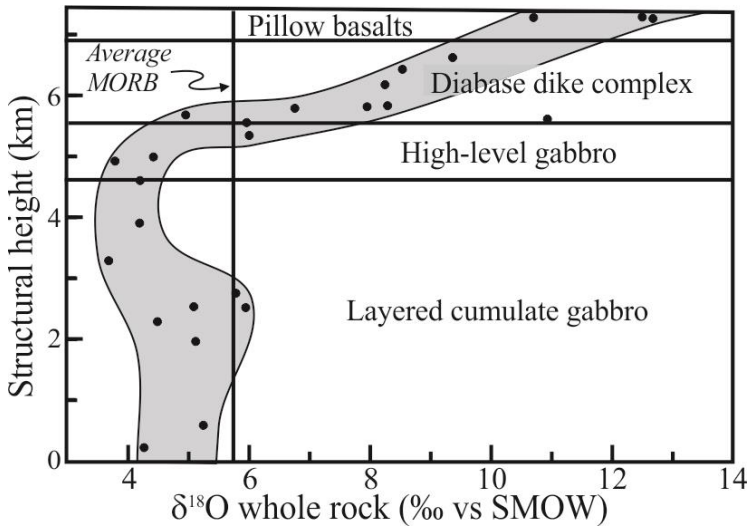

Fig. 5.9. Measured $\delta^{18}O$ values through a cross section of the Samail ophiolite. The lower, 'high temperature' section has low $\delta^{18}O$ values, while the upper, 'low temperature' section has high $\delta^{18}O$ values, consistent with the model of Muehlenbachs and Clayton. After Gregory and Taylor, (1981).

Analyses of altered seafloor material, represented by ophiolites, suggest that the oxygen isotope composition of the ocean has been invariant through time, with the exception of transient shifts due to accumulation of glacial ice on the continents.

5.7 Buffering the $^{18}O/^{16}O$ Ratio of Ocean Water

The two competing types of seawater-basalt interactions known to occur in the oceanic crust are not coincidental and are natural consequences of basaltic magmatism occurring on the seafloor. These interactions clearly bear on the oxygen isotope budget of the ocean and there is strong evidence that, in concert with continental weathering, they buffer the $^{18}O/^{16}O$ ratio of the ocean to a steady state value.

5.7.1 Summing the processes affecting the $^{18}O/^{16}O$ ratio of seawater

There are five natural processes that affect the oxygen isotope composition of seawater:

1. Continental weathering – lowers $\delta^{18}O_{ocean}$
2. Seafloor *weathering* (a misnomer meaning low-T alteration) – lowers $\delta^{18}O_{ocean}$
3. Hydrothermal alteration of ocean basalt (high-T alteration) – raises $\delta^{18}O_{ocean}$
4. Water cycling associated with subduction and magmatism
5. Continental growth (minor – long term)
6. Glaciation – raises $\delta^{18}O_{ocean}$ (short term fluctuations)

Glaciation is different in kind from the other processes. Removal of light water vapor to continental ice sheets results in unidirectional (positive) changes of 1-2 permil in the $\delta^{18}O$ value of seawater, and occurs on a relatively short time scale of 10^3 years.

The first four processes enumerated above comprise the backbone of the buffering hypothesis. These different processes operate in such a way that the $\delta^{18}O$ value of the oceans is maintained at a value near 0‰ (Fig. 5.10). In fact the buffering model is quite robust because the $\delta^{18}O$ value of MORB is fixed and the temperatures of both low-T and high-T alteration are also fixed within narrow limits and cannot change with time. If the

$\delta^{18}O$ value of seawater could be shifted to either higher or lower values by some unknown process, basalt-seawater interactions would force it back to a value near 0‰ in ~250 million years. The buffering rate is therefore on the order of ~100 Ma.

5.7.2 Unresolved controversy

From the very onset of stable isotope geochemistry, there have been strong proponents for and against the existence of major changes in oxygen isotope ratios of the ocean over geologic time. At this point in time, the arguments are centered on evidence for changes in $\delta^{18}O$ of only about 3-6 per mil over relatively short geologic periods of tens of millions of years. Most of the strong evidence comes from oxygen isotope variations in carefully selected brachiopod shells and inorganic cements deposited in Devonian times (see Chapter 6). The arguments are cogent and yet model calculations, discussed below, indicate that such changes are unlikely. Biogenic phosphate is much more resistant to diagenetic changes of oxygen isotope ratios and isotopic analyses of conodonts and fossil fish remains may provide penetrating evidence on this important question, one way or the other.

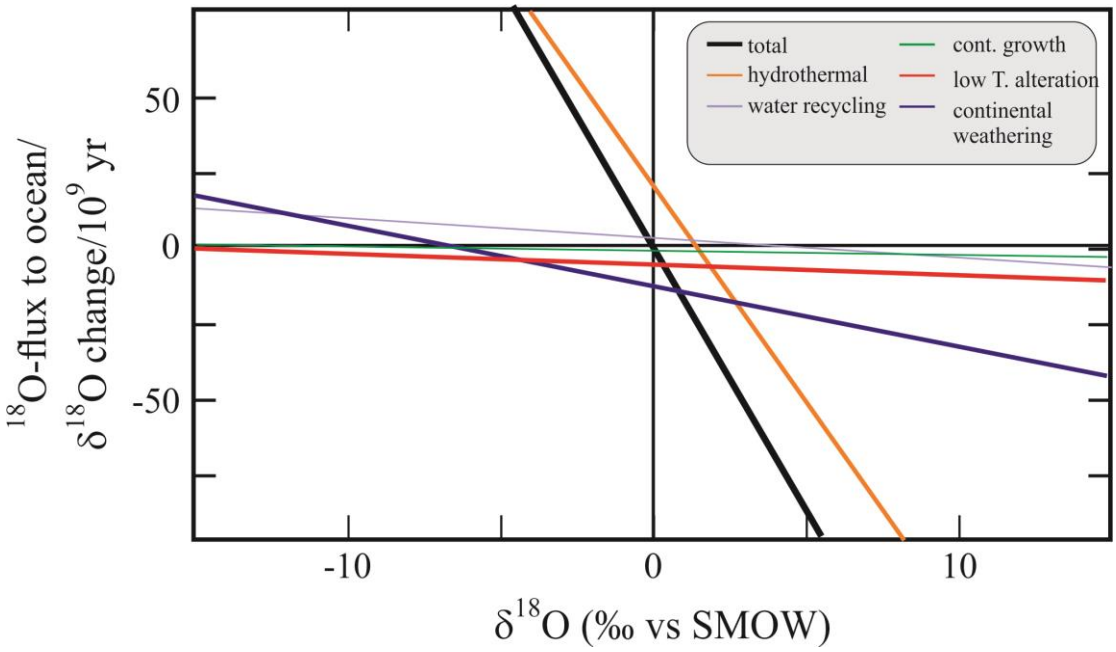

Fig. 5.10. Buffering effects of different alteration mechanisms to the $\delta^{18}O$ value of the ocean. Plotted are the effect of each flux and how it changes the ocean isotopic composition on the billion year time scale. The sum of all the alteration mechanisms is shown by the curve 'total', which buffers the $\delta^{18}O$ value of the ocean to a value of 0‰ See Muehlenbachs (1998) for details.

5.7.3. Model calculations

Gregory (1991) presented the following material balance equation relating the rate of change $\delta^{18}O$ of seawater to exchange processes between the lithosphere and hydrosphere

$$d\delta W/dt = \Sigma k_i(\delta W + \Delta_i - \delta_i^o) \qquad 5.1$$

where δW is the instantaneous $\delta^{18}O$ value of seawater, δ_i^o are the initial $\delta^{18}O$ values of the different rock reservoirs (i), Δ_i are bulk fractionation factors between the i reservoirs and water, and k_i are the rate constants in units of 1/t.

From the definition of Δ_i, it follows that $\delta_i^o - \Delta_i$ is the $\delta^{18}O$ value of seawater (δW) when steady state conditions are reached with the ith reservoir and

$$\delta W_{\text{steady state}} = [\Sigma k_i(\delta_i^o - \Delta_i)]/\Sigma k_i \qquad 5.2$$

In both simple and more refined models developed to address the fluxes of ^{18}O in and out of the ocean, relative rates of continental weathering and sea floor spreading are key parameters. There are obvious constraints on these rates, one being that the rate of continental weathering must be less than that of continental growth. Rates of seafloor spreading have very little effect on the overall buffering process as long as the average global spreading rate is greater than 1 km^2/yr. Present global spreading rates are 3-4 km^2/yr and were probably higher in the past. If seafloor spreading rates were doubled, the time required for the $\delta^{18}O$ of the ocean to return to zero from a perturbed value would be on the order of 60 million years. $\delta^{18}O$ values of the oceans could change only if seafloor spreading effectively ceased and continental weathering continued. The rate of change would be on the scale of billions of years, however. If seafloor spreading really did stop, there would be a reduction in global tectonic activity as well, and the effect of continental weathering would diminish accordingly.

5.7.4. An alternative explanation for the early-Earth low $\delta^{18}O$ values

An alternative view on the effect of plate tectonic-related buffering of the ocean by rock alteration was presented by Kasting *et al.* (2006). They suggested that conditions in the ocean have not been constant through time. In particular, they proposed that the depths of the oceans may have been shallower in the past, and as a result, the confining pressure at the mid ocean ridges from the overlying ocean would have been less than today. This would result is a significantly reduced depth of fluid penetration and reduced high temperature hydrothermal alteration at the ridges. The high temperature hydrothermal activity would have been less in the distant past and the overall $\delta^{18}O$ value of the oceans would have been lower. This idea in part explains the low $\delta^{18}O$ values measured in ancient sediments. This idea is predicated on a significant reduction in heat flow from the mantle since the Phanerozoic, an idea which is not well supported by geophysical models. Overall, the paleoclimate community remains divided over which mechanism – higher temperatures, lower $\delta^{18}O$ values of the ancient ocean, or diagenesis – are responsible for the secular variations in sediments through time.

References

Alt, J.C., Muehlenbachs, K. and Honnorez, J. (1986) An oxygen isotopic profile through the upper kilometer of the oceanic crust, DSDP Hole 504B. *Earth and Planetary Science Letters* **80**, 217-229.

Craig, H. and Gordon, L.I. (1965) Deuterium and oxygen-18 variations in the ocean and the marine atmosphere, Stable Isotopes in Oceanographic Studies and Paleotemperatures. Consiglio Nazionale delle Richerche, Pisa, Spoleto, Italy, pp. 9-130.

De La Rocha, C.L., Brzezinski, M.A. and DeNiro, M.J. (1997) Fractionation of silicon isotopes by marine diatoms during biogenic silica formation. *Geochimica et Cosmochimica Acta* **61**, 5051-5056.

De La Rocha, C.L., Brzezinski, M.A., DeNiro, M.J. and Shemesh, A. (1998) Silicon-isotope composition of diatoms as an indicator of past oceanic change. *Nature* **395**, 680-683.

Dole, M. (1935) The relative atomic weight of oxygen in water and air. *Journal of the American Chemical Society* **57**, 2731.

Dole, M. (1936) The relative atomic weight of oxygen in water and in air. A discussion of the atmospheric distribution of the oxygen isotopes and the chemical standard of atomic weights. *The Journal of Chemical Physics* **4**, 268-275.

Epstein, S. and Mayeda, T.K. (1953) Variation of ^{18}O content of waters from natural sources. *Geochimica et Cosmochimica Acta* **4**, 213-224.

Friedman, I., Schoen, B.S. and Harris, J.L. (1961) The deuterium concentration in Arctic sea ice. *Journal of Geophysical Research* **66**, 1861-1864.

Garlick, G.D. and Dymond, J.R. (1970) Oxygen isotope exchange between volcanic materials and ocean water. *Geological Society of America Bulletin* **81**, 2137-2141.

Gregory, R.T. (1991) Oxygen isotope history of seawater revisited; timescales for boundary event changes in the oxygen isotope composition of seawater, in: Taylor, H.P., Jr., O'Neil, J.R., Kaplan, I.R. (Eds.), Stable Isotope Geochemistry: A Tribute to Samuel Epstein. The Geochemical Society, San Antonio, pp. 65-76.

Gregory, R.T. and Taylor, H.P., Jr. (1981) An oxygen isotope profile in a section of Cretaceous oceanic crust, Samail ophiolite, Oman: evidence for ^{18}O buffering of the oceans by deep (>5km) seawater-hydrothermal circulation at mid-ocean ridges. *Journal of Geophysical Research* **86**, 2737-2755.

Holmden, C. and Muehlenbachs, K. (1993) The $^{18}O/^{16}O$ ratio of 2-billion-year-old seawater inferred from ancient oceanic crust. *Science* **259**, 1733-1736.

Ito, E., White, W.M. and Goepel, C. (1987) The O, Sr, Nd and Pb isotope geochemistry of MORB. *Chemical Geology* **62**, 157-176.

Kasting, J.F., Howard, M.T., Wallmann, K., Veizer, J., Shields, G. and Jaffrés, J. (2006) Paleoclimates, ocean depth, and the oxygen isotopic composition of seawater. *Earth and Planetary Science Letters* **252**, 82-93.

Keeling, R.F. (1995) The atmospheric oxygen cycle: The oxygen isotopes of atmospheric CO_2 and 0_2 and the $0_2/N_2$ ratio. *Reviews of Geophysics* **33**, 1253-1262.

Kroopnick, P. and Craig, H. (1972) Atmospheric oxygen: isotopic composition and solubility fractionation. *Science* **175**, 54-55.

Lane, G.A. and Dole, M. (1956) Fractionation of oxygen isotopes during respiration.

Science **123**, 574-576.

Lécuyer, C., Gruau, G., Frueh-Green, G.L. and Picard, C. (1996) Hydrogen isotope composition of early Proterozoic seawater. *Geology* **24**, 291-294.

Luz, B. and Barkan, E. (2011) The isotopic composition of atmospheric oxygen. *Biological Abstracts Vol. 95, Iss. 3, Ref. 30880.* **25**, doi:10.1029/2010GB003883 003814 pp.

Muehlenbachs, K. (1986) Alteration of the oceanic crust and the ^{18}O history of seawater, in: Valley, J.W., Taylor, H.P., Jr., O'Neil, J.R. (Eds.), Stable isotopes in high temperature geological processes. Mineralogical Society of America, Chelsea, pp. 425-444.

Muehlenbachs, K. (1998) The oxygen isotopic composition of the oceans, sediments and the seafloor. *Chemical Geology* **145**, 263-273.

Muehlenbachs, K. and Clayton, R.N. (1972) Oxygen Isotope Geochemistry of Submarine Greenstones. *Canadian Journal of Earth Sciences* **9**, 471-478.

Muehlenbachs, K. and Clayton, R.N. (1976) Oxygen isotope composition of the oceanic crust and its bearing on seawater. *Journal of Geophysical Research.* **81**, 4365-4369.

O'Neil, J.R. (1968) Hydrogen and oxygen isotope fractionation between ice and water. *Journal of Physical Chemistry* **72**, 3683-3684.

Pope, E.C., Bird, D.K. and Rosing, M.T. (2012) Isotope composition and volume of Earth's early oceans. *Proceedings of the National Academy of Sciences* **109**, 4371-4376.

Railsback, L.B., Anderson, T.F., Ackerly, S.C. and Cisne, J.L. (1989) Paleoceanographic modeling of temperature-salinity profiles from stable isotopic data. *Paleoceanography* **4**, 585-591.

Sheppard, S.M.F. and Epstein, S. (1970) D/H and $^{18}O/^{16}O$ ratios of minerals of possible mantle or lower crustal origin. *Earth and Planetary Science Letters* **9**, 232-239.

Silverman, S.R. (1951) The isotope geology of oxygen. *Geochimica et Cosmochimica Acta* **2**, 26-42.

Urey, H.C., Epstein, S. and McKinney, C.R. (1951) Measurement of paleotemperatures and temperatures of the Upper Cretaceous of England, Denmark, and the southeastern United States. *Geological Society of America Bulletin* **62**, 399-416.

Welp, L.R., Keeling, R.F., Meijer, H.A.J., Bollenbacher, A.F., Piper, S.C., Yoshimura, K., Francey, R.J., Allison, C.E. and Wahlen, M. (2011) Interannual variability in the oxygen isotopes of atmospheric CO_2 driven by El Niño. *Nature* **477**, 579-582.

Yui, T.F., Yeh, H.W. and Lee, C.W. (1990) A stable isotope study of serpentinization in the Fengtien Ophiolite, Taiwan. *Geochimica et Cosmochimica Acta* **54**, 1417-1426.

Chapter 6

BIOGENIC CARBONATES – OXYGEN

Contents

6.1 Introduction 1
6.2 The Phosphoric Acid Method 2
6.2.1 A major breakthrough 2
6.2.2 Acid Fractionation Factors 3
6.2.3. Applicability 5
6.3 The Oxygen Isotope Paleotemperature Scale 6
6.4 Factors Affecting Oxygen Isotope Paleotemperatures 11
6.4.1 Variations in $\delta\ ^{18}O$ of ocean water in space and time 11
6.4.2 Vital effects 13
6.4.3. Diagenesis 14
6.4.4 Ecology of the organism 19
6.5 Applications of Oxygen Isotope Paleothermometry 19
6.5.1 The Quaternary 20
6.5.2 The Paleogene and Neogene (Cenozoic) 21
6.5.3. Older samples 22
6.5.4 Application to continental carbonates 24
6.6 Clumped isotope thermometry 25
References 27

Chapter 6

BIOGENIC CARBONATES – OXYGEN

6.1 Introduction

Carbonates are one of the most studied phases in stable isotope geochemistry. They are found at all but the oldest chronological intervals, and the information from oxygen and carbon isotopes can be used to infer paleotemperatures, paleoproductivity, circulation patterns, water depth, etc. Oxygen isotope ratios of marine carbonates most often provide information about water temperature and ice volume, while carbon isotopes provide information about biological productivity conditions. Because of the vastness of the field, and the different information obtained from each isotope, they are presented in separate chapters (6 and 7), although some overlap is unavoidable.

The potential use of biogenic carbonates as a paleoclimate indicator played a pivotal role in the development of stable isotope geochemistry. The discipline as we know it today was spawned by Harold Urey, who recognized the possibility of determining temperatures of ancient oceans from the preserved oxygen isotope ratios of biogenic carbonates deposited by marine organisms. But, for meaningful application to paleoceanography, these temperatures had to be determined to within ± 0.5^{o}C, which required increasing the precision of the mass spectrometer analysis by an order of magnitude. Accomplishing this engineering feat not only made possible the development of the oxygen isotope paleotemperature scale, but allowed for the subtle variations in isotopic compositions of other light elements to be recognized as well.

Harold Urey was on his 1947 lecture tour sponsored annually by the Royal Society of London. He was speaking about the physical fractionation of stable isotopes between ideal gases and simple aqueous solutions. He finished his lecture at ETH Zürich and accepted a question from Paul Niggli, the renowned Alpine geologist. Niggli asked if the fractionation between carbonates and water might be large enough and sensitive enough to temperature variations so that the carbonates could be used for reconstructing ancient marine temperatures. The story goes that Urey thought a second, said that he didn't know, but that it seemed reasonable. Later calculations led him to believe that there was promise in this avenue of research. But numerous hurdles presented themselves before he would be able to apply his paleothermometer. Urey needed a more precise mass spectrometer. He needed a method to reproducibly convert carbonates to a gaseous phase that he could analyze in the mass spectrometer. And he needed to quantify the fractionation between carbonate and water as a function of temperature. Putting together a remarkable team of young scientists, including Samuel Epstein, Charles McKinney, John McCrea, Harold Lowenstam, and Harmon Craig, he was able to work out the details in record time, and clear the hurdles necessary to bring the paleotemperature technique to fruition.

The basic idea for the carbonate paleothermometer is as follows: The fractionation between calcite and water is a function of temperature. So the difference in the $\delta^{18}O$ values of calcite and water can be used for determining the temperatures of the ocean at the time the carbonate formed. In addition to the analytical problems mentioned above, there were several other concerns that needed to be addressed: 1) Did the marine organisms precipitate their shell material in isotopic equilibrium with the ocean water, or

is there a biological 'vital effect' that causes organisms to precipitate calcite out of isotopic equilibrium with water? Realize that many marine organisms precipitate aragonite shells rather than calcite, even though aragonite is not stable at the Earth's surface. Perhaps the isotopes are out of equilibrium as well. 2) Have the carbonates preserved their oxygen isotope composition over the millions of years since their initial deposition, or have they undergone diagenesis? 3) Was the $\delta^{18}O$ value of the ocean at the time the calcite formed the same as it is today? We only measure the $\delta^{18}O$ value of the carbonate. The $\delta^{18}O$ value of the water from which it formed is almost always inferred. All of these problems, noted by Urey in 1948, are addressed in the following sections.

6.2 The Phosphoric Acid Method

6.2.1 A major breakthrough

The quest for reliable methods to pretreat shells and to make precise oxygen isotope analysis of their constituent carbonate was described by Harold Urey as "the toughest chemical problem I ever faced." The development of the phosphoric acid method of carbonate analysis by his doctoral student John McCrea (1950) was a seminal chapter in the history of stable isotope geochemistry. This method, only slightly modified in the ensuing years, involves converting carbonate to CO_2 gas by reaction with phosphoric acid. The CO_2 is then analyzed in the mass spectrometer. The technique remains the protocol for analysis of carbonates in stable isotope laboratories the world over. Carbonate analysis today is routine, but the Urey group faced major obstacles to overcome this chemical challenge in 1949.

McCrea initially tried liberating CO_2 from carbonates by thermal decomposition

$$CaCO_3 + \text{heat} \rightarrow CaO + CO_2 \qquad 6.1.$$

Despite good chemical yields (*i.e.,* the reaction went to completion), the extracted CO_2 had scattered $\delta^{18}O$ values, far outside the required reproducibility of ± 0.1‰ and the approach was abandoned. McCrea next turned to acid decomposition

$$2H^+ + CaCO_3 \rightarrow Ca^{2+} + H_2O + CO_2 \qquad 6.2.$$

The procedure involves reacting the carbonate with an acid in an evacuated vessel, purifying, collecting and finally analyzing the CO_2 gas as a measure of the $\delta^{18}O$ value of the original carbonate. The only common acids whose vapor pressures of water and other compounds are low enough to use in a vacuum system are concentrated H_2SO_4 and H_3PO_4. It soon became apparent that 100% H_3PO_4 was the acid of choice. The early workers were concerned about contamination from organic matter present in commercial acids because fragments of organic molecules made in the source of the mass spectrometer could have masses in the 43-47 range that would interfere with determinations of 46/44 and 45/44 ratios. Thus the acid recipe (see Box 6.1) finally adopted by the Chicago group assured that no contamination arose from the specially prepared acid. The '100% phosphoric acid', common in many laboratories around the world is light green (from addition of chromium oxide), very viscous and known to spontaneously crystallize at any time. Most likely, some of the procedures developed by the early workers are unnecessary or have become obsolete by the commercial

availability of pure H_3PO_4, but most researchers take the approach 'if it ain't broke, don't fix it', so the acid ritual survives. Some laboratories have found that commercially available 85% phosphoric acid can be vacuum distilled to obtain a 100% phosphoric acid, which apparently works just fine.

Box 6.1: Preparation of 100% H_3PO_4 for stable isotope analysis of carbonates - Recipe

1. Pour 2.5 L (one bottle) of commercial 85% phosphoric acid into a large Pyrex beaker that is placed on a hotplate in a fume hood.
2. Slowly stir in about 1.4 kg of analytical grade P_2O_5. The ensuing reaction is exothermic and should be done with care.
3. Add a spatula-tip quantity of CrO_3. The solution turns pale yellow.
4. Slowly raise the temperature to 200°C and heat for about 7 hours. The solution turns green.
5. Raise the temperature to 220°C and heat 4-5 hours.
6. Stop heating when the density @25°C = 1.9, the density of 100% H_3PO_4.
7. When the acid cools, stir in 3mL of H_2O_2.
8. Store in brown glass bottles with rubber seals. 500 mL is a convenient size.
9. Age for about one month before using.

Notes

1. The density must be > 1.8. [H_3PO_4] > 100% is desirable as excess P_2O_5 readily takes up water. Solutions with [H_3PO_4] > 103%, however, are more prone to crystallize, and inhibit diffusion of CO_2 out of the acid into the head space.
2. The acid is very corrosive and will destroy the markings on glass thermometers. Use a glass sleeve or other means of protecting these markings.
3. The acid turns green as a result of reduction of Cr(VI) to Cr(III) by organic matter present in the commercial acid.
4. H_2O_2, a reducing agent in this case, is added to reduce residual Cr(VI) to Cr(III).
5. Avoid exposing the acid to air for extended periods, as it is hygroscopic.
6. No one understands what happens during the aging period, but aging seems to be necessary. At least, it can't hurt!

The phosphoric acid and calcite are reacted at a constant temperature. Most calcium in solution is present as calcium phosphate ion pairs $(CaPO_4)^-$ and $CaHPO_4$. The water produced is taken up by excess P_2O_5 to form H_3PO_4. During extraction of the CO_2, a very small amount of some other volatile compounds, mostly water vapor, is also liberated and is separated from the CO_2 by judicious use of cryogenic traps.

6.2.2 Acid Fractionation Factors

In both thermal and acid decompositions of carbonates, the liberated CO_2 contains *all* the carbon but only 2/3 of the oxygen in the carbonate (equations 6.1 & 6.2). As a consequence, the $\delta^{13}C$ value of the evolved CO_2 and parent carbonates are identical, but the oxygen isotope ratios are different due to a fractionation between the CO_2 gas and

oxygen from the carbonate that remains dissolved in the acid. $^{18}O/^{16}O$ ratios are always higher in liberated CO_2 than in the original carbonate (related to the stronger C=O double bonds in CO_2 gas). The magnitude of the oxygen isotope fractionation is probably controlled by both kinetic and equilibrium effects. A so-called *acid fractionation factor* must be applied to the CO_2 analysis to obtain the oxygen isotope ratio of the carbonate. The oxygen isotope fractionation between evolved CO_2 and a given carbonate is given by

$$\alpha_{CO_2-carbonate} = \frac{1000 + \delta^{18}O_{CO_2}}{1000 + \delta^{18}O_{carbonate}} \qquad 6.3,$$

and is constant at a given temperature of reaction. The α value becomes smaller with increasing temperature. Because of the temperature effect, H_3PO_4-carbonate reactions must be run at a constant temperature. For many years these reactions were carried out at 25ºC, but temperatures as high as 90ºC are commonly used today to a) ensure that reactions are complete in the relatively short times used in automated systems and b) to reduce the solubility of CO_2 in the acid allowing for smaller samples to be analyzed. It makes no difference what temperature is used because the method is calibrated to

Table 6.1*: Acid Fractionation Factors.*

Mineral	Temperature (°C)	Fractionation factor α	Reference
Calcite - $CaCO_3$	25	1.01025	1
	25	1.01049	4
'sealed vessel'	50	1.009311	2
'common acid bath'	50	1.009002	2
aragonite - $CaCO_3$	25	1.01034	1
	25	1.01107	4
dolomite -$CaMg(CO_3)_2$	25	1.01109	1
	50-100	$4.23 + 6.65\times10^5/T^2$	3
siderite - $FeCO_3$	50-150	$3.85 + 6.84\times10^5/T^2$	3
	25, 50	1.01017, 1.01016	6
	8.5-62	19670/T – 36.27	7
ankerite - $CaFe(CO_3)_2$	50-150	$4.15 + 6.68\times10^5/T^2$	3
magnesite - $MgCO_3$	50	1.01160	5
strontianite - $SrCO_3$	25	1.01049	1
witherite - $BaCO_3$	25	1.01097	1
	25	1.01063	4
smithsonite - $ZnCO_3$	25	1.01130	1
otavite - $CdCO_3$	25	1.01145	1
	25	1.01124 – 1.01369	4
rhodocrosite - $MnCO_3$	25	1.01012	1
cerussite - $PbCO_3$	25	1.01013	1

[1] (Sharma and Clayton, 1965) ; [2] (Swart et al., 1991); [3] (Rosenbaum and Sheppard, 1986); [4](Kim and O'Neil, 1997); [5](Perry and Tan, 1972); [6](Carothers et al., 1988) [7](van Dijk et al., 2018)

international reference standards reacted at the same temperature as the samples. As long as temperatures are kept constant, and an α value is determined based on accepted standards, measured (and corrected) $\delta^{18}O$ values of samples will be consistent with IAEA-accepted scales (SMOW or PDB), and will be comparable lab-to-lab.

For many years, the values of acid fractionation factors were unknown, because the $\delta^{18}O$ values of the carbonate themselves were unknown. All that could be measured was the $\delta^{18}O$ value of the evolved CO_2 gas. Sharma and Clayton (1965) and others later finally measured the $\delta^{18}O$ value of the *total* carbonate by the method of fluorination[1]. Once the baseline $\delta^{18}O_{carbonate}$ value was determined, it became a trivial exercise to determine the α value at any temperature[2]. Fractionation factors have values on the order of 1.010xx (10 per mil) and are different for different carbonates (Table 6.1). Remember that the α value in equation 6.3 is not the equilibrium CO_2-calcite fractionation, which is closer to 1.0109‰. It is the kinetic fractionation that occurs during dissolution of the calcite. As long as the fractionation is constant, however, it does not matter if it is equilibrium or not.

6.2.3. Applicability

The H_3PO_4 method is one of the most robust used in stable isotope geochemistry and is applicable to the analysis of all carbonates. Some carbonate minerals, like magnesite and smithsonite, *require* relatively high reaction temperatures because they react so slowly at room temperature. Using even the most basic extraction line, $\delta^{18}O$ and $\delta^{13}C$ values of samples weighing about 1 mg or more can be measured with a precision of better than 0.1 and 0.05‰, respectively. With sophisticated extraction systems connected directly to the mass spectrometer (*on-line systems*), samples as small as tens-to-hundreds of micrograms can be analyzed routinely with the same precision. A few authors have reported that grain size and carbonate/acid ratio can significantly influence the isotopic analyses (Wachter and Hayes, 1985; Barrera and Savin, 1987; Al-Aasm et al., 1990; Swart et al., 1991), but these effects are generally eliminated when the reactions are carried out at relatively high temperatures. Contamination by organic matter, chlorine- and sulfur-bearing compounds, or inclusions of other carbonates pose more serious problems (Charef and Sheppard, 1984). Organic matter is a particular concern for modern samples and should be removed before analysis. This can be done a number of ways including roasting the sample in a stream of helium, treatment with mild oxidizing agents, and exposure to an oxygen plasma. The small amount of organic matter present in fossil carbonate generally has no effect on the measured $\delta^{13}C$ and $\delta^{18}O$ values of the carbonate, but the samples are routinely sent through a pretreatment step in any case. One can always analyze treated and untreated splits of a given sample to ascertain if pretreatment is necessary. Recently, continuous flow techniques have been developed for rapid analysis of small samples (see Section 2.8.3). These automated peripherals are standard additions offered by all mass spectrometer manufactures.

---

[1] The fluorination reaction is approximated by $2CaCO_3 + 4F_2 \rightarrow 2CaF_2 + 2CF_4 + 3O_2$. *All* O_2 is extracted from the carbonate andmeasured for $\delta^{18}O$ value, hence the 'total carbonate' value.

[2] With a known $\delta^{18}O$ value of the carbonate (from fluorination) and a measured $\delta^{18}O$ value of evolved CO_2 gas from phosphoric acid digestion, the α value could be determined by plugging these values into equation. 6.3.

6.3 The Oxygen Isotope Paleotemperature Scale

Armed with an improved isotope ratio mass spectrometer and the phosphoric acid method of carbonate analysis, the Chicago group faced the challenge of calibrating a temperature scale based on the temperature-sensitive oxygen isotope fractionation between biogenic carbonate and ocean water. They had no established reference standards at that time nor knowledge of the fractionation factors for the analytical methods they employed: acid-carbonate reaction for carbonates (McCrea, 1950), and CO_2-H_2O equilibration for waters (Cohn and Urey, 1938). Undaunted, Samuel Epstein addressed the problem by making a simple empirical calibration. He collected shells and water from cold and warm water environments. He also cultured shells in laboratory aquariums. He then measured the difference between the oxygen isotope composition of CO_2 liberated from the carbonate by phosphoric acid at 25°C and CO_2 equilibrated with the ambient H_2O at 25°C. Fortuitously, this difference for normal marine calcite and ocean water is very small at 25°C. The point is illustrated in Fig. 6.1 using a $\delta^{18}O$ value of water = 0‰ as an example[3]. The $\alpha(CO_2 - H_2O)$ value at 25°C is 1.0412 (O'Neil et al., 1975), corresponding to a $\delta^{18}O$ value of CO_2 equilibrated with ocean water ($\delta^{18}O$ = 0‰)

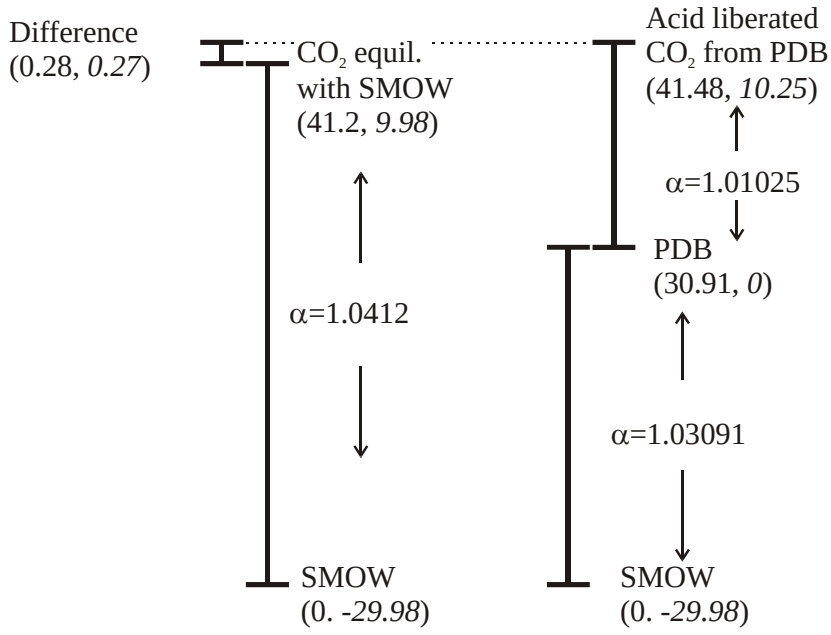

Fig. 6.1. Difference in the $\delta^{18}O$ value of acid liberated CO_2 from Pee Dee belemnite (PDB) and that equilibrated with SMOW. Delta values are shown on the SMOW scale (normal) and PDB scale (italic). In either case, the difference between the CO_2 gases measured in the mass spectrometer is only on the order of 0.2‰. Note: This difference between CO_2 equilibrated with SMOW and acid liberated CO_2 from a carbonate in equilibrium with SMOW at 25°C would be almost 2 ‰.

[3] The difference between the $\delta^{18}O$ value of CO_2 and H_2O varies slightly in relation to the $\delta^{18}O$ value of the phases relative to the standard, although the α value does not. For example the $\alpha(CO_2 - H_2O)$ value at 25°C is 1.0412. If the $\delta^{18}O$ value of the water is 0, then the coexisting CO_2 is 41.2‰ heavier. However, if the $\delta^{18}O$ value of the water is 20‰, for example, then the $\delta^{18}O$ value of the CO_2 is 62.02, 42.0‰ heavier. The α value is the same in both cases.

at 25°C of 41.2‰ on the SMOW scale. The standard PDB calcite is 30.91‰ heavier than SMOW (Coplen et al., 1983). Finally, the $\alpha(CO_2 - \text{calcite})$ value for acid fractionation is 1.01025 at 25°C (corresponding to $\Delta^{18}O_{CO2\text{-}cc}$ of 10.57 for $\delta^{18}O_{cc}$ = 30.91‰ on SMOW scale (0‰ on PDB scale) or $\alpha_{CO2\text{-}SMOW}$ = 1.03091×1.01025=1.04148), so that the CO_2 liberated from PDB calcite has a $\delta^{18}O$ value of 41.48‰. When all of these corrections are made, the difference between the $\delta^{18}O$ value of CO_2 equilibrated with SMOW and that liberated by phosphoric acid digestion from PDB is only 0.28‰[4]. Craig (1965) reported a value of 0.22‰ for this difference. The discrepancy is due to an earlier α(PDB-SMOW) = 1.03086, compared to the now accepted value of 1.03091. In fact, it shouldn't be surprising that the $\delta^{18}O$ values of the CO_2 liberated from the calcite and the CO_2 equilibrated with the water are almost the same. The CO_2 equilibrated with the water is in equilibrium with the water at 25°C, and the acid fractionation liberates a CO_2 that is close to equilibrium with the calcite. So if the calcite is in equilibrium with the CO_2, and the water is in equilibrium with the CO_2, *and* the calcite and water are in equilibrium with each other, then both CO_2 samples should have the same $\delta^{18}O$ value. The variation in the CO_2 'differences' is due to the temperature of equilibration between the calcite and the water from which it forms.

To calibrate the temperature dependence of the isotopic fractionation between biogenic carbonate and water, Epstein made analyses of shell material from attached or sedentary organisms including mussels, brachiopods, red and black abalone, and limpets that were living in the cool waters off Puget Sound (lowest T = 7.4°C), in the temperate waters of Monterey Bay, and in warm waters along the coast of Baja California (highest T = 20°C). Two higher temperature calibration points at 29 and 31°C were obtained from analyses of calcite regenerated by a cultured snail and a bivalve (*Pinna* sp.) to repair holes that were purposely drilled into their shells[5]. Oxygen isotope analyses of the natural and cultured carbonate samples in addition to the ambient waters provided adequate data to establish an empirical calibration for the fractionation between biogenic calcite and water over the range of temperatures found in modern oceans. After publication of the paleotemperature equation in 1951, the authors recognized that the helium roasting procedure used to remove organic matter from the shells had introduced extraneous oxygen to the system. Epstein *et al.* (1953) corrected the procedure and published the following revised equation which became the classic paleotemperature equation:

$$t(°C) = 16.5 - 4.3(\delta_c - \delta_w) + 0.14(\delta_c - \delta_w)^2 \qquad 6.4.$$

In this equation, δ_c is the $\delta^{18}O$ value of CO_2 liberated from reaction between the carbonate and phosphoric acid at 25°C, and δ_w is the $\delta^{18}O$ value of CO_2 equilibrated with water at 25°C. Their data and polynomial fit are reproduced in Fig. 6.2. There is no theoretical basis to the form of equation 6.4; it is simply a best-fit of the data to a second order polynomial. Over the 0-30°C range of modern ocean waters, $\delta^{18}O$ (PDB) values of marine carbonates range from about +3 to –3‰. The first measurements of paleotemperatures using this method are shown in Figure 6.3.

[4] Interestingly, the temperatures obtained from the Pee Dee belemnite (PDB standard) correspond to a temperature of 15.8°C, assuming a $\delta^{18}O$ value of the ocean of 0 on the SMOW scale.
[5] These warm water organisms were cultured in a tank in Bermuda.

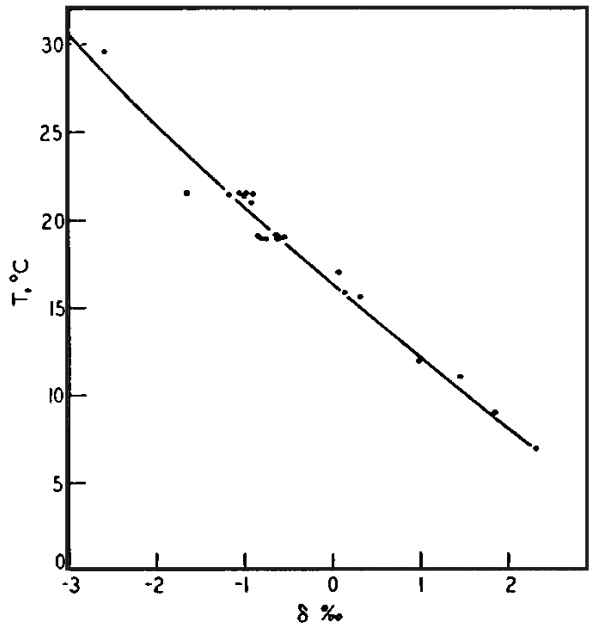

Fig. 6.2. Plot of Epstein *et al.* (1953) data set for determining the fractionation factor for carbonate - water. The x-axis (δ ‰) refers to the (δ_c - δ_w) of equation 6.4, T(°C) is measured water temperature.

Both δ_c and δ_w are the values relative to the same working standard of the mass spectrometer. CO_2 from PDB was the working standard used in the early days at the University of Chicago. Be aware that water analyses normalized to the SMOW scale and carbonates normalized to the PDB scale cannot be used in the classic paleotemperature equation, but the equation can be rewritten in a form appropriate for the delta values of the calcite and water relative to the PDB and SMOW scales respectively:

$$t(°C) = 15.75 - 4.3(\delta^{18}O_{c\text{-}PDB} - \delta^{18}O_{w\text{-}SMOW}) + 0.14(\delta^{18}O_{c\text{-}PDB} - \delta^{18}O_{w\text{-}SMOW})^2 \qquad 6.5.$$

Keep in mind that δ_c on the PDB scale is about 30 per mil lower than δ_c on the SMOW scale. In the first case (eq. 6.4), one uses the isotopic composition of CO_2 released from the carbonate by acid decomposition and, in the second case (eq. 6.5), the isotopic composition of total oxygen in the solid carbonate is reported (relative to PDB). To emphasize this important point that is frequently misunderstood, recall that $\delta^{18}O$ of the PDB carbonate standard is 0‰ on the PDB scale and 30.91‰ on the SMOW scale (Eq. 2.21). This difference seldom poses a problem in the practical world because the PDB scale for oxygen isotope analyses is restricted to analyses of carbonates only. The SMOW scale is used to report oxygen isotope analyses of every other substance including water.

The temperature dependence of the calcite-water system was revisited when O'Neil *et al.* (1969) measured the equilibrium oxygen isotope fractionation between inorganic calcite and water from 0 to 500°C using precipitation methods at low temperatures and recrystallization methods at high temperatures. The results of these

experiments were fit to an equation[6] whose form has a basis in statistical mechanics:

$$1000\ln\alpha_{\text{calcite-water}} = \frac{2.78\times10^{6}}{T^{2}} - 2.89 \qquad 6.6$$

where T is in Kelvins. Note that the δ values of calcite and water must be on the same scale (either PDB or SMOW) for this equation. The results are virtually indistinguishable from Epstein's earlier work. Kim and O'Neil (1997) synthesized carbonates at low temperature and developed a similar, though slightly different fractionation equation:

$$1000\ln\alpha_{\text{calcite-water}} = \frac{18.03\times10^{3}}{T} - 32.42 \qquad 6.7.$$

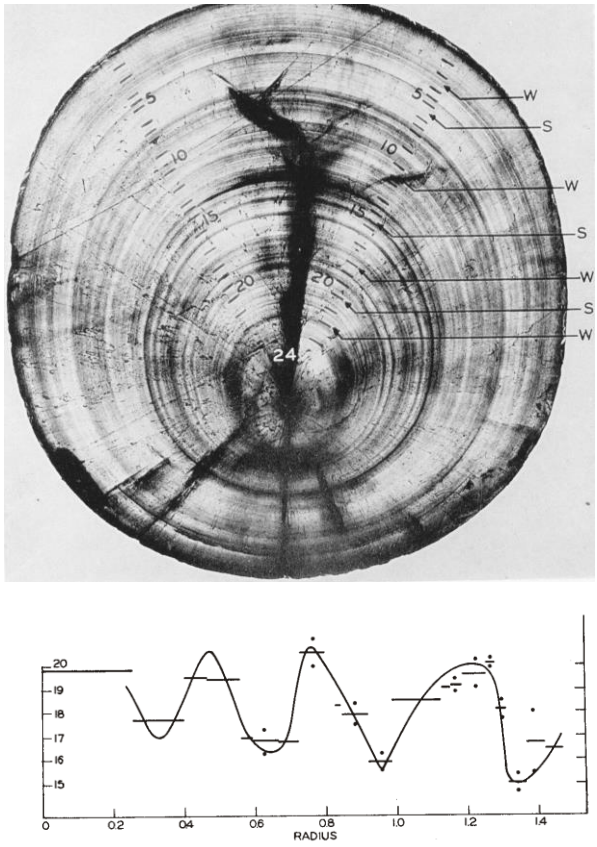

Figure 6.3. Cross section (top) of 150-million year old belemnite showing growth rings. The graph (bottom) illustrates isotopic temperatures obtained from oxygen isotope analyses of concentric layers of the skeleton. The regular variations reflect seasonal variations in growth temperature and indicate that the animal was born in the summer and died four years later in the spring (Urey et al., 1951).

[6] The additive term originally published was –3.39. This number was later corrected to –2.89 after recognition that an error was made in a mass spectrometer correction factor.

(Tarutani *et al.* (1969) obtained identical fractionations as Kim and O'Neil at 0 and 25°C). The difference between the O'Neil '69 *vs* Kim and O'Neil '97 results was explained by Kim and O'Neil as a result of kinetic factors that occur during synthesis. Their data result in a smaller fractionation that the earlier O'Neil *et al.* work. In contrast, Coplen (2007) came to the opposite conclusion. He measured the $\delta^{18}O$ values of vein calcite and water from Devils Hole, Nevada. His empirical estimate gives a $1000ln\alpha$ value of 28.09±0.13 at 33.7°C, significantly larger than the experimental data. He argued that kinetic effects result in laboratory fractionations that are smaller than equilibrium, a conclusion supported by a more recent work by Watkins *et al.* (2015). It their study, Watkins *et al.* synthesized calcite in the presence of dissolved bovine carbonic anhydrase, a catalyst that minimized isotopic disequilibrium between all the dissolved species CO_2, H_2CO_3, HCO_3^- and CO_3^{2-}.

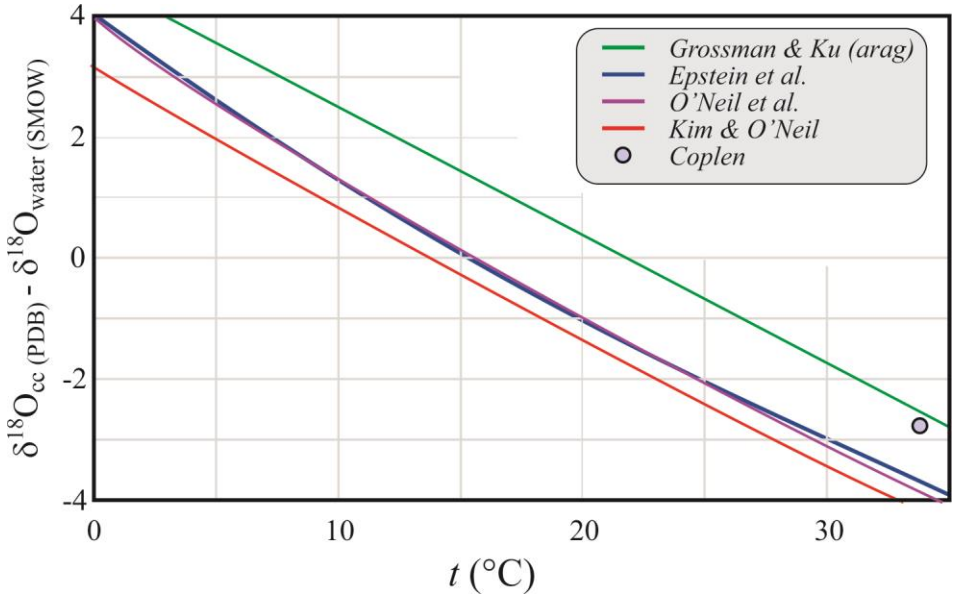

Fig. 6.4. Comparison of the calcite (aragonite)-water fractionation curves from various authors. Each has the same temperature dependence, but the absolute values are slightly different. Data sources: (Epstein et al., 1953; O'Neil et al., 1969; Grossman and Ku, 1986; Kim and O'Neil, 1997; Coplen, 2007). (The Kim and O'Neil and O'Neil *et al.* curves are only strictly valid for $\delta^{18}O_{water}$ = 0‰.)

What is clear from Fig. 6.4 is that the *precision* of an oxygen isotope temperature estimate can be as high as ±0.5°C but, given the uncertainties in the calibration and also the standardization, the *accuracy* is considerably lower. The empirical calibration of Epstein *et al.* seems to work for natural samples. Slowly precipitated cave calcites appear to have larger fractionations that biogenically-formed samples. It may be fortuitous that the empirical and experimental calibrations give reasonable temperatures for natural assemblages. What is clear is that relative temperature differences are accurate, and reliable estimates of temperature *change* are generally what is desired in palaeoclimate studies.

Many organisms deposit aragonite in their shells, so it is important to know if different polymorphs of $CaCO_3$ have significantly different oxygen isotope properties.

From limited experimental data, Tarutani *et al.* (1969) determined an inorganic aragonite-calcite fractionation of 0.6‰ at 25°C. While this fractionation is relatively small, as expected for two such similar minerals, it is significant in terms of paleotemperature determinations. That is, the paleotemperature equation developed for calcite is not appropriate for shells made of aragonite. Grossman and Ku (1986) empirically determined the aragonite-water fractionation between living organisms and seawater over a temperature range of 4-20°C (Fig. 6.4). Their equation, presented in terms of $\delta^{18}O$ aragonite on the PDB scale and $\delta^{18}O$ water on the SMOW scale for mollusks is given by

$$T(°C) = 21.8 - 4.69(\delta^{18}O_{aragonite} - \delta^{18}O_{water}) \qquad 6.7.$$

Equilibrium dolomite-water fractionations are larger than those for calcite -water. At 25°C, the $\Delta^{18}O_{dolomite\text{-}calcite}$ value is ~4‰, decreasing with increasing temperature. The dolomite -water equilibria is given by (Horita, 2014)

$$1000ln\alpha = 3.14(\pm0.02) \times 10^6/T^2 - 3.14\ (\pm0.11) \qquad 6.8.$$

6.4 Factors Affecting Oxygen Isotope Paleotemperatures

The carbonate paleotemperature equation has three variables; $\delta^{18}O_{carbonate}$, $\delta^{18}O_{water}$ and temperature (*t*). We estimate *t* from the measured $\delta^{18}O_{carbonate}$ value and an assumed $\delta^{18}O_{water}$ value. The validity of the *t* estimate depends on a number of factors, already recognized by Urey early on (1948): 1) The $\delta^{18}O_{water}$ value at the time of calcite growth: The $\delta^{18}O$ values of the ocean have undoubtedly changed in the past due to glacial – interglacial periods. Over the long term, the $\delta^{18}O$ values of the oceans appear to be buffered by hydrothermal interaction with the seafloor (Chapter 5), but the level of fluctuation is not known. Isolated basins, or shallow seas could be perturbed from the normal marine value by evaporation or influx of fresh water. We know that ancient carbonates have low $\delta^{18}O$ values, supporting (but in no way proving) that the $\delta^{18}O$ value of the ancient ocean was lower than today. 2) The degree to which the $\delta^{18}O$ values of carbonates have been altered: Even low temperature diagenesis can alter the $\delta^{18}O$ value of a carbonate due to the ease of dissolution in fresh waters. Great care is taken to avoid the effects of diagenesis, but no foolproof method exists to prove a lack of diagenesis. The low $\delta^{18}O$ values of ancient carbonates are equally explained by diagenesis as by changing ocean composition. 3) The degree to which the carbonates precipitated in equilibrium with water: It is known that some organisms (*e.g.,* corals) secrete carbonate that is not in isotopic equilibrium with water. This so-called 'vital' effect must be also be considered.

6.4.1 Variations in $\delta^{18}O$ of ocean water in space and time

We have seen that variations in oxygen isotope compositions of surface waters in modern oceans arise from both evaporation and influx of fresh water. These processes must be taken into consideration when working with the carbonates formed in the near-surface environment, or planktic organisms, especially in samples from shallow epicontinental seas or restricted marine basins where influx of fresh water and evaporation could have caused large isotopic shifts. The problem can be at least partly

addressed because oxygen isotope values and salinity are generally correlated (Chapter 5). For fossil materials, therefore, it is sometimes possible to estimate the $\delta^{18}O$ value of the ocean if an independent estimate of salinity can be made from salinity-dependent cation ratios in the carbonate (Carpenter and Lohmann, 1992), from Sr/Ca ratios (Beck et al., 1992; DeVilliers et al., 1994) or by some other means.

The Quaternary period presents a unique problem in that we have to deal with fluctuating $\delta^{18}O_{ocean}$ values related to glacial-interglacial cycles. On a time scale of tens of thousands of years, the $\delta^{18}O$ value of the entire ocean mass changed when isotopically light water was transferred from the ocean to continental ice sheets. Numerous isotopic studies have shown that during periods of advance and retreat of continental glaciers, $\delta^{18}O$ values of marine carbonate changed repeatedly and in a regular manner. Are the isotopic shifts due to changing ocean temperature or changing composition of the ocean related to growth of ice sheets? When the temperature of seawater decreases, the fractionation between carbonate and water increases (lower temperature, larger fractionation), so that organisms should precipitate carbonate with higher $\delta^{18}O$ values. At the same time, however, when temperatures decrease, ice caps grow, removing light water from the ocean and increasing the $\delta^{18}O_{ocean}$ value. Both effects – lowering temperature and raising the $\delta^{18}O$ value of the ocean – will cause the $\delta^{18}O$ values of carbonates to increase. We cannot tell *a priori* if high $\delta^{18}O$ values in glacial times are due to lower ocean temperatures or larger ice caps. Emiliani (1955, 1966) attempted to deconvolute this problem by analyzing carbonates that were precipitated in warm-water regions of the Caribbean and equatorial Atlantic (Fig. 6.5). He reasoned that temperatures would be relatively constant in the Central Atlantic, so that changes in the secular isotope record would be related to changes in the $\delta^{18}O$ values of the oceans and not temperature. He therefore, interpreted the regular variations in oxygen isotope ratios of the carbonates as a record of changing ice volumes.

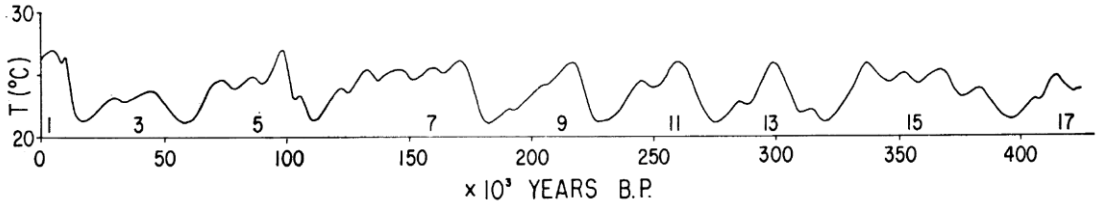

Fig. 6.5. Generalized temperature curve for surface waters from the Caribbean determined from the $\delta^{18}O$ values of foraminifera from Caribbean cores (reproduced from Emiliani, 1966). Odd numbers refer to interglacial stages.

This conclusion was reaffirmed in a later series of works by Shackleton and Opdyke (1973; 1976) using $\delta^{18}O$ values of benthic and planktic foraminifera from the western tropical Pacific. Following Emiliani's reasoning, they assumed that deep waters – generated at high latitudes and buffered by the presence of ice – have relatively constant, near-freezing temperatures. Variations in the $\delta^{18}O$ values of deep (benthic) foraminifera should therefore track the isotopic composition of the ocean. They found that deep (benthic) and shallow (planktic) foraminera had the same secular isotopic patterns, offset only by a constant amount related to their *relative* temperature differences. The magnitude of the isotopic variations were therefore related to changes in the ocean's isotopic composition and not temperature.

The usefulness of measuring coeval benthic and planktic foraminifera is illustrated in a comparative chemostratigraphic study of the Central and Intermediate Pacific ocean over a much longer time interval (Fig. 6.6). The similarity and gradual increase in $\delta^{18}O$ values of benthic and planktic foraminifera from intermediate latitudes over the past 80 million years shows that temperatures have decreased during this mostly ice-free time. In contrast, planktic foraminifera from the Central Pacific have a nearly constant $\delta^{18}O$ value, suggesting that the surface temperatures at the more tropical latitudes have remained constant as have the $\delta^{18}O$ values of the oceans.

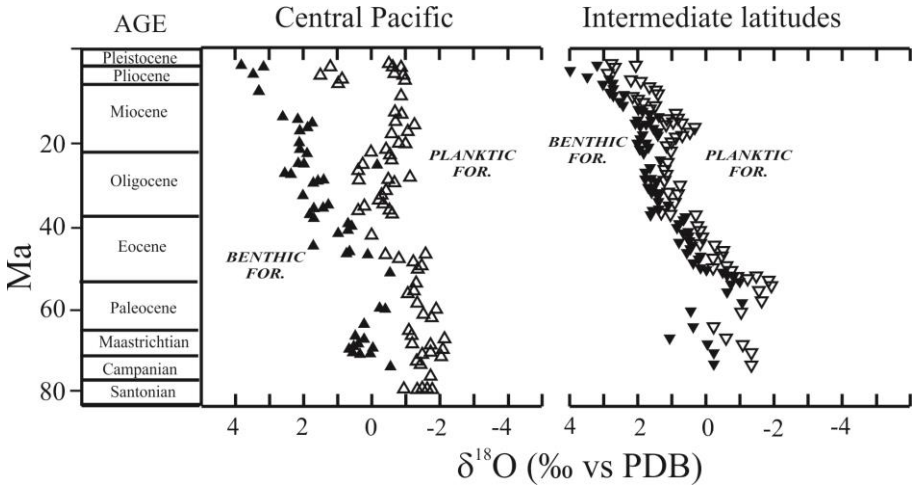

Fig. 6.6. $\delta^{18}O$ values of benthic and planktic foraminifera for central and intermediate latitudes of the Pacific Ocean. The deep and shallow water data parallel each other at the intermediate latitudes suggesting that temperatures at the surface and depth were the same. Temperatures generally decrease throughout the ice-free Paleocene and Neogene. Benthic foraminifera data for the central Pacific parallel the intermediate latitude data throughout the column, consistent with temperatures being controlled by downwelling waters from higher latitudes. In contrast, the equatorial planktic foraminifera data are relatively constant throughout, suggesting that surface temperatures are also constant. Modified from Anderson and Arthur (1983).

6.4.2 Vital effects

Epstein's early calibration of the paleotemperature scale was made using mollusks. Fortunately, mollusks, especially belemnites and brachiopods, *tend* to precipitate their carbonate shells in oxygen isotope equilibrium with ambient waters (Lowenstam, 1961) – see Carpenter and Lohmann (1995) for additional details. Some organisms secrete shells out of equilibrium with ambient water, leading to the so-called *vital effect*. For purposes of thermometry, it is critical to identify those organisms whose life processes *always* introduce an oxygen isotope offset by the vital effect and to recognize the conditions under which vital effects operate only *sometimes* for other organisms (*e.g.* foraminifera).

The commonly used planktic foraminifera often, but not always, secrete their tests in oxygen isotope equilibrium. Divergence from equilibrium is related to environmental factors including intensity of sunlight, temperature stress, nutrient supplies and the like. Thus planktic foraminifera can secrete carbonate out of equilibrium with ocean water, especially at tropical temperatures. Most benthic foraminifera, on the other hand, live in a

more uniform environment and are isotopically much better behaved. In fact, the extremely uniform temporal variations in data for certain benthic foraminfera (and corrected planktic data) allow precise correlations to be made between cores that are thousands of kilometers apart (Prell et al., 1986).

Coccoliths (single celled algae) not only deposit their calcium carbonate plates out of oxygen isotope equilibrium with environmental waters, but the magnitude of the vital effect for this class of organisms varies irregularly with both temperature and taxa. Echinoderms, corals, red algae, and certain benthic foraminifera notoriously precipitate their carbonate out of equilibrium with ambient waters (Fig. 6.7).

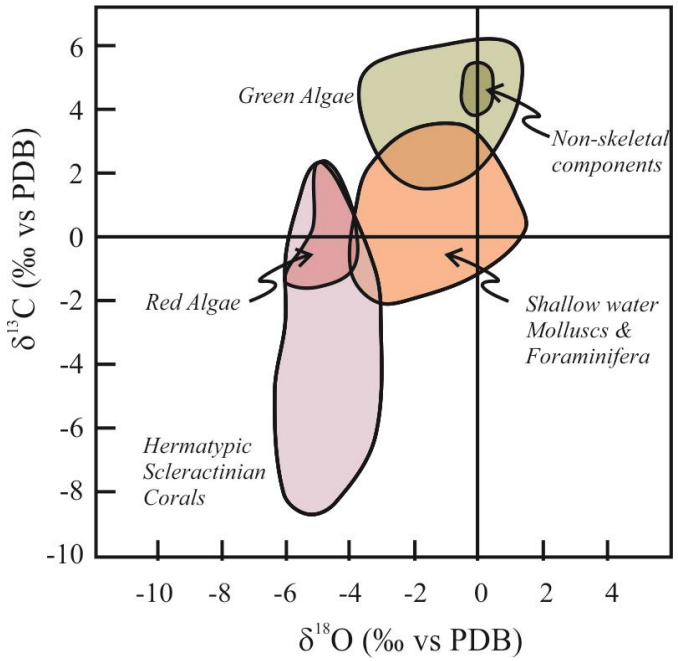

Fig. 6.7. Illustration of the range of disequilibrium oxygen and carbon isotope offsets for selected modern organisms due to the vital effect. After Anderson and Arthur (1983).

Over the course of 50 years or more, we have learned which species to use in oxygen isotope studies of paleoclimate and also to make sensible corrections to isotopic analysis that are predictably offset by a vital effect. Biogeochemists have even used disequilibrium deposition of carbonate to study details of life processes of modern and extinct marine organisms. Proposed explanations of the vital effect, particularly for carbon are discussed in more detail in Section 7.4.3.

6.4.3. Diagenesis

Original isotopic ratios must be preserved in carbonate shells for meaningful studies of palaeotemperature to be conducted. Reactions between biogenic carbonate and diagenetic fluids can easily erase the original isotopic record if fluid/carbonate ratios are large. During carbonate diagenesis, little or no direct isotopic exchange takes place between solid carbonates and aqueous fluids, because the rates of solid state diffusion of carbon and oxygen in carbonates at low temperatures are inconsequential (O'Neil, 1977). Carbon and oxygen isotope ratios of biogenic carbonate can be changed by two diagenetic processes: (1) addition of new carbonate by cementation, and (2) dissolution of unstable carbonate and reprecipitation of a stable mineral, normally low magnesium calcite.

Cementation is the most common diagenetic process leading to a change in the isotopic composition of a marine carbonate. Isotopic measurements of a cemented biogenic carbonate reflect mixtures of original (unaltered) and new carbonate rather than of original carbonate alone. Cementation of marine carbonates commonly occurs where sediments are exposed to high-energy conditions. Because carbonate cements are abiotic, there can be no vital effect and they are likely to be deposited in both carbon and oxygen isotope equilibrium with their parent fluids. The pore waters in equilibrium with the

earliest-formed cements often are the same as marine water, so that these early cements will be in isotopic equilibrium with ocean water. Unlike many biogenic carbonates, which are often unstable aragonite or high-Mg calcite (see below), cements are generally thermodynamically stable low-Mg calcite (although this varies between ice age and greenhouse conditions due to changing ocean chemistry) and therefore not prone to recrystallization at some later time. Clearly then, cements have a high potential for providing information relating to the original isotopic composition of seawater and/or temperature.

Unfortunately, not all cements give primary information. The cementing fluid may be locally confined and not in rapid communication with the major aqueous oceanic reservoir. In such cases, breakdown of organic matter can lead to formation of cements with very low $\delta^{13}C$ values. Secondary cements are often coarse-grained, but reflect equilibration with meteoric water. Carbonate cements are frequently large enough to sample cleanly, but infilling cements, particularly in shells of small organisms, can be analyzed separately only with very high spatial resolutions techniques, such as sophisticated micro-sampling or *in situ* ion probe analysis.

Solution and reprecipitation is a combined process that is thermodynamically driven towards a lower free energy state. For example, calcite is stable relative to aragonite, and low Mg-calcite is stable relative to high-Mg calcite. During the thermodynamically-driven chemical reactions to more stable phases, isotopic exchange will occur. Recrystallization can take place on a very fine scale (*e.g*. replacement reactions) such that original textures are retained despite chemical and isotopic changes. Recrystallization or neomorphism are terms used to describe the process of solution and redeposition and strictly used to describe the isochemical process of grain coarsening.

The magnitude of change in isotopic compositions of carbon and oxygen in biogenic carbonate that undergoes recrystallization depends on four factors: (1) temperature, (2) isotopic compositions of H_2O and HCO_3^- in the fluid, (3) fluid/solid (or fluid/rock) ratio, (4) the susceptibility of the carbonate to recrystallization to a more stable phase. As an end-member case, consider a biogenic marine carbonate that recrystallizes with a tiny amount of pore water of marine composition at a temperature close to the original deposition temperature. This process cannot significantly alter the isotopic ratios of the original carbonate and indeed such recrystallization occurs in marine sediments directly after deposition. On the other hand, isotopic ratios of the same biogenic carbonate would change dramatically if it underwent neomorphism bathed in a diagenetic fluid containing a component of low $\delta^{18}O$ fresh water that carried low $\delta^{13}C$ soil-derived bicarbonate. In general, open-system diagenesis (high water/rock ratios) leads to loss of primary isotopic information but, if diagenetic trends in isotopic ratios are regular, it may be possible to extrapolate back to original compositions (Fig. 6.8).

The *diagenetic potential* of a mineral in a given system can be described as the tendency of that mineral to undergo reaction with a given diagenetic fluid. The greater the departure from chemical (not isotopic) equilibrium between mineral and fluid, the greater is the diagenetic potential. Several factors control the diagenetic potential of biogenic calcium carbonate, and the strongest of these is chemical composition, specifically the Mg/Ca ratio. Low-magnesium calcite is *stable* and thus relatively insoluble and nonreactive in diagenetic fluids, whereas high-magnesium calcite is *metastable* relative to pure calcite and thus is more soluble and reactive. Crystal size is

also an important parameter because small particles have relatively high surface areas and can lower the free energy of the system by dissolving and recrystallizing to larger grains. The polymorphic form of $CaCO_3$ is another important factor that controls diagenetic potential. Aragonite and vaterite[7] are metastable in surface environments and are highly prone to dissolution and reprecipitation to more stable calcite, particularly when exposed to fluids with a fresh water component.

Fresh water or seawater containing a meteoric component is undersaturated with respect to marine carbonates and the disequilibrium promotes dissolution. Fresh rainwater is a particularly corrosive agent to carbonates as it is slightly acidic as well. Marine carbonates exposed to such fluids, either in shallow coastal waters or on land undergo *meteoric diagenesis.* Aragonite and high-magnesium calcite are common metastable constituents of biogenic carbonate and react with diagenetic fluids to form more stable low-magnesium calcite and a different isotopic composition.

Meteoric diagenesis almost always lowers both carbon and oxygen isotope ratios of carbonates because $\delta^{18}O$ values of meteoric waters are normally lower than those of seawater and $\delta^{13}C$ of soil bicarbonate is lower than that of seawater bicarbonate[8]. In arid regions where evaporation is intense, meteoric waters can have positive $\delta^{18}O$ values such that meteoric diagenesis of marine carbonate could shift $\delta^{18}O$ values to higher values, although this process is rare.

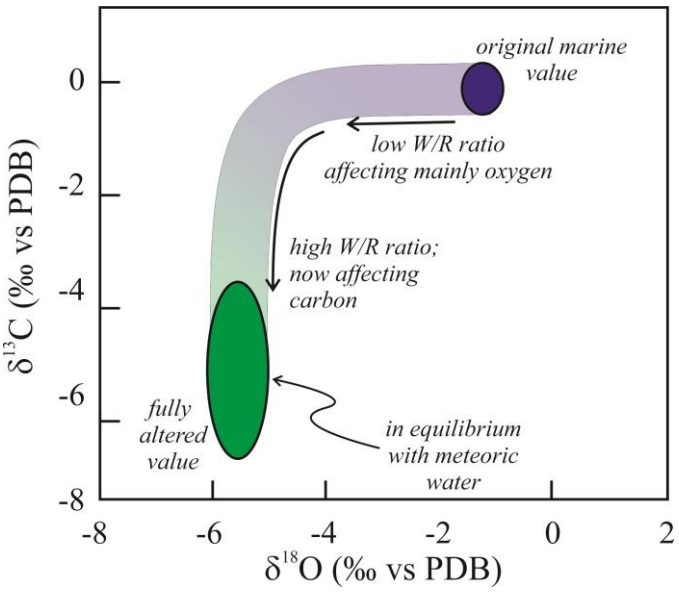

Figure 6.8. Illustration of changes in $\delta^{18}O$ and $\delta^{13}C$ that accompany alteration of a marine carbonate by meteoric water. Initial dissolution and reprecipitation by interaction with pore water fluids with a small meteoric component will shift carbonates to lower $\delta^{18}O$ values but leave $\delta^{13}C$ values relatively unchanged (point 1). Only after W/R ratios become very large, will $\delta^{13}C$ values decrease. The vertical line defined by increasing W/R interaction is the 'meteoric calcite line', which defines the $\delta^{18}O$ value of meteoric water responsible for precipitation of late calcite cements. From Lohmann (1988).

Alteration patterns on $\delta^{18}O$-$\delta^{13}C$ diagrams have characteristic shapes depending on the magnitude of the various diagenetic parameters. At the onset of diagenesis in a given region, a tiny amount of water enters the system and dissolves some carbonate. The fluid/rock ratio is perforce very low at this stage and the system is rock-dominated. The bicarbonate in solution generated by

[7] Measurements are made only of calcite and aragonite. Vaterite, a rare naturally occurring polymorph of $CaCO_3$, has been studied only under laboratory-controlled conditions.

[8] The $\delta^{13}C$ value of atmospheric CO_2 is -6 to -7‰ and is in near-equilibrium with marine dissolved inorganic carbon (see Chap. 7).

dissolution of solid carbonate will exchange oxygen isotopes with the water, mix with the soil bicarbonate already present in the fluid, and reprecipitate as a cement or replacement carbonate. Under rock-dominated conditions that prevail initially, newly precipitated carbonate will have isotopic ratios that are similar to those of the original carbonate. With ever increasing water/rock (W/R) ratios, both $\delta^{18}O$ and $\delta^{13}C$ values of the carbonate will decrease. But they will not change at the same rate. Oxygen is a major component of water, while dissolved carbon is only a trace component. Therefore, early diagenesis will affect the carbonate isotope ratios of oxygen far more than carbon (Brand and Veizer, 1981; Lohmann, 1988; Marshall, 1992). In effect, the W/R ratio are higher for oxygen than for carbon for the same amount of water. As diagenesis proceeds and fluid/rock ratios increase, $\delta^{18}O$ values of successively deposited carbonate (cement) become increasingly more negative while $\delta^{13}C$ values remain nearly constant. The $\delta^{18}O$ values reach a final limiting value that is controlled by the isotopic compositions of the diagenetic fluid and effective water/rock ratios. With still increasing fluid/rock ratios, $\delta^{13}C$ of ensuing cements become more negative, once again approaching a final, limiting value defined by the $\delta^{13}C$ value of the infiltrating fluid. In the context of a time sequence, a rotated J pattern develops on a $\delta^{13}C$-$\delta^{18}O$ diagram (Fig. 6.8). The data points on the upper right limb of the curve represent unaltered material. In combination with careful petrographic examination and chemical analysis, these stable isotope patterns can provide a detailed diagenetic history in a given carbonate terrane.

During diagenesis, a number of chemical changes occur and these changes can be used to identify altered and primitive portions of the carbonates. Most commonly, the concentrations of trace elements, Mn (promotes cathodoluminescence) and Fe (diminishes cathodoluminescence) of the cement increase during diagenesis under reducing conditions, and concentrations of Sr and Mg decrease. $^{87}Sr/^{86}Sr$ ratios can increase or decrease depending on the source of strontium in the local meteoric water. All these changes are specific to the conditions of diagenesis and sources of fluids, so no one geochemical tracer is completely diagnostic.

A number of strategies can be employed to circumvent and even exploit the effects of diagenesis, particularly for older material. Thick, nonluminescent portions of brachiopods and marine cements are likely to have preserved their original mineralogy, as well as chemical and isotopic compositions (Figure 6.9). Certain portions of brachiopods *can* and frequently *do* precipitate stable, low-magnesium calcite in equilibrium with seawater and, in addition, this carbonate is relatively massive and coarse grained. Analyses of nonluminescent portions of these shells can be used to determine original isotopic composition and analyses of altered portions are used to study diagenesis.

Another strategy involves specifically *searching out* the metastable phases. While it may seem counterintuitive, the thinking goes that if an unstable primary phase is still present, then it most likely hasn't undergone diagenesis. Aragonite is a metastable polymorph of $CaCO_3$ at surface conditions. It is easily altered to more stable calcite. Therefore, if aragonite can be found, its very preservation implies that diagenesis has been minimal. We have two seemingly diametrically opposed philosophies at our disposal. One is to search for metastable material, such as aragonite. The reasoning is simply that if it had been altered, it would have recrystallized as stable low-Mg calcite. The other approach is to find the most stable primary material, samples that were

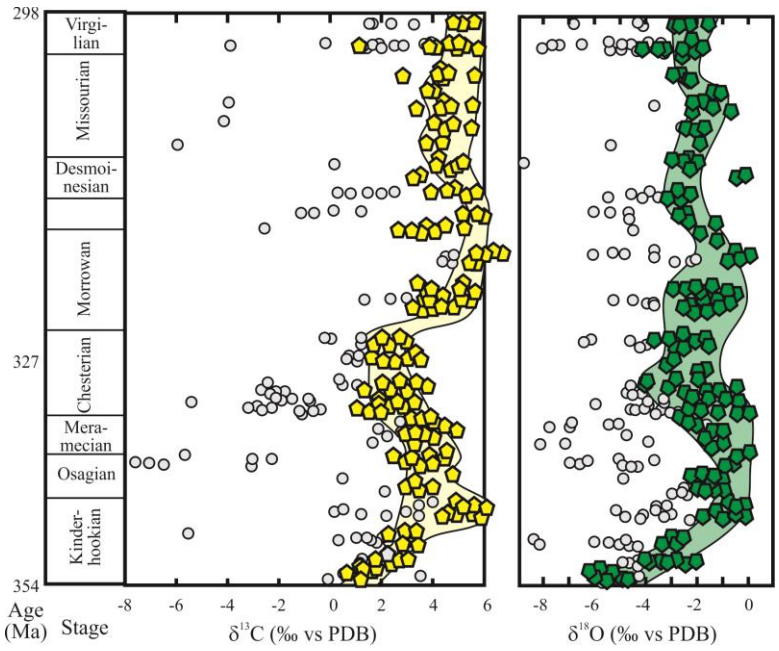

Fig. 6.9. North American Brachiopods (solid symbols) and coexisting cements (grey circles) from Carboniferous sediments. The $\delta^{18}O$ and $\delta^{13}C$ values of cements are lower than coexisting brachiopods, indicating diagenesis with meteoric water. The thick non-luminescent samples (colored symbols) tend to be the least modified by diagenesis. Modified from Mii *et al.* (1999)

precipitated as stable low-Mg calcite. Because it is already stable, it is less likely to undergo recrystallization.

Obviously, this strategy is only valid if we can be sure that the carbonate originally was low-Mg calcite. A simplified schematic of acceptable samples and strategies to use in studies of the stable isotope composition of marine biogenic carbonate is given in Figure 6.10.

For samples from marine cores of Cenozoic age, both diagenesis and ambiguities in the isotopic composition of ocean water are negligible. Consequently numerous isotopic studies have been made of pristine fossils of Cenozoic age in undisturbed cores from the deep sea. In Mesozoic or older sediments, isotopic measurements are mostly limited to shelf deposits where preservation is generally poor (and the oxygen isotope composition of the water is suspect).

Early workers active in oxygen isotope paleothermometry established guidelines to assess diagenesis of their carbonates, and these guidelines are still valid today. If any of the following are true, the carbonate is more likely (though not certain) to have retained its original $\delta^{18}O$ value:

1. The skeletal material or cement is made of unstable minerals like aragonite or high-Mg calcite. They would not survive exposure to diagenetic fluids. Their survival indicates that interaction with diagenetic fluids has been minimal.
2. The skeletal material *secreted by the organism* is stable low-Mg calcite. Stable minerals have a low diagenetic potential.
3. There are seasonal variations in isotopic ratios along the growth direction. Recrystallization would obliterate these signals. (This point has been challenged).
4. The material has the highest $\delta^{18}O$ value in the population. Diagenesis normally lowers the $\delta^{18}O$ value.
5. The material is not luminescent. Diagenesis often introduces cathodoluminescent Mn to neoformed carbonate.

6.4.4 Ecology of the organism

Carbon and oxygen isotope compositions of shells reflect local conditions of productivity and temperature *at the time of deposition*. Some organisms spend one part of their lives in one environment and other parts of their lives in different environments that can be, for example, darker, more saline, or colder. Even among the same species, larger and more robust individuals tend to build their shells in deeper, colder waters and therefore have higher $^{18}O/^{16}O$ ratios than their more fragile juvenile counterparts. Researchers must be aware of the ecology of the organisms they use if they are to interpret the stable isotope data properly. It was precisely for these reasons that the Chicago group analyzed shells of attached or sessile organisms to establish the paleotemperature scale.

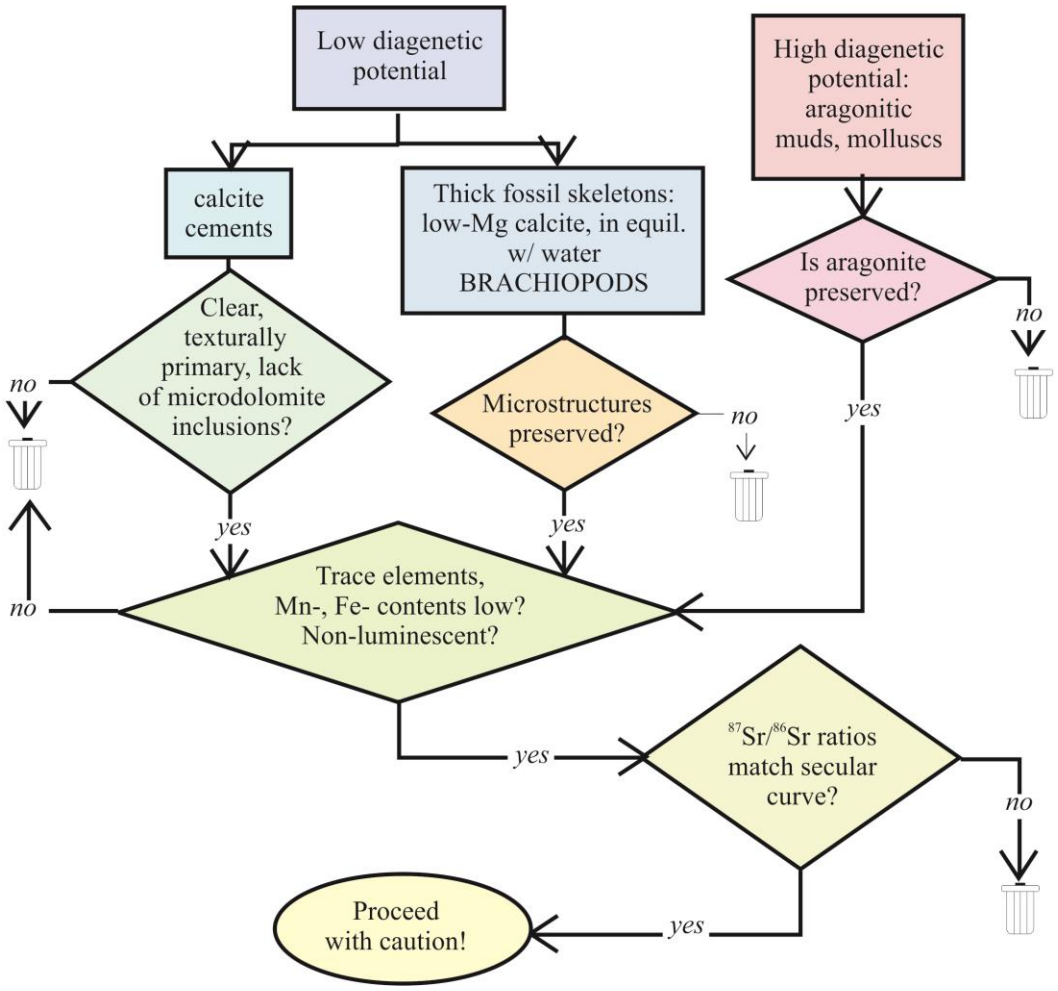

Fig. 6.10. Schematic flowchart of common procedures for identifying diagenesis. For further information, see (Carpenter et al., 1991; Marshall, 1992; Grossman, 1994).

6.5 Applications of Oxygen Isotope Paleothermometry

Taking into account all the factors that can affect $\delta^{18}O$ values of biogenic carbonate, including the application of appropriate correction factors, it is possible to address many

important issues of oceanography and paleoclimatology using the method of oxygen isotope paleothermometry. The principles employed are generally the same, so only a few examples of applications will be given here.

6.5.1 The Quaternary

The Quaternary record is very well preserved both in terms of complete detailed stratigraphy and minimal amount of diagenesis. The glacial periods (Ice House conditions) in the Quaternary pose a complication that is nearly unique in chemostratigraphic reconstruction. Most other times in history are free of extensive glacial ice, and the $\delta^{18}O$ values of the oceans can be considered to be constant in the short term. In the Quaternary period, the $\delta^{18}O$ values of marine carbonates are affected by changes in the isotopic composition of the ocean as much as changes in temperature as already discussed in section 6.4.1.

Arguably the most important discovery made through oxygen isotope analyses of biogenic carbonate was the delineation of important details of Pleistocene glaciation. The oxygen isotope curve originally presented by Emiliani (1966) and modified in (1978) is shown in Figure 6.6. Emiliani worked on shells of pelagic foraminifera from the perennially warm waters of the Caribbean in order to avoid the problem of temperature variations as the cause of changes in $\delta^{18}O$ of the shells. Several important features of glaciation over the last 700,000 years are apparent from Fig. 6.5:

1. The patterns are saw-toothed, implying that glaciation is a slow process and that deglaciation occurs much more rapidly.
2. A periodicity of ~100,000 years in the patterns can be reasonably linked to one of the Milankovich periodicities in orbital forcing,
3. There are many more glacial/interglacial stages in the Pleistocene than previously thought.

An extremely useful method of correlating stratigraphic sections can be made from the regularities observed in the oxygen isotope record in Quaternary foraminiferal tests from all over the world oceans. The uniformity in the record stems from two facts: (1) the effect measured is primarily a change in $\delta^{18}O$ of the oceans that resulted from changes in ice volumes on land, and (2) the mixing time of the oceans is very short ($\sim 10^3$ years). Since the early work of Emiliani, synchronous oxygen isotope stages, termed *marine isotope stages* (MIS) have been recognized by many workers. Odd numbers are assigned to warmer, interglacial times and even numbers to colder, glacial times. We are presently in MIS 1. There are five recognized oxygen isotope stages in the isotopic record of the last 130,000 years and substages are recognized as well, particularly in well-studied stage 5. MIS extends back over 100 cycles.

Age assignments are critical in stratigraphic work and are frequently the subject of considerable debate. A novel approach to age assignment is to assume that astronomically driven changes in climate (orbital forcing) are responsible for the waning and growth of ice sheets. Using this approach to tune several oxygen isotope records, Imbrie *et al.* (1984) established a reference chronostratigraphy for the late Quaternary called the SPECMAP (Spectral Mapping Project). In this work, they took the average of multiple deep sea cores tuned to the orbital forcing parameters to generate a ‘generic’

oxygen isotope record for the past 750,000 years (Fig. 6.10). The SPECMAP composite chronology is frequently used to adjust oxygen isotope records when no reliable ages are available. It is now common parlance to speak of events that occurred in a particular stage as oxygen isotope stage 2 or 5.

6.5.2 The Paleogene and Neogene (Cenozoic)

From an historical point of view, our state of knowledge of oceanographic features in the Paleogene-Neogene was greatly enhanced by oxygen isotope analyses of benthic and planktic foraminifera made in the early 1970s from marine cores. At that

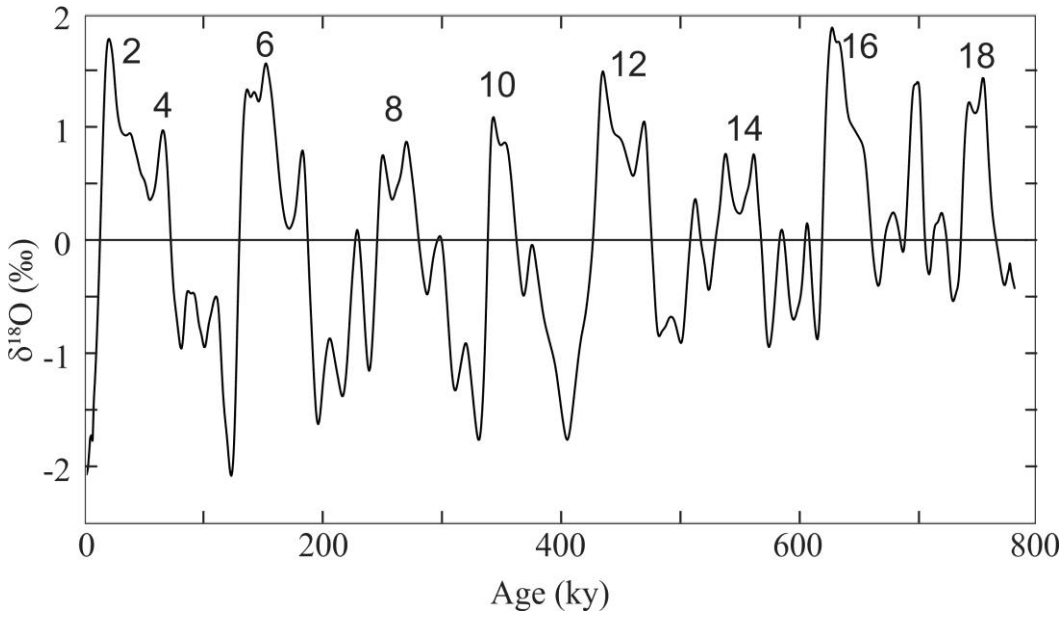

Fig. 6.11. Average (stacked) $\delta^{18}O$ records of multiple deep ocean cores turned to orbital parameters. The $\delta^{18}O$ values of each record are adjusted to have a mean value of 0‰. Even numbered (glacial) marine isotope stages are shown. After (Imbrie et al., 1984).

time sampling techniques were primitive by today's standards, but clear patterns were nevertheless evident in the data obtained. As a point of reference, the large difference in $\delta^{18}O$ between planktic and benthic shells forming in modern oceans from low latitudes reflect the large differences in temperature between surface and bottom waters. Bottom water temperatures are established by the sinking of cold, saline waters in the Antarctic and North Atlantic Seas. But ice volumes and ocean circulation patterns change with time, and these changes are reflected in the oxygen isotope data. Few such changes are as dramatic as those that occurred in Paleogene-Neogene time.

Data for planktic and benthic foraminiferal shells separated from cores collected at several sites in the North Pacific Ocean are shown in Figure 6.6. Differences in $\delta^{18}O$ between planktic and benthic shells were relatively small in the early Paleogene reflecting a relatively small differences in surface and bottom water temperatures. The cooling at the late Eocene to Oligocene and divergence of planktic and benthic foraminifera in Central Pacific samples suggests the beginning of cold downwelling waters originating at high latitudes. The dramatic cooling in the middle Miocene are related to the circumpolar Antarctic circulation and the formation of Antarctic ice sheets

(Savin et al., 1975).

The huge number of analyses of Paleogene-Neogene ocean core samples results in a extremely high-resolution record for the past 50-60 million years. Zachos *et al*. (2001) presents a detailed compilation of Paleogene to Present stable isotope variations (Fig. 6.12). Variations on the 10^4 to 10^5 y time scale are related to orbital parameters, while longer-scale, irreversible variations are related to tectonic processes. Spectral fitting of the data shows a strong periodicity at 100 ky and 41 ky for samples 0 to 4 Ma, with a loss of intensity of the 100 ky band in older samples.

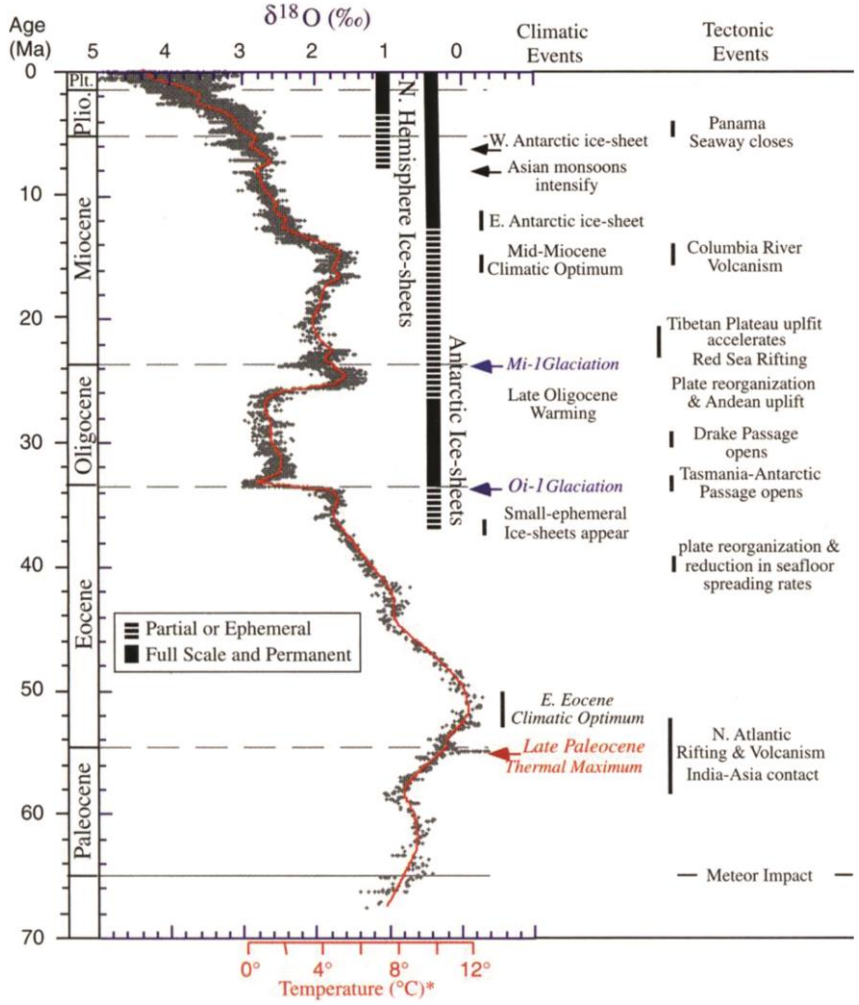

Fig. 6.12. High resolution $\delta^{18}O$ curve compiled from 40 ocean core samples. Most of the data are from the benthic foraminifera taxa *Cibicidoides* and *Nuttallides* corrected for vital effect. Absolute ages are corrected to the paleomagnetic time scale. Major events are correlated with $\delta^{18}O$ values, such as the E. Eocene climatic optimum and the timing and intensity of ice sheet formation. From Zachos *et al.* (2001).

6.5.3. Older samples

Well-preserved deep sea cores for Cretaceous samples exist, so that the foraminifera-based record extends back that far. Most Mesozoic and all Paleozoic samples are limited to shelf deposits. These lithologies have often undergone diagenesis, and great care must be taken to retrieve unaltered samples. In addition, the $\delta^{18}O$ value of the water in a shallow shelf setting may have been affected by a large meteoric contribution, lowering the apparent 'seawater' value. Workers in the field have been

careful to alleviate these problems by analyzing diagenetic-resistant material and by correlating salinity and $\delta^{18}O$ values of seawater using a temperature-salinity-density model or salinity-dependent cation ratios in the carbonate. As the age of samples increases, the uncertainties regarding diagenesis and $\delta^{18}O$ values of the ocean increase as well. Precambrian carbonates invariably have low $\delta^{18}O$ values, which can be correlated with one or more of three variables: diagenesis, low marine $\delta^{18}O$ values or warm ocean temperatures. Other stable isotope sedimentary proxies support the low $\delta^{18}O$ values of carbonates (cherts, iron formations), although the significance of the low values is still in debate.

Although extraction of the $\delta^{18}O$ value of unaltered carbonates is complicated by the effects of diagenesis, and the relationship between the $\delta^{18}O$ values of carbonates and ocean temperature is complicated by uncertainties about the oxygen isotope composition of the ocean through time, there have been a number of attempts to determine a secular curve for $\delta^{18}O$ values of marine carbonates. Figure 6.13 shows the extraordinary compilation of Veizer *et al.* (1999) for low magnesium calcite shells, mainly brachiopods and belemnites. High $\delta^{18}O$ values correspond to times of glaciation and generally cold conditions, and there is a diminution in $\delta^{18}O$ values of Ordovician and older samples.

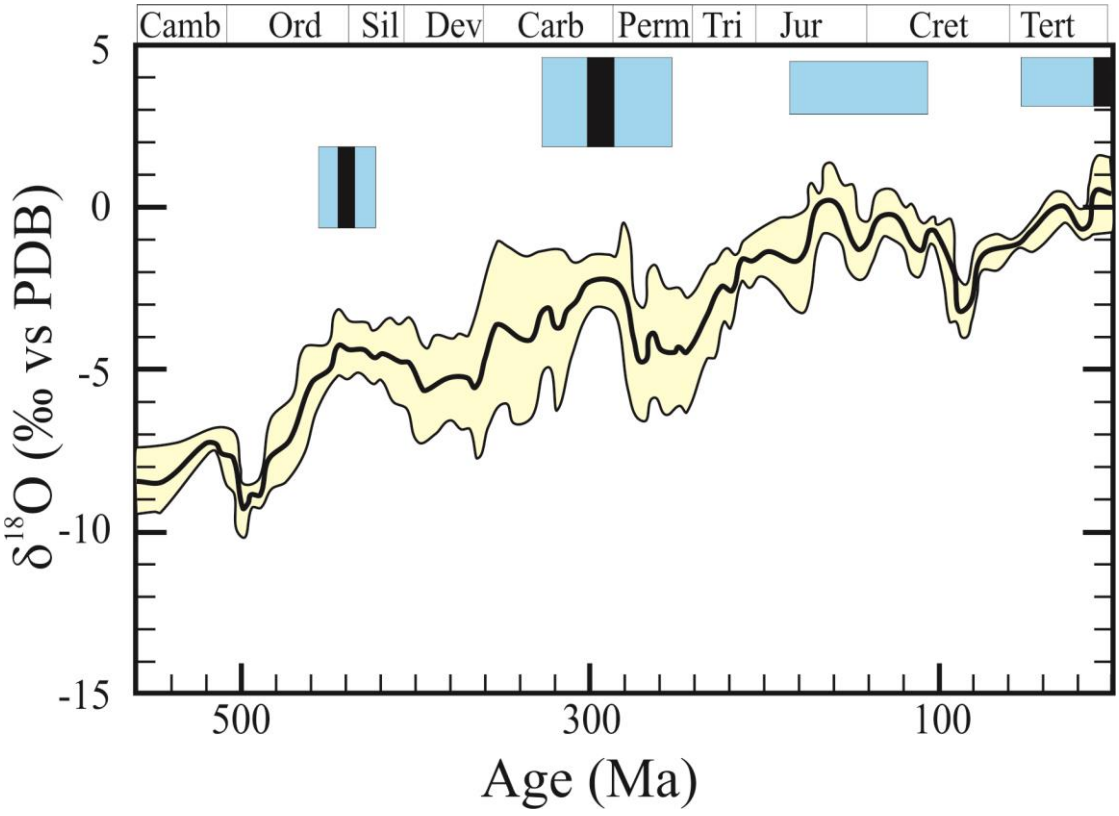

Fig. 6.13. Variations in the oxygen isotope ratio of shell carbonates. 1σ uncertainties are shown as the shaded region around the central line. Cold periods with evidence for glaciation are indicated by the shaded boxes above the curve, with ice ages illustrated with filled black boxes. Modified from Veizer *et al.* (1999).

6.5.4 Application to continental carbonates

Carbonates form in equilibrium with meteoric water in a number of different environments. Climatic information can be retrieved from these samples, but interpretation of the data is often complicated by the uncertainties in the $\delta^{18}O$ values of the water forming the carbonate. The $\delta^{18}O$ values of terrestrial (or continental) carbonates often are used to estimate the $\delta^{18}O$ value of the meteoric water, as opposed to the temperature of formation. Samples analyzed include speleothems, lake sediments, vein calcite, travertines and soil carbonates.

Interpretations of $\delta^{18}O$ values from terrestrial carbonates differ from those in the marine setting (Grootes, 1993). In Quaternary marine samples, high $\delta^{18}O$ values are caused by either increasing $\delta^{18}O$ values of the ocean due to glacial deposition on continents or lower ocean temperatures, or a combination of the two. In contrast, the $\delta^{18}O$ values of water from lakes are primarily a function of the $\delta^{18}O$ value of meteoric water. In the marine setting, low temperatures increase the $\delta^{18}O$ value of carbonates. In the continental setting, cold causes the $\delta^{18}O$ values of meteoric water to decrease (see Section 4.7.1), which in turn lowers the $\delta^{18}O$ value of the precipitating carbonate. The effect is essentially the reverse of that seen in the marine environment.

As an example, McKenzie and Hollander (1993) measured the oxygen isotope profile in a sedimentary sequence from a varved lake in Switzerland. There is a regular decrease in the $\delta^{18}O$ values of the lacustrine chalk from –8‰ prior to 1887 to values of close to -11‰ in modern sediments. McKenzie and Hollander attribute the lower $\delta^{18}O$ values in the young sediments to changes in atmospheric circulation in Central Europe. Pre-1887 meteoric waters were source primarily from cold prevailing northwesterly winds with low $\delta^{18}O$ values. The moisture source changed to one dominated by warmer westerly to southwesterly winds in modern times.

Cave deposits provide another important archive for terrestrial paleoclimate. There are dozens of magnificent oxygen isotope records of speleothem deposits. The National Climate Data Center lists over 100 isotope cave studies from all over the world (https://www.ncdc.noaa.gov/cdo/f?p=535:6:0:::::). Deep caves with poor air circulation have nearly constant year-round temperatures. Drip waters entering a cave are often at or near carbonate saturation. Ttwo processes contribute to the precipitation of calcite inside a cave: 1) outgassing of CO_2 from the drip water, and 2: evaporation, which increases the Ca^{2+} concentration of the fluid (Schwarcz, 2007). If CO_2 loss is slow, equilibrium between the dissolved species HCO_3^-, CO_2^{2-} and CO_2 is maintained, and carbonates precipitate in carbon and oxygen isotope equilibrium with formation waters (Hendy, 1971; Schwarcz, 1986). Combined with accurate mass spectrometric uranium-series dates of the carbonates, detailed records of terrestrial climates can be obtained.

Cave records provide a long term record in a specific location. Wang *et al.* (2017) measured the $\delta^{18}O$ values of the well-dated Paraíso Cave in eastern Amazonia and concluded that rainfall in the Amazon basin was lower by 58% in the last Glacial Maximum and higher by 142% in the warmest period in the Holocene 6000 years ago. These kinds of data provide continental records of paleoclimate that are unmatched by other records. The long term climatic data extractable from speleothems are illustrated by the remarkable Hulu cave in China (Fig. 6.14) which covers a time interval in excess of 70,000 years (Wang et al., 2001). The cave record follows the Greenland Ice core

(GISP2) closely in some regards and, significantly, diverges in others. The comparison between the Greenland record and the Monsoon-driven China record allow for climatic conditions to be compared over very different regions, and demonstrate a global insolation-driven system (Cheng et al., 2006)

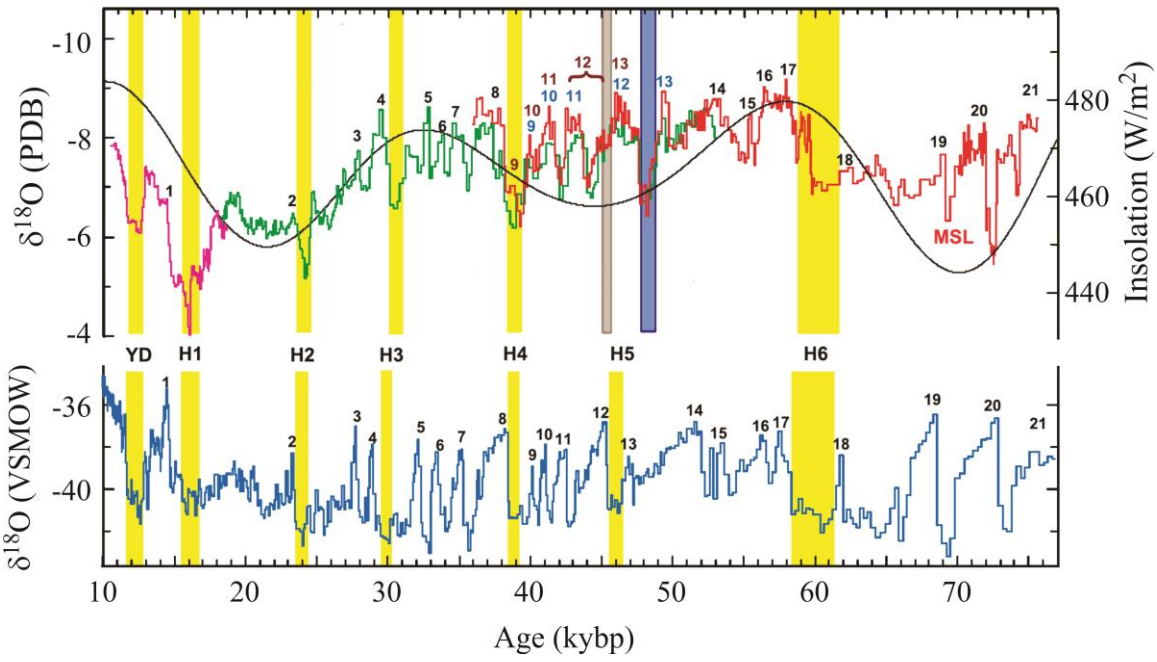

Fig. 6.14. Oxygen isotope record of the Hulu cave sequence (top) compared with the Greenland GISP2 ice core (bottom in blue). The Hulu cave is the combination of three stalagmites shown in different colors. Each analysis covers a period of ~ 130 y. 59 ^{230}Th analyses were made to date the core. The Younger Dryas (YD) and Heinrich events (H1-H6) are shown by yellow bands. The glacial/interglacial and sub-glacial events are clearly evident (numbers). Similarities as well as differences between the two records allow for global climate information to be retrieved. See Wang *et al.* (2001) for further details.

6.6 Clumped isotope thermometry

Clumped isotope thermometry is certainly one of the most exciting developments in paleothermometry over the last decade. The thermometer is based on the fact that the non-stochastic distribution of ^{13}C and ^{18}O in CO_2 is temperature dependent (Ghosh et al., 2006) and does not require an independent estimate of the isotopic composition of the water. It is truly a 'single mineral thermometer'. Unfortunately, during the acid digestion of the carbonate, only 2/3 of the oxygen in a carbonate is released to CO_2. Fortunately, any fractionation accompanying this decarbonation reaction appears to be mostly reproducible, so that the non-stochastic isotope distribution of the evolved CO_2 can still be used to estimate the temperature of last equilibration (Müller et al., 2017). The analytical technique is difficult and differences between laboratories and calibrations are still being worked out (e.g., Daëron et al., 2016). The theory of clumped isotope thermometry is introduced in section 3.7.

The exchange reaction governing the clumped isotope thermometer for carbonate can be expressed as (Schauble et al., 2006)

$$Ca^{13}C^{16}O_3 + Ca^{12}C^{18}O^{16}O_2 = Ca^{13}C^{18}O^{16}O_2 + Ca^{12}C^{16}O_3 \quad 6.9.$$

In essence, the above reaction describes the preference for ^{13}C and ^{18}O to 'clump' together (right side of reaction) relative to the randomly distributed configuration on the left side of reaction 6.8. Because the preference for the clumped configuration (~0.4% excess at room temperature) decreases with increasing temperature due to the increased entropy contribution, the excess clumped configuration varies with temperature. Results are presented in the Δ_{47} notation, where Δ_{47} is equal to the difference in the measured abundance of mass 47 ($^{13}C^{18}O^{16}O_2$) from that expected from a pure random (stochastic) distribution (see Eiler 2007 for details).

Applications of clumped isotope thermometry are numerous (Eiler, 2011). They have been used for climate reconstruction from cave carbonates (Affek et al., 2008), paleoaltitude reconstruction using soil carbonates (Quade et al., 2007), fluid sources along faults (Luetkemeyer et al., 2016), paleothermometry (Cummins et al., 2014) and even for martian meteorites (Halevy et al., 2011). As with any isotopic system, clumped isotopes are subject to alteration during diagenesis. In contrast to the oxygen and carbon isotope compositions, which are altered by exchange with large amounts of meteoric water, clumped isotopes can undergo simple scrambling during recrystallization (Dennis and Schrag, 2010; Winkelstern and Lohmann, 2016). In a closed system, resetting of calcite clumped isotopes occurs in excess of 100°C (Henkes et al., 2014) and dolomite resets only at significantly higher temperatures (Lloyd et al., 2017). Vital and kinetic effects must also be considered (e.g., Spooner et al., 2016). While numerous questions remain about the details of clumped isotopes, the technique has been used successfully in numerous applications and will certainly continue to grow.

The above discussion is really only half the picture. The information from carbon isotopes is complimentary to oxygen. Together, they provide far more information than either isotope alone. Chapter 7 continues with the carbon isotope story.

References

Affek, H.P., Bar-Matthews, M., Ayalon, A., Matthews, A. and Eiler, J.M. (2008) Glacial/interglacial temperature variations in Soreq cave speleothems as recorded by 'clumped isotope' thermometry. *Geochimica et Cosmochimica Acta* **72**, 5351-5360.

Al-Aasm, I.S., Taylor, B.E. and South, B. (1990) Stable isotope analysis of multiple carbonate samples using selective acid extraction. *Chemical Geology* **80**, 119-125.

Anderson, T.F. and Arthur, M.A. (1983) Stable isotopes of oxygen and carbon and their application to sedimentologic and paleoenvironmental problems, in: Arthur, M.A., Anderson, T.F., Kaplan, I.R., Veizer, J., Land, L.S. (Eds.), Stable Isotopes in Sedimentary Geology. SEPM Short Course, Columbia, pp. 1-151.

Barrera, E. and Savin, S.M. (1987) Effect of sample preparation on the delta^{18}O-value of fine-grained calcite. *Chemical Geology* **66**, 301-305.

Beck, J.W., Edwards, R.L., Ito, E., Taylor, F.W., Recy, J., Rougerie, F., Joannot, P. and Henin, C. (1992) Sea-surface temperature from coral skeltal strontium/calcium ratios. *Science* **257**, 644-647.

Brand, U. and Veizer, J. (1981) Chemical diagenesis of a multicomponent carbonate system -2: Stable isotopes. *Journal of Sedimentary Petrology* **51**, 987-997.

Carothers, W.W., Adami, L.H. and Rosenbauer, R.J. (1988) Experimental oxygen isotope fractionation between siderite-water and phosphoric acid liberated CO_2 -siderite. *Geochimica et Cosmochimica Acta* **52**, 2445-2450.

Carpenter, S.J., Lohmann, K.C., Holden, P., Walter, L.M., Huston, T.J. and Halliday, A.N. (1991) $\delta^{18}O$ values, $^{87}Sr/^{86}Sr$ and Sr/Mg ratios of Late Devonian abiotic marine calcite: Implications for the composition of ancient seawater. *Geochimica et Cosmochimica Acta* **55**, 1991-2010.

Carpenter, S.J. and Lohmann, K.C. (1992) Sr/Mg ratios of modern marine calcite: Empirical indicators of ocean chemistry and precipitation rate. *Geochimica et Cosmochimica Acta* **56**, 1837-1849.

Carpenter, S.J. and Lohmann, K.C. (1995) $\delta^{18}O$ and $\delta^{13}C$ values of modern brachiopod shells. *Geochimica et Cosmochimica Acta* **59**, 3749-3764.

Charef, A. and Sheppard, S.M.F. (1984) Carbon and oxygen isotope analysis of calcite or dolomite associated with organic matter. *Chemical Geology* **46**, 325-333.

Cheng, H., Edwards, R.L., Wang, Y., Kong, X., Ming, Y., Kelly, M.J., Wang, X., Gallup, C.D. and Liu, W. (2006) A penultimate glacial monsoon record from Hulu Cave and two-phase glacial terminations. *Geology* **34**, 217-220.

Cohn, M. and Urey, H.C. (1938) Oxygen exchange reactions of organic compounds and water. *Journal of the American Chemical Society* **60**, 679-687.

Coplen, T.B., Kendall, C. and Hopple, J. (1983) Comparison of stable isotope reference samples. *Nature* **302**, 236-238.

Coplen, T.B. (2007) Calibration of the calcite-water oxygen-isotope geothermometer at Devils Hole, Nevada, a natural laboratory. *Geochimica et Cosmochimca Acta* **71**, 3948-3957.

Craig, H. (1965) The measurement of oxygen isotope paleotemperatures, in: Tongiorgi, E. (Ed.), Stable isotopes in oceanographic studies and paleotemperatures. Consiglio Nazionale delle Richerche, Laboratorio de Geologia Nucleare, Pisa, pp. 161-182.

Cummins, R.C., Finnegan, S., Fike, D.A., Eiler, J.M. and Fischer, W.W. (2014)

Carbonate clumped isotope constraints on Silurian ocean temperature and seawater δ18O. *Geochimica et Cosmochimica Acta* **140**, 241-258.

Daëron, M., Blamart, D., Peral, M. and Affek, H.P. (2016) Absolute isotopic abundance ratios and the accuracy of Δ47 measurements. *Chemical Geology* **442**, 83-96.

Dennis, K.J. and Schrag, D.P. (2010) Clumped isotope thermometry of carbonatites as an indicator of diagenetic alteration. *Geochimica et Cosmochimica Acta* **74**, 4110-4122.

DeVilliers, S., Shen, G.T. and Nelson, B.K. (1994) The Sr/Ca-temperature relationship in corralline aragonite: Influence of variability in $(Sr/Ca)_{seawater}$ and skeletal growth parameters. *Geochimica et Cosmochimica Acta* **58**, 197-208.

Eiler, J.M. (2007) "Clumped-isotope" geochemistry—The study of naturally-occurring, multiply-substituted isotopologues. *Earth and Planetary Science Letters* **262**, 309-327.

Eiler, J.M. (2011) Paleoclimate reconstruction using carbonate clumped isotope thermometry. *Quaternary Science Reviews* **30**, 3575-3588.

Emiliani, C. (1955) Pleistocene temperatures. *Journal of Geology* **63**, 538-578.

Emiliani, C. (1966) Paleotemperature analysis of Caribbean cores P6304-8 and P6304-9 and a generalized temperature curve for the past 425,000 years. *Journal of Geology* **74**, 109-126.

Emiliani, C., Hudson, J.H., Shinn, E.A. and George, R.Y. (1978) Oxygen and carbon isotopic growth record in a reef coral from the Florida Keys and a deep-sea coral from Blake Plateau. *Science* **202**, 627-629.

Epstein, S., Buchsbaum, R., Lowenstam, H.A. and Urey, H.C. (1953) Revised carbonate-water isotopic temperature scale. *Geological Society of America Bulletin* **64**, 1315-1326.

Ghosh, P., Adkins, J., Affek, H., Balta, B., Guo, W., Schauble, E.A., Schrag, D.P. and Eiler, J.M. (2006) $^{13}C–^{18}O$ bonds in carbonate minerals: A new kind of paleothermometer. *Geochimica et Cosmochimica Acta* **70**, 1439-1456.

Grootes, P.M. (1993) Interpreting continental oxygen isotope records, in: Swart, P.K., Lohmann, K.C., McKenzie, J.A., Savin, S. (Eds.), Climate Change in Continental Isotopic Records. American Geophysical Union, Washington, D.C., pp. 37-46.

Grossman, E.L. and Ku, T.L. (1986) Oxygen and carbon isotope fractionation in biogenic aragonite; temperature effects. *Chemical Geology* **59**, 59-74.

Grossman, E.L. (1994) The carbon and oxygen isotopic record during the evolution of Pangea; Carboniferous to Triassic, in: Klein, G.D. (Ed.), Pangea: Paleoclimate, Tectonics, and Sedimentation during Accretion, Zenith, and Breakup of a supercontinent. Geological Society of America, Special Paper, pp. 207-228.

Halevy, I., Fischer, W.W. and Eiler, J.M. (2011) Carbonates in the Martian meteorite Allan Hills 84001 formed at 18 ± 4 °C in a near-surface aqueous environment. *Proceedings of the National Academy of Sciences of the United States of America* **108**, 16895-16899.

Hendy, C.H. (1971) The isotopic geochemistry of speleothems—I. The calculation of the effects of different modes of formation on the isotopic composition of speleothems and their applicability as palaeoclimatic indicators. *Geochimica et Cosmochimica Acta* **35**, 801-824.

Henkes, G.A., Passey, B.H., Grossman, E.L., Shenton, B.J., Pérez-Huerta, A. and Yancey, T.E. (2014) Temperature limits for preservation of primary calcite clumped

isotope paleotemperatures. *Geochimica et Cosmochimica Acta* **139**, 362-382.

Horita, J. (2014) Oxygen and carbon isotope fractionation in the system dolomite–water–CO_2 to elevated temperatures. *Geochemica et Cosmochimica Acta* **129**, 111-124.

Imbrie, J., Hays, J.D., Martinson, D.G., McIntyre, A., Mix, M., Morley, J.J., Pisias, N.G., Prell, W. and Shackleton, N.J. (1984) The orbital theory of Pleistocene climate: support from a revised chronology of the marine $\delta^{18}O$ record, in: Berger, A., Hays, J.D., Kukla, G., Salzman, B. (Eds.), Milankovich and Climate. Reidel, Dordrecht, pp. 269-305.

Kim, S.-T. and O'Neil, J.R. (1997) Equilibrium and nonequilibrium oxygen isotope effects in synthetic carbonates. *Geochimica et Cosmochimica Acta* **61**, 3461-3475.

Lloyd, M.K., Eiler, J.M. and Nabelek, P.I. (2017) Clumped isotope thermometry of calcite and dolomite in a contact metamorphic environment. *Geochimica et Cosmochimica Acta* **197**, 323-344.

Lohmann, K.C. (1988) Geochemical patterns of meteoric diagenetic systems and their application to studies of paleokarst, in: James, N.P., Choquette, P.W. (Eds.), Paleokarst. Springer-Verlag, Berlin, pp. 50-80.

Lowenstam, H.A. (1961) Mineralogy, O^{18}/O^{16} ratios, and strontium and magnesium contents of recent and fossil brachiopods and their bearing on the history of the oceans. *Journal of Geology* **69**, 241-260.

Luetkemeyer, P.B., Kirschner, D.L., Huntington, K.W., Chester, J.S., Chester, F.M. and Evans, J.P. (2016) Constraints on paleofluid sources using the clumped-isotope thermometry of carbonate veins from the SAFOD (San Andreas Fault Observatory at Depth) borehole. *Tectonophysics* **690, Part A**, 174-189.

Marshall, J.D. (1992) Climatic and oceanographic isotopic signals from the carbonate rock record and their preservation. *Geological Magazine* **129**, 143-160.

McCrea, J.M. (1950) On the isotopic chemistry of carbonates and a paleotemperature scale. *Journal of Chemical Physics* **18**, 849-857.

McKenzie, J.A. and Hollander, D.J. (1993) Oxygen-isotope record in Recent carbonate sediments from Lake Greifen, Switzerland (1750-1986); application of continental isotopic indicator for evaluation of changes in climate and atmospheric circulation patterns, in: Swart, P.K., Lohmann, K.C., McKenzie, J.A., Savin, S. (Eds.), Climate Change in Continental Isotopic Records. American Geophysical Union, Washington, D.C., pp. 101-111.

Mii, H.-S., Grossman, E.L. and Yancey, T.E. (1999) Carboniferous isotope stratigraphies of North America: Implications for Carboniferous paleoceanography and Mississippian glaciation. *Geological Society of America Bulletin* **111**, 960-973.

Müller, I.A., Violay, M.E.S., Storck, J.-C., Fernandez, A., van Dijk, J., Madonna, C. and Bernasconi, S.M. (2017) Clumped isotope fractionation during phosphoric acid digestion of carbonates at 70 °C. *Chemical Geology* **in press**.

O'Neil, J.R., Clayton, R.N. and Mayeda, T.K. (1969) Oxygen isotope fractionation in divalent metal carbonates. *Journal of Chemical Physics* **51**, 5547-5558.

O'Neil, J.R., Adami, L., H. and Epstein, S. (1975) Revised value for the O^{18} fractionation between CO_2 and H_2O at 25°C. *Journal of Research of the U. S. Geological Survey* **3**, 623-624.

O'Neil, J.R. (1977) Stable isotopes in mineralogy. *Physics and Chemistry of Minerals* **2**, 105-123.

Perry, E.C., Jr. and Tan, F.C. (1972) Significance of oxygen and carbon isotope variations in Early Precambrian cherts and carbonate rocks of Southern Africa. *Geological Society of America Bulletin* **83**, 647-664.

Prell, W.L., Imbrie, J., Martinson, D.G., Morley, J.J., Pisias, N.G., Shackleton, N.J. and Streeter, H.F. (1986) Graphic correlation of oxygen isotope stratigraphy application to the late Quaternary. *Paleoceanography* **1**, 137-162.

Quade, J., Garzione, C. and Eiler, J. (2007) Paleoelevation reconstruction using pedogenic carbonates. *Reviews in Mineralogy and Geochemistry* **66**, 53-87.

Rosenbaum, J. and Sheppard, S.M.F. (1986) An isotopic study of siderites, dolomites and ankerites at high temperatures. *Geochimica et Cosmochimica Acta* **50**, 1147-1150.

Savin, S.M., Douglas, R.G. and Stehli, F.G. (1975) Tertiary marine paleotemperatures. *Geological Society of America Bulletin* **86**, 1499-1510.

Schauble, E.A., Ghosh, P. and Eiler, J.M. (2006) Preferential formation of $^{13}C–^{18}O$ bonds in carbonate minerals, estimated using first-principles lattice dynamics. *Geochimica et Cosmochimica Acta* **70**, 2510-2529.

Schwarcz, H. (1986) Geochronology and isotopic geochemistry of speleothems, in: Fritz, P., Fontes, J.C. (Eds.), Handbook of Environmental Isotope Geochemistry. Elsevier, Amsterdam, pp. 271-303.

Schwarcz, H. (2007) CARBONATE STABLE ISOTOPES | Speleothems. *Encyclopedia of Quaternary Science*, 290-300.

Shackleton, N.J. and Opdyke, N.D. (1973) Oxygen Isotope and Palaeomagnetic Stratigraphy of Equatorial Pacific Core V28-238: Oxygen Isotope Temperatures and Ice Volumes on a 10^5 and 10^6 Year Scale. *Quaternary Research* **3**, 39-55.

Shackleton, N.J. and Opdyke, N.D. (1976) Oxygen-isotope and paleomagnetic stratigraphy of Pacific Core V28-239, late Pliocene to latest Pleistocene. *Geological Society of America Memoir* **145**, 449-464.

Sharma, T. and Clayton, R.N. (1965) Measurement of 0-18/0-16 ratios of total oxygen of carbonates. *Geochimica et Cosmochimica Acta* **29**, 1347-1353.

Spooner, P.T., Guo, W., Robinson, L.F., Thiagarajan, N., Hendry, K.R., Rosenheim, B.E. and Leng, M.J. (2016) Clumped isotope composition of cold-water corals: A role for vital effects? *Geochimica et Cosmochimica Acta* **179**, 123-141.

Swart, P.K., Burns, S.J. and Leder, J.J. (1991) Fractionation of the stable isotopes of oxygen and carbon in carbon dioxide during the reaction of calcite with phosphoric acid as a function of temperature and technique. *Chemical Geology* **86**, 89-96.

Tarutani, T., Clayton, R.N. and Mayeda, T.K. (1969) The effect of polymorphism and magnesium substitution on oxygen isotope fractionation between calcium carbonate and water. *Geochimica et Cosmochimica Acta* **33**, 987-996.

Urey, H.C., Epstein, S., McKinney, C. and McCrea, J. (1948) Method for measurement of paleotemperatures. *Bulletin of the Geological Society of America (abstract)* **59**, 1359-1360.

Urey, H.C., Epstein, S. and McKinney, C.R. (1951) Measurement of paleotemperatures and temperatures of the Upper Cretaceous of England, Denmark, and the southeastern United States. *Geological Society of America Bulletin* **62**, 399-416.

van Dijk, J., Fernandez, A., Müller, I.A., Lever, M. and Bernasconi, S.M. (2018) Oxygen isotope fractionation in the siderite-water system between 8.5 and 62 °C. *Geochimica et Cosmochimica Acta* **220**, 535-551.

Veizer, J., Ala, D., Azmy, K., Bruckschen, P., Buhl, D., Bruhn, F., Carden, G.A.F., Diener, A., Ebneth, S., Godderis, Y., Jasper, T., Korte, C., Pawellek, F., Podlaha, O.G. and Strauss, H. (1999) $^{87}Sr/^{86}Sr$, $\delta^{13}C$ and $\delta^{18}O$ evolution of Phanerozic seawater. *Chemical Geology* **161**, 59-88.

Wachter, E.A. and Hayes, J.M. (1985) Exchange of oxygen isotopes in carbon dioxide - phosphoric acid systems. *Chemical Geology* **52**, 365-374.

Wang, X., Edwards, R.L., Auler, A.S., Cheng, H., Kong, X., Wang, Y., Cruz, F.W., Dorale, J.A. and Chiang, H.-W. (2017) Hydroclimate changes across the Amazon lowlands over the past 45,000 years. *Nature* **541**, 204-207.

Wang, Y.J., Cheng, H., Edwards, R.L., An, Z.S., Wu, J.Y., Shen, C.-C. and Dorale, J.A. (2001) A high-resolution absolute-date late Pleistocene monsoon record from Hulu Cave, China. *Science* **294**, 2345-2348.

Watkins, J.M. and Hunt, J.D. (2015) A process-based model for non-equilibrium clumped isotope effects in carbonates. *Earth and Planetary Science Letters* **432**, 152-165.

Winkelstern, I.Z. and Lohmann, K.C. (2016) Shallow burial alteration of dolomite and limestone clumped isotope geochemistry. *Geology* **44**, 467-470.

Zachos, J., Pagani, M., Sloan, L., Thomas, E. and Billups, K. (2001) Trends, rhythms, and aberrations in global climate 65 Ma to Present. *Science* **292**, 686-693.

Chapter 7

CARBON IN THE LOW-TEMPERATURE ENVIRONMENT

Contents

7.1 Introduction 1
7.2 The carbon cycle 1
7.2.1 Carbon isotope budget of the Earth 3
7.3 Carbon reservoirs 3
7.3.1 Mantle 4
7.3.2 Plants 5
7.3.3 Organic carbon in sediments 8
7.3.4 Methane 10
7.3.5 Atmospheric CO_2 11
7.4 $\delta^{13}C$ values of carbonates 12
7.4.1 Introduction 12
7.4.2 General characterization of carbonates 13
7.4.3 The vital effect 13
7.4.4 Carbonate speciation effects 16
7.4.5 Controls on the $\delta^{13}C$ value of marine carbonates over long time scales 17
7.4.6 Variations in the $\delta^{13}C$ values of marine carbonates at short time scales 19
7.5 $\delta^{13}C$ studies of terrestrial carbonates 22
7.5.1 Paleo-p(CO_2) estimates from soil carbonates 23
References 24

Chapter 7

CARBON IN THE LOW-TEMPERATURE ENVIRONMENT

7.1 Introduction

Carbon dioxide has been called "the most important substance in the biosphere" (Revelle, 1985). It makes life on Earth possible and warms our planet to the habitable condition where H_2O is in the liquid state. Carbon is the foundation of the World's major energy source, and as fossil fuels continue to be burned at an alarming rate of 10 gigatons of CO_2 emitted per year, we have come to recognize the serious effects of anthropogenic-induced global warming. The carbon cycle is a complex system of feedback mechanisms at many levels, and has been an intense disciple of geologic study. Stable carbon isotopes have played a critical role in this research, being used to constrain sizes and fluxes into and out of the various carbon reservoirs. Other applications include evaluating variations in temperature and productivity in the past, photosynthetic pathways, diets, metabolic pathways, evidence for early life on earth and variations in greenhouse gas abundances through time. In this chapter we will review the carbon cycle, discuss plant photosynthesis and carbonate formation as it relates to carbon isotopes, and provide several examples of application of carbon isotope geochemistry to geological processes.

Carbon exists in oxidized, elemental and reduced forms. Oxidized forms include CO_2 and carbonates, elemental forms include graphite and diamond, and reduced forms include methane and organic matter. As is the case for almost all compounds, the heavy isotope ^{13}C is concentrated in the more oxidized forms[1]. Metabolic reduction of carbon (*i.e.* formation of organic matter) is a non-equilibrium process where ^{12}C is strongly partitioned into organic matter, leading to two major crustal reservoirs of carbon; a reduced low $\delta^{13}C$ reservoir and an oxidized high $\delta^{13}C$ reservoir. Assuming that most carbon in the surficial/crustal reservoir originated as volcanic CO_2 emissions with a near constant mantle value, the massive biologically-induced reduction of carbon over time led to a concomitant production of free oxygen (O_2 gas) critical to most life forms on Earth today.

7.2 The carbon cycle

The carbon cycle is complex and has been studied at many scales. The mantle reservoir, which swamps all others in size, is unimportant when considering changes in atmospheric $p(CO_2)$ related to short-term anthropogenic contributions. Transfer to and from the mantle reservoir (the flux rate) is simply too slow. Likewise, the abundance of CO_2 in the atmosphere is miniscule compared to the major reservoirs, and can be ignored when concerned with the long-term carbon budget. On the other hand, transfer of CO_2 between reservoirs is often made via the atmosphere, making it an important *flux*. In addition to size, therefore, fluxes into and out of the different reservoirs are of critical importance.

[1] Rare exceptions include carbon monoxide (relative to graphite), nitric oxide and ammonium ion for the nitrogen system.

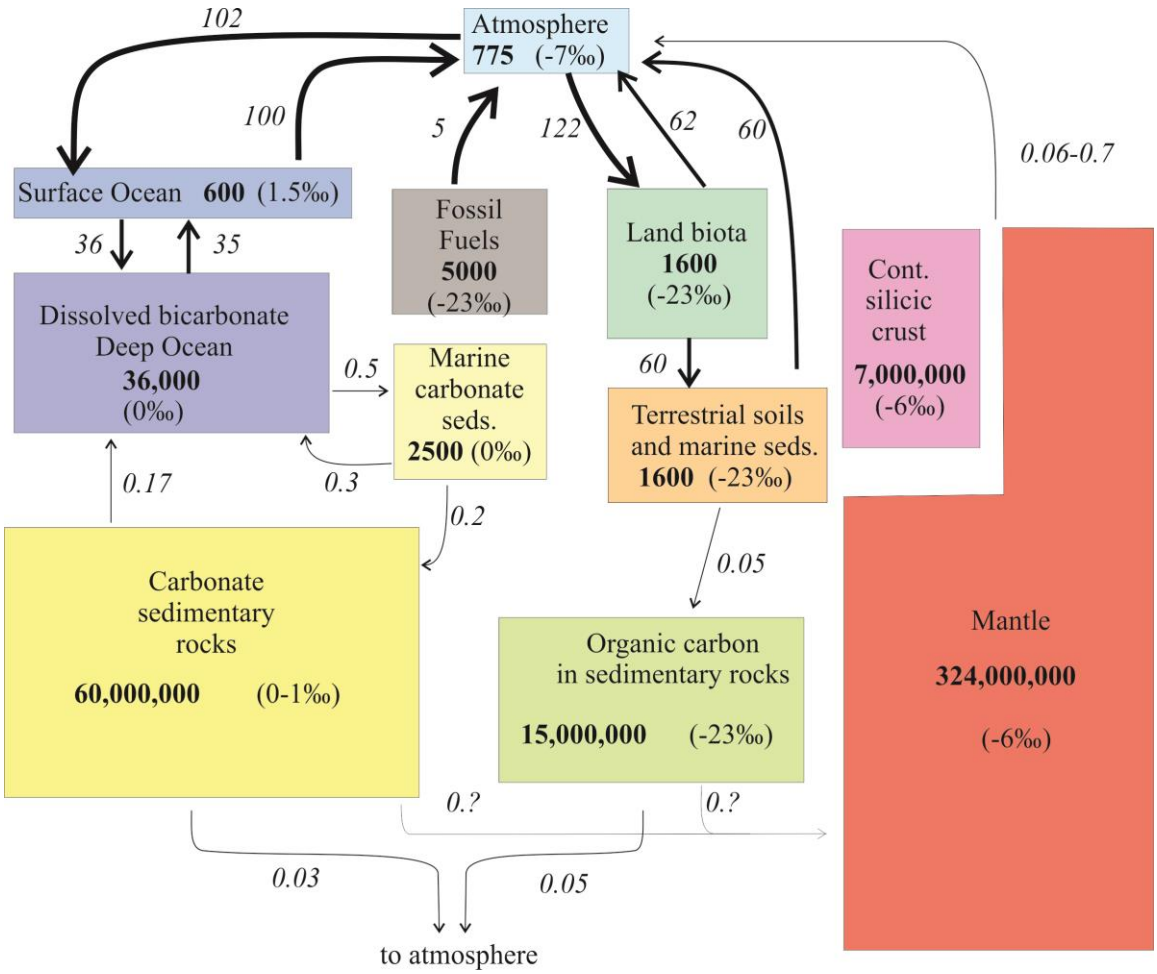

Fig. 7.1. Carbon cycle, showing amounts, fluxes and $\delta^{13}C$ values of different reservoirs. Abundance shown in bold in 10^{15}g. Flux is shown in italics in 10^{15}g/yr. $\delta^{13}C$ values are in parentheses.

The major reservoirs for carbon in the crust are sedimentary inorganic carbon in the form of carbonates (*e.g.*, limestones, dolomites), organic carbon, and carbon hosted in crystalline rocks. Reservoirs, their abundance, fluxes, and their $\delta^{13}C$ values are given in Table 1 and shown in Figures 7.1 and 7.2.

To a first approximation, we can assume that the carbon cycle is a balanced, steady-state system. Fluxes into and out of each reservoir equal each other, as seen in Figure 7.1. The exception, of course, is the anthropogenic flux of CO_2 from fossil fuel burning to the atmosphere, causing a minor, short-term ($10^3 – 10^5$ y) imbalance. Although small in size, the fluxes involving atmospheric CO_2 are immense, so that equilibrium between oceans and terrestrial organic carbon is maintained at near steady-state. There is a huge annual incorporation of CO_2 during plant respiration (122×10^{15}g C/year), which is nearly balanced by decomposition of plants and organic carbon in soils. The other large flux is between the atmosphere and surface ocean, where CO_2 is transferred to dissolved bicarbonate and back again. Finally, the flux between the surface and deep oceans is large and nearly balanced. The fluxes between the other reservoirs – carbonates, mantle,

organic carbon in sedimentary rocks – are orders of magnitude slower, and have relevance only in studies of long term climate variation.

***Table 7.1**. Mass and carbon isotope composition of major carbon reservoirs. After (Anderson and Arthur, 1983; Des Marais, 2001)*

Reservoir	Mass/10^{15} g C	δ^{13}C ‰ (PDB) average
Atmosphere (@ 290 PPM)	775	-6 to –7
Ocean (TDC)	35,000	0
(DOC)	1,000	-20
(POC)	3	-22
Land plants	1600	-25 (-12 for C_4 plants)
Soil humus	1000-3000	-25 (-12 for C_4 plants)
Sedimentary inorganic C (carbonates)	**60,000,000**	0 to 1
organic carbon	**15,000,000**	-23
continental silicic crust	**7,000,000**	-6
mantle	**324,000,000**	-5 to -6

7.2.1 Carbon isotope budget of the Earth

Fractionation between oxidized, inorganic carbon species is generally small. In contrast, the fractionation between inorganic (oxidized) and organic (reduced) carbon is very large. In fact, isotopically light carbon is a characteristic signature of life. The δ^{13}C values of 3.7 Ga carbonates from Greenland have been used to postulate a gradual buildup of organic matter through time (e.g., Schidlowski et al., 1979; Mojzsis et al., 1996). If all terrestrial carbon has come from the mantle with minimal fractionation, then the average δ^{13}C values of the terrestrial carbon reservoirs must equal those of the mantle. The two main terrestrial reservoirs, carbonate sedimentary rocks and organic carbon should equal to the assumed mantle value of -5.5‰ according to the equation

$$x\,(\delta^{13}C)_{carbonate} + (1 - x)(\delta^{13}C)_{organic\ carbon} = -5.5‰ \qquad 7.1,$$

where x is the fraction of carbonate relative to total carbon in both reservoirs. Average carbonate and organic carbon reservoirs give a rough Δ^{13}C (carbonate – organic carbon) value of 23‰ and an average δ^{13}C value of carbonates of 0‰, equation 7.1 becomes

$$x\,(\delta^{13}C)_{carbonate} + (1 - x)(\delta^{13}C_{carbonate} - 23) = -5.5‰ \qquad 7.2,$$

resulting in a carbonate fraction of 0.76, in good agreement with the data in Table 1.

7.3 Carbon reservoirs

General ranges for δ^{13}C values of typical reservoirs are shown in Figure 7.2 and described in further detail in the following sub-sections.

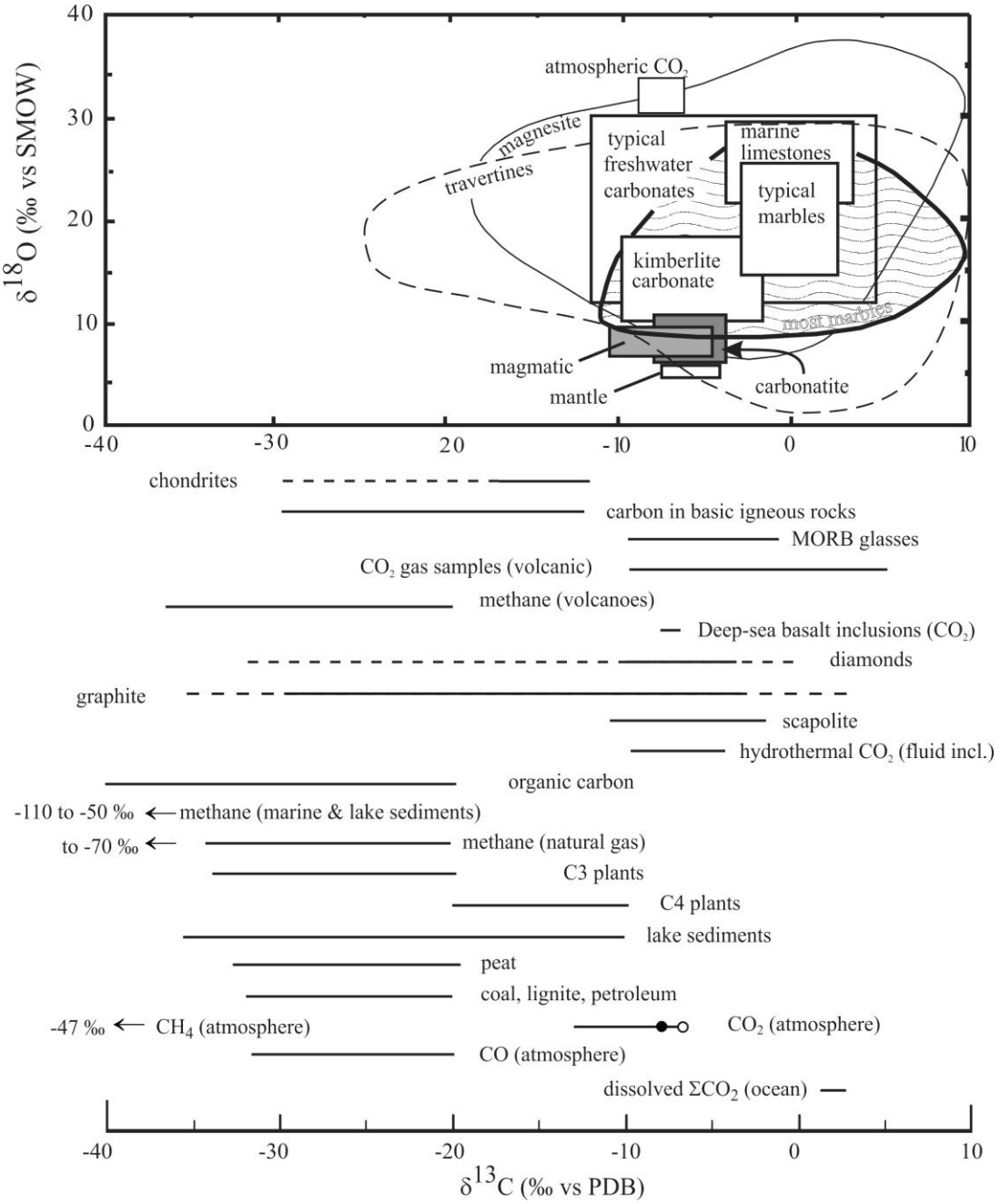

Fig. 7.2. General range of $\delta^{13}C$ (and $\delta^{18}O$) values of selected carbon-bearing materials.

7.3.1 Mantle

Mantle carbon enters the crustal reservoir mainly from mid-ocean spreading ridges and rift systems. The $\delta^{13}C$ value of CO_2 from the mantle is ~-6 to -5‰ (see Chapter 11). The $\delta^{13}C$ values of carbonatites and MORB are close to mantle value, with a minor light component (-22 to -26‰) for diamonds and MORB (Deines, 2002). The explanation for the low values may be related to subduction of organic carbon or degassing processes in the mantle (see Section 11.2.2 for more details).

7.3.2 Plants

The formation of reduced organic carbon occurs by reduction of CO_2 during photosynthesis[2]. Other forms of reduced carbon, from petroleum to animals, to black shales, ultimately can trace their origin back to photosynthesis. Therefore, we begin by reviewing the mechanisms and isotopic fractionations that occur during photosynthesis. Terrestrial plants derive their carbon from photosynthetic fixation of atmospheric CO_2, as does marine plankton. Other aquatic plants fix carbon from dissolved HCO_3^-.

Photosynthetic organisms remove ~10% of the CO_2 in the atmosphere per year, which is balanced by the decomposition of plant material at a later stage. The simple glucose producing reaction involves the reduction of CO_2 and production of O_2 using water as a hydrogen donor:

$$6CO_2 + 12H_2O \rightarrow C_6H_{12}O_6 + 6H_2O + 6O_2 \qquad 7.3.$$

The overall reaction is divided into two separate mechanisms: the "Light reaction" and the "Dark reaction". The Light reaction involves transfer of electrons from the donor molecule water to the acceptor molecule nicotinamide adenine dinucleotide phosphate (NADP), an important coenzyme in the plant cell. The Dark reaction uses NADPH and ATP to fix reduced C and transfer it into carbohydrates in the Calvin-Benson[3] cycle (C_3 cycle). The important step in terms of stable isotope chemistry is carboxylation, which involves the addition of CO_2 to the acceptor molecule, ribulose bis-phosphate (RuBP), catalyzed by the enzyme ribulose bisphosphate carboxylase-oxygenase (Rubisco). It is the partial removal of CO_2 during carboxylation that leads to the major carbon isotope fractionation in plants.

An additional process that occurs in plants is *photorespiration*, where O_2 is taken-up and CO_2 is generated. In this process, Rubisco catalyzes the oxygenation of RuBP, ultimately releasing CO_2, an overall energy consuming process. Two other photosynthetic pathways called the C_4 dicarboxylic acid pathway (C_4 pathway) and Crassulacean Acid Metabolism (CAM) have evolved that limit the inefficiencies of C_3 photorespiration. In these processes, CO_2 is concentrated at the active site of Rubisco to enhance the efficiency of photosynthesis. Photorespiration is significantly reduced in plants using these photosynthetic pathways.

A model of the C_4 pathway was first published in 1965 and 1966 (Hatch and Slack, 1966), where $^{14}CO_2$ was used as an isotopic tracer to identify the products of photosynthesis in sugarcane. The first labeled products are 4-carbon acids (oxaloacetate and then malate), rather than the 3-carbon acid 3-phosphoglyceric acid (3PGA) in the C_3 pathway. Malate enters the bundle sheath cells and is decarboxylated, releasing CO_2 which is used by the Calvin cycle as in C_3 plants. By concentrating CO_2 at the site of carboxylation (Rubisco), C_4 (and CAM) minimize photorespiration, a benefit under conditions of low stomatal conductance[4]. Low stomatal conductance is beneficial in hot arid environments, where minimizing water loss is critical, and under conditions of low $p(CO_2)$. The disadvantage is that C_4 photosynthesis is less efficient that C_3, so that there

[2] Minor CO_2 reduction also occurs by chemotrophs, which utilize chemical energy rather than light energy.
[3] Melvin Calvin won the Nobel prize in chemistry in 1961 for his work on assimilation of CO_2 by plants.
[4] Stomata are the pore openings of the epidermal layer of plant tissue where transpiration occurs.

is a competition between plants that use one or the other pathway. The basic rules useful for paleoclimate reconstruction are the following (Ehleringer et al., 1997):

- C_4 plants do well under conditions of low $p(CO_2)$
- C_4 plants have high water efficiency, and so are tolerant to high temperatures and aridity. There is a nearly perfect correlation between % C_4 flora in a community and minimum growing-season temperature (Teeri and Stowe, 1976).

Only about 0.4% of angiosperms are C_4 plants, but they account for 18% of total global productivity. C_4 plants include important crops such as maize, sugarcane, sorghum, and tropical pasture grasses. The C_3 pathway is used by trees, most shrubs, herbs and cool weather grasses and aquatic plants. C_3 plants are favored in high latitudes, cooler climates, and, because C_4 plants are so successful in regions with summer rainfall, regions with more arid summers. Forests, woodlands and high latitude grasses are generally C_3.

The different photosynthetic pathways were first recognized by stable isotope geochemists on the basis of two distinct populations of $\delta^{13}C$ values in plants (Bender, 1968; Smith and Epstein, 1970). The typical range of C_3 plants is -33 to -23‰, with an average of –27 to –26‰ (Fig. 7.3). The $\delta^{13}C$ values of C_4 plants are about 13‰ higher than those of C_3 plants, ranging from -16 to -9, averaging -13 to -12‰. There is no evidence of C_4 plants prior to the Cenozoic (Cerling and Quade, 1993; Cerling et al., 1993). Interestingly, Craig (1954) identified C_4 plants in an elegant work of the carbon isotope fractionation of plants, but incorrectly postulated that the high $\delta^{13}C$ values were related to uptake of dissolved carbonates.

Aquatic photosynthetic organisms derive their carbon from dissolved carbon in water. The $\delta^{13}C$ values of algae range from -22 to -10‰, plankton from -31 to -18‰, kelp from <-20 to -10‰. Most warm-water plankton have a $\delta^{13}C$ value of -22 to -17‰. It has been proposed that there is a temperature-dependent fractionation of the $\delta^{13}C$ value of plankton (Sackett et al., 1965; Degens et al., 1968). As plankton get a significant portion of their carbon from dissolved CO_2 as opposed to bicarbonate, the temperature dependence is a function of availability. There is no need to postulate temperature-sensitive enzymatic reactions to explain observed fractionations with change in water temperature. When molecular CO_2 is sufficiently abundant, there is constant fractionation of about 19‰ between CO_2 and cells over all reasonable temperatures. The average $\delta^{13}C$ value of marine plants is ~ -20‰.

The carbon isotope fractionation attending photosynthesis was first outlined by Park and Epstein (1960) who noted that two particular steps involved significant fractionation. These were 1) the preferential uptake of ^{12}C from air CO_2 and 2) the conversion of dissolved CO_2 by Rubisco to reduced carbon. A simple expression relating $\delta^{13}C$ value of a C_3 plant to that of CO_2 in air is given by (Farquhar et al., 1989);

$$\Delta^{13}C_{(CO_2 \text{ in air - plant})} = a\,\frac{p_a - p_i}{p_a} + b\,\frac{p_i}{p_a} \qquad 7.4$$

where $\Delta^{13}C$ is the overall discrimination during C assimilation, a (4.4‰) is the discrimination associated with gas phase diffusion in air and b (29‰) is the discrimination associated with carboxylation (mainly by Rubisco). The variables p_a and

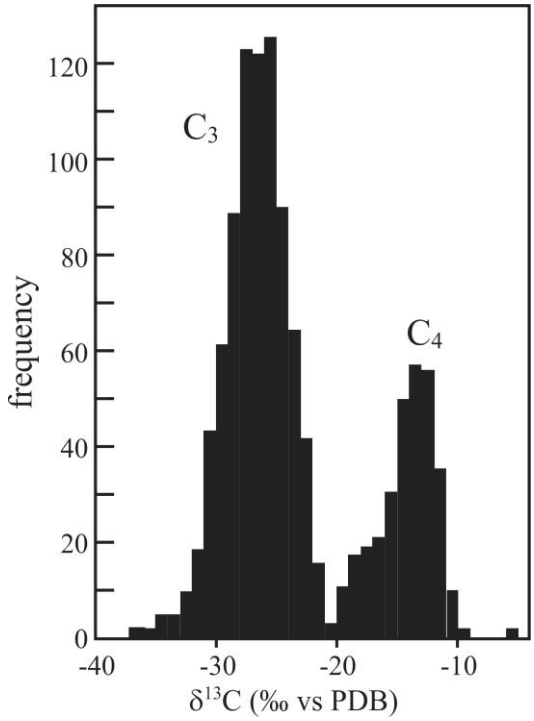

Fig. 7.3. $\delta^{13}C$ values of C_3 and C_4 terrestrial plants. The difference of 10‰ between the two groups makes for unambiguous identification. After Deines (1980)

p_i are the partial pressures of CO_2 in the bulk air and intercellular air spaces, respectively. If we take $p_i = 0.7p_a$ as a typical ratio, then $\Delta = 21.6$. For a $\delta^{13}C$ value of air is -7.9‰[5], plants will form with a $\delta^{13}C$ value of -28.9‰, in good agreement with typical values for modern C_3 plants. With lower internal pressure, the discrimination in the carboxylation step is reduced, and the overall fractionation associated with photosynthesis decreases.

It is worthwhile to view equation 7.4 under extreme variations in p_i and p_a. If p_i equals p_a (as might be the case in very low light), then there is no fractionation associated with diffusion of CO_2 into the stomata or cell because there is no CO_2 pressure gradient. The first part of equation 7.4 equals 0 ($p_a - p_i = 0$) and only the fractionation associated with discrimination during intake of carbon by carboxylation. The second part of equation 7.4 reaches its largest possible value (when $p_i/p_a = 1$) which is really quite intuitive. If there is lots of CO_2 in the cell, then the carboxylation step can easily discriminate in favor of the light isotope. Under these conditions the $\Delta^{13}C_{(CO_2 \text{ in air - plant})}$ reaches a maximum value of 29‰.

At the other extreme consider what happens when a plant is water stressed. The stomata close to minimize water loss, so that there is a large difference in p_i and p_a. Only a very small amount of CO_2 is admitted into the plant, and that which does make it into the cell is completely consumed in the carboxylation step. As p_i approaches 0, then the first part of equation 7.4 approaches a value of 4.4‰ and the second part (discrimination

[5] The Holocene, pre-industrial value was –6.5‰. The modern value is -8.5‰.

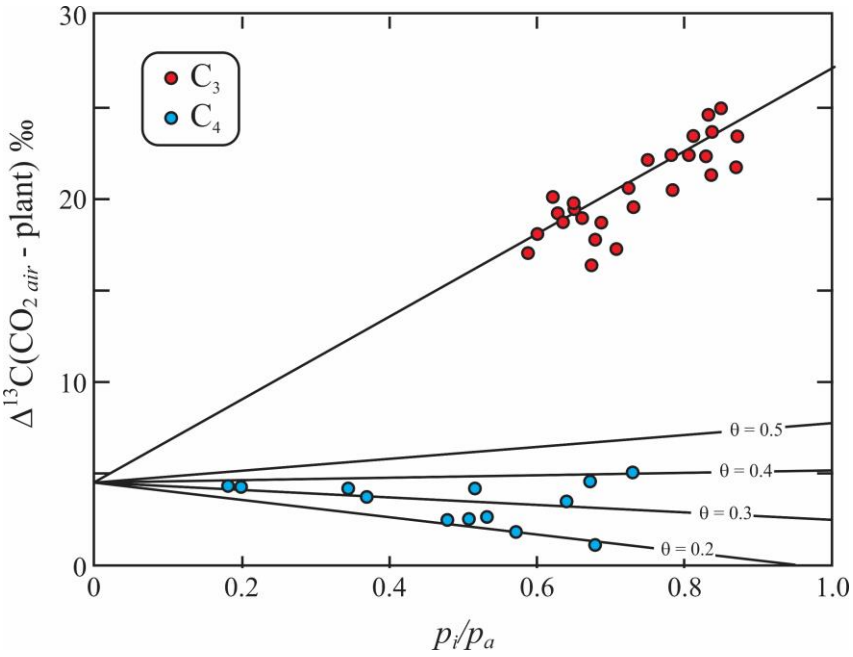

Fig. 7.4. Variation in isotopic composition of C_3 and C_4 plants as a function of p_i/p_a ratio. Curves are drawn based on equations 7.4 and 7.5 with a = 4.4, $b = b_3$ = 27, b_4 = -5.7, and varying θ. The insensitivity of C_4 plants to changing $p(CO_2)$ indicates that $a \cong b_4 + b_3\theta$. After (Farquhar et al., 1988).

unique to C_4 plants). θ is the fraction of carbon fixed by PEP carboxylation that ultimately leaks out of the bundle sheath cells, and contributes to the discrimination at Rubsico. If θ = 0, all carbon fixed by PEP carboxylation is refixed by Rubisco, so that the Rubisco discrimination ($b_3\theta$) equals zero. Typical values of p_i in C_4 plants are in the range of 0.3 to 0.4, and θ = 0.3, giving an Δ value of 4‰, or a $\delta^{13}C$ value of -11.9‰ for the plant, in good agreement with measured values. Note that when $b_4 + b_3\theta = a$, $\Delta = a$ and is independent of $p(CO_2)$, as has been observed in experimental studies (Fig. 7.4).

The sensitivity of C_3 plants to $p(CO_2)$ has led researchers to propose using $\delta^{13}C$ of plants as a proxy for $p(CO_2)$ variations in the recent past (e.g., Marino and McElroy, 1991; Feng and Epstein, 1995). Similarly, $\delta^{13}C$ values of marine phytoplankton have been used to estimate paleo- $p(CO_2)$ levels (Popp et al., 1989; Freeman and Hayes, 1992).

Local carbon isotope variations occur in dense forest canopies, where plants preferentially *incorporate* ^{12}C, whereas decay of leaf litter re-releases the ^{12}C enriched CO_2 . The net 'canopy effect' causes biomass formed close to the forest floor to have $\delta^{13}C$ values that are approximately 5‰ less than at the canopy top (Cerling et al., 2004).

7.3.3 Organic carbon in sediments

Soil and sedimentary organic carbon reflects the biogenic source. This is clearly evident when considering that coal and disseminated kerogen (*i.e.*, the insoluble organic matter in sediments) have $\delta^{13}C$ values that overlap the range defined by pre-industrial C_3 plants. Soils in sugar cane fields have $\delta^{13}C$ values that are consistent with a C_4 plant community. The isotopic range of most petroleum deposits is -30 to -27‰ compared to coal (-26 to -23‰); the difference is consistent with petroleum having a marine sediment

origin (Deines, 1980). Keep in mind that modern marine and terrestrial biomass have distinct isotopic ranges.

There are only minor isotopic shifts associated with preferential oxidation of different components of organic matter. The $\delta^{13}C$ value of soil CO_2 generally matches that of the soil organic matter, indicating little isotopic fractionation during decay. Increasing diagenesis (and catagenesis at higher temperatures) leads to the loss of CO_2, H_2O, and CH_4. H/C ratios decrease with increasing thermal maturity[6] until a value of zero is reached for graphite, the ultimate product of metamorphism. Inorganic thermal breakdown of the macromolecular carbon skeleton of kerogens favors the breaking of slightly weaker ^{12}C-^{12}C bonds, thereby liberating ^{13}C-depleted smaller molecules (*e.g.*, methane and CO_2), such that ^{13}C is slightly concentrated in the residual kerogen.

C/N ratios can be used to distinguish algal and land-plant origins of organic matter. The lower C/N ratios in aqueous plants are related to the absence of cellulose and lignin, in contrast to land plants where lignocellulosic structural biopolymers are needed to fight the effects of gravity. In combination with $\delta^{13}C$ values, different sources for organic matter in lake sediments can be unambiguously identified (Fig. 7.5).

The power of using C/N ratios and $\delta^{13}C$ values in lake sediments to determine origin is illustrated in a core from Lake Baikal, southern Siberia. Lake Baikal is extremely deep, and has a record of over 9000 years of continuous sedimentation. Sediment type, C/N ratios and $\delta^{13}C$ values all change dramatically at ~6.8 thousands years before present (Fig. 7.6). The low C/N ratios in the younger sediments and $\delta^{13}C$ values averaging -28‰ indicate a very high component of lacustrine algae with a minor vascular plant material component. Older sediments have a much larger land plant component, indicating lower productivity in the lake. The higher $\delta^{13}C$ values suggest a significant C_4 component (Qui et al., 1993).

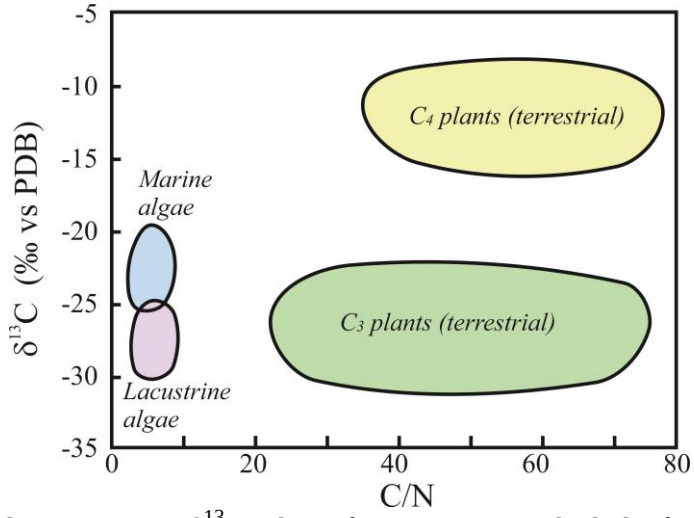

Fig. 7.5 Combined C/N ratios vs. $\delta^{13}C$ values of organic matter. The lack of cellulose in aquatic plants and algae lead to much lower C/N ratios than for terrestrial plants. Minor diagenesis will not appreciably affect either C/N or isotope ratios, so that detrital material can be traced in sediments. After (Meyers, 1994).

[6] In a straight chain n-alkane hydrocarbon molecule, the H/C ratio is 2 + 2/C. In the extreme case of graphite, the H/C ratio is 0.

The use of organic carbon in sedimentary sequences for chemostratigraphic reconstruction is complicated by the wide range of source material and preferential breakdown of certain components. One way of isolating unique organic components is with compound-specific gas chromatography techniques. Hayes *et al.* (1989) found that by analyzing only the geoporphyrin fraction, they were able to discriminate primary carbon of marine photosynthetic origin from that derived from non-photosynthetic sources. The geoporphyrin fractions were consistently depleted in ^{13}C relative to total organic carbon by up to 7‰, and provided far more information than bulk organic carbon alone. Additional works have shown that the organic carbon (as well as biogenic carbonates) could be used to evaluate differences in productivity in the past (e.g., Popp et al., 1989).

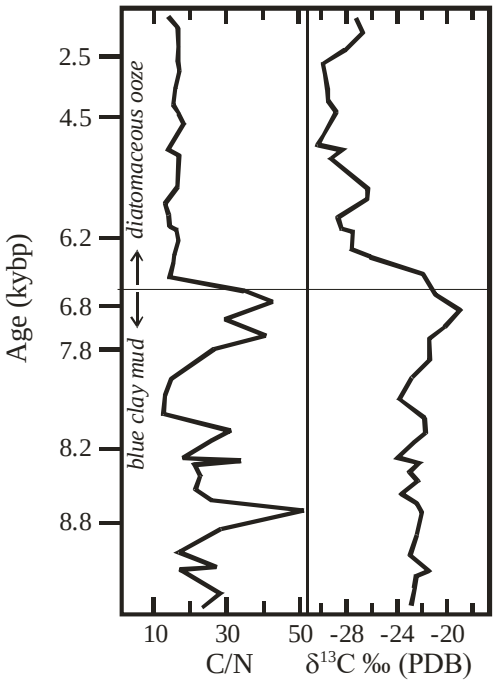

Fig. 7.6. Variations in C/N ratio and $\delta^{13}C$ value in a sediment column from the northern basin of Lake Baikal in southern Siberia. The change in sediment type ~6.5 thousand years ago is due to a reduction in glacial flour contribution and more *in situ* algal production. After Qui *et al.* (1993).

The $\delta^{13}C$ value of POC (particulate organic carbon) transferred by rivers is determined by its source. Values for C_3-based catchments are in the range of -25 to -30‰ (Sackett and Thompson, 1963; Strain and Tan, 1979; Spiker, 1981). POC derived from a high percentage of C_4 plants obviously has a higher value than that derived from a mainly C_3 source.

The $\delta^{13}C$ values of TDC (total dissolved carbon) as opposed to particulate organic matter may also have significant contributions from dissolved carbonate rocks, in addition to oxidation of organic material. Rivers draining carbonate-poor catchments typically have $\delta^{13}C$ values around -20‰, while carbonate-rich drainages have $\delta^{13}C$ values closer to -10 to -11‰. Under cool conditions, less organic matter is oxidized, and the $\delta^{13}C$ value of river waters reflects a larger contribution of dissolved carbonate. Estimated average global TDC values range from -6 to -9‰ (Anderson and Arthur, 1983) to ~-5‰ (Kump, 1991), a number that is used in considering the global carbon cycle (section 7.4).

7.3.4 Methane

The $\delta^{13}C$ values of methane are invariably far lower than their source (Rosenfeld and Silverman, 1959). Depending on the mechanism of methane formation, $\delta^{13}C$ values of methane can be as low as -100‰ (Fig. 7.7) and form organic matter via methanotrophic organisms with similarly low $\delta^{13}C$ values (Kaplan and Nissenbaum, 1966). Oxidation of light methane generates CO_2 and ultimately carbonates with anomalously low $\delta^{13}C$ values (Irwin et al., 1977). In freshwater systems, CH_4 is formed by acetate fermentation (*e.g.*, $CH_3COOH \rightarrow CH_4 + CO_2$) where the carbon in methane is derived from the methyl group of acetate. In saline environments, methane is produced by reduction of CO_2 (*e.g.* $CO_2 + 8(H) \rightarrow CH_4 + 2H_2O$. In the first case, carbon isotope

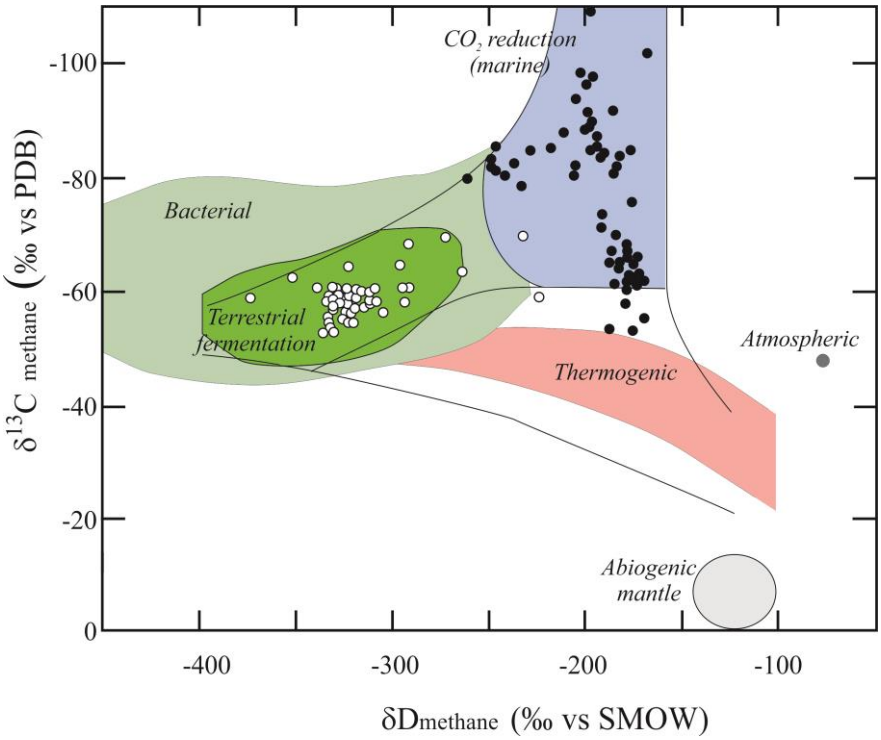

Fig. 7.7. Combined carbon-hydrogen isotope plot of methane. By use of combined carbon and hydrogen isotope ratios, formation from terrestrial fermentation, marine CO_2 reduction and thermal cracking can easily be distinguished. After Whiticar *et al.* (1986).

fractionation between acetate and newly-formed CH_4 is small. In contrast, there is a large fractionation between CO_2 and methane evolved during CO_2 reduction, so that methane formed by this mechanism has much lower $\delta^{13}C$ values (Whiticar et al., 1986; Whiticar, 1999). Fig. 7.7 shows the profound differences in the δD values of methane produced by different mechanisms. Bacterial fermentation can produce δD values lower than -400°C.

7.3.5 Atmospheric CO_2

The average global $\delta^{13}C$ value of CO_2 in the atmosphere has changed from -6.7‰ in 1956 to –7.9‰ in 1982 (Keeling et al., 1979), to less than -8.3‰ today as a result of fossil fuel burning. (The change is commonly referred to as the *Suess Effect*, although this term originally was used in the context of changing $\Delta^{14}C$ values due to the burning of 'dead' ^{14}C fossil fuels). Variations in the $\delta^{13}C$ values of the atmospheric CO_2 before Keeling's work at Mona Loa have been measured using C_4 plants[7] (Drake et al., 2016) and particularly ice cores (Fig. 7.8). Ancient variations in atmospheric $\delta^{13}C$ are more difficult to determine, but can be estimated from marine carbonates. The global atmospheric $\delta^{13}C$ value is related to the overall global carbon cycle, where different sources and sinks and their respective fluxes will lead to a quasi steady-state system (Affek and Yakir, 2014).

There are also variations associated with fossil fuel burning near large industrial-populated areas. Diurnal, seasonal and regional variations (N. Hemisphere vs. S.

[7] The $\delta^{13}C$ value of C_4 plants is relatively insensitive to $p(CO_2)$ as seen in Fig. 7.4.

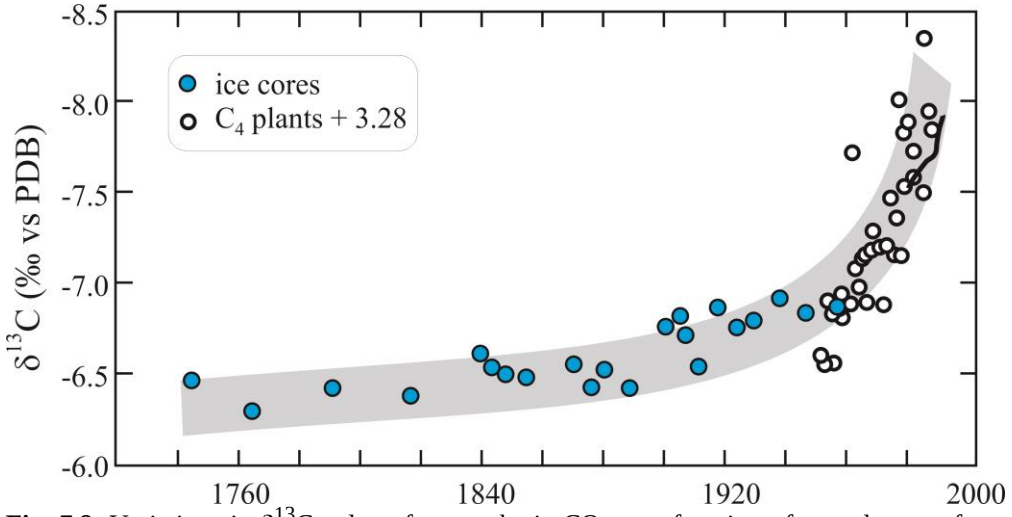

Fig. 7.8. Variations in $\delta^{13}C$ value of atmospheric CO_2 as a function of age. data are from direct measurements of atmospheric CO_2, measured $\delta^{13}C$ values of maize (a C_4 plant) and ice core air inclusions. After (Marino and McElroy, 1991).

Hemisphere) are also found to exist due to different natural sources and sinks of CO_2 (e.g., Ciais et al., 1995; Clark-Thorne and Yapp, 2003). The $\delta^{13}C$ value of atmospheric CO_2 changes by more than 1‰ on an annual timescale due to summer-winter changes in productivity. See Affek and Yakir (2014) for a detailed review.

7.4 $\delta^{13}C$ values of carbonates

7.4.1 Introduction

Most marine carbonates form in near-equilibrium with dissolved inorganic carbon, primarily HCO_3^-. Disequilibrium, related to *vital* effects (see section 7.4.3), can be corrected for, and with proper characterization, do not limit the information that is available from carbon isotope data from carbonates. The fractionation during carbonate precipitation is small and relatively insensitive to temperature (unlike the oxygen isotope fractionation), so that $\delta^{13}C$ values of ancient marine carbonates reflect the $\delta^{13}C$ value of dissolved inorganic carbon from which they formed. Locally, and on relatively short time scales, the $\delta^{13}C$ value of dissolved inorganic carbon will be related to productivity, ocean circulation, weathering, and other factors such as rapid input of exotic carbon sources. Over the 10-100 million year scale, the global $\delta^{13}C$ value of dissolved inorganic carbon varies in relation to the relative proportions of the two major carbon reservoirs, organic carbon and carbonate in the crust. And, because the residence time of dissolved inorganic carbon in the ocean is sufficiently long, major carbon isotope variations in marine sequences can be correlated over a wide geographic scale (Scholle and Arthur, 1980).

These ideas were, in part, formulated by Keith and Weber (1964) and Weber *et al.* (1965) 50 years ago. The use of carbon isotope geochemistry in reconstruction of paleoclimate is without doubt, one of the most important tools in the paleoclimatologist's modern arsenal.

7.4.2 General characterization of carbonates

A certain number of basic rules apply to carbonates.

1. The source of the carbon for marine limestones is dissolved bicarbonate, with a $\Delta^{13}C_{\text{carbonate-dissolved bicarbonate}}$ of 1 to 2‰. Average ocean TDC (predominantly HCO_3^-) for the bulk ocean has a $\delta^{13}C$ value of ~1‰ (Fig. 5.5). $\delta^{13}C$ values of TDC in the shallow oceans are higher than the overall ocean by about 1 to 2‰ due to the actions of the biological pump (Box 7.1).
2. The average $\delta^{18}O$ and $\delta^{13}C$ values of unaltered marine carbonates are close to 0‰ (on the PDB scale). The $\delta^{13}C$ value of carbonates in equilibrium with modern surface waters is 2-4‰. Lower values are related to vital effects and diagenesis. Deep water limestones have slightly positive $\delta^{18}O$ values because they form under cold conditions where the fractionation between carbonates and water is larger.
3. Terrestrial carbonates have low $\delta^{18}O$ values because they form in equilibrium with meteoric water. Tuffs and freshwater limestones incorporate a combination of dissolved inorganic carbon and atmospheric CO_2. If the dissolved inorganic carbon comes from the dissolution of marine carbonates, $\delta^{13}C$ value will be near zero. In contrast, dissolved inorganic carbon sourced by oxidation of organic matter will lead to strongly negative $\delta^{13}C$ values of precipitating carbonates. In general, freshwater limestones have negative $\delta^{13}C$ values, depending on the contribution from organic carbon.
4. The $\delta^{13}C$ value of soil carbonates is controlled by CO_2 respired from soil biota, as well as from decaying organic litter and soil organic carbon, so that the $\delta^{13}C$ values of soil carbonates (paleosols) are an indicator of the type of plant (C_3 vs. C_4) living at the time of carbonate formation. Soils formed in the presence of C_4 plants have $\delta^{13}C$ values 12 to 13‰ higher than those formed in predominantly C_3 plant communities (see section 7.5). The $\delta^{18}O$ value is a function of local meteoric water, with minor secondary evaporation effects.
5. Diagenesis almost always lowers the $\delta^{18}O$ values of marine carbonates (O'Neil, 1987). $\delta^{13}C$ values also tend to become lower during diagenesis as well, but the effect is often far less pronounced. This is a logical outcome of the fact that most diagenetic aqueous fluids contain only trace amounts of dissolved carbon (see Fig. 6.8). Much larger fluid/rock ratios are needed to alter the $\delta^{13}C$ than $\delta^{18}O$ value. In rare cases, $\delta^{13}C$ values of diagenetically altered marine carbonates will increase by reaction with residual CO_2 following methanogensis (removal of light carbon).

7.4.3 The vital effect

Certain organisms consistently deposit their carbonate shells out of carbon and/or oxygen isotope equilibrium with ambient fluids, the so-called vital effect. Vital effects have been explained by either metabolic processes or by a combination of *metabolic* and *kinetic processes* (McConnaughey, 1989a, b). Stable isotope relations observed in biogenic

Box 7.1. The biological pump. There is a steady-state, non-equilibrium carbon isotope fractionation between TDC in the shallow and deep ocean due to high biological activity in the near-surface photic zone of the ocean. Photosynthesizing organisms incorporate carbon and nutrients during their growth in the shallow ocean. In doing so, they preferentially incorporate ^{12}C in their tissues, causing a ^{13}C enrichment in the remaining TDC of the shallow ocean. Upon their death, the remains of organisms sink into the deep ocean where they are oxidized, releasing light carbon back to the ocean. The continuous removal of light carbon from the shallow ocean in essence acts as a CO_2 pump, transferring light carbon from shallow to deep levels in the ocean, and causing a 1 to 2‰ fractionation between the two ocean reservoirs. In times of reduced productivity, the intensity of the biological pump decreases, and the shallow oceans will reequilibrate with the larger deep ocean TDC reservoir. The transfer of carbonates from the shallow to deep ocean has a negligible effect because the $\delta^{13}C$ value of carbonates differ only slightly from that of TDC.

carbonates have fascinated isotope geochemists and biologists alike since the inception of the discipline. With appropriate caveats, it is reasonable to state that biogenic carbonate is commonly deposited in or near oxygen isotope equilibrium with ambient waters. And, when disequilibrium is the rule for a given organism, the departure from equilibrium is often fairly constant and the temperature sensitivity of the disequilibrium fractionation is nearly the same as that of equilibrium fractionations. Thus relative temperatures can often be determined with a good degree of confidence in these cases. Facts like these explain in part the success of the oxygen isotope paleotemperature method (Watkins et al., 2013).

In stark contrast to the oxygen isotope case, biogenic carbonate is rarely deposited in carbon isotope equilibrium with dissolved carbon in environmental waters. In addition, the overall magnitude of carbon isotope disequilibrium is greater than for oxygen because the carbon reservoir (HCO_3^-) in these systems is vastly smaller than the oxygen reservoir (H_2O). In all but a few cases, the direction of disequilibrium is such that ^{12}C is preferentially incorporated into the shells so that $\delta^{13}C$ values are more negative than equilibrium values. Departures from equilibrium precipitation are shown for many extant organisms in Figure 7.9.

Several basic rules apply. Slowly precipitating carbonates are most likely to be in equilibrium. There are many shells that *appear* to precipitate carbonates in equilibrium with water, but others that are lighter than equilibrium values by 4 and 14‰ for oxygen and carbon isotope ratios, respectively. Photosynthesis has no apparent effect on the $\delta^{18}O$ value of newly-forming carbonate material, but can lead to *higher* $\delta^{13}C$ values because organic matter formed during photosynthesis preferentially incorporates ^{12}C, leaving the inorganic carbon reservoir with higher $\delta^{13}C$ values.

The *kinetic* aspect of vital effects concerns the relative rates of both diffusion and chemical reactions of different isotopologues of dissolved carbonate species in the body fluids. Light isotopologues (both carbon and oxygen isotopes) diffuse faster than heavy isotopologues and react with other substances faster. As a consequence, $\delta^{18}O$ and $\delta^{13}C$ values of biogenic carbonate secreted *rapidly* with a kinetic isotope effect (1) are more negative than equilibrium values and (2) covary (Fig. 7.10). The word rapidly is emphasized because organisms whose isotopic ratios reflect a kinetic process must

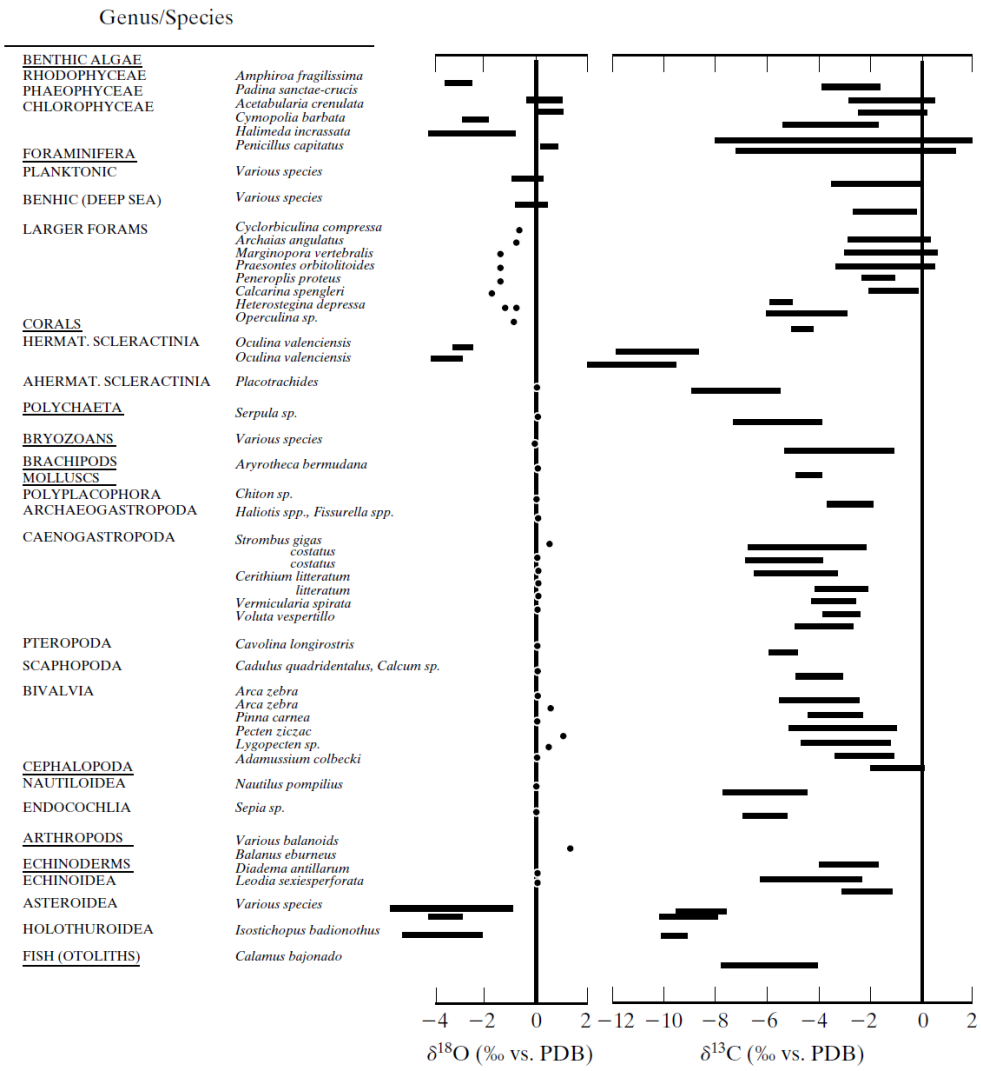

Fig. 7.9. Summary of differences between equilibrium and measured and values for various carbonate-secreting organisms. (Reprinted from Wefer and Berger, 1991, with permission from Elsevier.)

precipitate their carbonate almost immediately after some key reaction because the normally rapid oxygen isotope exchange between HCO_3^- and H_2O has not taken place. Information like this is helpful to marine biologists and biochemists attempting to understand physical and chemical controls on skeletogenesis in a variety of species. The difference between $\delta^{18}O/\delta^{13}C$ relations governed by both kinetic and metabolic effects and kinetic effects alone are shown nicely for two species of coral in Figure 7.10.

Metabolic processes have little effect on oxygen isotope ratios, but they can have a strong effect on carbon isotope ratios of dissolved inorganic carbon (DIC) in the internal pool of body fluids that are used for calcification. The processes of interest cause *removal* of light CO_2 from this pool during photosynthesis and *addition* of light CO_2 to the pool from respired CO_2. Photosynthetic organisms like algae preferentially use isotopically light $(CO_2)_{aq}$ to synthesize organic matter in soft tissues thereby leaving behind isotopically heavy carbon in the internal DIC pool. Thus if photosynthesis is a viable

control on $^{13}C/^{12}C$ ratios in these systems, $\delta^{13}C$ values of skeletal parts of photosynthetic organisms should be more positive than those of non-photosynthetic organisms living in similar environments. In fact $\delta^{13}C$ values of shells of hermatypic corals (those containing symbiont zooxanthellae) are usually higher than those of ahermatypic corals. In addition, the higher the rate of photosynthesis or growth rate (*e.g*. at higher illumination), the higher are the $\delta^{13}C$ values of certain corals. But just the reverse effect has been noted for large foraminifera in natural settings – the greater the growth rate, the lower the $\delta^{13}C$ if shell carbonate. The effects are clearly complicated.

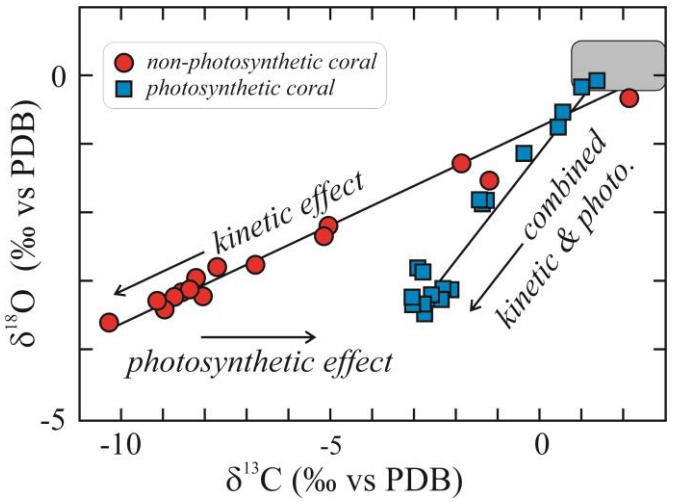

Figure 7.10. Stable isotope data for the photosynthetic coral *Pavona clavus* (squares) and the non-photosynthetic coral *Tubastrea* sp (circles). The covariation of $\delta^{18}O$ and $\delta^{13}C$ values for the ahermatypic coral is the normal *kinetic* relation. The departure to higher $\delta^{13}C$ values for the photosynthesizing coral is explained by the metabolic relation arising from preferential incorporation of ^{12}C during photosynthesis, causing an elevation of the $\delta^{13}C$ values of remaining inorganic carbon. After McConnaughey (1989b).

Respired CO_2 has lower $\delta^{13}C$ values than that of ambient DIC and can become a constituent of the internal carbon pool in some organisms. For example, Lee and Carpenter (2001) provided good evidence that carbon from respired CO_2 is incorporated into biogenic carbonate by certain taxa of marine calcareous algae. When metabolic factors dominate the vital effect of a population of organisms, $\delta^{13}C$ values can vary widely while $\delta^{18}O$ values remain relatively constant[8].

7.4.4 Carbonate speciation effects

In addition to vital effects related to kinetic and metabolic effects, isotope fractionations can be controlled by *speciation* effects. Through laboratory culturing experiments, Spero *et al.* (1997) showed that pH dependent variations in carbonate speciation in seawater can bear significantly on carbon and oxygen isotope ratios of shells secreted by certain foraminifera and presumably, other organisms as well. With increasing pH and concomitant increase in $[CO_3^{2-}]$[9], both $\delta^{18}O$ and $\delta^{13}C$ values steadily decrease below values predicted by equilibrium relations. The magnitude of the effect is sufficient to lower $\delta^{18}O$ and $\delta^{13}C$ values of *O. universa* shells by 0.2 and 0.6‰, respectively, with an increase of only 0.2 pH units.

[8] CO_2 and H_2O are usually in approximate oxygen isotope equilibrium in body fluids due to the presence of the carbonic anhydrase enzyme which catalyzes the exchange reaction.

[9] $[CO_3^{2-}]$ increases almost linearly with pH from a normal seawater pH value of 8.0 to a value of 8.6.

Zeebe (1999) explained these effects for oxygen by considering equilibrium oxygen isotope fractionation factors between the various species involved in carbonate precipitation. The oxygen isotope fractionation between HCO_3^- and CO_3^{2-} is an astonishingly high 16‰[10]. With increase in pH, the CO_3^{2-}/HCO_3^- ratio increases such that, if the carbonate species are taken up by the organism in proportion to their relative abundance, the slope of the $\delta^{18}O$-$[CO_3^{2-}]$ theoretical relation is –0.0024, a value that is indistinguishable from the value of –0.0022 observed in the laboratory for *O. universa*.

The speciation effect becomes particularly important when oxygen isotope analyses of foraminifera are used to reconstruct seawater temperatures during glacial periods. Several lines of evidence indicate that glacial oceans were more alkaline than modern oceans. If $p(CO_2)$ of the atmosphere was significantly lower in peak glacial times than during interglacial periods, as chemical analyses of inclusions in ice cores would suggest, the concentration of CO_3^{2-} might have increased enough to induce significant lowering of $\delta^{18}O$ of shell carbonate that could be incorrectly attributed to an increase in ocean temperature.

7.4.5 Controls on the $\delta^{13}C$ value of marine carbonates over long time scales

In spite of the complicating vital effects discussed above, to a first approximation, the $\delta^{13}C$ values of precipitating marine carbonates are determined by the value of total dissolved inorganic carbon (TDC, mainly HCO_3^-). The average $\delta^{13}C_{TDC}$ of whole-ocean is 0-1‰. The calcite-bicarbonate carbon isotope fractionation is small and relatively insensitive to temperature (Fig. 7.11), so that measured $\delta^{13}C$ values of marine carbonates directly reflect the $\delta^{13}C$ value of TDC. The near-surface TDC has a $\delta^{13}C$ value that is 1 to 2‰ higher than the overall ocean due to the effects of the biological pump (box 7.1). The positive $\delta^{13}C$ values of the near-surface water about 9‰ higher than atmospheric CO_2, in excellent agreement with estimates for equilibrium fractionation between the two reservoirs (Mook et al., 1974).

It is worthwhile to consider how all of the surface reservoirs interact. If we accept a +1‰ for the $\delta^{13}C$ value of the deep ocean (Fig. 5.5) then the shallow ocean is 1 to 2 ‰ heavier than this, assuming that the biological pump is active. That puts the shallow ocean at 2-3‰. Carbonates precipitating in the shallow ocean will be still higher, reaching $\delta^{13}C$ values as high as 4‰. From Fig. 7.11, we see that atmospheric CO_2 should be about 9‰ lighter than the dissolved shallow water bicarbonate, or -6 to -7‰, in excellent agreement with the pre-anthropogenic $\delta^{13}C$ value of the atmosphere as measured in glacial ice. Finally, we

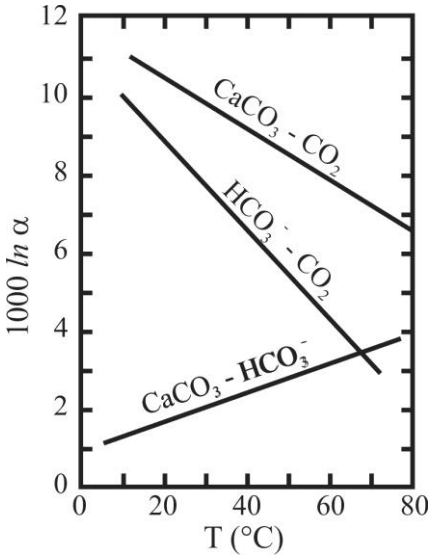

Fig 7.11. Carbon isotope fractionation curves for calcite, bicarbonate and CO_2 gas. Data from Emrich *et al.* (1970).

[10] There is a also a large oxygen isotope fractionation of about 8 per mil between the analogous $H_2PO_4^-$ and PO_4^{3-}. Large fractionations between such similar species are not well understood.

consider plants. The average $\delta^{13}C$ value of C_3 plants is -26 ‰, suggesting a $\Delta^{13}C_{CO2\text{-}C3\ plants}$ value of 20‰. From equation 7.4, a fractionation of 20‰ is achieved when $p_i = 0.65\ p_a$, in agreement with measured data. Not surprising then, all of the shallow carbon reservoirs are in near equilibrium or in a condition of steady-state disequilibrium (deep and shallow ocean). So it might seem worthwhile to ask which reservoirs control the $\delta^{13}C$ value of the whole system. The answer is that it depends very much on the timescale that one is considering. On the sub-annual time scale, the $\delta^{13}C$ value of the atmosphere will change due to different seasonal rates of photosynthesis and oxidation of organic matter. On a yearly to decadal timescale, the atmosphere will be controlled by exchange with the shallow ocean and plants. On a longer timescale, the activity of the biological pump will control the fractionation between the shallow and deep ocean, which in turn would affect the $\delta^{13}C$ value of the plant communities. And on a still longer timescale, the overall $\delta^{13}C$ value of the near surface system will be dictated by the proportions of carbon delivered to the oceans by the large organic and inorganic carbon reservoirs (Fig. 7.1).

Fig. 7.12 is a secular curve of the $\delta^{13}C$ value of marine carbonates on a million year time scale. The $\delta^{13}C$ value of precipitating carbonates is controlled by the value of the total dissolved carbon in the ocean and the TDC composition is related to proportions of inorganic and organic carbon by equation 7.2. Variations in Fig. 7.12 are related to tectonic activity, particularly erosion and/or deposition of organic-rich material and changing degrees of productivity. Note that formation or dissolution of carbonates will not affect the $\delta^{13}C$ value of TDC because the carbon isotope composition of the two reservoirs are almost the same. During the Carboniferous period when extremely high amounts of organic carbon were buried, the $\delta^{13}C$ values of inorganic carbon and TDC of the oceans reached their highest level in the Phanerozoic, and this is reflected in the carbonate record, where $\delta^{13}C$ values of carbonates reach over +4‰.

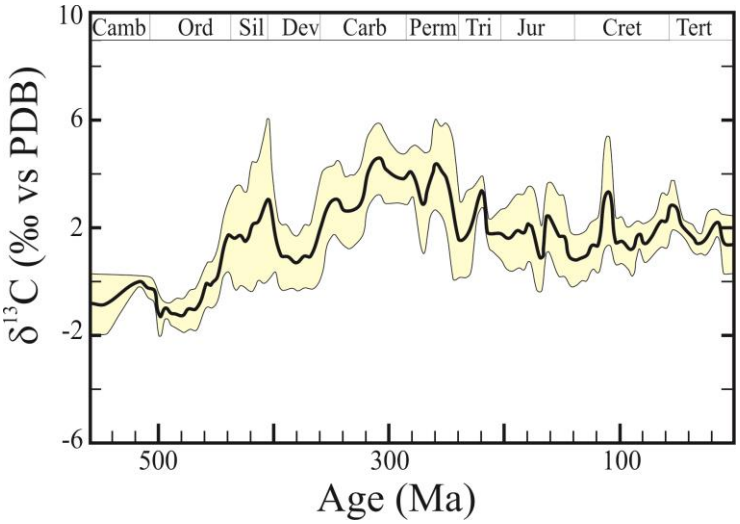

Fig. 7.12. Secular variations of $\delta^{13}C$ variations in marine carbonates. Data from low magnesium carbonate shells. The shaded area is 1σ uncertainty for a Gaussian distribution. After Veizer *et al.* (1999).

Because reduction of inorganic carbon releases oxygen, the $p(O_2)$ of the atmosphere is closely tied to the amount of carbon in the reduced form[11]. Photosynthetic reduction of CO_2 releases O_2, thereby raising the $p(O_2)$ of the atmosphere (Berner, 1987).

[11] Oxygen stored in sulfate can be re-released as O_2 during sulfate reduction. Removal of organic carbon by subduction also acts to shift the balance between $\delta^{13}C$ value and $p(O_2)$.

Accordingly, we see a close relationship between the long term $\delta^{13}C$ value of marine carbonates and atmospheric $p(O_2)$ (Fig. 7.13).

The most extreme ceabon isotope variations are found in Proterozoic carbonates (Fig. 7.14). Carbon isotope values in marine carbonates range from less than -4‰ to over 10‰. Changes in the Archean are related to increased biological fractionation as a result of methanotrophic[12] recycling (Krissansen-Totton et al., 2015). Large excursions in the Proterozoic have been explained in terms of large transfers of carbon between the inorganic and organic reservoirs, and concomitant fluctuations in atmospheric $p(O_2)$ (Des Marais, 2001). It is almost certain that the long-term deviations from isotopic steady-state conditions were caused by radical global changes in (i) the ability of biota to reduce vast amounts of carbon and (ii) Earth's dynamic processes that can temporarily shield reduced organic carbon from re-oxidation. Note that the global $\delta^{13}C$ values of organic carbon change far more than that of carbonates, due to their different reservoir sizes.

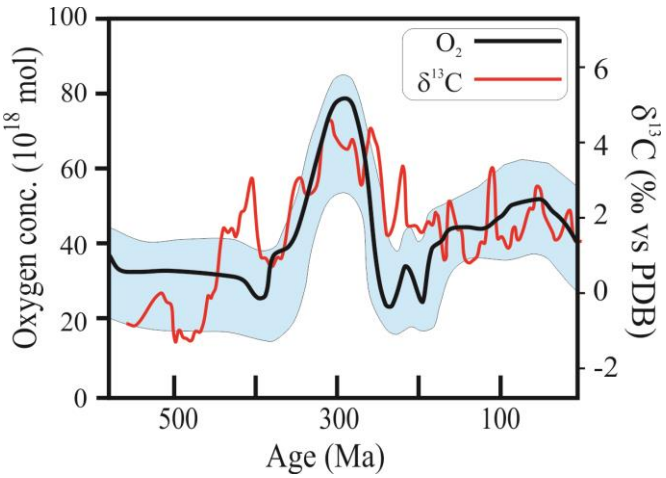

Fig. 7.13. Correlation between the oxygen concentration of the atmosphere and $\delta^{13}C$ value of marine carbonates. Curves from Berner and Canfield (1989) and Veizer *et al.* (1999).

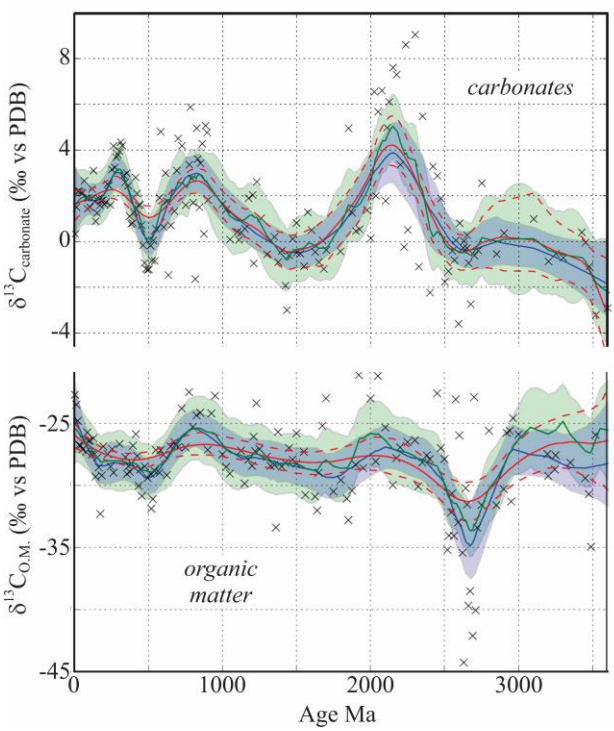

Fig. 7.14. Carbon isotope trends in Precambrian carbonates (upper) and organic matter (OM) (lower). Note the different scales. There is statistically significant increase in difference between $\delta^{13}C_{carb}$ and $\delta^{13}C_{OM}$ between early and late Archean. Modified from Krissansen-Totton *et al.* (2015). Used with permission from the American Journal of Science

7.4.6 Variations in the $\delta^{13}C$ values of marine carbonates at short time scales

Short term 'spikes' in $\delta^{13}C$ values of carbonates are related to catastrophic changes in ocean productivity or inputs of light

[12] Methanotrophs are prokaryotes that metabolize methane.

carbon. Over 60 such worldwide events have been recognized (Holser et al., 1996). We must be sure to clearly distinguish between a local and worldwide event. Isolated shallow marine basins can locally exhibit sharp carbon isotope excursions due to local geographic effects, such as changing circulation, overturn, changes in access to the open ocean etc. These do not have global significance. Because the residence time of TDC is long (1.8 ka and 55 ka for the shallow and deep oceans, respectively), complete homogenization on the worldwide scale should occur if an event affects the entire planet. To be sure that a carbon isotope excursion is truly of global significance, the event must be identified in geographically distinct carbonate sections throughout the world.

There are several mechanisms that can cause rapid global-wide changes to the $\delta^{13}C$ value of TDC. The first of these is a sudden loss of productivity due to a catastrophic event, such as the large impact at the K/T boundary, intense volcanic activity or rapid change in oceanic circulation. The sudden loss of productivity has been termed the 'Strangelove Ocean' (Hsü and McKenzie, 1985), after the Stanley Kubrick classic film Dr. Strangelove. Loss of productivity shuts down the biological pump, and the shallow ocean quickly equilibrates with the deep ocean on a 100 year time scale (Fig. 7.15). The shallow ocean thus acquires the $\delta^{13}C$ values of the much larger deep ocean reservoir. Recovery and restart of the biological pump occurs on much longer time scales, ranging from 0.5 to 1 Ma depending on the rapidity with which biological productivity once again resumes. The Cretaceous-Tertiary boundary is the classic example of perturbation of the biological pump, where all of the features expected by catastrophic productivity loss are observed (Zachos and Arthur, 1986). Certainly one of the best-refined examples of a global carbon isotope shift is that which occurs at the Paleocene/Eocene boundary (Fig. 7.16). Kennett and Stott (1991) recognized that there was a marked decrease in the $\delta^{13}C$ values for *both* shallow and deep water foraminifera

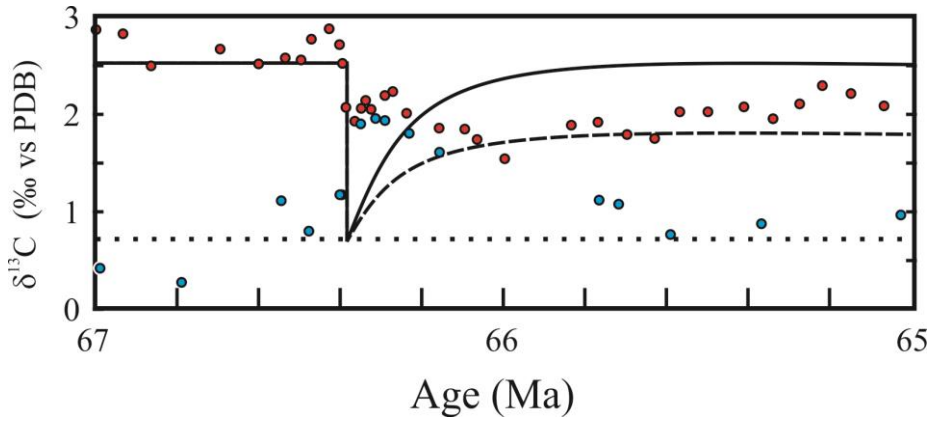

Fig 7.15. Variations in the $\delta^{13}C$ value of shallow-water foraminifera– red (*P. petaloidea*) and deep-water foraminifera– blue (*R. rotundata*) across the K/T boundary. Convergence of the shallow- and deep-water foraminifera data indicate a loss of productivity and shut-down of the biological pump. Lines show theoretical changes in carbonate $\delta^{13}C$ values across a catastrophic extinction boundary. Solid line = shallow-level carbonate trend with return to full recovery; dashed line, same with organic burial rate = 0.9 of the pre-event value; dotted line is the predicted deep-water carbonates. See (Zachos et al., 1989; Kump, 1991).

that occurred in just a few thousand years. This is a marked difference to the observations of K/T boundary sections. In the K/T sections, the $\delta^{13}C$ values of shallow and heavy carbon converge to a common value. The shifts can be explained in terms of reduction in productivity and shutting down the biological pump. In the case of the Paleocene/Eocene boundary sections, there is a lowering of *both* planktic and benthic foraminifera $\delta^{13}C$ values. These data cannot simply be explained by mixing of shallow and deep ocean. To explain Fig. 7.16 requires massive input of a ^{13}C-poor carbon source. Initial explanations for the isotopic anomaly at the Paleocene/Eocene were only partially satisfactory. Then in 1995, Dickens *et al.* (1995) proposed that dissociation of oceanic methane hydrate could explain both the low $\delta^{13}C$ values seen in Figure 7.16 as well as changes in the oxygen isotope ratios. Release of unstable methane hydrates (with $\delta^{13}C$ values averaging -65‰) related to changing ocean circulation patterns would cause a rapid lowering in the $\delta^{13}C$ values of the surface ocean and a more gradual change in the deep ocean as light CO_2 generated by the oxidation of methane was transferred through the thermocline. Similarly, the sharp decrease in $\delta^{18}O$ values in the planktic foraminifera data indicate a rapid warming of the surface ocean due to the increase in greenhouse gases, whereas the deep ocean took longer to respond.

As is so often the case, additional information – this time from boron isotope data – have led to a different interpretation for the Paleocene-Eocene boundary carbon excursion. Gutjahr *et al.* (2017) use boron isotopes as a proxy for shallow ocean pH and suggest that the Paleocene-Eocene excursion is more likely related to an enormous release of CO_2 during volcanism from the North Atlantic Igneous Province.

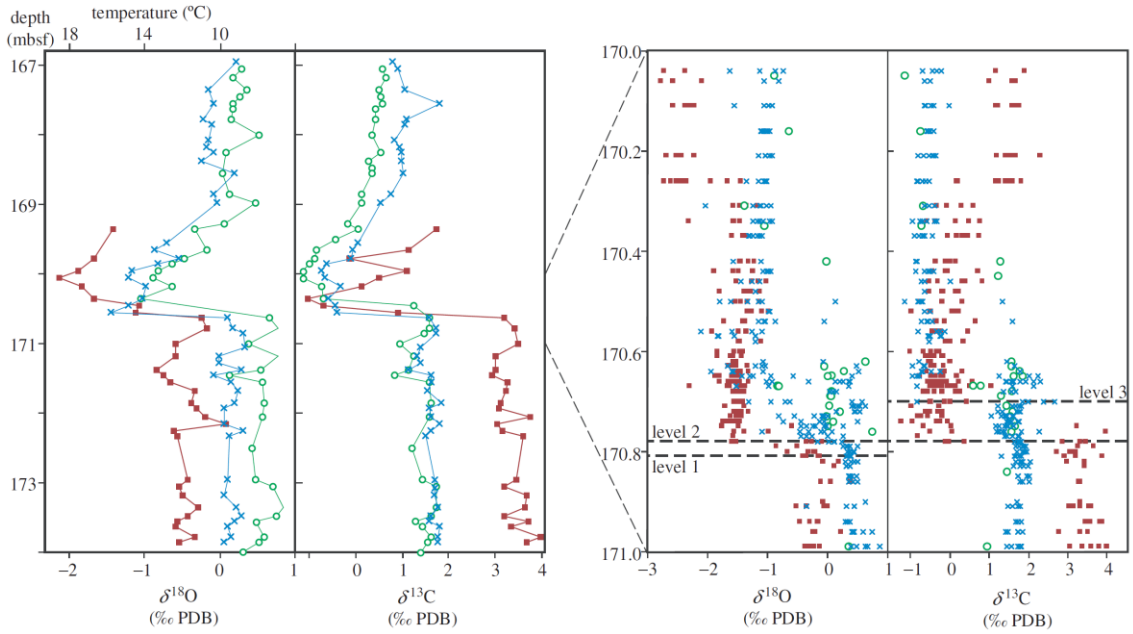

Fig. 7.16. $\delta^{13}C$ and $\delta^{18}O$ values of benthic and planktic foraminifera across the Paleocene-Eocene boundary. Changes in $\delta^{18}O$ values indicate a warming of 5-8°C over a few thousand years. The abrupt lowering of $\delta^{13}C$ values indicates a switching off of the biological pump and incorporation of light carbon, presumably from methane gas hydrates. Reprinted from Jenkyns (2003), with permission from the Royal Society of London.

7.5 $\delta^{13}C$ studies of terrestrial carbonates

Just about every type of carbonate precipitated on the land surface has been analyzed in order to extract climatological and paleoclimatalogical information (e.g., Swart et al., 1993). Studies aimed at elucidating information about modern conditions include the source of CO_2 for deposition of travertines (Turi, 1986), and information on rainfall and evaporation from oxygen isotope ratios of calcretes (Rossinsky and Swart, 1993). Breecker *et al.* (2009) identified a seasonal bias in the precipitation of soil carbonates on the basis of combined carbon and oxygen isotope ratios of soil CO_2. Chronological information can be obtained from speleothems (Schwarcz et al., 1976; Baskaran and Krishnamurthy, 1993), stromatolites (Casanova and Hillaire, 1993), ostracods, soil carbonates (Cerling and Quade, 1993), and varved lake deposits (McKenzie, 1985), just to name a few.

The $\delta^{13}C$ value of pedogenic carbonate is dominated by the vegetation isotopic signal, with significant differences due to varying proportions of C_3 and C_4 plants (Cerling and Quade, 1993). Soil carbonates, fossil tooth enamel and sediments in the Bengal Fan both show a remarkable increase of 10 to 12‰ between 7 and 5 Million years ago (Quade et al., 1989) that have been since recognized as a global feature (Cerling et

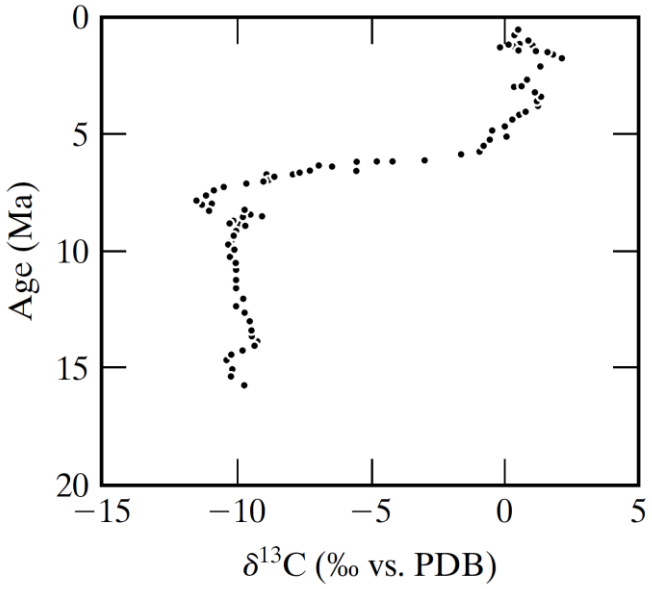

Fig. 7.17. Carbon isotope shift related to a global shift from a C_3 to C_4 dominated plant community. The increased success of C_4 plants beginning ~7 Ma is related to a decrease in the atmospheric $p(CO_2)$. Isotope data are from paleosol carbonates from Pakistan. Similar trends are found in North and South America from tooth enamel, demonstrating that the trend is global. From Cerling *et al.* (1993).

al., 1993; France-Lanord and Derry, 1994). The shift in the Bengal Fan sediments (Fig. 7.17) reflects the global expansion of C_4 biomass over a previously dominant C_3 plant community, due to a drop in atmospheric CO_2 levels. The cause of this global effect may be related to initiation of the Asian monsoon system.

7.5.1 Paleo-p(CO_2) estimates from soil carbonates

It has been demonstrated that the $\delta^{13}C$ value of soil carbonates is directly related to the partial pressure of CO_2 in the atmosphere (Cerling, 1991; Cerling, 1992). The concept is based on the idea that soil-derived CO_2 and atmospheric CO_2 have very different $\delta^{13}C$ values. The $\delta^{13}C$ value of the soil CO_2 close to the soil-air interface is strongly affected by the partial pressure of CO_2 in the atmosphere. Because soil carbonates precipitate in equilibrium with the ambient soil CO_2, their $\delta^{13}C$ values will be closely tied to the $p(CO_2)$ of the atmosphere. Fig. 7.18 shows the compilation of atmospheric $p(CO_2)$ over the Phanerozoic. What is striking is that while variations are large, the highest $p(CO_2)$ values over the last 400 million years are no higher than what is projected for the end of the century due to fossil fuel burning.

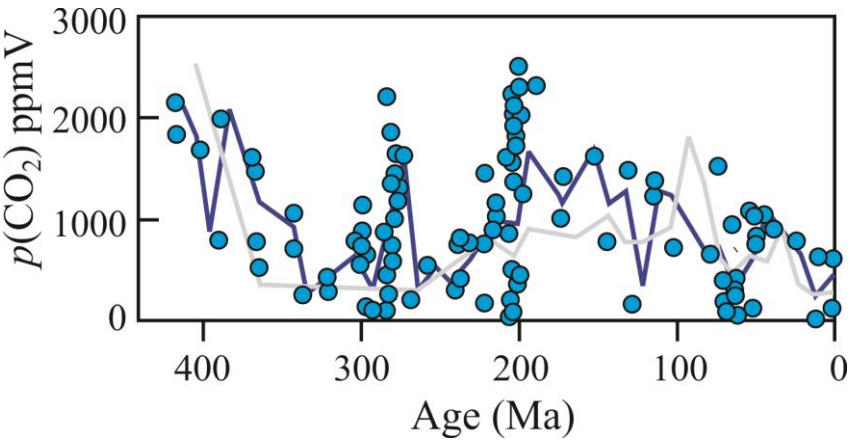

Fig. 7.18. Compilation of atmospheric $p(CO_2)$ estimates for the Phanerozoic based on the $\delta^{13}C$ values of soil carbonates. Blue line represents 10 Ma bin average. Also shown are average values based on other proxies (grey curve). The highest $p(CO_2)$ values over the last 400 million years are no greater than what is predicted from fossil fuel burning if left unchecked. Modified from Breecker *et al.* (2010).

References

Affek, H.P. and Yakir, D. (2014) The Stable Isotopic Composition of Atmospheric CO_2, in: Turekian, K.K. (Ed.), Treatise on Geochemistry. Elsevier, Oxford, pp. 179-212.

Anderson, T.F. and Arthur, M.A. (1983) Stable isotopes of oxygen and carbon and their application to sedimentologic and paleoenvironmental problems, in: Arthur, M.A., Anderson, T.F., Kaplan, I.R., Veizer, J., Land, L.S. (Eds.), Stable Isotopes in Sedimentary Geology. SEPM Short Course, Columbia, pp. 1-151.

Baskaran, M. and Krishnamurthy, R.V. (1993) Speleothems as proxy for the carbon isotope composition of atmospheric CO2. *Geophysical Research Letters* **20**, 2905-2908.

Bender, M.M. (1968) Mass spectrometric studies of carbon-13 variations in corn and other grasses. *Radiocarbon* **10**, 468-472.

Berner, R.A. (1987) Models for carbon and sulfur cycles and atmospheric oxygen; application to Paleozoic geologic history. *American Journal of Science* **287**, 177-196.

Berner, R.A. and Canfield, D.E. (1989) A new model for atmospheric oxygen over Phanerozoic time. *American Journal of Science* **289**, 333-361.

Breecker, D.O., Sharp, Z.D. and McFadden, L.D. (2009) Seasonal bias in the formation and stable isotopic composition of pedogenic carbonate in modern soils from central New Mexico, USA. *Geological Society of America Bulletin* **121**, 630-640.

Breecker, D.O., Sharp, Z.D. and McFadden, L.D. (2010) Atmospheric CO_2 concentrations during ancient greenhouse climates were similar to those predicted for AD 2100. *Proceedings of the National Academy of Sciences* **107**, 576-580.

Casanova, J. and Hillaire, M.-C. (1993) Carbon and oxygen isotopes in African lacustrine stromatolites; palaeohydrological interpretation, in: Swart, P.K., Lohmann, K.C., McKenzie, J.A., Savin, S. (Eds.), Climate Change in Continental Isotope Records. American Geophysical Union, Washington, D.C., pp. 123-133.

Cerling, T.E. (1991) Carbon dioxide in the atmosphere. *American Journal of Science* **291**, 377-400.

Cerling, T.E. (1992) Use of carbon isotopes in paleosols as an indicator of the carbon dioxide partial pressure of the paleoatmosphere. *Biological Abstracts Vol. 95, Iss. 3, Ref. 30880.* **6**, 307-314.

Cerling, T.E. and Quade, J. (1993) Stable carbon and oxygen isotopes in soil carbonates, in: Swart, P.K., Lohmann, K.C., McKenzie, J., Savin, S. (Eds.), Climate Change in Continental Isotopic Records. American Geophysical Union, Washington DC, pp. 217-231.

Cerling, T.E., Wang, Y. and Quade, J. (1993) Expansion of C_4 ecosystems as an indicator of global ecological change in the Late Miocene. *Nature* **361**, 344-345.

Cerling, T.E., Hart, J.A. and Hart, T.B. (2004) Stable isotope ecology in the Ituri forest. *Oecologia* **138**, 5-12.

Ciais, P., Tans, P.P., Trolier, M., White, J.W.C. and Francey, R.J. (1995) A large northern hemisphere terrestrial CO2 sink indicated by the 13C/12C ratio of atmospheric CO2. *Science* **269**, 1098-1101.

Clark-Thorne, S.T. and Yapp, C.J. (2003) Stable carbon isotope constraints on mixing and mass balance of CO_2 in an urban atmosphere: Dallas metropolitan area, Texas, USA. *Applied Geochemistry* **18**, 75-95.

Craig, H. (1954) Carbon 13 in plants and the relationships between carbon 13 and carbon 14 variations in nature. *The Journal of Geology* **62**, 115-149.

Degens, E.T., Guillard, R.R.L., Sackett, W.M. and Hellebust, J.A. (1968) Metabolic fractionation of carbon isotopes in marine plankton-- 1, Temperature and respiration experiments. *Deep Sea Research* **15**, 1-9.

Deines, P. (1980) The isotopic composition of reduced organic carbon, in: Fritz, P., Fontes, J.C. (Eds.), Handbook of environmental isotope geochemistry; Volume 1, The terrestrial environment, A. Elsevier, Amsterdam, pp. 329-406.

Deines, P. (2002) The carbon isotope geochemistry of mantle xenoliths. *Earth-Science Reviews* **58**, 247-278.

Des Marais, D.J. (2001) Isotopic evolution of the biogeochemical carbon cycle during the Precambrian, in: Valley, J.W., Cole, D.R. (Eds.), Stable Isotope Geochemistry, pp. 555-578.

Dickens, G.R., O'Neil, J.R., Rea, D.K. and Owen, R.M. (1995) Dissociation of oceanic methane hydrate as a cause of the carbon isotope excursion at the end of the Paleocene. *Paleoceanography* **10**, 965-971.

Drake, B.L., Hanson, D.T., Lowrey, T.K. and Sharp, Z.D. (2016) The carbon fertilization effect over a century of anthropogenic CO_2 emissions: higher intracellular CO2 and more drought resistance among invasive and native grass species contrasts with increased water use efficiency for woody plants in the US Southwest. *Global change biology*, 11 p.

Ehleringer, J.R., Cerling, T.E. and Helliker, B.R. (1997) C_4 photosynthesis, atmospheric CO_2, and climate. *Oecologia* **112**, 285-299.

Emrich, K., Ehalt, D.H. and Vogel, J.C. (1970) Carbon isotope fractionation during the precipitation of calcium carbonate. *Earth and Planetary Science Letters* **8**, 363-371.

Farquhar, G.D. (1983) On the nature of carbon isotope discrimination in C_4 plants. *Australian Journal of Plant Physiology* **10**, 205-226.

Farquhar, G.D., Hubick, K.T., Condon, A.G. and Richards, R.A. (1988) Carbon isotope fractionation and plant water-use efficiency, in: Rundel, P.W., Ehleringer, J.R., Nagy, K.A. (Eds.), Stable isotopes in Ecological Research. Springer Verlang, New York, pp. 21-40.

Farquhar, G.D., Ehleringer, J.R. and Hubick, K.T. (1989) Carbon isotope discrimination and photosynthesis. *Annual Review of Plant Physiology and Plant Molecular Biology* **40**, 503-537.

Feng, X. and Epstein, S. (1995) Carbon isotopes of trees from arid environments and implications for reconstructing atmospheric CO_2 concentration. *Geochimica et Cosmochimica Acta* **59**, 2599-2608.

France-Lanord, C. and Derry, L.A. (1994) $\delta^{13}C$ of organic carbon in the Bengal Fan: Source evolution and transport of C_3 and C_4 plant carbon to marine sediments. *Geochimica et Cosmochimica Acta* **58**, 4809-4814.

Freeman, K.H. and Hayes, J.M. (1992) Fractionation of carbon isotopes by phytoplankton and estimates of ancient CO_2 levels. *Global Biogeochemical Cycles* **6**, 185-198.

Gutjahr, M., Ridgwell, A., Sexton, P.F., Anagnostou, E., Pearson, P.N., Pälike, H., Norris, R.D., Thomas, E. and Foster, G.L. (2017) Very large release of mostly volcanic carbon during the Palaeocene–Eocene Thermal Maximum. *Nature* **548**, 573-577.

Hatch, M.D. and Slack, C.R. (1966) Photosynthesis in sugarcane leaves: a new carboxylation reaction and the pathway of sugar formation. *Biochemical Journal* **101**, 103-111.

Hayes, J.M., Freeman, K.H., Hoham, C.H. and Popp, B.N. (1989) Compound-specific isotopic analyses: a novel tool for reconstruction of ancient biogeochemical processes. *Organic Geochemistry* **16**, 1115-1128.

Holser, W.T., Magaritz, M. and Ripperdan, R.L. (1996) Global Isotopic Events, in: Walliser, O.H. (Ed.), Global Events and Event Stratigraphy in the Phanerozoic. Springer Verlag, pp. 63-88.

Hsü, K.J. and McKenzie, J.A. (1985) A "strangelove" ocean in the earliest Tertiary, in: Sundquist, E., Broecker, W.S. (Eds.), Chapman Conference on natural variations in carbon dioxide and the carbon cycle. American Geophysical Union, Tarpon Springs, FL, Jan. 9-13, pp. 487-492.

Irwin, H., Curtis, C. and Coleman, M. (1977) Isotopic evidence for source of diagenetic carbonates formed during burial of organic-rich sediments. *Nature* **269**, 209-213.

Jenkyns, H.C. (2003) Evidence for rapid climate change in the Mesozoic-Palaeogene greenhouse world. *Philosophical Transactions of the Royal Society of London, A.* **361**, 1885-1916.

Kaplan, I.R. and Nissenbaum, A. (1966) Anomalous carbon-isotope ratios in nonvolatile organic matter. *Science* **153**, 744-745.

Keeling, C.D., Mook, W.G. and Tans, P.P. (1979) Recent trends in the $^{13}C/^{12}C$ ratio of atmospheric carbon dioxide. *Nature* **277**, 121-123.

Keith, M.L. and Weber, J.N. (1964) Carbon and oxygen isotopic composition of selected limestones and fossils. *Geochimica et Cosmochimica Acta* **28**, 1787-1816.

Kennett, J.P. and Stott, L.D. (1991) Abrupt deep-sea warming, palaeoceanographic changes and benthic extinctions at the end of the Palaeocene. *Nature* **353**, 225-229.

Krissansen-Totton, J., Buick, R. and Catling, D.C. (2015) A statistical analysis of the carbon isotope record from the Archean to Phanerozoic and implications for the rise of oxygen. *American Journal of Science* **315**, 275-316.

Kump, L.R. (1991) Interpreting carbon-isotope excursions; Strangelove oceans. *Geology* **19**, 299-302.

Lee, D. and Carpenter, S.J. (2001) Isotopic disequilibrium in marine calcareous algae. *Chemical Geology* **172**, 307-329.

Marino, B.D. and McElroy, M.B. (1991) Isotopic composition of atmospheric CO_2 inferred from carbon in C4 plant cellulose. *Nature* **349**, 127-131.

McConnaughey, T. (1989a) ^{13}C and ^{18}O disequilibrium in biological carbonates I. Patterns. *Geochimica et Cosmochimica Acta* **53**, 151-162.

McConnaughey, T. (1989b) ^{13}C and ^{18}O disequilibrium in biological carbonates: II. In vitro simulation of kinetic isotope effects. *Geochimica et Cosmochimica Acta* **53**, 163-171.

McKenzie, J.A. (1985) Carbon isotopes and productivity in the lacustrine and marine environment, in: Stumm, W. (Ed.), Chemical processes in lakes. Wiley Interscience, New York, pp. 99-118.

Meyers, P.A. (1994) Preservation of elemental and isotopic source identification in sedimentary organic matter. *Chemical Geology* **114**, 289-302.

Mojzsis, S.J., Arrhenius, G., McKeegan, K.D., Harrison, T.M., Nutman, A.P. and Friend, C.R.L. (1996) Evidence for life on Earth before 3,800 million years ago. *Nature* **384**, 55-59.

Mook, W.G., Bommerson, J.C. and Staverman, W.H. (1974) Carbon isotope fractionation between dissolved bicarbonate and gaseous carbon dioxide. *Earth and Planetary Science Letters* **22**, 169-176.

O'Neil, J.R. (1987) Preservation of H, C, and O isotopic ratios in the low temperature environment., in: Kyser, T.K. (Ed.), Stable Isotope Geochemistry of Low Temperature Fluids. Mineralogical Association of Canada, Saskatoon, pp. 85-128.

Park, R. and Epstein, S. (1960) Carbon isotope fractionation during photosynthesis. *Geochimica et Cosmochimica Acta* **21**, 110-126.

Popp, B.N., Takigiku, R., Hayes, J.M., Louda, J.W. and Baker, E.W. (1989) The post-Paleozoic chronology and mechanism of ^{13}C depletion in primary marine organic matter. *American Journal of Science* **289**, 436-454.

Quade, J., Cerling, T.E. and Bowman, J.R. (1989) Development of Asian monsoon revealed by marked ecological shift during the latest Miocene in northern Pakistan. *Nature* **342**, 163-166.

Qui, L., Williams, D.F., Gvorzdkov, A. and Karabanov, E. (1993) Biogenic silica accumulationsand paleoproductivity in the northern basin of Lake Baikal during the Holocene. *Geology* **21**, 25-28.

Revelle, R. (1985) The scientific history of carbon dioxide, in: Sundquist, E.T., Broecker, W.S. (Eds.), The Carbon Cycle and Atmospheric CO_2: Natural Variations Archean to Present. American Geophysical Union, Washington, D.C., pp. 1-4.

Rosenfeld, W.D. and Silverman, S.R. (1959) Carbon isotope fractionation in bacterial production of methane. *Science* **130**, 1658-1659.

Rossinsky, V., Jr. and Swart, P.K. (1993) Influence of climate on the formation and isotopic composition of calcretes, in: Swart, P.K., Lohmann, K.C., McKenzie, J.A., Savin, S. (Eds.), Climate Change in Continental Isotopic Records. American Geophysical Union, Washington, D.C., pp. 67-75.

Sackett, W.M. and Thompson, R.R. (1963) Isotopic organic carbon composition of Recent continental derived clastic sediments of eastern Gulf Coast, Gulf of Mexico. *Bulletin of the American Association of Petroleum Geologists* **47**, 525-528.

Sackett, W.M., Eckelmann, W.R., Bender, M.L. and Be, A.W.M. (1965) Temperature dependence of carbon isotope composition in marine plankton and sediments. *Science* **177**, 52-56.

Schidlowski, M., Appel, P.W.U., Eichmann, R. and Junge, C.E. (1979) Carbon isotope geochemistry of the 3.7×10^9 yr-old Isua sediments, West Greenland; implications for the Archaean carbon and oxygen cycles. *Geochimica et Cosmochimica Acta.* **43**, 189-200.

Scholle, P.A. and Arthur, M.A. (1980) Carbon Isotope Fluctuations in Cretaceous Pelagic Limestones: Potential Stratigraphic and Petroleum Exploration Tool. *The American Association of Petroleum Geologists Bulletin* **64**, 67-87.

Schwarcz, H.P., Harmon, R.S., Thompson, P. and Ford, D.C. (1976) Stable isotope studies of fluid inclusions in speleothems and their paleoclimatic significance. *Geochimica et Cosmochimica Acta* **40**, 657-665.

Smith, B.N. and Epstein, S. (1970) Two categories of $^{13}C/^{12}C$ ratios for higher plants. *Plant Physiology* **47**, 380-383.

Spero, H.J., Bijma, J., Lea, D.W. and Bemis, B.E. (1997) Effect of seawater carbonate concentration on foraminiferal carbon and oxygen isotopes. *Nature* **390**, 497-500.

Spiker, E.C. (1981) Carbon isotopes as indicators of the source and fate of carbon in rivers and estuaries, in: Likens, G.E., Mackenzie, F.T., Richey, J.E., Sedell, J.R., Turekian, K.K. (Eds.), Carbon Dioxide Effects Research and Assessment Program; Flux of organic carbon by rivers to the oceans; report of a workshop. U.S. Dept. of Energy, Office of Energy Research, Washington, pp. 75-108.

Strain, P.M. and Tan, F.C. (1979) Carbon and oxygen isotope ratios in the Saguenay Fjord and the St. Lawrence Estuary and their implications for paleoenvironmental studies. *Estuarine Coastal Mar. Sci.* **8**, 119-126.

Swart, P.K., Lohmann, K.C., McKenzie, J.A. and Savin, S. (1993) Climate change in continental isotopic records, Geophysical Monograph, p. 374.

Teeri, J.A. and Stowe, L.G. (1976) Climatic patterns and the distribution of C_4 grasses in North America. *Oecologia* **23**, 1-12.

Turi, B. (1986) Stable isotope geochemistry of travertines, in: Fritz, P., Fontes, J.C. (Eds.), The Terrestrial Environment, B. Elsevier, Amsterdam, pp. 207-238.

Veizer, J., Ala, D., Azmy, K., Bruckschen, P., Buhl, D., Bruhn, F., Carden, G.A.F., Diener, A., Ebneth, S., Godderis, Y., Jasper, T., Korte, C., Pawellek, F., Podlaha, O.G. and Strauss, H. (1999) $^{87}Sr/^{86}Sr$, $\delta^{13}C$ and $\delta^{18}O$ evolution of Phanerozic seawater. *Chemical Geology* **161**, 59-88.

Watkins, J.M., Nielsen, L.C., Ryerson, F.J. and DePaolo, D.J. (2013) The influence of kinetics on the oxygen isotope composition of calcium carbonate. *Earth and Planetary Science Letters* **375**, 349-360.

Weber, J.N., Bergenback, R.E., Williams, E.G. and Keith, M.L. (1965) Reconstruction of depositional environments in the Pennsylvanian Vanport basin by carbon isotope ratios. *Journal of Sedimentary Petrology* **35**, 36-48.

Whiticar, M.J., Faber, E. and Schoell, M. (1986) Biogenic methane formation in marine and freshwater environments; CO_2 reduction vs. acetate fermentation; isotope evidence. *Geochimica et Cosmochimica Acta* **50**, 693-709.

Whiticar, M.J. (1999) Carbon and hydrogen isotope systematics of bacterial formation and oxidation of methane. *Chemical Geology* **161**, 291-314.

Zachos, J.C. and Arthur, M.A. (1986) Paleoceanography of the Cretaceous/Tertiary boundary event; inferences from stable isotopic and other data. *Paleoceanography* **1**, 5-26.

Zachos, J.C., Arthur, M.A. and Dean, W.E. (1989) Geochemical evidence for suppression of pelagic marine productivity at the Cretaceous/Tertiary boundary. *Nature* **337**, 61-64.

Zeebe, R.E. (1999) An explanation of the effect of seawater carbonate concentration on foraminiferal oxygen isotopes. *Geochimica et Cosmochimica Acta* **63**, 2001-2007.

Chapter 8

LOW TEMPERATURE MINERALS, EXCLUSIVE OF CARBONATES

Contents

8.1 Introduction 1
8.2 Phosphates 1
8.2.1 Analytical techniques 1
8.2.2 Applications to marine paleothermometry 2
8.2.3 Application to mammals-theory 4
8.2.4 Application to mammals - examples 6
8.3 Cherts 10
8.3.1 Application to Precambrian chert deposits 10
8.3.2 Application to Phanerozoic cherts 11
8.3.3 Diagenesis 12
8.3.4 Application to recent sediments 13
8.3.5 Other silica applications 14
8.4 Clay minerals 16
8.4.1 Early ‘bulk’ sample studies 16
8.4.2 Grain size considerations 17
8.4.3 Paleoaltimetry 18
8.5 Iron oxides 19
References 22

Chapter 8

LOW TEMPERATURE MINERALS, EXCLUSIVE OF CARBONATES

8.1 Introduction

Although carbonates are the most analyzed of all sedimentary phases, they are not the only option open to the stable isotope geochemist interested in reconstructing conditions or processes occurring in the past. There are a large number of other materials available, notably phosphates, cherts, iron and manganese oxides, and clay minerals. The benefits and disadvantages, as well as the information that can be retrieved from the non-carbonate low temperature minerals, varies widely. Phosphates and cherts are thought to be far more resistant to diagenesis than carbonates. Clay minerals contain both oxygen and hydrogen and are of both marine and terrestrial origin. Bone or tooth apatite is now widely used for reconstructing temperatures in continental settings *and* for improving our understanding of extinct (and extant) animal physiology and behavior.

8.2 Phosphates

Phosphates form over a wide range of pressure and temperatures and are somewhat of a 'garbage-can' mineral, incorporating hydroxyl, fluorine, chlorine and trace amounts of incompatible elements. Apatite is the most common phosphate mineral, consisting of the endmembers: 1) fluor-apatite, $Ca_5(PO_4)_3F$; 2) chlorapatite, $Ca_5(PO_4)_3Cl$; 3) hydroxyapatite, $Ca_5(PO_4)_3(OH)$; 4) carbonate apatite, $Ca_5(PO_4,CO_3,OH)_3(F,OH)$[1]. Apatite is found in almost all igneous and metamorphic rock types, in sedimentary rocks, in meteorites and lunar samples, and as hard parts in animals, both as shell material and bone. In the following section, we are only concerned with low temperature, carbonate apatite, or 'biological' apatite (Kohn et al., 1999). One important distinction between phosphates and carbonates from a stable isotope point of view is that carbonate can form directly from water, whereas low-temperature inorganic phosphate formation is extremely slow unless mediated by biochemical enzyme-catalyzed reactions.

8.2.1 Analytical techniques

Tudge (1960) was the first person to tackle phosphates for oxygen isotope analysis. He recognized that a major limitation of the carbonate paleothermometer was that one could not measure the $\delta^{18}O$ value of the water from which the carbonate precipitated. Tudge knew that two solid phases which precipitated at the same time and in equilibrium with each other could be used for paleotemperature estimates independent of the $\delta^{18}O$ value of water. Urey had calculated that the $^{18}O/^{16}O$ fractionation between the CO_3^{2-} and PO_4^{3-} ion were large and temperature sensitive, so that syngenetic carbonates and phosphates should act as an excellent paleothermometer (Fig. 8.1). One problem is that analysis by fluorination of phosphates is difficult. Earlier attempts by Craig and

[1] Driessens (1980) gives a general formula for tooth enamel of $Ca_{10}(PO_4)_6(CO_3)_{0.15}(Cl)_{0.1}(OH)_{1.6}$ and discusses chemical variations in detail. See Kohn *et al.* (1997) for additional analyses

Steinberg[2] to fluorinate $Ca_3(PO_4)_2$ were unsuccessful. Tudge developed a procedure whereby biogenic phosphate was dissolved in acids[3], and ultimately reprecipitated as $BiPO_4$, which was then fluorinated to yield O_2 gas. His technique was used successfully for some 30 years until a more straightforward method of producing Ag_3PO_4 rather than $BiPO_4$ was published (Crowson et al., 1991). Originally converted to O_2 by fluorination, Ag_3PO_4 is now converted to CO by high temperature reduction with graphite (O'Neil et al., 1994; Vennemann et al., 2002). In a majority of oxygen and carbon isotope studies of modern or relatively young biogenic apatite, the CO_3^{2-}-bound oxygen and carbon can also be measured using the analytically painless phosphoric acid technique normally reserved for carbonates. Oxygen in the carbonate ion in apatite is far easier to analyze than oxygen in the phosphate ion, but is also more easily reset during diagenesis.

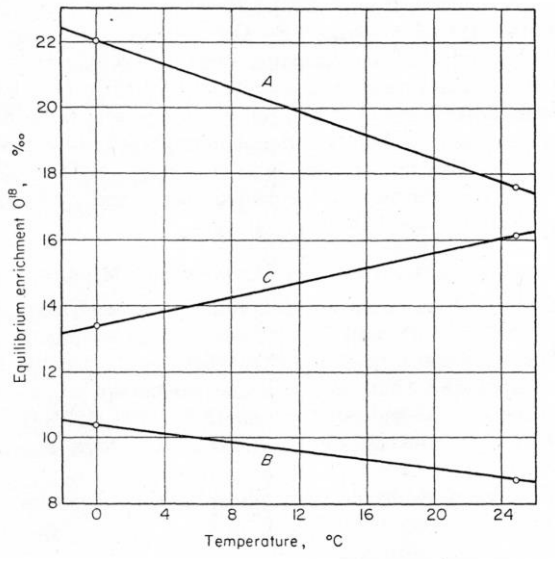

Fig. 8.1. Urey's calculations of ^{18}O enrichment in phosphate relative to carbonate (Tudge, 1960). Curve *A* is for $CO_3^{2-}{}_{(g)}$ - $H_2O_{(l)}$, curve *B* is $PO_4^{3-}{}_{(g)}$ - $H_2O_{(l)}$, curve *C* is for $PO_4^{3-}{}_{(g)}$ - $CO_3^{2-}{}_{(g)}$ + 25 ‰.

8.2.2 Applications to marine paleothermometry

Tudge never pursued the phosphate thermometer, and the idea remained dormant until Longinelli took it over several years later (Longinelli, 1965). He measured phosphate from shells of living marine organisms, assigning average growth temperature to each sample (Longinelli and Nuti, 1973), thereby deriving a fractionation equation between phosphate and water[4]:

$$t(°C) = 111.4 - 4.3(\delta_p - \delta_w + 0.5) \qquad 8.1.$$

Like Epstein's carbonate-water equation of 1953, Longinelli's phosphate-water equation has stood the test of time. In this equation, δ_p and δ_w are the $\delta^{18}O$ values of the phosphate and water on the same scale. Typical values for δ_p of marine phosphates are 20‰ (VSMOW), corresponding to a temperature of 23°C if equilibrated with ocean water.

Unfortunately, the temperature dependence (or $\partial\Delta/\partial T$) of phosphate-water fractionation is almost identical to that of carbonate-water. There is a ~9‰ fractionation between carbonates and phosphates, but that fractionation remains constant over the

[2] The work of Craig and Steinberg is discussed in Tudge, but not published.

[3] Even when dissolved in acid, oxygen in the dissolved PO_4^{3-} ion does not exchange with the aqueous solution.

[4] Incorrectly stated in original paper. Modified by Friedman and O'Neil (1977) for a new $\alpha_{CO2\text{-}H2O}$ value. Kolodny *et al.* (1983) derived an empirical calibration of $113.3 - 4.38(\delta_p - \delta_w)$, which is nearly identical to equation 8.1.

entire temperature range of biological activity. The idea of using combined phosphate-carbonate for paleothermometry was dead. However, phosphates could still be used as a paleothermometer by making the same assumptions about water composition as had been done for carbonates. Not ideal, for sure, but the resilience of phosphates to diagenetic alteration makes them an attractive mineral for paleoclimate reconstruction.

The team of Kolodny, Luz and Shemesh at the Hebrew University revisited biogenic phosphates in the early and mid-eighties. In Kolodny *et al*. (1983) they addressed the following fundamental question: If the exchange rate between inorganic aqueous solutions and PO_4^{3-} ions is so slow, then do organisms incorporate phosphate in oxygen isotope equilibrium with ambient water, or do they simply inherit the $\delta^{18}O$ value of the phosphate ion from food? They used several approaches to address this question. First, they measured the $\delta^{18}O$ values of fish bones living at different depths in Lake Baikal. Presumably, the $\delta^{18}O$ value of water and dissolved phosphate would be the same at all depths, but the lake is thermally stratified. If the phosphate oxygen incorporated by an organism was in equilibrium with ambient water due to enzyme-catalyzed exchange reactions, then there should be a regular increase in the $\delta^{18}O$ value of biological phosphate with depth (lower temperature, larger fractionation). If phosphate was incorporated wholesale, without reequilibration, then the $\delta^{18}O$ value of the fish bones should be constant, regardless of temperature. Indeed, the authors found that the $\delta^{18}O$ values of fish bones increased from 6.3‰ near the surface to 9.2‰ in the deepest levels, consistent with a 12°C measured temperature variations in the lake. Phosphate (at least in fish) appears to form in equilibrium with ambient water.

A second test was to raise fish living in otherwise identical conditions, with food of different $\delta^{18}O_{phosphate}$ values. Fish meal varied by 5‰ between fisheries, but the $\Delta^{18}O_{bone\ phosphate\ -\ water)}$ values from all fisheries were the same. From these results it is clear that during apatite formation, phosphate oxygen bonds are broken through enzymatic reactions, and complete isotopic exchange with ambient (body) water occurs. With their fears allayed, they were ready to tackle problems of paleoclimate.

One important observation was that for phosphorites, fish teeth and bones, and conodonts, there are clear trends toward lower $\delta^{18}O$ values in ancient samples. The trends could be due to changes in the $^{18}O/^{16}O$ ratio of the ocean with time, changing ocean temperatures, or diagenesis. Shemesh *et al.* (1983) made a strong case against diagenesis, demonstrating the diagenetic resistance of phosphorites by comparing coexisting cherts, carbonates and phosphates from the Campanian Mishash formation, Israel. If all three phases preserved their initial *equilibrium* $\delta^{18}O$ values, then each mineral should have a distinct and unique isotopic composition. Instead, it was found that both cherts and carbonates had a range of $\delta^{18}O$ values, with only the very highest ones corresponding to expected primary values. All other samples appeared to have been reset. In contrast, the phosphates all preserved the expected $\delta^{18}O$ value of formation with very little variation (Fig. 8.2).

The trend for marine phosphates plotted vs. age is remarkably similar to the marine carbonate curve (Fig. 8.3). The major difference, however, is that the carbonate curve excludes many samples that have been altered. The data used for generating the carbonate curve are “the cream-of-the-crop” – those few samples that most likely preserve primary $\delta^{18}O$ values. In contrast, the phosphate data include all analyses, clearly illustrating the resistance of phosphates to diagenesis.

8.2.3 Application to mammals-theory

All of the abovementioned examples are for marine samples, with the ultimate goal of defining changes in temperature or the $\delta^{18}O$ value of the ocean over time. Longinelli (1973) first proposed analyzing bones or teeth from mammals, with a different goal in mind. Rather than using the data for marine paleothermometry, as is the case with marine ectotherms[5], he envisioned using the oxygen isotope data to determine meteoric water values in ancient continental environments by using terrestrial endotherms. The $\delta^{18}O$ value of meteoric water is a function of temperature, latitude, altitude, etc. (see Chapter 4), so that the data from mammals would ultimately provide information about terrestrial paleoclimate. The basic idea is simple: The body temperature of a mammal is constant and consequently the $\delta^{18}O$ values of their apatite – either bones or teeth – is a function only of the $\delta^{18}O$ value of their body water, which in turn is controlled by drinking (meteoric) water and metabolism. Thus the phosphate is an indirect proxy for ancient meteoric water values. As intriguing as this idea sounds, it was another decade before anyone paid it serious attention, perhaps because these were viewed more as biological problems, whereas most stable isotope laboratories were housed in geological institutes at the time.

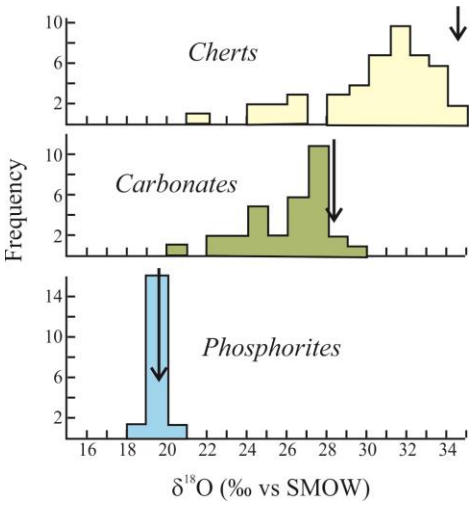

Fig. 8.2. Oxygen isotope composition of phosphorites, carbonates and cherts from the Mishash formation, Israel. The vertical arrows represent expected equilibrium values for the different minerals. Both carbonates and cherts are skewed to lower $\delta^{18}O$ values, consistent with diagenesis. The phosphates appear to preserve original, equilibrium $\delta^{18}O$ values, free from diagenesis. After Shemesh *et al* (1983).

Longinelli (1984) laid-out the basic ideas and premises of mammalian bone phosphate: 1) the body temperature of mammals is constant, 2) the mean isotopic composition of environmental water (*i.e.*, meteoric water) is the main variable controlling the oxygen isotope composition of body water, 3) bone or tooth phosphate occurs in equilibrium with body water. If these conditions are met, then mammalian phosphate is an indirect proxy for the $\delta^{18}O$ value of local meteoric water at the time the animal lived. Longinelli tested his idea by measuring blood samples from pigs, wild boar, deer and humans from various regions. The $\delta^{18}O$ values of body water for any local population were more-or-less constant. For each animal group, the $\delta^{18}O$ values of body water and local meteoric water varied linearly, but the best fit slope of the data was always less than 1. For pigs and humans the relationships are

$$\delta^{18}O_{blood} = 0.88\ \delta^{18}O_{meteoric\ water} + 2.1 \quad \text{pigs} \qquad 8.2$$

$$\delta^{18}O_{blood} = 0.60\ \delta^{18}O_{meteoric\ water} + 0.68 \quad \text{humans} \qquad 8.3.$$

[5] Ectotherms are what is commonly referred to as cold-blooded organisms, unable to internally regulate their body temperature. Endotherms are warm-blooded creatures, comprised by mammals and birds. Homeotherms are all animals that regulate their body temperature, regardless of metabolism.

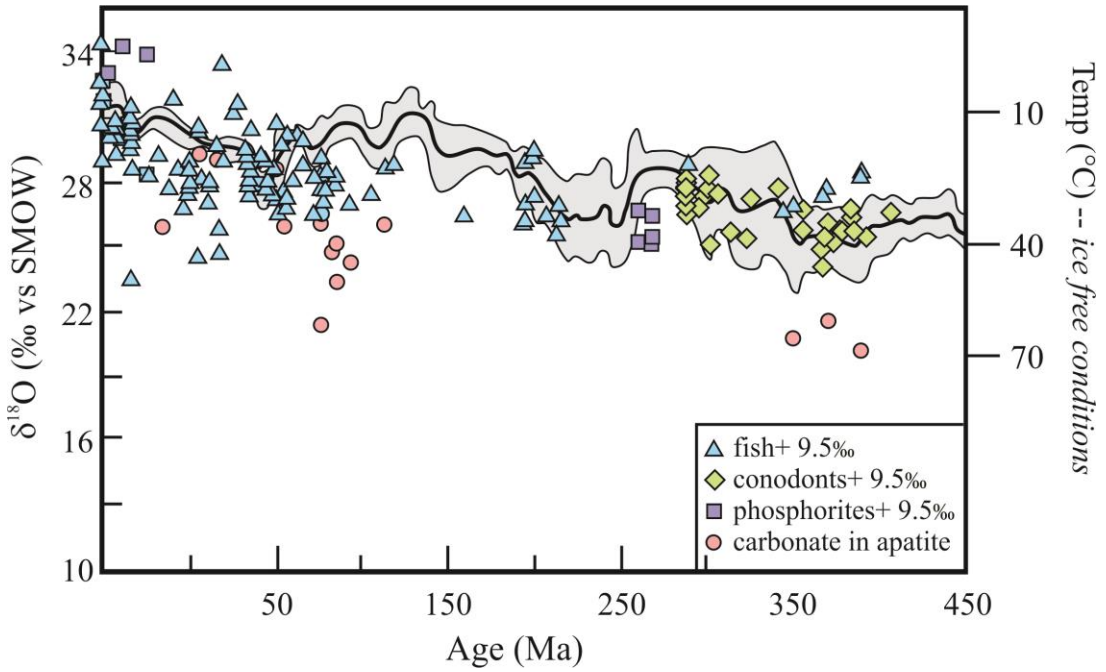

Fig. 8.3. Compilation of marine phosphate analyses as a function of time. 9.5‰ was added to all points in order to generate a curve directly comparable to carbonates, the latter shown by the continuous grey band. There is a general decrease in $\delta^{18}O$ value with increasing age. The 'carbonates in apatite' data are the $\delta^{18}O$ values of the carbonate component of the apatite. Unlike the phosphate-bound oxygen, which appears to preserve primary values, the carbonate component in old samples is clearly reset. Data from (Shemesh et al., 1983; Luz et al., 1984b; Kolodny and Luz, 1991; Lécuyer et al., 1993).

Longinelli recognized that body water has two sources: drinking water and metabolic water. Metabolic water is formed during the oxidation of food. The source of the oxygen for metabolic water is atmospheric O_2, which has a constant $\delta^{18}O$ value the world over. If an animal received all of its body water from the formation of H_2O by air O_2, then all individuals of that species would have a constant $\delta^{18}O$ value. For the pig and human cases (equations 8.2 and 8.3), it appears that pigs get more of their water from drinking, although humans add a further complication in that they are known to drink liquids (bottled water, beer, wine, etc.) from all over the globe, thereby partially homogenizing their $\delta^{18}O_{body\text{-}water}$ value and flattening out the slope.

Following Longinelli's work, Luz *et al.* (1984a) provided a quantitative explanation for the relationship between the $\delta^{18}O$ value of body water and drinking water using simple box models of inputs and outputs[6]. Figure 8.4 illustrates the system. An organism has oxygen inputs from three sources: drinking water, atmospheric oxygen (metabolic water) and food oxygen. The $\delta^{18}O$ values of drinking water and food oxygen are closely related to local meteoric water, while atmospheric oxygen is constant with a value of 23.8‰. The major outputs are: fluid loss (urine, sweat, etc.), water vapor in breath, and respired CO_2. Oxygen is also exhaled, but it is unused oxygen, and should

[6] More detailed calculations have since been made (e.g., Ayliffe and Chivas, 1990; Bryant and Froelich, 1995; Kohn et al., 1996), but results of these later models vary little from the original work.

have the same $\delta^{18}O$ value coming in as going out (see, however, Epstein and Zeiri, 1988), so does not enter into the overall flux calculations. Evolved fluids are assumed to have the $\delta^{18}O$ value of the body water, whereas the $\delta^{18}O$ values of water vapor and CO_2 are related to the body water by known and constant fractionation factors at 37°C ($\Delta^{18}O_{water\ vapor\ -\ water}$ = -8‰ and $\Delta^{18}O_{CO2\text{-}water}$ = 38‰). Fluxes normalized to O_2 are given for each input and output. Note that the amount of evolved fluid is equal to the original fluid plus a contribution from metabolic water (F4).

If the animal remains a constant size, then the inputs and outputs must equal each other. The overall isotopic composition of what goes in must equal what goes out, otherwise, the $\delta^{18}O$ value of the organism would change. Mass balance is given by

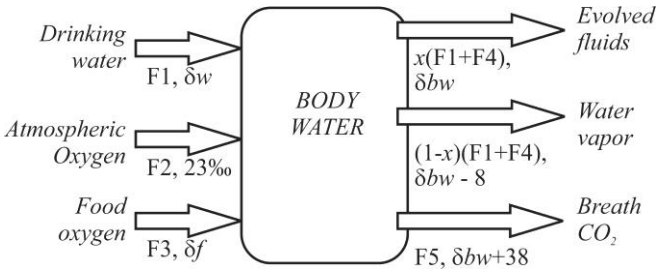

Fig. 8.4. Box model for estimating the $\delta^{18}O$ value of body water. Oxygen enters the body as drinking water, metabolic water (atmospheric O_2) and food oxygen, each with a defined flux. Water leaves the body as fluids, water vapor and exhaled CO_2, each with their own flux. The sum of the fluxes × $\delta^{18}O$ values of each input flux must equal the sum of the equivalent outputs, thus defining the $\delta^{18}O$ value of the body water. After (Luz et al., 1984a).

$$F1\delta w + 23F2 + F3\delta f = x(F1+F4)\delta bw + (1-x)(F1+F4)(\delta bw - 8) + F5(\delta bw + 35) \quad 8.4.$$

Equation 8.4 can be rearranged to solve for the $\delta^{18}O$ value of body water as

$$\delta bw = \frac{F1}{F1+F4+F5}\delta w + \frac{8(1-x)(F1+F4) + 23F2 - 38F5 + F3\delta f}{F1+F4+F5} \quad 8.5.$$

Equation 8.5 is in the same form to 8.2 and 8.3 (for constant δf). The slope is defined by the proportion of drinking water related to oxygen generated by metabolic processes. The larger the fraction of metabolic water (the less an animal drinks), the shallower the slope relating $\delta^{18}O_{body\ water}$ to $\delta^{18}O_{meteoric\ water}$.

There is a strong correlation between $\delta^{18}O$ and δD values of rabbits, kangaroos and deer (collagen) to relative humidity (Ayliffe and Chivas, 1990; Cormie et al., 1994; Huertas et al., 1995). These herbivores all derive a significant quantity of their water from plant water – water in leaves. Plants, in turn, undergo varying amounts of evaporative water loss as a function of relative humidity. The result is that this 'humidity signal' is recorded by the animal's bones.

8.2.4 Application to mammals - examples

Stable isotope analysis of mammalian bone and tooth enamel has been used to address a wide range of applications. One of the first was by Koch *et al*. (1989), who succeeded in demonstrating the power of using oxygen isotope geochemistry of mammalian apatite to address paleoclimate-related problems. Koch and his colleagues

found that seasonal variations in mastodont and mammoth tusks were preserved, with low $\delta^{18}O$ values correlating to cold-season growth, and they showed that CO_3^{2-}-bound oxygen in apatite retains its initial $\delta^{18}O$ value, at least for modern and fairly recent samples[7].

Since that work, a number of other seasonal variation studies have been made using spatial resolution measurements of tooth enamel. Tooth enamel is generally the phase of choice because it does not recrystallize during the life of the animal, and is far more resistant to diagenesis than bone. Enamel has a more-coarsely crystalline structure and lower organic content. The crystallinity of tooth enamel is unchanged over periods in excess of 1 million years (Ayliffe et al., 1994), whereas bone recrystallization occur in a matter of years (Tuross et al., 1989). The high organic content of bone also presents the opportunity for diagenetic alteration during early bacterial activity (e.g., Blake et al., 1997). In Triassic samples, only tooth enamel appears to preserve original $\delta^{18}O$ values, while bone is clearly reset (Sharp et al., 2000). High spatial resolution studies have now been made on horse, beaver, sheep and dinosaur teeth. The researchers were able to constrain seasonal climate variations in the past and place limits on migration routes and distances.

A simple, elegant application is given by the following example: A question that has been of great interest to evolutionary paleobiologists is when in Earth's history cetaceans (whales, dolphins and porpoises) changed their metabolism from one where only fresh water could be ingested to the modern situation where their osmoregulatory system can cope with the excess salt load of drinking pure seawater. From fossil localities and their associated sedimentary formations, the relative timing of evolution from land to ocean was well known, but when the cetacean osmoregulatory system evolved was not. With this in mind, Thewissen *et al.* (1996) measured $\delta^{18}O$ values of cetacean teeth from

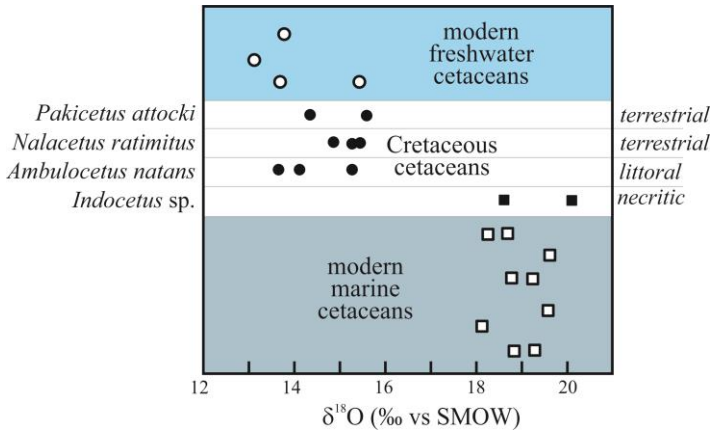

Fig. 8.5. $\delta^{18}O$ values of modern freshwater and marine cetaceans and samples from the Eocene Tethys showing the transition from freshwater to marine conditions. From Thewissen (1996).

[7] What defines a 'recent' sample in terms of whether diagenesis has occurred or not is quite variable, depending on conditions and material. Chemical changes in bone can occur in only a few years, with major crystallographic changes occurring over thousands to millions of years. How and when this might affect the $\delta^{18}O$ value of PO_4^{3-} or CO_3^{2-} oxygen is less clear. Pliocene, and perhaps Miocene samples often preserve initial $\delta^{18}O$ values in the CO_3^{2-} site of phosphate.

Eocene Tethyan cetaceans. The $\delta^{18}O$ values of modern freshwater and marine cetaceans are distinct (Fig. 8.5). They found a jump between *Ambulocetus natans* and *Indocetus* sp., the former having $\delta^{18}O$ values consistent with freshwater and the latter clearly related to marine water. This result was unexpected, because *Ambulocetus* is found in sedimentary beds of unambiguous marine origin. The authors concluded that *Ambulocetus* ingested only fresh water, or that it lived in fresh water while its teeth were mineralizing, only later migrating to the ocean. Metabolic studies have also been made towards better understanding whether or not dinosaurs were homeotherms (Barrick and Showers, 1994; Fricke and Rogers, 2000). Interpretations are complex, but generally support the idea of endothermy or at least homeothermy. Along the same line of reasoning, Fricke *et al.* (2011) found that the $\delta^{18}O$ values of giant sauropod dinosaur teeth were far lighter than the carbonate sediments hosting the fossil samples. They concluded that the best explanation for the low $\delta^{18}O$values is that the dinosaurs migrated to higher altitudes – on the order of 300 km.

The primary use of oxygen isotope analyses of mammalian apatite has been to reconstruct paleo-meteoric water values, which themselves tell us a great deal about paleoclimatological conditions. Examples of fields that have been addressed include glacial-interglacial transitions (Ayliffe et al., 1992), paleoaltitude estimates (Kohn et al., 2002; Fricke, 2003; Crowley et al., 2008), migration patterns (Koch et al., 1995) and

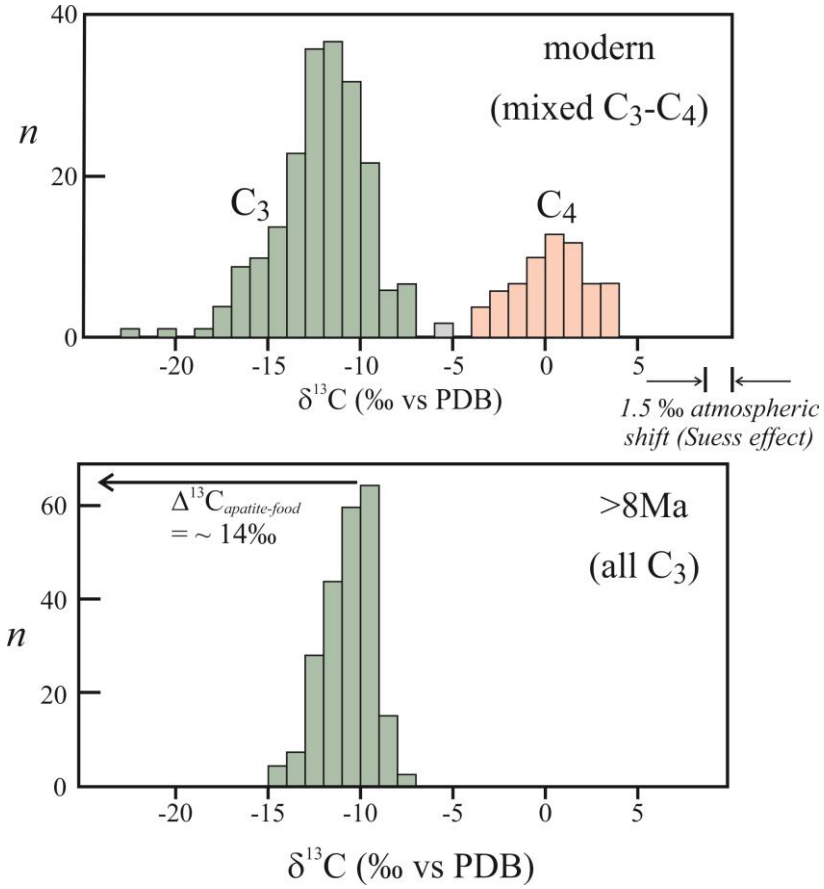

Fig. 8.6. Carbon isotope composition of modern mammals, showing a mostly bimodal dietary preference, and of fossil mammals older than 8 Ma, which show evidence of a C_3 diet only. The value of the diet is 14 ‰ lower than that of carbonate. After Cerling *et al.* (1998).

seasons of growth (Bryant et al., 1996; Fricke and O'Neil, 1996; Sharp and Cerling, 1997; Balasse et al., 2003).

Carbon isotope variations in the carbonate-site in apatite are also used to reconstruct paleoclimatic conditions and paleodiet. First-order variations in $\delta^{13}C$ values of mammalian carbonate are related to the proportion of C_3 and C_4 plants in the diet of the animal. C_3 plants have an average $\delta^{13}C$ value of -26.7‰, while C_4 plants have a $\delta^{13}C$ value of -12.5‰ (see Chapter 7). The $\delta^{13}C$ value of tooth enamel is approximately 14‰ higher than the food source (Cerling et al., 1998). Relative to C_4 plants, C_3 plants are favored under conditions of high atmospheric $p(CO_2)$ and low daytime growing-season temperature. Cerling *et al.* (1993) found a global change in the $\delta^{13}C$ values of fossil horse teeth around 8 Ma (see section 7.5). Prior to this time, the $\delta^{13}C$ value of horse (and other grazing animals) teeth was restricted to a range of -15 to -8‰, with a mode at -10‰, typical of a pure C_3 diet (Fig. 8.6). In more recent samples, there is a bimodal distribution. The C_3 diet is still seen, but a second mode centered around 0 to 2‰ emerges, distinctive of a pure C_4 diet. Over this same time interval, major evolutionary changes in flora and fauna occurred. Changes in vegetation due to lower CO_2 levels in the atmosphere (CO_2 starvation), and flora and fauna extinctions appear to be closely related.

Dietary reconstruction using stable isotopes is important for archaeological studies. Early hominid diet is constrained by the carbon isotope composition of tooth enamel. There had been a general consensus that the 3 Ma hominid *Australopithecus africanus* lived on a diet of fruits and leaves, in agreement with the belief that they occupied heavily wooded habitats. If this were indeed the case, the $\delta^{13}C$ values of tooth enamel would be consistent with a nearly pure C_3 diet, as is seen in modern primates. Instead, the $\delta^{13}C$ values from *A. africanus* suggest a mixed C_3 and C_4 diet, typical of carnivores and mixed C_3-C_4 feeders, but distinctly heavier than modern frugivore primates (Fig. 8.7).

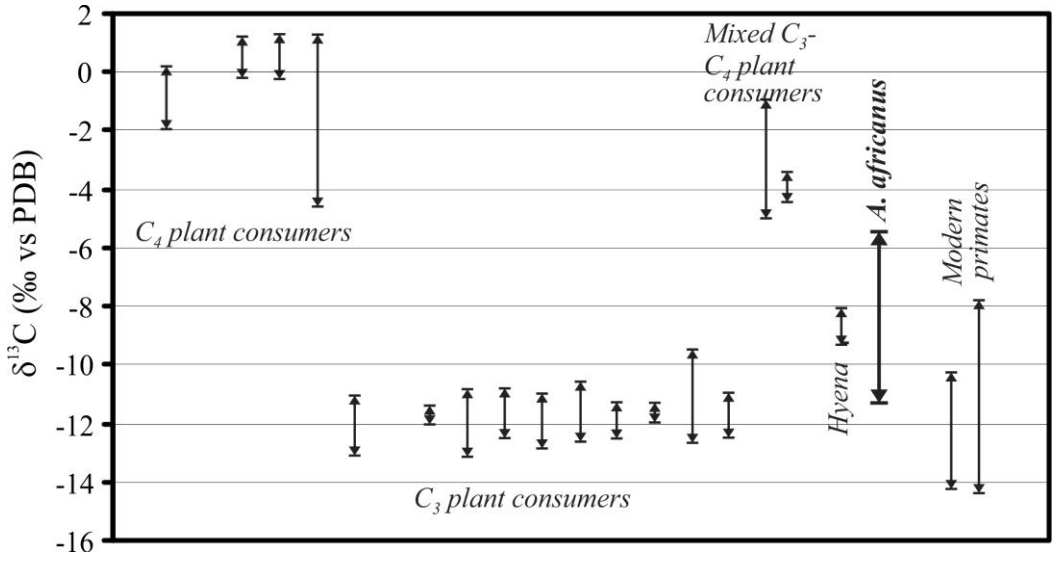

Fig. 8.7. Carbon isotope composition of different species from the 3-Ma Makapansgat Member 3, South Africa. C_3 and C_4 and plant eaters are distinct from one another. Mixed consumers and carnivores are intermediate, as is the hominid *A. africanus*. Modern primates (consumers) are also shown. After Sponheimer and Lee-Thorp (1999).

And finally, who can't resist the dogs? Consider the following archaeological problem. Domestic dog vertebrae from the Mesolithic site of Star Carr, Yorkshire, England have $\delta^{13}C$ values indicating a marine diet. Apparently these dogs fed predominantly on scraps from coastal people who made periodic trips inland (Clutton Brock and Noe Nygaard, 1990). Their dependency upon the people is clearly established from the carbon isotope data.

8.3 Cherts

Cherts are composed of microcrystalline quartz replacing authigenic silica, either opal or quartz. Cherts do not form by direct precipitation from ocean water, at least not since the Phanerozoic. Dissolved silica concentrations are and were simply too low. Instead, silica-secreting organisms concentrates dissolved silica in their cells which later reprecipitates/recrystallizes to form opaline silica and ultimately chert beds or concretions. Pre-Tertiary deposits formed from silica-secreting radiolarians and sponges. Extensive deep ocean layers of biogenic siliceous oozes of mid-Tertiary and younger ages corresponds to the explosion of diatom populations. Very old samples of thick chert beds, such as the Precambrian iron formations, may have been directly deposited from seawater, but no one knows.

8.3.1 Application to Precambrian chert deposits

Perry (1967) made the first systematic stable isotope study of Precambrian cherts. He analyzed massive chert beds where delicate microfossil remains were still evident, a good indication, he believed, that recrystallization and diagenesis had been minimal (see however, the discussion of neomorphism in Section 6.4.3). What Perry found was a systematic and dramatic decrease in the $\delta^{18}O$ values with increasing age, which he attributed to changing $\delta^{18}O$ values of ancient oceans. Later, more detailed work on Precambrian cherts (Knauth and Epstein, 1976; Knauth and Lowe, 1978) indicated that the very low $\delta^{18}O$ values were more likely artifacts of diagenesis. Lithographic facies and stratigraphic position strongly correlate with $\delta^{18}O$ values, consistent with at least partial diagenesis or precipitation from meteoric water. Nevertheless, the $\delta^{18}O$ values of the least-altered Precambrian samples were consistently 21-22‰ at 3.4 Ga, significantly lower than Phanerozoic equivalents of 30‰ or more (Fig. 8.8). The interpretation from the Knauth group was that the $\delta^{18}O$ value of the Archean oceans were buffered to a $\delta^{18}O$ value of ~ 0‰, as is the case today (section 5.6 for the idea of a buffered ocean), but temperatures of the ancient oceans were significantly hotter.

Perry (and other authors since) suggested lower $\delta^{18}O$ values of the ocean; Knauth, higher temperatures. Each conclusion is profound in its significance. If the ocean was indeed lighter than today, then tectonic processes, which buffer the ocean to a near-constant value, were very different in the past. Perry pointed out that tillites (products of glaciers) at 2 Ga were incompatible with overall high temperatures. Hren *et al.* (2009) measured both O and H isotope ratios in a 3.42-billion-year-old Buck Reef Chert rocks in South Africa and concluded that temperatures of the oceans were probably less than 40°C. The low $\delta^{18}O$ values of the cherts reflect a lighter Archean ocean. Knauth, using the argument that the oceans are buffered by hydrothermal processes at mid-ocean ridges, has offered the explanation for the low $\delta^{18}O$ values as indicative of high Earth-surface temperatures. The tillites that were noted by Perry, it was argued, could have been a

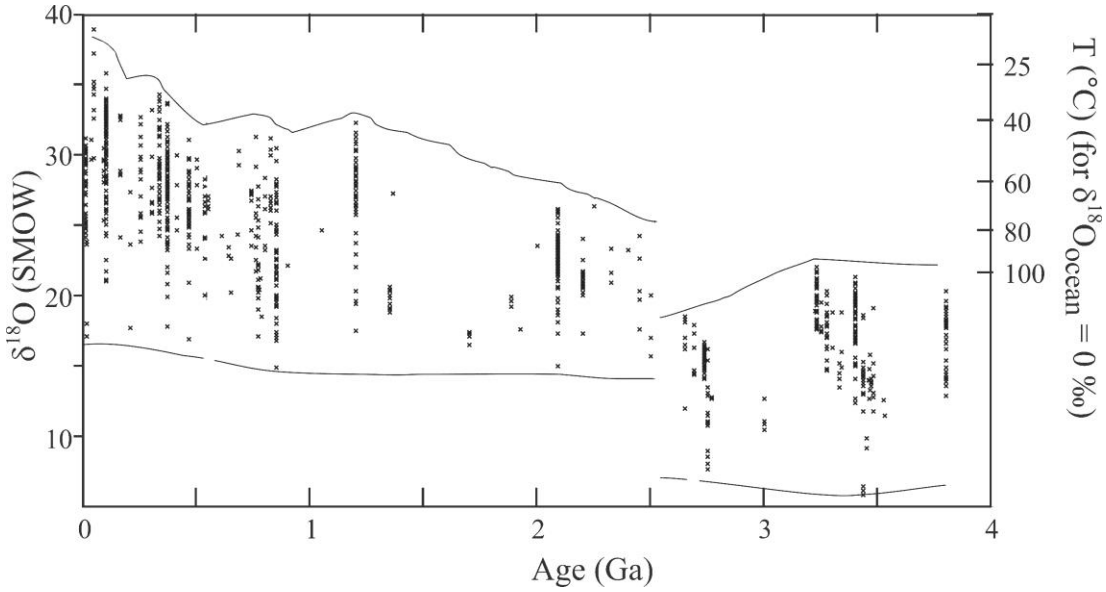

Fig. 8.8. Compilation of $\delta^{18}O$ values of cherts by Knauth (2005). The upper curve is thought to represent the least altered samples most likely to be in equilibrium with seawater. The apparent jump at 2.5 Ga is postulated by Knauth to be related to drawdown of CO_2 during weathering of the extensive, long-lived continental cratons developed at this time. Temperature estimates are for quartz-water fractionations.

transient feature. Temperature of 70°C or more are suggested for a near-zero $\delta^{18}O_{Ocean}$. A 70°C ocean would be scalding. For temperatures to change from steaming hot to glacial and back again is impossible today, with effective feedback mechanisms in place from plants, but could have happened in the past? The lack of a biological component to buffer $p(CO_2)$ could allow rapid changes in temperature. The chert data are some of the most compelling evidence for major temperature or isotopic differences in the ancient past. A completely unrelated methodology using the thermostability of phylogenetically dispersed ancestral elongation factors supports high temperatures in the Archean (Gaucher et al., 2008).

8.3.2 Application to Phanerozoic cherts

Phanerozoic cherts have been analyzed by combining stable oxygen *and* hydrogen isotope data (Knauth and Epstein, 1976). For each group of data organized by age, the combined $\delta^{18}O$-δD values define an array with $\delta D/\delta^{18}O$ slope of 8, equal to present meteoric water (Fig. 8.9). Knauth and Epstein argued that the slope 8 is a reflection of cherts having equilibrated with meteoric waters, similar to what is seen for kaolinites in section 8.4. Samples forming in equilibrium with ocean water would have the highest δD-$\delta^{18}O$ values for any age group, depending on the temperature of formation. Line-A in figure 8.9 defines the locus of samples in equilibrium with ocean water; higher temperatures plot at lower $\delta^{18}O$ and higher δD values[8]. For each age group, distinct

[8] The temperature - $\delta^{18}O$ relationship of Line A is from experimental fractionation factors. The hydrogen – temperature dependence is empirical.

temperature ranges are given, highest in the lower Paleozoic and Triassic, lowest in the post Jurassic. The field for each age group, trending down from Line A with a slope parallel to the meteoric water line, is interpreted as samples having formed in equilibrium with meteoric water (or a mixture of meteoric and ocean water) *at the average global temperature for that period of time*. The data presented in Fig. 8.9 indicate very high temperatures approaching 40°C in the Lower Paleozoic and Triassic. These values are at the limit of what might be expected for the temperature tolerance of most advanced organisms.

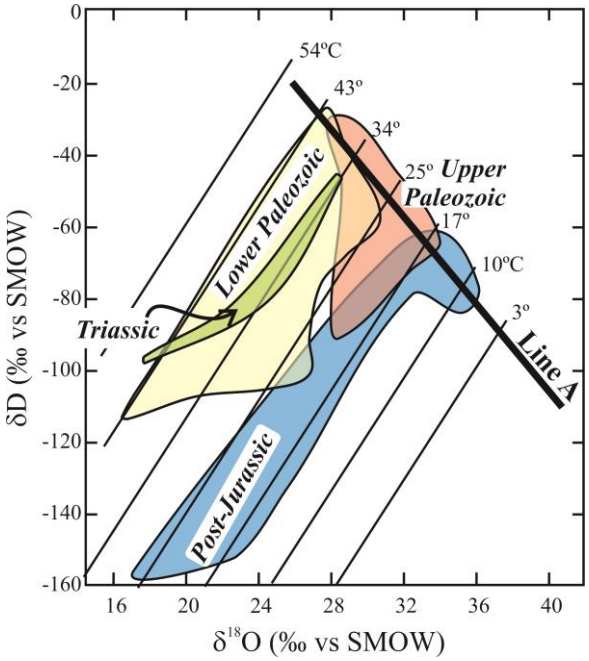

Fig. 8.9. δD - $\delta^{18}O$ plot of Phanerozoic cherts. Samples in equilibrium with ocean water should plot on line A, an empirical fit to the highest delta values for each group. Lines of constant temperature are drawn with a δD-$\delta^{18}O$ slope of 8, and are based on the quartz-water fractionation curve. Each age group plots in a field with slope 8, indicating that the samples formed in equilibrium with some combination of ocean water and meteoric water. After Knauth and Epstein (1976)

At the sub-cm scale, the complexities of single chert samples become apparent. High spatial resolution data from single chert nodules show systematic antiphase periodicity in $\delta^{18}O$ and δD values (Sharp et al., 2002). The hydrogen and oxygen isotope variations cannot be explained in terms of diagenesis, because δD and $\delta^{18}O$ values change in opposite directions (Fig. 8.10). Instead, the authors suggested that during formation of the chert nodule in shallow sediments, temperatures periodically varied by up to ~10°C. This work illustrates both the complexity of single nodules, and also the resilience of the Jurassic-age sample to diagenesis.

8.3.3 Diagenesis

All of the above conclusions are only valid if one can evaluate and account for diagenetic effects. As we have seen above, Knauth and Lowe (1978) recognized that significant diagenesis occurred in some Precambrian cherts, whereas others may not have changed by more than 3‰. Murata *et al.* (1977) measured $\delta^{18}O$ values of silica phases in the Miocene Monterey Shale formation in California, U.S.A, and found that there were abrupt changes in crystallography with depth, related to a progression from biogenic opal (opal-A) to opal-CT to microcrystalline quartz. For each silica 'polymorph', the $\delta^{18}O$ values are constant. Instead, a jump is observed across each transition (Fig. 8.11). If the samples had reequil-ibrated continuously as a function of temperature, then there should be a smooth variation in the $\delta^{18}O$ value with depth. Temperature of transformation were estimated as 35-50°C from opal-A to opal-CT and 45-80°C from opal-CT to microcrystalline quartz. Inherent in this assumption, is that the $\delta^{18}O$ values of the pore

waters remained constant at 0‰.

Monterey formation samples were reanalyzed using a stepwise fluorination technique developed to remove the effects of water contamination in the hydrous silica polymorphs. Results from the stepwise fluorination data give $\delta^{18}O$ values for the opal-CT that are considerably higher than earlier estimates, suggesting a temperature of this transition of 20°C (Matheney and Knauth, 1993).

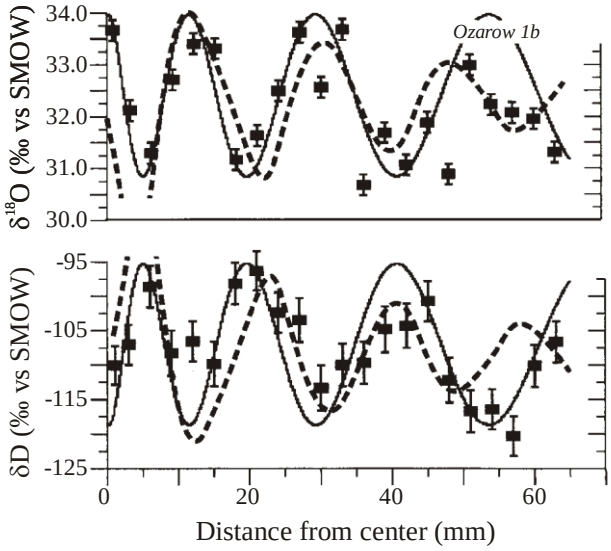

Fig. 8.10. Variations in hydrogen and oxygen isotope ratios as a function of the distance from center for chert nodules of Jurassic age. The antiphase periodicity of the nodules cannot be explained by diagenesis, which would lower both $\delta^{18}O$ and δD values in the same direction. Instead, the data are interpreted as reflecting temperature changes of ~10°C. After Sharp *et al.* (2002).

8.3.4 Application to recent sediments

Fresh biogenic silica has high organic matter and water content. Over millions of years, it recrystallizes to microcrystalline quartz. Water and organic matter are lost, so that the silica phase becomes essentially pure quartz. Whether or not changes in $\delta^{18}O$ values occur during the recrystallization processes is open to debate, but there is no problem with analyzing ancient cherts using conventional fluorination. Only minimal pretreatment is required because the sample is essentially pure quartz. For young and especially for modern samples, the complications of organic matter and high water content pose serious problems. Even purifying the silica phase is not a trivial task. Settling techniques are used to separate biogenic silica from detrital clays, and complicated chemical treatments are used to remove carbonate and iron oxide overgrowths. Organic matter is removed by treatment with NaOCl or hydrogen peroxide.

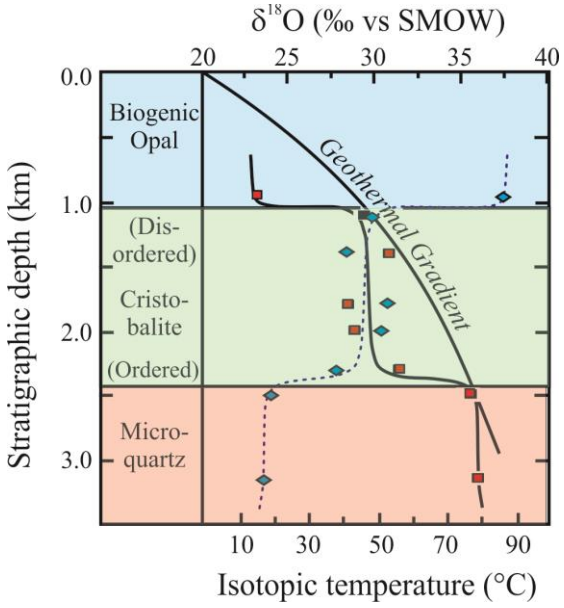

Fig. 8.11. Variations in $\delta^{18}O$ values of chert vs. depth for the Monterey formation, California, USA. $\delta^{18}O$ values (diamonds) jump across each phase transition. Temperatures of each transition agree with expected geothermal gradient. Complications associated with changing porewater values should be considered. After Murata *et al.* (1977).

The most difficult task is to remove water from the highly-hydrated silica, which may be up to 12 wt% of the total opal. Several techniques have been employed to remove water without causing irreproducible shifts in the $\delta^{18}O$ value of the remaining dehydrated silica.

Heating of opal at moderate temperatures in a vacuum will remove all water, but the resultant $\delta^{18}O$ values are not reproducible. Labeyrie (1974) showed that rapid cintering at 1000°C in vacuum removes all water with only a small $\delta^{18}O$ shift. Reproducibility of the method was later improved by first equilibrating the samples with water of known $\delta^{18}O$ value (Labeyrie and Juillet, 1982). Partial fluorination techniques have also been developed, where repeated partial fluorination reactions strip-away the hydrous component of the silica (Matheney and Knauth, 1989; Dodd and Sharp, 2010). The results from each method are generally similar (Chapligin et al., 2011), lending credence to their validity.

Given a method of analysis, modern and cultured samples could be analyzed in order to calibrate the silica-water thermometer. The first biogenic silica-water fractionation was made on diatoms[9] that formed in the ocean (Leclerc and Labeyrie, 1987). The empirical equation is similar to the extrapolation of the quartz-water curve determined experimentally at higher temperature

$$t = 17.2 - 2.4(\delta^{18}O_{si} - \delta^{18}O_w - 40) - 0.2(\delta^{18}O_{si} - \delta^{18}O_w - 40)^2 \ (t \text{ in } °C) \qquad 8.6.$$

Brandriss *et al.* (1998) cultured diatoms in the laboratory and measured the silica-water fractionation. Their data varied linearly with temperature, but suggested a fractionation that was about 9‰ less than the abiogenic silica-water curve and the Leclerc and Labeyrie curve. The difference was unexplained until Dodd *et al.* (2012) measured both antemortem and postmortem diatoms and found a bimodal distribution in their $\delta^{18}O$ values. Measuring a modest lake core (pond, really) they were able to measure antemortem diatoms and then the *same* samples by returning to the pond after a period of several years of burial. They found that the modern samples matched the Brandriss curve, whereas those samples that had been buried for less than one year had completely reequilibrated to the 'quartz-water' curve (Fig. 8.12), demonstrating that: a) diatoms precipitate out of equilibrium with their surrounding water and b) they completely reequilibrate at an extremely rapid rate to the quartz-water fractionation. Similar conclusions were reached by Schmidt *et al.* (1997; 2001) by comparing marine samples in surface water, sediment traps and surface sediments.

Like diatoms, sponges and radiolarian apparently do not precipitate in oxygen isotope equilibrium with ocean water.

8.3.5 Other silica applications

The $\delta^{18}O$ value of quartz has distinct ranges for different rock types. The $\delta^{18}O$ values of igneous rocks range from 8 to 10‰, metamorphic rocks, 10 to 16‰. Quartz from sandstones and beaches has a narrow range of 10 to 13‰. Shales are higher,

[9] Diatoms are marine algae that deposit internal silica frustules. Because they are photosynthetic, they are only found in near-surface waters. Thus the $\delta^{18}O$ value should then reflect sea-surface temperatures.

ranging from 15 to 24‰, very similar to authigenic quartz and quartz overgrowths. Cherts have the highest $\delta^{18}O$ values, ranging from 19 to 34‰. Blatt (1987) point out that the high $\delta^{18}O$ values of shales and mudstones cannot simply be reworked igneous and metamorphic rocks. Authigenic overgrowths formed during clay diagenesis and chert fragments must contribute to the high values, an idea that is supported by careful petrographic and isotopic analyses, as demonstrated by numerous studies (Fisher and Land, 1986; Hervig et al., 1995; Kelly et al., 2007) in which the overgrowth silica has $\delta^{18}O$ values in excess of 30‰.

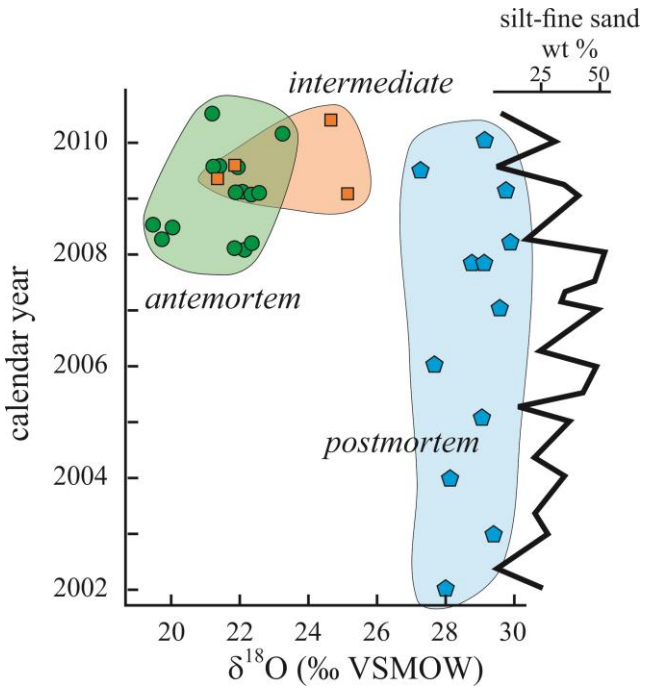

Fig. 8.12. $\delta^{18}O$ values of diatoms from a small pond in the Valles Caldera, New Mexico. Living (antemortem) samples (green) have $\delta^{18}O$ values that appear to be far out of equilibrium with their ambient water. The same material, sampled only 1-2 years later (blue), has reequilibrated to the equilibrium quartz-water fractionation. After Dodd *et al.* (2012).

Burial diagenesis does not change the $\delta^{18}O$ value of quartz unless accompanied by recrystallization. With this in mind, sources of eolian transported fine-grained quartz can be traced using oxygen isotope geochemistry. Mizota and Matsuhisa (1995) showed that quartz in the Canary Archipelago was sourced from the North African Sahara desert, on the basis of $\delta^{18}O$ values of quartz and $^{87}Sr/^{86}Sr$ ratios of mica. Sridhar *et al*. (1978) measured quartz from soils in Southwest United States and the Hawaiian Islands. Surprisingly, the $\delta^{18}O$ values of fine-grained materials from all locations ranged from 17 to 20‰. These values are not those of metamorphic and igneous rocks (8 to 16‰), nor of cherts (~30‰). Sources could be shales or mixtures of light igneous material with heavier quartz of low-temperature origin. The quartz from Hawaii is probably sourced from Asian soils.

One last application mentioned here is using silica phytoliths as a proxy for continental paleoclimate reconstruction. Phytoliths are the siliceous secondary cell wall found in many grasses, particularly abundant in grasslands and steppes. In a series of papers by Webb and Longstaffe (see 2003), the $\delta^{18}O$ value of phytolith silica was shown to be a function of soil water composition and temperature. Leaves were affected by humidity, as well, due to transpiration. Empirical relationships between phytolith $\delta^{18}O$ values and temperatures were derived. Applications to ancient samples have not yet been made, as far as I know.

8.4 Clay minerals

8.4.1 Early 'bulk' sample studies

The $\delta^{18}O$ of coarse-grained clastic sediments generally mimics the host rock, with $\delta^{18}O$ values ranging from 8-11‰ (igneous rocks) and up to about 17‰ for some metamorphic rocks (Savin and Epstein, 1970a). Authigneic overgrowths will bring these values up into the 20+ ‰ range. Hydrogen isotope ratios are generally in the range of -80 to -25‰, and is strongly controlled by mineralogy and particularly iron content. Biotites tend to have low δD values of -100 to -80, whereas muscovite, talc, and phengite have δD values as high as -30‰.

Savin and Epstein (1970a,b,c) were the first to tackle the stable isotope geochemistry of clay minerals. They hoped to answer the question of whether or not clay minerals form in equilibrium with their surroundings and how easily they are altered after formation. In order to avoid complexities associated with mineral purification, they tried to measure nearly monomineralic samples, such as those from kaolinite and montmorillonite (bentonite) deposits. When analyzing shales, the $\delta^{18}O$ values for clay minerals had a small correction due to quartz contamination.

Savin and Epstein's came to a number of general conclusions. They found that the $\delta^{18}O$ values of clay minerals mostly range from 16 to 26‰, higher than for igneous and most metamorphic rocks. Such high $\delta^{18}O$ values must have formed at low temperatures, where equilibrium $\Delta^{18}O_{mineral\text{-}water}$ values are large. But the scatter in the data was large

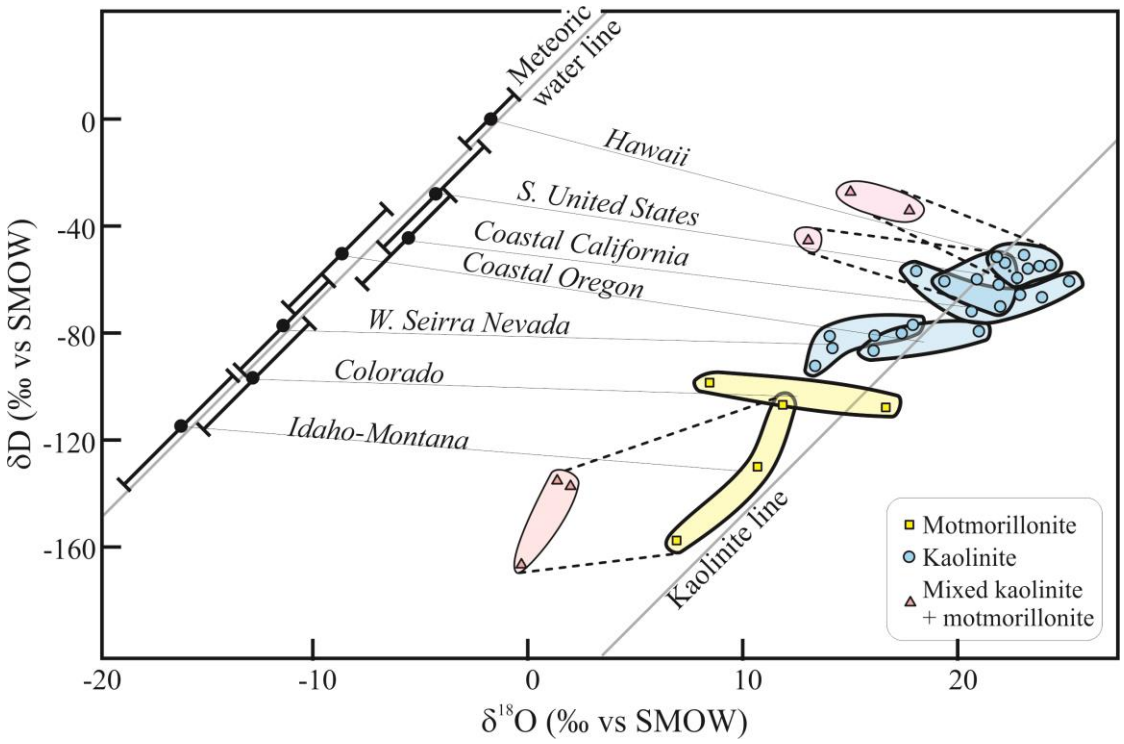

Fig. 8.13. Correlation between $\delta^{18}O$ and δD values of kaolinite/montmorillonite with assumed local meteoric water for the region. The data indicate a strong relationship between the isotope values of the clays and the coexisting meteoric water demonstrating that the clay minerals faithfully record both the δD and $\delta^{18}O$ values of local meteoric water. After (Lawrence and Taylor, 1971).

enough to indicate an 'exotic' terrigenous component as well. The δD values are similar to igneous and metamorphic rocks, ranging from -90 to -40‰. Combined δD-$\delta^{18}O$ values of kaolinites formed a linear array which paralleled the meteoric water line. Savin and Epstein proposed that if the massive kaolinite deposits formed in mild and wet continental climates, then the oxygen and hydrogen isotope composition of the clays would be buffered by meteoric water, a concept that was later expanded upon by Lawrence and Taylor (1971) (Fig. 8.13). On the basis of estimated meteoric water values and temperatures of kaolinitization, the $\alpha_{kaolinite\text{-}water}$ values for oxygen and hydrogen were estimated as 1.027 and 0.970, respectively. Similar fractionation factors were calculated for montmorillonite and glauconite.

In contrast to kaolinite deposits, which form in terrestrial environments as a result of massive exchange with meteoric water, Savin and Epstein found that the $\delta^{18}O$ values of illites from ocean cores average 15.5‰, far lower than the equilibrium value for samples in equilibrium with seawater (approx. 27‰ for kaolinite-water). Similarly, montmorillonites from ocean core samples are approximately 17‰, also lower than the equilibrium value. They concluded that these minerals were at least partially of detrital origin, and that they had not reequilibrated on the ocean floor even after millions of years. Later Yeh and Epstein (1978) demonstrated that even hydrogen isotope exchange of detrital clays does not occur on the ocean floor in millions of years, except for the smallest size fraction (<0.1μm).

Bindeman *et al.* (2016) measured the $\delta^{18}O$ and δD values of shales from all over the world covering the remarkable age range of 500 to 3500 Ma. They found that glacial periods in the Precambrian had $\delta^{18}O$ values that were significantly lower (~4 to 10‰) than in interglacial periods. The pre-and post-glacial samples had the same isotopic compositions, suggesting a rapid return to weathering conditions that prevailed prior to the onset of the glaciation. Other than the very oldest samples 3300-3500 Ma, the range and absolute values of $\delta^{18}O$ values have not changed appreciably over time, suggesting similar weathering conditions throughout much of Earth's history.

8.4.2 Grain size considerations

The next advance in studies of clay minerals occurred when people started picking apart the various phases in clastic deposits. Separation and purification of clay minerals is extremely laborious and requires a number of chemical and settling techniques (Sheppard and Gilg, 1996), but the information that is gained is substantial. The effects of burial diagenesis are beautifully illustrated in a detailed isotopic study of a sediment core from the Gulf coast, southwestern United States (Yeh and Savin, 1977; Yeh, 1980). $\delta^{18}O$ and δD values were measured as a function of grain size and depth (Fig. 8.14). The data show clear trends with depth:

- Oxygen and hydrogen isotope ratios in the shallowest levels most likely preserve detrital input from the Mississippi River.
- With increasing depth, both the oxygen and hydrogen isotope data tend to converge on a single value, which is thought to represent equilibration with pore waters.
- Hydrogen reequilibration occurs at ~70°C for all grain sizes, which is probably related to the breakdown of potassium feldspar (right panel, Fig. 8.14).
- Oxygen equilibrium occurs at higher temperatures, which is almost certainly

related to recrystallization due to the onset of active diagenesis, characterized by the reaction of aqueous fluids with unstable detrital components. The near constancy of both isotope ratios below ~3800 m (100°C) suggests attainment of equilibrium. The unchanging values with greater depth also suggest that the system was rock-buffered, with the isotopic composition of pore waters, rather than rock, changing with depth.

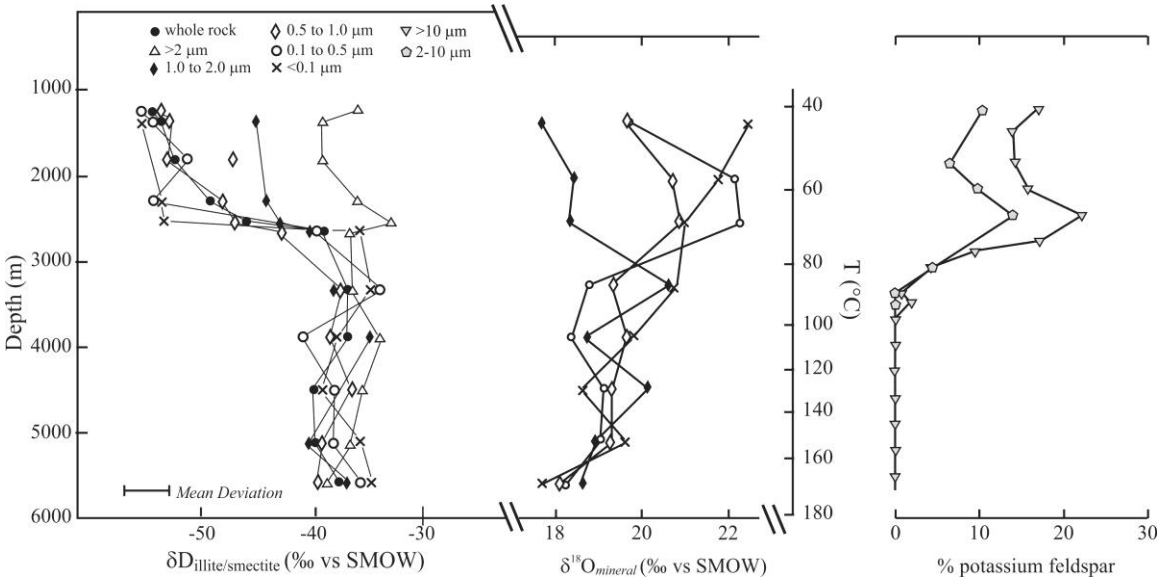

Fig. 8.14. Oxygen and hydrogen isotope ratios from Gulf Coast well 6 from Yeh and Savin (1977) and Yeh (1980). At shallow levels, the isotope data preserve the detrital input. With increasing depth, the oxygen, and more dramatically hydrogen, reequilibrate with porewaters until the differences between different size fractions disappear. The hydrogen reequilibration coincides with the conversion of K-spar to illite. (% feldspar from Hower et al., 1976).

Longstaffe and Ayalon (1987) made a detailed petrographic-isotopic study of diagenetic minerals in a Cretaceous transitional marine to continental sequence in west-central Alberta, Canada. They were able to recognize an increase in temperature with only a slight increase in $\delta^{18}O$ values of porewaters followed by a rapid decrease in $\delta^{18}O$ values of porewaters due to the infiltration of meteoric water, and finally a reduction of temperature to the present-day conditions (Fig. 8.15). What distinguishes this work from many purely geochemical studies is that they used petrographic information to infer the relative timing of formation of the different minerals, allowing them to infer conditions during multiple stages of a protracted pressure-temperature path for the formation.

The reader is referred to published review articles for more information (Longstaffe, 1987; Savin and Lee, 1988; Longstaffe, 1989). A discussion of fractionation factors for hydrous phyllosilicates can be found in Savin and Lee (1988).

8.4.3 Paleoaltimetry

Stable isotope paleoaltimetry is based on the idea that the $\delta^{18}O$ and δD values of meteoric water change dramatically with altitude (see section 4.7.4). Minerals that form at the Earth's surface should inherit a signature of the meteoric water, and hence preserve

information related to the altitude at the time the minerals formed. There are a number of minerals that have been used in paleoaltitude reconstruction, mostly soil and lacustrine carbonates, as well as animal teeth, and neoform phyllosilicates. The last of these – essentially clay minerals – provide added information in that they have both O and H isotope data, allowing for potential complicating factors, such as evaporation, to be evaluated (Mulch and Chamberlain, 2007). Additionally, many clay minerals can be directly dated (Clauer, 2013). As evident from Fig. 8.13, the isotopic composition of authigenic clay minerals is an indirect measurement of the isotopic composition of water attending formation of the minerals themselves. The isotopic composition of the meteoric water responsible for clay mineral formation is strongly dependent on the altitude at the time of formation (Poage and Chamberlain, 2001), so that the isotopic composition of the neoform minerals is an indirect estimate of the altitude of mineral formation. Stable isotope paleoaltimetry has been applied to virtually every major mountain range in the world.

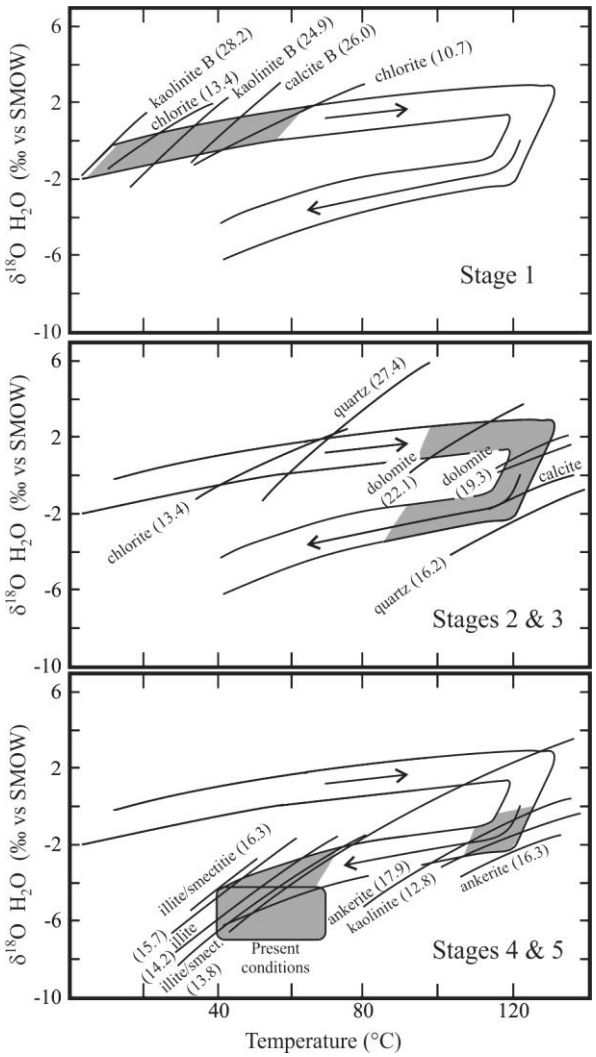

Fig. 8.15. Evolution of oxygen isotope ratios of porewaters from a transitional marine-terrestrial sequence from the Cretaceous-age Alberta Basin. Oxygen isotope ratios first increase due to exchange with newly-formed authigenic minerals, and then decrease as meteoric water infiltrates the system. After Longstaffe and Ayalon (1987).

Clay minerals applicable to paleoaltitude studies include kaolinites from weathered soil horizons, smectites formed during the weathering of volcanic ash layers, and micas formed in shear zones (Mulch and Chamberlain, 2007). Fig. 8.16 shows the $\delta^{18}O$ values of mulitiple authigenic minerals from the northern Great Basin region, USA with a dramatic change to lower values beginning in the middle to late Eocene (Horton et al., 2004). The authors attribute the change to a ~2km increase in the elevation of the region in the middle Eocene to early Oligocene.

8.5 Iron oxides

The iron oxides hematite (Fe_2O_3) and goethite (α-FeOOH) are common low-temperature alteration phases in the terrestrial and marine environment. They are found in

a bewildering array of environments when water and the oxidizing conditions of the near surface are encountered; from oceanic spreading centers, to soils, to precipitates on bones. Goethite has a small $Fe(CO_3)OH$ component. This means that oxygen, hydrogen and carbon isotopes can all be measured from the same sample, providing multiple constraints on the conditions attending formation. Yapp (2001) presents a nice review of the field.

As with many fine-grained materials, sample preparation is important. Selective dissolution methods are used to purify different ferric oxides. In addition, silicates are invariably intermixed with fine-grained ferric oxides, so that mass balance techniques are necessary to retrieve the pure ferric-oxide $\delta^{18}O$ value (e.g., Yapp, 1998; Bao et al., 2000). The analyzed data must be interpreted in terms of known fractionation factors, in order to retrieve temperatures of formation. The discrepancy between calibrations for goethite-water is quite remarkable (see Yapp, 2001, Fig. 2). No discrepancy exists for hydrogen isotope fractionation, but that might be because there is only one calibration that has been published!

The fractionation between goethites forming in modern soil and local mean meteoric water range from -1.5 to 6.3‰ (Bao et al., 2000). Such a large spread of $\Delta^{18}O$ values cannot be explained by temperature variations alone. Instead, processes such as evaporation in the soils where the goethites are forming causes dramatic shifts in the $\delta^{18}O$ values of soil water.

Yapp measured the $\delta^{18}O$ and δD values of goethites from a recent bog iron deposit and lateritic soil (Yapp, 1997). His temperature estimates for the recent materials were in excellent agreement with modern (summer) values. Turning to ancient samples (Ordovician to Cretaceous) he predicted that $\delta^{18}O$ values of goethites from low latitudes had formed under conditions of high rainfall, and that the meteoric water cycle affecting the late Cretaceous samples was different from today due to the effects of the Late Cretaceous seaway (Yapp, 1998).

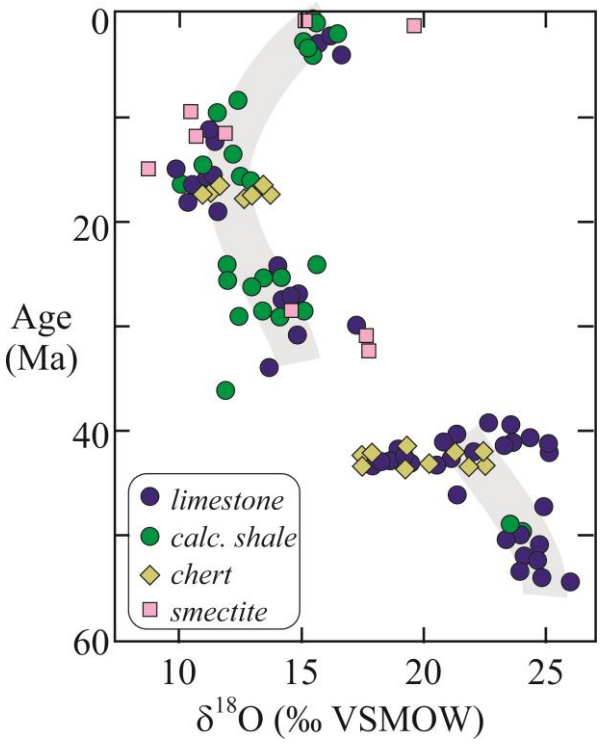

Fig. 8.16. Oxygen isotope values of various authigenic minerals from the northern Great Basin, USA. A clear break in the isotopic data is seen between 40-30 Ma, suggesting a change in altitude or circulation at this time. After Horton *et al.* (Horton et al., 2004).

Goethite geochemistry has also been used to calculate the partial pressure of CO_2 (pCO_2) in the atmosphere. CO_2 is formed in soil from the oxidation of organic matter. The pCO_2 in soils increases downward from the surface while the $\delta^{13}C$ value decreases. Yapp and Poths (1992) measured the concentration and $\delta^{13}C$ value of the $Fe(CO_3)OH$

component of a goethite deposit of Late Ordovician age. They found that the atmospheric pCO_2 during the goethite formation was ~16 times higher than present values.

The above examples of low temperature materials used for reconstructing paleoclimate or conditions of diagenesis are by no means complete. Researchers have analyzed pretty much anything that exists near the Earth's surface, and more often than not, the information is particularly useful. Amber, egg shells, snails, coal, collagen, hackberries, hair, manganese coatings, and volcanic ash are only a few of the additional materials that have been addressed with stable isotope geochemistry to address surficial processes.

References

Ayliffe, L.K. and Chivas, A.R. (1990) Oxygen isotope composition of the bone phosphate of Australian kangaroos: Potential as a palaeoenvironmental recorder. *Geochimica et Cosmochimica Acta* **54**, 2603-2609.

Ayliffe, L.K., Lister, A.M. and Chivas, A.R. (1992) The preservation of glacial-interglacial climatic signatures in the oxygen isotopes of elephant skeletal phosphate. *Palaeogeography, Palaeoclimatology, Palaeoecology* **99**, 179-191.

Ayliffe, L.K., Chivas, A.R. and Leakey, M.G. (1994) The retention of primary oxygen isotope compositions of fossil elephant skeletal phosphate. *Geochimica et Cosmochimica Acta* **58**, 5291-5298.

Balasse, M., Smith, A.B., Ambrose, S.H. and Leight, S.R. (2003) Determining sheep birth seasonality by analysis of tooth enamel oxygen isotope ratios: The late Stone Age site of Kasteelberg (South Africa). *Journal of Archaeolgical Science* **30**, 205-215.

Bao, H., Koch, P.L. and Thiemens, M.H. (2000) Oxygen isotopic composition of ferric oxides from recent soil, hydrologic, and marine environments. *Geochimica et Cosmochimica Acta* **64**, 2221-2231.

Barrick, R.E. and Showers, W.J. (1994) Thermophysiology of Tyrannosaurus rex; evidence from oxygen isotopes. *Science* **265**, 222-224.

Bindeman, I.N., Bekker, A. and Zakharov, D.O. (2016) Oxygen isotope perspective on crustal evolution on early Earth: A record of Precambrian shales with emphasis on Paleoproterozoic glaciations and Great Oxygenation Event. *Earth and Planetary Science Letters* **437**, 101-113.

Blake, R.E., O'Neil, J.R. and Garcia, G.A. (1997) Oxygen isotope systematics of biologically mediated reactions of phosphate; I, Microbial degradation of organophosphorus compounds. *Geochimica et Cosmochimica Acta* **61**, 4411-4422.

Blatt, H. (1987) Oxygen isotopes and the origin of quartz. *Journal of Sedimentary Petrology* **57**, 373-377.

Brandriss, M.E., O'Neil, J.R., Edlund, M.B. and Stoermer, E.F. (1998) Oxygen isotope fractionation between diatomaceous silica and water. *Geochimica et Cosmochimica Acta* **62**, 1119-1125.

Bryant, J.D. and Froelich, P.N. (1995) A model of oxygen isotope fractionation in body water of large mammals. *Geochimica et Cosmochimica Acta* **59**, 4523-4537.

Bryant, J.D., Froelich, P.N., Showers, W.J. and Genna, B.J. (1996) A tale of two quarries: Biologic and taphonomic signatures in the oxygen isotope composition of tooth enamel phosphate from modern and Miocene equids. *Palaios* **11**, 397-408.

Cerling, T.E., Wang, Y. and Quade, J. (1993) Expansion of C_4 ecosystems as an indicator of global ecological change in the Late Miocene. *Nature* **361**, 344-345.

Cerling, T.E., Ehleringer, J.R. and Harris, J.M. (1998) Carbon dioxide starvation, the development of C_4 ecosystems, and mammalian evolution. *Philosophical Transactions of the Royal Society of London* **3553**, 159-171.

Chapligin, B., Leng, M.J., Webb, E., Alexandre, A., Dodd, J.P., Sharp, Z.D. and others, a. (2011) Inter-laboratory comparison of oxygen isotope compositions from biogenic silica. *Chemical Geology* **75**, 7242–7256.

Clauer, N. (2013) The K-Ar and $^{40}Ar/^{39}Ar$ methods revisited for dating and tracing low-

temperature K-bearing clay minerals. *Chemical Geology* **354**, 163-185.

Clutton Brock, J. and Noe Nygaard, N. (1990) New osteological and carbon-isotope evidence on Mesolithic dogs: Companions to hunters and fishers at Star Carr (Yorkshire, England, UK), Seamer Carr (Yorkshire, England, UK) and Kongemose (Sjaelland, Denmark). *Biological Abstracts Vol. 91, Iss. 2, Ref. 20363.* **17**, 643-654.

Cormie, A.B., Schwarcz, H.P. and Gray, J. (1994) Relation between hydrogen isotopic ratios of bone collagen and rain. *Geochimica et Cosmochimica Acta* **58**, 377-391.

Crowley, B.E., Koch, P.L. and Davis, E.B. (2008) Stable isotope constraints on the elevation history of the Sierra Nevada Mountains, California. *Geological Society of America Bulletin* **120**, 588-598.

Crowson, R.A., Showers, W.J., Wright, E.K. and Hoering, T.C. (1991) Preparation of phsophate samples for oxygen isotope analysis. *Analytical Chemistry* **63**, 2397-2400.

Dodd, J.P. and Sharp, Z.D. (2010) A laser fluorination method for oxygen isotope analysis of biogenic silica and a new oxygen isotope calibration of modern diatoms in freshwater environments. *Geochimica et Cosmochimca Acta* **74**, 1381-1390.

Dodd, J.P., Sharp, Z.D., Fawcett, P.J., Brearley, A.J. and McCubbin, F.M. (2012) Rapid post-mortem maturation of diatom silica oxygen isotope values. *Geochem. Geophys. Geosyst.* **13**, Q09014.

Driessens, F.C.M. (1980) The mineral in bone, dentine and tooth enamel. *Bulletin des Sociétés Chimiques Belges* **89**, 663-689.

Epstein, S. and Zeiri, L. (1988) Oxygen and carbon isotopic compositions of gases respired by humans. *Proceedings of the National Academy of Sciences* **85**, 1727-1731.

Fisher, R.S. and Land, L.S. (1986) Diagenetic history of Eocene Wilcox sandstones, South-Central Texas. *Geochimica et Cosmochimica Acta* **50**, 551-561.

Fricke, H.C. and O'Neil, J.R. (1996) Inter- and intra-tooth variation in the oxygen isotope composition of mammalian tooth enamel: Some implications for paleoclimatological and paleobiological research. *Palaeogeography, Palaeoclimatology, Palaeoecology* **126**, 91-99.

Fricke, H.C. and Rogers, R.R. (2000) Multiple taxon-multiple locality approach to providing oxygen isotope evidence for warm-blooded theropod dinosaurs. *Geology* **28**, 799-802.

Fricke, H.C. (2003) Investigation of early Eocene water-vapor transport and paleoelevation using oxygen isotope data from geographically widespread mammal remains. *Geological Society of America Bulletin* **115**, 1088-1096.

Fricke, H.C., Hencecroth, J. and Hoerner, M.E. (2011) Lowland-upland migration of sauropod dinosaurs during the Late Jurassic epoch. *Nature* **480**, 513-515.

Friedman, I. and O'Neil, J.R. (1977) Compilation of stable isotope fractionation factors of geochemical interest, U. S. Geological Survey Professional Paper, Washington, D.C.

Gaucher, E.A., Govindarajan, S. and Ganesh, O.K. (2008) Palaeotemperature trend for Precambrian life inferred from resurrected proteins. *Nature* **451**, 704-707.

Hervig, R.L., Williams, L.B., Kirkland, I.K. and Longstaffe, F.J. (1995) Oxygen isotope microanalyses of diagenetic quartz: possible low temperature occlusion of pores. *Geochimica et Cosmochimica Acta* **59**, 2537-2543.

Horton, T.W., Sjostrom, D.J., Abruzzese, M.J., Poage, M.A., Waldbauer, J.R., Hren, M.T., Wooden, J. and Chamberlain, C.P. (2004) Spatial and temporal variation of

Cenozoic surface elevation in the Great Basin and Sierra Nevada. *American Journal of Science* **304**, 862-888.

Hower, J., Eslinger, E.V., Hower, M.E. and Perry, E.A. (1976) Mechanism of burial metamorphism of argillaceous sediment: 1. Mineralogical and chemical evidence. *Geological Society of America Bulletin* **87**, 725-737.

Hren, M.T., Tice, M.M. and Chamberlain, C.P. (2009) Oxygen and hydrogen isotope evidence for a temperate climate 3.42 billion years ago. *Nature* **462**, 205-208.

Huertas, A.D., Iacumin, P., Stenni, B., Chillón, B.S. and Longinelli, A. (1995) Oxygen isotope variations of phosphate in mammalian bone and tooth enamel. *Geochimica et Cosmochimica Acta* **59**, 4299-4305.

Kelly, J.L., Fu, B., Kita, N.T. and Valley, J.W. (2007) Optically continuous silcrete quartz cements of the St. Peter Sandstone: high precision oxygen isotope analysis by ion microprobe. *Geochimica et Cosmochimica Acta* **71**, 3812-3832.

Knauth, L.P. and Epstein, S. (1976) Hydrogen and oxygen isotope ratios in nodular and bedded cherts. *Geochimica et Cosmochimica Acta.* **40**, 1095-1108.

Knauth, L.P. and Lowe, D.R. (1978) Oxygen isotope geochemistry of cherts from the Onverwacht Group (3.4 billion years), Transvaal, South Africa, with implications for secular variations in the isotopic composition of cherts. *Earth and Planetary Science Letters* **41**, 209-222.

Knauth, L.P. (2005) Temperature and salinity history of the Precambrian ocean: implications for the course of microbial evolution. *Palaeogeography, Palaeoclimatology, Palaeoecology* **219**, 53-69.

Koch, P.L., Fisher, D.C. and Dettman, D.L. (1989) Oxygen isotopic variation in the tusks of extinct proboscideans; a measure of season of death and seasonality. *Geology* **17**, 515-519.

Koch, P.L., Heisinger, J., Moss, C., Carlson, R.W., Fogel, M.L. and Behrensmeyer, A.K. (1995) Isotopic tracking of change in diet and habitat use in African elephants. *Science* **267**, 1340-1343.

Kohn, M.J., Schoeninger, M.J. and Valley, J.W. (1996) Herbivore tooth oxygen isotope compositions; effects of diet and physiology. *Geochimica et Cosmochimica Acta* **60**, 3889-3896.

Kohn, M.J., Schoeninger, M.J. and Barker, W.W. (1999) Altered states: effects of diagenesis on fossil tooth chemistry. *Geochimica et Cosmochimica Acta* **63**, 2737-2747.

Kohn, M.J., Miselis, J.L. and Fremd, T.J. (2002) Oxygen isotope evidence for progressive uplift of the Cascade Range, Oregon. *Earth and Planetary Science Letters* **204**, 151-165.

Kolodny, Y., Luz, B. and Navon, O. (1983) Oxygen isotope variations in phosphate of biogenic apatites, I. Fish bone apatite - rechecking the rules of the game. *Earth and Planetary Science Letters* **64**, 393-404.

Kolodny, Y. and Luz, B. (1991) Oxygen isotopes in phosphates of fossil fish; Devonian to Recent, in: Taylor, H.P., Jr., O'Neil, J.R., Kaplan, I.R. (Eds.), Stable Isotope Geochemistry: A Tribute to Samuel Epstein. Lancaster Press, Inc., San Antonio, Texas, pp. 105-119.

Labeyrie, L. and Juillet, A. (1982) Oxygen isotopic exchangeability of diatom valve silica; Interpretation and consequences for paleoclimatic studies. *Geochimica et*

Cosmochimica Acta **46**, 967-975.

Labeyrie, L.J. (1974) New approach to surface seawater palaeotemperatures using $^{18}O/^{16}O$ ratios in silica of diatom frustules. *Nature* **248**, 40-42.

Lawrence, J.R. and Taylor, H.P., Jr. (1971) Deuterium and oxygen-18 correlation: Clay minerals and hydroxides in Quaternary soils compared to meteoric waters. *Geochimica et Cosmochimica Acta* **35**, 993-1003.

Leclerc, A.J. and Labeyrie, L. (1987) Temperature dependence of oxygen isotopic fractionation between diatom silica and water. *Earth and Planetary Science Letters* **84**, 69-74.

Lécuyer, C., Grandjean, P., O, N.J.R., Cappetta, H. and Martineau, F. (1993) Thermal excursions in the ocean at the Cretaceous-Tertiary boundary (northern Morocco): $\delta^{18}O$ record of phosphatic fish debris. *Palaeogeography, Palaeoclimatology, Palaeoecology* **105**, 235-243.

Longinelli, A. (1965) Oxygen isotopic composition of orthophosphate from shells of living marine organisms. *Nature* **207**, 716-719.

Longinelli, A. (1973) Preliminary oxygen-isotope measurements of phosphate from mammal teeth and bones. *Colloque International du CNRS* **219**, 267-271.

Longinelli, A. and Nuti, S. (1973) Revised phosphate-water isotopic temperature scale. *Earth and Planetary Science Letters* **19**, 373-376.

Longinelli, A. (1984) Oxygen isotopes in mammal bone phosphate; a new tool for paleohydrological and paleoclimatological research? *Geochimica et Cosmochimica Acta* **48**, 385-390.

Longstaffe, F.J. (1987) Stable isotope studies of diagenetic processes, in: Kyser, T.K. (Ed.), Short course in Stable isotope geochemistry of low temperature processes. Mineralogical Society of Canada, Saskatoon, SK, pp. 187-257.

Longstaffe, F.J. and Ayalon, A. (1987) Oxygen-isotope studies of clastic diagenesis in the Lower Cretaceous Viking Formation, Alberta; implications for the role of meteoric water, in: Marshall, J.D. (Ed.), Diagenesis of Sedimentary Sequences. Geological Society Special Publication, Liverpool, pp. 277-296.

Longstaffe, F.J. (1989) Stable isotopes as tracers in clastic diagenesis, in: Hutcheon, I.E. (Ed.), Short Course in Burial Diagenesis. Mineralogical Association of Canada, Montreal, pp. 201-277.

Luz, B., Kolodny, Y. and Horowitz, M. (1984a) Fractionation of oxygen isotopes between mammalian bone phosphate and environmental drinking water. *Geochimica et Cosmochimica Acta* **48**, 1689-1693.

Luz, B., Kolodny, Y. and Kovach, J. (1984b) Oxygen isotope variations in phosphate of biogenic apatites; III, Conodonts. *Earth and Planetary Science Letters* **69**, 255-262.

Matheney, R.K. and Knauth, L.P. (1989) Oxygen-isotope fractionation between marine biogenic silica and seawater. *Geochimica et Cosmochimica Acta* **53**, 3207-3214.

Matheney, R.K. and Knauth, L.P. (1993) New isotopic temperature estimates for early silica diagenesis in bedded cherts. *Geology* **21**, 519-522.

Mizota, C. and Matsuhisa, Y. (1995) Isotopic evidence for the eolian origin of quartz and mica in soils developed on volcanic materials in the Canary Archipelago. *Geoderma* **66**, 313-320.

Mulch, A. and Chamberlain, C.P. (2007) Stable isotope paleoaltimetry in orogenic belts - The silicate record in surface and crustal geological archives. *Reviews in Mineralogy*

and Geochemistry **66**, 89-118.

Murata, K.J., Friedman, I. and Gleason, J.D. (1977) Oxygen isotope relations between diagenetic silica minerals in Monterey Shale, Temblor Range, California. *American Journal of Science* **277**, 259-272.

O'Neil, J.R., Roe, L.J., Reinhard, E. and Blake, R.E. (1994) A rapid and precise method of oxygen isotope analysis of biogenic phosphates. *Israeli Journal of Earth Science* **43**, 203-212.

Perry, E.C., Jr. (1967) The oxygen isotope chemistry of ancient cherts. *Earth and Planetary Science Letters* **3**, 62-66.

Poage, M.A. and Chamberlain, C.P. (2001) Empirical relationships between elevation and the stable isotope composition of precipitation and surface waters; considerations for studies of paleoelevation change. *American Journal of Science* **301**, 1-15.

Savin, S.M. and Epstein, S. (1970a) The oxygen isotopic compositions of coarse grained sedimentary rocks and minerals. *Geochimica et Cosmochimica Acta* **34**, 323-329.

Savin, S.M. and Epstein, S. (1970b) The oxygen and hydrogen isotope geochemistry of clay minerals. *Geochimica et Cosmochimica Acta* **34**, 25-42.

Savin, S.M. and Epstein, S. (1970c) The oxygen and hydrogen isotope geochemistry of ocean sediments and shales. *Geochimica et Cosmochimica Acta* **34**, 43-63.

Savin, S.M. and Lee, M. (1988) Isotopic studies of phyllosilicates, in: Bailey, S.W. (Ed.), Hydrous phyllosilicates. Mineralogical Society of America, Chelsea, pp. 189-223.

Schmidt, M., Botz, R., Stoffers, P., Anders, T. and Bohrmann, G. (1997) Oxygen isotopes in marine diatoms: A comparative study of analytical techniques and new results on the isotope composition of recent marine diatoms. *Geochimica et Cosmochimica Acta* **61**, 2275-2280.

Schmidt, M., Botz, R., Rickert, D., Bohrmann, G., Hall, S.R. and Mann, S. (2001) Oxygen isotopes of marine diatoms and relations to opal-A maturation1. *Geochimica et Cosmochimica Acta* **65**, 201-211.

Sharp, Z.D. and Cerling, T.E. (1997) Fossil isotope records of seasonal climate and ecology: straight from the horse's mouth. *Geology* **26**, 219-222.

Sharp, Z.D., Atudorei, V. and Furrer, H. (2000) The effect of diagenesis on oxygen isotope ratios of biogenic phosphates. *American Journal of Science* **300**, 222-237.

Sharp, Z.D., Durakiewicz, T., Migaszewski, Z.M. and Atudorei, V.N. (2002) Antiphase hydrogen and oxygen isotope periodicity in chert nodules. *Geochimica et Cosmochimica Acta* **66**, 2865-2873.

Shemesh, A., Kolodny, Y. and Luz, B. (1983) Oxygen isotope variations in phosphate of biogenic apatites. II. Phosphorite rocks. *Earth and Planetary Science Letters* **64**, 405-416.

Sheppard, S.M.F. and Gilg, H.A. (1996) Stable isotope geochemistry of clay minerals. *Clay Minerals* **31**, 1-24.

Sponheimer, M. and Lee-Thorp, J.A. (1999) Isotopic evidence for the diet of an early hominid, *Australopithecus africanus*. *Science* **283**, 368-370.

Sridhar, K., Jackson, M.L., Clayton, R.N., Gillette, D.A. and Hawley, J.W. (1978) Oxygen isotopic ratios of quartz from wind-erosive soils in the Southwestern United States in relation to aerosol dust. *Soil Science Society of America Journal* **42**, 158-162.

Thewissen, J.G.M., Roe, L.J., O, N.J.R., Hussain, S.T., Sahni, A. and Bajpai, S. (1996)

Evolution of Cetacean osmoregulation. *Nature* **381**, 379-380.

Tudge, A.P. (1960) A method of analysis of oxygen isotopes in orthophosphate; its use in the measurement of paleotemperatures. *Geochimica et Cosmochimica Acta* **18**, 81-93.

Tuross, N., Behrensmeyer, A.K., Eanes, E.D., Fisher, L.W. and Hare, P.E. (1989) Molecular preservation and crystallographic alterations in a weathering sequence of wildebeest bones. *Applied Geochemistry* **4**, 261-270.

Vennemann, T.W., Fricke, H.C., Blake, R.E., O'Neil, J.R. and Colman, A. (2002) Oxygen isotope analysis of phosphates; a comparison of techniques for analysis of Ag_3PO_4. *Chemical Geology* **185**, 321-336.

Webb, E.A. and Longstaffe, F.J. (2003) The relationship between phytolith- and plant-water $\delta^{18}O$ values in grasses. *Geochimica et Cosmochimica Acta* **67**, 1437-1449.

Yapp, C.J. and Poths, H. (1992) Ancient atmospheric CO_2 pressures inferred from natural goethites. *Nature* **355**, 342-344.

Yapp, C.J. (1997) An assessment of isotopic equilibrium in goethites from a bog iron deposit and a lateritic regolith. *Chemical Geology* **135**, 159-171.

Yapp, C.J. (1998) Paleoenvironmental interpretations of oxygen isotope ratios in oolitic ironstones. *Geochimica et Cosmochimica Acta* **62**, 2409-2420.

Yapp, C.J. (2001) Rusty relics of Earth history: Iron(III) oxides, isotopes, and surficial environments. *Annual Review of Earth and Planetary Science* **29**, 165-199.

Yeh, H. and Savin, S.M. (1977) Mechanism of burial metamorphism of argillaceous sediments; 3, O-isotope evidence. *Geological Society of America Bulletin* **88**, 1321-1330.

Yeh, H.W. and Epstein, S. (1978) Hydrogen isotope exchange between clay minerals and sea water. *Geochimica et Cosmochimica Acta.* **42**, 140-143.

Yeh, H.W. (1980) D/H ratios and late-stage dehydration of shales during burial. *Geochimica et Cosmochimica Acta.* **44**, 341-352.

Chapter 9

NITROGEN

Contents

NITROGEN 1
9.1 Introduction 1
9.2 The nitrogen cycle 2
9.3 Nitrogen isotope fractionation 3
9.3.1 Nitrogen fixation 4
9.3.2 Mineralization 4
9.3.3 Assimilation 5
9.3.5 Denitrification 6
9.4 The characteristic $\delta^{15}N$ value of various materials 6
9.4.1 Plants and soil 7
9.4.2 Other terrestrial reservoirs 8
- Fertilizers 8
- Rain 8
- Fossil fuels 8

9.4.3 Nitrogen in the oceans 9
9.5 Nitrogen isotope ratios in animals 11
9.5.1 Compound specific studies 13
References 15

Chapter 9
NITROGEN

9.1 Introduction

Nitrogen is a trace phase in rocks and the major component of air. Estimates for the distribution of nitrogen between the major reservoirs – rocks, air, terrestrial – vary wildly, with some compilations suggesting that 98% of nitrogen is hosted by rocks (Hübner, 1986) to about ½ in rocks, with the remainder in the atmosphere (McDonough and Sun, 1995)[1]. Regardless of this discrepancy, there is roughly equal amounts of organic matter-hosted nitrogen in plants, soil, and the ocean (Hübner, 1986). Although minor in abundance, organic nitrogen is of tremendous importance, because almost all nitrogen isotope fractionation occurs by metabolic or metabolically-related processes. Over the eons, this has led to a range of nitrogen isotope compositions that span well over 100‰. Even in the mantle, the substantial range of $\delta^{15}N$ values has been attributed by some to subduction of surficial material (Beaumont and Robert, 1999; Marty and Dauphas, 2003).

The two stable isotopes of nitrogen are ^{14}N and ^{15}N, with a $^{14}N/^{15}N$ ratio in air of 272. Because the ratio is constant, air nitrogen is taken as our standard given by[2]

$$\delta^{15}N\,(\text{‰ vs AIR}) = \left(\frac{\left({}^{15}N/{}^{14}N \right)_{sample}}{\left({}^{15}N/{}^{14}N \right)_{\text{AIR}}} - 1 \right) 1000 \qquad 9.1.$$

A reference gas of N_2 from air is easily made by removing CO_2 and water from air cryogenically, and removing O_2 by reaction with copper oxide. The remaining gas will be N_2 with a trace of Ar. Solid reference samples are also available from NIST and the IAEA (Appendix 1).

Nitrogen is a trace element in rocks, and because nitrogen isotope ratios have traditionally been some of the most difficult to measure, nitrogen isotope geochemistry has not been thoroughly embraced by the geochemical community. Analytically, nitrogen is difficult to transfer in vacuum lines, because it cannot simply be frozen with liquid nitrogen. Instead, it needs to be *adsorbed* on zeolite-filled cold fingers. Also, at low nitrogen levels, even small leaks will compromise an analysis. Contamination with CO will have a drastic effect on measured $\delta^{15}N$ ratios due to the interference at mass 29 ($^{13}C^{16}O$).

Many analytical problems have been eliminated with the coupling of the elemental analyzer and mass spectrometer, which allows for combustion and analysis of N-bearing compounds to be made in continuous flow mode (Bebout et al., 2007, see section 2.8.3). Nitrogen analyses of many solids can now be made rapidly and with little

---

[1] The very high estimate for nitrogen in the mantle is not in agreement with contemporary models for how the volatile elements were delivered to a newly-forming Earth.

[2] In the agricultural literature, the $\delta^{15}N$ value is defined as $\delta^{15}N(\text{AIR ‰}) = \left(\frac{\left(\text{at\%}\,{}^{15}N \right)_{sample}}{\left(\text{at\%}\,{}^{15}N \right)_{\text{AIR}}} - 1 \right) 1000$, which is nearly, but not quite, identical to the definition in equation 9.1.

effort (except at low concentrations). This has raised the status of nitrogen as an important isotopic tracer, especially for pollution studies and within the biological community. It must be stressed however, that for nitrogen dissolved in water, sophisticated wet-chemical procedures are generally required to convert the nitrogen-bearing ion ($\left(NH_4^+\right)$, $\left(NO_3^-\right)$, etc.) to a solid form suitable for analysis (Kendall, 1998), although exciting new methods that employ bacterial denitrification have drastically simplified the procedure (Sigman et al., 2001; Coplen et al., 2004).

9.2 The nitrogen cycle

Nitrogen forms a number of oxidation states from +5 $\left(NO_3^-\right)$ to -3 $\left(NH_4^+\right)$. A simplified nitrogen cycle is shown in Fig. 9.1. Diatomic nitrogen is removed from air by microorganisms (particularly *Rhizobium* sp.) living symbiotically in higher plants or lichens. This process is called *nitrogen fixation*; a typical reaction is

$$N_{2\,(g)} + 3\,H_2O_{\,(g)} \xrightarrow{\textit{nitrogenase}} 2\,NH_{3\,(g)} + 3/2\,O_{2\,(g)} \qquad 9.2.$$

Nitrogen fixation is an energy consuming process. The ammonia or ammonium ion is extremely important in fertilizer, to the point where 5-14 $\times$ 10^{10} kg/yr of nitrogenous fertilizers are produced by industrial nitrogen fixation alone.

Assimilation or *immobilization* are the processes where NH_4^+ or NO_3^- are incorporated in living tissue. The reverse of this is the degredation of organic matter by heterotrophic bacteria and release of NH_4^+ in a process called *mineralization* (also called *ammonification*).

Nitrification is the oxidation of ammonia to NO_3^- by nitrifying organisms (*e.g.*,

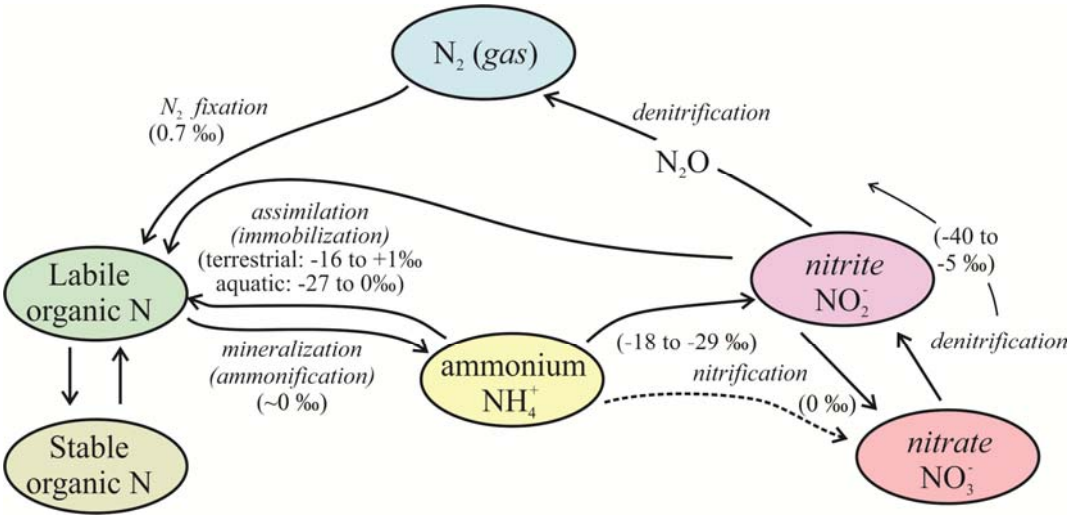

Fig. 9.1. Simplified diagram of the nitrogen cycle. Note that nitrification is generally thought of as the conversion of ammonium to nitrate, but that nitrite is an intermediate step. Likewise, denitrification is the conversion of nitrate to N_2 and/or N_2O gas, but that nitrite is an intermediate phase. Numbers in parentheses indicate average fractionations ($\delta^{15}N_{product}$ - $\delta^{15}N_{source}$) associated with each process.

chemotrophic bacteria). Nitrification is the two-step process given by a first oxidation, such as *Nitrosomonas*, $NH_4^+ \rightarrow NO_2^-$ and a second step *Nitrobacter*, $NO_2^- \rightarrow NO_3^-$. Oxygen comes from both H_2O and O_2 for this nitrification process. Nitrification is an energy-releasing process and is used by organisms as an energy source. A typical reaction sequence is (Kaplan, 1983)

$$NH_3 + 3/2\ O_2 \rightarrow HNO_2 + H_2O \qquad 9.3a$$
$$KNO_2 + ½\ O_2 \rightarrow KNO_3 \qquad 9.3b.$$

Denitrification is the process whereby NO_3^- and NO_2^- are converted to N_2O and ultimately N_2 gas by anaerobic bacteria, some fungi and aerobic bacteria. Denitrification accompanies degradation of organic matter, *e.g.* glucose,

$$5\ C_6H_{12}O_6 + 24\ NO_3^- + 24\ H^+ \rightarrow 30\ CO_2 + 42\ H_2O + 12\ N_2(g) \qquad 9.4.$$

Denitrification tends to occur in deeper layers of soil or in poorly aerated soils where $p(O_2)$ is low. In the ocean, denitrification is most active in stagnant water masses and where $p(O_2)$ is low. Correspondingly, denitrification increases with depth in the ocean. Atmospheric N_2 would be exhausted in 100 million years, if it were not for denitrification processes.

9.3 Nitrogen isotope fractionation

The nitrogen isotope fractionations attending the various processes shown in Fig. 9.1 are difficult to quantify because most of the transformations are metabolically driven and therefore kinetically controlled. They are not equilibrium reactions. As we have seen for biologically-mediated carbon reduction and will see in Chapter 10 for sulfate reduction, the magnitude (and even sign) of fractionation can be highly variable, depending upon the availability of nutrients and reaction rates. For example, nitrification, given by the multi-step transformation *organic nitrogen* $\rightarrow NH_4^+ \rightarrow NO_2^- \rightarrow NO_3^-$ may have different isotopic fractionations associated with each step, and within each step the fractionations can be variable, depending on ambient conditions. The $\delta^{15}N$ value of the product nitrate will be anywhere from -12 to -29‰ lighter than the ammonium from which it forms (Kendall, 1998).

Nitrogen isotope fractionation occurs during the transformation from the reactant to the product. The most significant fractionation effects in the low temperature nitrogen system are going to be kinetic. Following the idea for equilibrium fractionation, we can use the α terminology, recognizing that the fractionations are not equilibrium and do not follow basic thermodynamic rules. In this form, $\alpha_{p\text{-}s} = R_p/R_s$, where $R = {}^{15}N/{}^{14}N$ and p and s are the products and the substrate source of nitrogen (e.g., Kendall, 1998). Equilibrium fractionation in stable isotope geochemistry is often reported as $1000ln\alpha$, where $1000ln\alpha_{a\text{-}b}$ is very similar to $\delta_a - \delta_b$ (section 2.6). Because nitrogen isotope fractionations in nature are generally kinetically controlled, it is common to see fractionations reported using the '*enrichment factor'* notation ε, given by

$$\varepsilon = 1000\,(\alpha\text{-}1) \qquad 9.5a.$$

The use of an ε signifies that there is no suggestion of a reversible equilibrium process. Regardless of the subtleties that these different equations might convey, in practice they are the same. The ε and Δ values are almost identical (Kendall, 1998). The enrichment factor is also sometimes given by

$$\varepsilon = \left(\frac{\delta_p - \delta_r}{\delta_r + 1000}\right)1000 \qquad 9.5b,$$

where δ_p and δ_r are the delta values of the product and reactant, respectively. These two definitions of ε are not identical, but very close, except when δ_s values are very large (*e.g.*, in ^{15}N-enriched tracer experiments). ε is also nearly identical to $\delta_p - \delta_s$ or $\Delta^{15}N_{product\ -\ reactant}$. To be consistent with the rest of this book, we will use the simple difference between the δ values of the products and reactants, in which $\Delta^{15}N \approx \varepsilon$.

9.3.1 Nitrogen fixation

Nitrogen fixation is generally considered as a single process in terms of isotopic fractionation, because $\delta^{15}N$ values are measured on the product plant or bacterium, regardless of the pathway from $N_{2\ (g)}$ to organic matter. Nitrogen isotope fractionation associated with fixation is generally small. Hoering and Ford (1960) measured fractionations ($\delta^{15}N_{fixed} - \delta^{15}N_{Air}$) ranging from +3.7 to -2.2‰ (n = 4) and considered the average fractionation between atmospheric N_2 and fixed nitrogen in organic matter to be near 0‰. A compilation by Fogel and Cifuentes (1993) ranges form -3 to +1‰; one by Hübner (1986) gives an average value of -0.7 ± 1.6‰ (Fig. 9.2). The scatter does not indicate some sort of analytical error or uncertainty, but rather that real variations in fractionation for this and all other pathways exist.

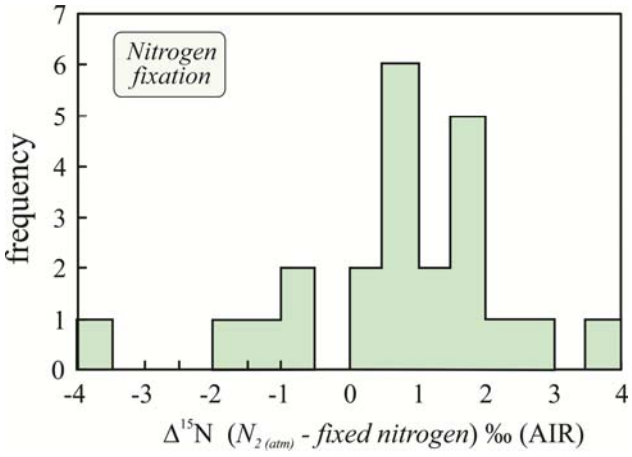

Fig. 9.2. Fractionation associated with N_2 fixation. The average value is 0.72‰ (meaning that the organisms have $\delta^{15}N$ values less than 0‰).

9.3.2 Mineralization

The fractionation associated with the breakdown of organic matter to soil ammonium is small (Δ = 0±1‰). As pointed out by Kendall (1998), mineralization is defined by some researchers as the breakdown of organic matter and conversion to nitrate. Under such circumstances, fractionations can be large and variable, but the differences are not due to the mineralization step itself, rather the nitrification of ammonium to nitrate.

9.3.3 Assimilation

Assimilation by microorganisms causes a strong and variable discrimination, favoring ^{14}N (Fig. 9.3). There is no appreciable difference between assimilation of NH_4^+, NO_2^-, and NO_3^-. Higher plants show much smaller fractionations, averaging only -0.25‰ ($\delta^{15}N_{plant} - \delta^{15}N_{assimilant}$). A compilation of data for ammonium assimilation by aquatic algae spans a very large range between -27 to 0‰ (Fogel and Cifuentes, 1993). The wide range of delta values can be modeled in terms of kinetic processes where rates are controlled by the availability of nitrogen, enzymes responsible for NH_3 fixation, and diffusion of NH_3 through the cell walls. Velinsky *et al*. (1991) found that ammonium assimilation in anoxic waters was strongly dependent on NH_4^+ concentrations. In waters with NH_4^+ concentrations of 40µM, the fractionation between particulate organic matter and NH_4^+ was modeled to be -20 to -30‰. In waters with concentrations of only 9µM, fractionations were -5 to -15‰.

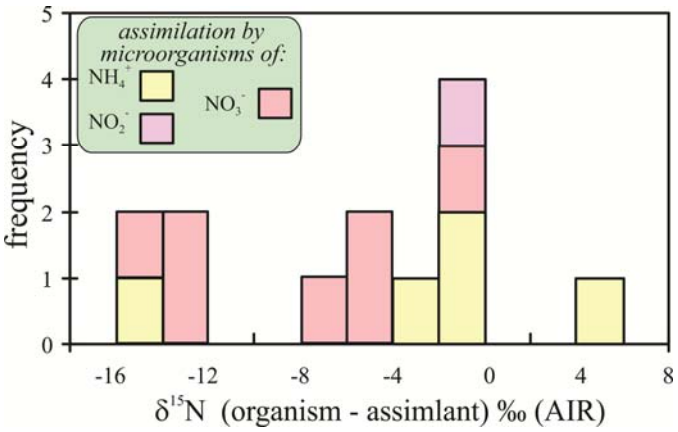

Fig. 9.3. Nitrogen isotope fractionation during assimilation by microorganisms. On the basis of limited data, the fractionation is similar regardless of whether ammonium, nitrate, or nitrite is the assimilant. Data from (Hübner, 1986).

9.3.4 Nitrification

Nitrification is a two step process from NH_4^+ through NO_2^- and finally NO_3^- (Equation 9.3). The second part of the reaction (Equation 9.3b $NO_2^- \rightarrow NO_3^-$) is quantitative, meaning all nitrite is converted to nitrate, and so there can be no nitrogen

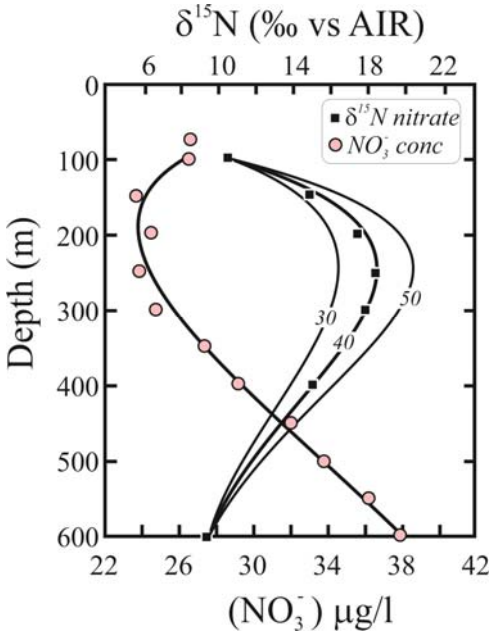

Fig. 9.4. **D**epth profile and dissolved nitrate concentration and $\delta^{15}N$ value in a depth profile from the eastern tropical North Pacific Ocean. As nitrate is converted to N_2, the nitrate concentration decreases and its $\delta^{15}N$ value increases, because the $\delta^{15}N$ value of the evolved N_2 gas is ~40‰ lighter. The data are modeled assuming $\Delta^{15}N_{NO_3\text{-}N_2}$ of 30, 40 and 50‰ as shown by curves through isotope data. After Cline and Kaplan (1975).

isotope fractionation associated with this step. Published estimates for the fractionation of ammonium to nitrite (Equation 9.3a) range from -18 to -29‰, with the nitrite (and ultimately nitrate) having lower $\delta^{15}N$ values than the ammonium precursor. The fractionation depends on the proportions of ammonium and nitrate after reaction. Obviously, if all ammonium is converted to nitrate in a 'closed system', then the $\delta^{15}N$ value of the nitrate will be identical to that of the original ammonium reservoir.

9.3.5 Denitrification

Laboratory experiments give a $\Delta^{15}N_{N_2\ gas\ -\ dissolved\ nitrate}$ value of -17 to -20‰. Measured fractionations from soil samples are often less, between -12 to -14‰ (e.g., Blackmer and Bremner, 1977). Mariotti *et al.* (1982) found the fractionation $\Delta^{15}N_{N_2O\ -\ NO_2^-}$ to range from -33‰ to -11‰. Cline and Kaplan (1975) measured the concentration and $\delta^{15}N$ values of dissolved nitrate in a water column from the eastern tropical North Pacific Ocean. They were able to model the variations in $\delta^{15}N$ values in terms of diffusion theory if the $\Delta^{15}N_{N_2\ (gas\ -\ dissolved\ nitrate)}$ value is -40‰ (Fig. 9.4).

Denitrification has large isotope fractionation effects due to the 'distillation' of N_2 gas. In shallow aquifers, N_2 gas produced by denitrification can be lost by diffusion to the atmosphere. This is a classic Rayleigh fractionation process with a large coefficient of fractionation. If a large amount of N_2 is produced, the nitrogen isotope composition of the remaining nitrate can change significantly. Figure 9.5 illustrates the magnitude of this effect. It also shows how we can use nitrogen isotopes to evaluate the amount of nitrate that has been removed from a system. In a contaminated aquifer, this obviously is an important tool for water quality studies.

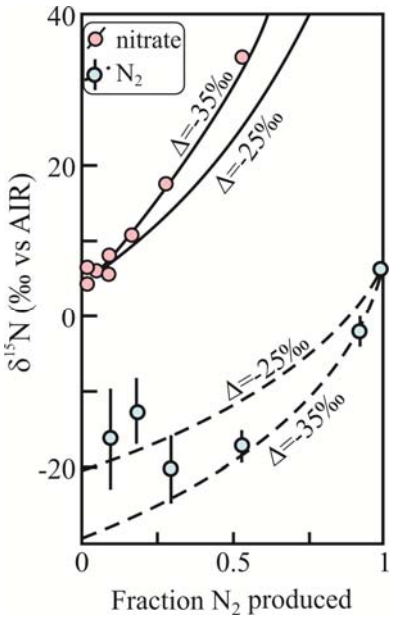

Fig. 9.5. Variations in the $\delta^{15}N$ values of dissolved nitrate and N_2 gas from water wells from the Kalahari desert. The data can be modeled by Rayleigh fractionation process, with a $\Delta^{15}N$ value between N_2 gas (product) and dissolved nitrate (reactant) of -35‰. When only a small amount of nitrate remains, its $\delta^{15}N$ value gets extremely heavy, while the sum of the N_2 approaches the original nitrate value. Solid lines are instantaneous nitrate value; dashed lines are *total* N_2 value for a given proportion of N_2 produced. After Heaton (1986).

9.4 The characteristic $\delta^{15}N$ value of various materials

Now that we have the chemistry and fractionation factors for a number of chemical transformations involving nitrogen, it should be a relatively straightforward task to make sense of the variability and range of $\delta^{15}N$ values of the different reservoirs. For example, from Figure 9.1, it is clear that the fractionation between N_2 gas and labile

organic nitrogen is close to zero. So we should expect that nitrogen-fixing plants[3] have $\delta^{15}N$ values close to zero, and indeed, this is the case. Especially when growing in nitrate-poor soil (so that the only source of nitrogen is N_2), nitrogen fixing plants have $\delta^{15}N$ values that are within 2‰ of air (Shearer and Kohl, 1986). As shown below, we can use similar logic to explain the $\delta^{15}N$ values of a number of different reservoirs.

9.4.1 Plants and soil

Nitrogen-fixing plants have $\delta^{15}N$ values close to zero. Other plants cannot fix N_2 and instead incorporate nitrogen by assimilation of NH_4^+ or NO_3^- from soil. The $\delta^{15}N$ values of plants are strongly dependent on those of the soil, which are in part controlled by the plants. In order to predict the $\delta^{15}N$ value of plants it is necessary to know the range of $\delta^{15}N$ values of soil *and* the mechanisms of uptake from the soil. $\delta^{15}N$ values of soil range from -10 to +15‰, with most soils between +2 and +5‰ (Kendall, 1998). The positive values are loosely tied to a preferential loss of ^{14}N during decomposition of particulate nitrogen sources. Unfortunately, specific factors controlling soil $\delta^{15}N$ values are complex and defy quantification. Even the source of extracted nitrogen are variable: tree roots preferentially assimilate soil nitrate while microorganisms tend to incorporate soil ammonium (Nadelhoffer and Fry, 1988). Nevertheless, some general guidelines can be established.

- Denitrification is most intense in poorly drained or poorly oxidized soils, as nitrate-consuming organisms become active only when oxygen levels are low. The subsequent loss of N_2 gas – the product of denitrification – increases the $\delta^{15}N$ value of any remaining nitrate (Fig. 9.5).
- Soils with abundant leaf litter tend to have lower $\delta^{15}N$ values than in surrounding regions with less foliage. An explanation for this trend is that the preferential uptake of ^{14}N by plants results in higher $\delta^{15}N$ values of the soil. In heavily vegetated areas, the ^{15}N-depleted plant material is returned to the soil as leaf litter.
- Anthropogenic activity can strongly affect the $\delta^{15}N$ of soil. In one study, the average $\delta^{15}N$ value of cultivated soils are 5.0±3.5‰ compared to 6.8±6.4‰ for uncultivated soils, due to addition of nitrogenous fertilizers with low $\delta^{15}N$ values (Hübner, 1986). In some soils, there are variations with depth, while in others, no such correlation is found. Factors include drainage, total N-content of soil and precipitation rate.

In nitrogen-limited soils, the $\delta^{15}N$ value of plants is close to that of the soils, as no discrimination is possible. In nutrient-rich soils, the fractionation between plants and dissolved inorganic nitrogen can be several per mil. Trees tend to have slightly lower $\delta^{15}N$ values than soil due to the negative fractionation during assimilation. Heterotrophic fungi, on the other hand, may have $\delta^{15}N$ values higher than those of the soil (Högberg, 1997). Overall, tree leaves have a range of $\delta^{15}N$ values of -8 to +3‰ (Peterson and Fry, 1987). There is a strong global-scale variation in the $\delta^{15}N$ values of soils that is related to the mean annual precipitation and mean annual temperature (Fig. 2 in Amundson et al.,

[3] Nitrogen fixing plants are those that are able to assimilate N_2 gas directly. In fact, nitrogen fixation is a symbiotic relationship with bacteria that live on the roots, but the isotopic effect is the same, nevertheless.

2003), although the trends cannot be explained in terms of only a few simple processes.

9.4.2 Other terrestrial reservoirs

- *Fertilizers*

Fertilizers generally have a $\delta^{15}N$ range of -4 to +4‰, the low values related to an atmospheric N_2 source. Organic fertilizers range from +6 to +30‰, related to the processes occurring in animal wastes (Kendall, 1998). The $\delta^{15}N$ value of animals increases by ~3‰ at each higher trophic level (see section 9.5). The most important factor for this increase is the excretion of isotopically light urine. Therefore, there is an enrichment in ^{15}N from plants to animals. Animal waste gets further enriched in ^{15}N by subsequent volatilization of isotopically light ammonia.

- *Rain*

The sources of nitrogen in rain are volatilization of ammonia, nitrification and denitrification of soils and anthropogenic sources. Hoering first measured the $\delta^{15}N$ values of NH_4^+ and NO_3^- in rain from the roof of the chemistry laboratory at the University of Arkansas, USA (Hoering, 1957). He found that, although there was significant variability in the $\delta^{15}N$ value of each component ($\delta^{15}N$ NH_4^+ = -0.1 to 9.0‰; $\delta^{15}N$ NO_3^- = -7.2 to +3.4), the fractionation between the two phases could be explained in terms of a kinetic fractionation between ammonium and nitrate. The range of $\delta^{15}N$ values of nitrate in rain has since been found to cover a range of ~ -10 to +9‰. Heaton (1986) gives an average of -5‰ (for South Africa) while a compilation by Kendall (1998) ranges from ~-3 to +9‰, with a strong mode at 0 to +2‰. In general, ammonium is lighter than nitrate by several per mil. The measured fractionation between NH_4^+ and NO_3^- in rain is dependent on the concentrations of the ions in precipitation. Variations from site to site are huge, because inputs can be so different. Pure air has $\delta^{15}N$ values of NH_3 and NO_2 of -10.0 ± 2.6‰ and -9.3 ± 3.5‰, respectively (Hübner, 1986). The effects of mixing different reservoirs are clear when just a few 'endmember' sources are considered. Barnyard-derived NH_3 has a $\delta^{15}N$ value of +25‰, NO_x from automobile exhaust is ~ +3.7‰, and fumaroles from southern Kamchatka have $\delta^{15}N$ values of $(NH_4)_2SO_4$ as low as -31‰ (Hübner, 1986). Freyer (1978) measured $\delta^{15}N$ values of NH_4^+ in rain water of -12.0 ± 1.9‰ from Jülich Germany. Published values of NH_4^+ in rain water range from -9.7 to +6.9. Not surprisingly, variations can be large between storms and even within individual storms, because the sources of nitrogen – fossil-fuel burning, ocean denitrification, etc. – themselves have a large range of $\delta^{15}N$ values. Peterson and Fry's average estimate (1987) for precipitation are -18 to +8‰ for NH_4^+ and -15 to +3‰ for NO_3^-.

- *Fossil fuels*

Peat and coal average +0.8‰ with a standard deviation of 1.6‰, ranging up to 6.3‰ (Hoering, 1955; Wada et al., 1975; Stiehl and Lehmann, 1980), similar to modern peats and bogs. Crude oils are generally in the range of +1.0 to +6.7‰, while natural gas

has far more variation (-10.5 to 14.4‰) (Hoering and Moore, 1958). The $\delta^{15}N$ value of natural gas changes quite drastically with the distance of migration from its source. An example from north Germany shows a systematic increase from -8.7 to +18.0‰ as migration distances increase, likely due to Rayleigh fractionation attending denitrification (Stahl, 1977).

9.4.3 Nitrogen in the oceans

The fact that the $\delta^{15}N$ values of most ocean materials are positive is easily explained in terms of the nitrogen cycle in the ocean. Nitrogen is one of the most important limiting nutrients in the ocean, so that productivity is limited by availability of metabolically available nitrogen[4]. The major inputs are river runoff, rain and fixation of molecular N_2 by marine blue-green algae (Fig. 9.6). Outputs or sinks of nitrogen in the ocean include burial in sediment and denitrification. We assume that the nitrogen cycle is balanced, with inputs equaling outputs, but how variable this is over time is not known. The fluxes of each exchange path are shown in Fig. 9.6. It is clear that the average values are not known well enough to quantify. Even more intractable is an attempt to quantify isotopic mass balance because the $\delta^{15}N$ values of each source are quite variable, as are the fractionations accompanying transfer from one reservoir to another.

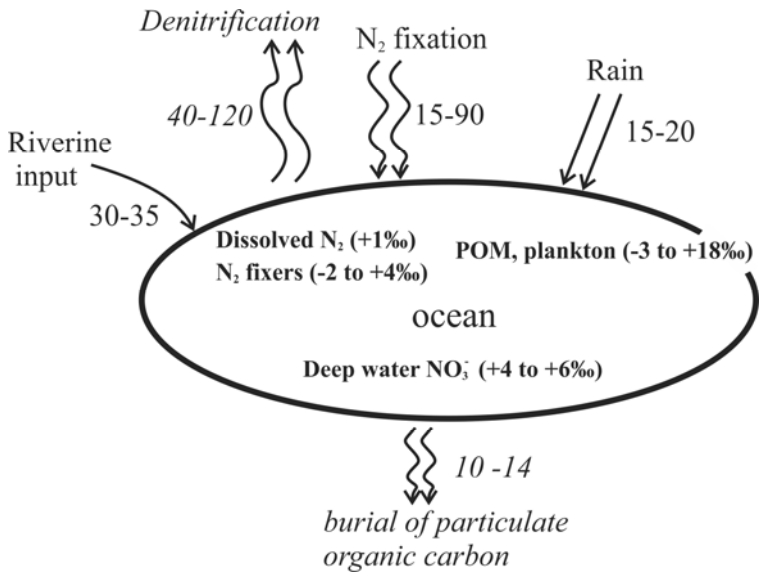

Fig. 9.6. Nitrogen system for the oceans. Sources and sinks (and their fluxes in 10^{12} gm-N_2/yr) are shown as normal and italicized text, respectively. $\delta^{15}N$ values of ocean materials are in bold text. Data from following sources: (Kaplan, 1983; Macko et al., 1984; Berner and Berner, 1987; Peterson and Fry, 1987; Fogel and Cifuentes, 1993).

[4] Nitrogen and phosphorus are strongly correlated with a nitrogen/phosphate ratio of ~15. Both nutrients become exhausted at the same time. The constant ratio is probably tied to a biochemical feedback mechanism. If dissolved nitrate levels become low, nitrogen-fixing blue green algae will produce nitrate, restoring the biochemical ratio. If nitrate values become high, non-nitrifying organisms would have an advantage, consuming nitrate disproportionately, again driving the ratio back to its balanced state.

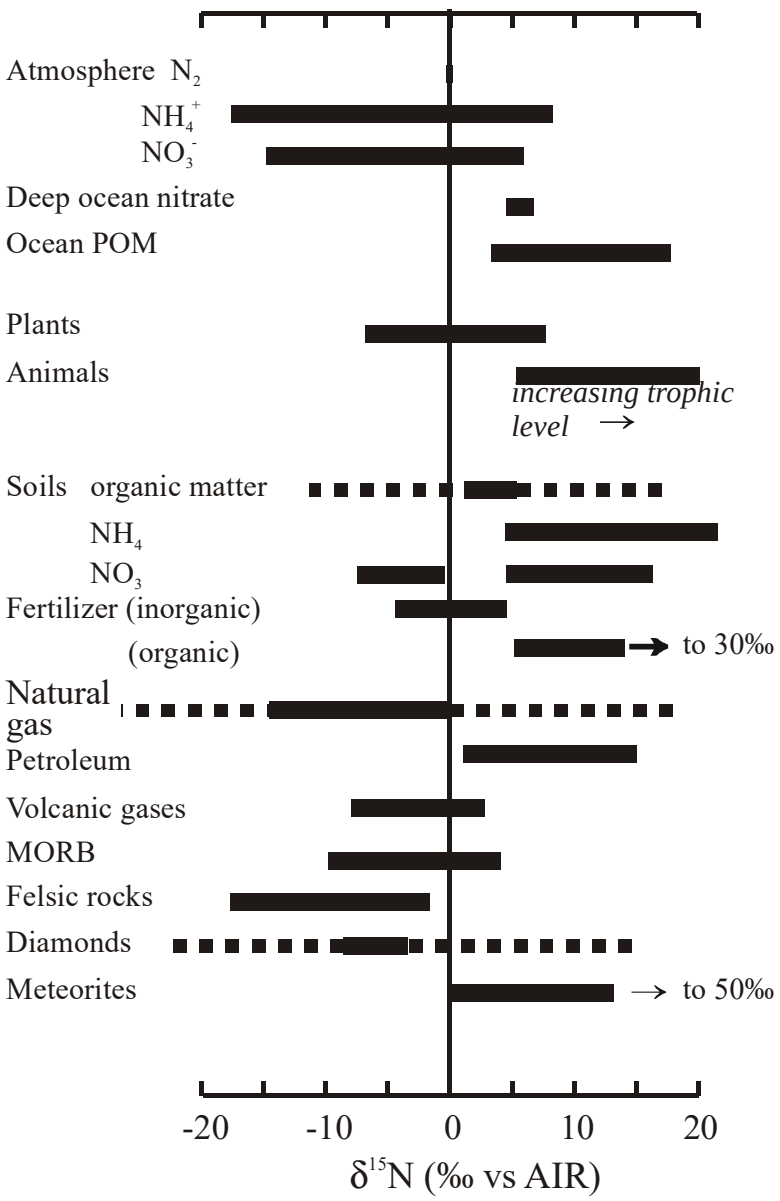

Fig. 9.7. Average $\delta^{15}N$ values for common reservoirs.

In spite of the uncertainties, several gross features are apparent. The major fractionation in the global ocean cycle occurs during denitrification, with N_2 being strongly depleted in ^{15}N relative to its source. All other sources and sinks are associated with rather small fractionation effects (see Fig. 9.1). Clearly loss of light N_2 back to the atmosphere will result in a positive average $\delta^{15}N$ value of the ocean. The positive $\delta^{15}N$ value of organic material in sediments is retained during subduction, seen both in rocks (Bebout and Fogel, 1992) and volcanic fumaroles sourced in oceanic sediments (Fischer et al., 2002).

There is significant spatial variation in the $\delta^{15}N$ value of dissolved nitrate. In the Eastern North Pacific Ocean, $\delta^{15}N$ values range from +6.5‰ in the Antarctic

intermediate water mass (at depth), up to +18.8‰ in the active denitrification zone (Cline and Kaplan, 1975).

Overall, average $\delta^{15}N$ values of various reservoirs are shown in Fig. 9.7. These data are a compilation from many sources. There are always unusual samples that have higher or lower values (Coplen et al., 2002), but the figure should serve as a guide for average ranges that are commonly found for each material.

9.5 Nitrogen isotope ratios in animals

The $\delta^{15}N$ values of animals are related to their diet (DeNiro and Epstein, 1981). The $\delta^{15}N$ value of an animal is generally heavier than the food it eats, and the $\delta^{15}N$ values increase by 3-4‰ for each successive trophic level[5]. Stable nitrogen isotope ratios are therefore an important ecological tool for quantifying trophic position and for reconstructing dietary preferences.

Not all tissues in a body have the same $\delta^{15}N$ value. Milk, blood and muscle tend to have $\delta^{15}N$ values 1-3‰ heavier than the diet, while urinary urea and bile have $\delta^{15}N$ values that are 2 to 4‰ more negative than the diet (Ambrose, 1991). The loss of ^{15}N-depleted urine is probably the primary cause for the elevated overall $\delta^{15}N$ value of animals relative to their diet, although it has been shown that there can be preferential uptake of ^{15}N relative to diet. At each successive trophic level, the $\delta^{15}N$ value of the food source increases, hence the animals' $\delta^{15}N$ values follow suit. The effect is most regular and intense for marine communities. As seen in Figure 9.8, there is a regular increase of ~3‰ per trophic level. The effect on terrestrial communities is not as large and is more variable, controlled by numerous factors. For example, several authors have found that there is a correlation in the $\delta^{15}N$ value of animals and the relative annual rainfall (Sealy et al., 1987). It appears that animals that are more water-stressed excrete a concentrated urine with higher $\delta^{15}N$ values.

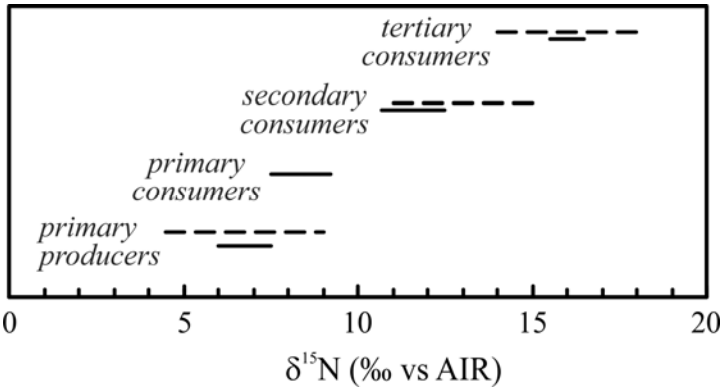

Fig 9.8. Nitrogen isotope compositions of marine plants and animals as a function of trophic level. There is a regular increase of approximately 3‰ per trophic level. Data from (Minagawa and Wada, 1984 (solid); Schoeninger and DeNiro, 1984 (dashed)).

The physiology of an organism has a large effect on its $\delta^{15}N$ value, especially the biochemical form of nitrogenous waste (Vanderklift and Ponsard, 2003). The fractionation between an organism and excreted urea is larger than the fractionation between an organism of excreted ammonia. Therefore, it is reasonable to assume, and

[5] A group of organisms that occupy the same position in a food chain. Each successive trophic level consumes the one below it. Hence: trophic level 1- autotrophs (*e.g.*, plants); trophic level 2 – herbivores; trophic level 3 – carnivores, etc.

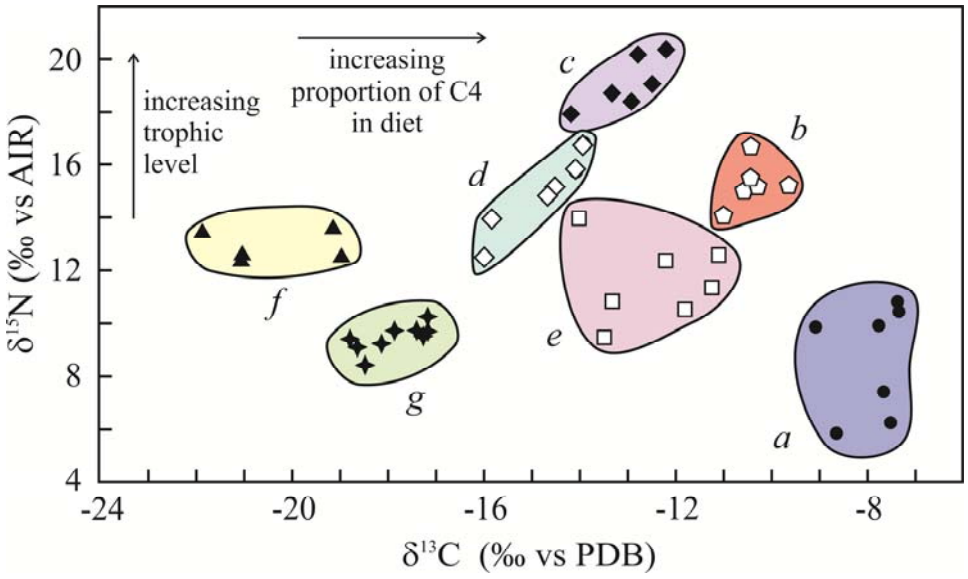

Fig. 9.9. $\delta^{13}C$ and $\delta^{15}N$ values of bone collagen from Native American communities.
a) Western Anasazi, S. Utah (A.D. 1 - 1300)
b) Nantucket Island, Mass. (A.D. 1000 - 1600)
c) N.W. coast Haida and Tlingit salmon fishers (historic)
d) S. California coastal (A.D. 1400 - 1800)
e) Plains Arikara, South Dakota (A.D. 1650 - 1733)
f) S. Ontario, Middle Woodland period (A.D. 1 - 400)
g) Modern Chicago, USA.
See text for details. Compilation and references from Martin (1999) and Schoeller *et al.* (1986).

supported by measurements of natural samples, that urea-excreting organisms have a larger trophic level effect than those which primarily excrete ammonia.

The combination of $\delta^{15}N$ and $\delta^{13}C$ values have been used in well over 100 publications to investigate trophic ecology of birds and mammals (Kelly, 2000). Combined $\delta^{15}N$-$\delta^{13}C$ values from prehistoric bone collagen are a valuable tool for distinguishing different populations and constraining a communities' diet. To a first degree, we can state that the $\delta^{15}N$ values are controlled by the trophic level of diet and the $\delta^{13}C$ values are controlled by the relative dietary proportions of C_3 and C_4 plants. Communities subsisting mainly on an animal diet will inherit the $\delta^{13}C$ value of their prey, perhaps with a subtle offset towards higher values (DeNiro and Epstein, 1978).

Figure 9.9 shows a compilation for a number of North American Native American communities. The combined carbon and nitrogen isotope values are easily explained in terms of assumed diet, and place constraints on diet in cases where ambiguities exist. For example, the Western Anasazi have the lowest $\delta^{15}N$ values and highest $\delta^{13}C$ values. It can be concluded that they had a maize-based diet[6] with only minor animal consumption (Martin, 1999). The Southern Ontario communities (Schwarcz et al., 1985) had a diet consisting of C_3 plants and animals that consumed C_3 plants. The elevated $\delta^{15}N$ values relative to the Anasazi community indicate at least a partial animal diet. The highest $\delta^{15}N$

[6] Maize is a C_4 plant. See Chapter 7 for a more thorough discussion of C_3-C_4 plants.

values are found in the Northwest coastal communities that consisted in large part on salmon (Schoeninger and Moore, 1992). Salmon are at a high trophic level, and this is reflected in the isotope data of the salmon-eating community.

The effect of trophic level on the $\delta^{15}N$ values of animals has been used for a large number of studies addressing different questions. The breadth of this field is illustrated in a study by Fogel *et al.* (1997) where the recognition that a nursing infant is technically at a higher trophic level than her mother was used to determine the duration of nursing by

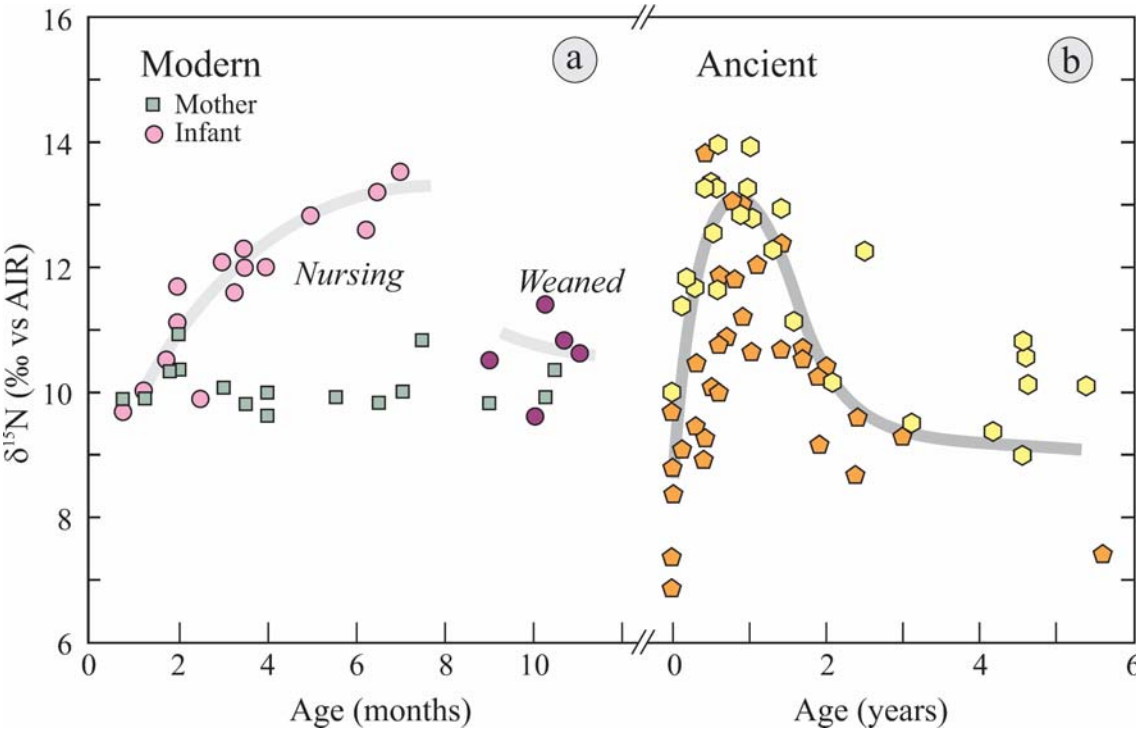

Fig. 9.10. a: $\delta^{15}N$ value of nursing mother and infant. Infant reaches a 3‰ higher $\delta^{15}N$ value, which disappears after weaning. **b:** Native American infants from pre- and post-historic sites, USA. Note different x-axis. After Fogel *et al.* (1997).

prehistoric people. Fig. 9.10a shows the $\delta^{15}N$ values of the fingernails of a mother and her infant from birth through weaning. The $\delta^{15}N$ value of the infant rises after birth to a value ~3‰ higher than the mother. Once the child is weaned, the diet of the two individuals is more-or-less the same, and the higher $\delta^{15}N$ value of the infant is soon lost. This concept was then used for two ancient populations, where the $\delta^{15}N$ values of individuals were measured as a function of age (Fig. 9.10b). In both populations, weaning occurs between one and two years.

9.5.1 Compound specific studies

The isotopic variations seen in individual amino acids are far larger and provide significantly more information than data from bulk samples alone. For example, some amino acids, such as glutamic acid, show an 8‰ increase in $\delta^{15}N$ value with each higher trophic level. In contrast, phenylalanine shown only a 0.4‰ increase with each trophic level (Chikaraishi et al., 2014). This is because the transamination/deamination processes

of glutamic acid always result in cleaving of the carbon-nitrogen bonds, whereas phenylalanine is converted to tyrosine without cleaving of these bonds. The result is that glutamic acid records the increase in $\delta^{15}N$ values of the host (fractionation), whereas, the $\delta^{15}N$ value of phenylalanine cannot change as it moves up into higher trophic levels. The effect is clearly seen in Fig. 9.11. Two food webs were studied: one marine and the other terrestrial. The marine food web has a constant $\delta^{15}N$ value for phenylalanine and a regular increase in the $\delta^{15}N$ of glutamic acid with increasing trophic level. The terrestrial foodweb has a 1-1 correlation between phenylalanine and glutamic acid for each trophic level and a distinct jump to higher glutamic acid values as trophic levels increase. The marine samples suggest a linear food chain with each successive trophic level having essentially identical $\delta^{15}N_{phenylalanine}$ values, whereas the large range of $\delta^{15}N_{phenylalanine}$ values in the terrestrial foodweb suggest that individual species within a given trophic level exploit specific and different food resources (Chikaraishi et al., 2014). The overall $\delta^{15}N$ values of an organism are the sum of all nitrogen-bearing compounds, whereas different amino acids single out processes that are unique to their different chemical behavior during metabolism.

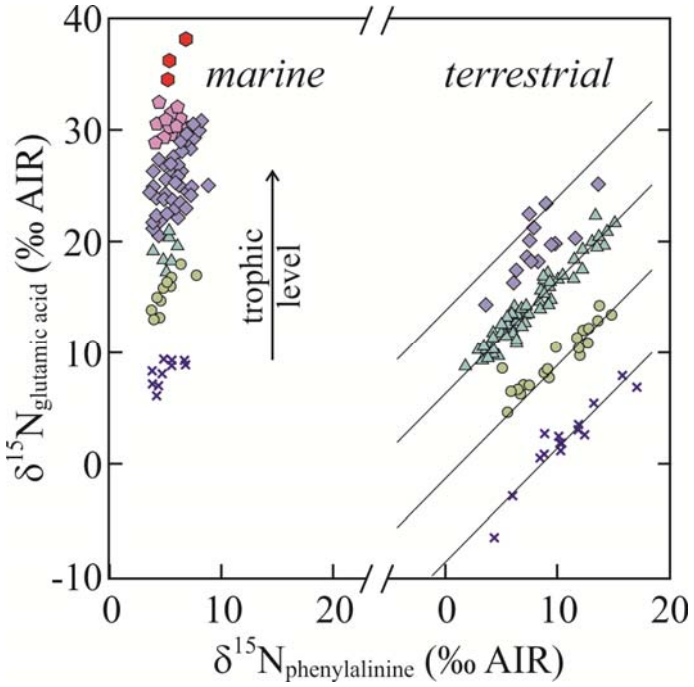

Fig. 9.11. Crossplot of the $\delta^{15}N$ values of isolated amino acids phenylalanine and glutamic acid from a marine (left) and terrestrial (right) food web. The $\delta^{15}N$ values of each food web show an ~8‰ jump with trophic level (from crosses to circles to triangles, squares, etc.). The marine food web has a constant phenylalanine value suggesting a linear and common food chain, whereas individuals in the terrestrial food web have distinct phenylalanine values indicative of distinct food sources at each successive trophic level. After Chikaraishi *et al.* (2014).

References

Ambrose, S.H. (1991) Effects of diet, climate and physiology on nitrogen isotope abundances in terrestrial foodwebs. *Biological Abstracts Vol. 91, Iss. 2, Ref. 20363.* **18**, 293-317.

Amundson, R., Austin, A.T., Schuur, E.A.G., Yoo, K., Matzek, V., Kendall, C., Uebersax, A., Brenner, D. and Baisden, W.T. (2003) Global patterns of the isotopic composition of soil and plant nitrogen. *Biological Abstracts Vol. 95, Iss. 3, Ref. 30880.* **17**, doi:10.1029/2002GB00190.

Beaumont, V. and Robert, F. (1999) Nitrogen isotope ratios of kerogens in Precambrian cherts: a record of the evolution of atmosphere chemistry? *Precambrian Research* **96**, 63-82.

Bebout, G.E. and Fogel, M.L. (1992) Nitrogen-isotope compositions of metasedimentary rocks in the Catalina Schist, California: Implications for metamorphic devolatilization history. *Geochimica et Cosmochimica Acta* **56**, 2839-2849.

Bebout, G.E., Idleman, B.D., Li, L. and Hilkert, A. (2007) Isotope-ratio-monitoring gas chromatography methods for high-precision isotopic analysis of nanomole quantities of silicate nitrogen. *Chemical Geology* **240**, 1-10.

Berner, E.K. and Berner, R.A. (1987) The Global Water Cycle. Prentice-Hall, Inc., Englewood Cliffs, NJ.

Blackmer, A.M. and Bremner, J.M. (1977) N-isotope discrimination in denitrification of nitrate in soils. *Soil Biology & Biochemistry* **9**, 73-77.

Chikaraishi, Y., Steffan, S.A., Ogawa, N.O., Ishikawa, N.F., Sasaki, Y., Tsuchiya, M. and Ohkouchi, N. (2014) High-resolution food webs based on nitrogen isotopic composition of amino acids. *Ecology and Evolution* **4**, 2423-2449.

Cline, J.D. and Kaplan, I.R. (1975) Isotopic fractionation of dissolved nitrate during denitrification in the eastern tropical North Pacific Ocean. *Marine Chemistry* **3**, 271-299.

Coplen, T.B., Hopple, J.A., Böhlke, J.K., Peiser, H.S., Rieder, S.E., Krouse, H.R., Rosman, K.J.R., Ding, T., Vocke, R.D.J., Révész, K.M., Lamberty, A., Taylor, P. and DeBièvre, P. (2002) Compilation of Minimum and Maximum Isotope Ratios of Selected Elements in Naturally Occurring Terrestrial Materials and Reagents. United States Geological Survey, Reston, p. 98.

Coplen, T.B., Bohlke, J.K. and Casciotti, K.L. (2004) Using dual-bacterial denitrification to improve $\delta^{15}N$ determinations of nitrates containing mass-independent ^{17}O. *Rapid Communications in Mass Spectrometry* **18**, 245-250.

DeNiro, M.J. and Epstein, S. (1978) Influence of diet on the distribution of carbon isotopes in animals. *Geochimica et Cosmochimica Acta.* **42**, 495-506.

DeNiro, M.J. and Epstein, S. (1981) Influence of diet on the distribution of nitrogen isotopes in animals. *Geochimica et Cosmochimica Acta* **45**, 341-351.

Fischer, T.P., Hilton, D.R., Zimmer, M.M., Shaw, A.M., Sharp, Z.D. and Walker, J.A. (2002) Contrasting nitrogen isotope behavior along the Central America margin: implications for the nitrogen balance of the Earth. *Science* **297**, 1154-1157.

Fogel, M.L. and Cifuentes, L.A. (1993) Isotope fractionation during primary production, in: Engel, M.H., Macko, S.A. (Eds.), Organic Geochemistry. Plenum Press, New

York, pp. 73-98.
Fogel, M.L., Tuross, N., Johnson, B.J. and Miller, G.H. (1997) Biogeochemical record of ancient humans. *Organic Geochemistry* **27**, 275-287.
Freyer, H.D. (1978) Seasonal trends in NH_4^+ and NO_3^- nitrogen isotope composition in rain collected at Jülich, Germany. *Tellus* **30**, 83-92.
Heaton, T.H.E. (1986) Isotopic studies of nitrogen pollution in the hydrosphere and atmosphere; a review. *Chemical Geology* **59**, 87-102.
Hoering, T. (1957) The isotopic composition of the ammonia and the nitrate ion in rain. *Geochimica et Cosmochimica Acta* **12**, 97-102.
Hoering, T.C. (1955) Variations in N-15 abundance in naturally occurring substances. *Science* **122**, 1233-1234.
Hoering, T.C. and Moore, H.E. (1958) The isotopic composition of the nitrogen in natural gases and associated crude oils. *Geochimica et Cosmochimica Acta* **13**, 225-232.
Hoering, T.C. and Ford, T.H. (1960) The isotope effect in the fixation of nitrogen by Azotobacter. *Journal of the American Chemical Society* **82**, 376-378.
Högberg, P. (1997) ^{15}N natural abundance in soil-plant systems. *New Phytologist* **137**, 179-203.
Hübner, H. (1986) Isotope effects of nitrogen in the soil and biosphere, in: Fritz, P., Fontes, J.C. (Eds.), Handbook of Environmental Isotope Geochemistry. Elsevier, Amsterdam, pp. 361-425.
Kaplan, I.R. (1983) Stable isotopes of sulfur, nitrogen and deuterium in Recent marine environments, in: Arthur, M.A., Anderson, T.F., Kaplan, I.R., Veizer, J., Land, L.S. (Eds.), Stable Isotopes in Sedimentary Geology. SEMP Short course, Columbia, pp. 2-1 - 2-108.
Kelly, J.F. (2000) Stable isotopes of carbon and nitrogen in the study of avian and mammalian trophic ecology. *Canadian Journal of Zoology* **78**, 1-27.
Kendall, C. (1998) Tracing nitrogen sources and cycling in catchments, in: Kendall, C., McDonnell, J.J. (Eds.), Isotope Tracers in Catchment Hydrology. Elsevier, Amsterdam, pp. 519-576.
Macko, S.A., Entzeroth, L. and Parker, P.L. (1984) Regional differences in nitrogen and carbon isotopes on the continental shelf of the Gulf of Mexico. *Naturwisenschaften* **71**, 374-375.
Mariotti, A., Germon, J.C., Leclerc, A., Catroux, G. and Létolle, R. (1982) Experimental determination of kinetic isotope fractionation of nitrogen isotopes during denitrification, in: Schmidt, H.-L., Förstel, H., Heinzinger, K. (Eds.), Stable Isotopes, Proceedings of the 4th International Conference. Elsevier, Jülich, pp. 459-464.
Martin, S.L. (1999) Virgin Anasazi diet as demonstrated through the analysis of stable carbon and nitrogen isotopes. *Kiva* **64**, 495-513.
Marty, B. and Dauphas, N. (2003) The nitrogen record of crust-mantle interaction and mantle convection from Archean to Present. *Earth and Planetary Science Letters* **206**, 397-410.
McDonough, W.F. and Sun, S.-s. (1995) The composition of the Earth. *Chemical Geology* **120**, 223-253.
Minagawa, M. and Wada, E. (1984) Stepwise enrichment of ^{15}N along the food chains:

Further evidence and the relation between $\delta^{15}N$ and animal age. *Geochimica et Cosmochimica Acta* **48**, 1135-1140.

Nadelhoffer, K.J. and Fry, B. (1988) Controls on natural nitrogen-15 and carbon-13 abundances in forest soil organic matter. *Soil Science Society of America Journal* **52**, 1633-1640.

Peterson, B.J. and Fry, B. (1987) Stable isotopes in ecosystem studies. *Annual Review of Ecology and Systematics* **18**, 293-320.

Schoeller, D.A., Minagawa, M., Slater, R. and Kaplan, I.R. (1986) Stable isotopes of carbon, nitrogen and hydrogen in the contemporary North American human food web. *Ecology of Food and Nutrition* **18**, 159-170.

Schoeninger, M.J. and DeNiro, M.J. (1984) Nitrogen and carbon isotopic composition of bone collagen from marine and terrestrial animals. *Geochimica et Cosmochimica Acta* **48**, 625-639.

Schoeninger, M.J. and Moore, K. (1992) Bone stable isotope studies in Archaeology. *Journal of World Prehistory* **6**, 247-296.

Schwarcz, H.P., Melbye, J., Katzenberg, M.A. and Knyf, M. (1985) Stable isotopes in human skeletons of southern Ontario; reconstructing palaeodiet. *Biological Abstracts Vol. 91, Iss. 2, Ref. 20363.* **12**, 187-206.

Sealy, J.C., Van Der Merwe, N.J., Thorp, J.A.L. and Lanham, J.L. (1987) Nitrogen isotopic ecology in southern Africa: Implications for environmental and dietary tracing. *Geochimica et Cosmochimica Acta* **51**, 2707-2718.

Shearer, G. and Kohl, D.H. (1986) N_2-fixation in field settings: Estimations based on natural ^{15}N abundance. *Australian Journal of Plant Physiology* **13**, 699-757.

Sigman, D.M., Casciotti, K.L., Andreani, M., Barford, C., Galanter, M. and Bohlke, J.K. (2001) A bacterial method for the nitrogen isotopic analysis of nitrate in seawater and freshwater. *Analytical Chemistry* **73**, 4145-4153.

Stahl, W.J. (1977) Carbon and nitrogen isotopes in hydrocarbon research and exploration. *Chemical Geology* **20**, 121-149.

Stiehl, G. and Lehmann, M. (1980) Isotopenvariationen des Stickstoffs humoser und bituminöser natürlicher organischer Substanzen. *Geochimica et Cosmochimica Acta* **44**, 1737-1746.

Vanderklift, M.A. and Ponsard, S. (2003) Sources of variation in consumer-diet $\delta^{15}N$ enrichment: a meta-analysis. *Oecologia* **136**, 169-182.

Velinsky, D.J., Fogel, M.L., Todd, J.F. and Tebo, B.M. (1991) Isotopic fractionation of dissolved ammonium at the oxygen-hydrogen sulfide interface in anoxic waters. *Geophysical Research Letters* **18**, 649-652.

Wada, E., Kadonaga, T. and Matsuo, S. (1975) ^{15}N abundance in nitrogen of naturally occurring substances and global assessment of denitrification from isotopic viewpoint. *Geochemical Journal* **9**, 139-148.

Chapter 10

SULFUR

Contents

10.1 Introduction 1
10.2 Analytical techniques 2
10.3 Equilibrium fractionation and geothermometry 4
10.4 Sulfate and sulfide formation at low temperature – the sedimentary sulfur cycle 7
10.4.1 Sulfate incorporation in sediments 8
10.4.2 Sulfide incorporation in sediments 8
10.5 Secular variations in sulfur 10
10.5.1 Long term variations 10
10.5.2 Alternative approaches – barite and trace carbonates 11
10.5.3 Time boundaries 13
10.5.4 Archean sulfates – clues to early atmosphere 13
10.5.5 Sulfur isotope anomalies – mass-independent fractionation 14
10.6 Sulfur isotope ratios in the terrestrial environment 15
10.7 Oxygen isotope variations in sulfates 16
References 18

Chapter 10

SULFUR

10.1 Introduction

Sulfur isotope (bio)geochemistry has broad applications to geological, biological and environmental studies. Sulfur is an important constituent of Earth's lithosphere, biosphere, hydrosphere and atmosphere and occurs as a major constituent in evaporites and ore deposits. Many of the characteristics of sulfur isotope geochemistry are analogous to those of nitrogen and especially carbon, because all three elements occur in reduced and oxidized forms[1], and undergo oxidation state changes as a result of biological processes.

There are four stable isotopes of sulfur (Table 10.1), and of course there are a number of isotope ratios that can be measured, including $^{33}S/^{32}S$, $^{34}S/^{32}S$, $^{36}S/^{32}S$, etc. However for most terrestrial samples, fractionations are mass dependent, resulting in simple covariance between these ratios (section 3.7). Measuring multiple isotope ratios provides no additional information over simply measuring any one – the relative ratios vary in constant proportions in both terrestrial and extraterrestrial samples. That said, important anomalies in $^{33}S/^{32}S$ and $^{36}S/^{32}S$ ratios from the predicted mass fractionation rules have been found in meteorites, ancient sulfate and some modern deposits (section 10.5.5). In general however, there is no need to analyze more than any two of the four stable isotopes of sulfur, the others being easily computed from simple relationships. The isotopes that are commonly measured are ^{34}S and ^{32}S, simply because these are the two most abundant of the four. All $\delta^{34}S$ values are reported relative to the CDT standard, or Cañon Diablo Troilite (Ault and Jensen, 1963) by the standard equation defining delta:

$$\delta^{34}S_{\text{sample}} = \left(\frac{(R)_{Sample}}{(R)_{CDT}} - 1 \right) \times 1000 \qquad 10.1,$$

where $R = {}^{34}S/{}^{32}S$ ratio. Cañon Diablo is the meteorite found at Meteor Crater, Arizona, USA. The isotopic composition of troilite[2] in iron meteorites has a very restricted range from 0.0 to 0.6‰ (Kaplan and Hulston, 1966), and is similar to that of the bulk Earth, making it an ideal reference material. However, high spatial resolution analyses of CDT have shown it to be slightly heterogeneous (Beaudoin et al., 1994). Secondary synthetic argentite (Ag_2S) and other sulfur-bearing standards have since been developed, with $\delta^{34}S$ values defined relative to the accepted CTD value of 0‰ (Appendix 1). The primary reference is IAEA-S-1, a synthetic silver sulfide with a $\delta^{34}S$ value of -0.3‰ relative to CDT (Cañon Diablo Troilite) (Robinson, 1995). Secondary standards with high and low $\delta^{34}S$ values have been synthesized so that both the absolute value on the CDT scale and laboratory-based corrections related to the 'stretching factor' can be determined.

---

[1] The valence of sulfur ranges from -2 to +6. In natural, inorganic compounds, intermediate valence compounds are generally not stable.

[2] Troilite is a sulfide with the mineral composition FeS. It differs from the common pyrrhotite with an approximate composition of Fe_7S_8 in that it is stoichiometric. Troilite is not found in terrestrial materials.

Table 10.1. *Abundance and mass (amu) of the different isotopes of sulfur (Coplen et al., 2002). Quantity in brackets represents uncertainty in the last two decimal places.*

Isotope	Abundance	Mass
^{32}S	95.03957(90)	31.97207
^{33}S	0.74865(12)	32.97146
^{34}S	4.19719(87)	33.96786
^{36}S	0.01459(21)	35.96708

10.2 Analytical techniques

A discussion of the analytical procedures for measure sulfur isotope ratios is necessary, because different isotope ratios may be obtained using different methods. This apparently serious problem is reduced by analyzing samples and internationally accepted standards using the same methods. A correction procedure can then be applied (see Appendix 2 for a sample calculation) to bring measured data into agreement with the officially recognized scale.

Part of the reason that sulfur has been the 'outcast' isotope are the problems associated with making mass spectrometric determinations. Two gases – SO_2 and SF_6 – have been used for sulfur isotope determinations. Both have advantages and disadvantages. SO_2 is easily produced and easily analyzed on most mass spectrometers. However it is a highly polar molecule, making it 'sticky' in the source of a mass spectrometer, and this results in a 'memory' between samples. The problem is compounded when trace amounts of water are in the vacuum line, leading to the formation of sulfuric acid, a non-volatile, corrosive acid. Extra-special care must be taken to keep the mass spectrometer clean, including heating the source and frequent cleaning. As a result, many laboratories have been reluctant to put SO_2 into their mass spectrometers. Those that make routine measurements of SO_2 often have a dedicated SO_2 mass spectrometer, or configure their mass spectrometer for SO_2 analysis for a block of time, followed by a thorough cleaning. The development of the continuous flow technique for SO_2 has changed the playing field somewhat (Giesemann et al., 1994). Only a very small amount of SO_2 enters the mass spectrometer, and the continuous He-stream keeps the source clean. In addition, analyses are very rapid and can be made on a small amount of material.

The second problem with SO_2 measurements is that there is an unavoidable mass spectrometer uncertainty. The $^{34}S/^{32}S$ ratio is determined by measuring the mass ratio 66/64, given by $^{34}S^{16}O^{16}O/^{32}S^{16}O^{16}O$. However, the isotopologue $^{32}S^{18}O^{16}O$ also has a mass of 66, and because the source of the oxygen is unrelated to the source of sulfur, the sulfur and oxygen isotope ratios are uncorrelated. There is no way to separate or distinguish $^{34}S^{16}O^{16}O$ from $^{32}S^{18}O^{16}O$ by measuring only the mass 64 and 66 intensities. A correction is made on the basis of measured $\delta^{34}S$ values of standard materials (Box 10.1). SO_2 is generated from sulfides by oxidation at high temperatures with either O_2 gas or an oxidized species such as copper oxide. If oxygen in the newly-formed SO_2 has a constant $\delta^{18}O$ value, then the correction based on the interference of ^{18}O to the mass 66 signal can easily be corrected for. However, different sulfides may react with oxygen at

different rates, and the $\delta^{18}O$ value of SO_2 generated could potentially vary between sulfides. The problem is minimized by converting all samples to Ag_2S (an easily oxidized species). In practice, this conversion step is all but abandoned by most laboratory researchers that use continuous flow techniques, mostly because it is a time-consuming step. Therefore, there may be a small bias when comparing $\delta^{34}S$ values of coexisting sulfides. The problem is more serious when comparing coexisting sulfides and sulfates. Oxygen may be inherited from the sulfate during thermal decomposition to SO_2. Thus the oxygen in SO_2 gas generated from sulfates and sulfides could have significantly different $\delta^{18}O$ values. The problem is alleviated by comparing results from sulfate standards with sulfate samples and sulfide standards with sulfide samples, although this assumes that the $\delta^{18}O$ value of sulfate samples and standards are similar.

Box 10.1. The ^{18}O problem for SO_2: $^{13}C/^{12}C$ ratios are determined from measurements of CO_2 gas. The 45/44 ratio is equal to ($^{12}C^{16}O^{17}O$ + $^{12}C^{17}O^{16}O$ + $^{13}C^{16}O^{16}O$) / $^{12}C^{16}O^{16}O$. The contribution to mass 45 by ^{17}O (the ^{17}O correction) can be made for terrestrial samples because the $\delta^{17}O$ is ~1/2 that of the $\delta^{18}O$ value. By measuring both 46/44 and 45/44 ratios of a gas, it is possible to extract the exact $\delta^{13}C$ value of a sample, regardless of the $\delta^{18}O$ value of the CO_2 (Craig, 1957).

The $\delta^{34}S$ value of SO_2 gas is determined from the 66/64 ratios. Mass 64 is equal to $^{32}S^{16}O^{16}O$, but mass 66 has contributions from $^{34}S^{16}O^{16}O$, $^{32}S^{18}O^{16}O$, $^{32}S^{16}O^{18}O$, and $H_2SO_2^+$ (Halas, 1985). Unlike CO_2, there is no way to correct for the ^{18}O contribution to mass 66, because the $^{34}S/^{32}S$ and $^{18}O/^{16}O$ ratios are non-correlated. If the $\delta^{18}O$ value of the gas could be independently determined, then a correction could be made if both standard and sample have the same $\delta^{18}O$ value. Alternatively, the ^{18}O-correction is determined by measuring samples that have been measured independently using the SF_6 method. For a further discussion on SO_2 and ^{18}O correction, the reader is referred to (Rees, 1978).

In contrast to SO_2, SF_6 is a very clean, inert gas. Because fluorine is monoisotopic, the different masses measured in the mass spectrometer for the ionized species SF_5^+ (127, 128, 129, 131) are all uniquely related to a single isotope of sulfur. SF_6 has a further advantage over SO_2 in that it has a very high ionization potential; 90% ionization compared to ~50% for SO_2 (Halas, 1985). The drawbacks to measuring SF_6 gas are twofold: First, SF_5^+ is a very heavy ion, and can only be measured on large radius mass spectrometers configured for analysis of SF_5^+. Second, the extraction technique involves fluorination and is therefore significantly more difficult than SO_2 combustion methods (although recent developments in laser fluorination make the SF_6 method more straightforward than earlier procedures (Beaudoin and Taylor, 1994).

A number of investigators have found that the relative difference between samples with very different $\delta^{34}S$ values is larger when measured as SF_6, as compared to SO_2. It is generally assumed that most analytical artifacts tend to shrink the differences between samples with significantly different isotope ratios. The analytical technique with the least amount of compression of the isotope scale is generally considered to be the most accurate. In a comparative study, Rees (1978) found that the spread of values determined using SF_6 extraction methods was larger than that obtained using SO_2 by a factor of 1.034 (*e.g.*, if a $\delta^{34}S$ value of a sample was 20.3‰ (VCDT) using SO_2, a value

of 21.0‰ would be obtained with SF_6). Overall, SF_6 is probably more accurate and precise. However, the rapidity, simplicity and safety of SO_2-based extraction techniques is a major factor for most researchers who would like to have large numbers of analyses and do not require the very high precision and multiple isotope data that can only be obtained by measuring SF_6.

By far the biggest advantage of the SF_6 technique is that it allows for accurate determinations of $\delta^{33}S$ and $\delta^{36}S$ analyses to be made. Subtle departures from the expected mass-dependent triple-isotope fractionation occur as a result of photolytic reactions in the stratosphere and provide valuable information about ancient atmospheres (See section 10.5.5).

10.3 Equilibrium fractionation and geothermometry

Equilibrium fractionations for selected sulfur-bearing compounds are shown in Fig. 10.1. The sulfur isotope fractionation between sulfates and sulfides is enormous and highly temperature sensitive. Unfortunately, sulfur isotope equilibrium between sulfates and sulfides occurs only at very high temperatures (see Rye, 2005 for a comprehensive review). Sulfides and sulfates, commonly found to coexist in ore deposits, are rarely in equilibrium, even when temperatures in excess of 500°C had been reached. If equilibrium exchange between sulfate and sulfides *did* occur at low temperatures, the fractionations would be huge. The expected equilibrium gypsum-galena fractionation is over 70‰ at 25°C. Equilibrium between oxidized and reduced sulfur species is most commonly observed for coexisting sulfides and sulfates in magmatic and hydrothermal systems

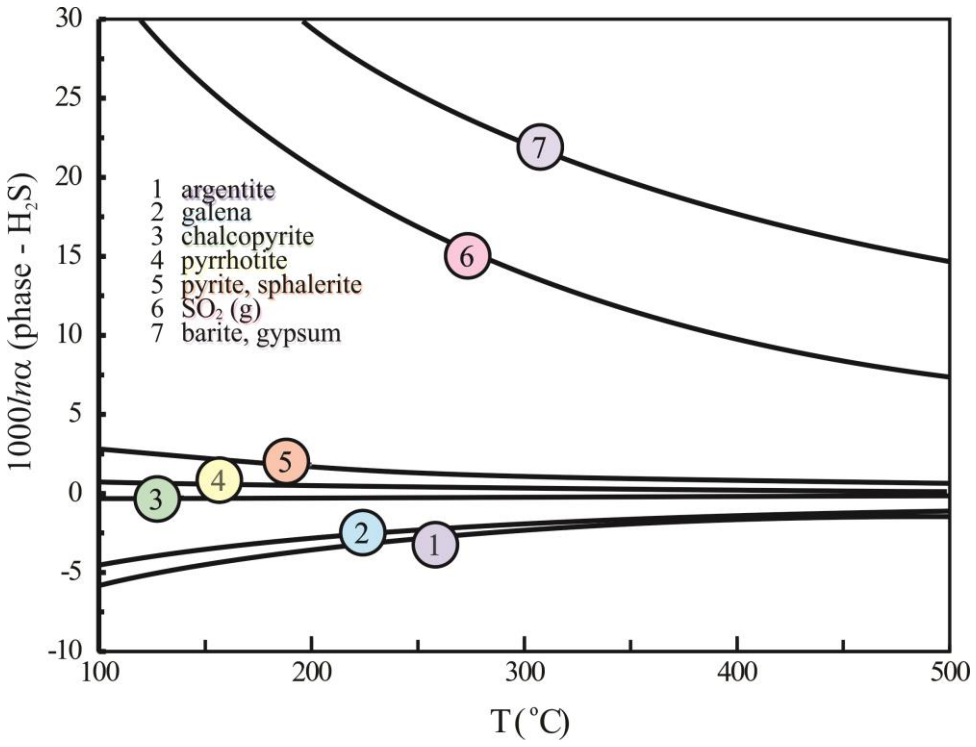

Fig. 10.1. Sulfur isotope fractionations between selected phases. Among the sulfides, galena-pyrite or galena-sphalerite have the largest fractionations.

formed above 250°C and H_2S and SO_2 gas from volcanic fumaroles (Nielsen, 1979).

Applications of sulfur isotope thermometry have mainly focused on coexisting sulfide pairs. One would expect that mineral pairs with the largest fractionations should be most suitable for thermometry, and indeed, sphalerite-galena pairs work very well as a geothermometer. In most cases, the calculated isotope temperature agrees well with other independent estimates, especially above 300°C. Reasonable temperature estimates from the sphalerite-galena thermometer may be obtained in ore deposits formed as low as 120°C, if the two minerals precipitated simultaneously. Below this temperature, the $\Delta^{34}S$ (sphalerite-galena) values are smaller than expected for equilibrium – that is, they correspond to temperatures that are too high.

Because of its large expected fractionation with other sulfides, pyrite should be an excellent mineral for thermometry, but it is not. In the majority of cases, pyrite-sulfide pairs (and chalcopyrite-sulfide pairs) give erroneous temperatures, the fractionations often being reversed. The reasons for this are not well understood, but are probably related to different sources of sulfur for pyrite and coexisting minerals.

The sulfur isotope composition of a sulfide precipitating from a sulfur-rich fluid is dependent on the temperature, the $\delta^{34}S$ value of the dissolve sulfur in solution *and* the sulfur species in solution. Because dissolved sulfur can exist in more than one oxidation state, the fractionation between the precipitating sulfide and solution is a function of temperature *and* the dominant aqueous sulfide species (Sakai, 1968; Ohmoto, 1972).

The four principal aqueous sulfur-bearing species above 250°C are $\sum SO_4^{2-}$, H_2S, HS^- and S^{2-}. $\sum SO_4^{2-}$ is the sum of SO_4^{2-}, HSO_4^{2-}, KSO_4^{2-}, etc). Which of these species

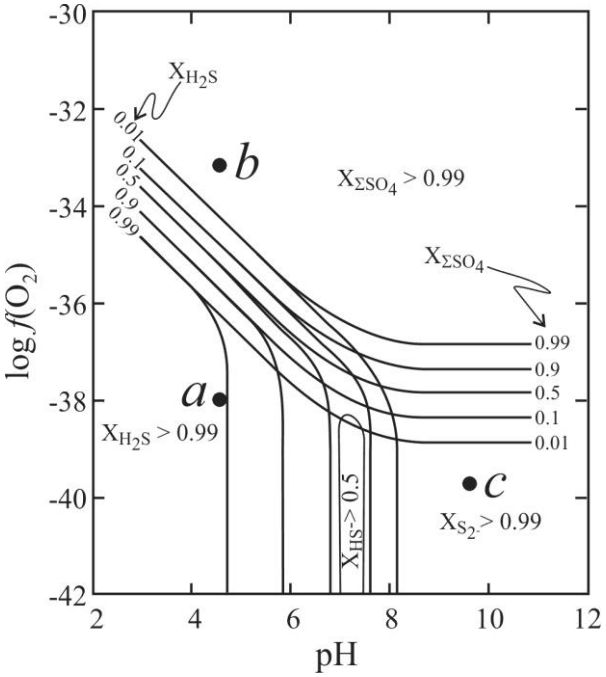

Fig. 10.2. Stability field of aqueous sulfur species as a function of pH and $f(O_2)$. At low pH & $f(O_2)$, H_2S is the dominant dissolved sulfur species (point *a*), at high pH, low $f(O_2)$, S_2 is the dominant species (point *c*), and at high $f(O_2)$, ΣSO_4 is the dominant species (point *c*). The three phase field represents an oversimplification of the system, because HS^- is a significant component at intermediate pH and low $f(O_2)$, as shown by the shaded region where X_{H_2S} >0.5. Modified from Ohmoto (1972).

dominates in a fluid depends on the pH, $f(O_2)$ and temperature of the fluid (Fig. 10.2). At low pH-$f(O_2)$ conditions, H_2S makes up the vast majority of the total dissolved sulfur, whereas $\sum SO_4^{2-}$ and S^{2-} exist in vanishingly small quantities. S^{2-} dominates at very high pH conditions (lower right of Fig. 10.2), and $\sum SO_4^{2-}$ is the principal aqueous sulfur species at high $f(O_2)$. The isotopic composition of minerals precipitating from the sulfur-bearing solution depends on which of the aqueous sulfur species is most abundant.

Fig. 10.3 shows the isotopic composition of sulfide minerals precipitating from a solution with a $\delta^{34}S$ value of 0 ‰. If the pH-$f(O_2)$ conditions are such that H_2S is the dominant dissolve sulfur species (low pH-low $f(O_2)$), then the $\delta^{34}S$ values of the sulfides pyrite, sphalerite and galena will be only slightly less than 0‰ (top pane, Fig. 10.3). If this same fluid were to become oxidized by passage through an oxidizing lithology such as a hematite-rich rock, then the dissolved sulfur species will be predominantly sulfate. Note that the $\delta^{34}S$ value of the dissolved species hasn't changed, only the oxidations state. Instead of a small fractionation between H_2S and sulfides, the fractionation between sulfate ions and sulfides becomes very large. The $\delta^{34}S$ values of the first-precipitating sulfides will be less than -30‰ because the sulfate-sulfide fractionation is so large (middle pane, Fig. 10.3). Similarly, if S^{2-} becomes stable (high pH and low $f(O_2)$), then the $\delta^{34}S$ value of the precipitating sulfides would be slightly positive (bottom pane, Fig. 10.3). The only difference in these three scenarios is the stable sulfur species in solution. Temperatures and bulk $\delta^{34}S$ values of the system are the same in each case, but the $\delta^{34}S$ values of the precipitating sulfides vary markedly depending on the stable dissolved sulfur species. If one were to see sulfides in an organic rich (reducing) layer with high $\delta^{34}S$ values, and an overlying hematite (oxidizing) layer with low $\delta^{34}S$ sulfides, it does not mean that a different sulfur source is indicated. It could simply be attributed to different dissolved sulfur species. It should be pointed out that if *all* dissolved sulfur in a system precipitated out as sulfide minerals, then the overall $\delta^{34}S$ values of the total

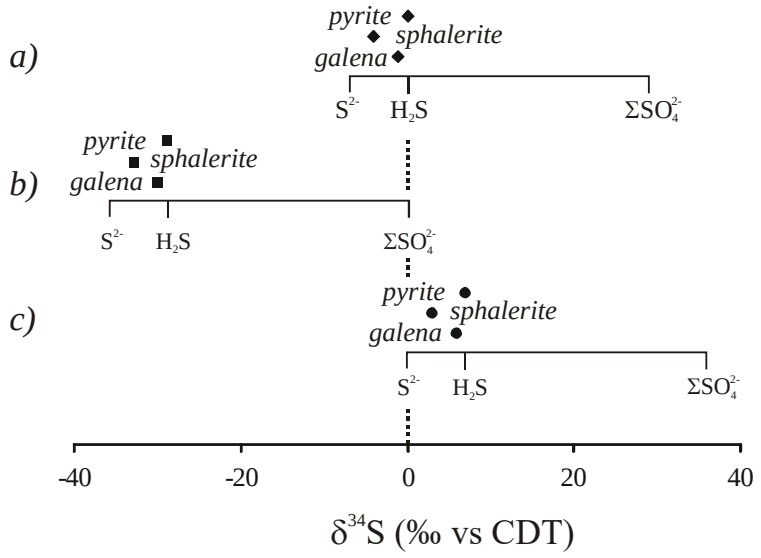

Fig. 10.3. Illustration of the initial $\delta^{34}S$ values of minerals forming from a fluid with a $\delta^{34}S_\Sigma$ value of 0‰. *a*) H_2S as dominant fluid species; *b*) $\sum SO_4^{2-}$ as dominant fluid species; *c*) S_2^- as dominant fluid species. Modified from Nielsen (1979).

sulfides would be independent of the dissolved sulfur species. Their $\delta^{34}S$ value would be identical to that of the original fluid. The conditions illustrated in Fig. 10.3 are those where only a small fraction of the total dissolve sulfur forms solid sulfide minerals.

10.4 Sulfate and sulfide formation at low temperature – the sedimentary sulfur cycle

Essentially all dissolved sulfur in the ocean is in the oxidized form sulfate. The residence time of reduced sulfur evolved from black smokers, etc. is only on the order of minutes[3]. The residence time of sulfate in seawater is on the order of 2×10^7 y, so that sulfur is well-mixed and the $\delta^{34}S$ value of the modern ocean has a constant value of 21.0‰ ±0.25‰ (Rees et al., 1978)[4]. Sulfur is removed from the ocean by precipitation of sulfate and sulfide minerals, and returned to the ocean by erosion of sediments.

The sulfur cycle has a number of similarities to the carbon cycle. In both cases, the element forms solids in both oxidized and reduced states. The oxidized forms are carbonates and sulfates; the reduced forms are organic matter and sulfides for carbon and sulfur, respectively. The isotopic fractionation between seawater and the oxidized forms is small and nearly constant, so that the delta value of the oxidized form (carbonates and sulfates) can be used as a proxy for the ocean value at the time of mineral formation. Reduction of dissolved carbon and sulfur is a biologically mediated process. Both are kinetically controlled, and the product phases – organic matter and sulfides – have much lighter and variable delta values than that of dissolved bicarbonate and sulfate in the ocean[5]. The long-term carbon and sulfur delta values of the ocean are controlled by the amount of organic matter (carbon) and sulfide (sulfur) stored in sediments (Fig. 10.4).

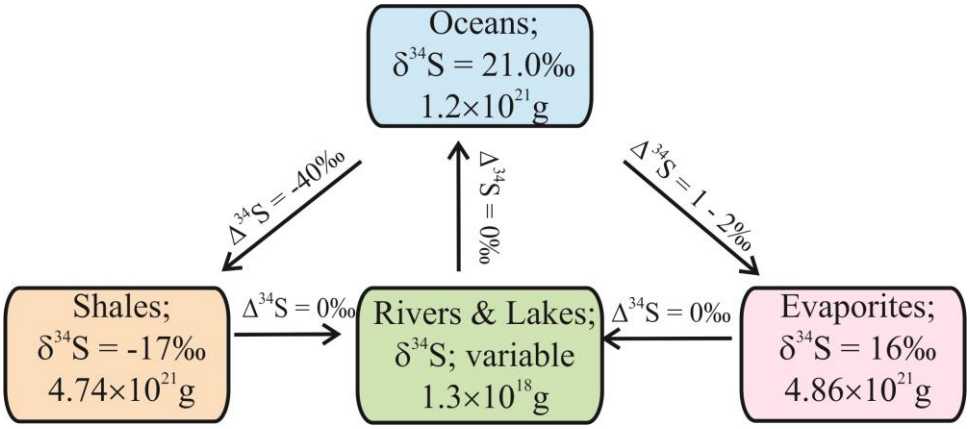

Fig. 10.4. Box model of the surficial sulfur cycle. The $\delta^{34}S$ value of the ocean is a function of transfer to and from sulfide (shales box); the modern ocean sulfate value is 21.0‰. After Claypool *et al.* (1980). Abundances of each reservoir are modern values after Holser *et al.* (1988). Note that published estimates for reduced/(Total sulfur) range from 0.29 to 0.55.

---

[3] In Archean times, reduced sulfur would have been the stable ionic species in the ocean.

[4] The value of 21.0‰ was determined using the SF_6 method. Earlier estimates using the SO_2 method are 20.0‰ and a large number of publications have used (and continue to use) the 20.0‰ value in their work.

[5] Note however that fractionation during assimilation of sulfur is small (2-3‰) but large for carbon ((Kaplan, 1983, page 2-4)

Just like carbon, the average crustal $\delta^{34}S$ value is given by $\frac{\sum m_i \times \delta^{34} S_i}{\sum m_i}$, where m_i is the mass of each reservoir. And like carbon, the average crustal value must equal the mantle value, assuming that the long-term transfer from the mantle to crust occurs without fractionation. Using the data in Fig. 10.4, the average crustal value is 2‰, slightly higher than the assumed mantle value of 0‰. We can 'tweak' the input parameters in Fig. 10.3 to adjust the crustal value. For example, a shale mass of 6×10^{21}g results in a $\delta^{34}S$ value of the crust of 0‰. Lowering the shale $\delta^{34}S$ value to -21.5 ‰ would also bring the crustal and mantle values into agreement. Alternatively, the long term subduction of light sulfur may have resulted in a crustal reservoir that is heavier than its mantle source (Alt et al., 2013). Uncertainties in reservoir size, flux and isotopic composition are too large to distinguish these possibilities.

10.4.1 Sulfate incorporation in sediments

The sulfur isotope fractionation between evaporitic sulfate minerals and dissolved sulfate is approximately 1-2‰ (Thode and Monster, 1965). Holser and Kaplan (1966) compiled the fractionations from experiments and analyses of modern evaporites. The fractionation obtained from experiments is 1.1±0.9‰. Recent evaporites were, on average, 0.4±1.2‰ heavier than dissolved ocean sulfate. Modern barites measured by the SF_6 method averaged 0.2‰ heavier than dissolved ocean sulfate (Paytan et al., 1998). The similarity between the $\delta^{34}S$ value of sulfate minerals and dissolved sulfate means that ancient sulfates can be used as a proxy for the $\delta^{34}S$ value of the ocean at the time the mineral formed.

10.4.2 Sulfide incorporation in sediments

Sulfides are mostly produced as a byproduct of bacterial sulfate reduction. *Assimilatory reduction* occurs in autotrophic organisms where sulfur is incorporated in proteins, particularly as S^{2-} in amino acids. Assimilatory reduction involves a valance change from +6 to –2. However, the bonding of the product sulfur is similar to the dissolved sulfate ion, and fractionations are small. In laboratory experiments, assimilation of sulfate occurs with a fractionation of -2 to -3 ‰ (Kaplan, 1983), far lower than what is seen for carbon fractionation during reduction of bicarbonate (or CO_2) to reduced carbon. One explanation for the relatively small fractionation is that once sulfur is transferred into the cell, it is completely reduced to the sulfur-bearing protein. The $\delta^{34}S$ value of organic sulfur in extant marine organisms incorporated by assimilatory processes is generally depleted by 0 to 5‰ relative to the ocean.

The second reduction mechanism, *dissimilatory reduction* is performed by heterotrophic organsisms, particularly *Desulfovibrio desulfuricans*. The overall reaction can be represented as

$$2\ CH_2O + SO_4^{2-} \rightarrow 2\ HCO_3^- + H_2S \qquad 10.3.$$

The dissimilatory reduction is called 'bacterial sulfate reduction' and is extremely important in terms of the Earth's sulfur budget. It is the major surficial process for changing sulfate to sulfide. Bacterial sulfate reduction is an energy-yielding, anaerobic

process that occurs only in reducing environments, such as in organic-rich ocean sediments. The bacteria use sulfate as an electron acceptor (oxidant). H_2S is given off as a byproduct, which is quickly consumed in the formation of metal sulfides. The sulfate reduction pathway consists of four steps (Goldhaber and Kaplan, 1974). The rates of these steps are quite different, as is the fractionation associated with each step. The slower the step, the larger the fractionation. In a disimilatory reduction reaction limited by the reactant sulfate, essentially all available sulfur will be consumed, and sulfur isotope fractionation between reactant and product will be very small. When there is excess sulfate, and reaction rates are slow, isotopic fractionation will be much larger. Reaction rates are most rapid near neutral pH conditions, and are independent of sulfate concentration when these are above ~0.5 mM (see Canfield, 2001 for an extensive review). Measured fractionations under experimental conditions range from between -20 to -46‰ at low rates of sulfate reduction to -10‰ at high reduction rates. The $\delta^{34}S$ value of sulfides of modern marine sediments is typically around -40‰, however, a wide range from -40‰ to ~ +3‰ is observed (Fig. 10.5). In general, and for the purposes of modeling, a fractionation of 40±10‰ between sulfate and sulfide is often assumed (Claypool et al., 1980).

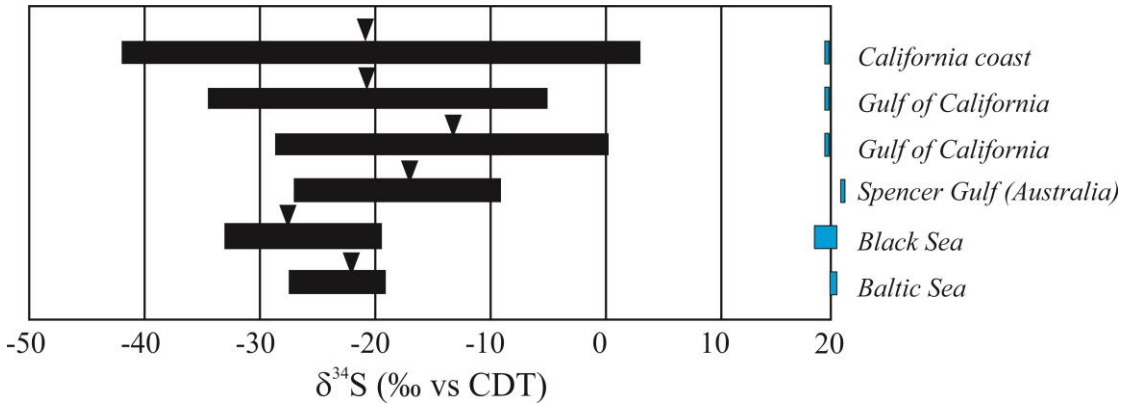

Fig. 10.5. Sulfur isotope composition of pyrite precipitated in modern sediments (solid black bars) and coexisting ocean-water sulfate (blue boxes). Average for pyrite analyses are given by arrowheads. In general, pyrite formed from bacterial sulfate reduction is 40‰ lighter than seawater sulfate (although this is not obvious from the figure!). After Schidlowski *et al.* (1977; 1983).

If, during disimilatory sulfate reduction, all of the pore-water sulfate were converted to sulfides – the 'closed system' case – then the $\delta^{34}S$ of the bulk sulfides would necessarily equal the dissolved seawater sulfate value of +21‰. The amount of sulfide precipitated (in wt %) would also necessarily equal the amount of sulfur initially present in the pore-water sulfate. What is observed in most oceanic sediment, however, are very low $\delta^{34}S$ values of the newly-formed sulfide (Fig. 10.5) and far more precipitated sulfide than expected from the amount of original dissolved sulfate in pore water alone (Fig. 10.6). The isotope and concentration data can only be explained if ocean water freely circulates through the upper sediment, via 'open system' behavior. Sulfate reduction continues due to influx of fresh sulfate from the overlying ocean water. Some ^{34}S-enriched sulfate must be returned to the ocean, thereby explaining the low $\delta^{34}S$ values of the sulfide mineralization. Bioturbation strongly aids the mixing process, which is most intense in the upper 6 cm of sediment.

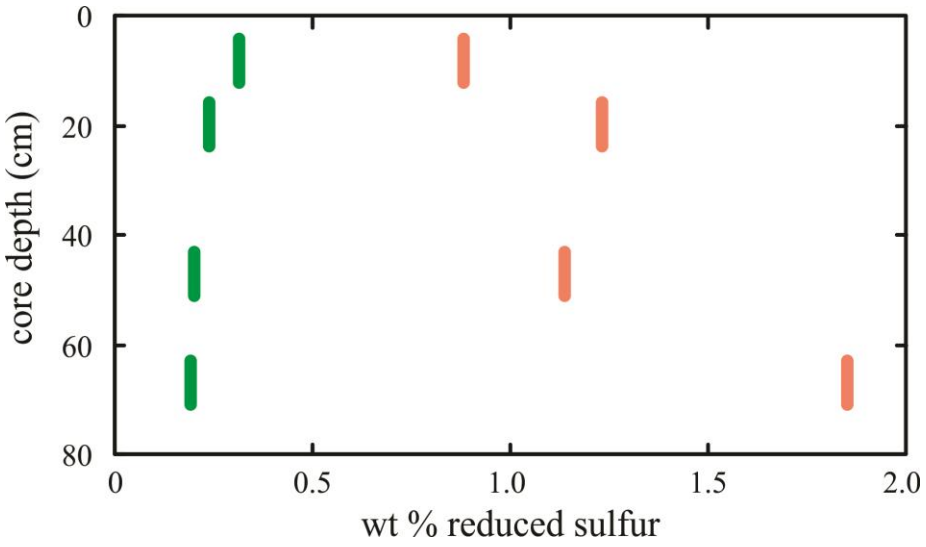

Fig. 10.6. Expected (green) and measured (rust) reduced sulfur abundance from sediment cores from the Gulf of California. The expected amount is calculated from the pore water volumes and sulfate concentrations, which decrease with depth. The higher measured abundance of reduced sulfur is evidence for continued influx of seawater sulfate after initial burial. The $\delta^{34}S$ values of H_2S decrease with depth, but the $\delta^{34}S$ values of pyrite are mostly constant between -20 to -30‰ (Raven et al., 2016). After Kaplan (1983).

Sulfate reduction and sulfide precipitation continues only as long as 1) organic matter is available for sulfate-reducing bacteria, 2) iron is present to react with H_2S, and of course, 3) sulfate is available as a reactant. Exchange of pore-water sulfate with ocean water decreases with depth, as the porosity is reduced due to sediment compaction. Sulfate reduction will quickly halt if the H_2S concentration is allowed to build up. As long as there are metal cations present to react with the evolving H_2S however, the sulfate reduction reactions will continue and sulfides will precipitate. Some of the H_2S byproduct will also leave the system by simple degassing at shallow levels. In the marine environment, neither sulfate nor ferric iron generally limit the sulfate-reduction reaction. Instead, it is the abundance of easily metabolized carbon that controls the extent of sulfate reduction reactions.

10.5 Secular variations in sulfur

10.5.1 Long term variations

The $\delta^{34}S$ values of marine evaporites reflect the isotopic composition of dissolved ocean sulfate at the time of their formation. Because the fractionation between sulfate minerals and dissolved sulfate is close to zero, creation or destruction of evaporites will have little effect on the $\delta^{34}S$ value of the oceans. On the other hand, the large difference in the $\delta^{34}S$ values of dissolved sulfate and bacterially-produced sulfide minerals means that production or destruction of sulfides will strongly influence the $\delta^{34}S$ value of the ocean sulfate. During periods of intense weathering of argillaceous sediments, notably shales, the $\delta^{34}S$ value of the ocean decreases, while during periods of vigorous bacterial sulfate reduction and preferential removal of ^{32}S, the $\delta^{34}S$ value of ocean sulfate increases.

The secular curve for the $\delta^{34}S$ value of sulfates is shown in Fig. 10.7. The $\delta^{34}S$

values range from <10‰ to over >35‰. The gross characteristics of the secular curve are explained in terms of removal or addition of reduced sulfur to the oceans. Realize that return of abundant +35‰ sulfate to a 10‰ ocean could have a measurable effect on the dissolve sulfate $\delta^{34}S$ value.

- Periods of high biological activity (sulfate reducing bacteria) increase the $\delta^{34}S$ value of the ocean (and evaporites) due to removal of ^{34}S-depleted sulfur as sedimentary sulfides. Favorable paleogeographic conditions, including extensive shallow marine settings, and abundant organic matter (as food source), are necessary for extensive production of sulfide. Periods of high $\delta^{34}S$ values (Cambrian, Devonian) also have widespread carbon-rich sediments.
- Intense weathering lowers the $\delta^{34}S$ value of the ocean. Low $\delta^{34}S$ values of evaporites due to extensive erosion of shales require elevated orogenic activity, such as the Devonian to Permian change associated with the Variscan orogeny (Fig.10.7).

The significance of the sulfate-sulfide ratio can be appreciated when one recognizes that 50% of the total photosynthetically produced O_2 is locked up in evaporite sulfate (Schidlowski et al., 1977). To put this in context, the shift from $\delta^{34}S$ values of 10‰ in the late Permian to 20‰ in the Tertiary requires a shift of 5×10^{20} grams of sulfur to the shale reservoir (Holser and Kaplan, 1966), releasing an equivalent amount of oxygen. 10^{20} grams of oxygen is equal to all of the diatomic oxygen in the modern atmosphere.

10.5.2 Alternative approaches – barite and trace carbonates

Relative to carbon and strontium, the secular sulfur isotope curve is poorly defined because evaporites were deposited only at certain periods in the Earth's past and are difficult to date with precision. Special conditions are required for their deposition and they are easily eroded. Other sulfur species, especially barite and trace sulfate in carbonates, have been used to expand and refine the sulfur curve. Unlike gypsum ($CaSO_4 \cdot 2H_2O$) evaporites, the $\delta^{34}S$ values of barites is strongly dependent on the type of deposit in which it is found. Thick stratiform barite deposits faithfully reproduce the evaporite curve, while thin beds or nodular barites have $\delta^{34}S$ values that are too high and most likely form in diagenetic settings within sulfate reducing sediments (Cecile et al., 1983; Goodfellow and Jonasson, 1984). Massive barite deposits require unusual geological conditions, such that the $\delta^{34}S$ values may have a high

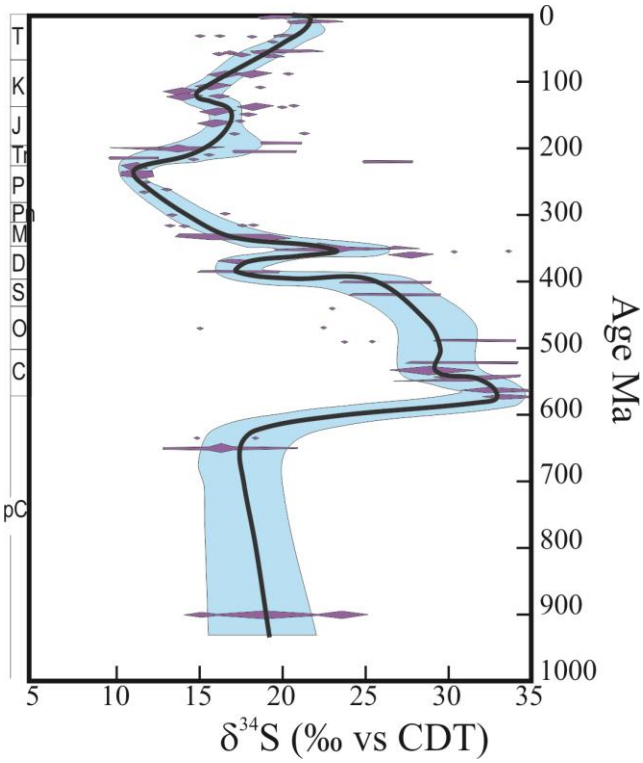

Fig. 10.7. Secular variations in the $\delta^{34}S$ value of evaporites. After Claypool *et al.* (1980).

contribution from a hydrothermal source. A sulfur isotope stratigraphic curve was generated for deep sea marine barites of Cretaceous and Cenozoic age with unprecedented temporal resolution (Paytan et al., 2004). The marine barites precipitate directly in the seawater column and are thought to have $\delta^{34}S$ values that are virtually identical to dissolved sulfate. The high resolution curve shows some very rapid changes, such as a 5‰ change between 125 and 120 Ma (Fig. 10.8). Such large rapid shifts require huge changes in input and output fluxes. The rapid changes may also occur in part because sulfate concentrations in the ocean were low at that time. These 'second order' features (10^7-yr scale) are similar to other more poorly defined equivalents in older evaporites (Holser, 1977) and suggest that the seawater sulfate curve may not be as 'smooth' as drawn in Fig. 10.7.

Sulfur is a ubiquitous trace element in sedimentary carbonates. Concentrations range from several tens of ppm in inorganic carbonates to several thousand ppm in some biogenic carbonates. As long as no fractionation accompanies the incorporation of sulfur into the carbonate, and no diagenetic alteration takes place, carbonates offer an attractive method for refining the secular sulfur curve. Carbonates may provide a representative $\delta^{34}S$ value of the ocean, precipitating in more open conditions as opposed to restricted marine basins (Strauss, 1997). Burdett *et al.* (1989) constructed a high resolution secular sulfur curve for the past 25 Ma using foraminifera. Their results agree well with Fig.

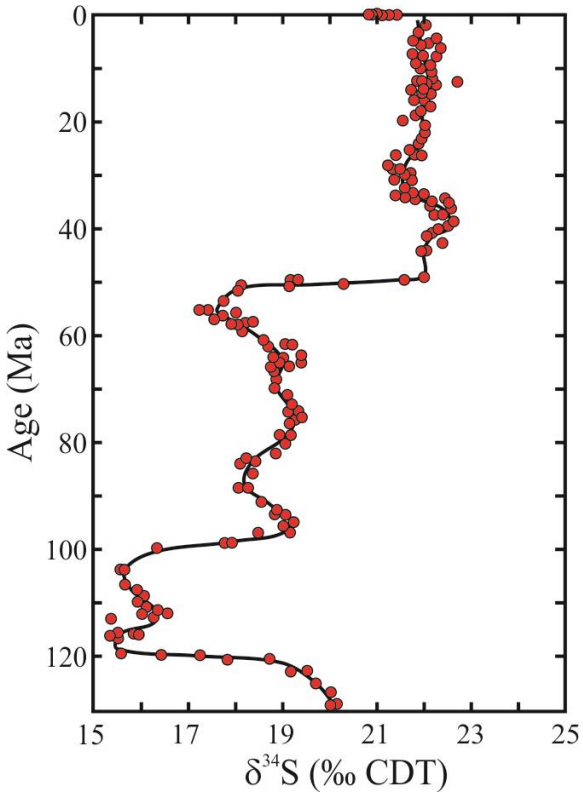

Fig. 10.8. $\delta^{34}S$ values of marine barite covering the Cenozoic. The high resolution curve clearly illustrates rapid changes in the sulfur isotope composition of the ocean. After Paytan *et al.* (2004).

10.8, but have much more scatter, which the authors attribute to possible diagenesis. A global secular $\delta^{34}S$ curve for the Paleozoic and Mesozoic has been generated from nearly 300 measurements of structurally substituted sulfate in the calcite lattice of carbonates (Kampschulte and Strauss, 2004). The curve matches earlier evaporite data, but provide a secular sulfur isotope curve with far higher resolution.

10.5.3 Time boundaries

Strauss (1997) reviewed secular variations across time boundaries characterized by profound biological or geological changes. Due to the paucity of evaporite data, all time boundary studies have been made on sedimentary sulfides. The non-constant fractionation between seawater sulfate and sulfides means that the data have more variation than would be expected from a sulfate curve. Nevertheless, the results are very informative. Consider that carbon isotope excursions can be expected in response to major extinction and radiation events, as the response time of carbon is relatively rapid. Enhanced sulfate reduction requires abundant organic matter as a food source, as evidenced by a correlation between the abundance of organic matter and sedimentary pyrite. During a catastrophic event, where productivity plunges, the $\delta^{34}S$ values of the oceans should decrease. The subsequent biological radiations should have the opposite effect. The $\delta^{34}S$ values of the oceans should first decrease across a time boundary associated with a catastrophic extinction, and then increase during the period of recovery. The magnitude of the effect is related to the intensity of the extinction event, the rate of recovery and the size of the oceanic sulfur reservoir.

Four extinction events have been studied (see Strauss, 1997 for references): the Precambrian-Cambrian, the Frasnian-Famennian, the Permian-Triassic, and the Cretaceous-Tertiary boundaries. Of these, only the Permian-Triassic event shows the expected sulfur trend (Bojar et al., 2016). Fluctuations occur at other boundaries, but no secular variations have been observed. Part of the reason for the irregular results between sections may be related to the inherent problems of analyzing sulfides instead of sulfates. In addition, local effects may mask any global sulfur variations.

10.5.4 Archean sulfates – clues to early atmosphere

Oxidation of mantle-derived sulfides is the major source of ‘crustal’ sulfate. Virtually all sulfate oxygen in post-Archean sediments is photosynthetically derived. Prior to the development of an oxygenated ocean and atmosphere, photolithotrophic (green and purple) sulfur bacteria would have been the principal source of oxygen for sulfate production (Monster et al., 1979). Sulfur isotope fractionation during photolithotrophic oxidation is small, so that in the absence of extensive bacterial sulfate reduction, all sulfide and sulfate minerals would have had $\delta^{34}S$ values close to the whole-earth value of 0‰. There should have been a buildup of sulfate in the oceans prior to the ultimate development of free oxygen in the atmosphere, if photosynthetic algae first become plentiful in the oceans. Abundant sulfate-reducing bacterial activity could only occur once sulfate became abundant and the ocean had been oxygenated in at least some locations. Once the sulfate-reducing bacteria became abundant, the dispersion of $\delta^{34}S$ values in sediments (due to isotope partitioning between sulfide and sulfate) would increase toward its modern range in excess of 70‰. The advent of sulfate-reducing bacteria was a major evolutionary step that preceded the oxygenation of the atmosphere.

A number of authors have measured the $\delta^{34}S$ values of ancient sulfides and sulfates, although Archean sulfate mineralization is rare[6]. Monster *et al.* (1979) showed that the divergence of sulfur isotope ratios in sediments occurred at some time between 3.1 and 2.8 billion years in the past (Fig. 10.9). Earlier sediments and igneous sulfide samples have an extremely limited range of $\delta^{34}S$ values of +0.5±1.0‰. By the middle Archean, the $\delta^{34}S$ values ranged from -20 to +20‰. It was concluded on the basis of these data, that low ocean sulfate concentrations persisted until ~2.8 Ga. Kakegawa and Ohmoto (1999) measured the $\delta^{34}S$ values of pyrite grains hosted in sedimentary pyritic shales of the 3.4 to 3.2 Ga Fig Tree Group of the Barberton Greenstone Belt, South Africa. The $\delta^{34}S$ values ranged from –0.8 to +4.4‰, suggesting that the sulfides were a product of microbial reduction of seawater sulfate. Such a conclusion suggests that seawater sulfate was an appreciable component of the Archean ocean, at least locally.

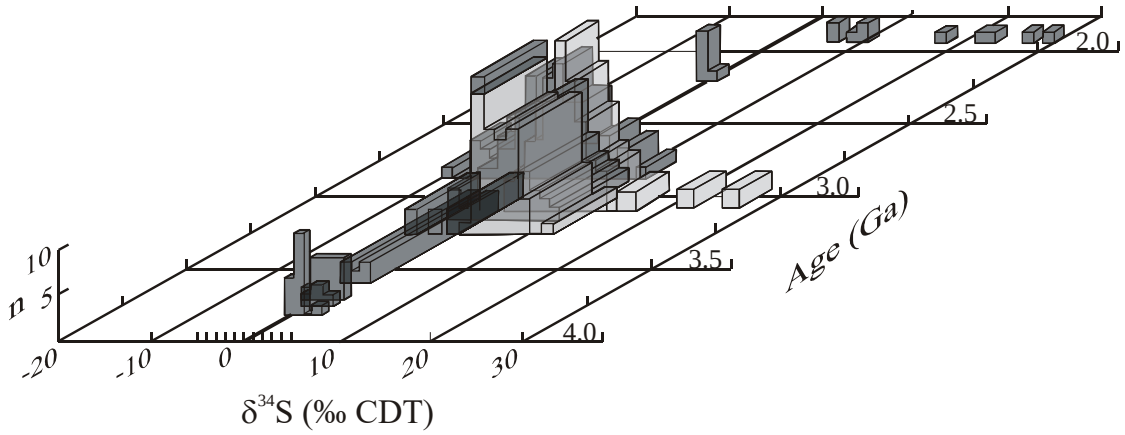

Fig. 10.9. Sulfur isotope variations of ancient deposits. Sulfides are given by dark grey fields, sulfates by lighter shades. The height of each polygon signifies the number of analyses. Around 3.1 Ga, the range of $\delta^{34}S$ values begins to increase as sulfate-reducing bacteria become more abundant. See Monster *et al*. (1979) for more details. Note that the age axis is in some cases poorly constrained.

10.5.5 Sulfur isotope anomalies – mass-independent fractionation

Further constraints on Archean surficial conditions can be made from multiple isotope measurements of sulfides. Under almost all geological conditions, the four isotopes of sulfur follow a predictable mass dependent fractionation, where $\delta^{33}S \approx 0.515 \times \delta^{34}S$, and $\delta^{36}S \approx 1.90 \times \delta^{34}S$ (Hulston and Thode, 1965). In contrast, mass-independent fractionations occur in a number of photochemical gas phase reactions. The isotopic composition of a mineral produced by mass-independent reactions do not follow the predicted relationships between the $\delta^{33}S$, $\delta^{34}S$ and $\delta^{36}S$ ratios. The $\Delta^{33}S$ and $\Delta^{36}S$ values are defined as the deviation from the expected isotope ratios by the following equation:

$$\Delta^{33}S = 1000 \times [(1 + \delta^{33}S/1000) - (1 + \delta^{34}S\ 1000)^{0.518} - 1] \qquad 10.4.$$

[6] No Archean evaporites exist. Instead, gypsum and anhydrite have been replaced by barite. There is some question as to whether primary $\delta^{34}S$ values were preserved during diagenetic alteration to barite.

Farquhar *et al*. (2000) measured the $\delta^{33}S$, $\delta^{34}S$, and $\delta^{36}S$ of sulfates and sulfides covering a wide age range. They found $\Delta^{33}S$ anomalies in samples older than about 2.1 Ga and especially older than 2.45 Ga, (Fig. 10.10). They attributed these anomalies to different atmospheric conditions in early atmosphere. Ozone would have been lacking in a diatomic oxygen-free atmosphere, so that ultraviolet rays could penetrate farther into the atmosphere resulting in mass-independent reactions. Alternatively, photochemical oxidation of reduced sulfide species could have produced sulfate species that did not follow normal mass-dependent fractionations. Regardless of the actual mechanism, the $\Delta^{33}S$ anomalies in Archean sulfates clearly indicate very different conditions of the early atmosphere.

Mass-independent sulfur isotope anomalies have also been found in sulfuric acid layers in South Pole ice cores (Savarino et al., 2003a; 2003c). The proposed explanation is that SO_2 expelled into the upper atmosphere during volcanic explosions has undergone

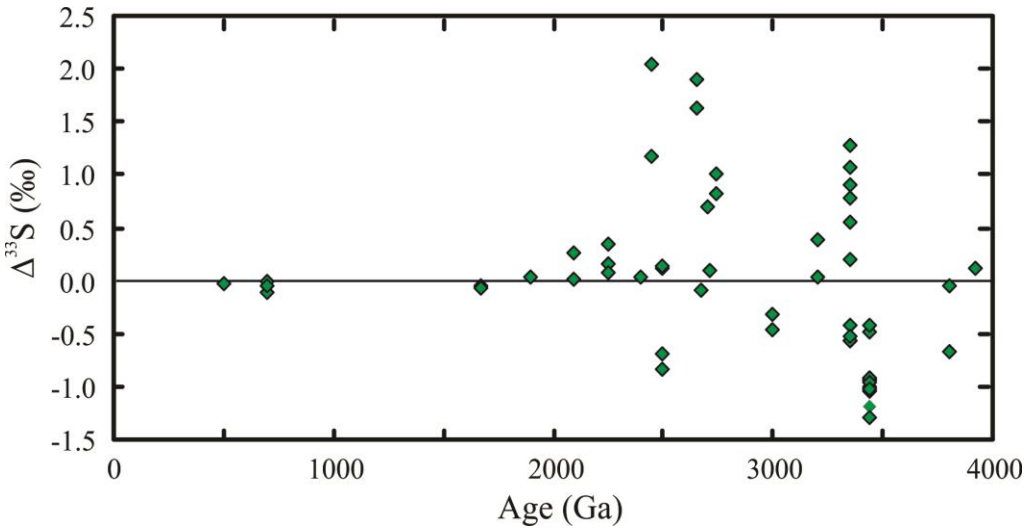

Fig. 10.10. $\Delta^{33}S$ values as a function of age for sulfur-bearing samples. At ~2.1Ga, $\Delta^{33}S$ anomalies are observed, which become significantly larger at ~2.5 Ga. The anomalous samples are believed to be related to an oxygen-free atmosphere in the Archean. After Farquhar *et al.* (2000).

photoxidation by UV radiation. Sulfate from the relatively weak 1991 Cerro Hudson event has no isotope anomaly, because the ejected SO_2 never left the troposphere. In contrast, sulfates from the Pinatubo eruption have a strong sulfur isotope anomaly, explained by the SO_2 ejecta reaching well into the stratosphere, where photolysis in the 190 to 220 nm spectral range would bring about the anomaly. Oxygen isotope anomalies in massive sulfates have also been measured, presumably related to sulfur oxidation reactions in the upper atmosphere (e.g., Bao et al., 2000b; Martin and Bindeman, 2009). Sulfur isotope anomalies have also been used as evidence of surficial recycling of crustal sulfur to great depths (Farquhar et al., 2002) and photolytic effects in martian meteorites (Franz et al., 2014).

10.6 Sulfur isotope ratios in the terrestrial environment

The variations in the terrestrial realm are far less predictable than in the oceanic environment. The largest natural flux of sulfur in the atmosphere is sulfate aerosols derived from sea spray with a $\delta^{34}S$ value close to that of the ocean. H_2S has a very short

residence time in the atmosphere, and will be converted to SO_2 (and sulfuric acid) without sulfur isotope fractionation. In arid climates, the $\delta^{34}S$ value of soils and water is controlled by atmospheric input from aerosols. In humid climates, where rock weathering is extensive, input from the dissolution of sulfur-bearing rocks overwhelms the contribution from atmospheric precipitates. The $\delta^{34}S$ values of rivers is controlled by the local rock type. Hoefs (1987) compiled results from a number of river waters. Not surprisingly, the $\delta^{34}S$ values of rivers cover the same range as rocks themselves. The $\delta^{34}S$ values of the Mackenzie river drainage system, Canada, span a wide range, from –20 to +20‰, clearly indicating that sulfur is supplied both from marine evaporites and shales. The Amazon river has a surprisingly narrow range of $\delta^{34}S$ values around 8‰. Longinelli and Edmond (1983) attributed the near-constant values to a strong Andean source of Permian evaporites. Sulfur isotope studies of individual drainage systems is most valuable for determining the sulfur source for that particular area.

Soil $\delta^{34}S$ values are generally locally derived. In arid regions, especially near the ocean, $\delta^{34}S$ soil values are high due to addition of sulfate from sea spray aerosols. High $\delta^{34}S$ values can also be traced to dissolution of evaporites or travertines (Krouse, 1989). Other sulfur sources include organic matter, and, for recent sediments, fossil fuel burning or other anthropogenic sources. It is now common for sulfur from anthropogenic fossil fuel emissions to overwhelm all other sources. Krouse and Case (1983) measured the $\delta^{34}S$ profile of soils near a sour gas processing plant in Alberta. Soil profiles of soluble sulfur were measured 2 km and 10 km from the processing plant. The 2 km profiles have $\delta^{34}S$ values of 20‰ at the surface, identical to those emitted from the processing plant. The $\delta^{34}S$ values decrease with depth down to approximately 0‰. The 10 km profiles range decrease steadily from ~5‰ at the surface to a plateau of -6 to -10‰ with depth. These lowest values are thought to represent the pre-industrial sulfur values. The use of sulfur isotopes as a tracer of anthropogenic sources is somewhat limited, however, given then huge number of possible sources and extensive mixing between the different sources.

10.7 Oxygen isotope variations in sulfates

Early measurements of the $\delta^{18}O$ values of dissolved sulfate in seawater ranged from 9.5 to 9.9‰ (Longinelli and Craig, 1967; Rafter and Mizutani, 1967; Cortecci, 1975). More recent analyses are closer to 8.6‰ (Holser et al., 1979; Zak et al., 1980). The cause of the discrepancy is not known (Longinelli, 1989), nevertheless, the measured values are far from those predicted on the basis of equilibrium fractionation between dissolved sulfate and water, where the $\Delta^{18}O\ (SO_{4\ aq}^{2-} - H_2O)$ is 38‰ (Lloyd, 1967, 1968). The reason for the disequilibrium is the dynamic conditions of input, output and partial reequilibration that occur in the sulfate oxygen cycle (Holser et al., 1979). The main inputs and outputs for sulfate oxygen can be modeled along the lines for sulfur (Fig. 10.4). The oxygen source for surficial oxidation of sulfides to sulfate is a combination of meteoric water and atmospheric O_2. Although the processes of oxidation, and the importance of bacterial oxidation, are not well known, average $\delta^{18}O$ values for oxidized sulfate globally are around -2‰ (Holser et al., 1979). Using an average $\delta^{18}O$ value of +12‰ for dissolved sulfate derived from weathered evaporites, Holser *et al*. (1979) estimate that the $\delta^{18}O$ value of sulfate flowing into the ocean is ~+5‰. Dissolved sulfate

will also fractionate oxygen during bacterial reduction to sulfide. Again, the magnitude of the effect is not well constrained. Holser *et al*. (1979) estimate the fractionation to be equal to -10‰. In other words, dissolved sulfate with low $^{18}O/^{16}O$ ratios will preferentially be reduced, leaving the remaining sulfate with a higher $\delta^{18}O$ value. The final fractionation occurs during precipitation of sulfate from dissolved sulfate. Results from various lines of evidence regarding this fractionation are often conflicting, ranging from 2 to nearly 10‰. An average $\Delta^{18}O_{\text{evaporite-dissolved sulfate}}$ value of 3.5 to 3.6‰ has been proposed (Holser et al., 1979; Claypool et al., 1980).

Taken together, a mass balance equation for oxygen in sulfate can be derived. The modern $\delta^{18}O$ value of 8.6‰ is obtained if the proportions of input from sulfide and sulfate are about equal. The secular sulfate oxygen isotope curve shows variations on the order of 7‰, although there is a great deal of uncertainty in its construction (Claypool et al., 1980). Covariations between oxygen and sulfur are poor. Nevertheless, some of the features seen in the sulfur secular curve are seen for oxygen as well, notably, the lowering of delta values during the Permian, followed by a rapid rise at the Permian-Triassic boundary. Late Devonian and Carboniferous samples have the highest $\delta^{18}O$ values of 17‰.

A stratigraphic curve for $\delta^{18}O$ in barite has been constructed for the last 10 million years using Deep Sea Drill Cores (Turchyn and Schrag, 2004). From a nearly constant value of 9‰ in the Miocene, there is a monotonic increase of 5‰ between 6 and 3 Ma and then a decrease back to modern values of 7.9‰ in the last 3 million years. The slightly elevated $\delta^{18}O_{\text{sulfate}}$ values in the Miocene are interpreted to represent oxidation of sulfide to a sulfate value between 10 and 14‰. The elevated $\delta^{18}O$ values may be related to changing intensities of bacterial disproportionation of sulfur compounds. The change in $\delta^{18}O$ values of 5‰ in several million years is far in excess of what is seen for oxygen in carbonates. The difference is clearly related to the fact that oxygen isotope equilibrium is attained between water and carbonate, which is not the case for sulfates.

The sulfate ion is one of the few naturally occurring oxygen-bearing ions that retains its oxygen isotope composition in the dissolved form. Sulfates that have formed by aqueous phase interaction with photochemically-derived oxygen (O_3 or H_2O_2) have been shown to retain a triple oxygen isotope anomaly (Bao et al., 2000b; Savarino et al., 2000). Applications include dry valley aerosols indicative of atmospheric oxidation of reduced gaseous sulfur compounds (Bao et al., 2000a), volcanic ashes erupted into the stratosphere (Savarino et al., 2003b) and ancient samples that predate diatomic atmospheric oxygen.

References

Alt, J.C., Schwarzenbach, E.M., Früh-Green, G.L., Shanks III, W.C., Bernasconi, S.M., Garrido, C.J., Crispini, L., Gaggero, L., Padrón-Navarta, J.A. and Marchesi, C. (2013) The role of serpentinites in cycling of carbon and sulfur: Seafloor serpentinization and subduction metamorphism. *Lithos* **178**, 40-54.

Ault, W.U. and Jensen, M.L. (1963) Summary of sulfur isotope standards, in: Jensen, M.L. (Ed.), Biogeochemistry of Sulfur Isotopes. Proceedings of the National Science Foundation Symposium at Yale University, New Haven, pp. 16-29.

Bao, H., Campbell, D.A., Bockheim, J.G. and Thiemens, M.H. (2000a) Origins of sulphate in Antarctic dry-valley soils as deduced from anomalous 17O compositions. *Nature* **407**, 499-502.

Bao, H., Thiemens, M.H., Farquhar, J., Campbell, D.A., Lee, C.C.-W., Heine, K. and Loope, D.B. (2000b) Anomalous ^{17}O compositions in massive sulphate deposits on the Earth. *Nature* **406**, 176-178.

Beaudoin, G. and Taylor, B.E. (1994) High precision and spatial resolution sulfur isotope analysis using MILES laser microprobe. *Geochimica et Cosmochimica Acta* **58**, 5055-5063.

Beaudoin, G., Taylor, B.E., Rumble, D.I. and Thiemens, M. (1994) Variations in the sulfur isotope composition of troilite from the Cañon Diablo iron meteorite. *Geochimica et Cosmochimica Acta* **58**, 4253-4255.

Bojar, A.-V., Halas, S., Bojar, H.-P. and Trembaczowski, A. (2016) Late Permian to Triassic isotope composition of sulfates in the Eastern Alps: palaeogeographic implications. *Geological Magazine*, 1-14.

Burdett, J.W., Arthur, M.A. and Richardson, M. (1989) A Neogene seawater sulfur isotope age curve from calcareous pelagic microfossils. *Earth and Planetary Science Letters* **94**, 189-198.

Canfield, D.E. (2001) Biogeochemistry of sulfur isotopes, in: Valley, J.W., Cole, D.R. (Eds.), Stable isotope geochemistry. Reviews in Mineralogy and Geochemistry, Washington, D.C., pp. 607-636.

Cecile, M.P., Shakur, M.A. and Krouse, H.R. (1983) The isotopic composition of western Canadian barites and the possible derivation of oceanic sulphate $\delta^{34}S$ and $\delta^{18}O$ age curves. *Canadian Journal of Earth Sciences* **20**, 1528-1535.

Claypool, G.E., Holser, W.T., Kaplan, I.R., Sakai, H. and Zak, I. (1980) The age curves of sulfur and oxygen isotopes in marine sulfate and their mutual interpretation. *Chemical Geology* **28**, 199-260.

Coplen, T.B., Hopple, J.A., Böhlke, J.K., Peiser, H.S., Rieder, S.E., Krouse, H.R., Rosman, K.J.R., Ding, T., Vocke, R.D.J., Révész, K.M., Lamberty, A., Taylor, P. and DeBièvre, P. (2002) Compilation of Minimum and Maximum Isotope Ratios of Selected Elements in Naturally Occurring Terrestrial Materials and Reagents. United States Geological Survey, Reston, p. 98.

Cortecci, G. (1975) Isotopic analysis of sulfate in a South Pacific core. *Marine Geology* **19**, 69-74.

Craig, H. (1957) Isotopic standards for carbon and oxygen and correction factors for mass-spectrometric analysis of carbon dioxide. *Geochimica et Cosmochimica Acta* **12**, 133-149.

Farquhar, J., Bao, H. and Thiemens, M. (2000) Atmospheric influence of Earth's earliest sulfur cycle. *Science* **289**, 756-758.

Farquhar, J., Wing, B.A., McKeegan, K.D., Harris, J.W., Cartigny, P. and Thiemens, M.H. (2002) Mass-independent sulfur of inclusions in diamonds and sulfur recycling on early Earth. *Science* **298**, 2369-2372.

Franz, H.B., Kim, S.-T., Farquhar, J., Day, J.M.D., Economos, R.C., McKeegan, K.D., Schmitt, A.K., Irving, A.J., Hoek, J. and Iii, J.D. (2014) Isotopic links between atmospheric chemistry and the deep sulphur cycle on Mars. *Nature* **508**, 364-368.

Giesemann, A., Jager, H.-J., Norman, A.L., Krouse, H.R. and Brand, W.A. (1994) On-line sulfur-isotope determination using an elemental analyzer coupled to a mass spectrometer. *Analytical Chemistry* **66**, 2816-2819.

Goldhaber, M.B. and Kaplan, I.R. (1974) The sulfur cycle, in: Goldberg, E.D. (Ed.), The Sea. John Wiley and Sons, New York, pp. 569-655.

Goodfellow, W.D. and Jonasson, I.R. (1984) Ocean stagnation and ventilation defined by $\delta^{34}S$ secular trends in pyrite and barite, Selwyn Basin, Yukon. *Geology* **12**, 583-586.

Halas, S. (1985) On bias in $^{34}S/^{32}S$ data obtained using SO_2 gas in mass spectrometry, in: IAEA (Ed.), Studies on sulphur isotope variations in Nature. International Atomic Energy Agency, Vienna, pp. 105-111.

Hoefs, J. (1987) Stable Isotope Geochemistry, 3rd ed. Springer-Verlag, Berlin.

Holser, W.T. and Kaplan, I.R. (1966) Isotope geochemistry of sedimentary sulfates. *Chemical Geology* **1**, 93-135.

Holser, W.T. (1977) Catastrophic Chemical Events in the History of the Ocean. *Nature* **267**, 403-408.

Holser, W.T., Kaplan, I.R., Sakai, H. and Zak, I. (1979) Isotope geochemistry of oxygen in the sedimentary sulfate cycle. *Chemical Geology* **25**, 1-17.

Holser, W.T., Schidlowski, M., Mackenzie, F.T. and Maynard, J.B. (1988) Geochemical cycles of carbon and sulfur, in: Gregor, B.C., Garrels, R.M., Mackenzie, F.T., Maynard, J.B. (Eds.), Chemical Cycles in the Evolution of the Earth. John Wiley & Sons, pp. 105-173.

Hulston, J.R. and Thode, H.G. (1965) Variations in the S^{33}, S^{34}, and S^{36} contents of meteorites and their relation to chemical and nuclear effects. *Journal of Geophysical Research* **70**, 3475-3484.

Kakegawa, T. and Ohmoto, H. (1999) Sulfur isotope evidence for the origin of 3.4 to 3.1 Ga pyrite at the Princeton gold mine, Barberton Greenstone Belt, South Africa. *Precambrian Research* **96**, 209-224.

Kampschulte, A. and Strauss, H. (2004) The sulfur isotopic evolution of Phanerozoic seawater based on the analysis of structurally substituted sulfate in carbonates. *Chemical Geology* **204**, 255-286.

Kaplan, I.R. and Hulston, J.R. (1966) The isotopic abundance and content of sulfur in meteorites. *Geochimica et Cosmochimica Acta* **30**, 479-496.

Kaplan, I.R. (1983) Stable isotopes of sulfur, nitrogen and deuterium in Recent marine environments, in: Arthur, M.A., Anderson, T.F., Kaplan, I.R., Veizer, J., Land, L.S. (Eds.), Stable Isotopes in Sedimentary Geology. SEMP Short course, Columbia, pp. 2-1 - 2-108.

Krouse, H.R. and Case, J.W. (1983) Sulphur isotope abundances in the environment and their relation to long term sour gas flaring near Valleyview, Alberta. *RMD Report*

83/18 to Research Management and Pollution Control Divisions of Alberta Environment, 110.

Krouse, H.R. (1989) Sulfur isotope studies of the pedosphere and biosphere, in: Rundel, P.W., Ehleringer, J.R., Nagy, K.A. (Eds.), Stable isotopes in ecological research. Ecological Studies, pp. 424-444.

Lloyd, R.M. (1967) Oxygen-18 composition of oceanic sulfate. *Science* **156**, 1228-1231.

Lloyd, R.M. (1968) Oxygen isotope behavior in the sulfate-water system. *Journal of Geophysical Research.* **73**, 6099-6110.

Longinelli, A. and Craig, H. (1967) Oxygen-18 variations in sulfate ions in sea-water and saline lakes. *Science* **146**, 56-59.

Longinelli, A. and Edmond, J.M. (1983) Isotope geochemistry of the Amazon Basin; a reconnaissance. *Journal of Geophysical Research. C. Oceans and Atmospheres* **88**, 3703-3717.

Longinelli, A. (1989) Oxygen-18 and sulphur-34 in dissolved oceanic sulphate and phosphate, in: Fritz, P., Fontes, J.C. (Eds.), The Marine Environment. Elsevier, Amsterdam, pp. 219-255.

Martin, E. and Bindeman, I. (2009) Mass-independent isotopic signatures of volcanic sulfate from three supereruption ash deposits in Lake Tecopa, California. *Earth and Planetary Science Letters* **282**, 102-114.

McKibben, M.A. and Eldridge, C.S. (1990) Radical sulfur isotope zonation of pyrite accompanying boiling and epithermal gold deposition; a SHRIMP study of the Valles Caldera, New Mexico. *Economic Geology* **85**, 1917-1925.

Monster, J., Appel, P.W.U., Thode, H.G., Schidlowski, M., Carmichael, C.M. and Bridgwater, D. (1979) Sulfur isotope studies in early Archaean sediments from Isua, West Greenland; implications for the antiquity of bacterial sulfate reduction. *Geochimica et Cosmochimica Acta.* **43**, 405-413.

Nielsen, H. (1979) Sulfur isotopes, in: Jager, E., Hunziker, J.C. (Eds.), Lectures in Isotope Geology. Springer, Berlin, pp. 283-312.

Ohmoto, H. (1972) Systematics of sulfur and carbon isotopes in hydrothermal ore deposits. *Economic Geology* **67**, 551-578.

Paytan, A., Kastner, M., Campbell, D.R. and Thiemens, M.H. (1998) Sulfur isotopic composition of Cenozoic seawater sulfate. *Science* **282**, 1459-1462.

Paytan, A., Kastner, M., Campbell, D. and Thiemens, M.H. (2004) Seawater sulfur isotope fluctuations in the Cretaceous. *Science* **304**, 1663-1665.

Rafter, T.A. and Mizutani, Y. (1967) Oxygen isotopic composition of sulphates, 2. Preliminary results on oxygen isotopic variation in sulphates and relationship to their environment and to their delta (34)S values. *New Zealand Journal of Science* **10**, 816-840.

Raven, M.R., Sessions, A.L., Fischer, W.W. and Adkins, J.F. (2016) Sedimentary pyrite $\delta^{34}S$ differs from porewater sulfide in Santa Barbara Basin: Proposed role of organic sulfur. *Geochimica et Cosmochimica Acta* **186**, 120-134.

Rees, C.E. (1978) Sulfur isotope measurements using SO_2 and SF_6. *Geochimica et Cosmochimica Acta.* **42**, 383-390.

Rees, C.E., Jenkins, W.J. and Monster, J. (1978) The sulphur isotopic composition of ocean water sulphate. *Geochimica et Cosmochimica Acta.* **42**, 377-382.

Robinson, B.W. (1995) Sulphur isotope standards, in: IAEA (Ed.), Reference and intercomparison materials for stable isotopes of light elements. International

Atomic Energy Agency, Vienna, pp. 39-46.

Rye, R.O. (2005) A review of the stable-isotope geochemistry of sulfate minerals in selected igneous environments and related hydrothermal systems. *Chemical Geology* **215**, 5-36.

Sakai, H. (1968) Isotopic properties of sulfur compounds in hydrothermal processes. *Geochemical Journal* **2**, 29-49.

Savarino, J., Lee, C.C.W. and Thiemens, M.H. (2000) Laboratory oxygen isotopic study of sulfur (IV) oxidation: Origin of the mass-independent oxygen isotopic anomaly in atmospheric sulfates and sulfate mineral deposits on Earth. *Journal of Geophysical Research: Atmospheres* **105**, 29079-29088.

Savarino, J., Bekki, S., Cole-Dai, J. and Thiemens, M.H. (2003a) Evidence from sulfate mass independent oxygen isotopic compositions of dramatic changes in atmospheric oxidation following massive volcanic eruptions. *Journal of Geophysical Research, D, Atmospheres* **108**, 6 pp.

Savarino, J., Bekki, S., Cole-Dai, J. and Thiemens, M.H. (2003b) Evidence from sulfate mass independent oxygen isotopic compositions of dramatic changes in atmospheric oxidation following massive volcanic eruptions. *Journal of Geophysical Research: Atmospheres* **108**, doi:10.1029/2003JD003737, D003721.

Savarino, J., Romero, A., Cole-Dai, J., Bekki, S. and Thiemens, M.H. (2003c) UV induced mass-independent sulfur isotope fractionation in stratospheric volcanic sulfate. *Geophysical Research Letters* **30**, doi:10.1029/2003GL018134.

Schidlowski, M., Junge, C.E. and Pietrek, H. (1977) Sulfur isotope variations in marine sulfate evaporites and the Phanerozoic oxygen budget. *Journal of Geophysical Research* **82**, 2557-2565.

Schidlowski, M., Hayes, J.M. and Kaplan, I.R. (1983) Isotopic Inferences of Ancient Biochemestries: Carbon, Sulfur, Hydrogen, and Nitrogen, in: Schopf, W.F. (Ed.), Earth's Earliest Biosphere: Its Origin and Evolution. Princeton University Press, Princeton, pp. 149-186.

Strauss, H. (1997) The isotopic composition of sedimentary sulfur through time. *Palaeogeography, Palaeoclimatology, Palaeoecology* **132**, 97-118.

Thode, H.G. and Monster, J. (1965) Sulfur-isotope geochemistry of petroleum, evaporites, and ancient seas. *American Association of Petroleum Geologists, Memoir* **4**, 367-377.

Turchyn, A.V. and Schrag, D.P. (2004) Oxygen Isotope Constraints on the Sulfur Cycle over the Past 10 Million Years. *Science* **303**, 2004-2007.

Zak, I., Sakai, H. and Kaplan, I.R. (1980) Factors controlling the $^{18}O/^{16}O$ and $^{34}S/^{32}S$ isotope ratios of ocean sulfates, evaporites and interstitial sulfates from modern deep sea sediments, in: Goldberg, E.D., Horibe, Y., Saruhashi, K. (Eds.), Isotope Marine Chemistry. Rokakuho, Tokyo, pp. 339-373.

Chapter 11

IGNEOUS PETROLOGY

Contents

11.1 Introduction 1
11.2 The Mantle 1
11.2.1 Oxygen 2
Meteorites and Lunar basalts 3
Mafic Lavas 3
Phenocrysts and xenoliths 5
Mantle Eclogites 6
11.2.2 Carbon 7
Carbon composition inferred from crustal reservoir 8
Diamonds and graphite 8
Carbonatites and kimberlites 9
Basaltic glass 10
11.2.3 Nitrogen 10
11.2.4 Hydrogen 11
11.2.5 Sulfur 13
11.3 Emplacement of plutonic rocks: Interactions with the crust and hydrosphere 14
11.3.1 Normal igneous rocks 15
11.3.2. Shallow level hydrothermal alteration by meteoric water – low $\delta^{18}O$ plutonic rocks 16
11.3.3 High $\delta^{18}O$ igneous rocks 19
11.4 Calculating Fluid-rock ratios 20
11.5 Other processes: Degassing, assimilation and fractional crystallization 22
11.5.1 Magmatic volatiles 22
11.5.2 Assimilation-Fractional Crystallization (AFC) processes 23
References 26

Chapter 11

IGNEOUS PETROLOGY

11.1 Introduction

Igneous rocks make up far-and-away the majority of the crust, and if we include the mantle, overwhelm all other rock types. Inevitably, every rock at the Earth's surface owes its origin to igneous rocks. Processes that occur in the near-surface environment can ultimately be best understood if we have a firm understanding of the composition and compositional range of different isotopic reservoirs, particularly those of the mantle. Igneous rocks can undergo a variety of modifications on their way to the surface. From a pristine mantle-derived magma, isotopic changes occur during fractional crystallization, assimilation of country rock, magma mixing, degassing, and hydrothermal alteration. Alteration can also occur at depth by subduction-related contamination and mantle metasomatism. All of these processes have been addressed using stable isotope geochemistry. This chapter is organized from the inside-out. That is to say, we start from the mantle and work towards the surface.

Oxygen is the major component of the mantle. The oxygen isotope composition of the oceans and all meteoric waters are ultimately controlled by hydrothermal interaction with oceanic igneous rocks of mantle origin. Carbon, sulfur, nitrogen and hydrogen are all trace components in the mantle. Nevertheless, due to the immensity of the mantle, even relatively small amounts of degassing of these elements can affect, or has affected in the past, their isotopic compositions in the terrestrial environment. Although there are important exceptions, the stable isotope compositional range of mantle materials are generally limited. The much larger isotopic variability seen in crustal igneous rocks is ultimately due to low temperature, upper crustal processes[1]. Many igneous rocks preserve an isotopic signature characteristic of a low-temperature alteration event. Where in their genesis these rocks inherited such a signature is an important aspect of stable isotope geochemistry as applied to igneous rocks and ore deposits.

11.2 The Mantle

The mantle is heterogeneous no matter how it is viewed. A seismologist sees distinct zones, layers and crosscutting slabs. This does not necessarily correlate with a geochemists view of the mantle. A seismic discontinuity related to density variations may not manifest itself chemically. From a geochemical standpoint, the mantle is heterogeneous with respect to elemental concentrations, radiogenic isotope geochemistry and stable isotope geochemistry.

The chemical composition of the mantle is more heterogeneous than it was early in Earth's history. Removal of melts leads to a mantle depleted in incompatible elements while addition of subducted material adds crustal-derived volatiles to the mantle. Perhaps the mantle was well homogenized after the Giant Impact between a Mars-sized impactor and the proto-Earth, which is responsible for the Earth-Moon system. It is thought that

[1] For oxygen and hydrogen, large variations are controlled by processes of fractionation related to the meteoric water cycle; for carbon, nitrogen and sulfur, biogenic processes are far more important.

the energy of the impact would have led to a magma ocean which presumably would have homogenized the mantle. However additional material was supplied to the Earth hundreds of millions of years after the Giant Impact, and this late delivery may be responsible for a significant amount of Earth's water. The chemical composition of a homogeneous, primordial mantle is termed the bulk silicate Earth, or BSE. Formation of continental crust led to development of a depleted mantle component, so that in the simplest case, we have three components – the BSE, the depleted mantle and continental crust.

The mantle has also been contaminated by reintroduction of crustal material during subduction. Radiogenic isotope, rare gas and trace element geochemistry allow for a number of mantle subdivisions to explain multicomponent chemical trends (see van Keken et al., 2002 for a review). Based on fundamental chemical differences between mid-ocean ridge basalts (MORB) and ocean-island basalts (OIB), the mantle has been divided into a primitive mantle, where the chemical composition is similar to the bulk silicate Earth (BSE) and a depleted mantle, manifest at mid-ocean ridges (DMM – depleted mid-ocean ridge MORB mantle). Further subdivisions include a sub-continental mantle, which has been affected by subduction and may have been isolated from other mantle regions for extended periods of time. High $^{3}He/^{4}He$ ratios of OIB have been interpreted in terms of a primitive, undegassed component. An enriched mantle source, defined by Rb/Sr, Sm/Nd and (U + Th)/Pb ratios that are higher than primitive mantle, is sampled at several hot spots (*e.g.*, Hawaii, Pitcairn, Samoa). Zindler and Hart (1986) further divided the enriched mantle into three components[2] and proposed that all oceanic mantle compositions could be derived by mixing between these components and a depleted MORB mantle (DMM). Hart *et al.* (1992) added a lower mantle component, presumably transported by plumes. Given the chemical complexity of the mantle, it is now unclear whether the simple primitive mantle, representative of the bulk silicate earth even exists today!

11.2.1 Oxygen

In the absence of contamination by crustal material, the oxygen isotope composition of the mantle has a very limited range. This is because the fractionation between the major minerals and melts in the mantle are small. Excepting spinel and CO_2, the fractionation between olivine and other phases such as pyroxene and silicate melts will be far less than 1‰ at mantle temperatures. Fractional crystallization, which is the process whereby crystals are removed from a melt by gravitational settling, will have a very minor effect on the $\delta^{18}O$ value of the magma until the melt evolves beyond the composition of basalt into the andesite or dacite field with the concomitant precipitation of quartz (Fig. 11.1). Isotopic shifts will be larger for hydrous melts, but probably never exceed 1.5‰ during simple fractional crystallization.

A pristine sample of mantle, not contaminated by subducted material, would provide us with the BSE composition and the oxygen isotope composition of the Earth . If such a sample existed, then deviations from it could be used to evaluate subtle degrees of contamination or chemical removal. Sampling the pristine mantle is not trivial. We only have access to samples now at the Earth's surface. Samples now at the surface that

[2] These are HIMU (high (U+Th)/Pb without high Rb/Sr) and EMI and EM2 (enriched mantle 1 and 2) which may contain recycled continental material, or have undergone mantle metasomatism.

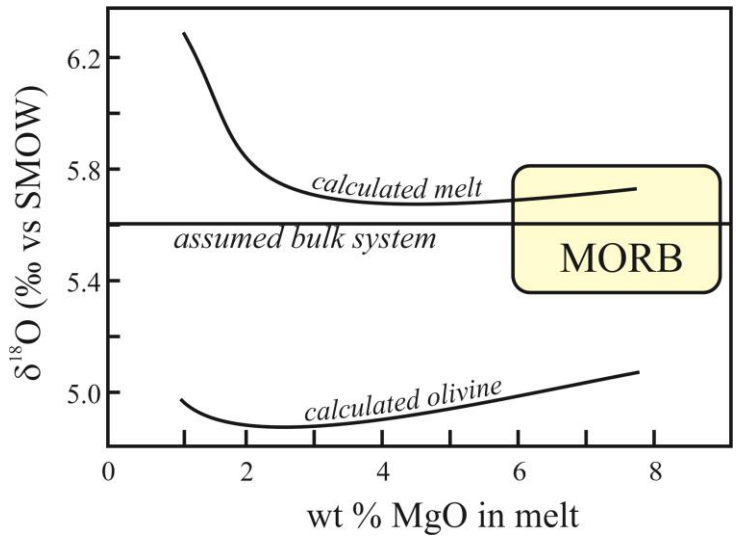

Fig. 11.1. Calculated $\delta^{18}O$ values of melt and olivine crystals during progressive fractionation crystallization (toward lower MgO contents). Only when the residual melt reaches a very high SiO_2 content (low wt% MgO in melt) does the $\delta^{18}O$ value change appreciably. After Eiler (2001).

originated at great depths have had abundant 'opportunities' to be modified during ascent by processes such as mixing, segregation, degassing, polymorphic transformation, assimilation, breakdown of high pressure minerals and rapid surficial alteration of unstable phases. Therefore, one of the most difficult tasks in mantle studies is seeing-through the modifications that can and often do occur. Three approaches have been used. The first is to use meteorite and lunar data as a proxy for the mantle. The second is to analyze mafic lavas, and the third is to analyze xenoliths or phenocrysts hosted in the lavas themselves. In spite of all the effort that has gone into answering the basic question of the oxygen isotope composition of the Earth's mantle, we still do not have a good feel for what the $\delta^{18}O$ value of the deep mantle is, clouding the refinement of the bulk $\delta^{18}O$ value of Earth.

Meteorites and Lunar basalts

Meteorites and lunar basalts can be used as a proxy for the bulk Earth $\delta^{18}O$ value. The $\delta^{18}O$ and $\delta^{17}O$ values of all meteorites are extremely scattered (Fig. 13.4). Enstatite chondrites, which most closely represent the bulk Earth in terms of the three oxygen isotopes, have a narrow range of $\delta^{18}O$ values centered around 5 to 6‰. The moon lies on the $\delta^{17}O$-$\delta^{18}O$ terrestrial fractionation line, strongly supporting a common origin for the Earth and Moon, or at least a well-mixed system. The $\delta^{18}O$ values of lunar samples have a very restricted value clustering at 5.7‰ (Spicuzza et al., 2007). If the Earth-Moon were truly homogenized during the Giant Impact, then the $\delta^{18}O$ value of 5.7‰ should also apply to the bulk Earth. See Chapter 13 for more on extraterrestrial samples.

Mafic Lavas

Mafic lavas and their mantle-sourced nodules are the material at the Earth's surface closest in composition to the mantle. However, there is a wealth of evidence indicating that the chemical compositions of most mafic lavas at the surface have been

modified from what they were at depth. Mafic magmas are often very fine-grained and glassy. Surface alteration, degassing and hydration occur very quickly. Phenocrysts tend to be less altered than the groundmass, and generally have a more restricted range of $\delta^{18}O$ values than bulk basalt (Kyser, 1986; Eiler et al., 1995). There is a strong correlation between Fe_2O_3/FeO or water content and $\delta^{18}O$ values of young submarine basalts (Fig. 5.7). Samples with the least degree of alteration are those with low water content and low Fe_2O_3/FeO ratios (Kyser et al., 1982). Bulk basalt samples have a wide range of $\delta^{18}O$ values (Fig. 11.2).

The oxygen isotope composition of MORB is very homogeneous. Ito *et al*. (1987) determined that the $\delta^{18}O$ value of fresh MORB glasses ranged from 5.3 to 6.2‰, averaging 5.7±0.2‰. Slight variations correlating with Sr, Nd and Pb isotope data were interpreted in terms of contamination by a small percentage of recycled crustal material. Analyses by laser fluorination also have a limited range of $\delta^{18}O$ values that average 5.5‰, and similar conclusions have been made regarding contamination by subducted material (Eiler, 2001).

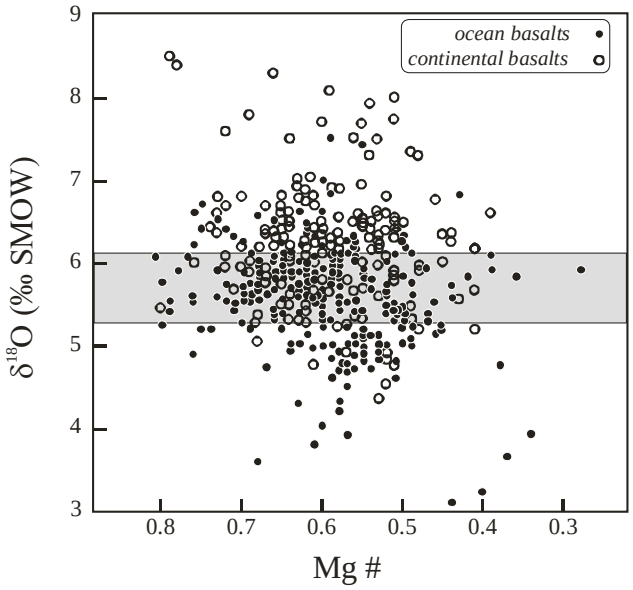

Fig. 11.2. Compilation of oxygen isotope values of oceanic and continental basalts vs. Mg #. The wide range of $\delta^{18}O$ values in the range of 'pristine basalts' (Mg#=0.68-0.75) has been used as evidence for mantle heterogeneity. Shaded area shows 'pristine' mantle value. After Harmon and Hoefs (1995).

Ocean Island Basalts range from 4.6 to 7.5‰ (mean of 5.5±0.5 1σ) and continental basalts range from 4.5 to 8.1‰ (mean 6.1±0.7) (Harmon and Hoefs, 1995). On the basis of the wide range of $\delta^{18}O$ range for 'unmodified, primary mantle partial melts' (Mg# of 0.68-0.75[3]) of 5 to 7‰, Harmon and Hoefs concluded that the upper mantle is clearly heterogeneous with respect to oxygen isotope ratios (Fig. 11.2).

[3] Mg # is defined as the molar ratio of Mg/(Mg+Fe).

Several lines of evidence indicate that the basalt data may not accurately reflect the isotopic composition of the mantle. There are a number of studies that illustrate subtle alteration features that could easily be overlooked. In samples that show little chemical evidence of alteration or contamination by crustal material during ascent, unusual hydrogen isotope compositions or large variations in the isotopic composition of xenocrystic material may indicate cryptic alteration (Dobson and O'Neil, 1987; Baldridge et al., 1996; Feldstein et al., 1996). Clear evidence of basalt glass alteration can be seen when comparing the glass data with coexisting phenocrystic material. For example, the oxygen isotope ratios of fresh, recently-erupted submarine volcanic glasses from the Pitcairn seamounts range from 5.8 to 7.4‰ (Woodhead-Jon and Devey-Colin, 1993). In contrast, the $\delta^{18}O$ values of olivine phenocrysts from basalts from Pitcairn island are homogeneous at 5.2‰, indistinguishable from typical mantle values (Eiler et al., 1995). For these reasons, recent studies tend to focus more on resistant phenocrysts or xenoliths than basalts themselves.

Phenocrysts and xenoliths

Olivine and pyroxene are the principal minerals making up mantle xenoliths. Very early on in the isotope game it became clear that olivine was notoriously difficult to fluorinate using the extraction techniques that were available at the time. Taylor and Epstein (1963) found that only 60 and 80‰ of olivine reacted with fluorine. Only one analysis gave an oxygen yield of 88%[4], which they considered reliable. Several researchers (Reuter et al., 1965; Garlick, 1966) circumvented the problem by first fusing olivine with quartz of a known composition to make a pyroxene glass, which could easily be fluorinated. The $\delta^{18}O$ value of the olivine could then be determeind by simple mass balance. Clearly the problems associated with analyzing olivine were well known.

Javoy analyzed a number of olivine samples from peridotite massifs and obtained $\delta^{18}O$ values of 5.2±0.08‰ (Javoy, 1980). Later work by a number of researchers showed that $\delta^{18}O$ values of olivine spanned a considerable range of 4.5 to 7.5‰. The spread of data was interpreted in terms of heterogeneous mantle reservoirs (Kyser, 1986) or mantle metasomatism (Gregory and Criss, 1986). It now appears, however, that much of the variability may have been an artifact of the analytical technique. Fluorination of olivine by laser heating results in a far smaller range of $\delta^{18}O$ values, with a mantle average of 5.18±0.28‰ (2σ) (Mattey et al., 1994), and a total range of 4.8 to 5.5‰. The $\Delta^{18}O_{cpx\text{-}ol}$ values average 0.4‰, consistent with a constant (temperature insensitive) fractionation at mantle temperatures.

The laser fluorination data indicate that the $\delta^{18}O$ value of the mantle is far less heterogeneous than had previously been thought. The large variations in oxygen isotope values found in OIB basalts therefore need to be considered in terms of alteration immediately prior to, during, or post eruption. The mantle value of 5.2‰ has been used as a benchmark from which to estimate the degree of crustal contamination. For example, olivine phenocrysts from Pitcairn basalts are indistinguishable from the mantle average value of 5.2‰ (Eiler et al., 1995), whereas the basalts themselves are quite scattered.

[4] The oxygen yield is the relationship between amount of O_2 gas produced (determined manometrically) and the theoretical yield based on sample weight and stoichiometry. For example, quartz has 16.64 μmol O_2/mg quartz, such that 10 mg of quartz should evolve 166.4 μmol of O_2 during the fluorination procedure.

Eiler *et al*. concluded on the basis of the 'mantle' oxygen values that incorporation of subducted sediment is not the explanation for the unusual Sr, Nd and Pb isotope ratios exhibited by these EM1 ocean island basalts. If the mantle is indeed as homogeneous as is presently thought, then even slight variations of a few tenths of a per mil – what would be considered 'noise' in most studies – have geological significance.

Mantle Eclogites

The discovery of oxygen isotope anomalies in mantle eclogites provided the earth science community with direct geochemical evidence for subduction and recycling of crustal material. Originally misinterpreted as being a function of fractional crystallization, the large variations in $\delta^{18}O$ values of mantle eclogites were instead considered by MacGregor and Manton (1986) and Ongley *et a.l* (1987) to be the result of

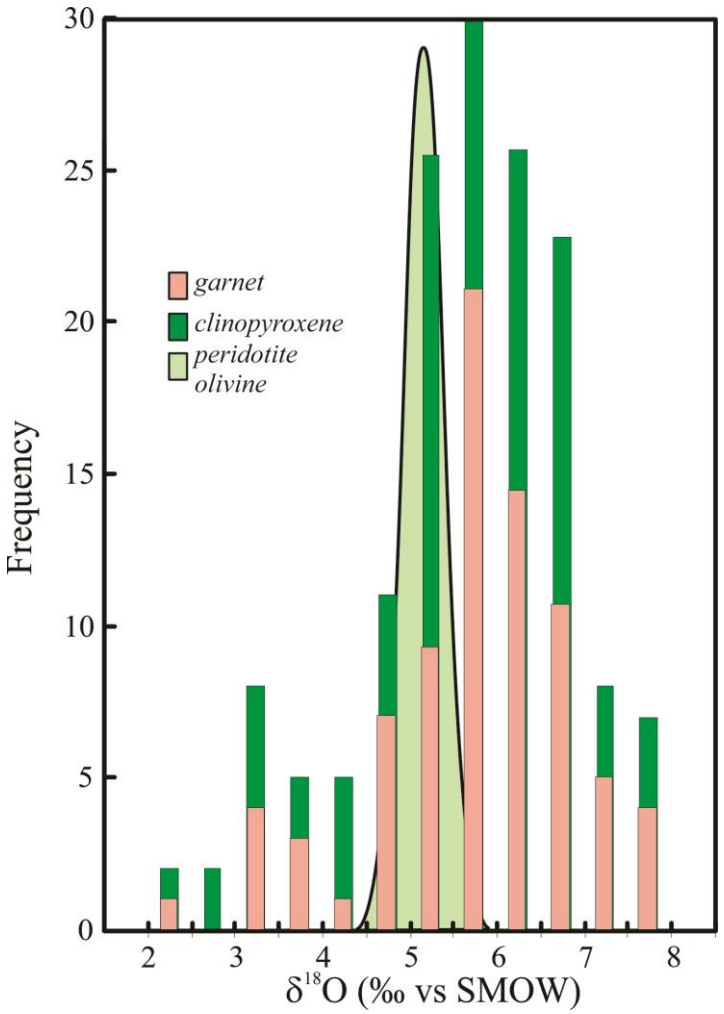

Fig. 11.3. Oxygen isotope values of garnet and clinopyroxene in mantle eclogites. Also shown is the distribution of peridotites (not at same frequency scale, *n*>100). Data from (MacGregor and Manton, 1986; Ongley et al., 1987; Shervais et al., 1988; Caporuscio, 1990; Mattey et al., 1994 ; Snyder et al., 1995; Viljoen et al., 1996; Smart et al., 2014).

metamorphosed subducted oceanic crust. Unlike peridotites, which have a very narrow range of $\delta^{18}O$ values, mantle eclogites span a range of 2 to 8‰ (Fig. 11.3). The large variation in $\delta^{18}O$ values cannot be explained in terms of any known mantle processes. Instead, the spread in $\delta^{18}O$ values is remarkably similar to those seen in altered oceanic crust (Figs. 5.8, 5.9). The carbon and sulfur isotope data presented in the following sections support the pre-subduction near-surface alteration signature for eclogites. Anomalously high $\delta^{18}O$ values have also been found in silicate inclusions from diamonds sourced at depths of >350 km (Burnham et al., 2015), indicating that mafic rocks altered near the Earth's surface have been subducted to great depths.

11.2.2 Carbon

There has been a considerable effort made towards understanding the carbon isotope systematics of the mantle. It is now quite clear that the range of carbon isotope values in mantle phases far exceeds that of oxygen. There are a number of proposed mechanisms for the large range. Compelling arguments have been made for each proposed mechanism, and, not surprisingly, the geological community has yet to reach consensus. One important difference between carbon and oxygen isotope systematics is that carbon isotope fractionation between relevant mantle phases is large even at high temperatures (Fig. 11.4) primarily because carbon exists in different oxidation states. Contrast this with oxygen, where fractionations are too small to have any significant consequence at mantle temperatures. A review of carbon in the mantle can be found in Deines (2002).

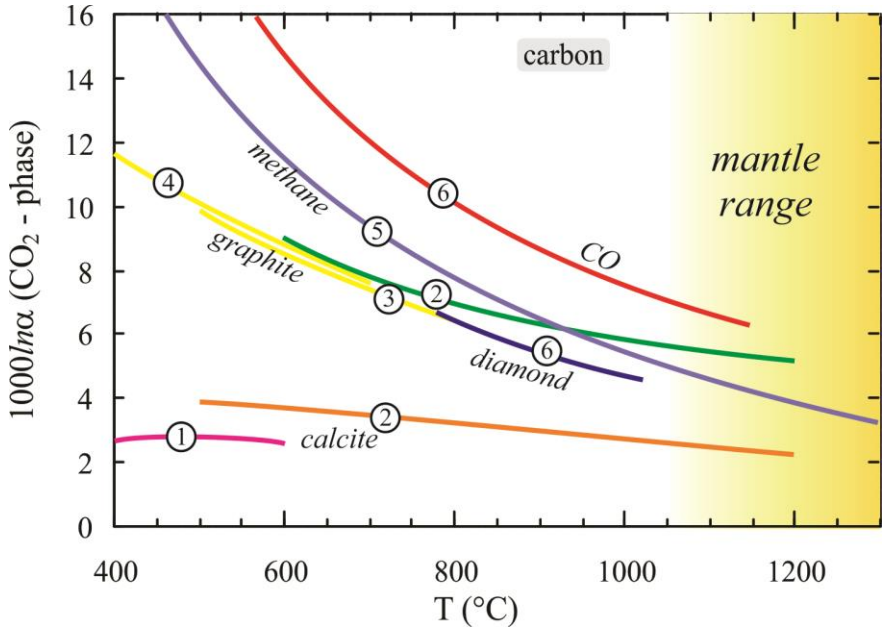

Fig. 11.4. Carbon isotope fractionations between phases at moderate to high temperatures. References: 1) (Bottinga, 1969); 2) (Scheele and Hoefs, 1992); 3) (Chacko et al., 1991) & (Scheele and Hoefs, 1992); 4) (Bottinga, 1968); 5) (Richet et al., 1977); 6) (Deines, 1980).

Carbon composition inferred from crustal reservoir

All crustal carbon is sourced by the mantle. The huge carbon flux along mid ocean ridges is sufficient to supply all terrestrial carbon in 300 to 700 million years (DesMarais, 1985)[5]. If all carbon in the crustal reservoir is derived from the mantle without appreciable isotopic fractionation, then the $\delta^{13}C$ value of the overall mantle can be determined from the bulk crustal value using mass balance equations, knowing the sizes and $\delta^{13}C$ values of the two major crustal reservoirs, carbonate and organic carbon (see section 7.2.1). If we assume that the $\delta^{13}C$ value of carbonates and organic matter are 0‰ and -25‰, respectively, with an abundance ratio of 4 to 1, then the bulk $\delta^{13}C$ value of the crust is -5‰. This should be the mantle value as well.. Other published estimates of this kind range from -4.5 to -7‰ (e.g., Hoefs, 1973).

Diamonds and graphite

Diamonds are arguably the best phase for addressing the $\delta^{13}C$ values of the mantle. They are unambiguously of mantle origin and once formed, are certain to retain their carbon isotope ratio. $\delta^{13}C$ values of diamonds have a huge range from -40 to +5‰ (Cartigny, 2005; Smart et al., 2011). A number of observations are apparent from the compiled data (Fig. 11.5):

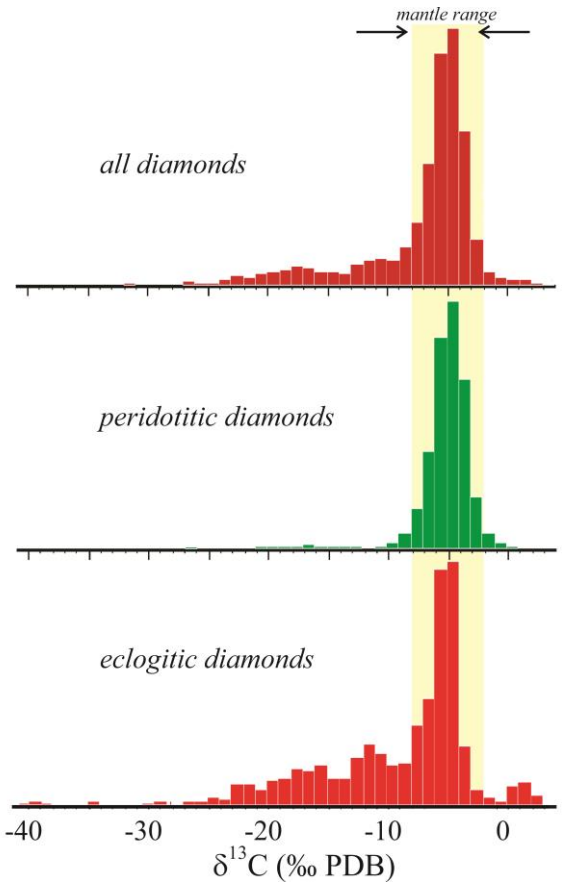

Fig. 11.5. Carbon isotope values of diamonds. The mode is between -5 and -6‰, skewed towards low values. The low values are due to eclogitic and metamorphic (not shown) diamonds. After Cartigny (2005).

1) There is a very pronounced mode at -5 to -6‰. 2) The data are skewed towards negative values down to less than -30‰. 3) There is a sharp upper limit to the data at approximately -1‰ with a few rare exceptions at higher $\delta^{13}C$ values. The low $\delta^{13}C$ values are almost exclusively eclogitic diamonds (E-type), and not peridotitic diamonds (P-type).

A number of mechanisms have been proposed to explain the data. Those considered most probable are the following:

1) Recycling of surficial carbon: The $\delta^{13}C$ value of the mantle is between -5 and -6‰ and samples with higher, but especially lower $\delta^{13}C$ values, are caused by contamination from subducted material. This

[5] Presumably there is a return flux to the mantle *via* subduction of a (near?) equivalent magnitude.

argument is strongly supported by correlation of the $\delta^{13}C$ values of diamonds with their occurrence. The P-type diamonds hosted in peridotites have a generally narrow range of $\delta^{13}C$ values that are close to the presumed mantle value of -5.5‰. The E-type diamonds have peak $\delta^{13}C$ values similar to peridotitic diamonds and tail down to an extremely low $\delta^{13}C$ values of -40 ‰ (Smart et al., 2011). The low $\delta^{13}C$ values are easily explained by subduction of light organic matter. As we have already seen earlier, the $\delta^{18}O$ values of eclogites are anomalous compared to the rest of the mantle, and have been explained in terms of subducted altered crust. As a logical extension, the low $\delta^{13}C$ values of the E-type diamonds are explained by a subducted organic source. The logic is simple and requires no extraordinary processes other than that oceanic material has been subducted to mantle depths. Low $\delta^{13}C$ organic matter of Archean age is known to exist and thought to the be result of methane-fixation by methanogenic bacteria (e.g., Eigenbrode and Freeman, 2006). Further evidence for a surficial subducted component is the non-zero $\Delta^{33}S$ of inclusions within diamonds (Farquhar et al., 2002a). Mass independent sulfur isotope fractionations presumably require photochemical-induced mass-independent reactions, which demonstrates that (at least) the inclusions within some diamonds must have been at the surface at one time. The idea of subducted light carbon works on all levels with few arguments to refute this hypothesis (see however, Deines et al., 1993).

2) Rayleigh distillation of mantle fluids: Loss of CO_2 from the carbon-bearing fluid (*e.g.,* carbonate-rich fluid) will lower the $\delta^{13}C$ value of the remaining fluid (Cartigny et al., 2001). As seen in Fig. 11.4, the $\Delta^{13}C_{CO2\text{-}calcite}$ value is on the order of 2-4‰ at mantle temperatures, so that under an extreme Raleigh fractionation process, the $\delta^{13}C$ values of a mantle fluid can be lowered substantially. This process can explain part of the spread in $\delta^{13}C$ values seen in E-type diamonds, but requires an unreasonably large amount of CO_2 extraction to produce diamonds that are as light as 40‰. A trend towards increasing $\delta^{13}C$ values in diamonds with decreasing depth from the Panda kimberlite, Canada is interpreted as a result of carbon isotope fractionation of an upward percolating carbonate-bearing metasomatic fluid/melt (Melton et al., 2013).

3) Inheritance of primordial light carbon: Extraterrestrial material has a wide range of $\delta^{13}C$ values. The low $\delta^{13}C$ values could therefore be inherited directly from the incorporation of light extraterrestrial material during Earth formation (Deines et al., 1993). It is not clear why only E-type diamonds would preserve this low primordial value. Furthermore, extraterrestrial material with $\delta^{13}C$ values as low as -40‰ are extremely rare, mainly found in pre-solar diamonds (Smart et al., 2011), making this explanation extremely unlikely.

Carbonatites and kimberlites

Carbonates in kimberlites and carbonatites are of deep-seated origin, and can be used to constrain the $\delta^{13}C$ value of the mantle. There are advantages and disadvantages to using carbonates compared to diamonds. Carbonatites are large masses of carbon-bearing material and most likely have undergone minimal carbon isotope fractionation during their formation or during ascent. The disadvantage of analyzing carbonates is that their $\delta^{13}C$ values can be modified during or following eruption. Degassing of CO_2, surficial meteoric water alteration, diagenesis, mixing with biogenic carbonates can all affect the

$\delta^{13}C$ values of carbonatites. None of these processes, on the other hand, will influence the $\delta^{13}C$ values of diamonds.

Taylor *et al.* (1967) measured carbon and oxygen isotope ratios of carbonatites (mantle-derived carbonates) and were able to distinguish the most pristine samples from those that had undergone significant exchange on the basis of C-O trends. The lowest isotope ratios were used to define the 'carbonatite box' with $\delta^{18}O$ and $\delta^{13}C$ values of 6 to 8‰ and -5 to -8‰, respectively. Other carbonatite studies have used additional criteria such as radiogenic isotope and trace element ratios, and depth of emplacement to subtract the effects of late alteration or degassing. Deines and Gold (1973) concluded that the average $\delta^{13}C$ value of carbonates is -5.1 ± 1.4‰, with statistically significant variation between carbonatite complexes. Carbonates in kimberlites are extremely fine-grained. The $\delta^{13}C$ value of kimberlites is statistically indistinguishable from carbonatites, but $\delta^{18}O$ values are invariably higher due to hydrothermal exchange during or post emplacement.

Basaltic glass

Carbon is present in basaltic glass trapped as fluid inclusions, along grain boundaries and as a dissolved component. Early studies gave a wide range of $\delta^{13}C$ which, it is now apparent, was due to analytical problems. There are two distinct populations of carbon that are released when samples are step-heated. At temperatures below 600°C degassing in an oxygen atmosphere generates a low $\delta^{13}C$ CO_2 gas (~-26‰). Upon further heating (in excess of 1000°C) CO_2 gas is liberated with a $\delta^{13}C$ value of approximately -6.6‰. The CO_2 evolved from low temperature heating is thought to be due to either organic contamination or late degassing/fractionation associated with emplacement. MORB glasses have a very consistent $\delta^{13}C$ value of -6.3‰; other basalt types show slight variations from this value (Exley et al., 1986).

11.2.3 Nitrogen

The paucity of nitrogen isotope measurements in deep-seated rocks is partly related to analytical difficulties which have only recently been overcome. Nitrogen is present in trace quantities in igneous rocks, and even minor atmospheric contamination will compromise an analysis. The low concentration of nitrogen in the mantle is an analytical problem, but it is also a benefit. Even small amounts of recycled material (crustal contamination), for example, could significantly alter the $\delta^{15}N$ of a sample. Thus, nitrogen isotope ratios are very sensitive indicators of mantle heterogeneities and mixing between reservoirs. In the last ten years, our understanding of nitrogen isotope systematics in the mantle has improved dramatically, nevertheless, a complete characterization of mantle isotope reservoirs and end-members is far from complete.

A thorough review of nitrogen isotope systematics in mantle materials can be found in Marty and Dauphas (2003). The average $\delta^{15}N$ value of the mantle is -5‰ relative to AIR, although clear heterogeneities exist (Fig. 11.6). The $\delta^{15}N$ value of gases extracted from MORB glass vesicles by crushing, range from -5 to +5‰. Samples with high $^{40}Ar/^{36}Ar$ ratios (indicating minimal air contamination) have $\delta^{15}N$ values of -5 to -3‰ (Marty and Humbert, 1997). Negative $\delta^{15}N$ values of N_2 gases are found in volcanic fumaroles (Sano et al., 2001; Fischer et al., 2002). When considered in conjunction with other rare gas geochemistry, the fumarole-derived samples require a mantle component that is significantly less than -5‰, possibly as low as -15‰ (Mohapatra and Murty,

2004). The $\delta^{15}N$ value of diamonds has a strong mode at -5‰ as well, although there is considerable scatter, with values ranging from -25 to +15‰. Li *et al.* (2016) proposed that the mantle $\delta^{15}N$ value of -5‰ can be explained by a light enstatite chondrite source (-25 to -15‰), with subsequent partitioning of light nitrogen into the core.

In contrast to MORB, deep mantle material, as sampled by mantle plumes has $\delta^{15}N$ values that are typically positive, ranging from –2 to 8‰. A number of explanations for the variations have been presented. Javoy (1997) suggested that heterogeneities in the mantle are remnants of heterogeneities of early accretion. Marty and Dauphas (2003) proposed that the difference between plume-related samples and MORB can be explained by secular variations in subduction. Archean sediments have $\delta^{15}N$ values as low as -6‰ (Beaumont and Robert, 1999), in comparison to modern sediments which are almost always positive. Archean sediments with negative $\delta^{15}N$ values would have only been subducted to shallow levels (due to the high temperatures early in the Earth's history), whereas younger material with positive $\delta^{15}N$ values could be subducted to much greater depths. In this scenario, the MORB data represent early subduction of material with negative $\delta^{15}N$ values, whereas mantle plumes tap a nitrogen reservoir related to much younger (and deeper) subduction. The reason that nitrogen may trace crustal subduction so clearly is simply that it has a very low concentration in unaltered mantle. Even slight additions to the mantle are therefore evident.

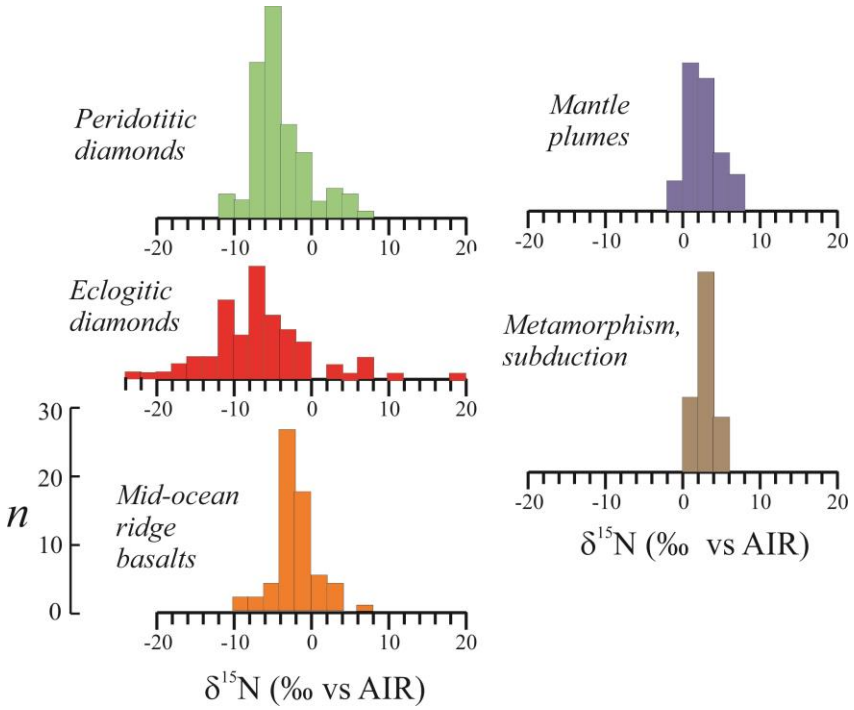

Fig. 11.6. $\delta^{15}N$ values of different mantle sources. After Marty and Dauphas (2003).

11.2.4 Hydrogen

Determining the hydrogen isotope composition of pristine mantle is a daunting endeavor, but one of significant importance. Knowing the abundance and isotopic composition of the mantle places significant constraints on the source of water to Earth.

The task of knowing the mantle hydrogen composition is complicated by the fact that almost any modification that occurs during ascent from depth to the surface will alter the hydrogen isotopic composition of whatever phase is hosting it. The very processes that bring a sample from the mantle to the surface are themselves aberrations from normal mantle conditions. For example, eruption of a xenolith-bearing kimberlitic magma is initiated by infiltration of a metasomatic fluid, which could alter the δD value of a mineral in a xenolith. Degassing and hydrothermal contamination would also alter the δD value of the sample. The problem is made more acute because of the rapid diffusion of hydrogen in minerals. In spite of these well-known problems, a number of researchers have addressed the hydrogen isotope systematics of mantle samples.

Hydrogen isotope measurements of bulk mantle minerals, fluid inclusions, and fresh glass from submarine basalts range from -120 to +13‰ (e.g., Sheppard and Epstein, 1970; Sheppard and Dawson, 1975; Kuroda et al., 1977; Boettcher and O'Neil, 1980; Kyser and O'Neil, 1984), a huge range. *In situ* spot analyses from single amphiboles span a range of more than 50‰ (Deloule et al., 1991; Xia et al., 2002). There are a number of processes which can modify the hydrogen isotope composition of mantle phases during ascent. Exchange with water can either raise or lower the δD value of a glass or hydrous mineral. Simple degassing will lower the δD value, whereas dehydrogenation, or the removal of molecular H_2 will *raise* the δD value of a hydrous phase (Feeley and Sharp, 1996).

Fresh submarine basalts encompass a wide range of both δD values and water contents. Kyser and O'Neil (1984) were able to explain δD value - water content trends in terms of degassing and addition of seawater (Fig. 11.7). By extrapolating these trends back to the 'unmodified' δD values of the original basalts, they concluded that the mantle has a 'surprisingly constant' δD value of ~-80‰. According to Kyser (1986), the hydrogen isotope composition of the mantle is "surprisingly uniform and best explained by the presence of a homogeneous reservoir of hydrogen that has existed in the mantle since the very early history of the earth".

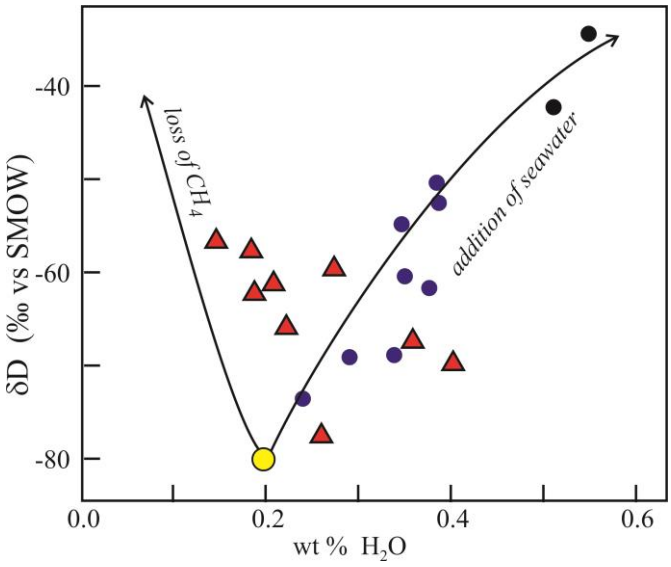

Fig. 11.7. Correlation of δD value and water content for Kilauea (circles) and Mid-Atlantic Ridge samples (triangles). The Kilauea samples can be explained by addition of water, while the MAR samples follow a CH_4 degassing (volatile loss) trend. Both trends converge at an unmodified value of ~-80‰. Trends are schematic. After Kyser and O'Neil (1984).

Boettcher and O'Neil (1980) analyzed a number of phlogopites and amphiboles from kimberlites and proposed a range of deep-seated H_2O of -58 to -79‰. In contrast to the phlogopites which had a relatively restricted range, the δD values of amphibole megacrysts were extremely scattered, ranging from

-113 to +8‰. The very variable δD values (combined with other chemical compositions) led the authors to conclude that there are complicated, near-surface processes that involve a discrete aqueous fluid. Late degassing behavior is supported by high-resolution ion-microprobe studies, where variations of 50‰ over 100s of microns are found (Deloule et al., 1991).

The δD value of the mantle above subduction zones is inferred from materials associated with these environments. Poreda (1985) found that basalts from the Mariana Trough had a number of geochemical characteristics clearly indicating a subducted component, including elevated water contents and $\delta^{18}O$ values, and low $^3He/^4He$ ratios. The δD values for these rocks are -46 to –32, consistent with an aqueous component from a low-T altered seafloor basalt. High δD values are also found in fresh boninite glasses, supporting a subducted component to these materials (Dobson and O'Neil, 1987). Giggenbach (1992) compiled data for volcanic and geothermal discharges around the Pacific rim and proposed a magmatic 'andesite' water component with a δD value of -20±10‰. Basaltic water (δD = -60‰) is brought to the mantle from hydrated basalt, whereas the andesitic water is a mixture of oceanic crust, pore water, and clay minerals accumulated in marine sediments. The distinctly different δD values for basaltic and andesitic water are due to dehydration of the different components occurring at different levels in the subduction zone.

In spite of the apparent homogeneous reservoir of the Earth's mantle with respect to hydrogen isotopes, there are some notable exceptions. Perhaps the most striking example comes from the primitive picritic lavas from the Baffin Islands (Hallis et al., 2015). These lavas have very high $^3He/^4He$ values which are characteristic of consistent with preservation of a primordial, undegassed volatile source[6]. The δD values of melt inclusions in olivines from these samples reach the exceptionally low value of -218‰. Some surficial materials have far lower values, but there are no known mantle processes that could lower the mantle D/H ratio to such low values. The low D/H ratios of these samples are interpreted as direct incorporation of nebular hydrogen (Hallis et al., 2015), in which nearly pure protium from the solar nebula is dissolved into an early magma ocean (Sharp, 2017). More on this in Chapter 13.

11.2.5 Sulfur

Hulston and Thode (1965) determined that the $\delta^{34}S$ values of meteorites are near 0‰. The $\delta^{34}S$ values of MORB are very constant at +0.3 ± 0.5‰ (Sakai et al., 1984). As is so often the case, what appeared at first glance to be a 'well-behaved' system got more complicated as more data were collected (Fig. 11.8). *In situ* analyses of sulfide minerals in E-type diamonds range from +2.3 to +8.2‰ (Chaussidon et al., 1987), which are interpreted as evidence of subducted sulfur of terrestrial origin. Evidence for long term recycling of oceanic and crustal sulfur was also found in metasomatized xenoliths from Dish Hill, California, where $\delta^{34}S$ values are near +7‰, sourced from subducted crustal sulfur (Wilson et al., 1996). Evidence for a subducted sulfur component is most definitive in a recent study by Farquhar *et al*. (2002b) who found mass-independent $\Delta^{33}S$ anomalies

[6] ^4He is a byproduct of radiactive decay from U, Th and K. ^3He in mantle samples is primordial, meaning it was acquired during the formation of the Earth. High $^3He/^4He$ ratios are therefore indicative of primitive material that has not been contaminated by ^4He from incompatible radioactive elements.

in sulfides in diamonds from Orapa kimberlite. Such anomalies are normally found in Archean sediments and are only known from samples formed at the Earth's surface (Chapter 10). Their discovery in deep-mantle xenoliths is compelling evidence for recycling of an Archean sulfur component. Additional mass independent sulfur anomalies have been found in mantle plume samples, indicating that Archean sediments were subducted to great depths and remained in place for billions of years (Delavault et al., 2016).

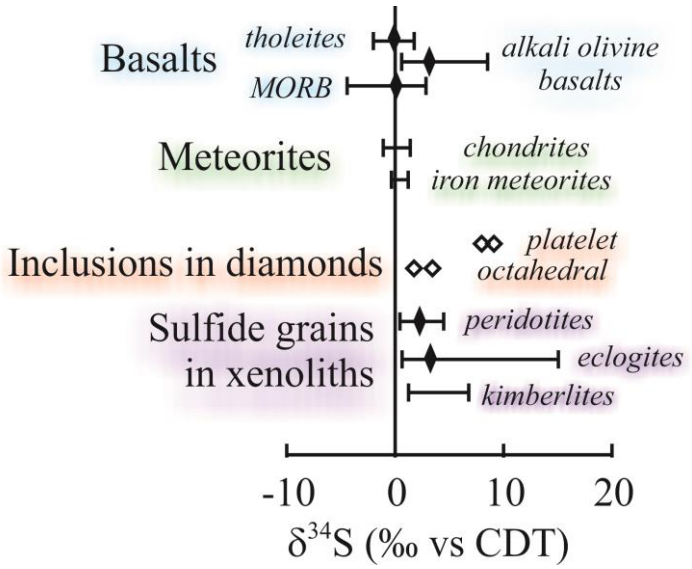

Fig. 11.8. Sulfur isotope composition of sulfides from various sources. Most data are near zero, with the notable exception of eclogites and inclusions in diamonds from eclogites. These data, supported by $\delta^{33}S$ anomalies, support a near-surface origin of sulfur in eclogites. After Chaussidon *et al*. (1987).

11.3 Emplacement of plutonic rocks: Interactions with the crust and hydrosphere

Magmas undergo a number of physio-chemical processes that change their isotopic composition on their arduous journey towards the Earth's surface. These include assimilation of crustal material, physical segregation by fractional crystallization, degassing, and hydrothermal alteration. Interaction of submarine basalts with seawater has already been discussed (Chapter 5), where $\delta^{18}O$ values of rocks can either be raised or lowered depending upon the temperature of interaction. The more general case of emplacement of plutonic rocks has been nicely outlined by Taylor in a number of publications, notably (Taylor, 1978) for plutonic granitic rocks. Compiled whole rock oxygen isotope data for a number of igneous rocks (Fig. 11.9) show a number of trends and patterns that can adequately be explained by well-understood processes.

Stable isotopes, particularly oxygen and hydrogen are well suited to the study of igneous rocks for the following reasons: 1) The oxygen and hydrogen isotope composition of the source region – the mantle – is well known and uniform. 2) As has been discussed for the mantle case, simple fractional crystallization does not affect the $\delta^{18}O$ value of a magma appreciably. Therefore, deviations from mantle values are evidence of open-system behavior at some time during or after emplacement. 3) The $\delta^{18}O$ values of sedimentary rocks are far higher than for igneous rocks. Combined with other isotopic systems, such as $^{87}Sr/^{86}Sr$, they can be used as a sensitive monitor for sedimentary contamination. 4) The oxygen and hydrogen isotope composition of meteoric and ocean water are unique and far different from those in equilibrium with deep-seated igneous rocks. Combined hydrogen and oxygen isotope data can be used to identify and sometimes quantify fluid-rock interaction in cases where other isotope or chemical systems completely fail.

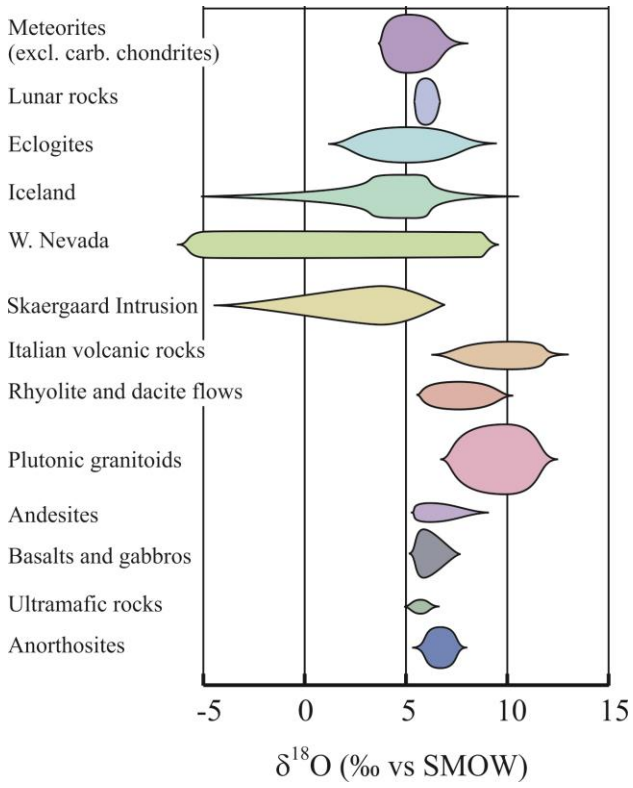

Fig. 11.9. Compilation of oxygen isotope compositions of various igneous rocks. The $\delta^{18}O$ values of lunar, meteoritic and most mafic and ultramafic rocks span a narrow range equal to the mantle. Plutonic granitoids in general range from 7 to 12‰, values higher than 9‰ found in S-type granites. There are a large number of altered rocks which plot both below and above the unaltered granitoids values. Volcanic andesite, rhyolite and dacite rocks tend to have $\delta^{18}O$ values that are several per mil lower than their intrusive equivalent. After Taylor (1974).

11.3.1 Normal igneous rocks

There are several common characteristics of unaltered igneous rocks. Whole rock $\delta^{18}O$ values range from 6 to 10‰[7]. The $\delta^{18}O$ values of coexisting minerals follow the expected order of ^{18}O enrichment: magnetite-biotite-hornblende-muscovite-plagioclase-potassium feldspar-quartz. The mineral fractionations correspond to high temperatures, but generally less than those expected for assumed granite emplacement temperatures. The explanation for the discrepancy is post-solidus exchange[8]. Typical $\Delta^{18}O$(quartz-plagioclase) values are 1.5-2.5‰; $\Delta^{18}O$(quartz-K-spar) values are 1.0-1.5‰. Volcanic rocks have $\delta^{18}O$ values that are generally 1-2‰ lower than chemically equivalent intrusive rocks. Finally, there is a general increase in $\delta^{18}O$ with increasing wt % Si. The increase, due in part simply to a higher modal abundance of quartz, has also been

[7] Values up to 14‰ are found in granitic rocks derived from melting of sedimentary material (section 11.3.3).

[8] Isotope fractionations corresponding to igneous emplacement temperatures are only preserved in very rapidly cooled, anhydrous rocks. For example, basalts from Hawaii and lunar basalts both preserve temperatures in excess of 1000°C.

explained by incorporation of crustal material at some point (Grunder, 1987). Taylor classifies granites (and more generally, plutonic rocks) into normal, low- and high-$\delta^{18}O$ groups (Table 11.1)

11.3.2. Shallow level hydrothermal alteration by meteoric water – low $\delta^{18}O$ plutonic rocks

Igneous bodies emplaced at shallow levels in the crust commonly undergo intense hydrothermal alteration. The high temperatures associated with the intrusion sets up hydrothermal convection cells that can drive significant amounts of aqueous fluids through the pluton and surrounding wallrock. Interaction with meteoric waters was recognized as early as 1963 (Taylor and Epstein, 1963), but the magnitude of water-rock interaction in shallow level plutons was not realized for another 20 years. Meteoric water infiltration may have no effect on the chemical composition of a pluton other than for stable isotope ratios (e.g., Criss and Taylor, 1983). Of course, hydrothermal waters can dissolve large amounts of other elements, explaining hydrothermal ore deposits.

Table 11.1 *Characterization of granitoids (Taylor, 1978).*

Type	$\delta^{18}O$	δD	Comments
Normal	6 to 10‰	-85 to -50‰	This represents the vast majority of all granites, granodiorites, quartz monzonites
Low $\delta^{18}O$	<6‰	>-150 to -85	The δD values can be higher. Hydrothermally altered granites
High $\delta^{18}O$	>10‰		S-type granites and low-T hydrothermal interaction

During shallow-level emplacement of a pluton, the pluton is the heat engine driving convection. The effect is largest for rocks emplaced at shallow levels in permeable host rocks, and will be most pronounced (from a stable isotope perspective) in regions where meteoric water is extremely light. For this reason, the majority of hydrothermal interaction studies have been made at high latitude/altitude. Modern examples of interaction of intrusions with meteoric water are associated with geothermal systems worldwide. Simply picture the spectacular thermal features at Yellowstone National Park to gain a sense of the magnitude of this effect, where shallow level plutons supply the heat for all of the magnificent hot springs and geysers seen at the surface today.

Intrusive igneous rocks hydrothermally altered by meteoric water share a number of characteristics, illustrated by an example from the Isle of Skye (Forester and Taylor, 1977). The $\delta^{18}O$ values of the altered rock are less than those of unaltered rocks, dropping to below -5‰. There is a characteristic, concentric depletion of $\delta^{18}O$ values towards the center of the complex. Low $\delta^{18}O$ values are seen both in the intrusive and country rocks, demonstrating that the hydrothermal exchange occurred post-emplacement. More alteration occurs in samples of higher permeability. δD values of amphiboles and chlorites are uniformly low relative to the mantle source, ranging from -132 to -119‰. Both quartz ($\delta^{18}O$ = -2.7 to +7.6‰) and plagioclase ($\delta^{18}O$ = -6.7 to +6.0‰) have $\delta^{18}O$ values well below those for normal granites, but the degree of hydrothermal alteration and isotopic lowering is far greater for feldspars. $\Delta^{18}O$(quartz-

feldspar) values are much larger than in normal granites, indicating that alteration of feldspars was more intense than for quartz. Low $\delta^{18}O$ values of exchange-resistant zircon (Gilliam and Valley, 1997) confirm earlier work by Forester and Taylor that the pre-emplacement $\delta^{18}O$ value of some of the later intrusions were lower than for normal granites.

A nice example of a fossil hydrothermal system is found centered around a series of shallow level granitic plutons in the Idaho batholith (Criss and Taylor, 1983). The $\delta^{18}O$ values of altered plagioclase are as low as -8.2‰, compared to the initial values of 9.3‰. The dimensions of the alteration cover over 15,000km. The $\delta^{18}O$ values can be contoured, with a general bulls-eye pattern centered on the intrusion. In at least one case, there is a 60 km diameter high-permeability ring fracture zone associated with caldera collapse, in which the lowest $\delta^{18}O$ values are found (Fig. 11.10).

The above results can be used to produce a general picture of shallow-level hydrothermal alteration of plutonic intrusive rocks. First, it should be recognized that meteoric waters do not alter the $\delta^{18}O$ value of a pluton until it has crystallized. This is because the partially-molten pluton is at lithostatic pressure, while water in the country rock is most likely at hydrostatic pressure. Furthermore, the viscosity of a siliceous magma is high and diffusion of water into the pluton is slow and an inefficient process. Finally, the amount of water necessary to significantly change the isotopic composition of the magma is on the order of 15%, far larger than the water-solubility of a silicate liquid.

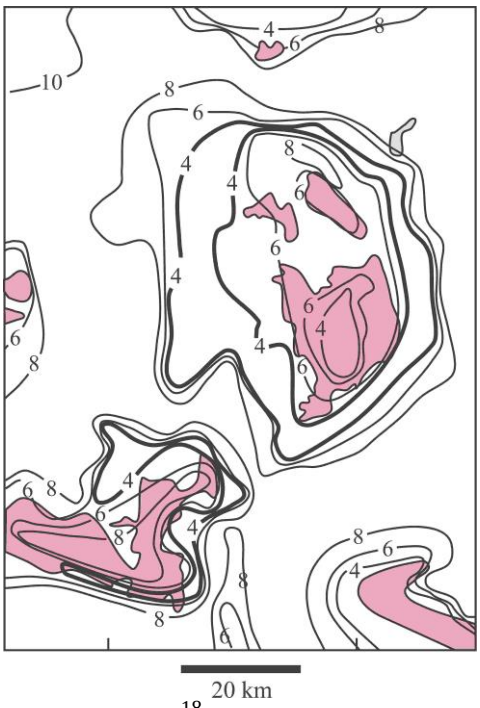

Fig. 11.10. $\delta^{18}O$ contours surrounding Eocene plutons (red shaded areas) in the Sawtooth Ring Zone (SRZ) of the Idaho Batholih, USA. The SRZ is a high-permeability zone due to collapse of the caldera, and is characterized by low $\delta^{18}O$ values (<4‰, shown by thick contour lines – values as low as -8‰ are measured) due to massive influx of meteoric water.

Once the magma crystallizes, however, fracture networks can develop leading to intense hydrothermal convection systems. In the case of the Isle of Skye system, there are two apparent mechanisms explaining the low $\delta^{18}O$ values; an initially low $\delta^{18}O$ magma and post-emplacement hydrothermal exchange. The progressively lower *initial* $\delta^{18}O$ values of each magma suite are explained by successive intrusions having incorporated wall-rock material of previously emplaced magmas whose $\delta^{18}O$ values had already been lowered by hydrothermal interaction. Post-solidus, a giant hydrothermal circulation system was set-up, resulting in continued lowering of the $\delta^{18}O$ values of feldspar. The convection system would be focused towards the center of the pluton, which retained its heat longest, resulting in higher fluid/rock ratios in the central zones and the observed concentrically lower $\delta^{18}O$ values towards the center. This characteristic pattern, with lower $\delta^{18}O$ values of feldspars towards the center has been seen in a large number of igneous complexes.

Not all low $\delta^{18}O$ volcanic rocks form by direct interaction with meteoric water. Pope *et al.* (2013) determined that the low, yet uniform silicic $\delta^{18}O$ volcanic rocks from the Krafla central volcano, Iceland are indicative of partial melting of basalts that had previously undergone hydrothermal interaction with meteoric water.

The use of refractory minerals is another way to 'see through' the effects of late alteration. Monani and Valley (2001) measured the oxygen isotope composition of zircons from the well-studied low $\delta^{18}O$ British Tertiary Complex, Scotland. The $\delta^{18}O$ values of zircons within an individual pluton are homogeneous, but generally lower than those from typical igneous rocks. The authors conclude that the intrusions had incorporated previously hydrothermally altered country rock, such that the igneous bodies crystallized zircons in equilibrium with the low $\delta^{18}O$ magma. In a study of Archean granitoids from the Anshan area, North China Craton, Wan *et al.* (2013) found igneous zircons with $\delta^{18}O$ values as low as -11.3‰. On the basis of correlations with radiogenic lead loss and U concentrations, the authors argue that post-emplacement isotope exchange has occurred.

Without doubt, the most amazing example of hydrothermal infiltration is found in the 1.9Ga Paleoproterozoic metamorphic rocks of the Belomorian Belt of Karelia, Russia (Bindeman and Serebryakov, 2011). The lowest $\delta^{18}O$ and δD values of these rocks are a remarkable -27‰ and -235‰, respectively. The rocks have strong isotopic heterogeneities on a sub-meter scale, demonstrating a near-surface hydrothermal imprint. The protolith igneous rocks were located near their equator at the time of their emplacement at 2.4-2.45 Ga. The extremely low isotope ratios for these rocks is explained by alteration with glacial waters that were present during the snowball Earth event at this time.

Extrapolation of the $\delta^{18}O$ values of the minerals to the actual meteoric water values were made using the triple oxygen isotope system (Herwartz et al., 2015). As shown in Fig. 11.11, the unaltered and altered samples from Karelia plot on a mixing line between the unaltered rock and the meteoric water. The $\delta^{18}O$ value of the actual meteoric water is estimated by finding the intersection of the "Archean meteoric water line" and the mixing line defined by their measured data. The results give an extremely low $\delta^{18}O$ value of ~ -43‰. Such low values today are only found in extreme high latitude environments, such as the inland regions of Antarctica.

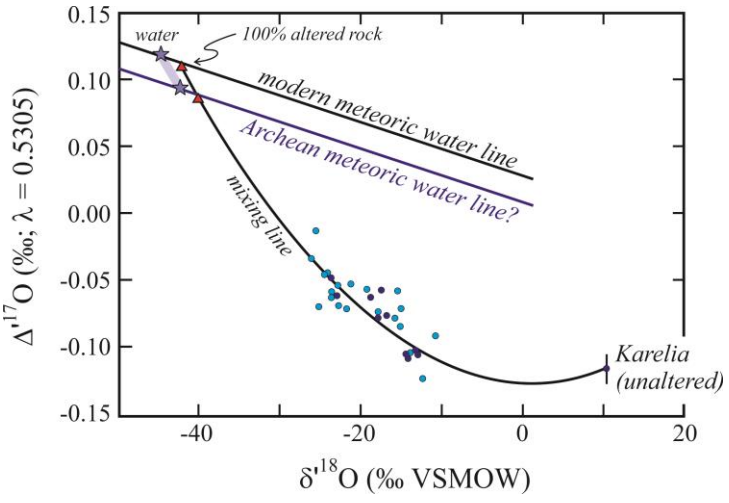

Fig. 11.11. $\Delta'^{17}O$-$\delta'^{18}O$ plot of hydrothermally altered and unaltered igneous rocks from Karelia, NW Russia. The data can be fit with a mixing line (curved line) that passes through the global triple oxygen isotope line at $\delta^{18}O$~-43‰, in agreement with earlier estimates for alteration during a snowball Earth event.

11.3.3 High $\delta^{18}O$ igneous rocks

There are three ways in which an igneous rock can attain high $\delta^{18}O$ values. These are 1) inheritance from the original magma (*e.g.*, anatexis of original high $\delta^{18}O$ material); 2) high-temperature hydrothermal exchange with high $\delta^{18}O$ country rocks and 3) low temperature exchange with a meteoric fluid. As we saw in Chapter 5 for the oceanic crust, the fractionations between minerals and water become so large at low temperature that water-rock interaction *raise* the $\delta^{18}O$ value of the rock, even when the $\delta^{18}O$ value of the water is low. Various methods have been used to ascertain which mechanism is responsible for causing high $\delta^{18}O$ values, and are briefly explained in the following section.

The two distinct processes, anatexis (melting of country rock) and low-temperature exchange with country rock can usually be distinguished by considering spatial variability. The isotopic composition of original homogeneous, high $\delta^{18}O$ magmas may vary between intrusive events, but should be constant for each distinct intrusion. Even if the magma body was heterogeneous, it should not correlate with distance to the country rock. On the other hand, if the high $\delta^{18}O$ character of an intrusion results from exchange with the country rocks following emplacement, then we would expect to see a spatial relationship between $\delta^{18}O$ values and distance from the contact. Combining oxygen, hydrogen and strontium isotope data (as well as old fashioned mineralogy!) may also be used to distinguish these two mechanisms.

Typical S-type (sedimentary) granites, with high Al contents and muscovite, are generated by incorporation of sedimentary material. Sediments generally have high $\delta^{18}O$, δD and $^{87}Sr/^{86}Sr$ values, all features that are seen in S-type granites. The $\delta^{18}O$ values of S-type granites are over 10‰, compared to 7-9‰ for I-type (igneous) granites (e.g., O'Neil and Chappell, 1977). The $^{87}Sr/^{86}Sr$ ratios of I-type granites are generally 0.704 to 0.706, while S-type granites have $^{87}Sr/^{86}Sr$ ratios over 0.708 up to 0.720. Groundmass minerals show the predicted isotopic enrichment trends, but in some cases, such as the Tuscan Magmatic Province, Italy, large sanidine crystals (1-5 cm in length) have $\delta^{18}O$ values that are 0.5 to 1.5‰ too high for the groundmass, indicating mixing of two distinct magmas (Taylor and Turi, 1976). These data cannot be explained in terms of either low temperature alteration or exchange with country rocks.

Several clear-cut examples of high-temperature exchange post-emplacement have been found. Southern California batholiths intruding high-grade pelitic rocks have high $\delta^{18}O$ values only at the margins (Turi and Taylor, 1971). Because quartz, as well as feldspar and biotite, have high $\delta^{18}O$ values, exchange with the country rock probably occurred at high temperatures. If the alteration had occurred at low temperatures, then the far more resistant quartz (relative to feldspar) would have retained its original isotopic composition. An important condition of high temperature exchange with country rock is that the country rock must be hot prior to intrusion. Otherwise, the heat necessary to melt the rock could not be generated by the intrusion.

Examples of high $\delta^{18}O$ granites caused by low-temperature hydrothermal alteration are found worldwide. There are a number of mineralogical features that are characteristic of low temperature alteration. In terms of stable isotopes, the strongest evidence comes from the large 'isotopic reversal' between quartz and feldspar. Low temperature hydrothermal exchange affects feldspar, but not quartz. In the Butler Hill

pluton, Missouri, the $\Delta^{18}O_{(quartz\text{-}feldspar)}$ values can be contoured throughout the pluton (Wenner and Taylor, 1976). They are near equilibrium values in the northeast, and decrease to negative values in the southwest. Meteoric waters responsible for the low temperature exchange are calculated to have had $\delta^{18}O$ = -6 to 0‰; δD = -25 to 0‰. These values are too high for modern meteoric water, but are equivalent to saline formation waters that existed in the region. Extensive Na and Fe metasomatism in the area supports a brine origin for the fluids.

11.4 Calculating Fluid-rock ratios

It is clear that fluid-rock interaction has occurred in many intrusive bodies. The low $\delta^{18}O$ values that are commonly seen attest to the fact that large amounts of water have passed through and interacted with the rock. To a first approximation, the amounts of fluid can be determined using the simple mass balance relationship (Taylor, 1978)

$$X_{rock} \cdot \delta^{i}_{rock} + \left(1 - X_{rock}\right)\delta^{i}_{water} = X_{rock} \cdot \delta^{f}_{rock} + \left(1 - X_{rock}\right)\delta^{f}_{water} \qquad 11.1$$

where X_{rock} is the molar fraction of the element in the rock, (1-X_{rock}) is the molar fraction of the element in water, *i* is the initial value, *f* is the final value. Equation 11.1 is equivalent to mixing a set amount of rock and water with initial isotopic compositions and allowing them to react at high temperature as a *closed system*. Because the system is closed, the $\delta^{18}O$ value of the system cannot change. The proportion of water and rock, given by the water/rock ratio can be calculated by rearranging the above equation to the form

$$W / R = \frac{\delta^{f}_{rock} - \delta^{i}_{rock}}{\delta^{i}_{water} - \left(\delta^{f}_{rock} - \Delta_{r-w}\right)} \qquad 11.2$$

where *W/R* is the water/rock ratio (in mole fraction) and $\Delta_{r\text{-}w}$ is the equilibrium fractionation between that rock and water after they have equilibrated (*i.e.* $\Delta_{r-w} = \delta^{f}_{rock} - \delta^{f}_{water}$). Although this equation allows us to quantify the water/rock ratio in the closed system case, keep in mind that several of the variables in equation 11.2 cannot be measured. First, the initial $\delta^{18}O_{rock}$ value is estimated, either on the basis of similar rock types, or from measured values of a sample far removed from the effects of alteration. Likewise, the initial $\delta^{18}O_{water}$ value is estimated, either from paleogeographic reconstruction of meteoric water values, or for a range of assumed values. The $\Delta_{r\text{-}w}$ value is estimated from an assumed temperature of reaction, an assumed equilibrium fractionation between water and rock and by making one final assumption that the water and rock were in isotopic equilibrium[9]. It is worth mentioning these uncertainties not so much as to discourage researchers from making such calculations, but to remind us that there are real limitations and uncertainties in such estimates. Fluid/rock ratio estimates

[9] The details are quite complex. Different minerals interact with hydrothermal fluids at different rates. Some minerals, such as feldspar, equilibrate quickly, while others, notably zircon (King et al., 1997), may never reequilibrate with the fluid.

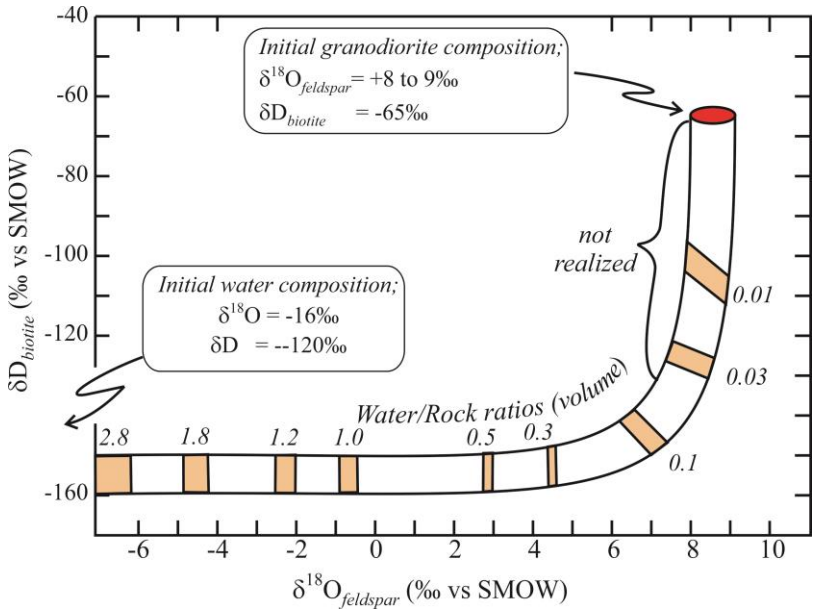

Fig. 11.12. Combined oxygen-hydrogen isotope composition of a granodiorite infiltrated by meteoric water with an initial composition $\delta^{18}O$ = -16‰, δD = -120‰. The δD values of the biotites are affected by even small amounts of water, whereas far larger *W/R* ratios are required to change the $\delta^{18}O$ value of the rock. Very low W/R ratios are not realized because the water will not flow when present in such small quantities. The trajectories are calculated for $\Delta^{18}O_{feldspar\text{-}H_2O}$ = +2‰ and $\Delta D_{biotite\text{-}H_2O}$ = -30 to -40‰ After Taylor, (1978).

can be very informative, but only as a rough indication of what actually occurred in the rock.

Equation 11.2 is for the physical condition where all water enters a rock as a single event, equilibrates with it, and is then expelled. This is the 'closed system', or *single* pass case of water-rock interaction based on mass balance. In the more dynamic 'open system', or *multi* pass case, an infinitesimally small amount of water infiltrates the rock, equilibrates with it, and is then expelled. This model is more realistic and better models the situation of fluids streaming through the rock. Mathematically, the open system case is obtained by differentiating and integrating equation 11.2 to give

$$W/R = \ln\left(\frac{\delta^i_{water} + \Delta_{r-w} - \delta^i_{rock}}{\delta^i_{water} - \left(\delta^f_{rock} - \Delta_{r-w}\right)}\right) \qquad 11.3$$

or

$$W/R = ln\left[\left(W/R\right)_{closed\ system} + 1\right] \qquad 11.4.$$

A more detailed examination of the caveats of the above equations and additional one-dimensional mixing models are given in Chapter 14.

Taylor (1978) considered the effects of water-rock interaction on the combined isotopic systems of oxygen and hydrogen. Because the hydrogen concentration of a rock

is only a fraction of the oxygen concentration, interaction with meteoric water affects the isotopic composition of hydrogen much more strongly than oxygen. That is to say, for a fixed amount of water infiltration, the effective molar *W/R* ratios for hydrogen will be much larger than for oxygen[10]. The combined effects of hydrothermal alteration on hydrogen and oxygen isotopic compositions is shown in Fig. 11.12 for infiltration by a light meteoric water. Even for very low *W/R* ratios, the δD values of the hydrous minerals change rapidly, while oxygen isotope ratios remains essentially unchanged. Only when *W/R* ratios become quite high do we see the $\delta^{18}O$ values of the rock change, by which time, hydrogen in the hydrous phases has essentially completely equilibrated with the infiltrating fluid. This is completely analogous to what we see during carbonate diagenesis, where carbon changes more slowly than oxygen (Chapter 6, Figure 6.8). The result is a dog-leg shaped profile of hydrogen oxygen isotope ratios for a complete sequence of *W/R* ratios. Measured $\delta D/\delta^{18}O$ values of intrusive complexes have been shown to follow the predicted trend (e.g., Criss and Taylor, 1986).

11.5 Other processes: Degassing, assimilation and fractional crystallization

11.5.1 Magmatic volatiles

Volatiles in magmas are the primary cause of explosive eruptions. Calculating the speciation of volatile phases and measuring their abundance in magmas is difficult, because solubilities change with pressure and temperature, phase changes occur in response to redox state, and degassing and/or late contamination will alter abundances and stable isotope ratios of magmatic volatiles. The major volatile species measured in volcanic gases are H_2O, CO_2, SO_2, H_2S, H_2, and HCl (Taylor, 1986). Gases measured in basaltic glass vesicles consist primarily of CO_2.

Volatile degassing has essentially no effect on the $\delta^{18}O$ value of a magma. This is because the atom proportion of oxygen leaving the system is too small to change the value of the silicate reservoir. Carbon, hydrogen and sulfur isotope ratios, on the other hand, both of the evolved gas and the residual magma, can change dramatically during degassing because the proportion of the element entering the gas phase can be significant. This is seen, for example, in the $\delta^{13}C$ values of fluid inclusions in MORB. The $\delta^{13}C$ values range from -9 to -4‰ (Pineau and Javory, 1983), which can be explained in terms of fractionation between a mafic melt and CO_2 gas under closed-system conditions.

Devolatilization effects can be especially large for hydrogen isotopes of residual melts and hydrous phases. Hydrogen isotope ratios in basaltic glasses range from the expected 'primary basalt value of -80‰ up to as high as -30‰ (compilation of Taylor, 1986). These data are consistent with degassing, as the lighter isotopologues of water should diffuse out of the melt faster than the heavier ones. In granitic plutons, there is a well-recognized correlation of δD values with water (Taylor, 1986). As an example of this effect, Nabelek *et al.* (1983) measured the $\delta^{18}O$ and δD values of samples from the composite granitic Notch Peak stock, Utah. Oxygen isotope ratios are more-or-less constant, but hydrogen isotope ratios vary by more than 50‰. The hydrogen isotope variations are well correlated with total water content and are concentrically zoned within each intrusion. The data can be explained entirely by a Rayleigh fractionation process. Loss of D-enriched H_2O vapor will lead to crystallization of hydrous minerals with ever

[10] This, of course, assumes that all the interstitial water is equilibrated with the hydrous minerals.

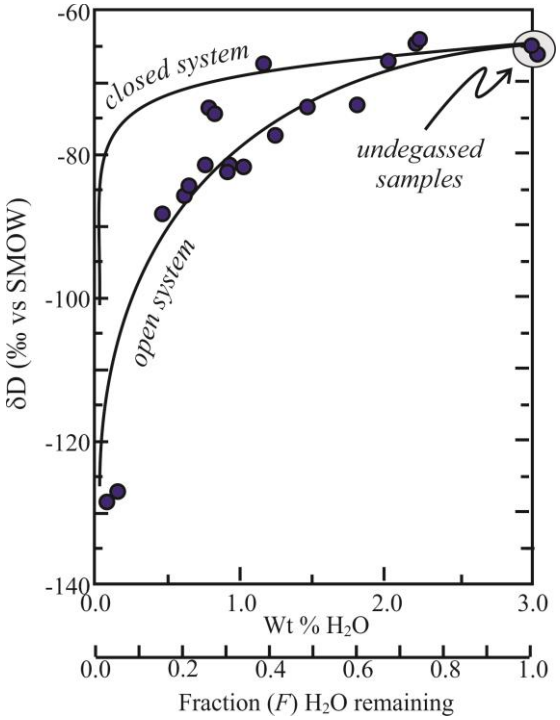

Fig. 11.13. δD values vs water content of fresh obsidian from Little Glass Mountain, Medicine Lake Highland, California, USA. The decrease of δD values from the undegassed samples follows an open system Rayleigh fractionation trajectory, suggesting that the low values are primary features of open system degassing, not of interaction with meteoric water. After (Taylor et al., 1983).

decreasing δD values[11]. By the time 90% of the H_2O is lost from the system, the δD values of biotites will decrease by 40 to 50‰.

Taylor *et al*. (1983) measured the water content and δD values of water-rich obsidian ejecta associated with rhyolite volcanism. There is a regular lowering of δD values associated with degassing as seen in Figure 11.13. The data are best explained by open system Rayleigh degassing. A major conclusion of Taylor *et al.* is that low δD values can be explained by open system behavior, and do not require an influx of meteoric water. Loss of hydrogen – as opposed to water – can lead to similar behavior, but because H_2 is depleted in deuterium compared to minerals or melt, the δD values of partially dehydrogenated biotites may have extremely high δD values (Feeley and Sharp, 1996). Overall it is clear that the minor volatile elements in magmas – H, C, N and S – which strongly partition into the fluid/vapor phase can undergo large fractionations under conditions of volatile loss.

11.5.2 Assimilation-Fractional Crystallization (AFC) processes

Taylor (1980) and DePaolo (1981) derived models for evaluating changes in isotope ratios of magmas due to assimilation of country rock and the effects of fractional crystallization. In particular, the authors showed that simple binary mixing models of $^{18}O/^{16}O$ and $^{87}Sr/^{86}Sr$ ratios do not adequately describe trends associated with assimilation. In the following discussion, the mechanisms of AFC are considered first in terms of simple fractional crystallization of a cooling magma and then for assimilation of country rock.

Crystallization and removal (by settling) of minerals in a magma chamber can be modeled using closed-system Rayleigh fractionation, where

$$\delta_{melt} - \delta^{o}_{melt} = \left(1000 + \delta^{o}_{melt}\right)\left(F^{(\alpha-1)} - 1\right) \qquad 11.5.$$

[11] Remember that the δD value of water is *higher* than coexisting melt, in contrast to $\delta^{18}O$.

Here, *F* refers to the fraction of element remaining in the melt, δ^{o}_{melt} is the initial melt composition, δ_{melt} refers to the isotopic composition of the melt at *F*, and α is the fractionation between melt and crystal. For oxygen isotopes, values of α are on the order of 1.001 ($\Delta^{18}O_{melt\ -\ solid}$ = 1‰), and even 95‰ crystallization will only nominally affect the $\delta^{18}O$ value of the remaining melt. Similarly, the δD value of the melt will change by less than 20‰, even if 80% of hydrogen is removed to the melt phase (assuming a melt-mineral fractionation of no more than 10‰). In other words, fractionation of H and O isotopes during crystallization cannot be large. Fractional crystallization will have no effect on Sr isotope ratios, because the fractionation between the isotopes of this heavy element are negligible.

Assimilation of wall-rock material can have much larger effects if the initial isotopic composition of the wall-rock is different from that of the magma, and a large proportion of wall-rock is incorporated into the melt. How much wall rock is assimilated is limited by available heat. Heat is generated from the latent heat of crystallization of a magma, which can then be made available for melting the country rock. The initial background temperature of a country rock determines how much of it will melt. Obviously, less heat is needed to melt a rock that is already hot.

Characteristic mixing for heavy radiogenic isotopes differs from stable isotopes in several respects. First, there is next to no isotopic fractionation between different phases (although small stable isotope fractionations do occur, e.g., Rüggeberg et al., 2008), and second, the *concentrations* of the elements and isotopic ratios in the assimilating wall rock, magma and crystals can be very different. Therefore, even small amounts of mixing can drastically affect radiogenic isotope ratios. Thus assimilation and fractional crystallization will affect oxygen and strontium isotope ratios in very different ways. The equations governing AFC processes are complex and can be found in DePaolo (1981) and Taylor (1986). The utility of AFC models is that combined isotopic trends in

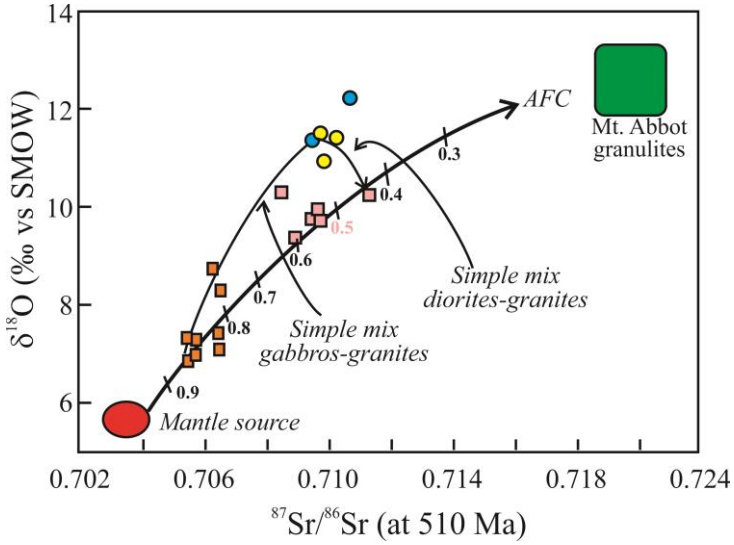

Fig. 11.14. $\delta^{18}O$-$^{87}Sr/^{86}Sr$ plot of gabbros (orange squares), diorites (pink squares), granodiorites (green circles) and granites (yellow circles) from the Granite Harbour Intrusives, Antarctica. The diorite data cannot be formed by mixing between granite and gabbro. Instead, they require an assimilation component of the local Mt. Abbot granulites. After (Dallai et al., 2003).

complex magmatic suites can be interpreted in terms of either simple mixing between endmembers or more complicated scenarios where assimilation of wallrock is required to explain the data. As an example, Dallai *et al*. (2003) posed the question whether a suite of Cambrian-Ordovician gabbros, diorites, granodiorites and granites forming the Mt. Abbott composite intrusions (Northern Victoria Land, Antarctica) could be generated from simple fractional crystallization and mixing or whether assimilation of country rock was necessary. The combined oxygen and strontium isotope data clearly require assimilation of the locally abundant Mt. Abbot granulites (Fig. 11.14). Simple mixing of the gabbros and granites will generate a hyperbolic mixing line that does not include the diorite data.

References

Baldridge, S.W., Sharp, Z.D. and Reid, K.D. (1996) Quartz-bearing basalts: oxygen isotopic evidence for crustal contamination of continental mafic rocks. *Geochimica et Cosmochimica Acta* **60**, 4765-4772.

Beaumont, V. and Robert, F. (1999) Nitrogen isotope ratios of kerogens in Precambrian cherts: a record of the evolution of atmosphere chemistry? *Precambrian Research* **96**, 63-82.

Bindeman, I.N. and Serebryakov, N.S. (2011) Geology, petrology and O and H isotope geochemistry of remarkably ^{18}O depleted Paleoproterozoic rocks of the Belomorian Belt, Karelia, Russia, attributed to global glaciation 2.4 Ga. *Earth and Planetary Science Letters* **306**, 163-174.

Boettcher, A.L. and O'Neil, J.R. (1980) Stable isotope, chemical and petrographic studies of high-pressure amphiboles and micas: Evidence for metasomatism in the mantle source regions of alkali basalt and kimberlites. *American Journal of Science* **280-A**, 594-621.

Bottinga, Y. (1968) Calculation of fractionation factors for carbon and oxygen isotopic exchange in the system calcite-carbon dioxide-water. *Journal of Physical Chemistry* **72**, 800-808.

Bottinga, Y. (1969) Carbon isotope fractionation between graphite, diamond and carbon dioxide. *Earth and Planetary Science Letters* **5**, 301-307.

Burnham, A.D., Thomson, A.R., Bulanova, G.P., Kohn, S.C., Smith, C.B. and Walter, M.J. (2015) Stable isotope evidence for crustal recycling as recorded by superdeep diamonds. *Earth and Planetary Science Letters* **432**, 374-380.

Caporuscio, F.A. (1990) Oxygen isotope systematics of eclogite mineral phases from South Africa. *Lithos* **25**, 203-210.

Cartigny, P., Harris, J.W. and Javoy, M. (2001) Diamond genesis, mantle fractionations and mantle nitrogen content: a study of δ13C–N concentrations in diamonds. *Earth and Planetary Science Letters* **185**, 85-98.

Cartigny, P. (2005) Stable isotopes and the origin of diamond. *Elements* **1**, 79-84.

Chacko, T., Mayeda, T.K., Clayton, R.N. and Goldsmith, J.R. (1991) Oxygen and carbon isotope fractionations between CO_2 and calcite. *Geochimica et Cosmochimica Acta* **55**, 2867-2882.

Chaussidon, M., Albarede, F. and Sheppard, S.M.F. (1987) Sulphur isotope heterogeneity in the mantle from ion microprobe measurements of sulphide inclusions in diamonds. *Nature* **330**, 242-244.

Criss, R.E. and Taylor, H.P., Jr. (1983) An $^{18}O/^{16}O$ and D/H study of Tertiary hydrothermal systems in the southern half of the Idaho Batholith. *Geological Society of America Bulletin* **94**, 640-663.

Criss, R.E. and Taylor, H.P., Jr. (1986) Meteoric-hydrothermal systems., in: Valley, J.W., Taylor, H.P.J., O'Neil, J.R. (Eds.), Stable Isotopes in High Temperature Geological Processes. Mineralogical Society of America, Chelsea, pp. 373-424.

Dallai, L., Ghezzo, C. and Sharp, Z.D. (2003) Oxygen isotope evidence for crustal assimilation and magma mixing in the Granite Harbour Intrusives, Northern Victoria Land, Antarctica. *Lithos* **67**, 135-151.

Deines, P. and Gold, D.P. (1973) The isotopic composition of carbonatite and kimberlite carbonates and their bearing on the isotopic composition of deep-seated carbon. *Geochimica et Cosmochimica Acta.* **37**, 1709-1733.

Deines, P. (1980) The isotopic composition of reduced organic carbon, in: Fritz, P., Fontes, J.C. (Eds.), Handbook of environmental isotope geochemistry; Volume 1, The terrestrial environment, A. Elsevier, Amsterdam, pp. 329-406.

Deines, P., Harris, J.W. and Gurney, J.J. (1993) Depth-related carbon isotope and nitrogen concentration variability in the mantle below the Orapa kimberlite, Botswana, Africa. *Geochimica et Cosmochimica Acta* **57**, 2781-2796.

Deines, P. (2002) The carbon isotope geochemistry of mantle xenoliths. *Earth-Science Reviews* **58**, 247-278.

Delavault, H., Chauvel, C., Thomassot, E., Devey, C.W. and Dazas, B. (2016) Sulfur and lead isotopic evidence of relic Archean sediments in the Pitcairn mantle plume. *Proceedings of the National Academy of Sciences* **113**, 12952-12956.

Deloule, E., Albarede, F. and Sheppard, S.M.F. (1991) Hydrogen isotope heterogeneities in the mantle from ion probe analysis of amphiboles from ultramafic rocks. *Earth and Planetary Science Letters* **105**, 543-553.

DePaolo, D.J. (1981) Trace element and isotopic effects of combined wallrock assimilation and fractional crystallization. *Earth and Planetary Science Letters* **53**, 189-202.

DesMarais, D. (1985) Carbon exchange between the mantle and the crust, and its effect upon the atmosphere: Today compared to Arechean time, The Carbon Cycle and Atmospheric CO_2: Natural Variations Archean to Present. Geophysical Monograph, pp. 602-611.

Dobson, P.F. and O'Neil, J.R. (1987) Stable isotope compositions and water contents of boninite series volcanic rocks from Chichi-Jima, Bonin Islands, Japan. *Earth and Planetary Science Letters* **82**, 75-86.

Eigenbrode, J.L. and Freeman, K.H. (2006) Late Archean rise of aerobic microbial ecosystems. *Proceedings of the National Academy of Sciences* **103**, 15759-15764.

Eiler, J.M., Farley, K.A., Valley, J.W., Stolper, E.M., Haurl, E.H. and Craig, H. (1995) Oxygen isotope evidence against bulk recycled sediment in the mantle sources of Pitcairn Island lavas. *Nature* **377**, 138-141.

Eiler, J.M. (2001) Oxygen isotope variations of basaltic lavas and upper mantle rocks, in: Valley, J.W., Cole, D.R. (Eds.), Stable Isotope Geochemistry. Mineralogical Society of America, Washington, D.C., pp. 319-364.

Exley, R.A., Mattey, D.P., Clague, D.A. and Pillinger, C.T. (1986) Carbon isotope systematics of a mantle "hotspot": a comparison of Loihi Seamount and MORB glasses. *Earth and Planetary Science Letters* **78**, 189-199.

Farquhar, J., Wing, B.A., McKeegan, K.D., Harris, J.W., Cartigny, P. and Thiemens, M.H. (2002a) Mass-independent sulfur of inclusions in diamonds and sulfur recycling on early Earth. *Science* **298**, 2369-2372.

Farquhar, J., Wing, B.A., McKeegan, K.D., Harris, J.W., Cartigny, P. and Thiemens, M.H. (2002b) Mass-independent sulfur of inclusions in diamond and sulfur recycling on early Earth. *Science* **298**, 2369-2372.

Feeley, T.C. and Sharp, Z.D. (1996) Chemical and hydrogen isotope evidence for in situ dehydrogenation of biotite in silicic magma chambers. *Geology* **24**, 1021-1024.

Feldstein, S.N., Lange, R.A., Vennemann, T. and O'Neil, J.R. (1996) Ferric-ferrous ratios, H_2O contents and D/H ratios of phlogopite and biotite from lavas of different tectonic regimes. *Contributions to Mineralogy and Petrology* **126**, 51-66.

Fischer, T.P., Hilton, D.R., Zimmer, M.M., Shaw, A.M., Sharp, Z.D. and Walker, J.A. (2002) Contrasting nitrogen isotope behavior along the Central America margin: implications for the nitrogen balance of the Earth. *Science* **297**, 1154-1157.

Forester, R.W. and Taylor, H.P., Jr. (1977) $^{18}O/^{16}O$, D/H and $^{13}C/^{12}C$ studies of the Tertiary igneous complex of Skye, Scotland. *American Journal of Science* **277**, 136-177.

Garlick, G.D. (1966) Oxygen isotope fractionation in igneous rocks. *Earth and Planetary Science Letters* **1**, 361-368.

Giggenbach, W.F. (1992) Isotopic shifts in waters from geothermal and volcanic systems along convergent plate boundaries and their origin. *Earth and Planetary Science Letters* **113**, 495-510.

Gilliam, C.E. and Valley, J.W. (1997) Low $\delta^{18}O$ magma, Isle of Skye, Scotland: Evidence from zircons. *Geochimica et Cosmochimica Acta* **61**, 4975-4981.

Gregory, R.T. and Criss, R.E. (1986) Isotopic exchange in open and closed systems, in: Valley, J.W., Taylor Jr., H.P., O'Neil, J.R. (Eds.), Stable Isotopes in High Temperature Geological Processes, 1 ed. Mineralogical Society of America, Chelsea, pp. 91-128.

Grunder, A.L. (1987) Low $\delta^{18}0$ silicic volcanic rocks at the Calabozos Caldera Complex, Southern Andes; evidence for upper-crustal contamination. *Contributions to Mineralogy and Petrology* **95**, 71-81.

Hallis, L.J., Huss, G.R., Nagashima, K., Taylor, G.J., Halldórsson, S.A., Hilton, D.R., Mottl, M.J. and Meech, K.J. (2015) Evidence for primordial water in Earth's deep mantle. *Science* **350**, 795-797.

Harmon, R.S. and Hoefs, J. (1995) Oxygen isotope heterogeneity of the mantle deduced from global ^{18}O systematics of basalts from different geotectonic settings. *Contributions to Mineralogy and Petrology* **120**, 95-114.

Hart, S.R., Hauri, E.H., Oschmann, L.A. and Whitehead, J.A. (1992) Mantle plumes and entrainment; isotopic evidence. *Science* **256**, 517-520.

Herwartz, D., Pack, A., Krylov, D., Xiao, Y., Muehlenbachs, K., Sengupta, S. and Di Rocco, T. (2015) Revealing the climate of snowball Earth from $\Delta^{17}O$ systematics of hydrothermal rocks. *Proceedings of the National Academy of Sciences* **112**, 5337-5341.

Hoefs, J. (1973) Ein Beitrag zur Isotopengeochemie des Kohlenstoffs in magmatischen Gesteinen. *Contributions to Mineralogy and Petrology* **41**, 277-300.

Hulston, J.R. and Thode, H.G. (1965) Variations in the S^{33}, S^{34}, and S^{36} contents of meteorites and their relation to chemical and nuclear effects. *Journal of Geophysical Research* **70**, 3475-3484.

Ito, E., White, W.M. and Goepel, C. (1987) The O, Sr, Nd and Pb isotope geochemistry of MORB. *Chemical Geology* **62**, 157-176.

Javoy, M. (1980) $^{18}O/^{16}O$ and D/H ratios in high temperature peridotites. *Colloques Internationaux du C.N.R.S.* **272**, 279-287.

Javoy, M. (1997) The major volatile elements of the Earth: Their origin, behavior, and fate. *Geophysical Research Letters* **24**, 177-180.

King, E.M., Barrie, C.T. and Valley, J.W. (1997) Hydrothermal alteration of oxygen isotope ratios in quartz phenocrysts, Kidd Creek mine, Ontario: Magmatic values are preserved in zircon. *Geology* **25**, 1079-1082.

Kuroda, Y., Suzuoki, T. and Matsuo, S. (1977) Hydrogen isotope composition of deep-seated water. *Contributions to Mineralogy and Petrology* **60**, 311-315.

Kyser, T.K., O'Neil, J.R. and Carmichael, I.S.E. (1982) Genetic relations among basic lavas and ultramafic nodules; evidence from oxygen isotope compositions. *Contributions to Mineralogy and Petrology* **81**, 88-102.

Kyser, T.K. and O'Neil, J.R. (1984) Hydrogen isotope systematics of submarine basalts. *Geochimica et Cosmochimica Acta* **48**, 2123-2133.

Kyser, T.K. (1986) Stable isotope variations in the mantle, in: Valley, J.W., Taylor, H.P., O'Neil, J.R. (Eds.), Stable isotopes in high temperature geological processes. Mineralogical Society of America, Chelsea, pp. 141-164.

Li, Y., Marty, B., Shcheka, S., Zimmermann, L. and Keppler, H. (2016) Nitrogen isotope fractionation during terrestrial core-mantle separation. *Geochemical Perspectives Letters* **2**, 138-147.

MacGregor, I.D. and Manton, W.I. (1986) Roberts Victor eclogites; ancient oceanic crust. *Journal of Geophysical Research, B* **91**, 14063-14079.

Marty, B. and Humbert, F. (1997) Nitrogen and argon isotopes in oceanic basalts. *Earth and Planetary Science Letters* **152**, 101-112.

Marty, B. and Dauphas, N. (2003) The nitrogen record of crust-mantle interaction and mantle convection from Archean to Present. *Earth and Planetary Science Letters* **206**, 397-410.

Mattey, D., Lowry, D. and Macpherson, C. (1994) Oxygen isotope composition of mantle peridotite. *Earth and Planetary Science Letters* **128**, 231-241.

Melton, G.L., Stachel, T., Stern, R.A., Carlson, J. and Harris, J.W. (2013) Infrared spectral and carbon isotopic characteristics of micro- and macro-diamonds from the Panda kimberlite (Central Slave Craton, Canada). *Lithos* **177**, 110-119.

Mohapatra, R.K. and Murty, S.V.S. (2004) Nitrogen isotopic composition of the MORB mantle: A reevaluation. *Geochemistry, Geophysics, Geosystems* **5**, doi:10.1029/2003GC000612.

Monani, S. and Valley, J.W. (2001) Oxygen isotope ratios of zircon: magma genesis of low $\delta^{18}O$ granites from the British Tertiary Igneous Province, western Scotland. *Earth and Planetary Science Letters* **184**, 377-392.

Nabelek, P.I., O'Neil, J.R. and Papike, J.J. (1983) Vapor phase exsolution as a controlling factor in hydrogen isotope variation in granitic rocks; the Notch Peak granitic stock, Utah. *Earth and Planetary Science Letters* **66**, 137-150.

O'Neil, J.R. and Chappell, B.W. (1977) Oxygen and hydrogen isotope relations in the Berridale batholith. *Journal of the Geological Society of London* **133**, 559-571.

Ongley, J.S., Basu, A.R. and Kyser, T.K. (1987) Oxygen isotopes in coexisting garnets, clinopyroxenes and phlogopites of Roberts Victor eclogites; implications for petrogenesis and mantle metasomatism. *Earth and Planetary Science Letters* **83**, 80-84.

Pineau, F. and Javory, M. (1983) Carbon isotopes and concentrations in mid-oceanic ridge basalts. *Earth and Planetary Science Letters* **62**, 239-257.

Pope, E.C., Bird, D.K. and Arnórsson, S. (2013) Evolution of low-^{18}O Icelandic crust. *Earth and Planetary Science Letters* **374**, 47-59.

Poreda, R. (1985) Helium-3 and deuterium in back-arc basalts; Lau Basin and the Mariana Trough. *Earth and Planetary Science Letters* **73**, 244-254.

Reuter, J.H., Epstein, S. and Taylor, H.P., Jr. (1965) O^{18}/O^{16} ratios of some chondritic meteorites and terrestrial ultramafic rocks. *Geochimica et Cosmochimica Acta* **29**, 481-488.

Richet, P., Bottinga, Y. and Javoy, M. (1977) A review of hydrogen, carbon, nitrogen, oxygen, sulphur, and chlorine stable isotope fractionation among gaseous molecules. *Annual Review of Earth and Planetary Science* **5**, 65-110.

Rüggeberg, A., Fietzke, J., Liebetrau, V., Eisenhauer, A., Dullo, W.-C. and Freiwald, A. (2008) Stable strontium isotopes ($\delta^{88}/^{86}$Sr) in cold-water corals — A new proxy for reconstruction of intermediate ocean water temperatures. *Earth and Planetary Science Letters* **269**, 570-575.

Sakai, H., DesMarais, D.J., Ueda, A. and Moore, J.G. (1984) Concentrations and isotope ratios of carbon, nitrogen and sulfur in ocean-floor basalts. *Geochemica et Cosmochimica Acta* **48**, 2433-2441.

Sano, Y.N., Takahata, N., Nishio, Y. and Fischer, T.P. (2001) Volcanic flux of nitrogen from the earth. *Chemical Geology* **171**, 263-271.

Scheele, N. and Hoefs, J. (1992) Carbon isotope fractionation between calcite, graphite and CO_2: an experimental study. *Contributions to Mineralogy and Petrology* **112**, 35-45.

Sharp, Z.D. (2017) Nebular ingassing as a source of volatiles to the Terrestrial planets. *Chemical Geology* **448**, 137-150.

Sheppard, S.M.F. and Epstein, S. (1970) D/H and ^{18}O/^{16}O ratios of minerals of possible mantle or lower crustal origin. *Earth and Planetary Science Letters* **9**, 232-239.

Sheppard, S.M.F. and Dawson, J.B. (1975) Hydrogen, carbon and oxygen isotope studies of megacryst and matrix minerals from Lesothan and South African kimberlites. *Physics and Chemistry of the Earth*, 747-763.

Shervais, J.W., Taylor, L.A., Lugmair, G.W., Clayton, R.N., Mayeda, T.K. and Korotev, R. (1988) Early proterozoic oceanic crust and the evolution of subcontinental mantle: Eclogites and related rocks from southern Africa. *Geological Society of America Bulletin* **100**, 411-423.

Smart, K.A., Chacko, T., Stachel, T., Muehlenbachs, K., Stern, R.A. and Heaman, L.M. (2011) Diamond growth from oxidized carbon sources beneath the Northern Slave Craton, Canada: A δ13C–N study of eclogite-hosted diamonds from the Jericho kimberlite. *Geochimica et Cosmochimica Acta* **75**, 6027-6047.

Smart, K.A., Chacko, T., Simonetti, A., Sharp, Z.D. and Heaman, L.A. (2014) A record of Paleoproterozoic subduction preserved in the Northern Slave Cratonic mantle: Sr-

Pb-O isotope and trace-element investigations of eclogite xenoliths from the Jericho and Muskox kimberlites. *Journal of Petrology* **55**, 549-583.

Snyder, G.A., Taylor, L.A., Jerde, E.A., Clayton, R.N., Mayeda, T.K., Deines, P., Rossman, G.R. and Sobolev, N.V. (1995) Archean mantle heterogeneity and the origin of diamondiferous eclogites, Siberia: Evidence from stable isotopes and hydroxyl in garnet. *American Mineralogist* **80**, 799-809.

Spicuzza, M.J., Day, J.M.D., Taylor, L.A. and Valley, J.W. (2007) Oxygen isotope constraints on the origin and differentiation of the Moon. *Earth and Planetary Science Letters* **253**, 254-265.

Taylor, B.E., Eichelberger, J.C. and Westrich, H.R. (1983) Hydrogen isotopic evidence of rhyolitic magma degassing during shallow intrusion and eruption. *Nature* **306**, 541-545.

Taylor, B.E. (1986) Magmatic volatiles: Isotopic variation of C, H, and S, in: Valley, J.W., Taylor, H.P.J., O'Neil, J.R. (Eds.), Stable Isotopes in High Temperature Geological Processes. Mineralogical Society of America, Chelsea, pp. 185-225.

Taylor, H.P., Jr. and Epstein, S. (1963) O^{18}/O^{16} ratios in rocks and coexisting minerals of the Skaergaard intrusion, East Greenland. *Journal of Petrology* **4**, 51-74.

Taylor, H.P., Jr., Frechen, J. and Degens, E.T. (1967) Oxygen and carbon isotope studies of carbonatites from the Laacher See district, west Germany and the Alnö district, Sweden. *Geochimica et Cosmochimica Acta.* **31**, 407-430.

Taylor, H.P., Jr. (1974) The application of oxygen and hydrogen isotope studies to problems of hydrothermal alteration and ore deposition. *Economic Geology* **69**, 843-883.

Taylor, H.P., Jr. and Turi, B. (1976) High-^{18}O igneous rocks from the Tuscan Magmatic Province, Italy. *Contributions to Mineralogy and Petrology* **55**, 33-54.

Taylor, H.P., Jr. (1978) Oxygen and hydrogen isotope studies of plutonic granitic rocks. *Earth and Planetary Science Letters* **38**, 177-210.

Taylor, H.P., Jr. (1980) The effects of assimilation of country rocks by magmas on $^{18}O/^{16}O$ and $^{87}Sr/^{86}Sr$ systematics in igneous rocks. *Earth and Planetary Science Letters* **47**, 243-254.

Taylor, H.P., Jr. and Sheppard, S.M.F. (1986) Igneous rocks: I. Processes of isotopic fractionation and isotope systematics, in: Valley, J.W., Taylor, H.P.J., O'Neil, J.R. (Eds.), Stable Isotopes in High Temperature Geological Processes. Mineralogical Society of America, Chelsea, pp. 227-271.

Turi, B. and Taylor, H.P.J. (1971) An oxygen and hydrogen isotope study of a granodiorite pluton from the Southern California Batholith. *Geochimica et Cosmochimica Acta* **35**, 383-406.

van Keken, P.E., Hauri, E.H. and Ballentine, C.J. (2002) Mantle mixing: The generation, preservation, and destruction of chemical heterogeneity. *Annual Review of Earth and Planetary Science* **30**, 493-525.

Viljoen, K.S., Smith, C.B. and Sharp, Z.D. (1996) Stable and radiogenic isotope study of eclogite xenoliths from the Orapa kimberlite, Botswana. *Chemical Geology* **131**, 235-255.

Wan, Y., Zhang, Y., Williams, I.S., Liu, D., Dong, C., Fan, R., Shi, Y. and Ma, M. (2013) Extreme zircon O isotopic compositions from 3.8 to 2.5 Ga magmatic rocks from the Anshan area, North China Craton. *Chemical Geology* **in press**.

Wenner, D.B. and Taylor, H.P., Jr. (1976) Oxygen and hydrogen isotope studies of a Precambrian granite-rhyolite terrane, St. Francois Mtns., S.E. Missouri. *Geological Society of America Bulletin* **87**, 1587-1598.

Wilson, M.R., Kyser, T.K. and Fagan, R. (1996) Sulfur isotope systematics and platinum group element behavior in REE-enriched metasomatic fluids; a study of mantle xenoliths from Dish Hill, California, USA. *Geochimica et Cosmochimica Acta* **60**, 1933-1942.

Woodhead-Jon, D. and Devey-Colin, W. (1993) Geochemistry of the Pitcairn seamounts; I, Source character and temporal trends. *Earth and Planetary Science Letters* **116**, 81-99.

Xia, Q.-K., Deloule, E., Wu, Y.-B., Chen, D.-G. and Cheng, H. (2002) Anomalously high δD values in the mantle. *Geophysical Research Letters* **29**, 4 pp.

Zindler, A. and Hart, S. (1986) Chemical Geodynamics. *Annual Review of Earth and Planetary Sciences* **14**, 493-571.

Chapter 12

METAMORPHIC PETROLOGY

Contents

12.1 Introduction 1
12.2 Stable isotopes as geochemical tracers 1
12.2.1 Closed system – protolith identification and alteration 1
12.2.2 Open systems: Volatilization and fluid infiltration processes 3
12.3 Fluid sources and fluid rock-interaction 8
12.3.1 Oxygen and hydrogen 8
12.3.2 Carbon 11
12.3.3 Sulfur 12
12.4 Scales of equilibration during metamorphism 13
12.4.1 Regional scale exchange 13
12.4.2 Localized exchange 14
12.5 Quantifying fluid-rock ratios and fluid fluxes 15
12.5.1 Simple mixing models: Zero dimensional water-rock interaction models 15
12.5.2 One dimensional (directional) water-rock interaction models 16
12.6 Thermometry 19
12.6.1 Introduction 19
12.6.2 Oxygen isotope thermometry in metamorphic rocks – testing for equilibrium 21
12.6.3 Applications of stable isotope thermometry 23
12.7 Retrograde Exchange – Geospeedometry 24
References 30

Chapter 12

METAMORPHIC PETROLOGY

12.1 Introduction

Early advances in the stable isotope geochemistry of rocks was certainly not limited to carbonates. In remarkable pioneering studies, Baertschi and Silverman (Baertschi, 1950; Baertschi and Silverman, 1951; Silverman, 1951) were able to analyze the oxygen isotope composition of silicates in metamorphic and igneous rocks, recognizing that significant differences existed between different rock types. But after these early publications, further work on high temperature rocks languished for the better part of a decade, during which time major breakthroughs were being made in hydrogen, carbon, oxygen, sulfur, and nitrogen isotope studies of carbonates, meteoric water, organic matter, etc. The stagnation was partly related to analytical difficulties of fluorination, and partly to the idea that the range of oxygen isotope values in rocks equilibrated at high temperatures was simply too small to be of interest.

Then, in 1958, Clayton and Epstein (1958) measured the oxygen isotope values of quartz, calcite, and magnetite from various metamorphic rocks, and found that the fractionations varied systematically with formation temperature. Follow-up studies made it clear that predictable oxygen isotope fractionations exist between minerals, and that these fractionations vary with temperature (Clayton and Epstein, 1961; James and Clayton, 1962; Taylor and Epstein, 1962a; Taylor and Epstein, 1962b; Taylor et al., 1963; O'Neil and Clayton, 1964). The field of stable isotope geochemistry in metamorphic studies had begun.

Metamorphic rocks form by recrystallization of an existing protolith in response to changes in pressure, temperature, and fluid composition. During metamorphism, processes such as deformation, volatilization, solid-solid mineral reactions and metasomatism occur at time scales that can exceed 100 M.y. The thermodynamic driving force of these chemical processes is far larger than that of isotopic substitution, so that stable isotope geochemistry passively follows the more energetic mineral reactions, and not the reverse. Application of stable isotope geochemistry to metamorphic rocks requires special considerations, but also offer unique opportunities for retrieving information about metamorphic phenomena. The problems of rock protoliths, fluid sources and fluid/rock ratios, mineral reaction progress, extent of isotopic exchange between contrasting lithologies, metamorphic temperatures and cooling rates have all been addressed with the methods of stable isotope geochemistry.

12.2 Stable isotopes as geochemical tracers

12.2.1 Closed system – protolith identification and alteration

In the simplest case, a rock behaves as a closed system during metamorphism and the bulk rock isotopic value is unchanged from the protolith. For example, quartz sand generally has a $\delta^{18}O$ values of 13-18‰, whereas authigenic cherts have $\delta^{18}O$ values well over 30‰. The protolith of a highly recrystallized quartzite could therefore be determined from the measured $\delta^{18}O$ value as long as the system remained closed to fluid infiltration. Vennemann *et al.* (1992) measured the $\delta^{18}O$ values of quartz pebbles from the gold- and uranium-bearing conglomerates from the Witwatersrand district, South

Africa. The meta-chert pebbles have a $\delta^{18}O$ value of 9 to 11.5‰, far lower than expected from a marine chert. Instead, the authors proposed that auriferous iron formations and exhalatives were the source of the ore bearing pebbles.

Attempts have been made to distinguish orthogneisses from paragneisses on the basis of their $\delta^{18}O_{wholerock}$ values. Paragneisses are derived from a mixture of carbonates and pelitic sediments and should have higher $\delta^{18}O$ values than metamorphosed granitoids (orthogneisses). Schwarcz and Clayton (1965) were able to clearly distinguish ortho- and para-amphibolites in one well constrained example from Ontario, but in other localities the isotopic compositions were ambiguous. They attributed the similar $\delta^{18}O$ values to reequilibration with external buffering fluids during metamorphism. In a reconnaissance study of 10,000 km^2 of Archean Canadian Shield, the $\delta^{18}O$ values of ortho- and paragneisses were found to be indistinguishable (Shieh and Schwarcz, 1977). The authors concluded that the rocks had exchanged with a metamorphic fluid or, more likely, that the sedimentary protolith to the paragneisses consisted essentially of detrital igneous material which had the same isotopic composition as its precursor.

Marbles cover a broad range of $\delta^{18}O$ values, but generally cluster around 20-25‰ (SMOW), typical of diagenetically altered limestones. Granulite-facies marbles may have slightly lower $\delta^{18}O$ values (Baertschi, 1951), and siliceous marbles and calc-silicates have the lowest $\delta^{18}O$ values of all, due to the higher permeability compared to pure marbles. The higher permeability leads to alteration by influx of meteoric waters, thereby lowering the $\delta^{18}O$and $\delta^{13}C$ values of the marble (Fig. 12.1). Carbonatites are of igneous origin, and have $\delta^{18}O$ values in the range of typical magmatic rocks (6 to 10‰), and $\delta^{13}C$ values thought to represent the mantle (-4 to -8‰) (Taylor et al., 1967). The origin of

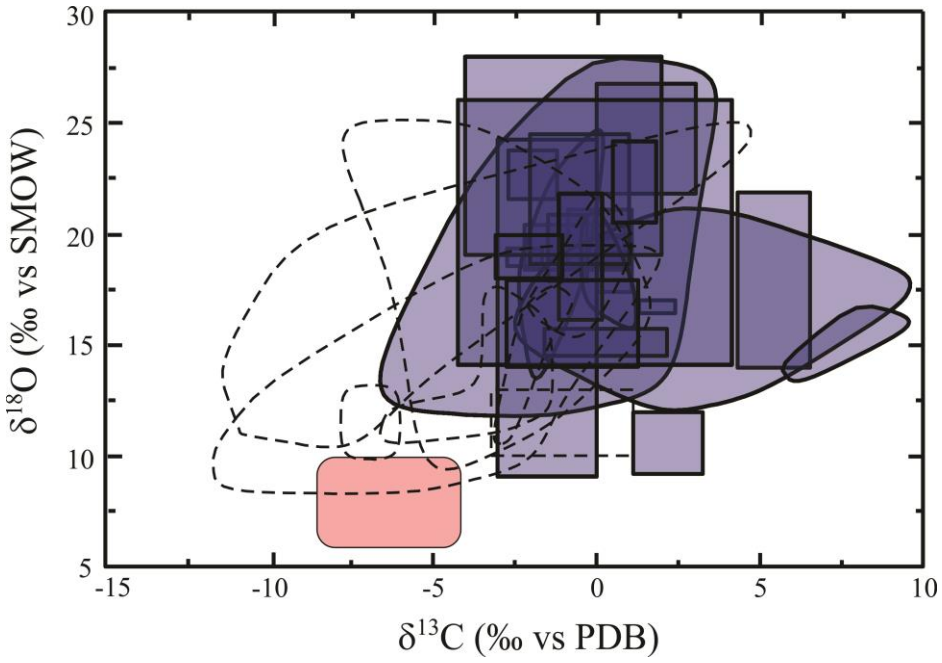

Fig. 12.1. Literature compilation of marbles. There is a clustering of $\delta^{18}O$ and $\delta^{13}C$ values around 20‰ (SMOW) and 0‰ (PDB), respectively. Siliceous marbles and calc-silicates (shown as dashed lines) have lower $\delta^{18}O$ and especially low $\delta^{13}C$ values. Also shown are igneous carbonatite box (pink box).

marbles – either carbonatitic or biogenic – can be constrained to some extent using stable isotope geochemistry.

The origin of sulfur in metamorphosed ore deposits can also be addressed using sulfur isotope geochemistry. Whereas thermochemical reduction of seawater sulfate to sulfide will preserve the high $\delta^{34}S$ values of the sulfate, reaction of metalliferous fluids with magmatic sulfide (*e.g.,* sulfide delivered from hydrothermal vents at Mid Ocean Ridges; so called 'sea-floor hydrothermal fluids') have values averaging only +1.5‰, far lower than typical seawater sulfate. High spatial resolution analyses of individual sulfides from a sea-floor hydrothermal spire, Axial Seamount, Juan de Fuca Ridge, eastern Pacific vary by 5 ‰, which is explained by mixing of hydrothermal sulfide with seawater sulfate (Crowe and Valley, 1992).

In a sulfur isotope study of the Sullivan Pb-Zn-Ag sedimentary exhalative (Sedex) deposit, Canada, which was metamorphosed to upper-greenschist conditions, the authors concluded that thermogenic sulfate reduction, bacterial sulfate reduction and remobilization of preexisting sulfide grains all contributed to the sulfur in the deposit (Taylor, 2004).

12.2.2 Open systems: Volatilization and fluid infiltration processes

An *open system* is one where fluids and/or melts can enter or leave a rock. Open system behavior is common, occurring over the full range of geological conditions. Examples include 1) carbonate diagenesis, where infiltration of meteoric waters and the expulsion of pore waters occurs during compaction, 2) incorporation of wallrock by ascending magmas, or 3) hydrothermal activity following emplacement of a shallow-level pluton. There is no limit on how much fluid may pass through a rock, but there are limits on how much internally-generated fluids can be lost from the rock. In the absence of a fluid or melt entering the rock, the bulk chemistry of the rock limits how much fluid can be expelled from the system, and consequently, how much the isotopic composition of a rock can change. Examples of fluid loss by dewatering, dehydration and decarbonation are given below.

Above sub-greenschist facies, loss of fluids take place by devolatilization and/or decarbonation reactions. The isotopic shifts caused by devolatilization reactions depend on the bulk composition of the rock and the P-T path followed during metamorphism. Fluids released during devolatilization reactions may escape either through a fracture network or, in cases of high permeability, pervasively. Two end-member models can be constructed for devolatilization-decarbonation reactions, with natural examples almost certainly lying between the two extremes (Valley, 1986). The first is termed *batch* devolatilization where fluid is evolved and remains in the system for the entirety of the devolatilization episode. Equilibrium between fluid-rock is maintained until reaction is complete, at which time the fluid escapes. While episodic fluid loss almost certainly occurs, retention of *all* fluid until decarbonation or devolatilization reactions go to completion could only be realized in cases where permeability is low and total fluid production is minimal. The second end-member case is *Rayleigh* devolatilization, where fluid leaves the system as it is formed, analogous to the Rayleigh fractionation models for precipitation (Chapter 4). By continuous removal of infinitely small 'packets' of fluid that are in equilibrium with the rock, the isotopic composition of the rock, and the bulk composition of the residual rock-fluid system, changes continuously.

Box 12.1: Mass (material) balance relationships; The lever rule:

The concept of material balance is fundamental in all geochemical applications, but is not well understood by many students. The isotopic compositions of smaller reservoirs change more than those of larger reservoirs in a system involving the interaction between two or more reservoirs of the same element. Removal of a vapor from the ocean will not measurably change the composition of the ocean, even though the light isotopes are preferentially incorporated into the vapor phase. The ocean must get heavier because light material is lost. But because there is so much more ocean than vapor, the increase is infinitesimally small. If we take enough vapor out of the ocean (*i.e.,* during the formation of ice caps), we *do* begin to see a change in the $\delta^{18}O$ and δD value of the ocean. In this case, the abundance of the lesser component – the ice caps comprise over 2% of hydrosphere – is beginning to approach that of the major component – the ocean (97.2%). In the same way, adding a small amount of hydrothermal fluid to a rock will not change appreciably the $\delta^{18}O$ value of the rock. The fluid-rock ratio is too low. Only when a great deal of fluid interacts with the rock, do we begin to see a change in the $\delta^{18}O$ (rock) value.

The δ value of a binary mixture *a* and *b* is given by:

$$\delta \text{ (mixture)} = \frac{N_a\delta_a + N_b\delta_b}{(N_a + N_b)} = X_a\delta_a + X_b\delta_b,$$

where *N* is the abundance of the element (*e.g.,* carbon, oxygen, etc.) *X* is the mole fraction. The general equation for *n* components is

$$\delta(system) = \sum_{i=1}^{n} X_i\delta_i \ .$$

The molar proportion of oxygen in a metamorphic rock is >50%. Hydrogen, on the other hand, will be present only in minor hydrous phases. The infiltration of an aqueous fluid will cause a larger change in the rock δD values than $\delta^{18}O$ values because of the mass balance rule. Only when the fluid-rock ratio gets very high, will the $\delta^{18}O$ values of the rock be affected appreciably.

Finally, there is a common misunderstanding that the fluid phase in a metamorphic rock is an important oxygen reservoir, which is not the case. The amount of fluid normally present along grain boundaries and fluid inclusions is too small to be of much consequence *as a fluid reservoir*. Therefore a fluid can only change the $\delta^{18}O$ value of a mineral appreciably if there is a large *flux* of fluid passing through the rock. At any one time, the amount of fluid in the rock is very small.

Keeping a simple mental image of the mass balance rule is very useful when interpreting isotopic results. “Is it reasonable on mass balance considerations” is a question that we should always keep in the back of our minds.

The batch volatilization model relies on calculations of equilibrium fractionation between all species based on simple mass balance constraints (see Box 12.1). When fluid leaves the system, the change in the isotopic composition of the rock can be calculated by

$$\delta_{\text{initial rock}} = \delta_{\text{final rock}}(x) + \delta_{\text{fluid}}(1\text{-}x) \qquad 12.1$$

where x = the mole fraction of the element (*e.g.*, oxygen) remaining in the rock during dehydration/volatilization and δ_{fluid} is the composition of newly-formed fluid in equilibrium with the final rock. The isotopic composition of the final rock is related to that of the fluid by the equation

$$\delta_{\text{final rock}} - \delta_{\text{fluid}} \approx 1000\ln\alpha_{\text{r-f}} \qquad 12.2$$

where $\alpha_{\text{r-f}}$ is the average fractionation between the final rock and fluid at the temperature of interest[1]. Equation 12.1 can be expressed as

$$\delta_{\text{fluid}} = \delta_{\text{initial rock}} - (x)1000\ln\alpha_{\text{r-f}} \qquad 12.3.$$

If the $\delta^{18}O$ values of both the initial and final rock can be determined, and the $1000ln\alpha_{\text{final rock – fluid}}$ is estimated with some confidence, then both the amount and $\delta^{18}O$ value of fluid lost from the system can be calculated. Generally, α is referred to the stoichiometrically-weighted average fractionation between the fluid and rock (Valley, 1986), although this is not a precise solution to equation 12.3. The fractionation factor changes in relation to the changing proportions of the solid components and with temperature (Rumble, 1982). Nevertheless, the approximation of constant α is generally sufficient to model fluid loss.

The Rayleigh model, or *open system* volatilization model will be approached if permeability is high and the P-T conditions result in a strong buoyancy of the expelled fluids. Lord Rayleigh derived the solution to the distillation equation (see Chapter 4) and applied it to the separation of different gases by diffusion through porous media. A modification of Rayleigh's equation, applicable to changes in the isotopic composition of a phase undergoing vaporization (or volatilization) is

$$\delta_f - \delta_i = \left(1000 + \delta_i\right)\left(F^{(\alpha-1)} - 1\right) \qquad 12.4,$$

where δ_f and δ_i are the final and initial δ value of the rock, α is the fractionation between rock and fluid, and F is the variable defined by fraction of the element remaining, ranging from 1 (unreacted) to 0 (all of the element lost to the vapor/fluid phase). That is, F equals 1 prior to any removal of the element of interest, and approaches 0 as all of the element is completely removed from the system. This equation, often called the *Rayleigh equation*, is a perfect solution for isothermal reactions where there is one reactant and one product, such as the decarbonation reaction 12.5 in terms of carbon, or the transformation of water

[1] The average α is computed assuming all phases are in equilibrium at all times. The α value will actually change during the reaction, but this is a second-order effect that can be ignored for the most part.

to water vapor at constant temperature (Chapter 4). The equation becomes far more complicated where there are multiple reactants and products, or changing temperatures, because the fractionation factor α changes with temperature and as a function of the relative proportions of the products and reactants (Young, 1993). Nonetheless, an average α value adequately approximates most geological situations.

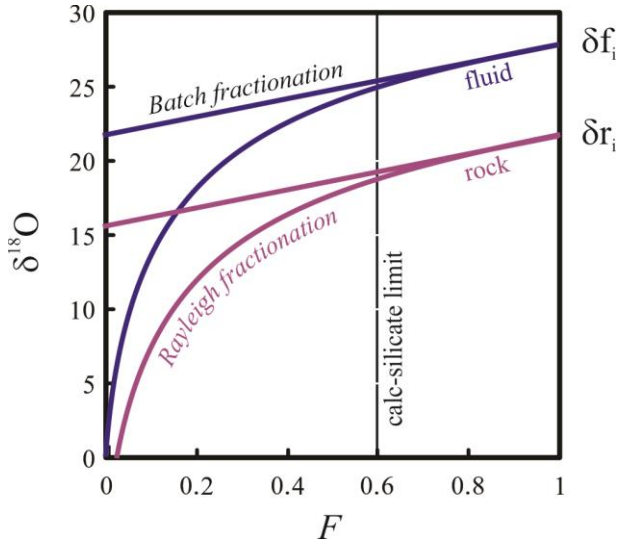

Fig 12.2. Changes in $\delta^{18}O$ value of rock (δr) and evolving CO_2 fluid (δf) for reaction 14.5, $\alpha = 1.006$. For high values of *F*, the batch and Rayleigh fractionation models have the same effect. Only for low *F* values (reactions proceeding to near completion) do the batch and Rayleigh curves diverge. For oxygen, the maximum degree of reaction for decarbonation reactions is given by the calc-silicate limit – *F* values cannot be less than 0.6. Initial values are given as δ_i. Note that the fractionation between fluid and rock is constant for all values of *F*.

The end-member batch and Rayleigh fractionation model paths are illustrated in Fig. 12.2. There are several fundamental consequences that are apparent from the figure. First, for moderate degrees of volatilization, the differences between batch and Rayleigh behavior are nearly indistinguishable. Only when the reactions are taken to near-completion do the Rayleigh and batch curves diverge significantly. Second, the magnitude by which volatilization reactions affect the isotopic composition of a system depends on what reactions take place, the mineral mode, the fractionation α, and the P-T conditions of the system (see Valley, 1986). However, there are fundamental limits as to how much oxygen can be removed from the system by decarbonation or dehydration, and thus how far along the Rayleigh fractionation curve a reaction can proceed. For a simple decarbonation reaction such as

$$\underset{\textit{calcite}}{CaCO_3} + \underset{\textit{quartz}}{SiO_2} \rightarrow \underset{\textit{wollastonite}}{CaSiO_3} + CO_2 \qquad 12.5$$

a maximum of 40% of the oxygen present in the reactants is lost to the fluid phase, so

that *F* cannot decrease to below 0.6, termed the *calc-silicate limit*[2]. The calc-silicate limit is, in fact, rarely reached. It requires that the reactants are in perfect stoichiometric proportions and that the reaction goes to completion. It is clear from Fig. 12.2 that decarbonation reactions alone cannot change the bulk rock $\delta^{18}O$ value of a rock by more than several per mil.

The maximum *F* value for oxygen loss from common dehydration reactions is even less than for decarbonation reactions. As an example, consider the two following volatilization reactions involving muscovite and talc;

$$\underset{\textit{muscovite}}{KAl_3Si_3O_{10}(OH)_2} + \underset{\textit{quartz}}{SiO_2} = \underset{\textit{microcline}}{KAlSi_3O_8} + \underset{\textit{kyanite}}{Al_2SiO_5} + H_2O \qquad 12.6$$

and

$$\underset{\textit{talc}}{Mg_3Si_4O_{10}(OH)_2} = 3\,\underset{\textit{enstatite}}{MgSiO_3} + \underset{\textit{quartz}}{SiO_2} + H_2O \qquad 12.7.$$

F values cannot go below 0.93 and 0.92 respectively (7 and 8% of the oxygen is lost to the fluid phase in these two reactions)[3]. The maximum shift in the $\delta^{18}O_{WR}$ value due to dehydration will almost always be less than 1‰. The bottom line is this: **volatilization reactions in metamorphic rocks cannot change the $\delta^{18}O_{WR}$ values of a lithology by more than several per mil under any conditions.** Larger shifts in $\delta^{18}O_{WR}$ values in geologic studies require the infiltration of a fluid or melt.

The effect of volatilization reactions on the isotopic composition of minor elements, such as hydrogen and carbon, can be much larger. In the case of both hydrogen and carbon, volatilization reactions can proceed until *F* approaches zero *for that element*, as is the case for carbon in reaction 12.5. The delta values will decrease asymptotically towards -1000‰ as *F* approaches 0. Such extreme lowering is never seen in metamorphic systems, but examples of Rayleigh volatilization trends for hydrogen and carbon isotope ratios are commonly observed as discussed in the following section.

In typical pelites, a series of dehydration reactions occurs with increasing temperatures until, by the time granulite-facies conditions are reached, nearly all hydrogen is driven from the rock. Hoernes and Hoffer (1979) found that the δD values of biotite in a prograde metamorphic sequence from Namibia decreased by 30‰ as temperatures of metamorphism increased from 480 to 650°C. The decreasing δD values can be explained by removal of water with high δD values during volatilization.

Nabelek *et al.* (1984) measured the $\delta^{18}O$ and $\delta^{13}C$ values of argillaceous sediments intruded by a granitic stock. The $\delta^{13}C$ values decreased by almost 12‰ as the intrusion was approached, concomitant with a decrease in the percentage of carbonate. All data fit inside an envelope defined by the end-member batch and Rayleigh decarbonation models (Fig. 12.3a) suggesting that the carbon isotope changes can be explained entirely by decarbonation reactions. In contrast, the low $\delta^{18}O$ values cannot be

[2] A maximum of 66% O_2 loss is possible for the reaction $CaCO_3 \rightarrow CaO + CO_2$, but this reaction is extremely rare.

[3] An extreme case would be the dehydration of brucite ($Mg(OH)_2$ or portlandite ($Ca(OH)_2$), where F can approach 50%, but this is an extreme example that is probably never encountered.

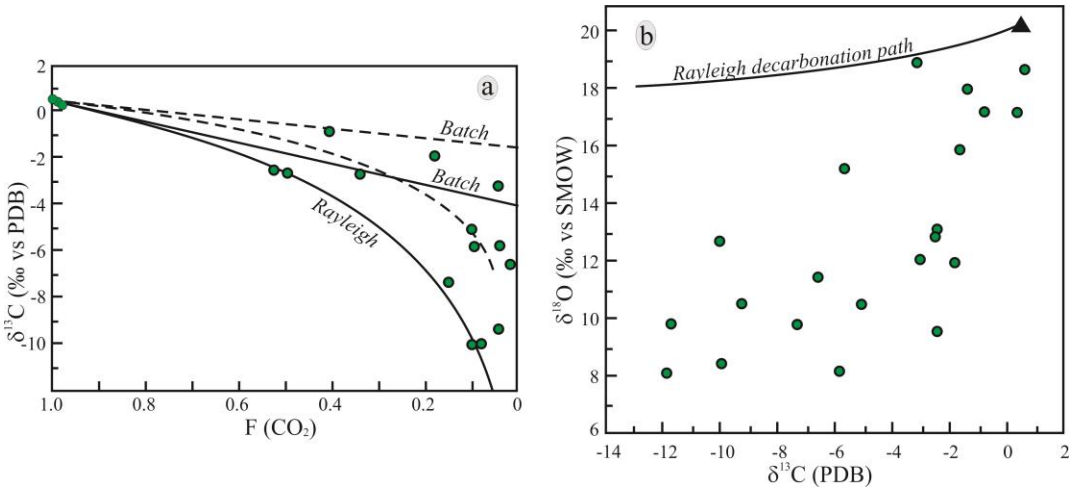

Fig. 12.3. a. Changes in $\delta^{13}C$ values of carbonate layers as a function of reaction progress for argillaceous sediments surrounding the Notch Peak Stock, Utah. Dashed and solid lines are for $\alpha_{CO2\text{-}cc}$ = 1.0025 and 1.0045, respectively. All data fall between the end-member batch and Rayleigh fractionation models, but not for any one value of α. **b.** In contrast to the carbon data, $\delta^{18}O$ values near the stock are far too low to be explained by Rayleigh fractionation during decarbonation reactions (curve). Instead, light fluids emanating from the stock must have infiltrated the permeable argillaceous sediments. (After Nabelek *et al.,* 1984). If they were 'pure' aqueous fluids, they would affect only the oxygen, but not carbon isotope composition.

explained by decarbonation alone. Decarbonation would only lower the $\delta^{18}O$ value of the sediments by a maximum of 2‰, far less than the 12‰ actually measured (Fig. 12.3b). The $\delta^{18}O$ values falling below 18‰ require open system behavior, explained by a low $\delta^{18}O$ fluid from the crystallizing granite infiltrating the permeable sediments.

A study of the Elkhorn contact aureole serves as a second example of complex volatilization and fluid infiltration behavior (Bowman et al., 1985). Changes in $\delta^{13}C$ and $\delta^{18}O$ values during decarbonation are calculated for both the batch (curve D-D′) and Rayleigh (curve D-R) equations (Fig. 12.4). Neither model reproduces the measured $\delta^{13}C$ and $\delta^{18}O$ values of the metamorphosed carbonates, shown as filled green circles. Bowman *et al.* proposed a two-stage model, incorporating partial decarbonation along a Rayleigh path (curve D-B) followed by mixing with an magmatic fluid (curve B-M).

Valley (1986) plotted trends for sixteen studies of contact metamorphism along with the predicted trends for pure volatilization. None of the coupled $\delta^{13}C$-$\delta^{18}O$ trends can be explained purely in terms of volatilization. In all cases, infiltration of an external fluid must be invoked.

12.3 Fluid sources and fluid rock-interaction

12.3.1 Oxygen and hydrogen

Through a combination of oxygen, hydrogen and carbon isotope analyses, it is often possible to constrain, or even unambiguously define, the origin of an infiltrating fluid. In order to go further and place numerical constraints on the *amount* of an infiltrating fluid, two conditions must be met. First, the composition of the infiltrating fluid must be different from that of the unaltered rock, and second, the isotopic composition of the infiltrating fluid and unaltered rock must be known.

A crude compartmentalization of hydrogen-oxygen isotope compositions of 'generic' fluids from different sources is given in Fig. 12.5. The isotopic compositions of meteoric waters, ocean water and brines have been measured directly. Metamorphic and igneous fluids are generally inferred. Direct measurements of metamorphic and igneous waters can be made on fumaroles and fluid inclusions, but this is rarely done. More often, the isotopic composition of a metamorphic fluid is calculated from the measured isotopic composition of solid phases and an assumed equilibrium fluid-rock fractionations (Sheppard, 1986).

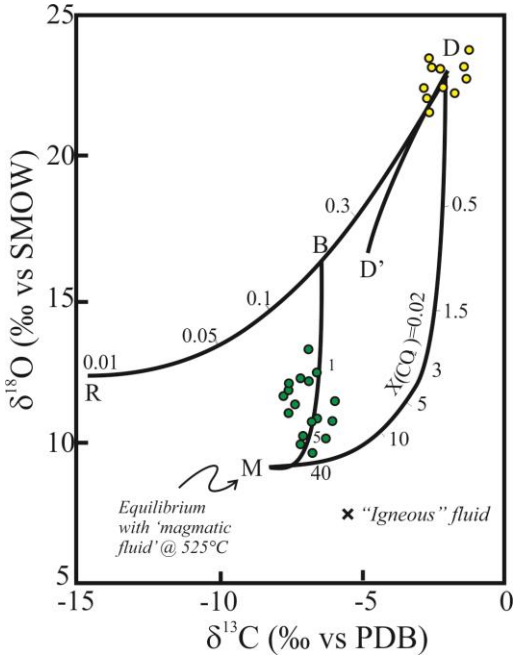

Fig. 12.4. $\delta^{13}C$ vs. $\delta^{18}O$ values for the Elkhorn contact aureole, Montana, USA (Bowman et al., 1985) . The unmetamorphosed limestone plots at D. Batch and Rayleigh volatilization curves are shown by trajectories D-D' and D-R, respectively. Mixing with an magmatic fluid plots along D-M. The metamorphosed calcites require a two stage model, first Rayleigh volatilization (D-B), followed by fluid infiltration (B-M).

Meteoric and ocean waters have distinct $\delta^{18}O$ values. Ocean waters have unambiguously high δD values whereas meteoric waters, depending upon latitude and elevation, may have extremely low δD and $\delta^{18}O$ values. Meteoric fluid-rock interactions can occur prior to metamorphism (Fourcade and Javoy, 1973; Valley and O'Neil, 1982; Sturchio and Muehlenbachs, 1985; Yui et al., 1995 and examples that follow), during peak metamorphism (Fricke et al., 1992), as a retrograde feature (Frey et al., 1976; Mora and Valley, 1991; Jenkin et al., 1992; Jenkin et al., 1994a), and in contact metamorphic rocks (Bowman et al., 1985; Jamtveit et al., 1992). It is reasonable to state with some certainty that interaction of a metamorphic rock with meteoric waters had occurred if the whole rock $\delta^{18}O$ or δD values are less than 3 to 4‰, or -100‰, respectively.

Probably the most striking example of meteoric water alteration in a metamorphic rock comes from the work of Yui *et al.* (1995) on the ultrahigh-pressure coesite-diamond-bearing rocks of the Dabie and Sulu terranes of eastern China. These rocks have been buried to depths far in excess of 100 km. The $\delta^{18}O$ values of all minerals are in equilibrium for the expected metamorphic temperatures. What is remarkable are the $\delta^{18}O$ values themselves. They range from -10.4 to -9.0‰, making them some of the lowest $\delta^{18}O$ values found in any rock. The authors suggest that the rocks underwent high latitude/altitude hydrothermal alteration with meteoric waters prior to subduction and metamorphism. This hypothesis requires that the system remained closed to external fluids throughout the extended journey from the surface to depth and back to the surface again.

Waters of oceanic origin have been recognized in metamorphic rocks by their uniquely high δD values. Wickham and Taylor (1985) found isotopic evidence for large-scale seawater infiltration to depths of 6-12 km. Homogeneous $\delta^{18}O$ values and very high

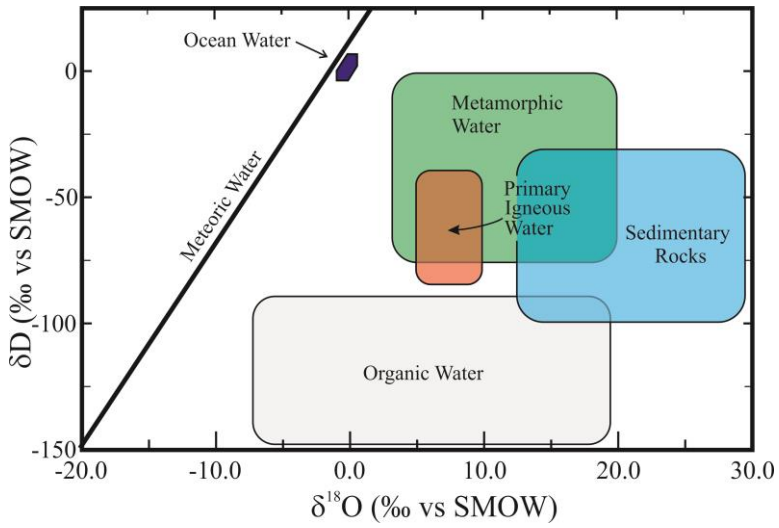

Fig 12.5. "Generic" water boxes for different geological environments. The range of ocean water is explained by changes in ice pack volume. Meteoric waters become lighter at higher latitudes and altitudes. Primary igneous water should be derived from the mantle with some degree of modification due to vapor loss. Organic water is related to the oxidation of organic material, and is a minor constituent in metamorphic rocks. Metamorphic waters are buffered by metamorphic rocks. Because of the extreme variety of metamorphic rock types, the metamorphic box is large. The sedimentary box is not sedimentary fluids, but rather the $\delta^{18}O$-δD values of the rock itself. During sedimentation in the marine environment, the $\delta^{18}O$-δD values are near zero (seawater). They increase during metamorphism as the fractionations between rock and fluid decrease. Diagram after Sheppard (1986).

δD values of the muscovite (-25‰) point to a oceanic source.

The distinct isotopic signature of ocean fluids can be traced throughout a rock's metamorphic/tectonic history. Oceanic hydrothermal alteration produces hydrous phases with high δD values. Dehydration of the hydrous phases during later subduction-related metamorphism will evolve a fluid with δD and $\delta^{18}O$ values characteristic of seawater. The high δD values (-30) and low $\delta^{18}O$ values (8.3‰ for quartz) from some Alpine eclogites are characteristic of rocks that have undergone seafloor metamorphism (Sharp et al., 1993). Dehydration of seafloor metamorphosed rocks during subduction presumably caused the release of fluids of an ocean affinity which then interacted with the surrounding rocks. Similar characteristic signatures of volatilization and infiltration from a subducting slab are seen at shallow levels (Bebout and Barton, 1989; Sharp and Barnes, 2004), where δD values as high as -25‰ are measured.

The compositional fields for waters other than oceanic or meteoric overlap, and are therefore ambiguous. The primary magmatic water box represents mantle aqueous fluids that have been modified by degassing during ascent (see Chapter 11). It overlaps with the far larger metamorphic water box, the range reflecting the varied compositions of the protoliths and their temperatures of metamorphism. The metamorphic water box could be subdivided further on the basis of different rock types and water sources. For example, the high δD end of the metamorphic water box is defined by hydrothermally altered ocean basalts, while the high $\delta^{18}O$ end of the metamorphic water box is for waters that have equilibrated with high $\delta^{18}O$ metasediments.

12.3.2 Carbon

Carbon isotope systematics differ from oxygen in several ways. First, carbon generally exists in only two solid forms, either as carbonate minerals or as reduced graphite (or organic matter at lower grades and diamonds at ultrahigh pressures). In carbonate- and graphite-free rocks, carbon is a minor or even trace element. While the molar abundance of oxygen is relatively constant for all but the most unusual rock types, carbon concentrations range from zero up to 12 wt % (in a pure marble) and approach 100% in graphite or coal deposits. Oxygen is the major component of most aqueous metamorphic fluids, while carbon is generally a trace component of the fluid, so that very high fluid-rock ratios (or alternatively carbon-rich fluids) are required to alter the $\delta^{13}C$ value of a rock. Finally, carbon can exist as a reduced or oxidized form in the fluid phase. The carbon isotope fractionation between CO_2 and CH_4 is large (Fig. 12.6), so that the oxidation state of the fluid will strongly affect the $\delta^{13}C$ value of a solid during fluid-rock interaction.

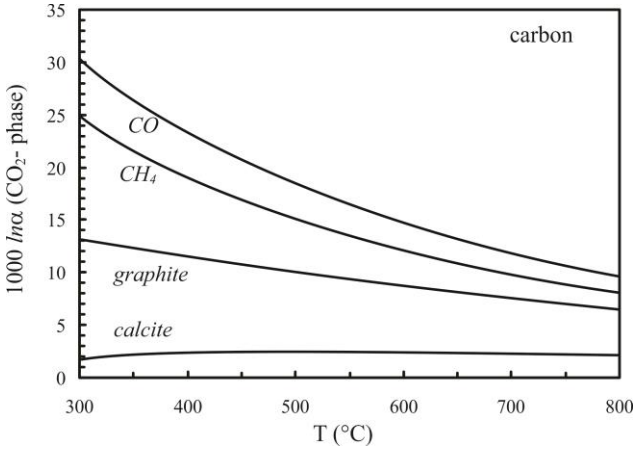

Fig 12.6. Carbon isotope fractionation between CO_2 and other phases. See Fig. 11.4 for references.

Carbon isotope measurements have traditionally been made on carbonates or graphite[4]. The diffusion rate of carbon in graphite is too slow for any exchange to occur at metamorphic temperatures. Carbon exchange between graphite and carbonate occurs only during recrystallization of the graphite. Because the diffusion rate of carbon in graphite is so slow, it is an excellent geothermometer for high temperature metamorphic terranes. Peak temperatures are often preserved even when overprinted by a secondary metamorphic event. This concept is discussed further in section 12.6.3.

Decarbonation reactions can change the $\delta^{13}C$ value of a carbonate, but only if a significant fraction of the carbonate is reacted away. The insensitivity of the carbon isotope composition to decarbonation is due to the small fractionation between CO_2 and carbonate (Fig. 12.6). A maximum (positive) fractionation of 2.6‰ occurs at ~450°C, which decreases with increasing temperature. 50% decarbonation will lower the $\delta^{13}C$ value of a carbonate by less than 2‰.

Another mechanism that changes the $\delta^{13}C$ value of carbonate is exchange with an exotic CO_2 or CH_4-rich fluid. Such behavior has been proposed to explain carbon isotope variations by a number of workers (Deines and Gold, 1969; Kreulen, 1980; Pineau et al., 1981) and can be quite diagnostic of fluid infiltration. Pineau *et al*. (1981) measured carbonates from deep granulites from Bamble, Norway where the $\delta^{13}C$ values were -8.2±1‰. They interpreted these low values as evidence of extensive infiltration of a mantle derived CO_2-rich fluid. Simple decarbonation of a typical carbonate (see Fig.

[4]$\delta^{13}C$ determinations have been made on other non-carbonate phases such as cordierite (Vry et al., 1988), scapolite (Hoefs et al., 1981; Moecher et al., 1994), and fluid inclusions (Hoefs and Touret, 1975; Rye et al., 1976; Kreulen, 1980).

11.1) would not lead to such low $\delta^{13}C$ values.

The generally accepted value for mantle carbon is approximately -6‰. A $\delta^{13}C$ value of -6‰ is by no means proof of mantle origin, however. Any one of a number of processes, such as exchange with CO_2 derived by oxidation of organic matter, will lower the $\delta^{13}C$ value of the carbonate as well (Frezzotti et al., 2000). While $\delta^{13}C$ values near -6‰ might result from simple infiltration of magmatic carbon, they do not prove the existence of a mantle-derived fluid. And finally, mysteries remain as to carbon sources, where $\delta^{13}C$ values have unexplained origins. Ghent and O'Neil (1985) found Precambrian marbles with $\delta^{13}C$ values of 8.9‰, which they tentatively explained as a primary, ancient sedimentary value (see Fig. 7.15). Deines (1968) found the record heavy sample. Carbonate inclusions in a mica peridotite have $\delta^{13}C$ values as high as +25‰. These high values may be related to volatilization of a CH_4-rich fluid, but the explanation is not totally satisfactory. Clearly, mysteries remain.

12.3.3 Sulfur

Sulfur isotope systematics are similar to those of carbon for the following reasons: 1) in most rocks, sulfur is a trace component. 2) It occurs in both oxidized (sulfate) and reduced (sulfide) form. 3) The concentration of sulfur in metamorphic fluids is low, and 4) sulfur-bearing species in the fluid can exist in a number of oxidation states.

At first glance, isolated sulfides appear to be far less 'reactive' than silicates or carbonates, although the apparent cause of this observation is somewhat deceiving. In a study of regionally metamorphosed graphitic sulfidic schists from south-central Maine, Oliver *et al*. (1992) found that the $\delta^{34}S$ values of coexisting pyrite and pyrrhotite did not approach equilibrium during metamorphism even in rocks that had reached 500°C. Instead, the grains preserved their pre-metamorphic $\delta^{34}S$ values averaging about -27‰, decreasing only slightly, if at all, with increasing metamorphic grade. The authors had expected equilibrium to be attained on the scale of 10s to 100s of meters, on the basis of published fluid fluxes for the region and the fact that exchange of sulfur between coexisting sulfides occurs rapidly even at low temperature in sulfide deposits. What Oliver *et al.* realized is that the lack of equilibrium on even the hand-sample scale is caused by the low sulfur concentrations in the fluid, analogous to what had been proposed by Monster *et al.* (1979). Although fluid flow was extensive and calculated *aqueous* fluid fluxes were high, the lack of sulfur species in the fluid resulted in a *sulfide* fluid flux that was vanishingly low. Sulfur concentrations in the fluid were simply so low that the fluids did not act as a conduit for sulfur transport between isolated sulfide grains.

The exchangeability of sulfur during metamorphism was further refined in an elegant *in situ* laser study of metamorphosed volcanogenic massive sulfide deposits (Crowe, 1994). Both touching and isolated chalcopyrite and pyrrhotite grains were analyzed from a suite of greenschist to amphibolite-grade rocks from Alaska (Fig. 12.7). Sulfide grains that were completely enclosed in quartz preserved their original hydrothermal $\delta^{34}S$ values. Touching sulfide pairs were reset to less-than-peak metamorphic temperatures due to continued exchange during retrogression. The degree of resetting was more pronounced in small touching pairs than large ones. Crowe concluded that the blocking temperature for sulfur isotope exchange is low, and that primary hydrothermal sulfur isotope compositions are only preserved in isolated grains that could not 'communicate' with each other during retrogression.

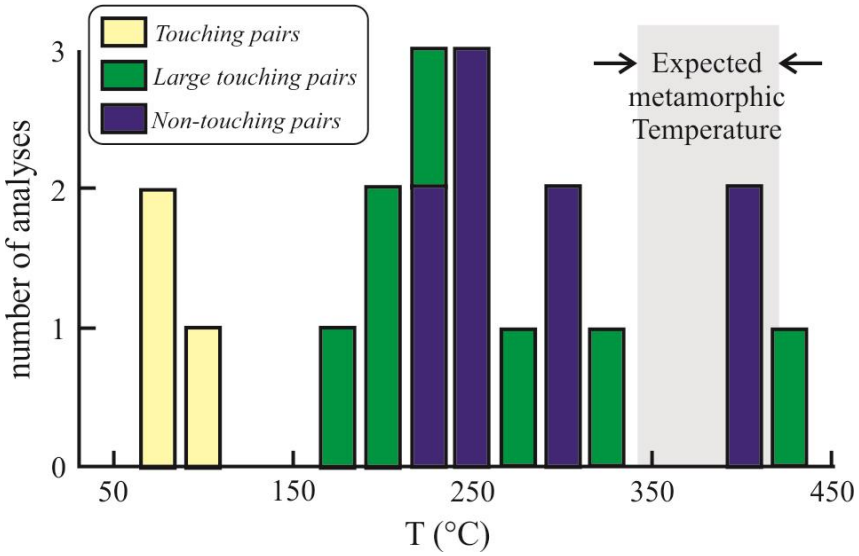

Fig. 12.7. Temperature estimates from $\Delta^{34}S$ values of coexisting pyrrhotite-chalcopyrite pairs from the greenschist facies Rua Cove deposit, Alaska, USA. While isolated grains may preserve fractionations corresponding to peak temperatures, samples in direct contact have reequilibrated during cooling. After Crowe (1994).

12.4 Scales of equilibration during metamorphism

Remarkably varied types of fluid movement have been identified in metamorphic terranes with the aid of stable isotope geochemistry. There are examples of fluid exchange at the kilometer scale, channeled fluid flow restricted to the cm scale, meteoric or seawater fluids penetrating down to depths in excess of 10 kilometers and channeled fluids in regional terranes clustered tightly in "hot spots" or controlled by large scale structural features or lithological boundaries. It is clear from the many different studies of metamorphic rocks that no simple rules apply to fluid flow behavior. Each terrane (and lithology) needs to considered on a case-by-case basis.

12.4.1 Regional scale exchange

Taylor *et al.* (1963) were the first to propose large-scale isotopic homogenization attending metamorphism. They measured the $\delta^{18}O$ values of mineral separates from three different bulk assemblages in kyanite zone pelitic schists in Central Vermont. Samples were collected over distances of several hundred meters from two metasedimentary units. The samples had a minimum of retrograde alteration and were all in textural equilibrium at the thin-section (mm-cm) scale. The measured isotopic fractionations between coexisting mineral pairs in a single lithology were the same in three of the four samples, indicating that they had equilibrated under the same temperature conditions. More surprising was that the $\delta^{18}O$ values of minerals common to all samples were nearly identical. This could be due to initial sedimentary isotopic compositions and modal abundances that coincidentally led to identical isotopic compositions at peak metamorphic conditions. Or, as the authors proposed, a fluid phase had promoted complete oxygen isotope homogenization between the different units. They suggested

that there was a pervasive metamorphic fluid that led to isotopic homogenization at the >100 meter scale. One way of testing this hypothesis would be to run mineral separates from rock types that were quite different, such as metapelites and coexisting calc-pelites. In this way, one could more reliably state that the initial $\delta^{18}O$ value of the two lithologies were different, yet the similar $\delta^{18}O$ values of hornblendes, epidotes, garnets, etc. were a strong indication of fluid homogenization.

Shieh and Schwarz (1977) found essentially identical bulk $\delta^{18}O$ values of different ortho- and para-gneisses over a 10,000 km^2 area. There is no mechanism that could explain fluid circulation and homogenization on such a large scale, rather these data do support the idea of a "fortuitously" homogeneous protolith. Bowman and Ghent (1986) measured the oxygen and hydrogen isotope composition of metapelites from staurolite to sillimanite zone in British Columbia and concluded that the general homogenity of the $\delta^{18}O_{quartz}$ values (13.3±0.3 1σ, n=9, 3 outliers) was caused by a homogeneous protolith. Demonstrating the presence of a pervasive fluid is difficult, and is best carried out when adjacent lithologies have clearly different protolith $\delta^{18}O$ values.

Isotope homogenization of hydrogen is probably more common than for oxygen. First, the buffering capacity of a rock for hydrogen is not very strong, given the low concentration of hydrogen in a rock. Second, the exchange rate of hydrogen between minerals and fluids is much more rapid than for oxygen. In the classic example of this phenomenom, Frey *et al*. (1976) state that rocks of the metamorphic Monta Rosa granite, Central Swiss Alps have 'stewed in their own juices'[5], in order to explain the homogeneity of hydrogen isotope ratios, and heterogeneity of oxygen isotope ratios.

12.4.2 Localized exchange

Fluid interaction between what are commonly deemed 'impermeable rock types', particularly marbles and cherts, is extremely limited. Marbles often retain their original $\delta^{18}O$ and $\delta^{13}C$ values, even when surrounded by lithologies that have a completely different isotopic composition or have evidence of extensive interaction with an external fluid. Marbles are more susceptible to isotopic exchange in samples where the permeability was enhanced by metamorphic decarbonation reactions (Rumble and Spear, 1983). Decarbonation reactions could produce a volatile phase which increases the fluid pressure. At the same time the volume change of the solid phases for the reaction, ΔV_{solids}, is negative, thereby increasing porosity. The degree of fluid infiltration is often proportional to the magnitude of calc-silicate reactions that have occurred. It should be pointed out, however, that ductile marbles probably cannot accommodate increased fluid pressures without flowing, and there is very serious issue regarding wetting angles in order for this process to persist for any significant period of time (see Holness and Graham, 1991 for a further discussion).

Rye *et al*. (1976) made a comprehensive stable isotope study of interbedded schist and marble units in a prograde metamorphic sequence at Naxos, Greece. The $\delta^{18}O$ values of the quartz and muscovite in the schists correlate well with metamorphic grade. The $\delta^{18}O$ values of quartz decrease from a typical sedimentary value of 19‰ in the least metamorphosed rocks to 9.4‰ in the migmatite[6] samples. The marbles, on the other

[5] One of the great 'lines' from a renowned stable isotope geochemist!
[6] Migmatites are rocks that have gotten sufficiently hot to partially melt.

hand, have relatively constant $\delta^{18}O$ values, even in the highest grade rocks. Rye *et al.* concluded that there was significant fluid infiltration into the schists from "deep-seated" sources, while the marbles were impermeable to the evolving fluids.

Fluid flow is often controlled by large scale structural features, such as thrust ramps, thermal domes related to igneous intrusions, antiforms and with kilometer-scale vein systems. Shear zones often act as important conduits for enormous amounts of fluid movement. Different $\delta^{18}O$ values between mylonites or ultramylonites and host rock clearly indicate that fluids passed through the shear zone. Both downward penetration of fluids – a meteoric source (McCaig et al., 1990; Morrison and Anderson, 1998) – and upward flow from deeper levels (Kerrich, 1986; Fourcade et al., 1989; Burkhard and Kerrich, 1990; Crespo-Blanc et al., 1995) have been identified.

12.5 Quantifying fluid-rock ratios and fluid fluxes

12.5.1 Simple mixing models: Zero dimensional water-rock interaction models

Taylor (1979) proposed a model for estimating fluid/rock ratios by assuming instantaneous and constant isotopic equilibration between a fluid and rock. His model was developed for fluids infiltrating a granite (Chapter 11), but has been applied to metamorphic rocks as well. The basic *mass balance* equation for mixing a rock and fluid is

$$W\delta^{i}_{H_2O} + R\delta^{i}_{rock} = W\delta^{f}_{H_2O} + R\delta^{f}_{rock} \qquad 12.8$$

where *i* is the initial value, *f* is the final value, *W* is the atom fraction of the element in water that has participated in the interaction, and *R* is the atom fraction of the element in rock. It is necessary to *assume* a value for $\delta^{i}_{H_2O}$, such as local meteoric water values. The $\delta^{i}_{H_2O}$ value can almost never be measured because the initial fluid is no longer present in the rock, other than as fluid inclusions which most likely have been modified during metamorphism. Similarly, the $\delta^{18}O$ value of the unaltered rock must be estimated. For shear zones, the non-sheared equivalent can be taken as the reasonable δ^{i}_{rock} value. In hydrothermal studies of epithermal granites, a normal granite is used for the δ^{i}_{rock} variable. The δ^{f}_{rock} value is measured. The only variable not known is $\delta^{f}_{H_2O}$, which must be calculated for an *assumed* temperature on the basis of known fractionation factors between rock and fluid ($\Delta_{rock\text{-}fluid}$).

Equation 12.8 can be rearranged to give a *closed system* water-rock relationship:

$$W / R = \frac{\delta^{f}_{rock} - \delta^{i}_{rock}}{\delta^{i}_{H_2O} - \left(\delta^{f}_{rock} - \Delta_{rock-fluid}\right)} \qquad 12.9,$$

where $\Delta_{rock\text{-}fluid}$ is the equilibrium fractionation between the rock and fluid at the temperature of interest. Equation 12.9 is valid for the special case where fluid enters a system, equilibrates with the rock and is expelled in a single event. It is equivalent to the *batch fractionation* described above for volatilization/dehydration reactions. Ohmoto (1986) compares the Taylor one-pass model to "an autoclave which contains water and

rock, and is maintained at a constant temperature". The other end-member scenario – the multi-pass case models the process of infinitely small quantities of fluid coming into contact with a rock, equilibrating with it, and then being expelled. This model can be derived by writing equation 12.8 in differential form and integrating it as follows:

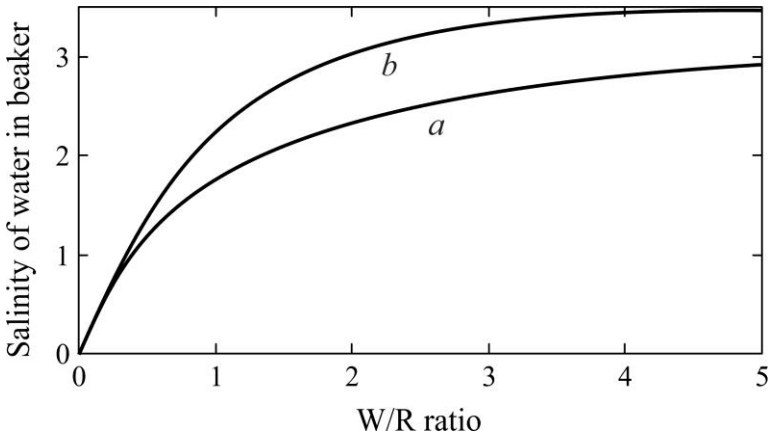

Fig. 12.8. Simple mixing of freshwater and seawater. The salinity of our beaker will only reach the salinity of the infiltrating fluid (3.5%) for infinite *W/R* ratios. Curve *a* 'one pass'; curve *b 'multi-pass'*

$$W/R = \ln\left[\frac{\delta^i_{H_2O} + \Delta - \delta^i_{rock}}{\delta^i_{H_2O} - \left(\delta^f_{rock} - \Delta\right)}\right] = \ln\left[(W/R)_{closed\ sytem} + 1\right] \qquad 12.10.$$

The equation is discussed in more detail by Nabelek (1991). Care should be taken when using these water-rock ratio models. The simple W/R ratio equations above are too often misapplied to metamorphic systems. In metamorphic rocks of deep-seated origin, estimates of the $\delta^i_{H_2O}$ and δ^i_{rock} values, as well as temperature of interaction may not be well constrained, and the researcher should be aware of the potentially large uncertainties that may be associated with calculated fluid/rock ratios.

In all cases, the *W/R* ratios calculated using equations 12.9 and 12.10 are considered *minimum* values. Fluids can pass through a rock and not interact with it due to sluggish kinetics, or only partially interact. In terms of the effect on the rock, it is the same as if the fluid had never passed through the rock. Such a scenario could be imagined where quartz precipitates along the walls of a newly-forming vein. Once a veneer of quartz has precipitated, further fluid flow could be channeled through the center of the vein without any effect on the rock.

12.5.2 One dimensional (directional) water-rock interaction models

The previously described fluid-rock interactions can be considered as 'zero dimensional' models. They consist of three stages: 1) introduction of some amount of fluid, 2) equilibration between the rock and fluid, and 3) expulsion of the fluid. It is a simple mass balance treatment and does not consider flow direction. The model works well in some cases, but does not adequately describe continuous fluid-rock interaction for fluids travelling unidirectionally. Instead, it is necessary to consider a one-dimensional system, where fluid comes from a source with a distinct isotopic composition and reacts with the rock along a specific *flow path*. When considering fluid-rock interaction in this way, we see how the isotopic compositions of the rock and the fluid change with time *and space*.

The concept behind a one-dimensional flow model is based in chromatographic

theory, and can easily be described by simple 'laboratory' analogs. First, we'll consider the zero dimensional model, discussed above. For our hypothetical example, we will just consider mixing between fresh water and salt water, ignoring isotopes. It is easy to visual this system, yet is no different that mixing of two reservoirs with different isotopic compositions. Our system consists of a beaker of fresh water and infiltrating seawater with a salinity of 3.5%. If we add a little bit of seawater to our beaker, the salinity increases slightly. The more salt water we add, the higher the salinity. Using equation 12.9, our δ^i_{rock} is the beaker's initial salt-free water, and our $\delta^i_{H_2O}$ is seawater with a salinity of 3.5%. The beaker filling up with ever-greater amounts of seawater equivalent to the one pass model. If the inflow of seawater is balanced by an outflow from the beaker, so that the level of water never changes, then the multipath model is realized. A graph depicting the *W/R* ratio using equations 12.9 and 12.10 is given in Fig. 12.8 for a 'one pass' (curve *a*) and 'multi-pass' model (curve b). Salinity at first increases rapidly with the addition of salt water, but ultimately approaches the 3.5 % salinity of the incoming fluid asymptotically. We need a *W/R* ratio of ∞ to reach the identical salinity as the infiltrating fluid.

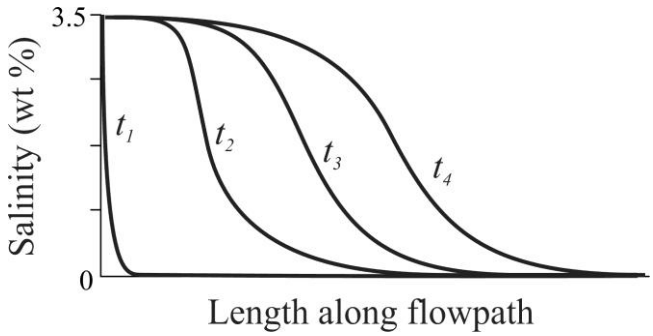

Fig. 12.10. One-dimensional infiltration model, illustrating the 'smoothing' effects of dispersion, diffusion, and finite reaction kinetics. t_x refers to time after the beginning of mixing. As time proceeds, the boundary becomes more diffuse.

Now, instead of a beaker, consider a long, thin capillary tube filled with fresh water. Seawater enters one end of the tube with a salinity of 3.5%. As the seawater enters from the tube from one end, fresh water is expelled from the other end. If there is no dispersion or diffusion at the seawater-freshwater interface, then a sharp salinity front exists at the boundary between the two fluids. The interface migrates forward with time, the rate of forward progress related to the *flux* (units of volume/area or simply distance), or rate of flow. This construction is illustrated in Fig.

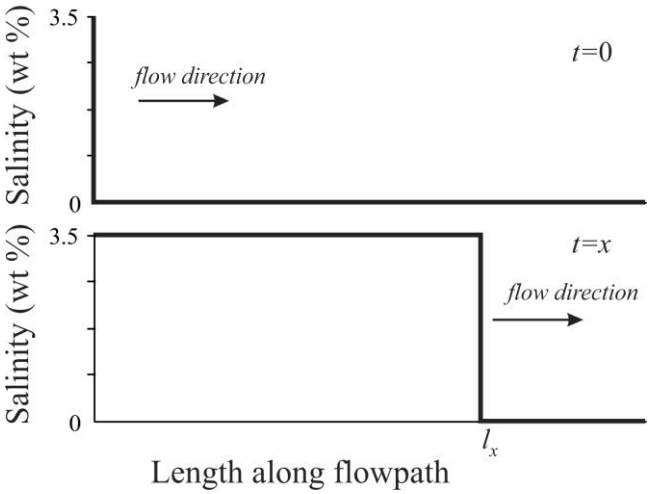

Fig. 12.9. One-dimension flow model of seawater infiltrating a column of freshwater. At time t=0, the entire length of the column will have freshwater. As the seawater flows into the column, a sharp front will migrate forward, the rate being proportional to the fluid flux. Although the salinity is not the same along the entire column, any plane perpendicular to the length of the column has seen the same amount of fluid (*e.g.*, had the same *W/R* ratio).

12.9. At t=0, the salinity of the entire tube is 0 and seawater is just beginning to enter from the left-hand side. As the flow continues, the seawater-freshwater front migrates to the right, so that at time $t=x$, there is a salinity front at position l_x. All of the fluid at $l<l_x$ has a salinity of 3.5%, and all fluid at $l>l_x$ has a salinity of 0%. If we were to apply the simple mixing equations, either 12.9 or 12.10 to this system, we would calculate a W/R ratio of 0 at all points $l>l_x$, and W/R ratios of ∞ at all point $l<l_x$. In fact, all points along the flowpath have seen the same fluid flux!

In real situations, the sharp front depicted in Fig. 12.9 becomes diffuse due to a number of processes, including diffusion, dispersion, sluggish exchange kinetics (between rock and fluid) and changing fractionation factors with changing temperature. As a result, the infiltration front becomes less sharp (Fig. 12.10) as flow proceeds.

Spooner *et al.* (1977) first modeled stable isotope data using flow path calculations. They divided the flow path up into a finite number of *en echelon* boxes, and considered each as a zero-dimensional system. A finite quantity of fluid enters the first box. It equilibrates with the rock volume in the first box, the $\delta^{18}O$ values of the rock and fluid being determined by the fractionation factor $\Delta^{18}O_{rock\text{-}fluid}$ and the W/R ratio. The amount of fluid entering the rock is determined by the porosity (ϕ) of the rock. When a small amount of fluid enters the first 'box', the $\delta^{18}O$ value of the rock changes very little, while the tiny packet of fluid equilibrates 'instantaneously' with the rock. The simple mass balance equation 12.9 applies. As the newly equilibrated fluid enters the second box, it has an isotopic composition that is *almost* – but not exactly – in equilibrium with the original rock, so that the $\delta^{18}O$ value of both the rock and the fluid box change nearly imperceptibly. As each new increment of fluid enters the system, the integrated W/R ratio of the first box increases, and the $\delta^{18}O$ (rock) value slowly shifts towards equilibrium with the initial fluid. If we have an infinite number of infinitely small boxes, the migrating front will be sharp. Increasing the size of each box causes the diffusion front to smooth out.

A number of authors have developed mathematical solutions in the form of partial differential equations which must be solved numerically to the problem of one-dimensional fluid flow (Lichtner, 1985; Baumgartner and Rumble, 1988; Blattner and Lassey, 1989). Some very nice applications have been made using this approach, particularly to fluid-rock interaction in shallow-level contact environments (Nabelek and Labotka, 1993; Bowman et al., 1994; Barnett and Bowman, 1995; Cook et al., 1997) and between contrasting lithologies (Ganor et al., 1989; Bickle and Baker, 1990; Vyhnal and Chamberlain, 1996).

As an example, Bickle and Baker (1990) made a detailed isotopic profile across a schist-marble contact in a Tertiary metamorphosed sequence from Naxos, Greece. The sigmoidal-shaped diffusion pattern is clearly displaced into the marble (Fig. 12.11). The authors concluded that the pattern requires that there was a net transport (advection) from the schist into the marble. The data can be explained by either a very modest degree of fluid *advection* toward the marble from the schist combined with diffusion, or by a much larger degree of fluid flow nearly *parallel* to bedding with only a small component perpendicular to bedding. The two cannot be distinguished. Only the contact-perpendicular component can be computed.

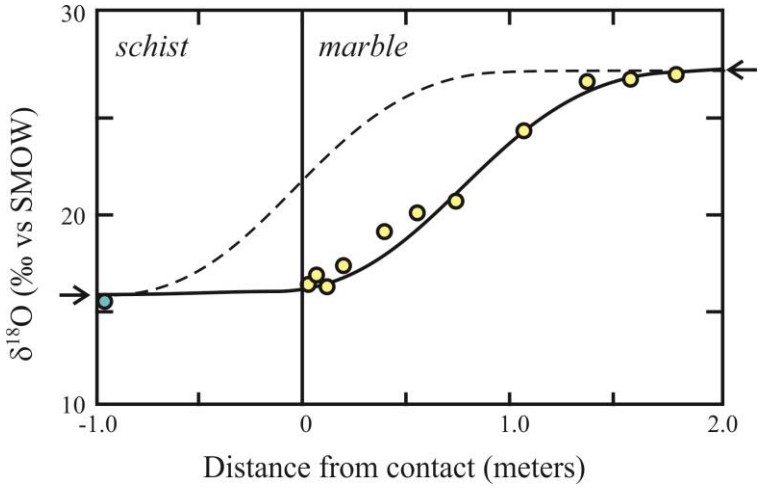

Fig. 12.11. Oxygen isotope profile of calcite across a schist-marble contact at Naxos, Greece. Data are shown by circles; the solid line is derived from a combined infiltration-diffusion model in which the fluid is moving from the schist into the marble. The arrows show the assumed initial compositions of the schist and marble, respectively. Note that if there was only pure diffusional exchange the sigmoidal profile would be symmetrical about the contact (as shown by the dashed line). The displacement into the marble requires a component of flow from schist to marble. From Bickle and Baker (1990).

In a similar study, Cartwright and Valley (1990) measured a sigmoidal shaped isotopic profile that was indeed centered on a granite-marble contact, in contrast to Bickle and Baker's displaced profile. They inferred this pattern to be related to diffusional exchange via an intergranular pore fluid without any advective flow perpendicular to the contact. The symmetry about the contact indicates that there was no preferential flow direction (see Box 12.2).

Models have been developed to quantify fluid flow directions and fluxes in a contact metamorphic event using stable isotope profiles. The situation has an additional complexity that significant temperature changes occur along the flow path (Dipple and Ferry, 1992), and consequently, isotopic fractionation between the fluid and rock varies with distance. Two endmember flow models can be envisioned: fluid flow out of the intrusion – that is the so-called 'down-temperature' flowpath; or fluid flow towards and eventually into the intrusion – the 'up-temperature' flowpath. Both models have been rigorously defended by various researchers. In fact, it seems likely that both flow regimes may occur at a single contact aureole at different times. Fluids flows out of a pluton as it crystallizes and expels water. Once crystallized, however, the temperature difference between the intrusive and country rock creates a buoyant driving force for fluids to flow towards the pluton and eventually upwards. The complexities of fluid rock interaction in a contact metamorphic setting are discussed in Nabelek (1991).

12.6 Thermometry

12.6.1 Introduction

Stable isotope thermometry began in the late 40's, with applications primarily to low-temperature carbonates. Baertschi and Silverman (Baertschi, 1951; Baertschi and Silverman, 1951) first measured the $\delta^{18}O$ values of bulk crystalline (silicate) rocks, but it

Box 12.2: Comparison of isotopic data across lithological contacts.

It is common to consider isotopic variations across a lithological contact and use differences to interpret mixing between the two lithologies. Care must be taken in terms of what is being compared, however! Many studies exist where comparisons are made incorrectly. Consider the juxtaposition of a quartzite and iron formation. The $\delta^{18}O_{bulk\ rock}$ values of the two lithologies are completely different and will show a marked decrease across the boundary, which could be mistakenly interpreted as isotopic disequilibrium. In fact, the iron formation has a lower $\delta^{18}O_{bulk\ rock}$ simply because it has a high percentage of magnetite. More meaningful information regarding cross-lithology equilibrium is obtained when either similar lithologies or like minerals are compared across lithologies. If the $\delta^{18}O$ values of quartz in the iron formation are the same as in the quartzite, then isotopic equilibrium exists between the two lithologies. It doesn't matter what the $\delta^{18}O$ value of the bulk rock is. If fluid exchange has resulted in isotopic equilibrium between the two lithologies, then the $\delta^{18}O$ values of each mineral will be the same in each rock type, even though the bulk rock values for each lithology could be completely different.

In a similar way, comparisons of the bulk rock $\delta^{18}O$ values of mafic and more felsic igneous rocks are flawed, yet frequently made. A higher proportion of low $\delta^{18}O$ minerals, such as olivine and pyroxene, in the more mafic magma will lead to a low $\delta^{18}O$ value, even when mafic and felsic co-mingled magmas are actually in isotopic equilibrium.

wasn't until some years later that Clayton and Epstein demonstrated that the fractionations between coexisting minerals in high temperature rocks were large enough to be valuable for thermometry (Clayton and Epstein, 1958, 1961). Garlick and Epstein (1967) made a detailed study of prograde metamorphic sequences and demonstrated that mineral-pair fractionations decrease with increasing metamorphic grade (Fig. 12.12). The $\delta^{18}O$ values increased in the following order: magnetite, ilmenite, chlorite, biotite, garnet, muscovite, quartz. They were able to quantify temperatures of metamorphism on the basis of quartz-magnetite fractionations, which had been calibrated experimentally. Myriad thermometric studies have since been made in a wide range of metamorphic rock types, ranging from subgreenschist facies to rocks heated to well over 1000°C (Sharp et al., 1992; 1998).

Stable isotope thermometry applied to metamorphic rocks is complicated by the slow cooling that occurs during retrogression. Taylor *et al* (1963) and Garlick and Epstein (1967) both recognized the problem of retrograde reequilibration. Taylor *et al.* asked whether or not chemical and mineralogical equilibrium are a prerequisite for oxygen isotope equilibrium. They reasoned that if recrystallization processes are strong enough to break Si-O bonds, they will surely result in anion reorganization as well. Taylor *et al* wrote "If the O^{18}/O^{16} ratios of these minerals are each "frozen in" at a different, but constant, characteristic temperature, then similar Δ-values might be obtained in each rock". This was the first mention of retrograde exchange in the sense of the concept of "closure temperatures". Although complications associated with retrograde exchange exist, careful treatment of oxygen isotope data has led to numerous successful thermometric studies in metamorphic rocks. In fact, with judicious sampling, more

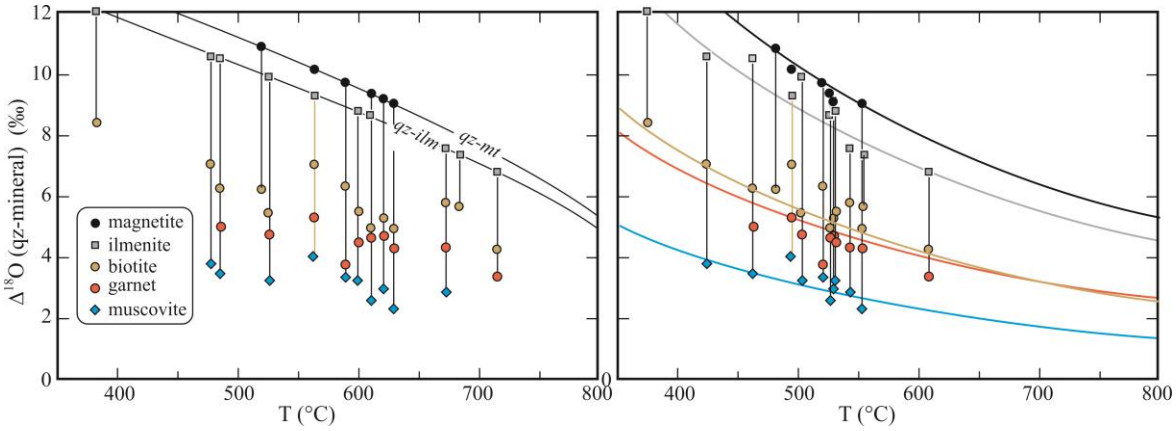

Fig. 12.12. Garlick and Epstein's (1967) measured fractionations of minerals relative to quartz for several metamorphic terranes. The authors noted that there is a general decrease in fractionation as temperatures increase. **Left:** The data as plotted in the original paper. Each sample is placed at the temperature determined by the quartz-magnetite calibration (based on published quartz-water and magnetite-water exchange experiments). **Right:** The data are refit here to more recent quartz-mineral calibration curves and show a generally smooth decrease in fractionation with increasing temperatures. Using the updated fractionation data, lower temperature estimates are obtained than in the original paper.

information than just peak metamorphic temperatures can be 'teased out' of a rock that has undergone partial retrograde exchange, as explained in section 12.7.

Two questions must be addressed when trying to extract metamorphic temperature information using stable isotope thermometry: 1) Was isotopic equilibrium attained during peak metamorphism, and 2) have the $\delta^{18}O$ values been modified during the subsequent slow cooling? In low-grade metamorphic rocks, condition one is commonly not met. Inheritance of pre-metamorphic values is all too common. In very high-grade metamorphic rocks, high intragranular diffusion rates may lead to at least partial reequilibration during slow cooling. There are a number of processes that can disturb the isotopic equilibrium of an assemblage. These include 1) diffusional reequilibration during simple cooling and in an otherwise stress-free system, 2) deformation and recrystallization, and 3) introduction of a disequilibrium fluid. If the diffusion rate of oxygen for a pair of minerals is fast, then some degree of resetting must occur during slow cooling from high temperature. The isotope community is divided with respect to the accuracy of high-temperature estimates obtained using stable isotope fractionations. Some groups have had apparent success in retrieving peak metamorphic temperatures; others maintain that peak-temperature equilibrium is almost never retained. Strategies have been developed to use stable isotope thermometry to extract peak metamorphic temperatures. Recent work indicates that certain minerals are extremely 'refractory', in the sense that they do not reequilibrate during cooling (Sharp, 1995; Valley, 2001). It is safe to say that careful selection of lithologies and minerals is crucial to any effort aimed at extracting peak temperature data from high-T metamorphic rocks (e.g., Farquhar et al., 1993).

12.6.2 Oxygen isotope thermometry in metamorphic rocks – testing for equilibrium

Several strategies have been developed to extract accurate temperature estimate from metamorphic rocks.

1) Measure multiple minerals in a single sample. If all mineral pairs give the same temperature, then there is more confidence in the validity of the results. The isotopic fractionation between two solid phases can be expressed by the equation

$$1000 \ln \alpha_{x-y} = \frac{a_{x-y} \times 10^6}{T^2} + b_{x-y} \qquad 12.11,$$

where a is the temperature coefficient of fractionation for phases x and y and b is a constant, usually equal to zero for anhydrous minerals, T is in Kelvins. Equation 12.11 can be rearranged in a simple linear format ($y = mx$)

$$1000 \ln \alpha - b = a \times \left(\frac{10^6}{T^2} \right) \qquad 12.12.$$

Our $y = 1000\ln\alpha - b$, $m = 10^6/T^2$, and $x = a$. If all minerals in an assemblage are in isotopic equilibrium at temperature T, then the data must form a linear array on a $1000\ln\alpha$-b *vs*. a plot. The best fit line passes through the origin and has a slope of $10^6/T^2$ (Javoy et al., 1970). Consider the mineral suite quartz, plagioclase, biotite, muscovite, and magnetite. In the example given in Fig. 12.13, all minerals plot on a straight line except magnetite. One could reasonably conclude that all minerals except magnetite are in isotopic equilibrium, and the slope defined by the data points for quartz, plagioclase, muscovite and biotite is equal to $10^6/T^2$.

This form of graphical representation has been used in numerous studies. It provides a statistical method for averaging temperatures in a multi-mineral system (assuming they are all in equilibrium) and clearly indicates any potential disequilibrium by one or more mineral.

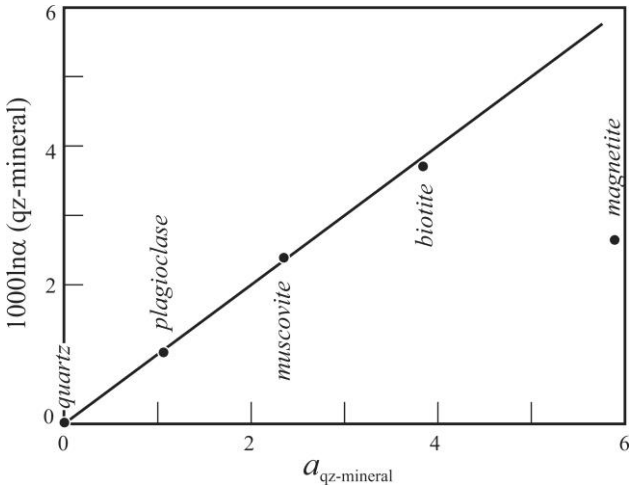

Fig. 12.13. Typical isotherm plot for coexisting minerals. All mineral data are plotted relative to quartz (although the choice of reference mineral is arbitrary and will not change the result). In the illustrated example, all minerals except magnetite define an isotherm, and magnetite is clearly out of equilibrium with the other phases. The slope of the best-fit line is equal to $10^6/T^2$ (T in Kelvin).

2) Analyze 'refractory' minerals. In the absence of recrystallization, isotopic exchange occurs by the process of self-diffusion, or intracrystalline diffusion. This is the process in which oxygen diffuses through a crystal lattice. The oxygen self-diffusion

rates of minerals are highly variable. The diffusion rates of biotite, leucite, and feldspar[7] are so rapid that retrograde isotopic exchange is likely to occur during slow cooling. Other minerals, such as garnet, olivine, zircon, and kyanite, have very slow self-diffusion rates. For these minerals, the $\delta^{18}O$ value of the mineral should 'lock in' at the time of crystallization, and not change at all during slow cooling. Bimineralic assemblages containing at least one refractory phase are excellent targets for extracting peak metamorphic temperatures from high-grade metamorphic rocks. Refractory minerals, defined as those that are least likely to exchange once crystallized, have their own set of problems, however. There are clear examples of refractory minerals forming during the prograde path of a metamorphic event and not reequilibrating during peak metamorphic conditions. Larson and Sharp (2003) demonstrated that the coexisting polymorphs andalusite, sillimanite and kyanite (all Al_2SiO_5), from a single lithology do not have the same $\delta^{18}O$ values. The differences are explained as being the result of different formation temperatures for each polymorph. The minerals did not reequilibrate with each other at the temperatures of peak metamorphism. The rocks went through discrete episodes of metamorphism. The stable isotope data of the aluminum silicates reflect these multiple events. It is necessary to consider phase equilibria and mineral reaction sequences when interpreting stable isotope data of refractory phases.

3) Avoid 'disturbed' samples. Late fluid infiltration and/or deformation will act to reset the $\delta^{18}O$ values of minerals. Fluids may preferentially interact with one mineral relative to another. It is not uncommon to find $\delta^{18}O$ values of feldspars that are higher than quartz, indicating that hydrothermal alteration has raised the $\delta^{18}O$ value of the feldspar, but not quartz. By analyzing mineral phases that are sensitive to hydrothermal exchange (*e.g.*, micas, feldspar, carbonates), a late fluid infiltration event can often be detected and the $\delta^{18}O$ value of the infiltrating fluid determined. Deformation and recrystallization also enhance reequilibration rates. Oxygen isotope disequilibrium is commonly observed in shear zones, where kinetically controlled reequilibration overwhelms equilibrium thermodynamic controls (e.g., Crespo-Blanc et al., 1995). Finally, it is well established that the diffusion rate of oxygen in a mineral is greatly enhanced when an aqueous fluid is present (Sharp et al., 1991). Anhydrous rocks are more likely to preserve peak temperatures than hydrous ones.

12.6.3 Applications of stable isotope thermometry

The most successful applications of stable isotope thermometry are generally made in rocks of amphibolite- and lower- granulite-facies. At lower metamorphic grades – greenschist and sub-greenschist facies – mineral separation becomes difficult due to the fine grain size, and temperatures may not have been high enough for all mineral phases to attain isotopic equilibrium[8]. By the time amphibolite-facies conditions are reached (~500°C), the rocks generally have coarse-grained minerals which can be easily separated

[7] The diffusion rate of oxygen in feldspar is strongly dependent on the presence of absence of an aqueous fluid – 'wet' vs 'dry' diffusion. See (Elphick et al., 1988; Sharp, 1991) for more information.

[8] In low-grade rocks, a strategy of analyzing *less* refractory phases may be the most successful approach. For example, quartz-calcite pairs can provide temperature information of less than 250°C (Kirschner et al., 1995).

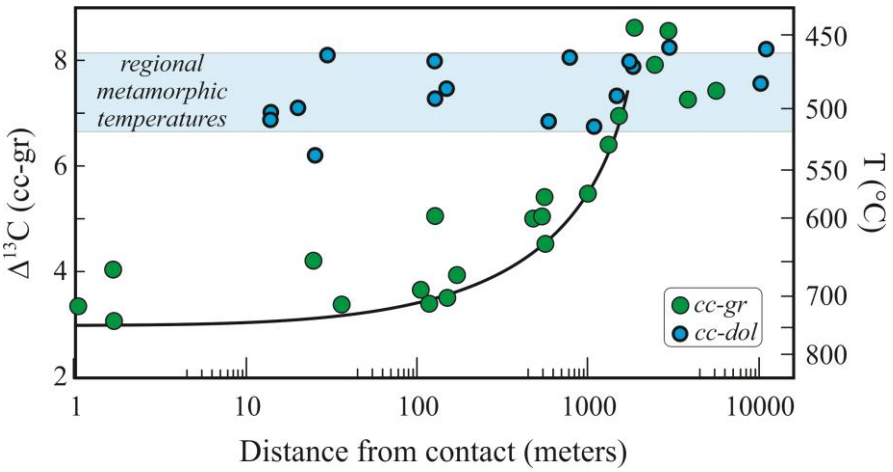

Fig. 12.14. Profile of calcite-graphite carbon isotope thermometry and calcite-dolomite solvus thermometry away from a gabbro-marble contact (Tudor Gabbro, Ontario Canada). The carbon isotope thermometer preserves high contact metamorphic temperatures (curve), while the calcite-dolomite solvus thermometer has been completely reset during later regional metamorphism (shaded area). After Dunn and Valley (1992).

for isotope analysis. Temperatures are sufficiently high during amphibolite-facies metamorphism that there is a strong likelihood that isotopic equilibrium was reached during metamorphism, but not so high that retrograde diffusional effects should be a serious factor. In very high temperature rocks, retrograde resetting is common, although there are examples of successful applications to very hot rocks (Fourcade and Javoy, 1973; Sharp et al., 1992; Farquhar et al., 1993).

An elegant application of geothermometry using refractory minerals was made by Dunn and Valley (1992) with calcite-graphite. Graphite stands out as one of the minerals most resistant to retrograde resetting. Once prograde recrystallization ceases, there is no change in the $\delta^{13}C$ value of graphite. Dunn and Valley compared temperature estimates from calcite-graphite fractionations ($\Delta^{13}C_{calcite\text{-}graphite}$) with those from calcite-dolomite solvus thermometry (not a stable isotope thermometer) in a contact aureole that was overprinted by a subsequent regional amphibolite grade metamorphic event (Fig. 12.14). The calcite-dolomite solvus thermometer gives uniform temperatures that correspond to the regional amphibolite-grade overprinting event. All memory of the earlier high temperature contact metamorphic event was erased in the subsequent regional event. The calcite-graphite isotope thermometer also records the amphibolite-facies event far from the gabbroic intrusion. But as the intrusion is approached, the calcite-graphite temperatures increase systematically, in accordance with the predicted thermal halo associated with the pre-metamorphic intrusion. In this instance, the calcite-graphite thermometer has preserved early high temperatures in spite of a later, protracted amphibolite-facies overprint.

12.7 Retrograde Exchange – Geospeedometry

Deformation, exsolution and recrystallization during late-stage fluid infiltration processes can completely reset the isotopic composition of a mineral. In the absence of these processes, however, the degree of retrograde exchange is controlled purely by

intracrystalline diffusion which can be treated quantitatively. Although retrograde diffusion-based resetting hinders our ability to obtain peak metamorphic temperatures, it can be used to extract cooling-rate information, the so-called stable isotope 'geospeedometer'.

The basic idea of determining cooling rates was first presented by Giletti (1986), and is illustrated in Fig. 12.15. A bimineralic assemblage *a-b* is heated to a peak temperature given by *T(p)*. Diffusion rates are rapid at *T(p)*, and the two minerals quickly reach isotopic equilibrium by the process of diffusional exchange[9]. The equilibrium fractionation at *T(p)* is $\Delta(p)$. Now, if the rock were rapidly cooled to room temperature (essentially quenched), then the peak temperature equilibrium fractionations $\Delta(p)$ would be preserved. The cooling rate was too fast for any retrograde reequilibration to take place. Now consider what happens if the rock is cooled very slowly. Starting at *T(p)*, the temperature is lowered by a small increment ΔT, and the new temperature ($T(p) - \Delta T$) is maintained for an extended period of time. The diffusion rates of oxygen in minerals *a* and *b* are rapid enough so that they will re-equilibrate at the new, lower temperature in a relatively short time. The rock is cooled again by a small increment ΔT and remains at the

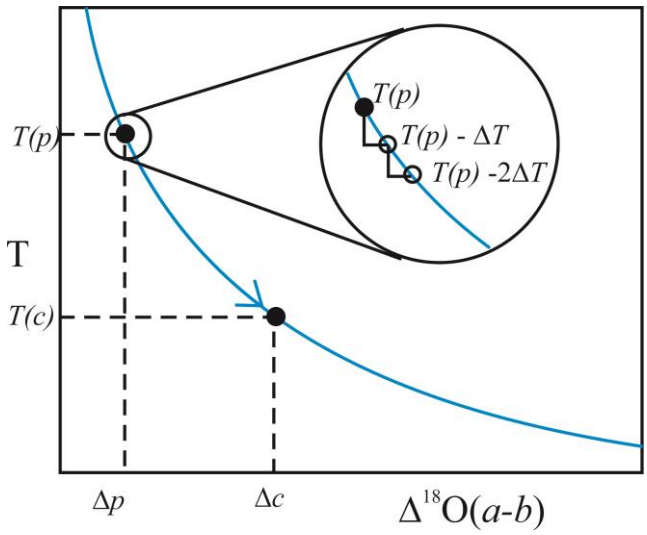

Fig. 12.15. Schematic plot of $\Delta^{18}O$ value for phases *a* and *b* vs temperature. Initial, peak temperatures are *T(p)*. If the sample is cooled rapidly (quenched) to room temperature, it will preserve fractionations Δp, corresponding to equilibrium at *T(p)*. If the sample is cooled slowly, it will continue to re-equilibrate during cooling, following the equilibrium fractionation vs. temperature path shown by the curved blue line. The sample cools by a small amount (*e.g.*, from *T(p)* to $T(p) - \Delta T$ etc) and re-equilibrates at the new temperature. The sample will continue to re-equilibrate at each new temperature until the closure temperature *T(c)* is reached, at which point intracrystalline diffusion effectively ceases. Further cooling will not modify the fractionation. The measured $\Delta^{18}O_{a\text{-}b}$ value is set by the closure temperature.

[9] Diffusional exchange in this case is limited by the **intractrystalline** diffusion rate, or self-diffusion rate. This is the diffusion rate of oxygen within a crystal. The **intercrystalline**, or grain boundary diffusion rate, which allows oxygen to migrate between phases, is considered to be orders of magnitude more rapid than the intracrystalline diffusion rate. Limited experimental studies support this assumptions (e.g., Farver and Yund, 1991a).

new temperature until isotopic equilibrium is again attained. It is clear that by cooling a rock slowly, the $\Delta(a\text{-}b)$ value will track along the equilibrium curve, shown by the arrow in Fig. 12.15. At some point, however, temperatures drop low enough so that the diffusion rates become too slow for any further exchange to occur. The temperature interval over which we move from a situation where there is complete exchange during cooling to one where there is effectively no exchange is narrow. This is because the diffusion rate exponentially increases with increasing temperature. The narrow temperature interval over which the assemblage goes from complete isotopic equilibrium (rapid diffusion rates), to one where the diffusion rate effectively stops, is defined as the **closure temperature** *T(c)* (Dodson, 1973). Further cooling does not change the $\delta^{18}O$ values of either phase. The fractionation that is measured in the laboratory is $\Delta(c)$, given by the closure temperature of the system. It is unrelated to the peak temperature *T*(*p*), but *is* related to the cooling rate. In both of the cooling scenarios considered above, the mineralogy and peak temperature and final temperature (room temperature) are the same. The only difference is in the rate of cooling, and the different measured fractionations are related only to differences in cooling rates. If we could quantify this effect, then we would have a *geospeedometer*, a tool to calculate how fast a rock cooled.

In a simple bimineralic assemblage, the *closure temperature* (*Tc*) is determined by the mineral with the *slower* diffusion rate. This may seem counterintuitive but is easily explained. During cooling, the *Tc* of the more refractory mineral is reached. Diffusion stops for that mineral, and its isotopic composition does not change with further cooling. The diffusion rate of oxygen in the second phase may still be rapid, but because there is nothing for it to exchange with, its isotopic composition is also fixed.

The closure temperature of a mineral is a function of the following parameters: 1) cooling rate; 2) grain size; 3) grain geometry; 3) diffusion rate; 4) modal abundance of the minerals. Dodson (1973) derived the following equation relating the cooling rate to closure temperature for a phase in an infinite reservoir:

$$T_c = \frac{Q/R}{\ln\left[\dfrac{ART_c^2\left(D_o/a^2\right)}{Q(\mathrm{d}T/\mathrm{d}t)}\right]} \qquad 12.13.$$

Tc is the closure temperature (in Kelvins), d*T*/d*t* is the cooling rate, *a* is the grain radius, *R* is the gas constant, *A* is a diffusional anisotropy parameter (55, 27, or 8.7 for volume diffusion from a sphere, cylinder or plane sheet respectively), *Q* is the activation energy for diffusion, and *Do* is the preexponential factor. *Q* and *Do* are related to diffusion rate by the Arrhenius relation

$$D = D_o \times e^{-\left(\frac{Q}{RT}\right)} \qquad 12.14.$$

Q and *Do* are normally determined experimentally. An extensive list of diffusion data is compiled in Cole and Chakraborty (2001).

Figure 12.16 illustrates the evolution of the oxygen isotope values for a bimineralic quartz-magnetite assemblage as it is slowly cooled. The top figure shows the $\delta^{18}O$ progression with equal oxygen proportion of quartz and magnetite from an initial temperature of 750°C. The solid lines represent the $\delta^{18}O$ values for a cooling rate of 10°C/M.Y. and a grain radius of 0.35 cm and the dashed line is for the same system cooled at 100°C/M.Y. The quartz closure temperatures for the rapidly and slowly cooled rocks are 588°C and 542°C, respectively calculated from equation 12.13 and the diffusion data in Table 12.1. Above 588°C, the cooling curves are identical. The only difference is the temperature at which diffusion effectively stops. The closure temperature for magnetite is significantly lower than for quartz, but once the closure temperature for quartz is reached, it cannot exchange further with the magnetite, and the $\delta^{18}O$ values of both minerals remain unchanged with further cooling. Cooling below the closure temperature will not change the minerals' $\delta^{18}O$ values, as illustrated by the flat lines below the closure temperature. The lower figure shows the same conditions except that now there is 90 atom % O in quartz and 10 atom % O in magnetite. In this case, the $\delta^{18}O$ values of magnetite changes considerably, while the $\delta^{18}O$ value of quartz is almost unchanged, a consequence of mass balance considerations. In both cases, the closure temperatures are the same.

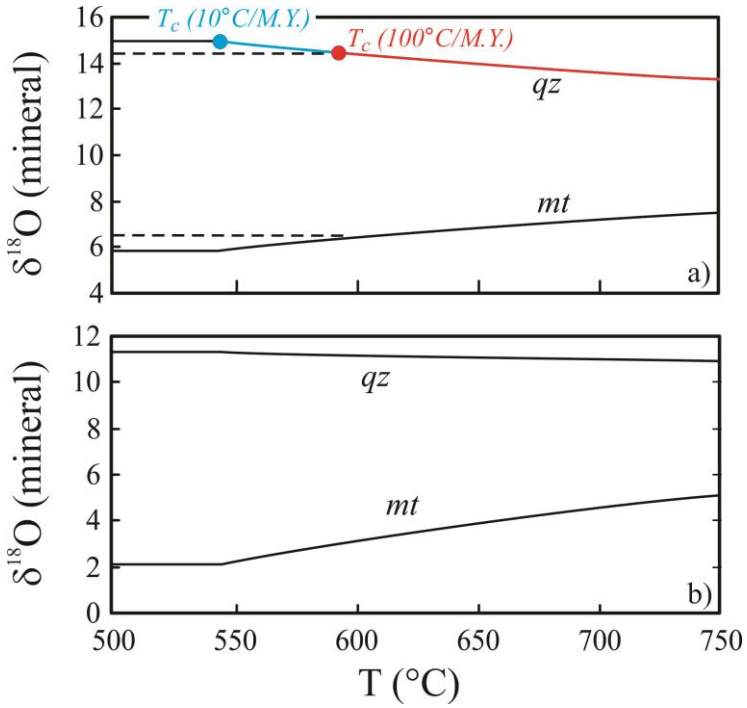

Fig. 12.16. Variations in $\delta^{18}O$ values of coexisting quartz and magnetite (initial $\delta^{18}O_{bulk\ rock}$ = 10.34‰, grain radius 3.5 mm) during slow cooling. Fig. 12.16a shows the progression of $\delta^{18}O$ values for equal atomic proportions of O in both phases. Solid line = cooling rate of 10°C/M.Y.; dashed line is for cooling rate of 100°C/M.Y. The closure temperature for quartz is 542°C (10°C/M.Y) and 588°C (100°C/M.Y.). The closure temperature for magnetite is lower. Lower figure is for cooling rate of 10°C/M.Y. with 90 % modal O_2 in quartz and only 10 % in magnetite. Closure temperatures are the same, but the change in the $\delta^{18}O$ values of each phase depend critically on modal abundance. Diffusion data from Table 12.1.

Things become more complicated (and more interesting) when a rock has multiple phases. Cooling rate curves for a 4 phase assemblage are plotted in Fig. 12.17 using modal proportions, grain size, and diffusion rate data given in Table 12.1. All phases maintain isotopic equilibrium until the closure temperature of hornblende is reached (*Tchnbd*). The $\delta^{18}O$ value of hornblende does not change with cooling below this temperature. All other phases continue to exchange until the closure temperature of quartz is reached (*Tcqz*). Its composition is then fixed, and magnetite and plagioclase continue to exchange until the closure temperature of magnetite is reached, after which no further isotope exchange occurs.

The significance of Figure 12.17 is that the measured $\delta^{18}O$ values bear no relationship to peak metamorphic temperatures. Instead they represent 'apparent temperatures' related to the effects of retrograde cooling. The cooling rate of a rock can be estimated by finding the best fit between the measured and calculated $\delta^{18}O$ values of each phase by varying the cooling rate estimates.

The simple equation of Dodson includes certain assumptions which are not strictly correct. It applies only to minerals hosted by an infinite reservoir, and was initially developed for argon diffusion related to thermochronology. For oxygen, it is only strictly valid for a single mineral 'bathed' in a sea of oxygen. More rigorous numeric solutions for diffusion considering modal abundance and a finite reservoir have been made (Eiler et al., 1992; Jenkin et al., 1994b). Although the calculations using these more exact solutions are complex, simple computer models have been developed making their application relatively straightforward (Eiler et al., 1995). For most common mineral assemblages, the solutions attained using equation 12.13 and the more exact solutions provide essentially the same answer.

The diffusion rate of oxygen in minerals appears to be strongly affected by the presence or absence of an aqueous fluid. There are clear indications of an aqueous fluid enhancing diffusion rates from both experimental and empirical methods (Elphick et al., 1988; Farver and Yund, 1991b; Sharp et al., 1991; Sharp and Moecher, 1994). Some authors have suggested that H_2O fugacity rather than actual presence of a fluid phase may control diffusion rate (Kohn, 1999), although such an interpretation requires that diffusion of oxygen in most metamorphic terranes would follow the 'wet' diffusion data, which is certainly not the case.

The above examples illustrate the advantage of using 'refractory' minerals for estimating peak temperatures of metamorphism. The diffusion rate of garnet, for example, is so slow, that it will not undergo any retrograde exchange for typical metamorphic conditions. In a bimineralic garnet-quartz rock, peak temperatures should be retained if the system cooled as a closed system. Once the garnet 'closes', the quartz has nothing to exchange with. The $1000 ln\alpha_{qz\text{-}garnet}$ value should reflect the temperature of garnet crystallization.

Additional information about the cooling history of a rock could be obtained if the zoning in a mineral could be determined. A number of studies have used microsampling or *in situ* laser techniques to measure the variations in the $\delta^{18}O$ values of a single mineral or vein (Chamberlain and Conrad, 1991; Conrad and Chamberlain, 1992; Kirschner et al., 1993; Kohn et al., 1993; Young and Rumble, 1993). Ion microprobe techniques have also been refined to the point where they can be applied to stable isotope studies (Valley and Graham, 1998).

Table 12.1. *Parameters for diffusion calculations for Figure 12.17. Coefficients a and b from equation 12.11 relative to quartz.*

Mineral	*Do* (cm^2/sec)	*Q* (kJ/mol)	Grain radius (mm)	anisotropy parameter *A*	*a*	*b*	fraction O_2
Quartz	190	284.0	2.5	8.7	0	0	0.25
Plagioclase	1.4 E-7	109.6	0.5	55	-1.39	0	0.25
Hornblende	1.0 E-7	171.5	0.5	8.7	-3.15	0.3	0.25
Magnetite	2.7E-5	202.5	0.5	55	-6.11	0	0.25

References

Baertschi, P. (1950) Isotopic composition of the oxygen in silicate rocks. *Nature* **166**, 112-113.

Baertschi, P. (1951) Relative abundances of oxygen and carbon isotopes in carbonate rocks. *Nature* **168**, 288-289.

Baertschi, P. and Silverman, S.R. (1951) The determination of relative abundances of the oxygen isotopes in silicate rocks. *Geochimica et Cosmochimica Acta* **1**, 4-6.

Barnett, D.E. and Bowman, J.R. (1995) Coupled mass transport and kinetically limited isotope exchange: Applications and exchange mechanisms. *Geology* **23**, 225-228.

Baumgartner, L.P. and Rumble, D. (1988) Transport of stable isotopes; 1, Development of a kinetic continuum theory for stable isotope transport. *Contributions to Mineralogy and Petrology* **98**, 417-430.

Bebout, G.E. and Barton, M.D. (1989) Fluid flow and metasomatism in a subduction zone hydrothermal system; Catalina schist terrane, California. *Geology* **17**, 976-980.

Bickle, M.J. and Baker, J. (1990) Advective-diffusive transport of isotopic fronts; an example from Naxos, Greece. *Earth and Planetary Science Letters* **97**, 78-93.

Blattner, P. and Lassey, K.R. (1989) Stable-isotope exchange fronts, Damköhler numbers, and fluid to rock ratios. *Chemical Geology* **78**, 381-392.

Bowman, J.R., O'Neil, J.R. and Essene, E.J. (1985) Contact skarn formation at Elkhorn, Montana. II: Origin and evolution of C-O-H skarn fluids. *American Journal of Science* **285**, 621-660.

Bowman, J.R. and Ghent, E.D. (1986) Oxygen and hydrogen isotope study of minerals from metapelitic rocks, staurolite to sillimanite zones, Mica Creek, British Columbia. *Journal of Metamorphic Geology* **4**, 131-141.

Bowman, J.R., Willett, S.D. and Cook, S.J. (1994) Oxygen isotopic transport and exchange during fluid flow: One-dimensional models and applications. *American Journal of Science* **294**, 1-55.

Burkhard, M. and Kerrich, R. (1990) Fluid-rock interactions during thrusting of the Glarus nappe- evidence from geochemical and stable isotope data. *Schweiz. Mineral. Petrogr. Mitt.* **70**, 77-82.

Cartwright, I. and Valley, J.W. (1990) Fluid-rock interaction in the North-west Adirondack Mountains, New York State, in: Ashworth, J.R., Brown, M. (Eds.), High temperature metamorphism and crustal anatexis. The Mineralogical Society Series, Birmingham, pp. 180-197.

Chamberlain, C.P. and Conrad, M.E. (1991) Oxygen isotope zoning in garnet. *Science* **254**, 403-406.

Clayton, R.N. and Epstein, S. (1958) The relationship between O^{18}/O^{16} ratios in coexisting quartz, carbonate, and iron oxides from various geological deposits. *Journal of Geology* **66**, 352-373.

Clayton, R.N. and Epstein, S. (1961) The use of oxygen isotopes in high-temperature geological thermometry. *Journal of Geology* **69**, 447-452.

Cole, D.R. and Charkraborty, S. (2001) Rates and mechanisms of isotopic exchange, in: Valley, J.W., Cole, D.R. (Eds.), Stable Isotope Geochemistry. Mineralogical Society of America, Washington, D.C., pp. 83-223.

Conrad, M.E. and Chamberlain, C.P. (1992) Laser-based, in situ measurements of fine-scale variations in the $\delta^{18}O$ values of hydrothermal quartz. *Geology* **20**, 812-816.

Cook, S.J., Bowman, J.R. and Forster, C.B. (1997) Contact metamorphism surrounding the Alta stock: finite element model simulation of heat- and $^{18}O^{16}O$ mass-transport during prograde metamorphism. *American Journal of Science* **297**, 1-55.

Crespo-Blanc, A., Masson, H., Sharp, Z.D., Cosca, M. and Hunziker, J. (1995) A stable and $^{40}Ar/^{39}$ Ar isotope study of a major thrust in the Helvetic nappes. *Geological Society of America Bulletin* **107**, 1129-1144.

Crowe, D.E. and Valley, J.W. (1992) Laser microprobe study of sulfur isotope variation in a sea-floor hydrothermal spire, Axial Seamount, Juan de Fuca Ridge, eastern Pacific. *Chemical Geology* **101**, 63-70.

Crowe, D.E. (1994) Preservation of original hydrothermal $\delta^{34}S$ values in greenschist and amphibolite volcanogenic massive sulfide deposits. *Geology* **22**, 873-876.

Deines, P. (1968) The carbon and oxygen isotopic composition of carbonates from a mica peridotite dike near Dixonville, Pennsylvania. *Geochimica et Cosmochimica Acta* **32**, 613-625.

Deines, P. and Gold, D.P. (1969) The change in carbon and oxygen isotopic composition during contact metamorphism of Trenton limestone by the Mount Royal pluton. *Geochimica et Cosmochimica Acta* **33**, 421-424.

Dipple, G.M. and Ferry, J.M. (1992) Fluid flow and stable isotopic alteration in rocks at elevated temperatures with applications to metamorphism. *Geochimica et Cosmochimica Acta* **56**, 3539-3550.

Dodson, M.H. (1973) Closure temperature in cooling geochronological and petrological systems. *Contributions to Mineralogy and Petrology* **40**, 259-274.

Dunn, S.R. and Valley, J.W. (1992) Calcite-graphite isotope thermometry; a test for polymetamorphsim in marble, Tudor gabbro aureole, Ontario, Canada. *Journal of Metamorphic Geology* **10**, 487-501.

Eiler, J.M., Baumgartner, L.P. and Valley, J.W. (1992) Intercrystalline stable isotope diffusion; a fast grain boundary model. *Contributions to Mineralogy and Petrology* **112**, 543-557.

Eiler, J.M., Baumgarntner, L.P. and Valley, J.W. (1995) Fast Grain Boundary: A Fortran-77 program for calculating the effects of retrograde interdiffusion of stable isotopes. *Computers and Geosciences* **20**, 1415-1434.

Elphick, S.C., Graham, C.M. and Dennis, P.F. (1988) An ion microprobe study of anhydrous oxygen diffusion in anorthite; a comparison with hydrothermal data and some geological implications. *Contributions to Mineralogy and Petrology* **100**, 490-495.

Farquhar, J., Chacko, T. and Frost, B.R. (1993) Strategies for high-temperature oxygen isotope thermometry; a worked example from the Laramie anorthosite complex, Wyoming, USA. *Earth and Planetary Science Letters* **117**, 407-422.

Farver, J.B. and Yund, R.A. (1991a) Measurement of oxygen grain boundary diffusion in natural, fine-grained, quartz aggregates. *Geochimica et Cosmochimica Acta* **55**, 1597-1607.

Farver, J.R. and Yund, R.A. (1991b) Oxygen diffusion in quartz: dependence on temperature and water fugacity. *Chemical Geology* **90**, 55-70.

Fourcade, S. and Javoy, M. (1973) Rapports $^{18}O/^{16}O$ dans les roches du vieux socle

catazonal d'In Ouzzal (Sahara algérien). *Contributions to Mineralogy and Petrology* **42**, 235-244.

Fourcade, S., Marquer, D. and Javoy, M. (1989) $^{18}O/^{16}O$ variations and fluid circulation in a deep shear zone: The case of the Alpine ultramylonites from the Aar massif (Central Alps, Switzerland). *Chemical Geology* **77**, 119-131.

Frey, M., Hunziker, J.C., O'Neil, J.R. and Schwander, H.W. (1976) Equilibrium-disequilibrium relations in the Monte Rosa Granite, Western Alps: Petrological, Rb-Sr and stable isotope data. *Contributions to Mineralogy and Petrology* **55**, 147-179.

Frezzotti, M.L., Dallai, L. and Sharp, Z.D. (2000) Fluid-inclusion and stable-isotope evidence for fluid infiltration and veining during metamorphism in marbles and metapelites. *European Journal of Mineralogy* **12**, 231-246.

Fricke, H.C., Wickham, S.M. and O'Neil, J.R. (1992) Oxygen and hydrogen isotope evidence for meteoric water infiltration during mylonitization and uplift in the Riby Mountains-East Humboldt Range core complex, Nevada. *Contributions to Mineralogy and Petrology* **111**, 203-221.

Ganor, J., Matthews, A. and Paldor, N. (1989) Constraints on effective diffusivity during oxygen isotope exchange at a marble-schist contact, Sifnos (Cyclades), Greece. *Earth and Planetary Science Letters* **94**, 208-216.

Garlick, G.D. and Epstein, S. (1967) Oxygen isotope ratios in coexisting minerals of regionally metamorphosed rocks. *Geochimica et Cosmochimica Acta* **31**, 181-214.

Ghent, E.D. and O'Neil, J.R. (1985) Late Precambrian marbles of unusual carbon-isootpe composition, southeastern British Columbia. *Canadian Journal of Earth Sciences* **22**, 324-329.

Giletti, B.J. (1986) Diffusion effects on oxygen isotope temperatures of slowly cooled igneous and metamorphic rocks. *Earth and Planetary Science Letters* **77**, 218-228.

Hoefs, J. and Touret, J. (1975) Fluid inclusion and carbon isotope study from Bamble granulites (South Norway); a preliminary investigation. *Contributions to Mineralogy and Petrology* **52**, 165-174.

Hoefs, J., Coolen, J.J.M.M.M. and Touret, J. (1981) The sulfur and carbon isotope composition of scapolite-rich granulites from southern Tanzania. *Contributions to Mineralogy and Petrology* **78**, 332-336.

Hoernes, S. and Hoffer, E. (1979) Equilibrium relations of prograde metamorphic mineral assemblages. A stable isotope study of rocks of the Damara Orogen, Namibia. *Contributions to Mineralogy and Petrology* **68**, 377-389.

Holness, M.B. and Graham, C.M. (1991) Equilibrium dihedral angles in the system H_2O-CO_2-NaCl-calcite, and implications for fluid flow during metamorphism. *Contributions to Mineralogy and Petrology* **108**, 368-383.

James, H.L. and Clayton, R.N. (1962) Oxygen isotope fractionation in metamorphosed iron formations of the Lake Superior region and in other iron-rich rocks, in: Engel, A.E.J., James, H.L., Leonard, B.F. (Eds.), Petrologic Studies, Buddington Volume. Geological Society of America, New York, pp. 217-233.

Jamtveit, B., Bucher, N.K. and Stijfhoorn-Derk, E. (1992) Contact metamorphism of layered shale-carbonate sequences in the Oslo Rift; I, Buffering, infiltration, and the mechanisms of mass transport. *Journal of Petrology* **33**, 377-422.

Javoy, M., Fourcade, S. and Allegre, C.J. (1970) Graphical method for examination of $^{18}O/^{16}O$ fractionations in silicate rocks. *Earth and Planetary Science Letters* **10**, 12-

16.

Jenkin, G.R.T., Fallick, A.E. and Leake, B.E. (1992) A stable isotope study of retrograde alteration in SW Connemara, Ireland. *Contributions to Mineralogy and Petrology* **110**, 269-288.

Jenkin, G.R.T., Craw, D. and Fallick, A.E. (1994a) Stable isotopic and fluid inclusion evidence for meteoric fluid penetration into an active mountain belt; Alpine Schist, New Zealand. *Journal of Metamorphic Geology* **12**, 429-444.

Jenkin, G.R.T., Farrow, C.M., Fallick, A.E. and Higgins, D. (1994b) Oxygen isotope exchange and closure temperatures in cooling rocks. *Journal of Metamorphic Geology* **12**, 221-235.

Kerrich, R. (1986) Fluid transport in lineaments. *Philosophical Transactions of the Royal Society of London, Series A* **317**, 219-251.

Kirschner, D.L., Sharp, Z.D. and Teyssier, C. (1993) Vein growth mechanisms and fluid sources revealed by oxygen isotope laser microprobe. *Geology* **21**, 85-88.

Kirschner, D.L., Sharp, Z.D. and Masson, H. (1995) Oxygen isotope thermometry of quartz-calcite veins: Unraveling the thermal-tectonic history of the subgreenschist facies Morcles nappe (Swiss Alps). *Geological Society of America Bulletin* **107**, 1145-1156.

Kohn, M.J., Valley, J.W., Elsenheimer, D. and Spicuzza, M.J. (1993) O isotope zoning in garnet and staurolite: Evidence for closed-system mineral growth during regional metamorphsim. *American Mineralogist* **78**, 988-1001.

Kohn, M.J. (1999) Why most "dry" rocks should cool "wet". *American Mineralogist* **84**, 570-580.

Kreulen, R. (1980) CO_2-rich fluids during regional metamorphism on Naxon (Greece): carbon isotopes and fluid inclusions. *American Journal of Science* **280**, 745-771.

Larson, T. and Sharp, Z.D. (2003) Stable isotope constraints on the Al_2SiO_5 'triple-point' rocks from the Proterozoic Priest pluton contact aureole, New Mexico. *Journal of Metamorphic Geology* **21**, 785-798.

Lichtner, P.C. (1985) Continuum model for simultaneous chemical reactions and mass transport in hydrothermal systems. *Geochimica et Cosmochimica Acta* **49**, 779-800.

McCaig, A.M., Wickham, S.M. and Taylor, H.P., Jr. (1990) Deep fluid circulation in Alpine shear zones, Pyrenees, France: field and oxygen isotope studies. *Contributions to Mineralogy and Petrology* **106**, 41-60.

Moecher, D.P., Valley, J.W. and Essene, E.J. (1994) Extraction and carbon isotope analysis of CO_2 from scapolite in deep crustal granulites and xenoliths. *Geochimica et Cosmochimica Acta* **58**, 959-967.

Monster, J., Appel, P.W.U., Thode, H.G., Schidlowski, M., Carmichael, C.M. and Bridgwater, D. (1979) Sulfur isotope studies in early Archaean sediments from Isua, West Greenland; implications for the antiquity of bacterial sulfate reduction. *Geochimica et Cosmochimica Acta.* **43**, 405-413.

Mora, C.I. and Valley, J.W. (1991) Prograde and retrograde fluid-rock interaction in calc-silicates northwest of the Idaho Batholith; stable isotopic evidence. *Contributions to Mineralogy and Petrology* **108**, 162-174.

Morrison, J. and Anderson, J.L. (1998) Footwall refrigeration along a detachment fault; implications for the thermal evolution of core complexes. *Science* **279**, 63-66.

Nabelek, P.I., Labotka, T.C., O'Neil, J.R. and Papike, J.J. (1984) Contrasting fluid/rock

interaction between the Notch Peak granitic intrusion and argillites and limestones in western Utah; evidence from stable isotopes and phase assemblages. *Contributions to Mineralogy and Petrology* **86**, 25-34.

Nabelek, P.I. (1991) Stable Isotope Monitors, in: Kerrick, D.M. (Ed.), Contact Metamorphism. Mineralogical Society of America, Chelsea, pp. 395-435.

Nabelek, P.I. and Labotka, T.C. (1993) Implications of geochemical fronts in the Notch Peak contact-metamorphic aureole, Utah, USA. *Earth and Planetary Science Letters* **119**, 539-559.

O'Neil, J.R. and Clayton, R.N. (1964) Oxygen isotope geothermometry, Isotopic and Cosmic chemistry. North Holland Publishing Co., Amsterdam, pp. 157-168.

Ohmoto, H. (1986) Stable isotope geochemistry of ore deposits, in: Valley, J.W., Taylor, H.P., Jr., O'Neil, J.R. (Eds.), Stable Isotopes in High Temperature Geological Processes. Mineralogical Society of America, Chelsea, pp. 491-559.

Oliver, N.H.S., Hoering, T.C., Johnson, T.W., Rumble III, D. and Shanks, W.C.I. (1992) Sulfur isotopic disequilibrium and fluid-rock interaction during metamorphism of sulfidic black shales from the Waterville-Augusta area, Maine, USA. *Geochimica et Cosmochimica Acta* **56**, 4257-4265.

Pineau, F., Javoy, M., Behar, F. and Touret, J. (1981) La geochimie isotopique du facies granulite du Bamble (Norvege) et l'origine des fluides carbones dans la croute profonde. *Bulletin de Mineralogie* **104**, 630-641.

Rumble, D.I. (1982) Stable isotope fractionation during metamorphic devolatilization reactions, in: Ferry, J.M. (Ed.), Characterization of Metamorphism Through Mineral Equilibria. Mineralogical Society of America, Chelsea, pp. 327-353.

Rumble, D.I. and Spear, F.S. (1983) Oxygen-isotope equilibration and permeability enhancement during regional metamorphism. *Journal of the Geological Society of London* **140**, 619-628.

Rye, R.O., Schuiling, R.D., Rye, D.M. and Jansen, J.B.H. (1976) Carbon, hydrogen, and oxygen isotope studies of the regional metamorphic complex at Naxos, Greece. *Geochimica et Cosmochimica Acta.* **40**, 1031-1049.

Schwarcz, H.P. and Clayton, R.N. (1965) Oxygen isotopic studies of amphibolites. *Canadian Journal of Earth Science* **2**, 72-84.

Sharp, Z.D. (1991) Determination of oxygen diffusion rates in magnetite from natural isotopic variations. *Geology* **19**, 653-656.

Sharp, Z.D., Giletti, B.J. and Yoder, H.S., Jr. (1991) Oxygen diffusion rates in quartz exchanged with CO_2. *Earth and Planetary Science Letters* **107**, 339-348.

Sharp, Z.D., Essene, E.J. and Smyth, J.R. (1992) Ultra-high temperatures from oxygen isotope thermometry of a coesite-sanidine grospydite. *Contributions to Mineralogy and Petrology* **112**, 358-370.

Sharp, Z.D., Essene, E.J. and Hunziker, J.C. (1993) Stable isotope geochemistry and phase equilibria of coesite-bearing whiteschists, Dora Maira Massif, Western Alps. *Contributions to Mineralogy and Petrology* **114**, 1-12.

Sharp, Z.D. and Moecher, D.P. (1994) O-isotope variations in a porphyroclastic meta-anorthosite; diffusion effects and false isotherms. *American Mineralogist* **79**, 951-959.

Sharp, Z.D. (1995) Oxygen isotope geochemistry of the Al_2SiO_5 polymorphs. *American Journal of Science* **295**, 1058-1076.

Sharp, Z.D. (1998) Application of stable isotope geochemistry to low grade metamorphic rocks, in: Frey, M., Robinson, D. (Eds.), Low-Grade Metamorphism. Blackwell Publishers, London, pp. 227-260.

Sharp, Z.D. and Barnes, J.D. (2004) Water-soluble chlorides in massive seafloor serpentinites: a source of chloride in subduction zones. *Earth and Planetary Science Letters* **226**, 243-254.

Sheppard, S.M.F. (1986) Characterization and isotopic variations in natural waters, in: Valley, J.W., Taylor, H.P.J., O'Neil, J.R. (Eds.), Stable Isotopes in High Temperature Geological Processes. Mineralogical Society of America, Chelsea, pp. 165-183.

Shieh, Y. and Schwarcz, H.P. (1977) An estimate of the oxygen isotope composition of a large segment of the Canadian Shield in northwestern Ontario. *Canadian Journal of Earth Science* **14**, 927-931.

Silverman, S.R. (1951) The isotope geology of oxygen. *Geochimica et Cosmochimica Acta* **2**, 26-42.

Spooner, E.T.C., Beckinsale, R.D., England, P.C. and Senior, A. (1977) Hydration, Oxygen 18 Enrichment and Oxidation During Ocean Floor Hydrothermal Metamorphism of Ophiolitic Metabasic Rocks from E. Liguria, Italy. *Geochimica et Cosmochimica Acta* **41**, 857-871.

Sturchio, N.C. and Muehlenbachs, K. (1985) Origin of low-^{18}O metamorphic rocks from a late Proterozoic shear zone in the Eastern Desert of Egypt. *Contributions to Mineralogy and Petrology* **91**, 188-195.

Taylor, B.E. (2004) Biogenic and thermogenic sulfate reduction in the Sullivan Pb–Zn–Ag deposit, British Columbia (Canada): Evidence from micro-isotopic analysis of carbonate and sulfide in bedded ores. *Chemical Geology* **204**, 215-236.

Taylor, H.P., Jr. and Epstein, S. (1962a) Relationship between O^{18}/O^{16} ratios in coexisting minerals of igneous and metamorphic rocks Part 1. Principles and experimental results. *Geological Society of America Bulletin* **73**, 461-480.

Taylor, H.P., Jr., Frechen, J. and Degens, E.T. (1967) Oxygen and carbon isotope studies of carbonatites from the Laacher See district, west Germany and the Alnö district, Sweden. *Geochimica et Cosmochimica Acta.* **31**, 407-430.

Taylor, H.P., Jr. (1979) Oxygen and hydrogen isotope relationships in hydrothermal mineral deposits, in: Barnes, H.L. (Ed.), Geochemistry of Hydrothermal Ore Deposits, 2 ed. J. Wiley and Sons, New York, pp. 236-277.

Taylor, J., H.P. and Epstein, S. (1962b) Relationship between O^{18}/O^{16} ratios in coexisting minerals of igneous and metamorphic rocks Part 2. Application to petrologic problems. *Geological Society of America Bulletin* **73**, 675-694.

Taylor, J., H.P., Albee, A.L. and Epstein, S. (1963) O^{18} /O^{16} ratios of coexisting minerals in three assemblages of kyanite-zone pelitic schist. *Journal of Geology* **71**, 513-522.

Valley, J.W. and O'Neil, J.R. (1982) Oxygen isotope evidence for shallow emplacement of Adirondack anorthosite. *Nature* **300**, 497-500.

Valley, J.W. (1986) Stable isotope geochemistry of metamorphic rocks, in: Valley, J.W., Taylor, H.P., Jr., O, N.J.R. (Eds.), Stable Isotopes in High Temperature Geological Processes. Mineralogical Society of America, Chelsea, pp. 445-490.

Valley, J.W. and Graham, C.M. (1998) Ion microprobe analysis of oxygen, carbon, and hydrogen isotope ratios, in: McKibben, M.A., Shanks, W.C.I., Ridlye, W.I. (Eds.), Applications of microananalytical techniques to understanding mineralizing

processes. Bookcrafters, Inc., Chelsea, pp. 73-98.

Valley, J.W. (2001) Stable isotope thermometry at high temperatures, in: Valley, J.W., Cole, D.R. (Eds.), Stable Isotope Geochemistry. Mineralogical Society of America, Washington, D.C., pp. 365-413.

Vennemann, T.W., Kesler, S.E. and O, N., J.R. (1992) Stable isotope compositions of quartz pebbles and their fluid inclusions as tracers of sediment provenance; implications for gold- and uranium-bearing quartz pebble conglomerates. *Geology* **20**, 837-840.

Vry, J.K., Brown, P.E., Valley, J.W. and Morrison, J. (1988) Constraints on granulite genesis from carbon isotopic compositions of cordierite and graphite. *Nature* **332**, 66-68.

Vyhnal, C.R. and Chamberlain, C.P. (1996) Preservation of early isotopic signatures during prograde metamorphism, eastern Vermont. *American Journal of Science* **296**, 394-419.

Wickham, S.M. and Taylor, H.P., Jr. (1985) Stable isotopic evidence for large-scale seawater infiltration in a regional metamorphic terrane; the Trois Seigneurs Massif, Pyrenees, France. *Contributions to Mineralogy and Petrology* **91**, 122-137.

Young, E.D. (1993) On the $^{18}O/^{16}O$ record of reaction progress in open and closed metamorphic systems. *Earth and Planetary Science Letters* **117**, 147-167.

Young, E.D. and Rumble, D., III (1993) The origin of correlated variations in in-situ $^{18}O/^{16}O$ and elemental concentrations in metamorphic garnet from southeastern Vermont, USA. *Geochimica et Cosmochimica Acta* **57**, 2585-2597.

Yui, T.-F., Rumble III, D. and Lo, C.-H. (1995) Unusually low $\delta^{18}O$ ultra-high-pressure metamorphic rocks from the Sulu Terrain, eastern China. *Geochimica et Cosmochimica Acta* **59**, 2859-2864.

Chapter 13

EXTRATERRESTRIAL MATERIALS

Contents

13.1 Introduction 1
13.2 Classification of meteorites 2
13.3 Oxygen isotopes in the solar system 3
13.3.1 Introduction 3
13.3.2 Discovery of an ^{17}O anomaly 4
13.3.3 Possible explanations: mixing of two distinct reservoirs 6
13.3.4 Mass-independent fractionation 7
13.3.5 Oxygen isotopes in meteorites – undifferentiated bodies 9
13.3.6. Oxygen isotopes in meteorites – differentiated bodies 10
13.4 Hydrogen 11
13.4.1 Introduction 11
13.4.2 Hydrogen in chondrites 13
13.4.3 Hydrogen in differentiated meteorites. 14
13.5 Carbon 17
13.6 Nitrogen 19
13.7 Sulfur 20
13.8 Chlorine 21
References 23

Chapter 13

EXTRATERRESTRIAL MATERIALS

13.1 Introduction

Some of the earliest problems addressed with stable isotope chemistry involved the origin and heterogeneities of the solar system. Hyperbolic orbits identified (erroneously) for certain meteorites suggested that there might be matter from outside the solar system that ultimately reached the Earth. Early attempts to find exotic carbon, oxygen and chlorine isotope ratios in meteorites failed (Harkins and Stone, 1926; Manian et al., 1934; Jenkins and King, 1936), in part because precision of the measurements was not sufficiently high at the time, and also because the anomalous material that does exist was simply not analyzed. Hydrogen isotope analyses followed in the 1950's, when δD values approaching 300‰ from the carbonaceous chondrites Ivuna and Orgueil were measured (Boato, 1954). Additional isotopic systems were studied in the coming decades, including sulfur (Trofimov, 1949), nitrogen (Injerd and Kaplan, 1974) and carbon (Krouse and Modzeleski, 1970). There was a flurry of interest in lunar materials when Apollo samples were returned to Earth. Most lunar samples had $\delta^{18}O$ values very similar to equivalent terrestrial rock types, indicating a close genetic relationship between Earth and Moon. Then in 1973, Clayton *et al*. (1973) published a paper that completely changed the meteorite community. For the first time, an 'exotic' stable isotope component in meteorites had clearly been identified. From then on, stable isotope geochemistry has become one of the most important tools for constraining mechanisms of formation and history of the early solar system.

There are no distinct boundaries between traditional earth sciences, cosmochemistry, space sciences and astrophysics, and so it is difficult to limit the scope of this chapter. For example, the isotope chemistry of interstellar grains (Anders and Zinner, 1993; Nittler, 2003) is important in the study of nucleosynthesis and stellar evolution. And, at the other end of the spectrum, the chemistry of certain meteorite types is used to estimate the bulk chemical composition of the Earth. This data are then applied to terrestrial studies completely unrelated to meteorite research. All of these fields overlap one other to a certain extent. In this chapter we will limit our examinations to more traditional meteorite research. Readers interested in processes of star formation and nucleosynthesis of elements and their isotopes are referred to Anders and Zinner (1993, in appendix) and Nittler (2003) for a review and additional references. It must be stressed that the 'normal' stable isotopes (H,C,N,O,S) are not used independently of other isotopic systems, such as noble gas, non-traditional isotopes (*e.g.*, Mg, Si), and short-lived radiogenic isotopes. But again, discussion of these systems is beyond the scope of this chapter. Further information beyond the short review here can be found in Clayton (1993) for oxygen isotopes and McKeegan and Leshin (2001) for H, C, N, O stable isotope systems.

13.2 Classification of meteorites

The alphabet soup of meteorite names can be very confusing to the uninitiated, but is really not complex after a simple review. Table 13.1 and Fig. 13.1 illustrate the basic classification of meteorites.

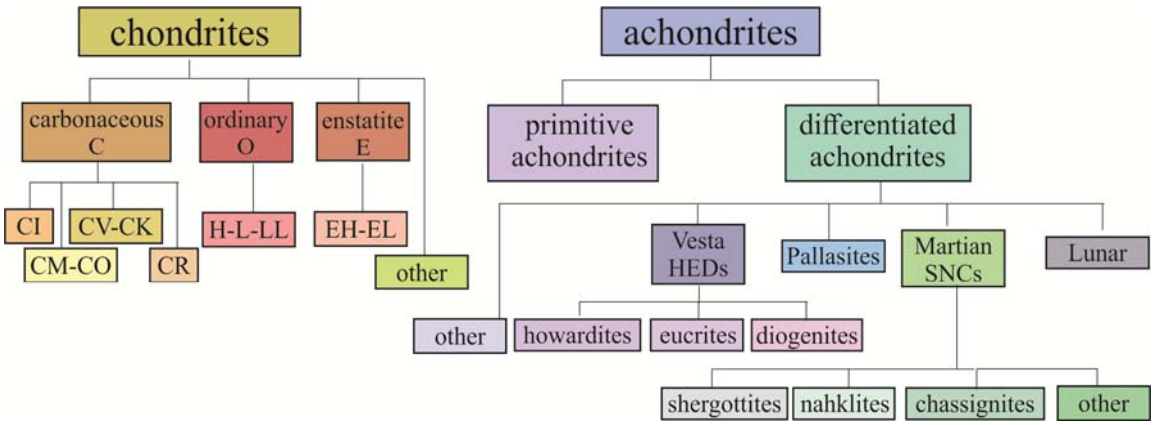

Fig. 13.1. Simplified meteorite classification. Meteorites are divided into chondrule-bearing chondrites and chondrule-free achondrites. The chondrites are further divided into carbonaceous, ordinary and enstatite chondrites. Achondrites include differentiated bodies including samples from the bodies 4-Vesta, Mars, and Moon.

The primary division of meteorites is between chondrites and achondrites. Chondrites contain chondrules[1] embedded in a fine-grained matrix. Chondrules are spherules of olivine and/or pyroxene with or without glass and metal inclusions thought to have formed by melting of nebular dust during flash heating. The fine-grained interstitial matrix consists of silicates, oxides, metal, sulfides and organic matter. The chondrites are considered to be agglomeration of rocky and icy material from unprocessed remnants of planetesimals from the asteroid belt. Chondrites also contain interstellar grains, calcium-aluminum inclusions (CAIs), and other refractory primitive objects. Achondrites are more processed material, often representing crustal magmatic or metamorphic rocks from dismembered planetesimals. Achondrites have undergone planetary differentiation, where early heating by radioactive decay of short lived isotopes caused segregation between an iron-rich core and silicate mantle. ***Iron meteorites*** are the fragments of the cores of asteroids/planetesimals. ***Stony iron meteorites***, such as pallasites, may be core-mantle boundary material, and ***stony meteorites*** are considered to be silicate mantle material of a segregated body. The origin of many achondrites can be attached to one of several large bodies, including Mars (the SNC meteorities), the Moon, and the asteroid 4 Vesta (HED[2] meteorites).

[1] CI chondrites have been so heavily aqueously altered on their parent body that no chondrules survive. Nevertheless, they come from a parent body that contained chondrules and did not go through differentiation.
[2] Howardites, Eucrites and Diogenites

Table 13.1. *Classification of different meteorite types (Brearley and Jones, 1998; Shearer et al., 1998).*

Name	**Mineralogy**	**Source**	
Iron meteorites	Iron-nickel metal; iron sulfide	Cores of disrupted asteroids	Groups distinguished by trace element abundances and textures
Stony-iron meteorites-pallasites mesosiderites	Roughly equal proportions of Fe,Ni-metal and silicate	Core-mantle boundary of disrupted asteroids?; impacts on asteroids	
Stony meteorites - achondrites			
Basaltic achondrites-howardites eucrites diogenites	Pigeonite-plagioclase-bearing basalts, orthopyroxenites, or mélange of each	Thought to be a basaltic magma system from asteroid 4 Vesta	Distinguished from other achondrite groups on the basis of oxygen isotopes
Other achondrites-aubrites, ureilites, angrites, etc.	Exotic basalts and related igneous rocks	Main belt differentiated asteroids	Each group distinguished on the basis of oxygen isotopes
Martian meteorites (SNC meteorites) – Shergottites, nakhlites chassignites, other	Magmatic basalts, lherzolites, clinopyroxenites, orthopyroxenite, dunite	Mars	Young (most <1.3Ga) *(ALH84001 is 4.5 Ga)*. Characteristic stable and rare gas isotope ratios
Lunar	Basalts, anorthosites, and lunar breccias	Moon	Compare closely with returned samples from the Apollo and Luna missions.
Stony meteorites – chondrites			
Agglomeratic rocks containing rocky and metallic materials. Unprocessed remnants of planetesimals from the asteroid belt. Some of the least processed material in the solar system. Consist of high-temperature chondrules hosted in a fine-grained matrix which represents low-T fraction of nebular material. Also contain interstellar grains, calcium-aluminum inclusions (CAIs), and other refractory objects. Groups are distinguished by chemistry and oxygen isotope ratios. Divided into types 1-6, where 3 is least altered, 2 and 1 are higher levels of low-T aqueous alteration and 4-6 are increasing levels of thermal metamorphism.			
Carbonaceous or C chondrites	8 groups – CI, CM, CR, CV, CO, CK, CH, CB; named after type fall-locality.		
Ordinary or O chondrites	3 groups – H, L and LL: H – high total Fe content; L – low total Fe content; LL – low metallic Fe		
Enstatite or E chondrites	2 groups – EH, EL: EH – high total iron; EL – low total iron		
Other classes	Rumuruti-like (R), Kakangari-like (K), Tagish Lake		
Other extraterrestrial material			
Interplanetary dust particles (IDPs)	Divided into chondritic and non-chondritic types	Active periodic comets from Oort cloud and Kuiper belt.	Primordial 'icy dust balls' (Rietmeijer, 1998). Average size is 10μm

13.3 Oxygen isotopes in the solar system

13.3.1 Introduction

The pioneers of fluorination included meteorites (or tektites) in their rock suites to fill out the general overview of natural oxygen isotope variations (Baertschi, 1950;

Silverman, 1951). Vinogradov *et al.* (1960) measured a suite of meteorites using the method of carbon reduction and found noticeable, but small $\delta^{18}O$ variations between different types. Similar conclusions were reached in a later thorough examination of different meteorite types (Reuter et al., 1965). Silicate separates from 27 chondrites varied by only 1.2‰. Chondrules had the same values as the whole rock. Pallasites were several per mil lower than the chondrites, but overall, it appeared that meteorites were not particularly interesting from a stable isotope viewpoint. In the same year, the same group (Taylor et al., 1965) found much larger variations in chondrites when they measured only pyroxene and not olivine[3]. Now the variations were larger; 9‰ for pyroxenes and 13‰ between different bulk rock samples. They developed a meteorite classification scheme of three groups with distinct $\delta^{18}O$ values.

The return of the Apollo lunar samples led to a flurry of activity by a number of stable isotope laboratories in the United States (e.g., Epstein and Taylor, 1970; Friedman et al., 1970; Onuma et al., 1970; Kaplan and Petrowski, 1971). It was quickly recognized that the $\delta^{18}O$ values of lunar basalts and anorthosites were the same as terrestrial equivalents[4]. These data demonstrated that the Earth and Moon were closely related, but said little about the genesis of the solar system.

13.3.2 Discovery of an ^{17}O anomaly

The importance of oxygen isotope geochemistry as it pertained to meteorites was recognized when Clayton *et al*. (1973) made one of the most striking discoveries in the field of planetary science. They analyzed anhydrous high temperature phases (calcium aluminum inclusions, or CAIs) from carbonaceous chondrites, mostly Allende (which had only fallen to Earth on Feb. 8, 1969, in Chihuahua, Mexico[5]). The range of $\delta^{18}O$ values was extraordinary, covering over 30‰. This in itself was far more than anyone had measured previously. But as a result of their extremely careful analytical procedure, Clayton's group found something else that was far more surprising – namely that the $\delta^{17}O$ values of these primitive samples varied in a non-mass dependent way. This discovery was made not by measuring the $\delta^{17}O$ values directly, but rather by noting that the 'apparent' $\delta^{13}C$ values of the CO_2 gas that they were analyzing was not constant. The reason and significance is worth the short explanation in the following paragraphs.

The Chicago group analyzed silicates by reacting them with BrF_5 at high temperatures[6]. The evolved oxygen was converted to CO_2 by reaction with spectroscopic graphite at high temperatures and the CO_2 was analyzed for its $\delta^{18}O$ value. This was standard procedure in most laboratories at the time. What was unusual in the Allende samples was that there was a systematic variation in the apparent $\delta^{13}C$ value of the CO_2 gas that correlated with the measured $\delta^{18}O$ value. This was puzzling because the two isotopic systems carbon and oxygen are independent of each other. The carbon comes from the graphite rod and should have a constant value, whereas the oxygen is derived

[3] Olivine is a notoriously difficult mineral to fluorinate using conventional methods. See 11.2.1 for more details.

[4] Later analyses confirmed that $\delta^{17}O$ values were also identical to terrestrial ones (Clayton and Mayeda, 1975).

[5] The other important CC meteorite that was analyzed was Murchison, which fell in Australia only a few months later.

[6] A typical reaction would be $2\ MgSiO_3 + 12/5\ BrF_5 \rightarrow 2\ MgF_2 + 2\ SiF_4 + 6/5\ Br_2 + 3O_2$.

from the fluorinated silicate. The three isotopologues of CO_2 have masses of 44 ($^{12}C^{16}O_2$), 45 ($^{13}C^{16}O_2$ *and* $^{12}C^{16}O^{17}O$) and 46 ($^{12}O^{16}O^{18}O$) [7]. In almost all known chemical fractionation mechanisms, the following relationship is valid

$$\left(\frac{^{17}O}{^{16}O}\right) \approx \left(\frac{^{18}O}{^{16}O}\right)^{0.52} \qquad 13.1,$$

which translates to $\delta^{17}O \approx 0.52(\delta^{18}O)$. (See section 3.7 for details about the three isotope system). Normally, there is no reason to measure the $\delta^{17}O$ value of a sample, because it varies with $\delta^{18}O$ according to equation 13.1. By subtracting out the ^{17}O contribution to the mass 45 isotopologue of CO_2 – the so-called ^{17}O correction – we can calculate the $\delta^{13}C$ value of CO_2 gas from the 45/44 ratio. Clayton *et al*. noticed that the calculated $\delta^{13}C$ values were changing in concert with the $\delta^{18}O$ values. What they were actually measuring, and quickly realized, was that the variations in the 45/44 ratio were $^{17}O/^{16}O$ ratios that did not conform to equation 13.1. When plotting $\delta^{17}O$ vs $\delta^{18}O$ (assuming that the $^{13}C/^{12}C$ ratio was constant), the chondrite data did not plot on the normal *Terrestrial Fractionation Line* (TFL) with slope of ~0.52 as is seen for almost all materials in the

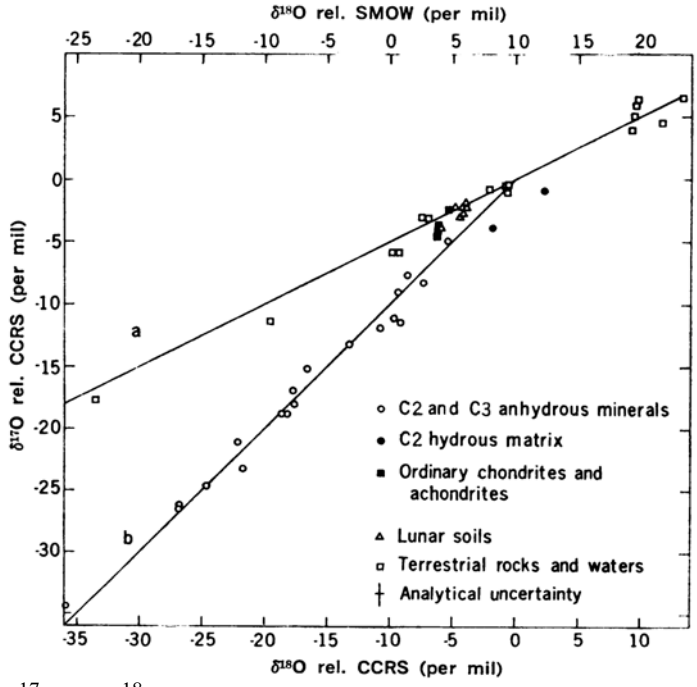

Fig 13.2. Plot of $\delta^{17}O$ vs $\delta^{18}O$ values for anhydrous (high T) chondritic samples (open circles), aqueously altered chondritic samples (filled circles) and terrestrial material. The chondrite data plot with a slope 1, whereas the terrestrial samples plot on the terrestrial fractionation line (TFL) (slope ~1/2). All data are plotted relative to a carbonaceous chondrite reference standard (CCRS) defined as the intersection of the slope 1 line from chondrite data with the TFL. Plotted in this way, the chondrite data are explained in terms of mixing between two components; a nebular gas near CCRS and a very ^{16}O enriched source, possibly from outside the solar system. Reprinted from Clayton *et al.* (1973) with permission. Note that by defining their data in terms of the carbonaceous chondrite reference standard (CCRS), the mixing line b in figure 13.1 meets the criterion $\delta^{17}O = \delta^{18}O$.

Box 13.1 The three isotope plot for oxygen.
All chemical fractionation processes (except for certain photochemical effects) fractionate the three isotopes of oxygen according to equation 13.1. On the three isotope plot $\delta^{17}O$ vs. $\delta^{18}O$, this leads to all data defining a $\delta^{17}O/\delta^{18}O$ slope of ~0.525 (mass fractionation line – *mfl*). All terrestrial samples plot on a *mfl* which approximately intersects $\delta^{17}O = \delta^{18}O = 0‰$ (vs. SMOW) and is called the *Terrestrial Fractionation Line (TFL)*. Any object that undergoes mass dependent fractionation will spread out on a *mfl* line, illustrated by the dashed line with slope 0.52 emanating from point *a*. Mixing between two reservoirs with distinct $\delta^{17}O$-$\delta^{18}O$ values will result in samples plotting on a straight line, whose slope is defined by the compositions of the two endmembers. The mixing line of slope 1 could be explained by mixing between an average nebular composition given by CCRS in Fig. 13.1 and a second component rich in ^{16}O. How far a sample plots off the *TFL* line is defined in terms of $\Delta^{17}O$ by the equation $\Delta^{17}O = \delta^{17}O - (0.52x)\cdot\delta^{18}O$. The inset box shows the $\delta^{17}O$-$\delta^{18}O$ values of samples from Mars. They plot on a *mfl* with a $\Delta^{17}O$ value of +0.3‰.

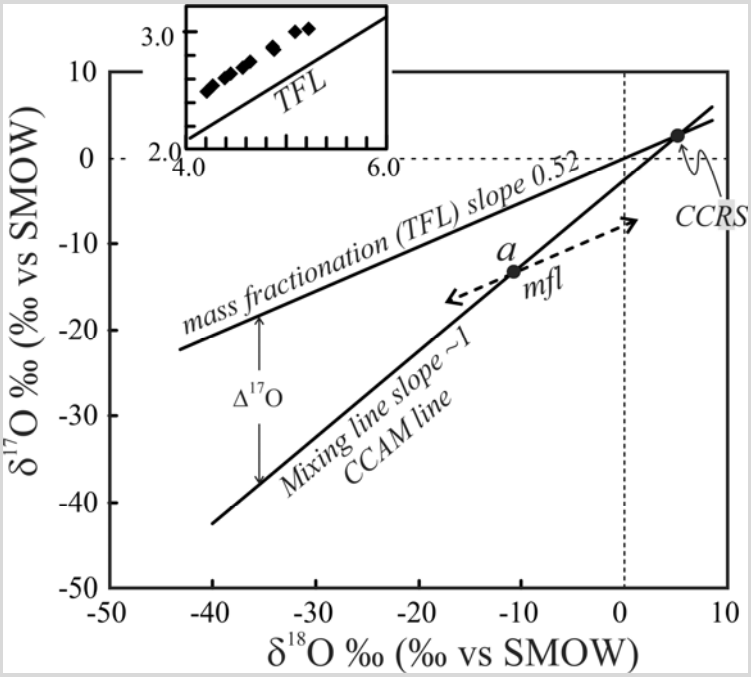

Fig. B.13.1.

Earth and Moon, but rather on a slope 1 line, below the TFL line (Fig. 13.2). (See Box 13.1 for discussion of $\delta^{18}O$ vs $\delta^{17}O$ plots).

13.3.3 Possible explanations: mixing of two distinct reservoirs

Clayton *et al.* interpreted their data as evidence for mixing between two distinct reservoirs: the first was the heavy nebular (solar) reservoir and the second was a primitive, pre-solar ^{16}O-rich dust source that originated outside of the solar system.

Clayton *et al*. postulated that the ^{16}O-rich component was probably extremely impoverished in ^{17}O and ^{18}O, as might be expected from oxygen formed from a young helium burning star, where only ^{16}O is produced. Clayton (1993) assigned $\delta^{17}O$ and $\delta^{18}O$ values to the solar nebula of 24.2 and 30‰, respectively while the light exotic dust component had $\delta^{17}O$ and $\delta^{18}O$ values of a composition with $\delta^{18}O$ = ~-42‰, and ~-40‰. A linear trend is seen in the triple oxygen isotope data of CAIs with a slope of 0.96, resulting from simple mixing between the ^{16}O-rich and nebular components.

The original 'mixing of two reservoirs' explanation for the oxygen isotope trends in early-formed material has some inconsistencies, which alternative models have sought to explain. Some of the concerns are the following:

- If the ^{16}O-rich component formed by stellar nucleosynthesis of helium burning, then the $\delta^{18}O$-$\delta^{17}O$ values should correlate with other isotope systems, such as Mg and Si. However, no such correlations are found.
- The presolar component should be nearly pure ^{16}O. However all measurements of CAI inclusions have $\delta^{18}O$-$\delta^{17}O$ values that 'bottom-out' around -50 to -40‰ (McKeegan and Leshin, 2001). Only presolar grains have lower values (Nittler et al., 1997; Amari, 2014), but the estimated abundance of such grains is less than 0.25 parts per billion. If the exotic ^{16}O rich source was not pure ^{16}O, then why is the $^{18}O/^{17}O$ ratio the same as the solar nebular value (thereby giving the slope 1 line)?
- If an ^{16}O-rich melt exchanged with the solar nebular gas during crystallization, the degree of ^{17}O and ^{18}O enrichment should correlate with the order of crystallization, which is not the case. Melilite has the highest $\delta^{18}O$-$\delta^{17}O$ values, but should crystallize before pyroxene (Stolper, 1982). Alternatively, exchange with the heavy nebular gas occurred by diffusion. Appropriate diffusion data are not sufficient to properly evaluate this possibility.

13.3.4 Mass-independent fractionation

An alternative to the two reservoir mixing hypothesis was born when Thiemens and Heidenreich (1983) discovered that ozone (O_3) produced by dissociation of molecular oxygen (O_2) in a high frequency discharge occurred with a mass-independent fractionation. The $\delta^{18}O$-$\delta^{17}O$ values of the residual oxygen and newly-formed ozone plot on a slope 1 line (Fig. 13.3), nearly identical to the slope for carbonaceous chondrite mineral inclusions found by Clayton *et al* (1973).

Thiemens and Heidenreich initially suggested a mechanism of optical self-shielding to explain the mass-independent fractionation. O_2 gas undergoes strong absorption of ultraviolet light by the Schumann-Runge absorption bands between 1.76×10^{-7}m and 1.926×10^{-7} m, causing photodissociation of O_2. The absorption bands are slightly different for ^{16}O-^{16}O and the other isotopologues ^{17}O-^{16}O and ^{18}O-^{16}O. Because >99.5% of O_2 consists of $^{16}O_2$, radiation corresponding to $^{16}O_2$ will strongly be absorbed (or self-shielded), so that only the wavelengths absorbed by ^{17}O-^{16}O and ^{18}O-^{16}O will filter through to the center of the reaction chamber. These UV rays will then cause mass-independent dissociation of the rare isotopologues ^{17}O-^{16}O and ^{18}O-^{16}O. The dissociated ^{17}O and ^{18}O ultimately react with $^{16}O_2$ to form ozone. Figure 13.3 shows the ozone

enriched in the heavy isotopes and the residual O_2 with preferential removal of ^{18}O and ^{17}O.

More recently, it has been shown that it is the role of symmetry that is the primary cause of the non-mass dependent fractionation (e.g., Michalski and Bhattacharya, 2009). The O_2 starting material is photo-dissociated by UV radiation. The O radicals react with surrounding O_2 to O_3 via a metastable transition state. The stability of the transition state is function of the symmetry. Highly symmetric transition state $^{16}O_3$ is less stable than ^{16}O-1^6O-^{17}O and ^{16}O-^{16}O-^{18}O, both of which have a lower symmetry. As a consequence, stable O_3 is enriched in both of the rare isotopes without distinction between ^{17}O and ^{18}O. The data therefore define a MIF line with a slope of 1. Such ^{17}O and ^{18}O enriched O_3 is observed in the stratosphere (Thiemens, 2006). The positive anomaly of stratospheric O_3 is counterbalanced by a marked negative anomaly of tropospheric O_2 (Luz et al., 1999).

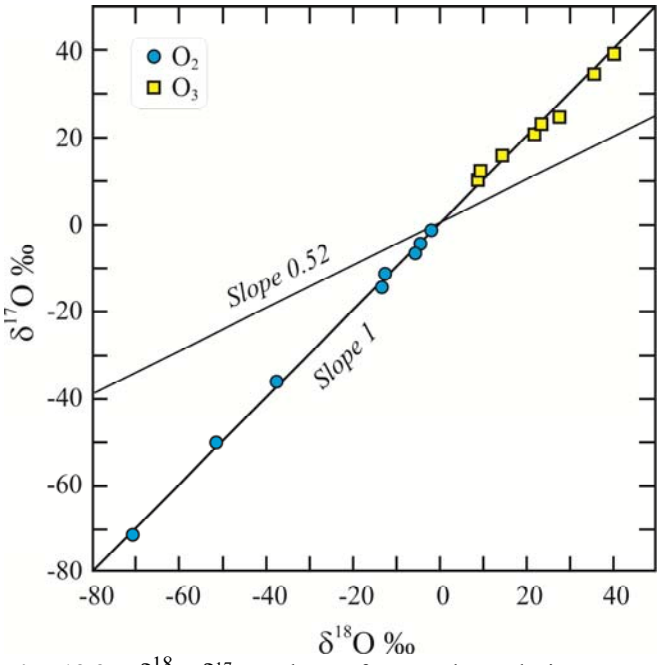

Fig. 13.3. $\delta^{18}O$-$\delta^{17}O$ values of O_2 and O_3 during ozone formation by high-frequency discharge. The product ozone is enriched in both ^{17}O and ^{18}O by a mass-independent mechanism, which was believed to be due to self-shielding (Thiemens and Heidenreich, 1983).

Mass independent isotope fractionation has been predicted to occur in interstellar clouds by the process of self-shielding. Some interstellar clouds appear to be enriched in ^{13}CO by a factor of 2.3 compared to the Sun. Langer (1977) suggested that the enrichment is the result of self-shielding in the interstellar clouds. Bally and Langer (1982) showed that the CO gas of interstellar clouds is enriched in ^{16}O as well.

The idea behind the self-shielding hypothesis is the following: CO is dissociated by distinct frequencies of UV radiation. The molecular cloud would be more opaque to the frequencies absorbed by $C^{16}O$ rather than $C^{17}O$ and $C^{18}O$ due to the former's much higher concentration. Radiation that is only absorbed by the rare isotopologues is able to penetrate far more deeply into the molecular cloud. As a result, only the rare isotopes $C^{17}O$ and $C^{18}O$ are dissociated in the cloud's interior. The oxygen produced by this dissociation then combines with hydrogen to produce ^{17}O- and ^{18}O-enriched water ice, which ultimately becomes incorporated in solid phases (Yurimoto and Kuramoto, 2004). Chakraborty *et al.* (2008) suggested that self-shielding was not necessary, arguing that the ^{17}O and ^{18}O enrichment in CO could be due to a stronger coupling coefficient, in which $C^{17}O$ and $C^{18}O$ are more efficiently dissociated than $C^{16}O$. This idea has been questioned (Lyons et al., 2009), but regardless of the actual mechanism, preferential photodissociation of $C^{17}O$ and $C^{18}O$ in the molecular cloud can lead to ^{17}O- and ^{18}O-

enriched H_2O. The H_2O is ultimately incorporated in chondrites which will lead to a heavy oxygen component relative to the overall nebular value.

With the new model, we would expect the solar nebula and Sun to have $\delta^{18}O$-$\delta^{17}O$ values of ~-50‰, in contrast to the Clayton mixing model where the solar component is the heaviest (> +20‰). Evidence for a low $\delta^{18}O$-$\delta^{17}O$ solar wind was found by Hashizume and Chaussidon (2005), who measured the $\delta^{18}O$ and $\delta^{17}O$ values of solar energetic particles that had been implanted in metal grains on the lunar regolith. The measured $\Delta^{17}O$ value of the solar particles was -33±16‰, corresponding to a protosolar nebula of ~-67‰ for $\delta^{18}O$ and $\delta^{17}O$ (when appropriate fractionations are considered). More recently, direct analysis of solar wind implanted on SiC targets during the NASA Genesis mission were made (McKeegan et al., 2011). The calculated value for the Sun is $\delta^{17}O$ = -59.1‰ and $\delta^{18}O$ = -58.5‰ (vs SMOW). The $\delta^{17}O$-$\delta^{18}O$ slope 1 data for the CCAM samples is then explained by simple mixing with the light nebular reservoir (Sun) and a molecular cloud enriched in ^{18}O and ^{17}O due to photochemical reactions. Young and Russell (1998) suggested that the mixing between these two reservoirs has a slope of exactly 1.0, and that the shallower slope of 0.996 suggested by Clayton's early work is explained by aqueous alteration of some meteoric material.

13.3.5 Oxygen isotopes in meteorites – undifferentiated bodies

The bulk isotopic compositions of meteorite parent bodies generally fall on a mixing line between the isotopically light solar component and heavy 'ice-derived' component. Further modification due to volatile loss to space and low temperature reequilibration/alteration expands the isotopic range to higher $\delta^{18}O$ and $\delta^{17}O$ values with a slope less than 1. Each meteorite group occupies a distinct isotopic range (Fig. 13.4), although there is some overlap between groups. Indeed, one of the most diagnostic tools used for categorizing meteorites is the triple oxygen isotope composition.

The overall oxygen isotope compositions of different extraterrestrial materials are explained in the following way. The earliest-formed anhydrous phases plot with low $\delta^{17}O$-$\delta^{18}O$ values that are equilibrated with the unmodified nebula (Krot et al., 2002). Later-formed silicate minerals follow a mixing line with a slope close to or equal to 1 (the CCAM line) to higher delta values due to mixing with the isotopically heavy H_2O-derived component. Alteration occurring on a parent body with an aqueous fluid causes the isotope composition of that body to spread out along a mass dependent fractionation line, and loss of light water from a small body will draw the combined $\delta^{17}O$-$\delta^{18}O$ values upward (Young et al., 1999). Under equilibrium conditions, the slope defined by a set of samples from a single body will be ~0.52, characteristic of mass-dependent fractionation. The highest $\delta^{17}O$ and $\delta^{18}O$ values are found in highly altered CM and CI chondrites. These hydrous, highly oxidized samples have experienced high fluid/rock ratios and their oxygen isotope compositions reflect the heavy aqueous component. Chondrite classes that plot with distinct slopes between 0.52 and 1, such as the CR chondrites, are thought to represent partial mixing between material plotting along the CCAM line and unrelated altered material. Alteration with an aqueous fluid will tend to cause the isotope data to spread out on a mass dependent fractionation line, and loss of light water to space will draw the combined $\delta^{17}O$-$\delta^{18}O$ values towards higher values (Young et al., 1999).

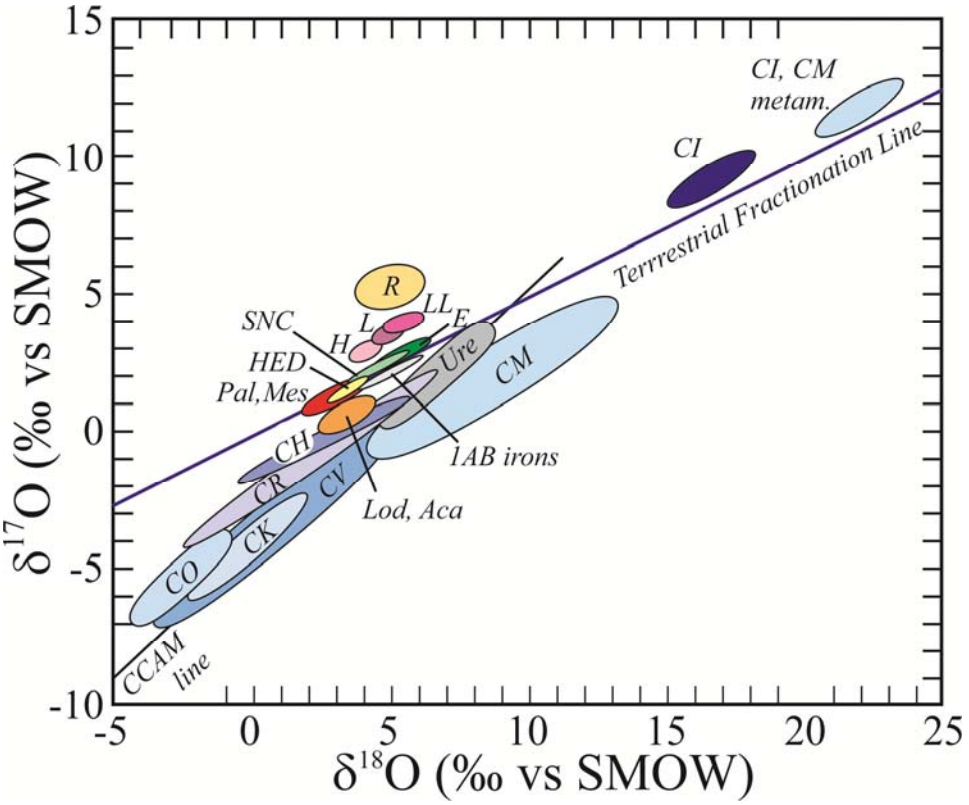

Fig. 13.4. Oxygen isotope fields for different meteorite types. Apollo (lunar) samples plot essentially on the Terrestrial Fractionation Line. Most Martian meteorites have $\delta^{18}O$ values between 3.5 and 5.5 with a $\Delta^{17}O = 0.32$ (Franchi et al., 1999). A Martian basaltic breccia has higher $\delta^{18}O$ values (5.6-7.5) and a distinctly high $\Delta^{17}O$ value of 0.58±0.01 (Agee et al., 2013). The Moon is virtually indistinguishable from Earth. Abbreviations: Ure – urelites; Pal, Mes – pallasites, mesosiderites; HED – howardites, eucrites, diogenites; SNC – shergottites, nakhlites, chassignites (most Martian meteorites), Lod, Aca – lodranites, acapulcoites; E – enstatite chondrites; C – carbonaceous chondrites; H, L, LL – ordinary chondrites; R – R chondrites. Compiled from various sources.

13.3.6. Oxygen isotopes in meteorites – differentiated bodies

Samples from a well-mixed, differentiated body should plot on a mass dependent fractionation line passing through the bulk $\delta^{17}O$-$\delta^{18}O$ value of that body, and indeed this is the case. Most samples from differentiated bodies, including the Moon, Mars, HEDs (4 Vesta), angrites, aubrites, mesosiderites, and pallasites, all fall on $\delta^{17}O$-$\delta^{18}O$ arrays with a slope of ~0.525, parallel to that of the Earth (Fig. 13.5). The $\delta^{17}O$-$\delta^{18}O$ array for the Earth and Moon are virtually indistinguishable. It is generally accepted that the Earth-Moon system formed during the collision of a Mars-sized body (informally called Theia) with the proto Earth approximately 60-100 Ma after the formation of our solar system (the collapse of the proto solar nebula). The remarkably similar $\Delta^{17}O$ values for lunar and terrestrial samples suggests that the two bodies either had identical initial $\Delta^{17}O$ values or that the two bodies were well mixed during the Giant Impact responsible for the Earth-Moon system.

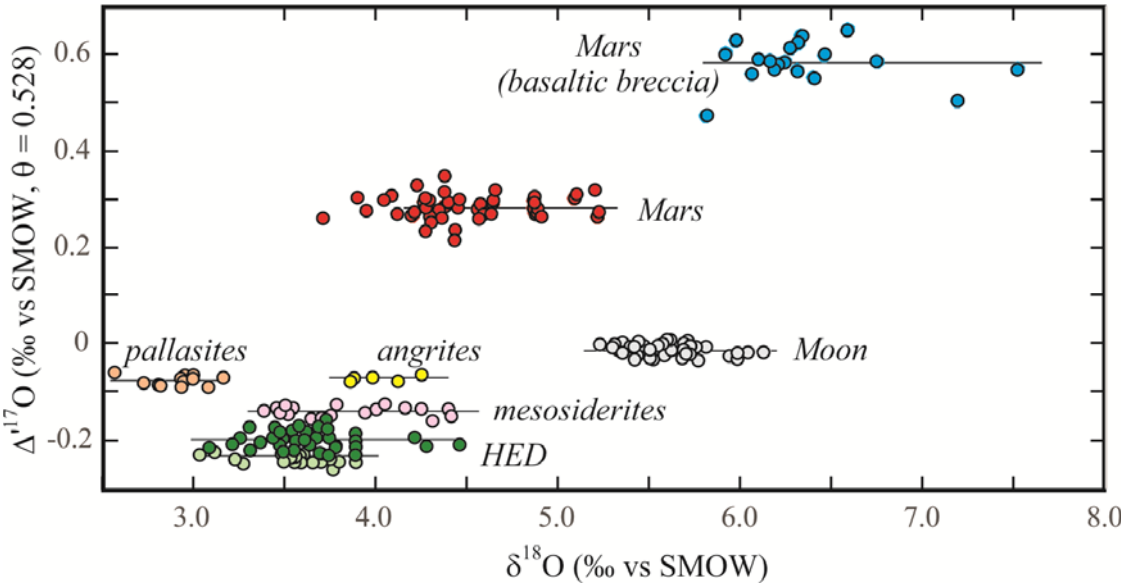

Fig. 13.5 Triple oxygen isotope composition of differentiated meteorites. The $\Delta'^{17}O$ values are defined as $\Delta'^{17}O = \delta'^{17}O - 0.528 \times \delta'^{18}O$, where the ' refers to the linearized delta value (see Text box 3.1). The data for each group of differentiated meteorites defines a linear array consistent with isotopic equilibrium for the three isotope system. Two HED data sets are plotted: (Wiechert et al., 2004, dark green) and (Greenwood et al., 2005, pale green). Both show flat trends. The difference in the two data sets is probably due to slightly different calibration standards. Data from the following sources: (Franchi et al., 1999; Wiechert et al., 2001; Wiechert et al., 2004; Greenwood et al., 2005; Greenwood et al., 2006; Spicuzza et al., 2007; Rumble III and Irving, 2009; Greenwood et al., 2012; Agee et al., 2013; Herwartz et al., 2014; Young et al., 2016).

13.4 Hydrogen

13.4.1 Introduction

The D/H ratios of materials in our Galaxy span such an enormous range as to strain the utility of the delta notation. Solar wind is virtually deuterium-free, with δD values approaching -1000‰. At the other end of the spectrum, cold molecular clouds have spectroscopically-measured D/H ratios as high as 10^{-1}, corresponding to >600,000‰ (see Robert et al., 2000 for a review of galactic values). Hydrogen isotope systematics differ significantly from those of oxygen, and the information available from D/H ratios is quite different as well. Hydrogen has only two stable isotopes, in place of oxygen's three, so that mixing of distinct sources can only be tracked in 'one dimension' instead of two. Hydrogen, while far and away the most abundant phase in molecular clouds and our solar system, is rare in solids preserved in meteorites. And finally, the isotopes of hydrogen have a very different formation history than oxygen. Oxygen is produced during star-forming events, with each isotope identified with specific nucleosynthetic processes. Deuterium, in contrast, was formed in the Big Bang (Burbidge et al., 1957). There is no additional stellar input to the primordial mix. For oxygen, the solar isotope abundances define the starting point for the composition and evolution of the solar system. For the hydrogen-deuterium system, the Sun is of no help in giving us average

solar system values, as all deuterium was 'burned' during contraction of our proto-Sun[8].

The D/H ratios of various materials are shown in Fig. 13.6. The D/H ratio following the Big Bang is estimated as 67-90×10^{-6} or -520 to -420‰ (Copi et al., 1995). Deuterium is destroyed during star burning, so that the average D/H ratio of the Universe has decreased with time. Spectroscopic analysis of local interstellar medium gives a D/H ratio of (14-17)×10^{-6}. The presolar D/H ratio is estimated at ~ (20±3.5)×10^{-6} using the ^{3}He/H ratio of the solar wind. Jupiter can also be used as a proxy for the presolar D/H

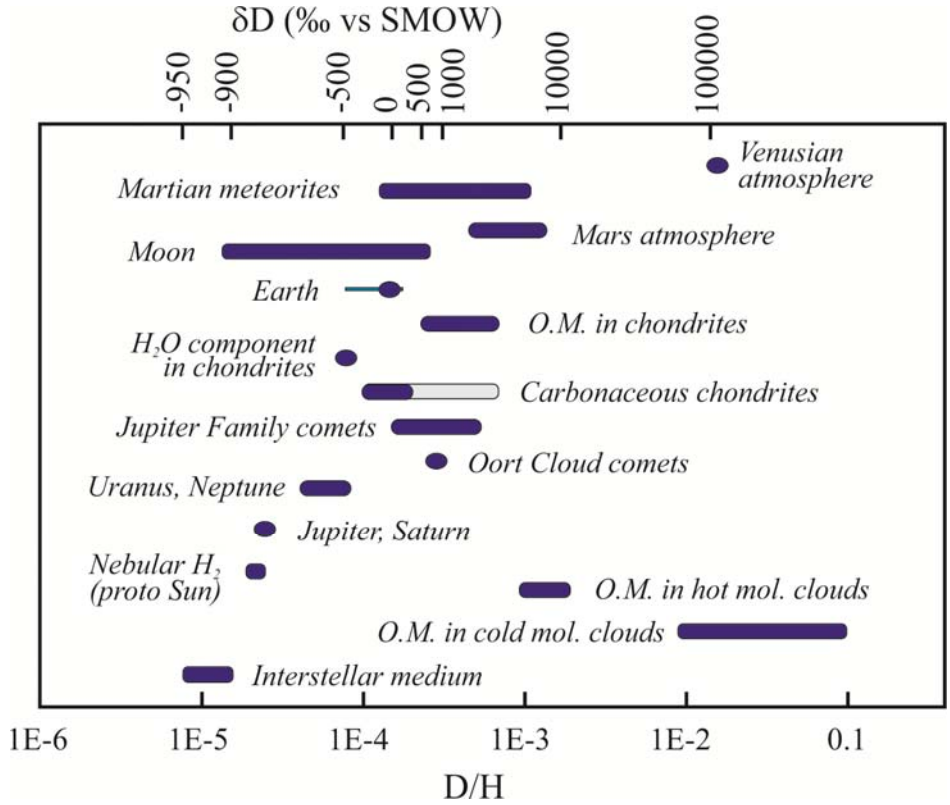

Fig. 13.6 D/H ratios for galactic and solar system bodies. The solar nebula (measured for Jupiter and Saturn and inferred for the proto Sun are nearly pure H_2. High δD values of organic matter in molecular clouds is explained by extreme fractionation during ion exchange reactions. The high D/H ratios of Venus are thought to be due to hydrodynamic escape of protium to space. Comets are generally light although several Jupiter family comets have measured D/H ratios that overlap the bulk Earth value. The bulk Earth is ~ -40‰. The full range of Earth values is given by the thin dark line. Most carbonaceous chondrites fall in the dark blue range, although anomalous heavy chondrites (Ornans, Semarkona) have δD values as high as >2000‰ (grey band). Data from compilations of Robert *et al.* (2000) and Sharp (2017).

ratio. Jupiter formed very shortly after the birth of our solar system, and because of its enormous size, Jupiter would have incorporated all hydrogen in its orbit without fractionation. Spectroscopic analysis of Jupiter gives a D/H ratio of Jupiter (26±7)×10^{-6}, which is in excellent agreement with the solar estimate. Knowing the baseline for the D/H ratio of the solar system, allows us to explain higher D/H ratios of terrestrial and

[8] Of all the isotopes of all elements, deuterium is the most easily destroyed in thermonuclear reactions.

extraterrestrial materials in terms of preferential incorporation of deuterium during various discrimination processes in the solar nebula.

There are enormous deuterium enrichments in dense molecular clouds. D/H ratios as high as 10^{-1} and 10^{-3} are detected in organic matter from cold (10 K) and hot (>80 K) molecular clouds, respectively. Such high δD values (>600,000‰) can only be achieved by isotopic enrichments occurring at extremely low temperatures. Normal gaseous exchange reactions do not occur at such low temperatures. Instead, ion exchange reactions, in which gaseous molecules are ionized by ultraviolet radiation and then undergo isotopic exchange, are called upon to explain the extreme deuterium enrichments. Two such reactions are (Robert et al., 2000)

$$H_3^+ + HD \Leftrightarrow H_2D^+ + H_2 \qquad 13.2$$

and

$$CH_3^+ + HD \Leftrightarrow CH_2D^+ + H_2 \qquad 13.3.$$

With this process in mind, organic matter formed under low temperature conditions in the nebula should be extremely heavy, and indeed, δD values well above 1,000‰ and approaching 12,000‰ have been measured (Alexander et al., 2010). These extreme values are explained as a result of low temperature reactions similar to equation 13.3 and/or oxidation of H_2O at low temperatures producing very light H_2 which was removed from the system.

At low temperatures, the fractionation between H_2O and H_2 are extremely large. $\alpha_{H2O\text{-}H2}$ values range from 9.5 at 180 K to 5.5 at 230 K (Reeves and Bottinga, 1972). Oxidation of H_2 to H_2O at such low temperatures could therefore lead to extreme D enrichments resulting in δD values easily approaching +500‰. *In situ* D/H analyses of phyllosilicates in the matrix of the ordinary chondrite Semarkona are remarkably high, reaching values of 3300 to 4600‰ (Deloule and Robert, 1995). Such extreme values can be explained by the ion exchange reaction given by equation 13.2 above at temperatures on the order of 110-140 K.

13.4.2 Hydrogen in chondrites

The first hydrogen isotope measurements of meteorites gave 'unearthly' high δD values up to +300‰ (Boato, 1954). The range was greatly expanded in the 70's and 80's. For example, Kolodny *et al.* (1980) measured δD values between -70 and +771‰ from seven carbonaceous chondrites. McNaughton *et al.* (1981) measured values as high as 3,000‰ in several ordinary chondrites. δD values of bulk chondrites typically range from ~-200 to in excess of +600‰ and vary with chondrite type (Fig. 13.7). The bulk values are a mixture of phyllosilicate hydrogen (*e.g.,* water) and organic matter. Alexander *et al.* (2012) measured the hydrogen isotope composition and C/H ratios of a large number of chondrites. They plotted the δD values against the C/H ratios and extrapolated the best-fit line to a C/H ratio of 0, following the approach of Kolodny *et al.* (1980). They interpreted the y-intercept (C/H = 0) as the phyllosilicate portion of the mixture, which is essentially the hydrous component of the phyllosilicate. The H_2O contents have δD values of -500‰ (CM, CI and CO chondrites) and +100‰ (CR chondrites). The result is in excellent agreement with the earlier work of Kolodny *et al.* (1980), and can be explained by low

temperature equilibrium fractionation between solar H_2 and small amounts of oxidized H_2O.

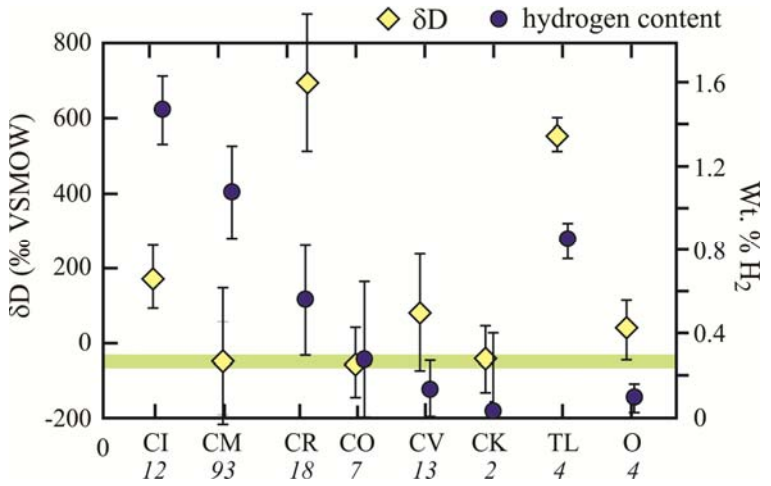

Fig. 13.7. H_2O content and δD values of chondritic meteorites. The green band is the bulk Earth δD value. O- ordinary chondrites; TL – Tagish Lake. From Sharp (2017). Italicized numbers refer to number of analyses made.

13.4.3 Hydrogen in differentiated meteorites.

The source of hydrogen in differentiated bodies is an unsettled question. The Earth, Moon and Mars all have some 'water component', where 'water' is loosely defined as the hydrogen-bearing phase. On Earth, a significant portion of H does occur as water in the ocean today, with equal or likely greater amounts in the mantle and perhaps core. Mars has evidence for large quantities of water in the past (Villanueva et al., 2015), and even the Moon, which was long thought to be devoid of hydrogen, has now been shown to contain hydrogen in trace quantities in minor phases, such as melt inclusions and apatite grains[9] (Saal et al., 2008; McCubbin et al., 2010). Other differentiated bodies, such as the HEDs, also have H-bearing phases.

The surprising thing is that the terrestrial planets are thought to have formed inside the 'snow line' or 'frost line' and therefore should not contain any indigenous water. During collapse of the proto-nebular cloud, adiabatic heating during infall of the nebular cloud to a disk would have raised the temperature of the disk to 1250-1450°C. Subsequent cooling would lead to condensation of the elements in relation to their volatility. Hydrogen condenses as water ice at temperatures of ~150 K and the solid ice is then incorporated into the growing planetesimals. The snow line is the inferred region inside of which temperature were too high for H_2O to condense *prior* to dissipation of the nebular cloud. The snow line is thought to have been at the radial position of the asteroid belt. As a result, the growing terrestrial planets sunward of this radial distance should not have incorporated any water. And yet we see that all of the terrestrial planets (perhaps with the exception of Mercury) have or had significant amounts of water. The question then becomes 'how did these bodies, inside of the snow line, acquire their water?

[9] Water ice has been detected in the permanently shadowed regions of the south pole. The origin for this water is likely due to delivery from comets.

A number of hypotheses have been proposed to explain the incorporation of water by the terrestrial planets (see Sharp, 2017 for a detailed review). These include direct incorporation of nebular H_2 gas, addition of hydrous bodies from beyond the snow line and late addition to the planets by bombardment from carbonaceous chondrites – the so called 'late veneer' or 'late accretion' hypothesis.

The late veneer hypothesis has received considerable attention because it explains the high concentration of highly siderophile (HSE) elements in the mantle. The HSEs (Os, Ir, Ru, Rh, Pt, Pd, Re, Au) are strongly partitioned into iron metal. As a result, they should have been completely sequestered into the core during early planetary formation. The higher-than-expected concentration of the HSEs in the mantle was first explained by late addition of chondritic material following core formation. Addition of 0.7% chondritic material after the Giant Impact event responsible for the Moon formation is sufficient to explain the elevated HSE abundance of Earth's mantle. If the impactors were hydrous chondrites, represented by CM chondrites, then the δD value of late accreted material would match that of Earth with ~2% delivery needed to account for the minimum estimate of the Earth's water content.

If a significant fraction of chondrite types *other* than CM were delivered during late accretion, then the integrated δD value of the delivered material would be too high to match Earth. This deuterium excess could be counterbalanced by light hydrogen if direct ingassing of nebular H_2 occurred as the planetesimals were nearing their final size (Sharp, 2017). Ingassing of light nebular H_2 also allows for the possibility of some heavy cometary volatiles to be added to the Earth system. Marty *et al.* (2012) conclude that the H and N isotope composition of Earth is explained by a combination of chondritic and solar compositions without isotopic fractionation during hydrodynamic escape. Sharp (2017) proposed that a combination of nebular ingassing followed by hydrodynamic escape and late addition of chondritic and cometary material explains the isotopic composition of Earth as well as the high $f(O_2)$ of the mantle. Primordial ^3He, found in many mantle hot spots may also be sourced directly from nebular ingassing. The remarkably high δD value 125,000‰ for the atmosphere of Venus is explained by near complete loss of H by heating of the upper atmosphere by extreme ultraviolet radiation from the early Sun and hydrodynamic escape of H or H_2 through a CO_2-rich atmosphere (Donahue et al., 1982). Whether the Earth has had its D/H ratio modified by hydrodynamic escape remains unresolved.

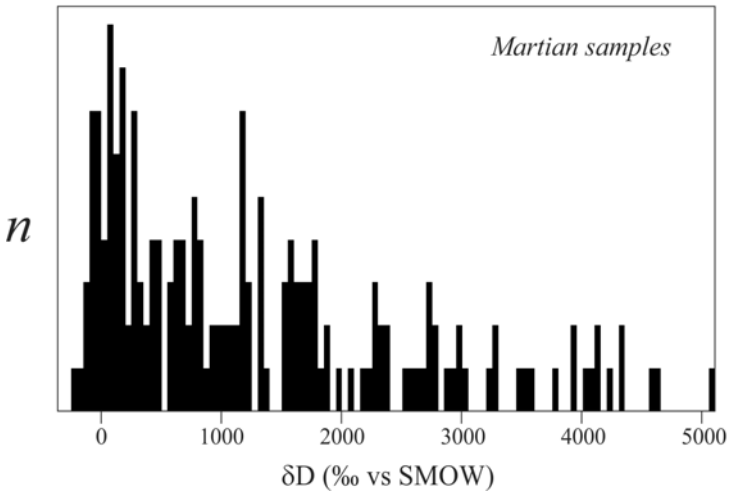

Fig. 13.8. Compilation of δD values of Martian meteorites. Most analyses are from ion microprobe measurements of apatite grains. Compilation from Sharp, (2017).

Like Venus, although to a much lesser extent, the Martian atmosphere also has a high δD value (δD = 4000‰), again explained by preferential loss of H_2 to space. Martian meteorites have a wide range of δD values ranging from near zero up to 5,000‰ (Fig. 13.8).

Until recently, most hydrogen in lunar samples was thought to be due to solar wind implantation (Epstein and Taylor, 1970). The δD value of hydrogen extracted from lunar soils is between -890‰ and -1000‰, explained as being entirely sourced by deuterium-free solar wind. Hydrogen was recognized as a primary phase in lunar glass (Saal et al., 2008; 2013) and the volatile-rich phase apatite ($Ca_5(PO_4)_3(OH,F,Cl)$) (McCubbin et al., 2010). The δD values of lunar apatites cover an extremely wide range (Fig. 13.9). The unmodified bulk Moon is thought to have a δD value equal to or higher than Earth (Hauri et al., 2017). The lowest values (not shown in Fig. 13.9 are measured on bulk lunar soil samples. The δD values approach -1,000‰ and are explained as direct implantation of protium-rich solar wind. The highest δD values are either due to heavy cometary input (Greenwood et al., 2011) or loss of H_2 to space during degassing (Sharp et al., 2013). Low δD values (~-600 to -300) may represent a distinct volatile source (Robinson et al., 2016) that may be tapping a nebular ingassing component (Sharp, 2017).

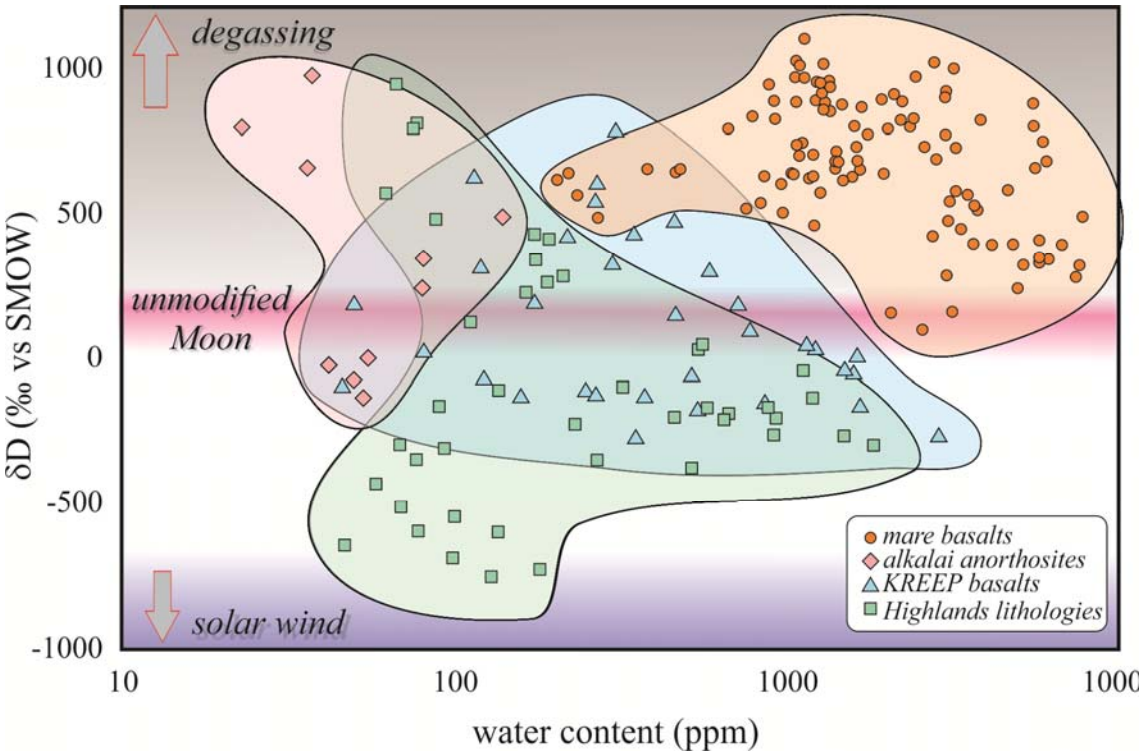

Fig. 13.9. Hydrogen isotope values *vs.* water content [H_2O] of lunar apatite grains. Different lithologies have distinct [H_2O]-δD fields. Mare basalts have the highest [H_2O] and δD values. Modified from Robinson *et al.* (2016).

13.5 Carbon

Carbon isotope analyses of meteorites began extremely early-on in the stable isotope game, motivated by the identification of a distinct spectroscopic bands found in N-type stars attributable to high concentrations of $^{12}C^{13}C$. In 1936, several attempts were made to measure the $^{13}C/^{12}C$ ratio of graphite from Canyon Diablo iron meteorite using spectrographic measurements of graphite discharge. Unfortunately, the spectrographic image was identical to that obtained from terrestrial graphite (e.g., Jenkins and King, 1936), suggesting that no ^{13}C anomaly existed in meteorites. Murphey and Nier (1941) determined the carbon isotope composition of 'meteorite carbon' from seven samples, which ranged from -33 to -11 ‰ (approximate PDB scale). Additional analyses in the coming decades also found that meteoritic carbon had $\delta^{13}C$ values that overlapped with terrestrial values. The first anomalous values were found in the carbonate fraction of two carbonaceous chondrites (Orgueil and Ivuna), where $\delta^{13}C$ values of ~+60‰ (PDB) were measured on the dolomite fraction (Clayton, 1963). Along with Boato's early high δD values in meteorites, this was one of the first findings of anomalous stable isotope ratios in extraterrestrial material.

In the same year, Briggs (1963) reported $\delta^{13}C$ values of solvent-extractable organic material from carbonaceous chondrites that were only slightly less than 0‰, higher than terrestrial equivalent organic matter. The anomalous $\delta^{13}C$ values provided some of the strongest evidence to date that organic material in meteorites was indeed of extraterrestrial origin.

Two papers appearing in 1970 expanded the data base for carbonaceous chondrites (Krouse and Modzeleski, 1970; Smith and Kaplan, 1970). Both showed very high $\delta^{13}C$ values of carbonates and less convincing, but still high, $\delta^{13}C$ values of organic extracts (Fig. 13.10). The data were clearly incompatible with a terrestrial carbon origin. Instead, the 'endogenous' carbon (Smith and Kaplan, 1970) in carbonaceous meteorites was firmly established.

The emerging picture was that the $\delta^{13}C$ values of organic carbon averaged around -16‰, while the much less abundant carbonate had $\delta^{13}C$ values as high as +60 or +70‰. The fractionation of >80‰ between the oxidized and reduced form was far larger than what was observed on Earth, where the differences were only on the order of 25 to 30‰. Urey (1967) considered two distinct carbon synthesis events in the solar system as a possible explanation. Several year later, Lancet and Anders (1970) proposed an alternative explanation that did not require an exotic carbon source. They showed experimentally that oxidation-reduction reactions of CO (Fischer-Tropsch synthesis) given by

$$n\ CO + (2n + 1)\ H_2 \rightarrow C_nH_{2n+2} + n\ H_2O \qquad 13.4$$

and

$$2n\ CO + (n + 1)\ H_2 \rightarrow C_nH_{2n+2} + n\ CO_2 \qquad 13.5$$

could produce large carbon isotope fractionations. In this reaction, both oxidized and reduced carbon are formed abiogenically. Another possible low-temperature exchange reaction is

$$^{12}CO + {}^{13}C^{+} \rightarrow {}^{13}CO + {}^{12}C^{+} \qquad 13.6.$$

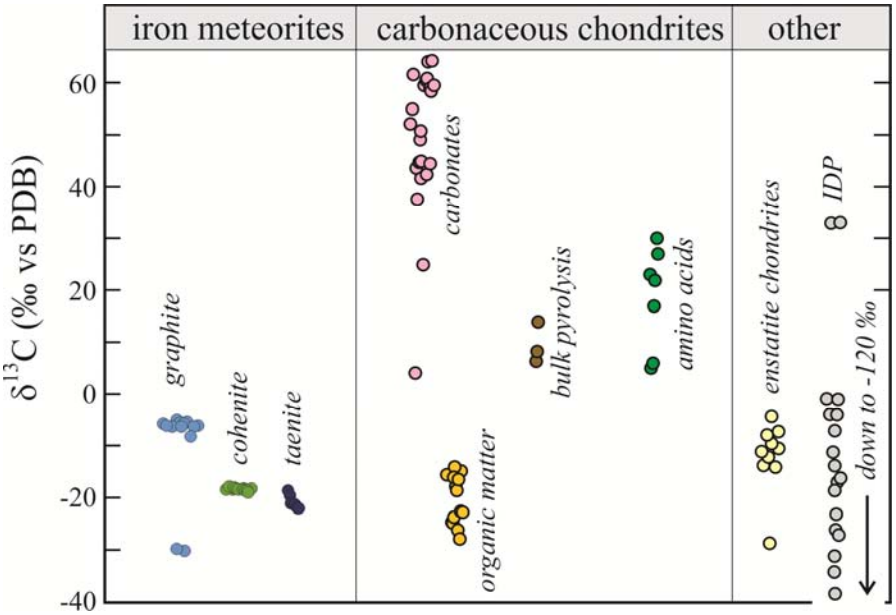

Fig. 13.10. Carbon isotope composition of different extraterrestrial materials. The Sun has a $\delta^{13}C$ value of -105±20‰. All other materials have higher $^{13}C/^{12}C$ ratios (except one IDP), consistent with low temperature reactions that enrich solid phases in ^{13}C. Data from the following sources: (Craig, 1953; Clayton, 1963; Krouse and Modzeleski, 1970; Smith and Kaplan, 1970; Deines and Wickman, 1975; Grady et al., 1986; Epstein et al., 1987; Engel et al., 1990; Messenger, 2000; Hashizume et al., 2004).

The low temperature oxidation-reduction reactions can explain the high $\delta^{13}C$ value of most solar system materials relative to the Sun. The Sun is thought to have a $\delta^{13}C$ value of -105±20‰ (Hashizume et al., 2004). Interplanetary dust particles (IDPs) have a very wide range of $\delta^{13}C$ values from -120 to +33‰ (Messenger, 2000), consistent with a low protosolar nebula value and heavier samples resulting from low temperature reactions such as 13.4 -13.6.

The isotopic composition of individual amino acids from CM chondrites have been measured (Engel et al., 1990). The $\delta^{13}C$ values are as high as +30‰, clearly of extraterrestrial origin. Interestingly, the measured samples are not racemic[10], which had been used as previous evidence for terrestrial contamination. The high $\delta^{13}C$ values eliminate contamination as a possibility of their origin. The isotopic ratios of nitrogen, and hydrogen from the hydroxy acids from Murchison are also extraterrestrial, with $\delta^{15}N$ values of 37-184‰ (Engel and Macko, 1997) and δD topping out at >500‰ (Cronin et al., 1993).

In a number of stepwise combustion analyses of carbonaceous chondrites, an extremely high $\delta^{13}C$ value of 1100‰ was measured (Swart et al., 1983). Later work

[10] A racemic amino acid is one that has equal abundance of left- and right-handed optical isomers (enantiomers). The Murchison sample has a D/L value of 0.85, significantly different from the racemic value of 0.5. It is normally assumed that non-racemic amino acids are due to biological synthesis.

using high spatial resolution ion microprobe analyses revealed $\delta^{13}C$ values in interstellar residual grains in excess of 7000‰ (Zinner and Epstein, 1987). These are primitive and rare grains of 'stardust'.

13.6 Nitrogen

The wide range of nitrogen isotope variations in the solar system is exceeded only by hydrogen. Studies of the nitrogen isotope geochemistry of meteorites lagged behind the other 'traditional' light stable isotope elements mostly because nitrogen concentrations in meteorites are low and the analyses are difficult. Some of the first measurements of carbonaceous chondrites found a range considerably broader than what existed on Earth. Injerd and Kaplan (1974) measured $\delta^{15}N$ ratios between -20 and +46‰ from four chondrites. Kung and Clayton (1978) expanded the number of analyses and extended the total range observed for carbonaceous chondrites from lows of –40 to -30‰ for enstatite chondrites to highs of +30 and +50‰ (Renazzo with an anomalous 170‰). They felt that the variations were too large to be explained by mass dependent fractionation, and instead suggested that the meteorites were recording nitrogen isotope heterogeneities in the solar nebula.

As we have seen for hydrogen and carbon, the nitrogen isotope composition of the Sun represents the overall $\delta^{15}N$ value of the solar system. The Sun has the lowest $^{15}N/^{14}N$ ratio of any materials in our solar system. All processes that have occurred in the protoplanetary disk and after its dissipation, lead to a an enrichment in ^{15}N which is then incorporated into growing planetary bodies. The solar system can be broadly characterized of consisting of three distinct 'regions' in terms of $\delta^{15}N$ values (Mandt et al., 2014). The Sun, Jupiter and Saturn, with their very low $^{15}N/^{14}N$ ratio, the inner solar system, with $\delta^{15}N$ values of 0-50‰ and cometary ices, with $\delta^{15}N$ values of 850±150‰ (Fig. 13.11).

Hashizume *et al.* measured the $\delta^{15}N$ value of metal grain from the lunar soil in order to obtain the value of the solar wind. Their estimate was very light, at ≤ -240‰. A more recent measurement of solar wind implanted on the SiC plates of the Genesis mission corresponds to a $\delta^{15}N$ value of the solar wind of -407±7‰ and a $\delta^{15}N$ value for the Sun (and protosolar nebula) of -383±8‰ (Marty et al., 2011). For comparison, the $\delta^{15}N$ value of Jupiter was measured to be -374±80‰ from the *Galileo* Probe Mass Spectrometer (Owen et al., 2001).

The heavy nitrogen isotope composition of some solar system materials, such as organic matter, 'organic globules' in the Tagish Lake chondrite (Nakamura-Messenger et al., 2006) and comets (Fig. 13.11) has been attributed to low temperature ion molecule exchange reactions that could occur in a cold molecular cloud or in the protostellar nebula far from the Sun. One such reaction is

$$HN_2^+ + N^{15}N \rightarrow H^{15}NN^+ + N_2 \qquad 13.7$$

where the HN_2^+ ion (isodiazene) becomes enriched in ^{15}N and then becomes incorporated into ices and organic matter (Furi and Marty, 2015).

Nitrogen enrichment can also occur by escape from a planetary surface, such as Mars (as evidenced by the high $\delta^{15}N$ of the Martian atmosphere) and Titan. The moderately elevated $\delta^{15}N$ values of many asteroidal materials is probably related to kinetic and equilibrium isotope fractionations between nitrogen. The large fractionations relative to what is seen on Earth are difficult to account for and almost certainly require, at minimum, fractionation associated with an oxidation state change (*e.g.,* N_2 to NH_2^+) and low temperature dynamic interactions. Alternatively, the large range of $\delta^{15}N$ values has been suggested to reflect primordial nebular inhomogeneities (Thiemens and Clayton, 1981; Prombo and Clayton, 1993).

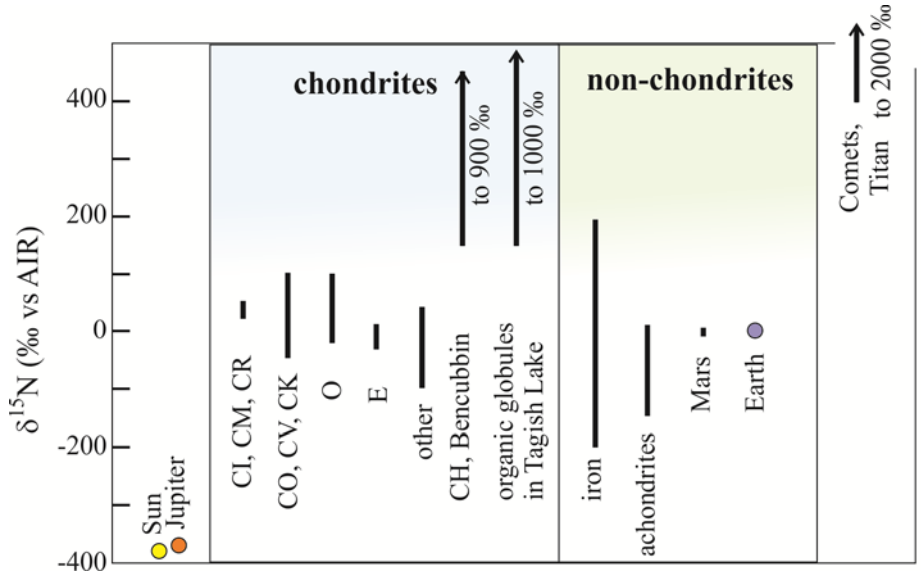

Fig. 13.11. Nitrogen isotope composition of different extraterrestrial materials. The Sun has the lowest $\delta^{15}N$ value of -383‰. All other solar system materials have higher $\delta^{15}N$ values. Samples formed at low temperatures far from the Sun, such as comets and Titan ($\delta^{15}N$ = 620‰) have the highest $\delta^{15}N$ values consistent with molecular ion reactions at low temperatures. The intermediate values found in meteorites may be related to kinetic or equilibrium molecular exchange reactions. Data from the following sources: (Owen et al., 2001; Grady and Wright, 2003; Nakamura-Messenger et al., 2006; Marty et al., 2011; Mandt et al., 2014; Furi and Marty, 2015).

13.7 Sulfur

In the meteorite world, the most remarkable thing about sulfur is how unremarkable it is. Hulston and Thode (1965) noted in a comprehensive study of meteoritic $\delta^{34}S$ values "that the isotopic composition of the total sulfur is remarkably constant from meteorite to meteorite." Most meteorites have a $\delta^{34}S$ value that falls in the range of -2 to +3‰. Hulston and Thode did not find any $\delta^{33}S$ or $\delta^{36}S$ anomalies that might be evidence of an exotic nucleosynthetic source. The data suggest that sulfur underwent some fractionation on the parent bodies, but that the source within the solar system was more-or-less constant (Kaplan and Hulston, 1966). This conclusion is consistent with the idea that sulfur condensed out of the solar nebula as FeS without fractionation and that no oxidation state changes occurred prior to incorporation into the parent bodies. The one interesting theme that has been observed in sulfur isotopes is the non-mass dependent fractionation (see section 10.5.5 for more information) seen in some differentiated bodies. Farquhar *et al.* (2000a) measured urelite samples with a small ^{33}S

anomaly which they attributed to gas phase reactions in the solar nebula that resulted in small anomalies in the protoplanetary disk. Both positive and negative ^{33}S anomalies have also been seen in Martian meteorites, which are explained by deposition of oxidized sulfur produced by atmospheric chemical reactions (Farquhar et al., 2000b). The common sulfur anomaly on Mars indicates widespread incorporation of surficial sulfur into Martian materials that have been delivered to Earth (Franz et al., 2014). A sulfur-36 anomaly has also been seen in some primitive differentiated bodies, presumably due to decay of ^{36}Cl early in solar system history (Defouilloy et al., 2016).

13.8 Chlorine

Chlorine isotopes are considered in this chapter because of the large isotope variations that have been seen in extraterrestrial materials. There are two stable isotopes of chlorine, ^{35}Cl and ^{37}Cl. The isotope ratios are reported in the standard delta notation with seawater – Standard Mean Ocean Chloride or SMOC – assigned a $\delta^{37}Cl$ value of 0‰. The bulk Earth $\delta^{37}Cl$ value is also close to 0‰. There are large variations in terrestrial materials due to near-surface processes (Barnes and Sharp, 2017), but most of these fractionation mechanisms are not relevant to extraterrestrial materials.

The $\delta^{37}Cl$ value of chondrites range from -4.5 to 2.5‰ (Fig. 13.12). The majority fall between -2 and +1‰, roughly consistent with the bulk Earth. What is perhaps most interesting is that three of the chondrite samples have $\delta^{37}Cl$ values less than -4‰. Mars has a wide range of $\delta^{37}Cl$ values, covering over 10‰ total variation. This is far larger range than for equivalent lithologies on Earth. The high $\delta^{37}Cl$ values are thought to be due to preferential loss of the light isotope (^{35}Cl) to space, leaving a heavy residue. The low $\delta^{37}Cl$ values (deep red color in Fig. 13.12) are the olivine phyric shergottites, which are thought to be the samples least contaminated by crustal material. Finally, the iron meteorites are negative, and reach the lowest $\delta^{37}Cl$ values of any extraterrestrial material measured to date (Gargano et al., 2017). It is suggested that the negative $\delta^{37}Cl$ values reflect direct incorporation of Cl from the solar nebula, and that the Sun presumably also has a negative $\delta^{37}Cl$ value (Sharp et al., 2016). The higher $\delta^{37}Cl$ values of most chondrites are explained by addition of an HCl-bearing ice ($HCl{\cdot}3H_2O$) formed beyond the snowline prior to dissipation of the solar nebula. The ice would preferentially incorporate ^{37}Cl ultimately leading to the heavy Cl isotope compositions of most chondrites.

The most remarkable Cl isotope variations are seen on the Moon, with a spread in excess of 40‰ (Fig. 13.12). The lowest values are close to 0‰ with one negative sample. Other than hydrogen, no other isotopic system shows such a large lunar range in its isotopic composition. The high $\delta^{37}Cl$ values are most likely due to degassing. In detail, a number of ideas have been proposed, including the following:

1. Local degassing of a solidifying magma, with the light isotopes preferentially lost to the vapor phase (Sharp et al., 2010);
2. Some samples may be related to vapor phase deposition related to meteorite impacts (Treiman et al., 2014);
3. Degassing into a vacuum
4. Degassing during the waning stages of the magma ocean stage following the Giant Impact (Boyce et al., 2015; Barnes et al., 2016).

Each of these ideas has merits and all are not mutually exclusive. Clearly the cause or causes of the enormous enrichment in ^{37}Cl in lunar samples is unique and is not well understood.

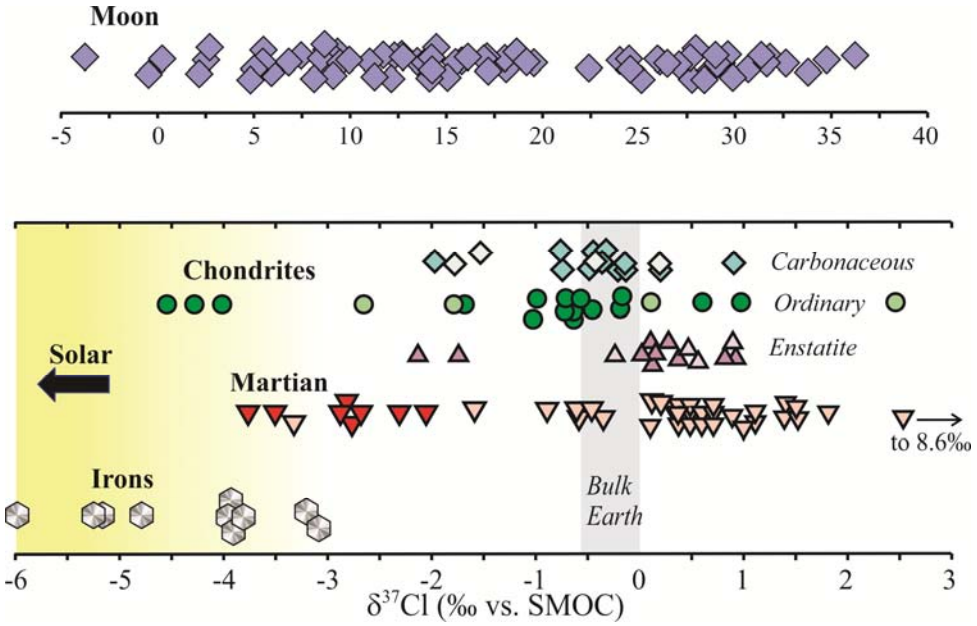

Fig. 13.12. Chlorine isotope composition of extraterrestrial materials. The lowest $\delta^{37}Cl$ values probably reflect the composition of the protonebular disk and Sun. Iron meteorites, mantle-derived Martian meteorites (deep red) and several ordinary chondrites preserve this signature. The other samples have been contaminated by a ^{37}Cl-enriched HCl-bearing ice or have lost light isotopes through vaporization. Each of these possibilities drives the $\delta^{37}Cl$ values of the residue to higher values. Lunar samples show a huge range of $\delta^{37}Cl$ values (note different scale for lunar materials. The high $\delta^{37}Cl$ values are due to vaporization of Cl during degassing.

Other isotope systems have been used to study extraterrestrial materials including Li, Mg, Si, Ti, Cr, Fe, Ni, Zn, and Mo. These are not normally considered as traditional stable isotopes and will not be considered here. Readers are referred to the recent book "*Non-Traditional Stable Isotopes"* (2017) which is a general overview of some of the recent developments of the non-HCNOS isotope systems.

References

Agee, C.B., Wilson, N.V., McCubbin, F.M., Ziegler, K., Polyak, V.J., Sharp, Z.D., Asmerom, Y., Nunn, M.H., Shaheen, R., Thiemens, M.H., Steele, A., Fogel, M.L., Bowden, R., Glamoclija, M., Zhang, Z. and Elardo, S.M. (2013) Unique meteorite from the Early Amazonian epoch on Mars: Water-rich basaltic breccia NWA 7034. *Science* **339**, 780-785.

Alexander, C.M.O.D., Newsome, S.D., Fogel, M.L., Nittler, L.R., Busemann, H. and Cody, G.D. (2010) Deuterium enrichments in chondritic macromolecular material—Implications for the origin and evolution of organics, water and asteroids. *Geochimica et Cosmochimica Acta* **74**, 4417-4437.

Alexander, C.M.O.D., Bowden, R., Fogel, M.L., Howard, K.T., Herd, C.D.K. and Nittler, L.R. (2012) The provenances of asteroids, and their contributions to the volatile inventories of the terrestrial planets. *Science* **337**, 721-723.

Amari, S. (2014) Recent progress in presolar grain studies. *Mass Spectrometry*.

Anders, E. and Zinner, E. (1993) Interstellar grains in primitive meteorites: diamond, silicon carbide, and graphite. *Meteoritics* **28**, 490-514.

Baertschi, P. (1950) Isotopic composition of the oxygen in silicate rocks. *Nature* **166**, 112-113.

Bally, J. and Langer, W.D. (1982) Isotope-selective photodestruction of carbon monoxide. *The Astrophysical Journal* **255**, 143-148.

Barnes, J.D. and Sharp, Z.D. (2017) Chlorine Isotope Geochemistry. *Reviews in Mineralogy and Geochemistry* **82**, 345-378.

Barnes, J.J., Tartèse, R., Anand, M., McCubbin, F.M., Neal, C.R. and Franchi, I.A. (2016) Early degassing of lunar urKREEP by crust-breaching impact(s). *Earth and Planetary Science Letters* **447**, 84-94.

Boato, G. (1954) The isotopic composition of hydrogen and carbon in the carbonaceous chondrites. *Geochimica et Cosmochimica Acta* **6**, 209-220.

Boyce, J.W., Treiman, A.H., Guan, Y., Ma, C., Eiler, J.M., Gross, J., Greenwood, J.P. and Stolper, E.M. (2015) The chlorine isotope fingerprint of the lunar magma ocean. *Science Advances* **1**, 8 pp.

Brearley, A. and Jones, R.H. (1998) Chondritic meteorites, in: Papike, J.J. (Ed.), Planetary Materials. Mineralogical Society of America, Washington, D.C., pp. 3.01-03.370.

Briggs, M.H. (1963) Evidence of an extraterrestrial origin for some organic constituents of meteorites. *Nature* **197**, 1290.

Burbidge, E.M., Burbidge, G.R., Fowler, W.A. and Hoyle, F. (1957) Synthesis of the elements in stars. *Reviews of Modern Physics* **29**, 547-650.

Chakraborty, S., Ahmed, M., Jackson, T.L. and Thiemens, M.H. (2008) Experimental test of self-shielding in vacuum ultraviolet photodissociation of CO. *Science* **321**, 1328-1331.

Clayton, R.N. (1963) Carbon isotope abundance in meteoritic carbonates. *Science* **140**, 192-193.

Clayton, R.N., Grossman, L. and Mayeda, T.K. (1973) A component of primitive nuclear composition in carbonaceous meteorites. *Science* **182**, 485-488.

Clayton, R.N. and Mayeda, T.K. (1975) Genetic relations between the moon and meteorites. *Proceedings of the Lunar Science Conference* **6**, 1761-1769.

Clayton, R.N. (1993) Oxygen isotopes in meteorites. *Annual Review of Earth and Planetary Sciences* **21**, 115-149.

Copi, C.J., Schramm, D.N. and Turner, M.S. (1995) Big-bang nucleosynthesis and the baryon density of the universe. *Science* **267**, 192-199.

Craig, H. (1953) The geochemistry of the stable carbon isotopes. *Geochimica et Cosmochimica Acta* **3**, 53-92.

Craig, H. (1957) Isotopic standards for carbon and oxygen and correction factors for mass-spectrometric analysis of carbon dioxide. *Geochimica et Cosmochimica Acta* **12**, 133-149.

Cronin, J.R., Pizzarello, S., Epstein, S. and Krishnamurthy, R.V. (1993) Molecular and isotopic analyses of the hydroxy acids, dicarboxylic acids, and hydroxydicarboxylic acids of the Murchison Meteorite. *Geochimica et Cosmochimica Acta* **57**, 4745-4752.

Defouilloy, C., Cartigny, P., Assayag, N., Moynier, F. and Barrat, J.A. (2016) High-precision sulfur isotope composition of enstatite meteorites and implications of the formation and evolution of their parent bodies. *Geochimica et Cosmochimica Acta* **172**, 393-409.

Deines, P. and Wickman, F.E. (1975) A contribution to the stable carbon isotope geochemistry of iron meteorites. *Geochimica et Cosmochimica Acta* **39**, 547-557.

Deloule, E. and Robert, F. (1995) Interstellar water in meteorites? *Geochimica et Cosmochimica Acta* **59**, 4695-4706.

Donahue, T.M., Hoffman, J.H., Hodges, R.R. and Watson, A.J. (1982) Venus was wet: A measurement of the ratio of deuterium to hydrogen. *Science* **216**, 630-633.

Engel, M.H., Macko, S.A. and Silfer, J.A. (1990) Carbon isotope composition of individual amino acids in the Murchison meteorite. *Nature* **348**, 47-49.

Engel, M.H. and Macko, S.A. (1997) Isotopic evidence for extraterrestrial nonracemic amino acids in the Murchison meteorite. *Nature* **389**, 265-268.

Epstein, S. and Taylor, H.P., Jr. (1970) $^{18}O/^{16}O$, $^{30}Si/^{28}Si$, D/H, and $^{13}C/^{12}C$ studies of lunar rocks and minerals. *Science* **167**, 533-535.

Epstein, S., Krishnamurthy, R.V., Cronin, J.R., Pizzarello, S. and Yuen, G.U. (1987) Unusual stable isotope ratios in amino acid and carboxylic acid extracts from the Murchison meteorite. *Nature* **326**, 477-479.

Farquhar, J., Jackson, T.L. and Thiemens, M.H. (2000a) A ^{33}S enrichment in ureilite meteorites: evidence for a nebular sulfur component. *Geochimica et Cosmochimica Acta* **64**, 1819-1825.

Farquhar, J., Savarino, J., Jackson, T.L. and Thiemens, M.H. (2000b) Evidence of atmospheric sulphur in the martian regolith from sulphur isotopes in meteorites. *Nature* **404**, 50-52.

Franchi, I.A., Wright, I.P., Sexton, A.S. and Pillinger, C.T. (1999) The oxygen-isotopic composition of Earth and Mars. *Meteoritics & Planetary Science* **34**, 657-661.

Franz, H.B., Kim, S.-T., Farquhar, J., Day, J.M.D., Economos, R.C., McKeegan, K.D., Schmitt, A.K., Irving, A.J., Hoek, J. and Iii, J.D. (2014) Isotopic links between atmospheric chemistry and the deep sulphur cycle on Mars. *Nature* **508**, 364-368.

Friedman, I., O'Neil, J.R., Adami, L.H., Gleason, J.D. and Hardcastle, K. (1970) Water, hydrogen, deuterium, carbon, carbon-13, and oxygen-18 content of selected Lunar material. *Science* **167**, 538-540.

Furi, E. and Marty, B. (2015) Nitrogen isotope variations in the Solar System. *Nature Geoscience* **8**, 515-522.

Gargano, A.M., Sharp, Z.D. and Taylor, L.A. (2017) Further Constraining the Chlorine Isotope Composition of the Solar Nebula: Main Group Iron Meteorites
80th Meteoritical Society Annual Meeting 2017.

Grady, M.M., Wright, I.P., Carr, L.P. and Pillinger, C.T. (1986) Compositional differences in enstatite chondrites based on carbon and nitrogen stable isotope measurements. *Geochimica et Cosmochimica Acta* **50**, 2799-2813.

Grady, M.M. and Wright, I.P. (2003) Elemental and isotopic abundances of carbon and nitrogen in meteorites. *Space Science Reviews* **106**, 231-248.

Greenwood, J.P., Itoh, S., Sakamoto, N., Warren, P., Taylor, L. and Yurimoto, H. (2011) Hydrogen isotope ratios in lunar rocks indicate delivery of cometary water to the Moon. *Nature Geoscience* **4**, 79-82.

Greenwood, R.C., Franchi, I.A., Jambon, A. and Buchanan, P.C. (2005) Widespread magma oceans on asteroidal bodies in the early Solar System. *Nature* **435**, 916-918.

Greenwood, R.C., Franchi, I.A., Jambon, A., Barrat, J.A. and Burbine, T.H. (2006) Oxygen Isotope Variation in Stony-Iron Meteorites. *Science* **313**, 1763-1765.

Greenwood, R.C., Franchi, I.A., Gibson, J.M. and Benedix, G.K. (2012) Oxygen isotope variation in primitive achondrites: The influence of primordial, asteroidal and terrestrial processes. *Geochimica et Cosmochimica Acta* **94**, 146-163.

Harkins, W.D. and Stone, S.B. (1926) The isotopic composition and atomic weight of chlorine from meteorites and from minerals of non-marine origin: (Papers on atomic stability). *Journal of the American Chemical Society* **48**, 938-949.

Hashizume, K., Chaussidon, M., Marty, B. and Terada, K. (2004) Protosolar carbon isotopic composition: Implications for the origin of meteoritic organics. *The Astrophysical Journal* **600**, 480-484.

Hashizume, K. and Chaussidon, M. (2005) A non-terrestrial ^{16}O-rich isotopic composition for the protosolar nebula. *Nature* **434**, 619 - 622.

Hauri, E.K., Saal, A.E., Nakajima, M., Anand, M., Rutherford, M.J., Van Orman, J.A. and Le Voyer, M. (2017) Origin and Evolution of water in the Moon's interior. *Annual Review of Earth and Planetary Sciences* **45**, 89-111.

Herwartz, D., Pack, A., Friedrichs, B. and Bischoff, A. (2014) Identification of the giant impactor Theia in lunar rocks. *Science* **344**, 1146-1150.

Hulston, J.R. and Thode, H.G. (1965) Variations in the S^{33}, S^{34}, and S^{36} contents of meteorites and their relation to chemical and nuclear effects. *Journal of Geophysical Research* **70**, 3475-3484.

Injerd, W.G. and Kaplan, I.R. (1974) Nitrogen isotope distribution in meteorites. *Meteoritics* **9**, 308-309.

Jenkins, F.A. and King, A.S. (1936) A test of the abundance of the heavy isotope of carbon in a graphite meteorite. *Publications of the Astronomical Society of the Pacific*, 323-325.

Kaplan, I.R. and Hulston, J.R. (1966) The isotopic abundance and content of sulfur in meteorites. *Geochimica et Cosmochimica Acta* **30**, 479-496.

Kaplan, I.R. and Petrowski, C. (1971) Carbon and sulfur isotope studies on Apollo 12 lunar samples. *Proceedings of the Lunar Science Conference*, 1397-1406.

Kolodny, Y., Kerridge, J.F. and Kaplan, I.R. (1980) Deuterium in carbonaceous chondrites. *Earth and Planetary Science Letters* **46**, 149-158.

Krot, A.N., McKeegan, K.D., Leshin, L.A., MacPherson, G.J. and Scott, E.R.D. (2002) Existence of an ^{16}O-rich gaseous reservoir in the solar nebula. *Science* **295**, 1051-1054.

Krouse, H.R. and Modzeleski, V.E. (1970) C^{13}/C^{12} abundances in components of carbonaceous chondrites and terrestrial samples. *Geochimica et Cosmochimica Acta* **34**, 459-474.

Kung, C.C. and Clayton, R.N. (1978) Nitrogen abundances and isotopic compositions in stony meteorites. *Earth and Planetary Science Letters* **38**, 421-435.

Lancet, M.S. and Anders, E. (1970) Carbon isotope fractionation in the Fischer-Tropsch synthesis and in meteorites. *Science* **170**, 980-982.

Langer, W.D. (1977) Isotopic abundance of CO in interstellar clouds. *The Astrophysical Journal* **212**, L39-L42.

Luz, B., Barkan, E., Bender, M.L., Thiemens, M.H. and Boering, K.A. (1999) Triple-isotope composition of atmospheric oxygen as a tracer of biosphere productivity. *Nature* **400**, 547-550.

Lyons, J.R., Lewis, R.S. and Clayton, R.N. (2009) Comment on "Experimental test of self-shielding in vacuum ultraviolet photodissociation of CO". *Science* **324**, 1516-1516.

Mandt, K.E., Mousis, O., Lunine, J.I. and Gautier, D. (2014) Protosolar ammonia as the unique source of Titan's nitrogen. *Astrophysical Journal Letters* **788**, L24 (25pp).

Manian, S.H., Urey, H.C. and Bleakney, W. (1934) An investigation of the relative abundance of the oxygen isotopes O^{16}/O^{18} in stone meteorites. *Journal of the American Chemical Society* **56**, 2601-2609.

Marty, B., Chaussidon, M., Wiens, R.C., Jurewicz, A.J.G. and Burnett, D.S. (2011) A ^{15}N-poor isotopic composition for the Solar System as shown by Genesis solar wind samples. *Science* **332**, 1533-1536.

Marty, B. (2012) The origins and concentrations of water, carbon, nitrogen and noble gases on Earth. *Earth and Planetary Science Letters* **313-314**, 56–66.

McCubbin, F.M., Steele, A., Hauri, E.H., Nekvasil, H., Yamashita, S. and Hemley, R.J. (2010) Nominally hydrous magmatism on the Moon. *Proceedings of the National Academy of Science* **107**, 11223-11228.

McKeegan, K.D. and Leshin, L.A. (2001) Stable isotope variations in extraterrestrial materials, in: Valley, J.W., Cole, D.R. (Eds.), Stable Isotope Geochemistry. Mineralogical Society of America, Washington, D.C., pp. 279-318.

McKeegan, K.D., Kallio, A.P.A., Heber, V.S., Jarzebinski, G., Mao, P.H., Coath, C.D., Kunihiro, T., Wiens, R.C., Nordholt, J.E., Moses, R.W., Reisenfeld, D.B., Jurewicz, A.J.G. and Burnett, D.S. (2011) The oxygen isotopic composition of the Sun inferred from captured solar wind. *Science* **332**, 1528-1532.

McNaughton, N.J., Borthwick, J., Fallick, A.E. and Pillinger, C.T. (1981) Deuterium/hydrogen ratios in unequilibrated ordinary chondrites. *Nature* **294**, 639-641.

Messenger, S. (2000) Identification of molecular-cloud material in interplanetary dust particles. *Nature* **404**, 968-971.

Michalski, G. and Bhattacharya, S.K. (2009) The role of symmetry in the mass independent isotope effect in ozone. *Proceedings of the National Academy of Sciences* **106**, 5493-5496.

Murphey, B.F. and Nier, A.O. (1941) Variations in the relative abundance of the carbon isotopes. *Physical Review* **59**, 771-772.

Nakamura-Messenger, K., Messenger, S., Keller, L.P., Clemett, S.J. and Zolensky, M.E. (2006) Organic globules in the Tagish Lake meteorite: Remants of the protosolar disk. *Science* **314**, 1439-1442.

Nittler, L.R., Alexander, C.M.O.D., Gao, X., Walker, R.M. and Zinner, E. (1997) Stellar sapphires: The properties and origins of presolar Al_2O_3 in meteorites. *The Astrophysical Journal* **483**, 475-495.

Nittler, L.R. (2003) Presolar stardust in meteorites: recent advances and scientific frontiers. *Earth and Planetary Science Letters* **209**, 259-273.

Onuma, N., Clayton, R.N. and Mayeda, T.K. (1970) Oxygen isotope fractionation between minerals and an estimate of the temperature of formation. *Science* **167**, 536-538.

Owen, T., Mahaffy, P.R., Niemann, H.B., Atreya, S. and Wong, M. (2001) Protosolar nitrogen. *The Astrophysical Journal Letters* **553**, L77-L79.

Prombo, C.A. and Clayton, R.N. (1993) Nitrogen isotopic compositions of iron meteorites. *Geochimica et Cosmochimica Acta* **57**, 3749-3761.

Reeves, H. and Bottinga, Y. (1972) The D/H Ratio in Jupiter's Atmosphere. *Nature* **238**, 326-327.

Reuter, J.H., Epstein, S. and Taylor, H.P., Jr. (1965) O^{18}/O^{16} ratios of some chondritic meteorites and terrestrial ultramafic rocks. *Geochimica et Cosmochimica Acta* **29**, 481-488.

Rietmeijer, F.J.M. (1998) Interplanetary Dust Particles, in: Papike, J.J. (Ed.), Planetary Materials. Mineralogical Society of America, Washington, D.C., pp. 2-1- 2-95.

Robert, F., Gautier, D. and Dubrulle, B. (2000) The solar system D/H ratio: observations and theories. *Space Science Reviews* **92**, 201-224.

Robinson, K.L., Barnes, J.J., Nagashima, K., Thomen, A., Franchi, I.A., Huss, G.R., Anand, M. and Taylor, G.J. (2016) Water in evolved lunar rocks: Evidence for multiple reservoirs. *Geochimica et Cosmochimica Acta* **188**, 244-260.

Rumble III, D. and Irving, A.J. (2009) Dispersion of oxygen isotopic compositions among 42 martian meteorites determine by laser fluorination: evidence for assimilation of (ancient) altered crust. *Lunar and Planetary Science Conference* **40**, 2293.pdf.

Saal, A.E., Hauri, E.H., Cascio, M.L., Van Orman, J.A., Rutherford, M.C. and Cooper, R.F. (2008) Volatile content of lunar volcanic glasses and the presence of water in the Moon's interior *Nature* **454**, 192-195.

Saal, A.E., Hauri, E.H., Van Orman, J.A. and Rutherford, M.A. (2013) Hydrogen isotopes in lunar volcanic glasses and melt inclusions reveal a carbonaceous chondrite heritage. *Science* **340**, 1317-1320.

Sharp, Z.D., Shearer, C.K., McKeegan, K.D., Barnes, J.D. and Wang, Y.Q. (2010) The chlorine isotope composition of the Moon and implications for an anhydrous mantle. *Science* **329**, 1050-1053.

Sharp, Z.D., McCubbin, M. and Shearer, C.K. (2013) A hydrogen-based oxidation mechanism relevant to planetary formation. *Earth and Planetary Science Letters* **380**, 88-97.

Sharp, Z.D., Williams, J., Shearer, C.K., Agee, C.B. and McKeegan, K.D. (2016) The chlorine isotope composition of Martian meteorites 2. Implications for the early solar system and the formation of Mars. *Meteoritics and Planetary Sciences* **doi: 10/1111/maps.12591**, 16 pages.

Sharp, Z.D. (2017) Nebular ingassing as a source of volatiles to the Terrestrial planets. *Chemical Geology* **448**, 137-150.

Shearer, C.K., Papike, J.J. and Rietmeijer, F.J.M. (1998) The planetary sample suite and environments of origin, in: Papike, J.J. (Ed.), Planetary Materials. Mineralogical Society of America, Washington, D.C., pp. 1-1 - 1-28.

Silverman, S.R. (1951) The isotope geology of oxygen. *Geochimica et Cosmochimica Acta* **2**, 26-42.

Smith, J.W. and Kaplan, I.R. (1970) Endogenous carbon in carbonaceous meteorites. *Science* **167**, 1367-1370.

Spicuzza, M., Day, J.M.D., Taylor, L.A. and Valley, J.W. (2007) Oxygen isotope constraints on the origin and differentiation of the Moon. *Earth and Planetary Science Letters* **253**, 254-265.

Stolper, E. (1982) Crystallization sequences of Ca-, Al-rich inclusions from Allende: an experimental study. *Geochimica et Cosmochimica Acta* **46**, 2159-2180.

Swart, P.K., Grady, M.M., Pillinger, C.T., Lewis, R.S. and Anders, E. (1983) Interstellar carbon in meteorites. *Science* **220**, 406-410.

Taylor, H.P., Jr., Duke, M.B., Silver, L.T. and Epstein, S. (1965) Oxygen isotope studies of minerals in stony meteorites. *Geochimica et Cosmochimica Acta* **29**, 489-512.

Teng, F.-Z., Watkins, J.M. and Dauphas, N. (2017) Non-Traditional Stable Isotopes, Reviews in Mineralogy and Geochemistry. Mineralogical Society of America, p. 885.

Thiemens, M. and Clayton, R.N. (1981) Nitrogen isotopes in the Allende meteorite. *Earth and Planetary Science Letters* **55**, 363-369.

Thiemens, M. (2006) History and applications of mass-independent isotope effects. *Annual Reviews of Earth and Planetary Sciences* **34**, 217–262.

Thiemens, M.H. and Heidenreich, J.E.I. (1983) The mass-independent fractionation of oxygen: A novel isotope effect and its possible cosmochemical implications. *Science* **219**, 1073-1075.

Treiman, A.H., Boyce, J.W., Gross, J., Guan, Y., Eiler, J.M. and Stolper, E.M. (2014) Phosphate-halogen metasomatism of lunar granulite 79215: Impact-induced fractionation of volatiles and incompatible elements. *American Mineralogist* **99**, 1860-1870.

Trofimov, A. (1949) Isotopic constitution of sulfur in meteorites and in terrestrial objects. *Doklady Akademii nauk SSSR* **66**, 181-184.

Urey, H.C. (1967) The abundance of the elements with special reference to the problem of the iron abundance. *Quarterly Journal of the Royal Astronomical Society* **8**, 23-47.

Villanueva, G.L., Mumma, M.J., Novak, R.E., Käufl, H.U., Hartogh, P., Encrenaz, T., Tokunaga, A., Khayat, A. and Smith, M.D. (2015) Strong water isotopic anomalies in the martian atmosphere: Probing current and ancient reservoirs. *Science* **348**, 218-221.

Vinogradov, A.P., Dontsova, E.I. and Chupakhin, M.S. (1960) Isotopic ratios of oxygen in meteorites and igneous rocks. *Geochimica et Cosmochimica Acta* **18**, 278-293.

Wiechert, U.H., Halliday, A.N., Lee, D.-C., Snyder, G.A., Taylor, L.A. and Rumble, D.I. (2001) Oxygen isotopes and the Moon-forming Giant Impact. *Science* **294**, 345-348.

Wiechert, U.H., Halliday, A.N., Palme, H. and Rumble, D. (2004) Oxygen isotope evidence for rapid mixing of the HED meteorite parent body. *Earth and Planetary Science Letters* **221**, 373-382.

Young, E., Kohl, I.E., Warren, P.H., Rubie, D.C., Jacobson, S.A. and Morbidelli, A. (2016) Oxygen isotopic evidence for vigorous mixing during the Moon-forming giant impact. *Science* **351**, 493-496.

Young, E.D. and Russell, S.S. (1998) Oxygen reservoirs in the early solar nebula inferred from an Allende CAI. *Science* **282**, 452-455.

Young, E.D., Ash, R.D., England, P. and Rumble, D. (1999) Fluid Flow in Chondritic Parent Bodies: Deciphering the Compositions of Planetesimals. *Science* **286**, 1331-1335.

Yurimoto, H. and Kuramoto, K. (2004) Molecular cloud origin for the oxygen isotope heterogeneity in the Solar System. *Science* **305**, 1763-1766.

Zinner, E. and Epstein, S. (1987) Heavy carbon in individual oxide grains from the Murchison Meteorite. *Earth and Planetary Science Letters* **84**, 359-368.

Chapter 13

EXTRATERRESTRIAL MATERIALS

Contents

13.1 Introduction 1
13.2 Classification of meteorites 2
13.3 Oxygen isotopes in the solar system 3
13.3.1 Introduction 3
13.3.2 Discovery of an ^{17}O anomaly 4
13.3.3 Possible explanations: mixing of two distinct reservoirs 6
13.3.4 Mass-independent fractionation 7
13.3.5 Oxygen isotopes in meteorites – undifferentiated bodies 9
13.3.6. Oxygen isotopes in meteorites – differentiated bodies 10
13.4 Hydrogen 11
13.4.1 Introduction 11
13.4.2 Hydrogen in chondrites 13
13.4.3 Hydrogen in differentiated meteorites. 14
13.5 Carbon 17
13.6 Nitrogen 19
13.7 Sulfur 20
13.8 Chlorine 21
References 23

Chapter 13

EXTRATERRESTRIAL MATERIALS

13.1 Introduction

Some of the earliest problems addressed with stable isotope chemistry involved the origin and heterogeneities of the solar system. Hyperbolic orbits identified (erroneously) for certain meteorites suggested that there might be matter from outside the solar system that ultimately reached the Earth. Early attempts to find exotic carbon, oxygen and chlorine isotope ratios in meteorites failed (Harkins and Stone, 1926; Manian et al., 1934; Jenkins and King, 1936), in part because precision of the measurements was not sufficiently high at the time, and also because the anomalous material that does exist was simply not analyzed. Hydrogen isotope analyses followed in the 1950's, when δD values approaching 300‰ from the carbonaceous chondrites Ivuna and Orgueil were measured (Boato, 1954). Additional isotopic systems were studied in the coming decades, including sulfur (Trofimov, 1949), nitrogen (Injerd and Kaplan, 1974) and carbon (Krouse and Modzeleski, 1970). There was a flurry of interest in lunar materials when Apollo samples were returned to Earth. Most lunar samples had $\delta^{18}O$ values very similar to equivalent terrestrial rock types, indicating a close genetic relationship between Earth and Moon. Then in 1973, Clayton *et al*. (1973) published a paper that completely changed the meteorite community. For the first time, an 'exotic' stable isotope component in meteorites had clearly been identified. From then on, stable isotope geochemistry has become one of the most important tools for constraining mechanisms of formation and history of the early solar system.

There are no distinct boundaries between traditional earth sciences, cosmochemistry, space sciences and astrophysics, and so it is difficult to limit the scope of this chapter. For example, the isotope chemistry of interstellar grains (Anders and Zinner, 1993; Nittler, 2003) is important in the study of nucleosynthesis and stellar evolution. And, at the other end of the spectrum, the chemistry of certain meteorite types is used to estimate the bulk chemical composition of the Earth. This data are then applied to terrestrial studies completely unrelated to meteorite research. All of these fields overlap one other to a certain extent. In this chapter we will limit our examinations to more traditional meteorite research. Readers interested in processes of star formation and nucleosynthesis of elements and their isotopes are referred to Anders and Zinner (1993, in appendix) and Nittler (2003) for a review and additional references. It must be stressed that the 'normal' stable isotopes (H,C,N,O,S) are not used independently of other isotopic systems, such as noble gas, non-traditional isotopes (*e.g.*, Mg, Si), and short-lived radiogenic isotopes. But again, discussion of these systems is beyond the scope of this chapter. Further information beyond the short review here can be found in Clayton (1993) for oxygen isotopes and McKeegan and Leshin (2001) for H, C, N, O stable isotope systems.

13.2 Classification of meteorites

The alphabet soup of meteorite names can be very confusing to the uninitiated, but is really not complex after a simple review. Table 13.1 and Fig. 13.1 illustrate the basic classification of meteorites.

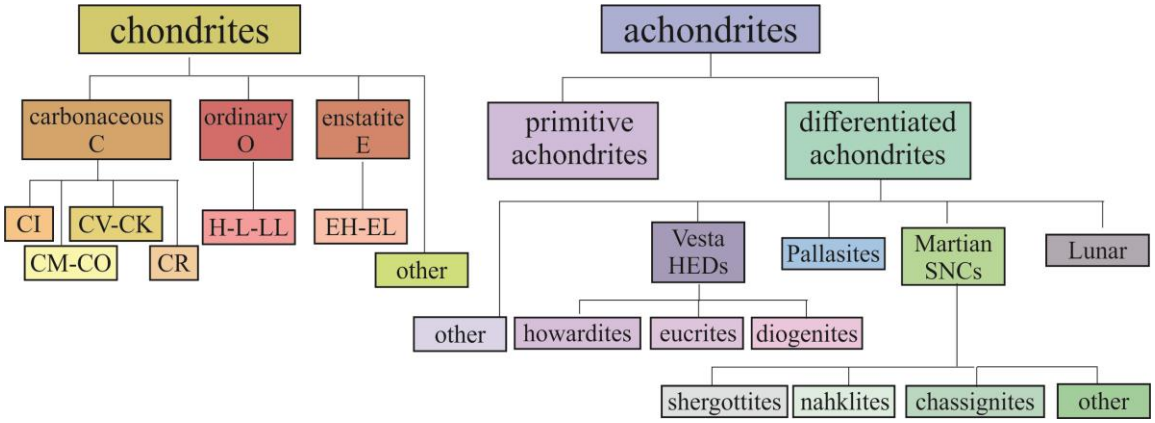

Fig. 13.1. Simplified meteorite classification. Meteorites are divided into chondrule-bearing chondrites and chondrule-free achondrites. The chondrites are further divided into carbonaceous, ordinary and enstatite chondrites. Achondrites include differentiated bodies including samples from the bodies 4-Vesta, Mars, and Moon.

The primary division of meteorites is between chondrites and achondrites. Chondrites contain chondrules[1] embedded in a fine-grained matrix. Chondrules are spherules of olivine and/or pyroxene with or without glass and metal inclusions thought to have formed by melting of nebular dust during flash heating. The fine-grained interstitial matrix consists of silicates, oxides, metal, sulfides and organic matter. The chondrites are considered to be agglomeration of rocky and icy material from unprocessed remnants of planetesimals from the asteroid belt. Chondrites also contain interstellar grains, calcium-aluminum inclusions (CAIs), and other refractory primitive objects. Achondrites are more processed material, often representing crustal magmatic or metamorphic rocks from dismembered planetesimals. Achondrites have undergone planetary differentiation, where early heating by radioactive decay of short lived isotopes caused segregation between an iron-rich core and silicate mantle. ***Iron meteorites*** are the fragments of the cores of asteroids/planetesimals. ***Stony iron meteorites***, such as pallasites, may be core-mantle boundary material, and ***stony meteorites*** are considered to be silicate mantle material of a segregated body. The origin of many achondrites can be attached to one of several large bodies, including Mars (the SNC meteorities), the Moon, and the asteroid 4 Vesta (HED[2] meteorites).

[1] CI chondrites have been so heavily aqueously altered on their parent body that no chondrules survive. Nevertheless, they come from a parent body that contained chondrules and did not go through differentiation.
[2] Howardites, Eucrites and Diogenites

Table 13.1. *Classification of different meteorite types (Brearley and Jones, 1998; Shearer et al., 1998).*

Name	**Mineralogy**	**Source**	
Iron meteorites	Iron-nickel metal; iron sulfide	Cores of disrupted asteroids	Groups distinguished by trace element abundances and textures
Stony-iron meteorites-pallasites mesosiderites	Roughly equal proportions of Fe,Ni-metal and silicate	Core-mantle boundary of disrupted asteroids?; impacts on asteroids	
Stony meteorites - achondrites			
Basaltic achondrites-howardites eucrites diogenites	Pigeonite-plagioclase-bearing basalts, orthopyroxenites, or mélange of each	Thought to be a basaltic magma system from asteroid 4 Vesta	Distinguished from other achondrite groups on the basis of oxygen isotopes
Other achondrites-aubrites, ureilites, angrites, etc.	Exotic basalts and related igneous rocks	Main belt differentiated asteroids	Each group distinguished on the basis of oxygen isotopes
Martian meteorites (SNC meteorites) – Shergottites, nakhlites chassignites, other	Magmatic basalts, lherzolites, clinopyroxenites, orthopyroxenite, dunite	Mars	Young (most <1.3Ga) *(ALH84001 is 4.5 Ga)*. Characteristic stable and rare gas isotope ratios
Lunar	Basalts, anorthosites, and lunar breccias	Moon	Compare closely with returned samples from the Apollo and Luna missions.
Stony meteorites – chondrites			
Agglomeratic rocks containing rocky and metallic materials. Unprocessed remnants of planetesimals from the asteroid belt. Some of the least processed material in the solar system. Consist of high-temperature chondrules hosted in a fine-grained matrix which represents low-T fraction of nebular material. Also contain interstellar grains, calcium-aluminum inclusions (CAIs), and other refractory objects. Groups are distinguished by chemistry and oxygen isotope ratios. Divided into types 1-6, where 3 is least altered, 2 and 1 are higher levels of low-T aqueous alteration and 4-6 are increasing levels of thermal metamorphism.			
Carbonaceous or C chondrites	8 groups – CI, CM, CR, CV, CO, CK, CH, CB; named after type fall-locality.		
Ordinary or O chondrites	3 groups – H, L and LL: H – high total Fe content; L – low total Fe content; LL – low metallic Fe		
Enstatite or E chondrites	2 groups – EH, EL: EH – high total iron; EL – low total iron		
Other classes	Rumuruti-like (R), Kakangari-like (K), Tagish Lake		
Other extraterrestrial material			
Interplanetary dust particles (IDPs)	Divided into chondritic and non-chondritic types	Active periodic comets from Oort cloud and Kuiper belt.	Primordial 'icy dust balls' (Rietmeijer, 1998). Average size is 10μm

13.3 Oxygen isotopes in the solar system

13.3.1 Introduction

The pioneers of fluorination included meteorites (or tektites) in their rock suites to fill out the general overview of natural oxygen isotope variations (Baertschi, 1950;

Silverman, 1951). Vinogradov *et al.* (1960) measured a suite of meteorites using the method of carbon reduction and found noticeable, but small $\delta^{18}O$ variations between different types. Similar conclusions were reached in a later thorough examination of different meteorite types (Reuter et al., 1965). Silicate separates from 27 chondrites varied by only 1.2‰. Chondrules had the same values as the whole rock. Pallasites were several per mil lower than the chondrites, but overall, it appeared that meteorites were not particularly interesting from a stable isotope viewpoint. In the same year, the same group (Taylor et al., 1965) found much larger variations in chondrites when they measured only pyroxene and not olivine[3]. Now the variations were larger; 9‰ for pyroxenes and 13‰ between different bulk rock samples. They developed a meteorite classification scheme of three groups with distinct $\delta^{18}O$ values.

The return of the Apollo lunar samples led to a flurry of activity by a number of stable isotope laboratories in the United States (e.g., Epstein and Taylor, 1970; Friedman et al., 1970; Onuma et al., 1970; Kaplan and Petrowski, 1971). It was quickly recognized that the $\delta^{18}O$ values of lunar basalts and anorthosites were the same as terrestrial equivalents[4]. These data demonstrated that the Earth and Moon were closely related, but said little about the genesis of the solar system.

13.3.2 Discovery of an ^{17}O anomaly

The importance of oxygen isotope geochemistry as it pertained to meteorites was recognized when Clayton *et al*. (1973) made one of the most striking discoveries in the field of planetary science. They analyzed anhydrous high temperature phases (calcium aluminum inclusions, or CAIs) from carbonaceous chondrites, mostly Allende (which had only fallen to Earth on Feb. 8, 1969, in Chihuahua, Mexico[5]). The range of $\delta^{18}O$ values was extraordinary, covering over 30‰. This in itself was far more than anyone had measured previously. But as a result of their extremely careful analytical procedure, Clayton's group found something else that was far more surprising – namely that the $\delta^{17}O$ values of these primitive samples varied in a non-mass dependent way. This discovery was made not by measuring the $\delta^{17}O$ values directly, but rather by noting that the 'apparent' $\delta^{13}C$ values of the CO_2 gas that they were analyzing was not constant. The reason and significance is worth the short explanation in the following paragraphs.

The Chicago group analyzed silicates by reacting them with BrF_5 at high temperatures[6]. The evolved oxygen was converted to CO_2 by reaction with spectroscopic graphite at high temperatures and the CO_2 was analyzed for its $\delta^{18}O$ value. This was standard procedure in most laboratories at the time. What was unusual in the Allende samples was that there was a systematic variation in the apparent $\delta^{13}C$ value of the CO_2 gas that correlated with the measured $\delta^{18}O$ value. This was puzzling because the two isotopic systems carbon and oxygen are independent of each other. The carbon comes from the graphite rod and should have a constant value, whereas the oxygen is derived

[3] Olivine is a notoriously difficult mineral to fluorinate using conventional methods. See 11.2.1 for more details.

[4] Later analyses confirmed that $\delta^{17}O$ values were also identical to terrestrial ones (Clayton and Mayeda, 1975).

[5] The other important CC meteorite that was analyzed was Murchison, which fell in Australia only a few months later.

[6] A typical reaction would be $2\ MgSiO_3 + 12/5\ BrF_5 \rightarrow 2\ MgF_2 + 2\ SiF_4 + 6/5\ Br_2 + 3O_2$.

from the fluorinated silicate. The three isotopologues of CO_2 have masses of 44 ($^{12}C^{16}O_2$), 45 ($^{13}C^{16}O_2$ *and* $^{12}C^{16}O^{17}O$) and 46 ($^{12}O^{16}O^{18}O$) [7]. In almost all known chemical fractionation mechanisms, the following relationship is valid

$$\left(\frac{^{17}O}{^{16}O}\right) \approx \left(\frac{^{18}O}{^{16}O}\right)^{0.52} \qquad 13.1,$$

which translates to $\delta^{17}O \approx 0.52(\delta^{18}O)$. (See section 3.7 for details about the three isotope system). Normally, there is no reason to measure the $\delta^{17}O$ value of a sample, because it varies with $\delta^{18}O$ according to equation 13.1. By subtracting out the ^{17}O contribution to the mass 45 isotopologue of CO_2 – the so-called ^{17}O correction – we can calculate the $\delta^{13}C$ value of CO_2 gas from the 45/44 ratio. Clayton *et al*. noticed that the calculated $\delta^{13}C$ values were changing in concert with the $\delta^{18}O$ values. What they were actually measuring, and quickly realized, was that the variations in the 45/44 ratio were $^{17}O/^{16}O$ ratios that did not conform to equation 13.1. When plotting $\delta^{17}O$ vs $\delta^{18}O$ (assuming that the $^{13}C/^{12}C$ ratio was constant), the chondrite data did not plot on the normal *Terrestrial Fractionation Line* (TFL) with slope of ~0.52 as is seen for almost all materials in the

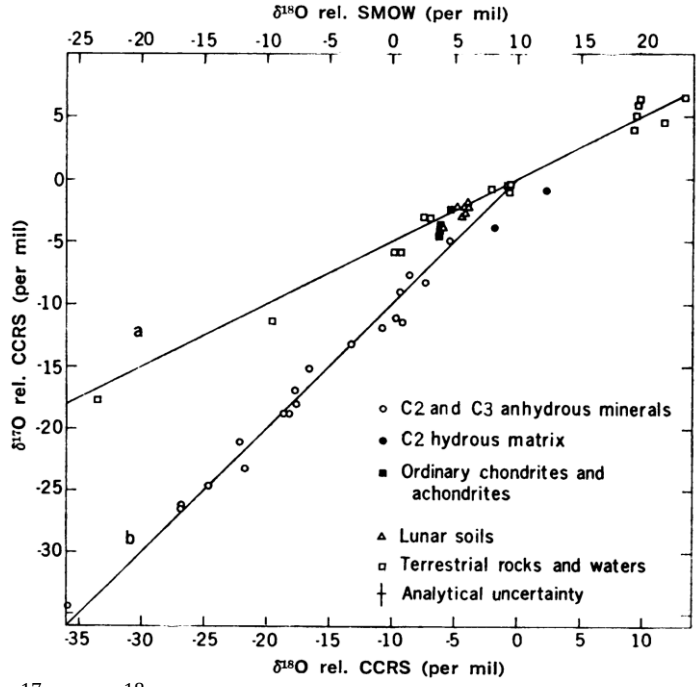

Fig 13.2. Plot of $\delta^{17}O$ vs $\delta^{18}O$ values for anhydrous (high T) chondritic samples (open circles), aqueously altered chondritic samples (filled circles) and terrestrial material. The chondrite data plot with a slope 1, whereas the terrestrial samples plot on the terrestrial fractionation line (TFL) (slope ~1/2). All data are plotted relative to a carbonaceous chondrite reference standard (CCRS) defined as the intersection of the slope 1 line from chondrite data with the TFL. Plotted in this way, the chondrite data are explained in terms of mixing between two components; a nebular gas near CCRS and a very ^{16}O enriched source, possibly from outside the solar system. Reprinted from Clayton *et al.* (1973) with permission. Note that by defining their data in terms of the carbonaceous chondrite reference standard (CCRS), the mixing line b in figure 13.1 meets the criterion $\delta^{17}O = \delta^{18}O$.

Box 13.1 The three isotope plot for oxygen.
All chemical fractionation processes (except for certain photochemical effects) fractionate the three isotopes of oxygen according to equation 13.1. On the three isotope plot $\delta^{17}O$ vs. $\delta^{18}O$, this leads to all data defining a $\delta^{17}O/\delta^{18}O$ slope of ~0.525 (mass fractionation line – *mfl*). All terrestrial samples plot on a *mfl* which approximately intersects $\delta^{17}O = \delta^{18}O = 0‰$ (vs. SMOW) and is called the *Terrestrial Fractionation Line (TFL)*. Any object that undergoes mass dependent fractionation will spread out on a *mfl* line, illustrated by the dashed line with slope 0.52 emanating from point *a*. Mixing between two reservoirs with distinct $\delta^{17}O$-$\delta^{18}O$ values will result in samples plotting on a straight line, whose slope is defined by the compositions of the two endmembers. The mixing line of slope 1 could be explained by mixing between an average nebular composition given by CCRS in Fig. 13.1 and a second component rich in ^{16}O. How far a sample plots off the *TFL* line is defined in terms of $\Delta^{17}O$ by the equation $\Delta^{17}O = \delta^{17}O - (0.52x)\cdot\delta^{18}O$. The inset box shows the $\delta^{17}O$-$\delta^{18}O$ values of samples from Mars. They plot on a *mfl* with a $\Delta^{17}O$ value of +0.3‰.

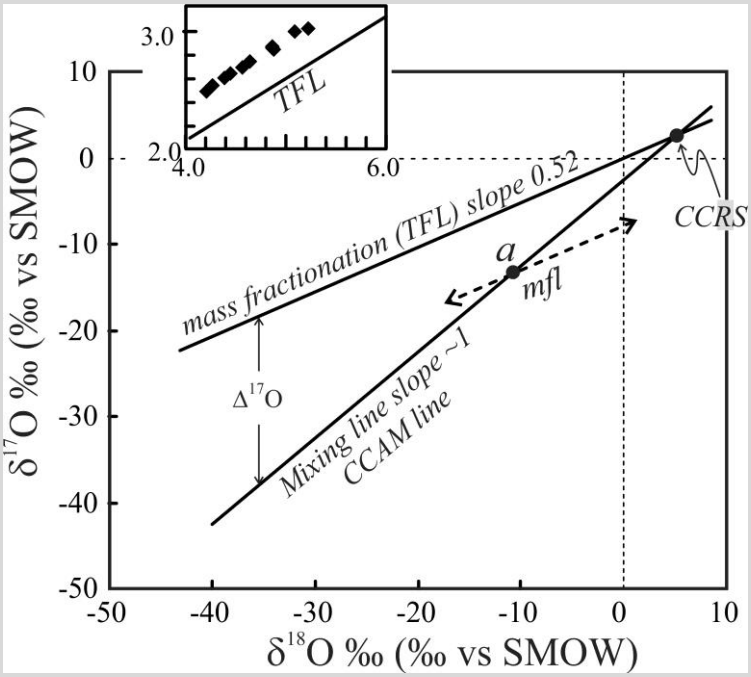

Fig. B.13.1.

Earth and Moon, but rather on a slope 1 line, below the TFL line (Fig. 13.2). (See Box 13.1 for discussion of $\delta^{18}O$ vs $\delta^{17}O$ plots).

13.3.3 Possible explanations: mixing of two distinct reservoirs

Clayton *et al.* interpreted their data as evidence for mixing between two distinct reservoirs: the first was the heavy nebular (solar) reservoir and the second was a primitive, pre-solar ^{16}O-rich dust source that originated outside of the solar system.

Clayton *et al*. postulated that the ^{16}O-rich component was probably extremely impoverished in ^{17}O and ^{18}O, as might be expected from oxygen formed from a young helium burning star, where only ^{16}O is produced. Clayton (1993) assigned $\delta^{17}O$ and $\delta^{18}O$ values to the solar nebula of 24.2 and 30‰, respectively while the light exotic dust component had $\delta^{17}O$ and $\delta^{18}O$ values of a composition with $\delta^{18}O$ = ~-42‰, and ~-40‰. A linear trend is seen in the triple oxygen isotope data of CAIs with a slope of 0.96, resulting from simple mixing between the ^{16}O-rich and nebular components.

The original 'mixing of two reservoirs' explanation for the oxygen isotope trends in early-formed material has some inconsistencies, which alternative models have sought to explain. Some of the concerns are the following:

- If the ^{16}O-rich component formed by stellar nucleosynthesis of helium burning, then the $\delta^{18}O$-$\delta^{17}O$ values should correlate with other isotope systems, such as Mg and Si. However, no such correlations are found.
- The presolar component should be nearly pure ^{16}O. However all measurements of CAI inclusions have $\delta^{18}O$-$\delta^{17}O$ values that 'bottom-out' around -50 to -40‰ (McKeegan and Leshin, 2001). Only presolar grains have lower values (Nittler et al., 1997; Amari, 2014), but the estimated abundance of such grains is less than 0.25 parts per billion. If the exotic ^{16}O rich source was not pure ^{16}O, then why is the $^{18}O/^{17}O$ ratio the same as the solar nebular value (thereby giving the slope 1 line)?
- If an ^{16}O-rich melt exchanged with the solar nebular gas during crystallization, the degree of ^{17}O and ^{18}O enrichment should correlate with the order of crystallization, which is not the case. Melilite has the highest $\delta^{18}O$-$\delta^{17}O$ values, but should crystallize before pyroxene (Stolper, 1982). Alternatively, exchange with the heavy nebular gas occurred by diffusion. Appropriate diffusion data are not sufficient to properly evaluate this possibility.

13.3.4 Mass-independent fractionation

An alternative to the two reservoir mixing hypothesis was born when Thiemens and Heidenreich (1983) discovered that ozone (O_3) produced by dissociation of molecular oxygen (O_2) in a high frequency discharge occurred with a mass-independent fractionation. The $\delta^{18}O$-$\delta^{17}O$ values of the residual oxygen and newly-formed ozone plot on a slope 1 line (Fig. 13.3), nearly identical to the slope for carbonaceous chondrite mineral inclusions found by Clayton *et al* (1973).

Thiemens and Heidenreich initially suggested a mechanism of optical self-shielding to explain the mass-independent fractionation. O_2 gas undergoes strong absorption of ultraviolet light by the Schumann-Runge absorption bands between 1.76×10^{-7}m and 1.926×10^{-7} m, causing photodissociation of O_2. The absorption bands are slightly different for ^{16}O-^{16}O and the other isotopologues ^{17}O-^{16}O and ^{18}O-^{16}O. Because >99.5% of O_2 consists of $^{16}O_2$, radiation corresponding to $^{16}O_2$ will strongly be absorbed (or self-shielded), so that only the wavelengths absorbed by ^{17}O-^{16}O and ^{18}O-^{16}O will filter through to the center of the reaction chamber. These UV rays will then cause mass-independent dissociation of the rare isotopologues ^{17}O-^{16}O and ^{18}O-^{16}O. The dissociated ^{17}O and ^{18}O ultimately react with $^{16}O_2$ to form ozone. Figure 13.3 shows the ozone

enriched in the heavy isotopes and the residual O_2 with preferential removal of ^{18}O and ^{17}O.

More recently, it has been shown that it is the role of symmetry that is the primary cause of the non-mass dependent fractionation (e.g., Michalski and Bhattacharya, 2009). The O_2 starting material is photo-dissociated by UV radiation. The O radicals react with surrounding O_2 to O_3 via a metastable transition state. The stability of the transition state is function of the symmetry. Highly symmetric transition state $^{16}O_3$ is less stable than ^{16}O-1^6O-^{17}O and ^{16}O-^{16}O-^{18}O, both of which have a lower symmetry. As a consequence, stable O_3 is enriched in both of the rare isotopes without distinction between ^{17}O and ^{18}O. The data therefore define a MIF line with a slope of 1. Such ^{17}O and ^{18}O enriched O_3 is observed in the stratosphere (Thiemens, 2006). The positive anomaly of stratospheric O_3 is counterbalanced by a marked negative anomaly of tropospheric O_2 (Luz et al., 1999).

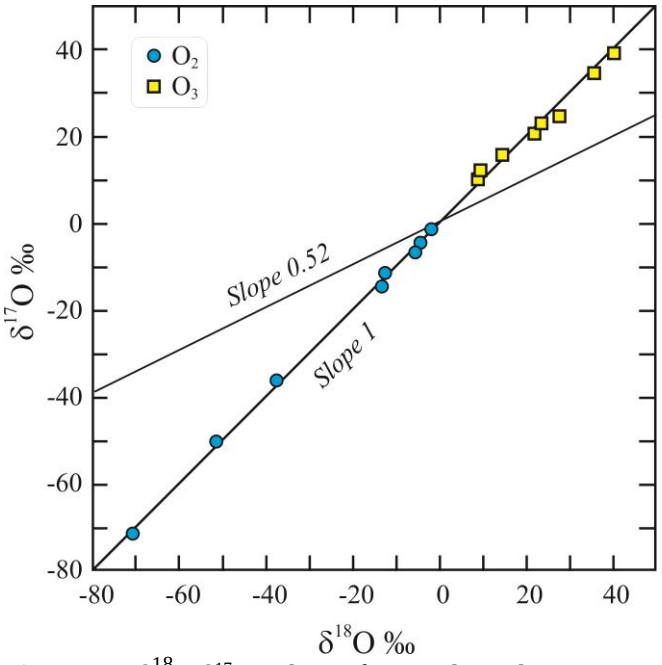

Fig. 13.3. $\delta^{18}O$-$\delta^{17}O$ values of O_2 and O_3 during ozone formation by high-frequency discharge. The product ozone is enriched in both ^{17}O and ^{18}O by a mass-independent mechanism, which was believed to be due to self-shielding (Thiemens and Heidenreich, 1983).

Mass independent isotope fractionation has been predicted to occur in interstellar clouds by the process of self-shielding. Some interstellar clouds appear to be enriched in ^{13}CO by a factor of 2.3 compared to the Sun. Langer (1977) suggested that the enrichment is the result of self-shielding in the interstellar clouds. Bally and Langer (1982) showed that the CO gas of interstellar clouds is enriched in ^{16}O as well. Thiemens (1999) and Clayton (2002) extended the model to our own solar system.

The idea behind the self-shielding hypothesis is the following: CO is dissociated by distinct frequencies of UV radiation. The molecular cloud would be more opaque to the frequencies absorbed by $C^{16}O$ rather than $C^{17}O$ and $C^{18}O$ due to the former's much higher concentration. Radiation that is only absorbed by the rare isotopologues is able to penetrate far more deeply into the molecular cloud. As a result, only the rare isotopes $C^{17}O$ and $C^{18}O$ are dissociated in the cloud's interior. The oxygen produced by this dissociation then combines with hydrogen to produce ^{17}O- and ^{18}O-enriched water ice, which ultimately becomes incorporated in solid phases (Yurimoto and Kuramoto, 2004). Chakraborty *et al.* (2008) suggested that self-shielding was not necessary, arguing that the ^{17}O and ^{18}O enrichment in CO could be due to a stronger coupling coefficient, in which $C^{17}O$ and $C^{18}O$ are more efficiently dissociated than $C^{16}O$. This idea has been questioned (Lyons et al., 2009), but regardless of the actual mechanism, preferential photodissociation of $C^{17}O$ and $C^{18}O$ in the molecular cloud can lead to ^{17}O- and ^{18}O-

enriched H_2O. The H_2O is ultimately incorporated in chondrites which will lead to a heavy oxygen component relative to the overall nebular value.

With the new model, we would expect the solar nebula and Sun to have $\delta^{18}O$-$\delta^{17}O$ values of ~-50‰, in contrast to the Clayton mixing model where the solar component is the heaviest (> +20‰). Evidence for a low $\delta^{18}O$-$\delta^{17}O$ solar wind was found by Hashizume and Chaussidon (2005), who measured the $\delta^{18}O$ and $\delta^{17}O$ values of solar energetic particles that had been implanted in metal grains on the lunar regolith. The measured $\Delta^{17}O$ value of the solar particles was -33±16‰, corresponding to a protosolar nebula of ~-67‰ for $\delta^{18}O$ and $\delta^{17}O$ (when appropriate fractionations are considered). More recently, direct analysis of solar wind implanted on SiC targets during the NASA Genesis mission were made (McKeegan et al., 2011). The calculated value for the Sun is $\delta^{17}O$ = -59.1‰ and $\delta^{18}O$ = -58.5‰ (vs SMOW). The $\delta^{17}O$-$\delta^{18}O$ slope 1 data for the CCAM samples is then explained by simple mixing with the light nebular reservoir (Sun) and a molecular cloud enriched in ^{18}O and ^{17}O due to photochemical reactions. Young and Russell (1998) suggested that the mixing between these two reservoirs has a slope of exactly 1.0, and that the shallower slope of 0.996 suggested by Clayton's early work is explained by aqueous alteration of some meteoric material.

13.3.5 Oxygen isotopes in meteorites – undifferentiated bodies

The bulk isotopic compositions of meteorite parent bodies generally fall on a mixing line between the isotopically light solar component and heavy 'ice-derived' component. Further modification due to volatile loss to space and low temperature reequilibration/alteration expands the isotopic range to higher $\delta^{18}O$ and $\delta^{17}O$ values with a slope less than 1. Each meteorite group occupies a distinct isotopic range (Fig. 13.4), although there is some overlap between groups. Indeed, one of the most diagnostic tools used for categorizing meteorites is the triple oxygen isotope composition.

The overall oxygen isotope compositions of different extraterrestrial materials are explained in the following way. The earliest-formed anhydrous phases plot with low $\delta^{17}O$-$\delta^{18}O$ values that are equilibrated with the unmodified nebula (Krot et al., 2002). Later-formed silicate minerals follow a mixing line with a slope close to or equal to 1 (the CCAM line) to higher delta values due to mixing with the isotopically heavy H_2O-derived component. Alteration occurring on a parent body with an aqueous fluid causes the isotope composition of that body to spread out along a mass dependent fractionation line, and loss of light water from a small body will draw the combined $\delta^{17}O$-$\delta^{18}O$ values upward (Young et al., 1999). Under equilibrium conditions, the slope defined by a set of samples from a single body will be ~0.52, characteristic of mass-dependent fractionation. The highest $\delta^{17}O$ and $\delta^{18}O$ values are found in highly altered CM and CI chondrites. These hydrous, highly oxidized samples have experienced high fluid/rock ratios and their oxygen isotope compositions reflect the heavy aqueous component. Chondrite classes that plot with distinct slopes between 0.52 and 1, such as the CR chondrites, are thought to represent partial mixing between material plotting along the CCAM line and unrelated altered material. Alteration with an aqueous fluid will tend to cause the isotope data to spread out on a mass dependent fractionation line, and loss of light water to space will draw the combined $\delta^{17}O$-$\delta^{18}O$ values towards higher values (Young et al., 1999).

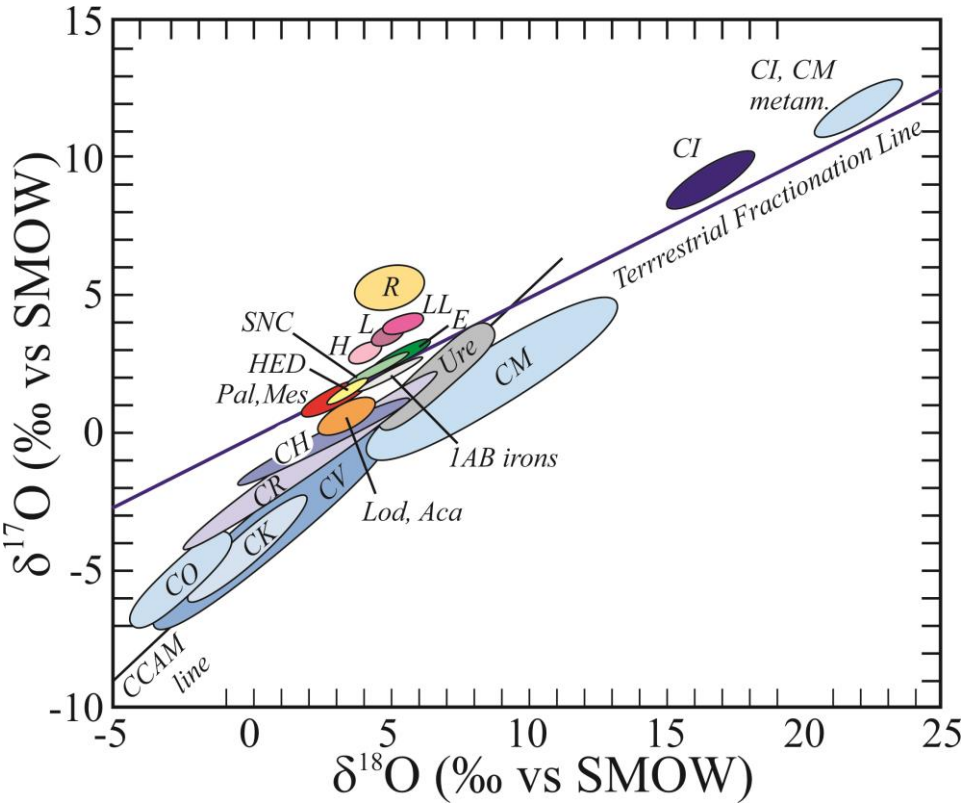

Fig. 13.4. Oxygen isotope fields for different meteorite types. Apollo (lunar) samples plot essentially on the Terrestrial Fractionation Line. Most Martian meteorites have $\delta^{18}O$ values between 3.5 and 5.5 with a $\Delta^{17}O = 0.32$ (Franchi et al., 1999). A Martian basaltic breccia has higher $\delta^{18}O$ values (5.6-7.5) and a distinctly high $\Delta^{17}O$ value of 0.58±0.01 (Agee et al., 2013). The Moon is virtually indistinguishable from Earth. Abbreviations: Ure – urelites; Pal, Mes – pallasites, mesosiderites; HED – howardites, eucrites, diogenites; SNC – shergottites, nakhlites, chassignites (most Martian meteorites), Lod, Aca – lodranites, acapulcoites; E – enstatite chondrites; C – carbonaceous chondrites; H, L, LL – ordinary chondrites; R – R chondrites. Compiled from various sources.

13.3.6. Oxygen isotopes in meteorites – differentiated bodies

Samples from a well-mixed, differentiated body should plot on a mass dependent fractionation line passing through the bulk $\delta^{17}O$-$\delta^{18}O$ value of that body, and indeed this is the case. Most samples from differentiated bodies, including the Moon, Mars, HEDs (4 Vesta), angrites, aubrites, mesosiderites, and pallasites, all fall on $\delta^{17}O$-$\delta^{18}O$ arrays with a slope of ~0.525, parallel to that of the Earth (Fig. 13.5). The $\delta^{17}O$-$\delta^{18}O$ array for the Earth and Moon are virtually indistinguishable. It is generally accepted that the Earth-Moon system formed during the collision of a Mars-sized body (informally called Theia) with the proto Earth approximately 60-100 Ma after the formation of our solar system (the collapse of the proto solar nebula). The remarkably similar $\Delta^{17}O$ values for lunar and terrestrial samples suggests that the two bodies either had identical initial $\Delta^{17}O$ values or that the two bodies were well mixed during the Giant Impact responsible for the Earth-Moon system.

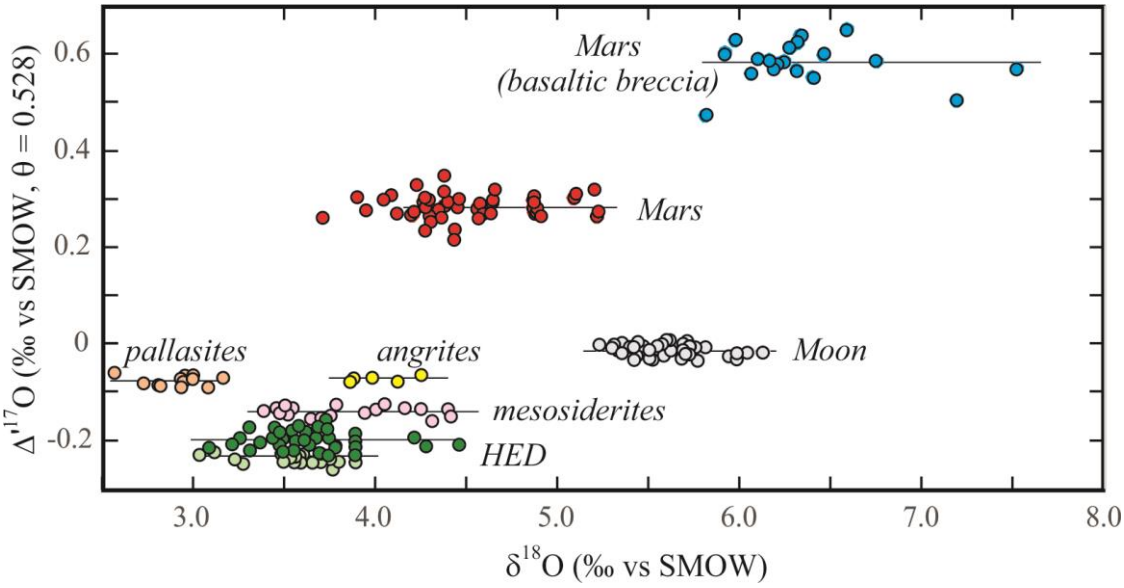

Fig. 13.5 Triple oxygen isotope composition of differentiated meteorites. The $\Delta'^{17}O$ values are defined as $\Delta'^{17}O = \delta'^{17}O - 0.528\times\delta'^{18}O$, where the ' refers to the linearized delta value (see Text box 3.1). The data for each group of differentiated meteorites defines a linear array consistent with isotopic equilibrium for the three isotope system. Two HED data sets are plotted: (Wiechert et al., 2004, dark green) and (Greenwood et al., 2005, pale green). Both show flat trends. The difference in the two data sets is probably due to slightly different calibration standards. Data from the following sources: (Franchi et al., 1999; Wiechert et al., 2001; Wiechert et al., 2004; Greenwood et al., 2005; Greenwood et al., 2006; Spicuzza et al., 2007; Rumble III and Irving, 2009; Greenwood et al., 2012; Agee et al., 2013; Herwartz et al., 2014; Young et al., 2016).

13.4 Hydrogen

13.4.1 Introduction

The D/H ratios of materials in our Galaxy span such an enormous range as to strain the utility of the delta notation. Solar wind is virtually deuterium-free, with δD values approaching -1000‰. At the other end of the spectrum, cold molecular clouds have spectroscopically-measured D/H ratios as high as 10^{-1}, corresponding to >600,000‰ (see Robert et al., 2000 for a review of galactic values). Hydrogen isotope systematics differ significantly from those of oxygen, and the information available from D/H ratios is quite different as well. Hydrogen has only two stable isotopes, in place of oxygen's three, so that mixing of distinct sources can only be tracked in 'one dimension' instead of two. Hydrogen, while far and away the most abundant phase in molecular clouds and our solar system, is rare in solids preserved in meteorites. And finally, the isotopes of hydrogen have a very different formation history than oxygen. Oxygen is produced during star-forming events, with each isotope identified with specific nucleosynthetic processes. Deuterium, in contrast, was formed in the Big Bang (Burbidge et al., 1957). There is no additional stellar input to the primordial mix. For oxygen, the solar isotope abundances define the starting point for the composition and evolution of the solar system. For the hydrogen-deuterium system, the Sun is of no help in giving us average

solar system values, as all deuterium was 'burned' during contraction of our proto-Sun[8].

The D/H ratios of various materials are shown in Fig. 13.6. The D/H ratio following the Big Bang is estimated as $67\text{-}90\times10^{-6}$ or -520 to -420‰ (Copi et al., 1995). Deuterium is destroyed during star burning, so that the average D/H ratio of the Universe has decreased with time. Spectroscopic analysis of local interstellar medium gives a D/H ratio of $(14\text{-}17)\times10^{-6}$. The presolar D/H ratio is estimated at ~ $(20\pm3.5)\times10^{-6}$ using the ^{3}He/H ratio of the solar wind. Jupiter can also be used as a proxy for the presolar D/H

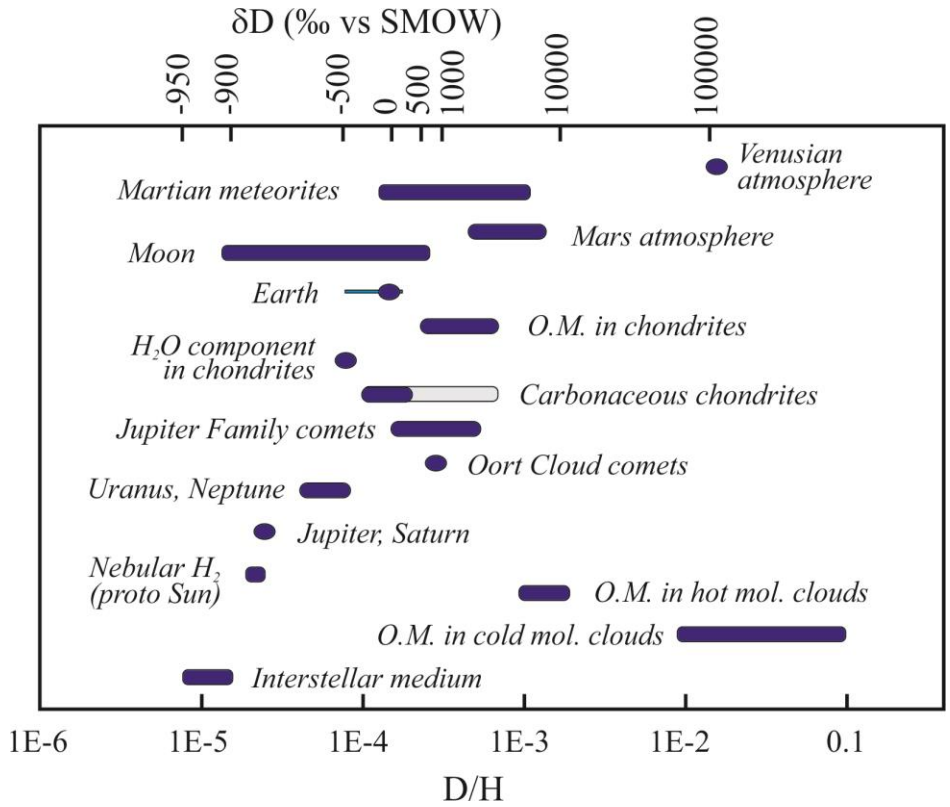

Fig. 13.6 D/H ratios for galactic and solar system bodies. The solar nebula (measured for Jupiter and Saturn and inferred for the proto Sun are nearly pure H_2. High δD values of organic matter in molecular clouds is explained by extreme fractionation during ion exchange reactions. The high D/H ratios of Venus are thought to be due to hydrodynamic escape of protium to space. Comets are generally light although several Jupiter family comets have measured D/H ratios that overlap the bulk Earth value. The bulk Earth is ~ -40‰. The full range of Earth values is given by the thin dark line. Most carbonaceous chondrites fall in the dark blue range, although anomalous heavy chondrites (Ornans, Semarkona) have δD values as high as >2000‰ (grey band). Data from compilations of Robert *et al.* (2000) and Sharp (2017).

ratio. Jupiter formed very shortly after the birth of our solar system, and because of its enormous size, Jupiter would have incorporated all hydrogen in its orbit without fractionation. Spectroscopic analysis of Jupiter gives a D/H ratio of Jupiter $(26\pm7)\times10^{-6}$, which is in excellent agreement with the solar estimate. Knowing the baseline for the D/H ratio of the solar system, allows us to explain higher D/H ratios of terrestrial and

[8] Of all the isotopes of all elements, deuterium is the most easily destroyed in thermonuclear reactions.

extraterrestrial materials in terms of preferential incorporation of deuterium during various discrimination processes in the solar nebula.

There are enormous deuterium enrichments in dense molecular clouds. D/H ratios as high as 10^{-1} and 10^{-3} are detected in organic matter from cold (10 K) and hot (>80 K) molecular clouds, respectively. Such high δD values (>600,000‰) can only be achieved by isotopic enrichments occurring at extremely low temperatures. Normal gaseous exchange reactions do not occur at such low temperatures. Instead, ion exchange reactions, in which gaseous molecules are ionized by ultraviolet radiation and then undergo isotopic exchange, are called upon to explain the extreme deuterium enrichments. Two such reactions are (Robert et al., 2000)

$$H_3^+ + HD \Leftrightarrow H_2D^+ + H_2 \qquad 13.2$$

and

$$CH_3^+ + HD \Leftrightarrow CH_2D^+ + H_2 \qquad 13.3.$$

With this process in mind, organic matter formed under low temperature conditions in the nebula should be extremely heavy, and indeed, δD values well above 1,000‰ and approaching 12,000‰ have been measured (Alexander et al., 2010). These extreme values are explained as a result of low temperature reactions similar to equation 13.3 and/or oxidation of H_2O at low temperatures producing very light H_2 which was removed from the system.

At low temperatures, the fractionation between H_2O and H_2 are extremely large. $\alpha_{H2O\text{-}H2}$ values range from 9.5 at 180 K to 5.5 at 230 K (Reeves and Bottinga, 1972). Oxidation of H_2 to H_2O at such low temperatures could therefore lead to extreme D enrichments resulting in δD values easily approaching +500‰. *In situ* D/H analyses of phyllosilicates in the matrix of the ordinary chondrite Semarkona are remarkably high, reaching values of 3300 to 4600‰ (Deloule and Robert, 1995). Such extreme values can be explained by the ion exchange reaction given by equation 13.2 above at temperatures on the order of 110-140 K.

13.4.2 Hydrogen in chondrites

The first hydrogen isotope measurements of meteorites gave 'unearthly' high δD values up to +300‰ (Boato, 1954). The range was greatly expanded in the 70's and 80's. For example, Kolodny *et al.* (1980) measured δD values between -70 and +771‰ from seven carbonaceous chondrites. McNaughton *et al.* (1981) measured values as high as 3,000‰ in several ordinary chondrites. δD values of bulk chondrites typically range from ~-200 to in excess of +600‰ and vary with chondrite type (Fig. 13.7). The bulk values are a mixture of phyllosilicate hydrogen (*e.g.*, water) and organic matter. Alexander *et al.* (2012) measured the hydrogen isotope composition and C/H ratios of a large number of chondrites. They plotted the δD values against the C/H ratios and extrapolated the best-fit line to a C/H ratio of 0, following the approach of Kolodny *et al.* (1980). They interpreted the y-intercept (C/H = 0) as the phyllosilicate portion of the mixture, which is essentially the hydrous component of the phyllosilicate. The H_2O contents have δD values of -500‰ (CM, CI and CO chondrites) and +100‰ (CR chondrites). The result is in excellent agreement with the earlier work of Kolodny *et al.* (1980), and can be explained by low

temperature equilibrium fractionation between solar H_2 and small amounts of oxidized H_2O.

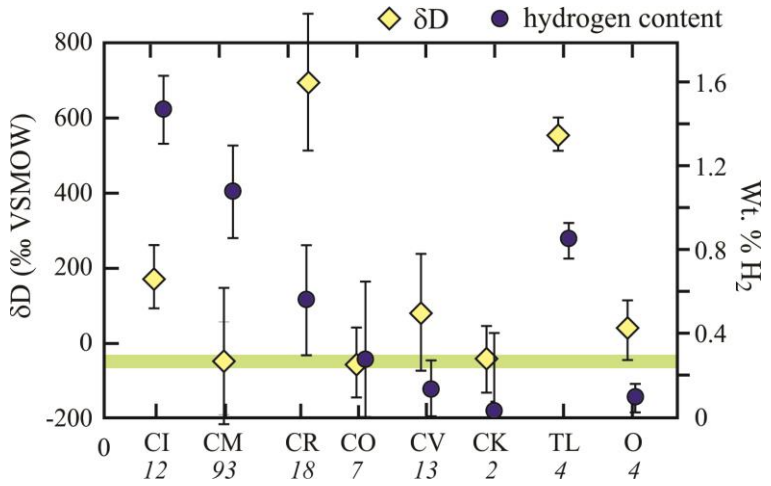

Fig. 13.7. H_2O content and δD values of chondritic meteorites. The green band is the bulk Earth δD value. O- ordinary chondrites; TL – Tagish Lake. From Sharp (2017). Italicized numbers refer to number of analyses made.

13.4.3 Hydrogen in differentiated meteorites.

The source of hydrogen in differentiated bodies is an unsettled question. The Earth, Moon and Mars all have some 'water component', where 'water' is loosely defined as the hydrogen-bearing phase. On Earth, a significant portion of H does occur as water in the ocean today, with equal or likely greater amounts in the mantle and perhaps core. Mars has evidence for large quantities of water in the past (Villanueva et al., 2015), and even the Moon, which was long thought to be devoid of hydrogen, has now been shown to contain hydrogen in trace quantities in minor phases, such as melt inclusions and apatite grains[9] (Saal et al., 2008; McCubbin et al., 2010). Other differentiated bodies, such as the HEDs, also have H-bearing phases.

The surprising thing is that the terrestrial planets are thought to have formed inside the 'snow line' or 'frost line' and therefore should not contain any indigenous water. During collapse of the proto-nebular cloud, adiabatic heating during infall of the nebular cloud to a disk would have raised the temperature of the disk to 1250-1450°C. Subsequent cooling would lead to condensation of the elements in relation to their volatility. Hydrogen condenses as water ice at temperatures of ~150 K and the solid ice is then incorporated into the growing planetesimals. The snow line is the inferred region inside of which temperature were too high for H_2O to condense *prior* to dissipation of the nebular cloud. The snow line is thought to have been at the radial position of the asteroid belt. As a result, the growing terrestrial planets sunward of this radial distance should not have incorporated any water. And yet we see that all of the terrestrial planets (perhaps with the exception of Mercury) have or had significant amounts of water. The question then becomes 'how did these bodies, inside of the snow line, acquire their water?

[9] Water ice has been detected in the permanently shadowed regions of the south pole. The origin for this water is likely due to delivery from comets.

A number of hypotheses have been proposed to explain the incorporation of water by the terrestrial planets (see Sharp, 2017 for a detailed review). These include direct incorporation of nebular H_2 gas, addition of hydrous bodies from beyond the snow line and late addition to the planets by bombardment from carbonaceous chondrites – the so called 'late veneer' or 'late accretion' hypothesis.

The late veneer hypothesis has received considerable attention because it explains the high concentration of highly siderophile (HSE) elements in the mantle. The HSEs (Os, Ir, Ru, Rh, Pt, Pd, Re, Au) are strongly partitioned into iron metal. As a result, they should have been completely sequestered into the core during early planetary formation. The higher-than-expected concentration of the HSEs in the mantle was first explained by late addition of chondritic material following core formation. Addition of 0.7% chondritic material after the Giant Impact event responsible for the Moon formation is sufficient to explain the elevated HSE abundance of Earth's mantle. If the impactors were hydrous chondrites, represented by CM chondrites, then the δD value of late accreted material would match that of Earth with ~2% delivery needed to account for the minimum estimate of the Earth's water content.

If a significant fraction of chondrite types *other* than CM were delivered during late accretion, then the integrated δD value of the delivered material would be too high to match Earth. This deuterium excess could be counterbalanced by light hydrogen if direct ingassing of nebular H_2 occurred as the planetesimals were nearing their final size (Sharp, 2017). Ingassing of light nebular H_2 also allows for the possibility of some heavy cometary volatiles to be added to the Earth system. Marty *et al.* (2012) conclude that the H and N isotope composition of Earth is explained by a combination of chondritic and solar compositions without isotopic fractionation during hydrodynamic escape. Sharp (2017) proposed that a combination of nebular ingassing followed by hydrodynamic escape and late addition of chondritic and cometary material explains the isotopic composition of Earth as well as the high $f(O_2)$ of the mantle. Primordial ^3He, found in many mantle hot spots may also be sourced directly from nebular ingassing. The remarkably high δD value 125,000‰ for the atmosphere of Venus is explained by near complete loss of H by heating of the upper atmosphere by extreme ultraviolet radiation from the early Sun and hydrodynamic escape of H or H_2 through a CO_2-rich atmosphere (Donahue et al., 1982). Whether the Earth has had its D/H ratio modified by hydrodynamic escape remains unresolved.

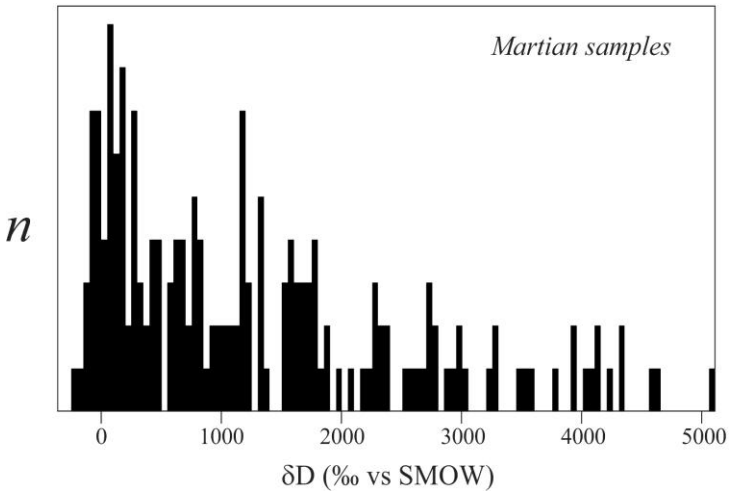

Fig. 13.8. Compilation of δD values of Martian meteorites. Most analyses are from ion microprobe measurements of apatite grains. Compilation from Sharp, (2017).

Like Venus, although to a much lesser extent, the Martian atmosphere also has a high δD value (δD = 4000‰), again explained by preferential loss of H_2 to space. Martian meteorites have a wide range of δD values ranging from near zero up to 5,000‰ (Fig. 13.8).

Until recently, most hydrogen in lunar samples was thought to be due to solar wind implantation (Epstein and Taylor, 1970). The δD value of hydrogen extracted from lunar soils is between -890‰ and -1000‰, explained as being entirely sourced by deuterium-free solar wind. Hydrogen was recognized as a primary phase in lunar glass (Saal et al., 2008; Saal et al., 2013) and the volatile-rich phase apatite ($Ca_5(PO_4)_3(OH,F,Cl)$) (McCubbin et al., 2010). The δD values of lunar apatites cover an extremely wide range (Fig. 13.9). The unmodified bulk Moon is thought to have a δD value equal to or higher than Earth (Hauri et al., 2017). The lowest values (not shown in Fig. 13.9 are measured on bulk lunar soil samples. The δD values approach -1,000‰ and are explained as direct implantation of protium-rich solar wind. The highest δD values are either due to heavy cometary input (Greenwood et al., 2011) or loss of H_2 to space during degassing (Sharp et al., 2013). Low δD values (~-600 to -300) may represent a distinct volatile source (Robinson et al., 2016) that may be tapping a nebular ingassing component (Sharp, 2017).

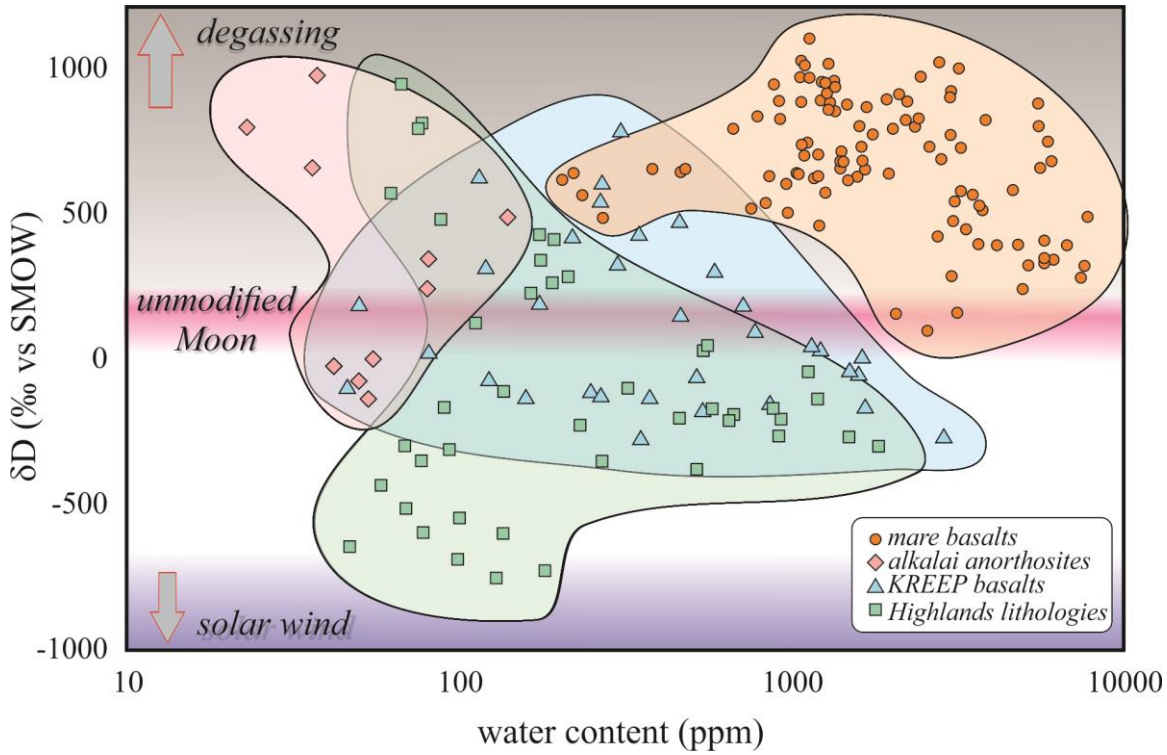

Fig. 13.9. Hydrogen isotope values *vs.* water content [H_2O] of lunar apatite grains. Different lithologies have distinct [H_2O]-δD fields. Mare basalts have the highest [H_2O] and δD values. Modified from Robinson *et al.* (2016).

13.5 Carbon

Carbon isotope analyses of meteorites began extremely early-on in the stable isotope game, motivated by the identification of a distinct spectroscopic bands found in N-type stars attributable to high concentrations of $^{12}C^{13}C$. In 1936, several attempts were made to measure the $^{13}C/^{12}C$ ratio of graphite from Canyon Diablo iron meteorite using spectrographic measurements of graphite discharge. Unfortunately, the spectrographic image was identical to that obtained from terrestrial graphite (e.g., Jenkins and King, 1936), suggesting that no ^{13}C anomaly existed in meteorites. Murphey and Nier (1941) determined the carbon isotope composition of 'meteorite carbon' from seven samples, which ranged from -33 to -11 ‰ (approximate PDB scale). Additional analyses in the coming decades also found that meteoritic carbon had $\delta^{13}C$ values that overlapped with terrestrial values. The first anomalous values were found in the carbonate fraction of two carbonaceous chondrites (Orgueil and Ivuna), where $\delta^{13}C$ values of ~+60‰ (PDB) were measured on the dolomite fraction (Clayton, 1963). Along with Boato's early high δD values in meteorites, this was one of the first findings of anomalous stable isotope ratios in extraterrestrial material.

In the same year, Briggs (1963) reported $\delta^{13}C$ values of solvent-extractable organic material from carbonaceous chondrites that were only slightly less than 0‰, higher than terrestrial equivalent organic matter. The anomalous $\delta^{13}C$ values provided some of the strongest evidence to date that organic material in meteorites was indeed of extraterrestrial origin.

Two papers appearing in 1970 expanded the data base for carbonaceous chondrites (Krouse and Modzeleski, 1970; Smith and Kaplan, 1970). Both showed very high $\delta^{13}C$ values of carbonates and less convincing, but still high, $\delta^{13}C$ values of organic extracts (Fig. 13.10). The data were clearly incompatible with a terrestrial carbon origin. Instead, the 'endogenous' carbon (Smith and Kaplan, 1970) in carbonaceous meteorites was firmly established.

The emerging picture was that the $\delta^{13}C$ values of organic carbon averaged around -16‰, while the much less abundant carbonate had $\delta^{13}C$ values as high as +60 or +70‰. The fractionation of >80‰ between the oxidized and reduced form was far larger than what was observed on Earth, where the differences were only on the order of 25 to 30‰. Urey (1967) considered two distinct carbon synthesis events in the solar system as a possible explanation. Several year later, Lancet and Anders (1970) proposed an alternative explanation that did not require an exotic carbon source. They showed experimentally that oxidation-reduction reactions of CO (Fischer-Tropsch synthesis) given by

$$n\,CO + (2n + 1)\,H_2 \rightarrow C_nH_{2n+2} + n\,H_2O \qquad 13.4$$

and

$$2n\,CO + (n + 1)\,H_2 \rightarrow C_nH_{2n+2} + n\,CO_2 \qquad 13.5$$

could produce large carbon isotope fractionations. In this reaction, both oxidized and reduced carbon are formed abiogenically. Another possible low-temperature exchange reaction is

$$^{12}CO + {}^{13}C^{+} \rightarrow {}^{13}CO + {}^{12}C^{+} \qquad 13.6.$$

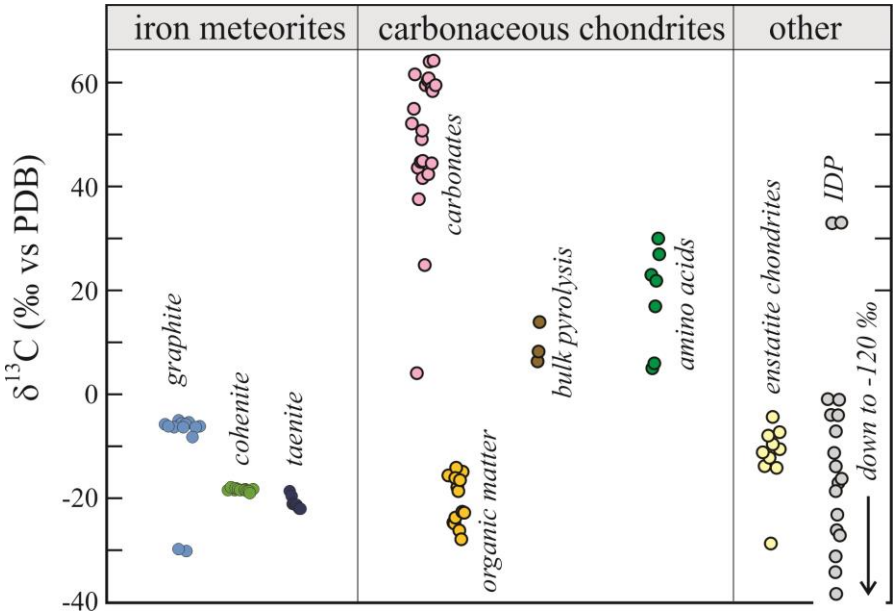

Fig. 13.10. Carbon isotope composition of different extraterrestrial materials. The Sun has a $\delta^{13}C$ value of -105±20‰. All other materials have higher $^{13}C/^{12}C$ ratios (except one IDP), consistent with low temperature reactions that enrich solid phases in ^{13}C. Data from the following sources: (Craig, 1953; Clayton, 1963; Krouse and Modzeleski, 1970; Smith and Kaplan, 1970; Deines and Wickman, 1975; Grady et al., 1986; Epstein et al., 1987; Engel et al., 1990; Messenger, 2000; Hashizume et al., 2004).

The low temperature oxidation-reduction reactions can explain the high $\delta^{13}C$ value of most solar system materials relative to the Sun. The Sun is thought to have a $\delta^{13}C$ value of -105±20‰ (Hashizume et al., 2004). Interplanetary dust particles (IDPs) have a very wide range of $\delta^{13}C$ values from -120 to +33‰ (Messenger, 2000), consistent with a low protosolar nebula value and heavier samples resulting from low temperature reactions such as 13.4 -13.6.

The isotopic composition of individual amino acids from CM chondrites have been measured (Engel et al., 1990). The $\delta^{13}C$ values are as high as +30‰, clearly of extraterrestrial origin. Interestingly, the measured samples are not racemic[10], which had been used as previous evidence for terrestrial contamination. The high $\delta^{13}C$ values eliminate contamination as a possibility of their origin. The isotopic ratios of nitrogen, and hydrogen from the hydroxy acids from Murchison are also extraterrestrial, with $\delta^{15}N$ values of 37-184‰ (Engel and Macko, 1997) and δD topping out at >500‰ (Cronin et al., 1993).

In a number of stepwise combustion analyses of carbonaceous chondrites, an extremely high $\delta^{13}C$ value of 1100‰ was measured (Swart et al., 1983). Later work

[10] A racemic amino acid is one that has equal abundance of left- and right-handed optical isomers (enantiomers). The Murchison sample has a D/L value of 0.85, significantly different from the racemic value of 0.5. It is normally assumed that non-racemic amino acids are due to biological synthesis.

using high spatial resolution ion microprobe analyses revealed $\delta^{13}C$ values in interstellar residual grains in excess of 7000‰ (Zinner and Epstein, 1987). These are primitive and rare grains of 'stardust'.

13.6 Nitrogen

The wide range of nitrogen isotope variations in the solar system is exceeded only by hydrogen. Studies of the nitrogen isotope geochemistry of meteorites lagged behind the other 'traditional' light stable isotope elements mostly because nitrogen concentrations in meteorites are low and the analyses are difficult. Some of the first measurements of carbonaceous chondrites found a range considerably broader than what existed on Earth. Injerd and Kaplan (1974) measured $\delta^{15}N$ ratios between -20 and +46‰ from four chondrites. Kung and Clayton (1978) expanded the number of analyses and extended the total range observed for carbonaceous chondrites from lows of –40 to -30‰ for enstatite chondrites to highs of +30 and +50‰ (Renazzo with an anomalous 170‰). They felt that the variations were too large to be explained by mass dependent fractionation, and instead suggested that the meteorites were recording nitrogen isotope heterogeneities in the solar nebula.

As we have seen for hydrogen and carbon, the nitrogen isotope composition of the Sun represents the overall $\delta^{15}N$ value of the solar system. The Sun has the lowest $^{15}N/^{14}N$ ratio of any materials in our solar system. All processes that have occurred in the protoplanetary disk and after its dissipation, lead to a an enrichment in ^{15}N which is then incorporated into growing planetary bodies. The solar system can be broadly characterized of consisting of three distinct 'regions' in terms of $\delta^{15}N$ values (Mandt et al., 2014). The Sun, Jupiter and Saturn, with their very low $^{15}N/^{14}N$ ratio, the inner solar system, with $\delta^{15}N$ values of 0-50‰ and cometary ices, with $\delta^{15}N$ values of 850±150‰ (Fig. 13.11).

Hashizume *et al.* measured the $\delta^{15}N$ value of metal grain from the lunar soil in order to obtain the value of the solar wind. Their estimate was very light, at ≤ -240‰. A more recent measurement of solar wind implanted on the SiC plates of the Genesis mission corresponds to a $\delta^{15}N$ value of the solar wind of -407±7‰ and a $\delta^{15}N$ value for the Sun (and protosolar nebula) of -383±8‰ (Marty et al., 2011). For comparison, the $\delta^{15}N$ value of Jupiter was measured to be -374±80‰ from the *Galileo* Probe Mass Spectrometer (Owen et al., 2001).

The heavy nitrogen isotope composition of some solar system materials, such as organic matter, 'organic globules' in the Tagish Lake chondrite (Nakamura-Messenger et al., 2006) and comets (Fig. 13.11) has been attributed to low temperature ion molecule exchange reactions that could occur in a cold molecular cloud or in the protostellar nebula far from the Sun. One such reaction is

$$HN_2^+ + N^{15}N \rightarrow H^{15}NN^+ + N_2 \qquad 13.7$$

where the HN_2^+ ion (isodiazene) becomes enriched in ^{15}N and then becomes incorporated into ices and organic matter (Furi and Marty, 2015).

Nitrogen enrichment can also occur by escape from a planetary surface, such as Mars (as evidenced by the high $\delta^{15}N$ of the Martian atmosphere) and Titan. The moderately elevated $\delta^{15}N$ values of many asteroidal materials is probably related to kinetic and equilibrium isotope fractionations between nitrogen. The large fractionations relative to what is seen on Earth are difficult to account for and almost certainly require, at minimum, fractionation associated with an oxidation state change (*e.g.,* N_2 to NH_2^+) and low temperature dynamic interactions. Alternatively, the large range of $\delta^{15}N$ values has been suggested to reflect primordial nebular inhomogeneities (Thiemens and Clayton, 1981; Prombo and Clayton, 1993).

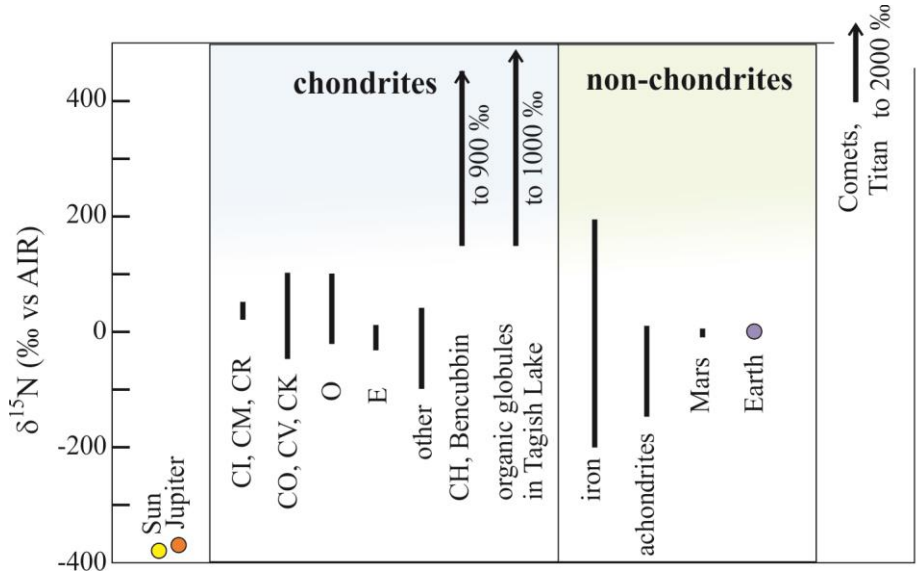

Fig. 13.11. Nitrogen isotope composition of different extraterrestrial materials. The Sun has the lowest $\delta^{15}N$ value of -383‰. All other solar system materials have higher $\delta^{15}N$ values. Samples formed at low temperatures far from the Sun, such as comets and Titan ($\delta^{15}N$ = 620‰) have the highest $\delta^{15}N$ values consistent with molecular ion reactions at low temperatures. The intermediate values found in meteorites may be related to kinetic or equilibrium molecular exchange reactions. Data from the following sources: (Owen et al., 2001; Grady and Wright, 2003; Nakamura-Messenger et al., 2006; Marty et al., 2011; Mandt et al., 2014; Furi and Marty, 2015).

13.7 Sulfur

In the meteorite world, the most remarkable thing about sulfur is how unremarkable it is. Hulston and Thode (1965) noted in a comprehensive study of meteoritic $\delta^{34}S$ values "that the isotopic composition of the total sulfur is remarkably constant from meteorite to meteorite." Most meteorites have a $\delta^{34}S$ value that falls in the range of -2 to +3‰. Hulston and Thode did not find any $\delta^{33}S$ or $\delta^{36}S$ anomalies that might be evidence of an exotic nucleosynthetic source. The data suggest that sulfur underwent some fractionation on the parent bodies, but that the source within the solar system was more-or-less constant (Kaplan and Hulston, 1966). This conclusion is consistent with the idea that sulfur condensed out of the solar nebula as FeS without fractionation and that no oxidation state changes occurred prior to incorporation into the parent bodies. The one interesting theme that has been observed in sulfur isotopes is the non-mass dependent fractionation (see section 10.5.5 for more information) seen in some differentiated bodies. Farquhar *et al.* (2000a) measured urelite samples with a small ^{33}S

anomaly which they attributed to gas phase reactions in the solar nebula that resulted in small anomalies in the protoplanetary disk. Both positive and negative ^{33}S anomalies have also been seen in Martian meteorites, which are explained by deposition of oxidized sulfur produced by atmospheric chemical reactions (Farquhar et al., 2000b). The common sulfur anomaly on Mars indicates widespread incorporation of surficial sulfur into Martian materials that have been delivered to Earth (Franz et al., 2014). A sulfur-36 anomaly has also been seen in some primitive differentiated bodies, presumably due to decay of ^{36}Cl early in solar system history (Defouilloy et al., 2016).

13.8 Chlorine

Chlorine isotopes are considered in this chapter because of the large isotope variations that have been seen in extraterrestrial materials. There are two stable isotopes of chlorine, ^{35}Cl and ^{37}Cl. The isotope ratios are reported in the standard delta notation with seawater – Standard Mean Ocean Chloride or SMOC – assigned a $\delta^{37}Cl$ value of 0‰. The bulk Earth $\delta^{37}Cl$ value is also close to 0‰. There are large variations in terrestrial materials due to near-surface processes (Barnes and Sharp, 2017), but most of these fractionation mechanisms are not relevant to extraterrestrial materials.

The $\delta^{37}Cl$ value of chondrites range from -4.5 to 2.5‰ (Fig. 13.12). The majority fall between -2 and +1‰, roughly consistent with the bulk Earth. What is perhaps most interesting is that three of the chondrite samples have $\delta^{37}Cl$ values less than -4‰. Mars has a wide range of $\delta^{37}Cl$ values, covering over 10‰ total variation. This is far larger range than for equivalent lithologies on Earth. The high $\delta^{37}Cl$ values are thought to be due to preferential loss of the light isotope (^{35}Cl) to space, leaving a heavy residue. The low $\delta^{37}Cl$ values (deep red color in Fig. 13.12) are the olivine phyric shergottites, which are thought to be the samples least contaminated by crustal material. Finally, the iron meteorites are negative, and reach the lowest $\delta^{37}Cl$ values of any extraterrestrial material measured to date (Gargano et al., 2017). It is suggested that the negative $\delta^{37}Cl$ values reflect direct incorporation of Cl from the solar nebula, and that the Sun presumably also has a negative $\delta^{37}Cl$ value (Sharp et al., 2016). The higher $\delta^{37}Cl$ values of most chondrites are explained by addition of an HCl-bearing ice ($HCl{\cdot}3H_2O$) formed beyond the snowline prior to dissipation of the solar nebula. The ice would preferentially incorporate ^{37}Cl ultimately leading to the heavy Cl isotope compositions of most chondrites.

The most remarkable Cl isotope variations are seen on the Moon, with a spread in excess of 40‰ (Fig. 13.12). The lowest values are close to 0‰ with one negative sample. Other than hydrogen, no other isotopic system shows such a large lunar range in its isotopic composition. The high $\delta^{37}Cl$ values are most likely due to degassing. In detail, a number of ideas have been proposed, including the following:

1. Local degassing of a solidifying magma, with the light isotopes preferentially lost to the vapor phase (Sharp et al., 2010);
2. Some samples may be related to vapor phase deposition related to meteorite impacts (Treiman et al., 2014);
3. Degassing into a vacuum
4. Degassing during the waning stages of the magma ocean stage following the Giant Impact (Boyce et al., 2015; Barnes et al., 2016).

Each of these ideas has merits and all are not mutually exclusive. Clearly the cause or causes of the enormous enrichment in ^{37}Cl in lunar samples is unique and is not well understood.

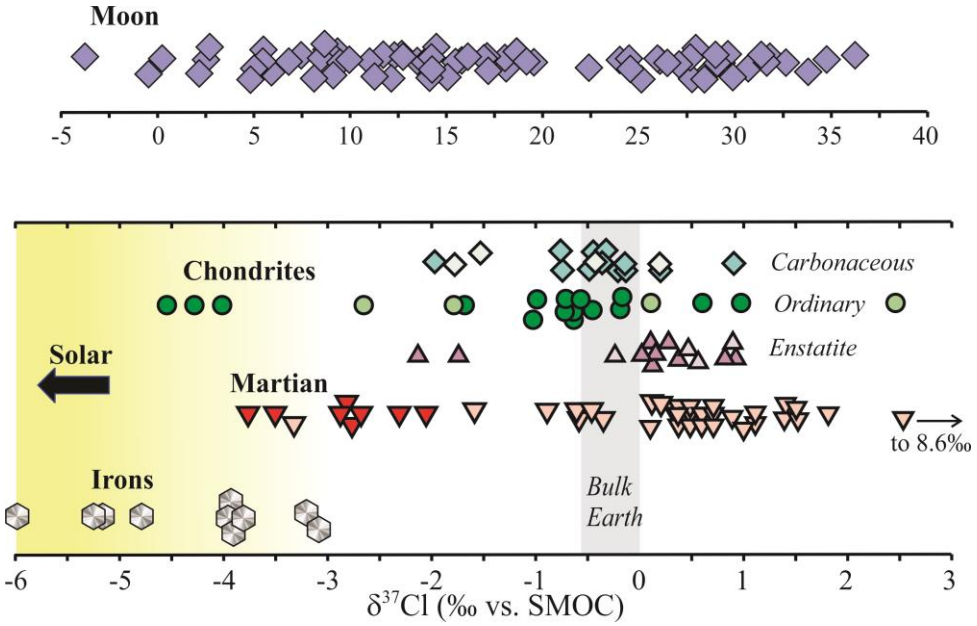

Fig. 13.12. Chlorine isotope composition of extraterrestrial materials. The lowest $\delta^{37}Cl$ values probably reflect the composition of the protonebular disk and Sun. Iron meteorites, mantle-derived Martian meteorites (deep red) and several ordinary chondrites preserve this signature. The other samples have been contaminated by a ^{37}Cl-enriched HCl-bearing ice or have lost light isotopes through vaporization. Each of these possibilities drives the $\delta^{37}Cl$ values of the residue to higher values. Lunar samples show a huge range of $\delta^{37}Cl$ values (note different scale for lunar materials. The high $\delta^{37}Cl$ values are due to vaporization of Cl during degassing.

Other isotope systems have been used to study extraterrestrial materials including Li, Mg, Si, Ti, Cr, Fe, Ni, Zn, and Mo. These are not normally considered as traditional stable isotopes and will not be considered here. Readers are referred to the recent book "*Non-Traditional Stable Isotopes"* (2017) which is a general overview of some of the recent developments of the non-HCNOS isotope systems.

References

Agee, C.B., Wilson, N.V., McCubbin, F.M., Ziegler, K., Polyak, V.J., Sharp, Z.D., Asmerom, Y., Nunn, M.H., Shaheen, R., Thiemens, M.H., Steele, A., Fogel, M.L., Bowden, R., Glamoclija, M., Zhang, Z. and Elardo, S.M. (2013) Unique meteorite from the Early Amazonian epoch on Mars: Water-rich basaltic breccia NWA 7034. *Science* **339**, 780-785.

Alexander, C.M.O.D., Newsome, S.D., Fogel, M.L., Nittler, L.R., Busemann, H. and Cody, G.D. (2010) Deuterium enrichments in chondritic macromolecular material—Implications for the origin and evolution of organics, water and asteroids. *Geochimica et Cosmochimica Acta* **74**, 4417-4437.

Alexander, C.M.O.D., Bowden, R., Fogel, M.L., Howard, K.T., Herd, C.D.K. and Nittler, L.R. (2012) The provenances of asteroids, and their contributions to the volatile inventories of the terrestrial planets. *Science* **337**, 721-723.

Amari, S. (2014) Recent progress in presolar grain studies. *Mass Spectrometry*.

Anders, E. and Zinner, E. (1993) Interstellar grains in primitive meteorites: diamond, silicon carbide, and graphite. *Meteoritics* **28**, 490-514.

Baertschi, P. (1950) Isotopic composition of the oxygen in silicate rocks. *Nature* **166**, 112-113.

Bally, J. and Langer, W.D. (1982) Isotope-selective photodestruction of carbon monoxide. *The Astrophysical Journal* **255**, 143-148.

Barnes, J.D. and Sharp, Z.D. (2017) Chlorine Isotope Geochemistry. *Reviews in Mineralogy and Geochemistry* **82**, 345-378.

Barnes, J.J., Tartèse, R., Anand, M., McCubbin, F.M., Neal, C.R. and Franchi, I.A. (2016) Early degassing of lunar urKREEP by crust-breaching impact(s). *Earth and Planetary Science Letters* **447**, 84-94.

Boato, G. (1954) The isotopic composition of hydrogen and carbon in the carbonaceous chondrites. *Geochimica et Cosmochimica Acta* **6**, 209-220.

Boyce, J.W., Treiman, A.H., Guan, Y., Ma, C., Eiler, J.M., Gross, J., Greenwood, J.P. and Stolper, E.M. (2015) The chlorine isotope fingerprint of the lunar magma ocean. *Science Advances* **1**, 8 pp.

Brearley, A. and Jones, R.H. (1998) Chondritic meteorites, in: Papike, J.J. (Ed.), Planetary Materials. Mineralogical Society of America, Washington, D.C., pp. 3.01-03.370.

Briggs, M.H. (1963) Evidence of an extraterrestrial origin for some organic constituents of meteorites. *Nature* **197**, 1290.

Burbidge, E.M., Burbidge, G.R., Fowler, W.A. and Hoyle, F. (1957) Synthesis of the elements in stars. *Reviews of Modern Physics* **29**, 547-650.

Chakraborty, S., Ahmed, M., Jackson, T.L. and Thiemens, M.H. (2008) Experimental test of self-shielding in vacuum ultraviolet photodissociation of CO. *Science* **321**, 1328-1331.

Clayton, R.N. (1963) Carbon isotope abundance in meteoritic carbonates. *Science* **140**, 192-193.

Clayton, R.N., Grossman, L. and Mayeda, T.K. (1973) A component of primitive nuclear composition in carbonaceous meteorites. *Science* **182**, 485-488.

Clayton, R.N. and Mayeda, T.K. (1975) Genetic relations between the moon and meteorites. *Proceedings of the Lunar Science Conference* **6**, 1761-1769.

Clayton, R.N. (1993) Oxygen isotopes in meteorites. *Annual Review of Earth and Planetary Sciences* **21**, 115-149.

Clayton, R.N. (2002) Solar System: Self-shielding in the solar nebula. *Nature* **415**, 860-861.

Copi, C.J., Schramm, D.N. and Turner, M.S. (1995) Big-bang nucleosynthesis and the baryon density of the universe. *Science* **267**, 192-199.

Craig, H. (1953) The geochemistry of the stable carbon isotopes. *Geochimica et Cosmochimica Acta* **3**, 53-92.

Craig, H. (1957) Isotopic standards for carbon and oxygen and correction factors for mass-spectrometric analysis of carbon dioxide. *Geochimica et Cosmochimica Acta* **12**, 133-149.

Cronin, J.R., Pizzarello, S., Epstein, S. and Krishnamurthy, R.V. (1993) Molecular and isotopic analyses of the hydroxy acids, dicarboxylic acids, and hydroxydicarboxylic acids of the Murchison Meteorite. *Geochimica et Cosmochimica Acta* **57**, 4745-4752.

Defouilloy, C., Cartigny, P., Assayag, N., Moynier, F. and Barrat, J.A. (2016) High-precision sulfur isotope composition of enstatite meteorites and implications of the formation and evolution of their parent bodies. *Geochimica et Cosmochimica Acta* **172**, 393-409.

Deines, P. and Wickman, F.E. (1975) A contribution to the stable carbon isotope geochemistry of iron meteorites. *Geochimica et Cosmochimica Acta* **39**, 547-557.

Deloule, E. and Robert, F. (1995) Interstellar water in meteorites? *Geochimica et Cosmochimica Acta* **59**, 4695-4706.

Donahue, T.M., Hoffman, J.H., Hodges, R.R. and Watson, A.J. (1982) Venus was wet: A measurement of the ratio of deuterium to hydrogen. *Science* **216**, 630-633.

Engel, M.H., Macko, S.A. and Silfer, J.A. (1990) Carbon isotope composition of individual amino acids in the Murchison meteorite. *Nature* **348**, 47-49.

Engel, M.H. and Macko, S.A. (1997) Isotopic evidence for extraterrestrial nonracemic amino acids in the Murchison meteorite. *Nature* **389**, 265-268.

Epstein, S. and Taylor, H.P., Jr. (1970) $^{18}O/^{16}O$, $^{30}Si/^{28}Si$, D/H, and $^{13}C/^{12}C$ studies of lunar rocks and minerals. *Science* **167**, 533-535.

Epstein, S., Krishnamurthy, R.V., Cronin, J.R., Pizzarello, S. and Yuen, G.U. (1987) Unusual stable isotope ratios in amino acid and carboxylic acid extracts from the Murchison meteorite. *Nature* **326**, 477-479.

Farquhar, J., Jackson, T.L. and Thiemens, M.H. (2000a) A ^{33}S enrichment in ureilite meteorites: evidence for a nebular sulfur component. *Geochimica et Cosmochimica Acta* **64**, 1819-1825.

Farquhar, J., Savarino, J., Jackson, T.L. and Thiemens, M.H. (2000b) Evidence of atmospheric sulphur in the martian regolith from sulphur isotopes in meteorites. *Nature* **404**, 50-52.

Franchi, I.A., Wright, I.P., Sexton, A.S. and Pillinger, C.T. (1999) The oxygen-isotopic composition of Earth and Mars. *Meteoritics & Planetary Science* **34**, 657-661.

Franz, H.B., Kim, S.-T., Farquhar, J., Day, J.M.D., Economos, R.C., McKeegan, K.D., Schmitt, A.K., Irving, A.J., Hoek, J. and Iii, J.D. (2014) Isotopic links between atmospheric chemistry and the deep sulphur cycle on Mars. *Nature* **508**, 364-368.

Friedman, I., O'Neil, J.R., Adami, L.H., Gleason, J.D. and Hardcastle, K. (1970) Water, hydrogen, deuterium, carbon, carbon-13, and oxygen-18 content of selected Lunar material. *Science* **167**, 538-540.

Furi, E. and Marty, B. (2015) Nitrogen isotope variations in the Solar System. *Nature Geoscience* **8**, 515-522.

Gargano, A.M., Sharp, Z.D. and Taylor, L.A. (2017) Further Constraining the Chlorine Isotope Composition of the Solar Nebula: Main Group Iron Meteorites
80th Meteoritical Society Annual Meeting 2017.

Grady, M.M., Wright, I.P., Carr, L.P. and Pillinger, C.T. (1986) Compositional differences in enstatite chondrites based on carbon and nitrogen stable isotope measurements. *Geochimica et Cosmochimica Acta* **50**, 2799-2813.

Grady, M.M. and Wright, I.P. (2003) Elemental and isotopic abundances of carbon and nitrogen in meteorites. *Space Science Reviews* **106**, 231-248.

Greenwood, J.P., Itoh, S., Sakamoto, N., Warren, P., Taylor, L. and Yurimoto, H. (2011) Hydrogen isotope ratios in lunar rocks indicate delivery of cometary water to the Moon. *Nature Geoscience* **4**, 79-82.

Greenwood, R.C., Franchi, I.A., Jambon, A. and Buchanan, P.C. (2005) Widespread magma oceans on asteroidal bodies in the early Solar System. *Nature* **435**, 916-918.

Greenwood, R.C., Franchi, I.A., Jambon, A., Barrat, J.A. and Burbine, T.H. (2006) Oxygen Isotope Variation in Stony-Iron Meteorites. *Science* **313**, 1763-1765.

Greenwood, R.C., Franchi, I.A., Gibson, J.M. and Benedix, G.K. (2012) Oxygen isotope variation in primitive achondrites: The influence of primordial, asteroidal and terrestrial processes. *Geochimica et Cosmochimica Acta* **94**, 146-163.

Harkins, W.D. and Stone, S.B. (1926) The isotopic composition and atomic weight of chlorine from meteorites and from minerals of non-marine origin: (Papers on atomic stability). *Journal of the American Chemical Society* **48**, 938-949.

Hashizume, K., Chaussidon, M., Marty, B. and Terada, K. (2004) Protosolar carbon isotopic composition: Implications for the origin of meteoritic organics. *The Astrophysical Journal* **600**, 480-484.

Hashizume, K. and Chaussidon, M. (2005) A non-terrestrial ^{16}O-rich isotopic composition for the protosolar nebula. *Nature* **434**, 619 - 622.

Hauri, E.K., Saal, A.E., Nakajima, M., Anand, M., Rutherford, M.J., Van Orman, J.A. and Le Voyer, M. (2017) Origin and Evolution of water in the Moon's interior. *Annual Review of Earth and Planetary Sciences* **45**, 89-111.

Herwartz, D., Pack, A., Friedrichs, B. and Bischoff, A. (2014) Identification of the giant impactor Theia in lunar rocks. *Science* **344**, 1146-1150.

Hulston, J.R. and Thode, H.G. (1965) Variations in the S^{33}, S^{34}, and S^{36} contents of meteorites and their relation to chemical and nuclear effects. *Journal of Geophysical Research* **70**, 3475-3484.

Injerd, W.G. and Kaplan, I.R. (1974) Nitrogen isotope distribution in meteorites. *Meteoritics* **9**, 308-309.

Jenkins, F.A. and King, A.S. (1936) A test of the abundance of the heavy isotope of carbon in a graphite meteorite. *Publications of the Astronomical Society of the Pacific*, 323-325.

Kaplan, I.R. and Hulston, J.R. (1966) The isotopic abundance and content of sulfur in meteorites. *Geochimica et Cosmochimica Acta* **30**, 479-496.

Kaplan, I.R. and Petrowski, C. (1971) Carbon and sulfur isotope studies on Apollo 12 lunar samples. *Proceedings of the Lunar Science Conference*, 1397-1406.

Kolodny, Y., Kerridge, J.F. and Kaplan, I.R. (1980) Deuterium in carbonaceous chondrites. *Earth and Planetary Science Letters* **46**, 149-158.

Krot, A.N., McKeegan, K.D., Leshin, L.A., MacPherson, G.J. and Scott, E.R.D. (2002) Existence of an ^{16}O-rich gaseous reservoir in the solar nebula. *Science* **295**, 1051-1054.

Krouse, H.R. and Modzeleski, V.E. (1970) C^{13}/C^{12} abundances in components of carbonaceous chondrites and terrestrial samples. *Geochimica et Cosmochimica Acta* **34**, 459-474.

Kung, C.C. and Clayton, R.N. (1978) Nitrogen abundances and isotopic compositions in stony meteorites. *Earth and Planetary Science Letters* **38**, 421-435.

Lancet, M.S. and Anders, E. (1970) Carbon isotope fractionation in the Fischer-Tropsch synthesis and in meteorites. *Science* **170**, 980-982.

Langer, W.D. (1977) Isotopic abundance of CO in interstellar clouds. *The Astrophysical Journal* **212**, L39-L42.

Luz, B., Barkan, E., Bender, M.L., Thiemens, M.H. and Boering, K.A. (1999) Triple-isotope composition of atmospheric oxygen as a tracer of biosphere productivity. *Nature* **400**, 547-550.

Lyons, J.R., Lewis, R.S. and Clayton, R.N. (2009) Comment on "Experimental test of self-shielding in vacuum ultraviolet photodissociation of CO". *Science* **324**, 1516-1516.

Mandt, K.E., Mousis, O., Lunine, J.I. and Gautier, D. (2014) Protosolar ammonia as the unique source of Titan's nitrogen. *Astrophysical Journal Letters* **788**, L24 (25pp).

Manian, S.H., Urey, H.C. and Bleakney, W. (1934) An investigation of the relative abundance of the oxygen isotopes O^{16}/O^{18} in stone meteorites. *Journal of the American Chemical Society* **56**, 2601-2609.

Marty, B., Chaussidon, M., Wiens, R.C., Jurewicz, A.J.G. and Burnett, D.S. (2011) A ^{15}N-poor isotopic composition for the Solar System as shown by Genesis solar wind samples. *Science* **332**, 1533-1536.

Marty, B. (2012) The origins and concentrations of water, carbon, nitrogen and noble gases on Earth. *Earth and Planetary Science Letters* **313-314**, 56–66.

McCubbin, F.M., Steele, A., Hauri, E.H., Nekvasil, H., Yamashita, S. and Hemley, R.J. (2010) Nominally hydrous magmatism on the Moon. *Proceedings of the National Academy of Science* **107**, 11223-11228.

McKeegan, K.D. and Leshin, L.A. (2001) Stable isotope variations in extraterrestrial materials, in: Valley, J.W., Cole, D.R. (Eds.), Stable Isotope Geochemistry. Mineralogical Society of America, Washington, D.C., pp. 279-318.

McKeegan, K.D., Kallio, A.P.A., Heber, V.S., Jarzebinski, G., Mao, P.H., Coath, C.D., Kunihiro, T., Wiens, R.C., Nordholt, J.E., Moses, R.W., Reisenfeld, D.B., Jurewicz,

A.J.G. and Burnett, D.S. (2011) The oxygen isotopic composition of the Sun inferred from captured solar wind. *Science* **332**, 1528-1532.

McNaughton, N.J., Borthwick, J., Fallick, A.E. and Pillinger, C.T. (1981) Deuterium/hydrogen ratios in unequilibrated ordinary chondrites. *Nature* **294**, 639-641.

Messenger, S. (2000) Identification of molecular-cloud material in interplanetary dust particles. *Nature* **404**, 968-971.

Michalski, G. and Bhattacharya, S.K. (2009) The role of symmetry in the mass independent isotope effect in ozone. *Proceedings of the National Academy of Sciences* **106**, 5493-5496.

Murphey, B.F. and Nier, A.O. (1941) Variations in the relative abundance of the carbon isotopes. *Physical Review* **59**, 771-772.

Nakamura-Messenger, K., Messenger, S., Keller, L.P., Clemett, S.J. and Zolensky, M.E. (2006) Organic globules in the Tagish Lake meteorite: Remants of the protosolar disk. *Science* **314**, 1439-1442.

Nittler, L.R., Alexander, C.M.O.D., Gao, X., Walker, R.M. and Zinner, E. (1997) Stellar sapphires: The properties and origins of presolar Al_2O_3 in meteorites. *The Astrophysical Journal* **483**, 475-495.

Nittler, L.R. (2003) Presolar stardust in meteorites: recent advances and scientific frontiers. *Earth and Planetary Science Letters* **209**, 259-273.

Onuma, N., Clayton, R.N. and Mayeda, T.K. (1970) Oxygen isotope fractionation between minerals and an estimate of the temperature of formation. *Science* **167**, 536-538.

Owen, T., Mahaffy, P.R., Niemann, H.B., Atreya, S. and Wong, M. (2001) Protosolar nitrogen. *The Astrophysical Journal Letters* **553**, L77-L79.

Prombo, C.A. and Clayton, R.N. (1993) Nitrogen isotopic compositions of iron meteorites. *Geochimica et Cosmochimica Acta* **57**, 3749-3761.

Reeves, H. and Bottinga, Y. (1972) The D/H Ratio in Jupiter's Atmosphere. *Nature* **238**, 326-327.

Reuter, J.H., Epstein, S. and Taylor, H.P., Jr. (1965) O^{18}/O^{16} ratios of some chondritic meteorites and terrestrial ultramafic rocks. *Geochimica et Cosmochimica Acta* **29**, 481-488.

Rietmeijer, F.J.M. (1998) Interplanetary Dust Particles, in: Papike, J.J. (Ed.), Planetary Materials. Mineralogical Society of America, Washington, D.C., pp. 2-1- 2-95.

Robert, F., Gautier, D. and Dubrulle, B. (2000) The solar system D/H ratio: observations and theories. *Space Science Reviews* **92**, 201-224.

Robinson, K.L., Barnes, J.J., Nagashima, K., Thomen, A., Franchi, I.A., Huss, G.R., Anand, M. and Taylor, G.J. (2016) Water in evolved lunar rocks: Evidence for multiple reservoirs. *Geochimica et Cosmochimica Acta* **188**, 244-260.

Rumble III, D. and Irving, A.J. (2009) Dispersion of oxygen isotopic compositions among 42 martian meteorites determine by laser fluorination: evidence for assimilation of (ancient) altered crust. *Lunar and Planetary Science Conference* **40**, 2293.pdf.

Saal, A.E., Hauri, E.H., Cascio, M.L., Van Orman, J.A., Rutherford, M.C. and Cooper, R.F. (2008) Volatile content of lunar volcanic glasses and the presence of water in the Moon's interior *Nature* **454**, 192-195.

Saal, A.E., Hauri, E.H., Van Orman, J.A. and Rutherford, M.A. (2013) Hydrogen isotopes in lunar volcanic glasses and melt inclusions reveal a carbonaceous chondrite heritage. *Science* **340**, 1317-1320.

Sharp, Z.D., Shearer, C.K., McKeegan, K.D., Barnes, J.D. and Wang, Y.Q. (2010) The Chlorine Isotope Composition of the Moon and implications for an anhydrous mantle. *Science* **329**, 1050-1053.

Sharp, Z.D., McCubbin, M. and Shearer, C.K. (2013) A hydrogen-based oxidation mechanism relevant to planetary formation. *Earth and Planetary Science Letters* **380**, 88-97.

Sharp, Z.D., Williams, J., Shearer, C.K., Agee, C.B. and McKeegan, K.D. (2016) The chlorine isotope composition of Martian meteorites 2. Implications for the early solar system and the formation of Mars. *Meteoritics and Planetary Sciences* **doi: 10/1111/maps.12591**, 16 pages.

Sharp, Z.D. (2017) Nebular ingassing as a source of volatiles to the Terrestrial planets. *Chemical Geology* **448**, 137-150.

Shearer, C.K., Papike, J.J. and Rietmeijer, F.J.M. (1998) The planetary sample suite and environments of origin, in: Papike, J.J. (Ed.), Planetary Materials. Mineralogical Society of America, Washington, D.C., pp. 1-1 - 1-28.

Silverman, S.R. (1951) The isotope geology of oxygen. *Geochimica et Cosmochimica Acta* **2**, 26-42.

Smith, J.W. and Kaplan, I.R. (1970) Endogenous carbon in carbonaceous meteorites. *Science* **167**, 1367-1370.

Spicuzza, M., Day, J.M.D., Taylor, L.A. and Valley, J.W. (2007) Oxygen isotope constraints on the origin and differentiation of the Moon. *Earth and Planetary Science Letters* **253**, 254-265.

Stolper, E. (1982) Crystallization sequences of Ca-, Al-rich inclusions from Allende: an experimental study. *Geochimica et Cosmochimica Acta* **46**, 2159-2180.

Swart, P.K., Grady, M.M., Pillinger, C.T., Lewis, R.S. and Anders, E. (1983) Interstellar carbon in meteorites. *Science* **220**, 406-410.

Taylor, H.P., Jr., Duke, M.B., Silver, L.T. and Epstein, S. (1965) Oxygen isotope studies of minerals in stony meteorites. *Geochimica et Cosmochimica Acta* **29**, 489-512.

Teng, F.-Z., Watkins, J.M. and Dauphas, N. (2017) Non-Traditional Stable Isotopes, Reviews in Mineralogy and Geochemistry. Mineralogical Society of America, p. 885.

Thiemens, M. and Clayton, R.N. (1981) Nitrogen isotopes in the Allende meteorite. *Earth and Planetary Science Letters* **55**, 363-369.

Thiemens, M. (1999) Planetary atmospheres and the early solar system. *Science* **283**, 341-345.

Thiemens, M. (2006) History and applications of mass-independent isotope effects. *Annual Reviews of Earth and Planetary Sciences* **34**, 217–262.

Thiemens, M.H. and Heidenreich, J.E.I. (1983) The mass-independent fractionation of oxygen: A novel isotope effect and its possible cosmochemical implications. *Science* **219**, 1073-1075.

Treiman, A.H., Boyce, J.W., Gross, J., Guan, Y., Eiler, J.M. and Stolper, E.M. (2014) Phosphate-halogen metasomatism of lunar granulite 79215: Impact-induced

fractionation of volatiles and incompatible elements. *American Mineralogist* **99**, 1860-1870.

Trofimov, A. (1949) Isotopic constitution of sulfur in meteorites and in terrestrial objects. *Doklady Akademii nauk SSSR* **66**, 181-184.

Urey, H.C. (1967) The abundance of the elements with special reference to the problem of the iron abundance. *Quarterly Journal of the Royal Astronomical Society* **8**, 23-47.

Villanueva, G.L., Mumma, M.J., Novak, R.E., Käufl, H.U., Hartogh, P., Encrenaz, T., Tokunaga, A., Khayat, A. and Smith, M.D. (2015) Strong water isotopic anomalies in the martian atmosphere: Probing current and ancient reservoirs. *Science* **348**, 218-221.

Vinogradov, A.P., Dontsova, E.I. and Chupakhin, M.S. (1960) Isotopic ratios of oxygen in meteorites and igneous rocks. *Geochimica et Cosmochimica Acta* **18**, 278-293.

Wiechert, U.H., Halliday, A.N., Lee, D.-C., Snyder, G.A., Taylor, L.A. and Rumble, D.I. (2001) Oxygen isotopes and the Moon-forming Giant Impact. *Science* **294**, 345-348.

Wiechert, U.H., Halliday, A.N., Palme, H. and Rumble, D. (2004) Oxygen isotope evidence for rapid mixing of the HED meteorite parent body. *Earth and Planetary Science Letters* **221**, 373-382.

Young, E., Kohl, I.E., Warren, P.H., Rubie, D.C., Jacobson, S.A. and Morbidelli, A. (2016) Oxygen isotopic evidence for vigorous mixing during the Moon-forming giant impact. *Science* **351**, 493-496.

Young, E.D. and Russell, S.S. (1998) Oxygen reservoirs in the early solar nebula inferred from an Allende CAI. *Science* **282**, 452-455.

Young, E.D., Ash, R.D., England, P. and Rumble, D. (1999) Fluid Flow in Chondritic Parent Bodies: Deciphering the Compositions of Planetesimals. *Science* **286**, 1331-1335.

Yurimoto, H. and Kuramoto, K. (2004) Molecular cloud origin for the oxygen isotope heterogeneity in the Solar System. *Science* **305**, 1763-1766.

Zinner, E. and Epstein, S. (1987) Heavy carbon in individual oxide grains from the Murchison Meteorite. *Earth and Planetary Science Letters* **84**, 359-368.

Appendix 1.

Standard Reference Materials for Stable Isotopes.

Isotopic composition of selected reference materials after the compilation of Coplen *et al*. (2002) and data from IAEA. Additional standards not presented here have been made, however they are not official IAEA-approved. Additional IAEA standards are developed continually. Refer to the IAEA website for up-to-date delta values.

Reference Standard	Substance	$\delta^{18}O$ (VSMOW)	$\delta^{18}O$ (VPDB)	$\delta^{13}C$ (VPDB)	δD (VSMOW)
VSMOW, VSMOW2 (Standard Mean Ocean Water)	water	≡ 0.00			≡ 0.00
SLAP (Standard Light Antarctic Precipitation)	water	≡ -55.50			≡ -428.00
SLAP2		-55.50			-427.5
GISP (Greenland Ice Sheet Precipitation)	water	-24.76			-189.5
IAEA 604	Enriched H_2O	-5.86			799.9
NGS1	CH_4 in nat. gas			-29.0	-138
NGS2	CH_4 in nat. gas			-44.7	-173
NGS2	C_2H_6 in nat. gas			-31.7	-121
NGS3	CH_4 in nat. gas			-72.7	-176
NBS-18	calcite	7.20	-23.00	-5.01	
NBS-19	calcite	28.64	≡ -2.20	≡ +1.95	
IAEA-603	calcite		-2.37	2.46	
IAEA-CO-1	calcite	28.39	-2.44	2.48	
IAEA-CO-8	calcite	7.54	-22.67	-5.75	
IAEA-CO-9	$BaCO_3$	15.16	-15.28	-47.12	
LSVEC	Li_2CO_3	3.63	-26.46	-46.48	
USGS-24	graphite			-15.99	
NBS-22	oil			-29.74	
IAEA-CH-7	polyethylene			-31.83	-100.3
IAEA-C-6	sucrose			-10.43	
NBS-28	quartz	9.58			
NBS-30	biotite	5.24			-65.7
NIST RM 8562	CO_2	22.20	-8.45	-3.76	
NIST RM 8563	CO_2	6.46	-23.72	-41.56	
NIST RM 8564	CO_2	31.11	0.19	-10.45	

Appendix 1, continued.

		$\delta^{18}O$ (SMOW)	$\delta^{13}C$ (VPDB)	$\delta^{15}N$ (air)	δD (VSMOW)
USGS-24	graphite		-15.99		
NBS-22	oil		-29.74		
IAEA 600	caffeine		-27.77	1.0	
IAEA 601	benzoic acid	23.3			
IAEA 602	benzoic acid	71.4			
IAEA-CH-3	cellulose		-24.724		
IAEA-CH-6	sucrose		-10.449		
IAEA-CH-7	polyethylene		-32.151		-100.3
IAEA-303-A	$NaHCO_3$		93.3		
IAEA-303-B	$NaHCO_3$		466.		
IAEA-N-1	$(NH_4)_2SO_4$			0.4	
IAEA-N-2	$(NH_4)_2SO_4$			20.3	
IAEA-NO-3	KNO_3	25.6		4.7	
NSVEC	N_2 gas			-2.8	
NBS-14	N_2 gas			-1.18	
IAEA-N-1	$(NH_4)_2SO_4$			0.43	
IAEA-N-2	$(NH_4)_2SO_4$			20.32	
IAEA-305A	$(NH_4)_2SO_4$			39.8	
IAEA-305B	$(NH_4)_2SO_4$			375.3	
IAEA-311	$(NH_4)_2SO_4$			4693	
USGS25	$(NH_4)_2SO_4$			-30.4	
USGS26	$(NH_4)_2SO_4$			53.7	
IAEA-310A	$CO(NH_2)_2$			47.2	
IAEA-310B	$CO(NH_2)_2$			244.6	
IAEA-NO-3	KNO_3	25.3		4.69	
USGS32	KNO_3			179.2	
USGS34	KNO_3	-27.9		-1.8	
USGS35	$NaNO_3$	57.5		2.7	

Appendix 1, continued.

		$\delta^{18}O$ (SMOW)	$\delta^{15}N$ (air)	$\delta^{34}S$ (CDT)	$\delta^{37}Cl$ (SMOC)
USGS25	$(NH_4)_2SO_4$		-30.25		
USGS26	$(NH_4)_2SO_4$		53.62		
USGS32	KNO_3		179.2		
USGS34	KNO_3	-27.9	-1.8		
USGS35	$NaNO_3$	57.5	2.7		
IAEA-S-1	Ag_2S			≡ -0.30	
IAEA-S-2	Ag_2S			22.67	
IAEA-S-3	Ag_2S			-32.55	
IAEA-S-4	native sulfur			16.9	
NBS-123	sphalerite			17.44	
NBS-127	$BaSO_4$	8.7		21.1*	
IAEA-SO-5	$BaSO_4$	12.0		0.49	
IAEA-SO-6	$BaSO_4$	-11.0		-34.05	
Soufre de lacq	Sulfur			16.90	
SRM 975	NaCl				0.43
SRM 975a	NaCl				0.2
ISL 354	NaCl				0.05

2

*The original published $\delta^{34}S$ value of NBS 127 was 20.32‰ using SO_2 gas (Hut, 1987). A revised value of 21.1‰ was determined using SF_6 gas.

Coplen T. B., Hopple J. A., Böhlke J. K., Peiser H. S., Rieder S. E., Krouse H. R., Rosman K. J. R., Ding T., Vocke R. D. J., Révész K. M., Lamberty A., Taylor P., and DeBièvre P. (2002) Compilation of Minimum and Maxium Isotope Ratios of Selected Elements in Naturally Occurring Terrestrial Materials and Reagents, pp. 98. United States Geological Survey.

Hut G. (1987) Consultants' group meeting on stable isotope reference samples for geochemical and hydrological investigations. International Atomic Energy Agency.

Appendix 2.

Sample calculation of the correction procedure for adjusting measured isotope data to accepted IAEA reference scales.

There are a number of factors which lessen the measured spread between the isotopic composition of two samples with very different isotopic ratios. Leaking of changeover valves, memory, blanks, etc. could all cause the apparent isotopic difference between two samples to be less what it actually is. A correction for the compression effects can be made by 'stretching' all data so that they conform to a universally accepted scale. The problem is most severe for hydrogen isotope determinations. Two standards with very different compositions, VSMOW = 0 ‰ and SLAP = -428‰, were developed to allow each laboratory to correct for the compression unique to their system. For the hydrogen example, the difference between VSMOW and SLAP must be 428 ‰. If the difference measured in the laboratory is less than 428‰, a stretching factor needs to be applied to the data. Similar stretching factors can be applied to all isotope systems. The example below is for sulfur.

Consider the measured $\delta^{34}S$ values of SO_2 gas samples given in Table A2-1.

Table A.2.1 *Sample stretching factor calculations*

Sample	Measured $\delta^{34}S$ value	Measured × stretching factor*	Shifted to VCDT scale	Accepted $\delta^{34}S$ value
1	-14.2	-14.83	-14.61	
2	+2.3	2.40	2.62	
IAEA-S-1	-0.5	-0.52	-0.30	-0.30
IAEA-S-2	21.5	22.45	22.67	22.67

*Two decimal places are recorded in column 3. This does not imply that the data have a higher level of precision than the measured data in column 2. The extra decimal place is added to avoid rounding errors. Reported data should have the level of decimal places appropriate to their uncertainty.

Step 1. The accepted difference ($\Delta_{accepted}$) between IAEA-S-2 and IAEA-S-1 is (22.67 – -0.3) = 22.97‰. The measured difference ($\Delta_{measured}$) between IAEA-S-2 and IAEA-S-1 in our example is (21.5 – -0.5) = 22.0‰. The measured isotope scale is compressed relative to the accepted one by a ratio of $\Delta_{accepted}/\Delta_{measured}$ given by 22.97/22.0 = 1.0441. This is the 'stretching' factor, required to bring the scale of the measured values into agreement with the accepted one. All measurements are multiplied by the stretching factor (column 3 – Measured × stretching factor).

Step 2. The data now need to be shifted by a constant amount to bring them into agreement with the VCDT scale. The difference between the accepted and measured values 'stretched' to the IAEA scale is given by (-0.3 – -0.52) = 0.22 or (22.67 – 22.45) = 0.22. 0.22 is added to all data in column 3 to bring them into agreement with the VCDT scale (column 4 – Shifted to VCDT scale). Note that the two measured IAEA samples have been corrected so that they are identical to the accepted IAEA values.

The two steps outlined above are illustrated graphically in Fig. A2. In the top row,

the measured delta values of two references and two samples are given. In step one, all delta values are multiplied by a constant to increase the difference between them, so that the measured difference between the two standards is the same as the accepted difference. (The difference between the measured values of the references could be larger than the accepted values. In such a case, step 1 involves multiplication by a constant less than 1, and the delta values are compressed). In the step 2, a constant is added to each value to bring the measured values of the two references in agreement with the accepted values. At this point, the corrected delta values of the samples will be on the IAEA scale.

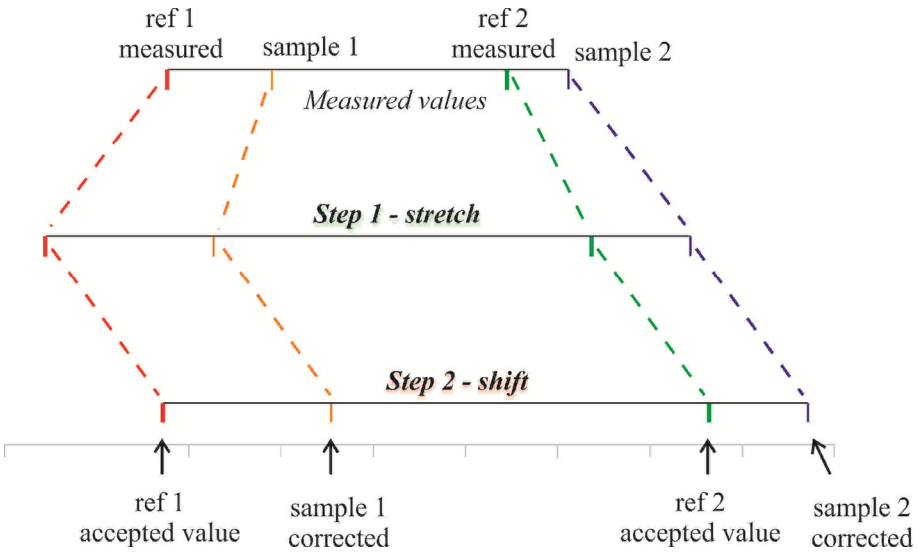

Fig. A2. Schematic of stretching